National Library of Canada
Acquisitions and Bibliographic Services Branch
395 Wellington Street
Ottawa, Ontario
K1A 0N4

Bibliothèque nationale du Canada
Direction des acquisitions et des services bibliographiques
395, rue Wellington
Ottawa (Ontario)
K1A 0N4

Your file Votre référence

Our file Notre référence

NOTICE

The quality of this microform is heavily dependent upon the quality of the original thesis submitted for microfilming. Every effort has been made to ensure the highest quality of reproduction possible.

If pages are missing, contact the university which granted the degree.

Some pages may have indistinct print especially if the original pages were typed with a poor typewriter ribbon or if the university sent us an inferior photocopy.

Reproduction in full or in part of this microform is governed by the Canadian Copyright Act, R.S.C. 1970, c. C-30, and subsequent amendments.

AVIS

La qualité de cette microforme dépend grandement de la qualité de la thèse soumise au microfilmage. Nous avons tout fait pour assurer une qualité supérieure de reproduction.

S'il manque des pages, veuillez communiquer avec l'université qui a conféré le grade.

La qualité d'impression de certaines pages peut laisser à désirer, surtout si les pages originales ont été dactylographiées à l'aide d'un ruban usé ou si l'université nous a fait parvenir une photocopie de qualité inférieure.

La reproduction, même partielle, de cette microforme est soumise à la Loi canadienne sur le droit d'auteur, SRC 1970, c. C-30, et ses amendements subséquents.

Canada

UNIVERSITY OF ALBERTA

AN INVESTIGATION OF HOIST-INDUCED DYNAMIC LOADING

by

DOUGLAS A. BARRETT

A thesis submitted to the Faculty of Graduate Studies and Research in partial fulfillment of the requirements for the degree of Master of Science

in

Civil Engineering.

DEPARTMENT OF CIVIL ENGINEERING

EDMONTON, ALBERTA

SPRING 1993

National Library
of Canada

Acquisitions and
Bibliographic Services Branch

395 Wellington Street
Ottawa, Ontario
K1A 0N4

Bibliothèque nationale
du Canada

Direction des acquisitions et
des services bibliographiques

395, rue Wellington
Ottawa (Ontario)
K1A 0N4

Your file Votre référence

Our file Notre référence

The author has granted an irrevocable non-exclusive licence allowing the National Library of Canada to reproduce, loan, distribute or sell copies of his/her thesis by any means and in any form or format, making this thesis available to interested persons.

L'auteur a accordé une licence irrévocable et non exclusive permettant à la Bibliothèque nationale du Canada de reproduire, prêter, distribuer ou vendre des copies de sa thèse de quelque manière et sous quelque forme que ce soit pour mettre des exemplaires de cette thèse à la disposition des personnes intéressées.

The author retains ownership of the copyright in his/her thesis. Neither the thesis nor substantial extracts from it may be printed or otherwise reproduced without his/her permission.

L'auteur conserve la propriété du droit d'auteur qui protège sa thèse. Ni la thèse ni des extraits substantiels de celle-ci ne doivent être imprimés ou autrement reproduits sans son autorisation.

ISBN 0-315-82067-5

Canada

Whiting

WHITING CORPORATION

15700 LATHROP, HARVEY, IL 60426-5198 • (312) 468-9400 • FAX: (312) 785-0755 • TELEX: 25-3274

November 25, 1992

Mr. Douglas Barrett
10605 85th Avenue
Edmonton, Alberta, Canada
T6E 2K6

Dear Mr. Barrett,

I have received your request to reproduce Table 34, page 206 from the 4th edition of the Crane Handbook, in your thesis on dynamic loads on bridge cranes and supporting structures.

Permission is granted for you to reproduce this table in your thesis, please credit the Whiting Corporation, Harvey, Illinois.

Very Truly Yours,

Peter S. Hammond
Advertising Manager

Moncton • Montreal • Toronto • Winnipeg • Edmonton • Vancouver • Taiwan • Hong Kong

October 29, 1991

Mr. Douglas Barrett
10605 85th Avenue
Edmonton, Alberta
T6E 2K6

Dear Mr. Barrett,

This letter serves to acknowledge your correspondence of August 21, 1991 and our subsequent discussion surrounding your request to reproduce selected components of CSA Standard B167-1964 (General Purpose Electric Overhead Travelling Cranes).

Permission is granted to reproduce, under the following conditions, those sections you outline in your letter (Page 8 - Tables 1, 2, Page 9 - Tables 3, 4, Page 17 - Table 10) strictly for the application you describe. Any further reproduction must be reviewed by CSA before permission may be granted.

1. Reproduction is limited to B167-1964 edition only.
2. The following credit statement shall be predominantly displayed on the reproduced section: "With the permission of the Canadian Standards Association, this material is reproduced from B167-1964 (General Purpose Electric Overhead Travelling Cranes), which is copyrighted by CSA, 178 Rexdale Boulevard, Rexdale, Ontario, Canada, M9W 1R3".
3. As updates to this Standard would be the responsibility of the user, a statement shall be predominantly displayed advising the reader that: "This copy of CSA Standard B167-1964 (General Purpose Electric Overhead Travelling Cranes), as reproduced with CSA permission, will not be updated to reflect amendments made to the original content of the CSA Standard after November 1966. For up-to-date information, see the current edition of the CSA Catalogue of Standards".
4. CSA will receive one complimentary copy of your reproduced excerpt.

I trust this letter serves your requirements and if I can be of further assistance in this matter, please don't hesitate to contact me.

Best regards,

Peter S. Nicol
Manager, Standards Sales
Standards Division
(416) 747-2629

Canadian Standards Association, 178 Rexdale Blvd. Rexdale (Toronto) Ontario, Canada M9W 1R3
Telephone: (416) 747-4000 Telefax: (416) 747-2475 Telex: 06-989344

PN/Oct.91/17/cm

UNIVERSITY OF ALBERTA

RELEASE FORM

NAME OF AUTHOR : DOUGLAS BARRETT

TITLE OF THESIS : AN INVESTIGATION OF HOIST-INDUCED DYNAMIC LOADING

DEGREE : MASTER OF SCIENCE IN CIVIL ENGINEERING

YEAR THIS DEGREE GRANTED : 1993

Permission is hereby granted to the University of Alberta to reproduce single copies of this thesis and to lend or sell such copies for private, scholarly or scientific research only.

The author reserves all other publication and other rights in association with the copyright in the thesis, and except as hereinbefore provided neither the thesis nor any substantial portion thereof may be printed or otherwise reproduced in any material form whatsoever without the author's prior written permission.

D. Barrett

10605 85 Ave. Edmonton, Alberta, T6E 2K6. Canada

April 23 1993

UNIVERSITY OF ALBERTA

FACULTY OF GRADUATE STUDIES AND RESEARCH

The undersigned certify that they have read, and recommend to the Faculty of Graduate Studies and Research for acceptance, a thesis entitled **An Investigation of Hoist-Induced Dynamic Loading** submitted by Douglas A. Barrett in partial fulfillment of the requirements for the degree of Master of Science in Civil Engineering.

T. Hrudey
Dr. T. M. Hrudey

AW Lipsett
Dr. A.W. Lipsett

Jamie Kennedy
Dr. D.J.L. Kennedy

April 21 1993

ABSTRACT

Bridge cranes and their craneways are incorporated into many building structures. The dynamic loading upon these structures, resulting from the hoisting of payloads, is examined in this thesis. Some of the standards which deal with this loading case are reviewed. A computer program which may be used to perform dynamic analyses is described. A finite element model of a crane and craneway are developed and the results of several dynamic analyses are presented. Difficulties associated with this approach are also indicated. Those difficulties relate to the non-linear natures of the tension-elongation relationship of the cable and the torque-velocity relationship of the motor.

A simpler model, called the Three Degree-of-Freedom model, is then proposed. For the Three Degree-of-Freedom model, the structure is treated as a single degree-of-freedom system, and two hoisting scenarios, jerk-starting and braking, are defined. These hoisting scenarios allow simplifying assumption to be made about the motor and the cable.

The results from a testing program are compared with the results predicted using the Three Degree-of-Freedom model. The Three Degree-of-Freedom model provides very good predictions for the jerk-starting results, but much poorer predictions for the braking results. Some aspects of the data indicate reasons why the model is not as accurate in the case of braking, and possible improvements to the model are suggested.

ACKNOWLEDGEMENT

I would like to acknowledge a number of people who made the completion of this thesis possible.

First, from long ago when I was in the real world and working as a professional engineer, my boss, Dolf Daam, got me interested in the problem of dynamic loading on bridge cranes while we looked at designing extensions for craneways. The Daams ran a shop which encouraged experimentation and creativity. It was a great working environment for a new engineer, and I will always remember those times and the people there, most fondly.

At the University of Alberta, Terry Hrudey, my thesis adviser, patiently read through a great number of iterations of all the chapters, correcting my errors and pointing out the many locations where I had expressed ideas in forms too garbled to be understood by human readers. I appreciate what he went through. We also had some good sessions solving spring and mass problems. I am also indebted to Dale Lathe, who wrote up the data logger data handling routines, and who worked with me on trying to make the ten channel amplifier perform.

I am very fortunate to have friends who helped me throughout, by exercising my intellect and keeping up my spirits with their companionship. Some of these friends were other people going through graduate studies at the time I was. Most warmly I remember Jay Snell, Scott Alexander, Steve Talman, and Gilbert Grondin, who taught me to juggle. Some of the friends are not from grad studies. I am very much indebted to John Collier, who allowed me access to his computer for over a year. His act of generosity made this project possible. I am also indebted to my friend and downstairs neighbour, Shirley Goski, who cheerfully typed many revisions, and who made living in the house a joy. Karly Coleman also typed revisions, and actually came to enjoy the formulas. She also spent one of her days off with me, photocopying and running around the university delivering packages to committee members. Finally, Linda MacDonald proof read parts of the thesis, and stuck notes and labels on graphs and diagrams. She said I would finish, because she had faith in me. As I said, I am very fortunate.

TABLE OF CONTENTS

Page

CHAPTER 1 INTRODUCTION 1

1.1 Parts and Functions of a Bridge Crane 2

1.2 Bridge Crane Loading Cases 4

1.3 The Dynamic Factor 7

CHAPTER 2 DESCRIPTION OF THE STRUCTURES LAB SHOP CRANE 11

2.1 Structural Configuration 11

2.2 Trolley 11

2.3 Hoist Motor 17

2.4 Payload 17

2.5 Cable and Load Cell Assembly and Slings 18

CHAPTER 3 A REVIEW OF PRESENT STANDARDS 30

3.1 CSA Standard S16.1-1977 Steel Structures for Buildings 30

3.2 CSA Standard CAN3-S16.1-M89 — Steel Structures for Buildings - Limit States Design 31

3.3 National Building Code of Canada - 1992 32

3.4 CSA Standard B167-1964 — General Purpose Electric Overhead Travelling Cranes 33

3.5 DIN 15.018 part 1 - Cranes, Steel Structures, Verification and Analysis 38

3.6 DIN 4132 — Craneways, Steel Structures, Principles for Calculating Design and Construction 41

3.7 CMAA Specification #74 - 1987 — Specification for Top Running and Under Running Single Girder Electric Overhead Travelling Cranes 41

3.8 AISC Specifications for the Design, Fabrication, and Erection of Structural Steel for Buildings 42

Page

3.9 JIS B 8821 - 1976 — Electric Overhead Travelling Cranes 45
3.10 BS 2573 - 1983 46
3.11 Other Approaches 47
3.12 Summary of Standards 49

CHAPTER 4 NUMERICAL DYNAMIC ANALYSIS 53
4.1 Modelling of Crane Components 53
  4.1.1 Hoist Motor Model 53
  4.1.2 Crane and Craneway Structure Model 65
  4.1.3 Cable Model 78
  4.1.4 Payload 79
4.2 Assembly of the Global Matrices 82
4.3 Outline of Numerical Time Stepping Procedure 87
  4.3.1 Degrees of Freedom Approximation Procedures 87
  4.3.2 Evaluating the Force Terms 91
    4.3.2.1 Solving for the Fo Term 92
    4.3.2.2 Solving for the R Term 97
  4.3.3 Solving for Variable Cable Stiffness 99
4.4 Computer Program Results 109

CHAPTER 5 DERIVATION OF DYNAMIC FACTOR FORMULA 114
5.1 Reduction of Crane and Craneway Model to 1 DoF 115
5.2 The Ratios κ and μ 121
5.3 Assembly of 3DoF Model 123
5.4 Derivation of Natural Frequencies and Mode Shapes 127
5.5 Assumptions Concerning Motor Behaviour 131
5.6 Solution for Modal Degrees of Freedom 135
5.7 General Solution for the Uncoupled Equations of Motion 136
5.8 Initial Conditions 138

Page

5.8.1 Initial Conditions for Starting 140

5.8.1.1 Assumption that Jerk Starting is the Critical Case 140

5.8.1.2 Assumptions Concerning Cable Behaviour 141

5.8.1.2.1 Validity of the Assumption of Quasi-Static Behaviour 147

5.8.1.3 Solution Using Starting Initial Conditions 151

5.8.2 Initial Conditions for Braking 154

5.8.2.1 Solution for Braking with Static Initial Conditions 157

5.8.2.2 General Solution for Braking 158

5.9 Discussion of Structure Coefficients 164

5.9.1 Dependence of Structure Coefficient on κ and μ 164

5.9.2 Solution for S when μ Approaches Zero 170

5.9.4 Effects of Varying κ on the Dynamic Factor 185

5.10 Summary of Derived Dynamic Factors 189

CHAPTER 6 TESTING PROGRAM 194

6.1 Setup and Calibration 201

6.1.1 Acceleration Measurement 201

6.1.2 Displacement Measurement 202

6.1.3 Wheel Loads 203

6.1.4 Bridge Bending Moment 209

6.1.5 Cable Tension 212

6.2 Recording and amplifying equipment 212

6.2.1 FM Tape Recorder 212

6.2.2 Validyne Amplifier 213

6.2.3 Dash 8 Data Logger 213

6.3. Data Reduction 214

Page
6.3.1 Setting Zero Points 214
6.3.2 Electrical Interference and Filtering 215
6.3.3 Acceleration Signals 220
6.3.4 Displacement Signals 220
6.5 Data Presentation 223
6.5.1 Natural Frequency Data 223
6.4.2 Peak Values 223

CHAPTER 7 COMPARISON OF TEST RESULTS AND PREDICTED BEHAVIOUR 260

7.1 Dynamic Ratios 260

7.1.1 Comparison of D_{3xj} with Measured Dynamic Ratios for Jerk-Starting Tests 260

7.1.1.1 The Anomaly of the Results for Set ELC 262

7.1.2 Comparison of Measured Dynamic Ratios for Braking Conditions and D_{3xb} 266

7.1.3 Comparison of Measured Dynamic Ratios and Dynamic Factors from the Standards 276

7.2 Evaluation of Assumptions Underlying 3 DoF Model 284

7.2.1 Single DoF System Structure Assumption 284

7.2.2 Assumption of No Damping 286

7.2.3 Assumption of Infinite Motor Mass and Constant Motor Speed 287

7.2.4 Assumption that Jerk-Starting is the Most Severe Starting Case 287

7.2.5 Assumptions Regarding the Values of k_c and m_s 290

Page

7.2.6 Assumptions Relating to Structure Motion......................294

CHAPTER 8 CONCLUSIONS AND RECOMMENDATIONS..........................309
8.1Conclusions..309
8.2 Recommendations..311
8.2.1 Recommendations for Further Study....................................311
8.2.2 Recommendations Relating to Procedures for Numerical Dynamic Analysis..314
8.2.3 Recommendations Relating to Test Procedure..................316

REFERENCES...319

APPENDIX A CALIBRATIONS...322
Appendix A.1 Calibration Curves for Wheel Assembly Load Cells...322
Appendix A.2 Calibration Curves for LVDT's.......................................323
Appendix A.3 Measured Static Displacement of Crane Structure..324

APPENDIX B MATRICES FOR MODELS "2" AND "E"..................................327

APPENDIX C COMPUTER PROGRAM LISTINGS...332
Appendix C.1 Listing for MAKEKAM.BAS...332
Appendix C.2 Listing for GENJAC.BAS..341
Appendix C.3 Listing for CRIMSIM.BAS...346
Appendix C.4 Listing for CRIS5.BAS..353

APPENDIX D DERIVATIONS...365
Appendix D.1 Derivation of Parabolic Compound Curve...................365
Appendix D.2 Proof that ω_2^2 and ω_3^2 Bound ω_s^2 and ω_c^2.............................368
Appendix D.3 Proof that $(1 - \gamma_2)(1 - \gamma_3) = \mu$..369

Page
Appendix D.4 Proof that $\mu > \gamma_2 - 1$ 371
Appendix D.5 Modal Masses....................372
Appendix D.6 Proof that $(1 - \gamma_2)B_2 + (1 - \gamma_3)B_3 = \frac{m_p g}{k_s}$....................374
Appendix D.4 Proof that $\kappa > | \gamma_3 |$ 377

APPENDIX E LETTER FROM CMAA....................379

LIST OF TABLES

		Page
Table 2.1	Trolley Mass Calculations	17
Table 2.2	Summary of Cable Stiffness Values	29
Table 3.1	Summary of Dynamic Loads and Factors from Various Standards Applied to the Shop Crane Carrying the Large or Small Payload	52
Table 4.1	Calculations of Effective Motor Mass and Motor Force	67
Table 4.2	Natural Frequencies for Structure Models	76
Table 4.3	Dynamic Ratios From Computer Simulations	113
Table 5.1	Effective Structure Mass from Models "2" and "E"	119
Table 5.2	Values of $\frac{H_o\omega_c}{g}\frac{\kappa\sqrt{\mu}}{\sqrt{(1+\kappa)^3}}$ for Test Setups for Shop Crane	148
Table 5.3	Summary of Calculated Frequencies	192
Table 5.4	Summary of Predicted Dynamic Ratos	193
Table 6.1	Test Name Designations	197
Table 6.2	Measured Natural Frequencies	224
Table 6.3	Peak Values due to Jerk-Starting, for 2BC	238
Table 6.4	Peak Values for Starting Conditions Other than Jerk-Starting, for 2BC	239
Table 6.5	Peak Values After Braking, for 2BC	240
Table 6.6	Peak Values due to Jerk-Starting, for 2BS	241
Table 6.7	Peak Values for Starting Conditions Other than Jerk-Starting, for 2BS	242
Table 6.8	Peak Values After Braking, for 2BS	243

List of Tables, continued

Page

Table 6.9 Peak Values due to Jerk-Starting, for EBC 244

Table 6.10 Peak Values for Starting Conditions Other than Jerk-Starting, for EBC 245

Table 6.11 Peak Values After Braking, for EBC 246

Table 6.12 Peak Values due to Jerk-Starting, for EBS 247

Table 6.13 Peak Values for Starting Conditions Other than Jerk-Starting, for EBS 248

Table 6.14 Peak Values After Braking, for EBS 249

Table 6.15 First Peak Values due to Jerk-Starting, for 2LC 250

Table 6.16 Later Peak Values due to Jerk-Starting, for 2LC 251

Table 6.17 Peak Values for Starting Conditions Other than Jerk-Starting, for 2LC 252

Table 6.18 Peak Values After Braking, for 2LC 253

Table 6.19 Peak Values due to Jerk-Starting, for 2LS 254

Table 6.20 Peak Values After Braking, for 2LS 255

Table 6.21 Peak Values due to Jerk-Starting, for ELC 256

Table 6.20 Peak Values After Braking, for ELC 257

Table 6.19 Peak Values due to Jerk-Starting, for ELS 258

Table 6.20 Peak Values After Braking, for ELS 259

Table 7.1 Comparison of D_{3xj} and Measured Dynamic Ratio 262

Table 7.2 Measured Damping Ratios 286

Table 7.3 Comparison of Measured and Predicted Natural Frequencies 290

Table 7.4 Recalculation of Cable Stiffness and Effective Motor Mass Using Measured Natural Frequencies 293

List of Tables, continued

Page

Table 7.5 Recalculation of Cable Stiffness Using Structure Velocity 298

Table 7.6 Comparison of Reduced Dynamic Ratios Using Various Values of Cable Stiffness 299

LIST OF FIGURES

		Page
Figure 1.1	Parts of a Bridge Crane and Craneway	3
Figure 2.1	East View of Section Through Shop Crane	12
Figure 2.2	North View of Craneway and Building Structure	13
Figure 2.3	Crane Bridge Section Properties	14
Figure 2.4	Craneway Beam Section Properties	14
Figure 2.5	Photograph of Shop Crane	15
Figure 2.6	Frame for Weighing Trolley	16
Figure 2.7	Large Payload	19
Figure 2.8	Test Setup to Measure Cable Stiffness	20
Figure 2.9	Derivation of Net Cable Stiffness Structures Lab Shop Crane Small Payload	22
Figure 2.10	Derivation of Net Cable Stiffness Structures Lab Shop Crane Large Payload in Chain Slings	23
Figure 2.11	Derivation of Net Cable Stiffness Structures Lab Shop Crane Large Payload in Web Slings	24
Figure 2.12	Delayed Elasticity Model for Time Dependent Behaviour of Slings Case of Payload Being Lowered	25
Figure 2.13	Delayed Elasticity Model for Time Dependent Behaviour of Slings Case of Payload Being Raised	26
Figure 2.14	Definition of Effective Stiffness and Implied Hysteresis Loop	28
Figure 3.1	Classification Table from CSA Standard B67-1964	35
Figure 3.2	Factor Tables from CSA Standard B67-1964	36

List of Figures, continued

Page

Figure 3.3 Service Factor Table from CSA Standard B67-1964 37

Figure 3.4 Graph of Dynamic Factors Ψ and 1 + (HLF) versus Hoisting Speed 39

Figure 3.5 Table of Runway Design Factors from Whiting Crane Handbook 48

Figure 4.1 Typical Torque versus Motor Speed Curve 55

Figure 4.2 Torque versus Motor Speed as Pullout Slip Varies 57

Figure 4.3 "Constant Speed" Behaviour from Typical Torque versus Motor Speed Curve 57

Figure 4.4 Torque Over Extended Range of Motor Speeds 59

Figure 4.5 Modified Torque versus Motor Speed Curve 59

Figure 4.6 Compound Parabolic Curve to Approximate Torque versus Motor Speed Relationship 61

Figure 4.7 Hoist Motor, Gears, and Drum 62

Figure 4.8 Forces Acting on Effective Motor Mass 66

Figure 4.9 Beam Element 68

Figure 4.10 Multi-Degree of Freedom Model for Shop Crane Loaded at East End of Bridge - Model "E" 71

Figure 4.11 Locations Represented by Nodes and Elements of Model "E" 72

Figure 4.12 Multi-Degree of Freedom Model for Shop Crane Loaded at East End of Bridge - Model "2" 73

Figure 4.13 Locations Represented by Nodes and Elements of Model "2" 74

Figure 4.14 Model for Cable 78

Figure 4.15 Models for Payload 80

List of Figures, Continued

Page

Figure 4.16 Assembled Multi-Degree of Freedom Model 83

Figure 4.17 Assumed Cable Tension versus Elongation Relationship 104

Figure 4.18 Variables for Assumed Tension Elongation Relationship
Structures Lab Shop Crane
For Cases in which Small Payload is Used 110

Figure 4.19 Variables for Assumed Tension Elongation Relationship
Structures Lab Shop Crane
Large Payload in Chain Slings 111

Figure 4.20 Variables for Assumed Tension Elongation Relationship
Structures Lab Shop Crane
Large Payload in Web Slings 112

Figure 5.1 Single Degree of Freedom Model of Crane and Craneway Structure 116

Figure 5.2 Stiffness, Effective Mass, and Natural Frequency on a Simply Supported Beam 118

Figure 5.3 Normalized Time History Graphs of Displacements, Forces and Moments 120

Figure 5.4 Assembled 3 Degree of Freedom Model 124

Figure 5.5 Assumption of Constant Speed Motor 132

Figure 5.6 Two Interpretations of Infinite Mass and No Acceleration 134

Figure 5.7 Assumed Time Histories of Jerk-Starting Velocities 146, 300

List of Figures, continued

Page

Figure 5.8 Comparison of One Linear and Three Non-Linear Cable Tension versus Elongation Curves 150

Figure 5.9 Jerk-Starting Structure Coefficient versus κ, with μ as a Parameter 167

Figure 5.10 Structure Coefficient for Braking versus κ, with μ as a Parameter 168

Figure 5.11 Path of Values for S_{xj} when $\kappa = 2\mu$ 169

Figure 5.12 Approximation for S_{xj} 171

Figure 5.13 Approximation for S_{xb} 172

Figure 5.14 Path of Maximum Values for S_{xj} 178

Figure 5.15 Path of Maximum Values for S_{xb} 179

Figure 5.16 Influences Upon the Path of Maximum Values for S_{xj} 183

Figure 5.17 Influences Upon the Path of Maximum Values for S_{xb} 184

Figure 5.18 Example Case in Which Decreasing k_c Increases Dynamic Factor 188

Figure 5.19 Example Case in Which Decreasing k_c Decreases Dynamic Factor 188

Figure 6.1 Schematic Plan View of Shop Crane Showing Locations of Data Collecting Stations 198

Figure 6.2 Typical Test Setup 199

Figure 6.3 Processing and Data Analysis Steps 200

Figure 6.4 Endtruck Wheel Assembly 204

Figure 6.5 Free Body Diagram of Endtruck Wheel Assembly 205

List of Figures, continued

Page

Figure 6.6 Y Plate Load Cell 207

Figure 6.7 Wheel Assembly Load Cell Calibration 208

Figure 6.8 Wiring Arrangement for Strain Gauges on Bridge Beam 210

Figure 6.9 2BSb2 - Wheel Loads versus Time 217

Figure 6.10 2BSb2 - Northeast Wheel Load versus Time, As Recorded and Numerically Filtered 219

Figure 6.11 ELSs1 - Structure Displacement versus Time 221

Figure 6.12 ELSs3 - Structure Displacement versus Time 222

Figure 6.13 2LCs3 - Example Where Second Peak After Payload Liftoff is Greatest 227

Figure 6.14 2BCb2 - Structure Displacement versus Time 228

Figure 6.15 2BCb2 - Cable Tension versus Time 229

Figure 6.16 2BCb2 - Bridge Beam Midspan Bending Moment versus Time 230

Figure 6.17 2BCb2 - Wheel Loads versus Time 231

Figure 6.18 2BCb1 - Accelerations and Payload Displacement versus Time 232

Figure 6.19 EBSb3 - Structure Displacement versus Time 233

Figure 6.20 EBSb3 - Cable Tension versus Time 234

Figure 6.21 EBSb3 - Bridge Beam Midspan Bending Moment versus Time 235

Figure 6.22 EBSb3 - Wheel Loads versus Time 236

Figure 6.23 EBSb3 - Accelerations and Payload Displacement versus Time 237

Figure 7.1 Predicted versus Measured Dynamic Ratios for Jerk-Starting 261

List of Figures, continued

Page

Figure 7.2 ELCs1 - Cable Tension versus Time 263

Figure 7.3 ELCs2 - Cable Tension versus Time 264

Figure 7.4 ELCs3 - Cable Tension versus Time 265

Figure 7.5 Comparison of Dynamic Ratios before and After Braking 267

Figure 7.6 Assumed Displacement Vibrations due Solely to Braking 269

Figure 7.7 Dynamic Ratios due Solely to Braking 271

Figure 7.8 Predicted versus Measured Dynamic Ratios due Solely to Braking 272

Figure 7.9 Phase Shift β versus Dynamic Ratio due Solely to Braking 274

Figure 7.10 Comparison of Angles β and $\Delta t_b \omega + \frac{\pi}{2}$ 275

Figure 7.11 Comparison of Measured Dynamic Ratios with Specified Dynamic Factors - Case of Bridge Beam and Large Payload 277

Figure 7.12 Comparison of Measured Dynamic Ratios with Specified Dynamic Factors - Case of Bridge Beam and Small Payload 278

Figure 7.13 Comparison of Measured Dynamic Ratios with Specified Dynamic Factors - Case of Craneway Structure and Large Payload 279

Figure 7.14 Comparison of Measured Dynamic Ratios with Specified Dynamic Factors - Case of Craneway Structure and Small Payload 280

Figure 7.15 Graph of Specified Dynamic Factors and Measured Dynamic Ratios versus Hoisting Speed 283

Figure 7.16 Normalized Jerk-Starting Dynamic Ratios Plotted by Parameter 285

List of Figures, continued

Page

Figure 7.17 Dynamic Ratio versus Initial Cable Tension 288

Figure 7.18 2BCb1 - Structure Velocity and Cable Elongation Rate 301

Figure 7.19 2BSb2 - Structure Velocity and Cable Elongation Rate 302

Figure 7.20 EBCb1 - Structure Velocity and Cable Elongation Rate 303

Figure 7.21 EBSb1 - Structure Velocity and Cable Elongation Rate 304

Figure 7.22 2LCs1 - Structure Velocity and Cable Elongation Rate 305

Figure 7.23 2LSs1 - Structure Velocity and Cable Elongation Rate 306

Figure 7.24 ELCs1 - Structure Velocity and Cable Elongation Rate 307

Figure 7.25 ELSs3 - Structure Velocity and Cable Elongation Rate 308

Figure 8.1 Proposed Multi-Degree of Freedom System With Which to Derive Effective Structure Mass 313

Figure 8.2 Alternate Model for Cable 315

Figure A.1 Calibration Curve for NW Wheel Load Cell 322

Figure A.2 Calibration Curve for NE Wheel Load Cell 322

Figure A.3 Calibration Curve for SW Wheel Load Cell 322

Figure A.4 Calibration Curve for SE Wheel Load Cell 322

Figure A.5 Calibration Curve for LVDT 24T 1010 at SE Wheel 323

Figure A.6 Calibration Curve for LVDT 24T 2501 at Trolley 323

Figure A.5 Calibration Curve for LVDT 6T 3005 at Payload 323

Figure D.1 Derivation of Compound Curve Approximate Force versus Motor Speed Relationship 366

LIST OF SYMBOLS

A	total cross sectional area of all the lines of cable
$\bar{A}$	second mode amplitude prior to braking
$\bar{\bar{A}}$	third mode amplitude prior to braking
$\{A\}$	column vector used in the solution for F_o

$$\{A\} = \left[[\omega^2] + \frac{\beta_2}{\Delta t^2}[\,I\,]\right]^{-1}\{\Phi_1\}$$

a_0, a_1	coefficients for the linear expression for Fo in terms of $\dot{y}_m$
A_j	amplitude of the vibration of the j^{th} modal degree of freedom
$\{A_s\}$	column vector used in the solution for F_o

$$\{A_s\} = \left[\begin{bmatrix} [0] & [0] \\ [0] & [\omega_s^2] \end{bmatrix} + \frac{\beta_2}{\Delta t^2}[\,I\,]\right]^{-1}\{\Phi_1\}$$

B	amplitude of the vibrations due solely to braking
$\{B\}$	column vector used in the solution for F_o

$$\{B\} = \left[[\omega^2] + \frac{\beta_2}{\Delta t^2}[\,I\,]\right]^{-1}\{\Phi_2\}$$

b_0, b_1 and b_2	coefficients, used to define the parabolas which approximate the force versus motor speed relationship
B_j	value of the j^{th} modal degree of freedom when the static crane carries the weight of the payload
$\{B_s\}$	column vector used in the solution for F_o

$$\{B_s\} = \left[\begin{bmatrix} [0] & [0] \\ [0] & [\omega_s^2] \end{bmatrix} + \frac{\beta_2}{\Delta t^2}[\,I\,]\right]^{-1}\{\Phi_2\}$$

C	amplitude of the vibrations occuring after braking
[C]	diagonal matrix used in the solution for F_o $[C] = \frac{\beta_2}{\Delta t^2}\left[[\omega^2] + \frac{\beta_2}{\Delta t^2}[I]\right]^{-1}[I]$
c_0, c_1 and c_2	coefficients, used to define the parabolas which approximate the torque versus motor speed relationship
$[C_s]$	matrix used in the solution for F_o $[C_s] = \frac{\beta_2}{\Delta t^2}\left[\begin{bmatrix} [0] & [0] \\ [0] & [\omega_s^2] \end{bmatrix} + \frac{\beta_2}{\Delta t^2}[I]\right]^{-1}$
d	section depth of the bridge of the crane
D	dynamic factor: the ratio of the maximum deflection to the static deflection
D_{3xj}	dynamic factor derived from the exact solution from the 3 degree of freedom model for the case of jerk-starting
D_{3xb}	dynamic factor derived from the exact solution from the 3 degree of freedom model for the case of braking
$\{D_s\}$	column vector used in the solution for F_o $\{D_s\} = \left[\begin{bmatrix} [0] & [0] \\ [0] & [\omega_s^2] \end{bmatrix} + \frac{\beta_2}{\Delta t^2}[I]\right]^{-1}\{\Phi_3\}$
E	Young's modulus of elasticity
E_s	Young's modulus for the structure
E_c	Young's modulus for the cable
{F}	force vector in the equations of motion of a system
F_o	force acting at a moment arm of length r_e required to develop a torque equivalent to the motor torque

F_x	force, or group of forces, which comprise a static loading case, and which are applied at location, or set of locations, x
g	acceleration due to gravity
h	height of the crane, and the maximum travel of the payload
HLF	Hoist Load Factor, defined in Clause 3.3.2.1.1.4.2 of CMAA#74
H_o	nominal hoisting speed of the crane
I	cross sectional moment of inertai
I_c	moment of inertia of a cantilever model for a simply supported beam
I_{drum}	polar mass moments of inertia of the hoist drum
I_{gear}	polar mass moments of inertia of a gear within the hoist transmission
I_e	effective moment of inertia of a composite section
I_w	moment of inertia of the steel section within a composite section
I_t	moment of inertia of the transformed composite section
$[K]$	global stiffness matrix for the system
k^*	a stiffness term in the expression for a_0 and a_1.

$$k^* = \frac{1}{\langle \Phi_1 \rangle \{A\}}$$

$\langle K_2 \rangle$	second row of $[K]$
k_c	cable stiffness: net stiffness of the cable, load cell assembly, and slings
$k_{c_{slacken}}$	slope of the best fit line through the points near the maximum load on the slackening side of the cable elongation curve
$k_{c_{tighten}}$	slope of the best fit line through the points near the maximum loadon the tightening side of the cable elongation curve

$k_{c_{effective}}$	stiffness which results, with a given payload mass, in the same frequency of free vibration that occurs when $k_{c_{tighten}}$ is used for the portion of each period during which the cable tension increases, and $k_{c_{slacken}}$ is used for the portion during which cable tension decreases $k_{c_{effective}} = \left(\frac{2}{\sqrt{\frac{1}{k_{c_{slacken}}}} + \sqrt{\frac{1}{k_{c_{tighten}}}}} \right)^2 \qquad (2.1)$
$\langle K^F \rangle$	a term in the expression for a_0 $\langle K^F \rangle = \frac{\langle \Phi_1 \rangle [C]}{\langle \Phi_1 \rangle \{A\}}$
$[K_s]$	global stiffness matrix for the structure
$[K_s\text{-}1]$	structure stiffness matrix [Ks] without its first row and column
$\langle K_{s1}\text{-}1 \rangle$	a row vector containing all but the first term of the first row of $[K_s]$
$\{K_{s1}\text{-}1\}$	a column vector containing all but the first term of the first column of $[K_s]$
$\langle K^R \rangle$	a term in the expression for a_0 $\langle K^R \rangle = \frac{\langle K_2 \rangle [\Phi][C]}{1 - \langle K_2 \rangle [\Phi]\{B\}}$
k_s^*	stiffness term used in the expression for F_o $k_s^* = \frac{1}{\langle \Phi_1 \rangle \{A_s\}}$
$\langle K_s^F \rangle$	a term in the expression for a_0 $\langle K_s^F \rangle = \frac{\langle \Phi_1 \rangle [C_s]}{\langle \Phi_1 \rangle \{A_s\}}$
k_x	vertical stiffness of a simply supported beam at a location a distance x along the span

$k(x,x)$	stiffness of the structure at x due to applied load at *x*
L_c	length a cantilever model for a simply supported beam
M	bending moment of the bridge at midspan
$[M]$	global mass matrix for the system
$\bar{m}$	distributed mass of a member or an element
$\bar{m}_c$	distributed mass of a cantilever model for a simply supported beam
m_i	initial slope of the motor foce versus motor speed curve
m_m	effective motor mass : as defined in equation (4.6), an imaginary mass used in calculating the rotational inertial effects, but not the weight, of the motor, gears and drum
m_p	mass of the payload
m_pg	weight of the payload
m_s	mass in a single degree of freedom system which has the same stiffness as the crane structure and the same frequency as the first natural frequency of the crane structure
$[M_s]$	global mass matrix for the structure
$[M_s\text{-}1]$	structural mass matrix [Ms] without its first row and column
M_x	bending moment at location x
n	number of lines of cable between the hoist and the hook
p	a factor which accounts for the fraction of full shear connection between the concrete and the wide flange beam within a composite section
R	reaction force of the floor upon the payload
r_e	effective moment arm that relates the motor torque to a force with a line of action along the cable $r_e = \left(\frac{\dot{y}_m}{\omega_r}\right)$

s	slip: the difference in rotational velocities between the rotor and stator fields, relative to the synchronous speed
S	structure coefficient
s_p	pullout slip
S_{xj}	structure coefficient derived from the exact solution from the 3 degree of freedom model for the case of jerk-starting
S_{xb}	structure coefficient derived from the exact solution from the 3 degree of freedom model for the case of braking
T_c guess	first guess for cable tension in the iteration procedure to solve for cable tension
T_f	tension axis intercept, on a cable tension versus elongation graph, for a straight line which the curve defining cable tension in terms of elongation approaches assymptotically
$\bar{T}$	constant within the exponent which determines the rate at which the curve defining cable tension in terms of elongation approaches the line $k_c y_c + T_f$
T_c	net cable tension
T	torque between the rotor and stator magnetic fields
T_{max}	maximum torque that can be developed between the rotor and stator fields
V_o	velocity at which cable is wound onto the drum when the motor is at synchronous speed
V_x	Shear at location x
$\{W\}$	column vector of modal displacements
$\{\ddot{W}\}$	second derivative of the modal degrees of freedom
w_j	j^{th} modal degree of freedom of the system
w_{jmax}	maximum value of the j^{th} modal degree of freedom
x_o	constant coefficient which multiplies the exponential term in the expression for F_o when cable stiffness is not constant

$\{Y\}$	column vector of mass displacements
y^{**}	linear combination of y_o, $\dot{y}_o$, and $\ddot{y}_o$, used to relate the values for displacement and acceleration at the end of a timestep
y^{*}	linear combination of y_o, $\dot{y}_o$, and $\ddot{y}_o$, used to relate the values for displacement and acceleration at the end of a timestep
y_o	value of displacement y at the beginning of a timestep
$\dot{y}_o$	value of velocity $\dot{y}$ at the beginning of a timestep
$\ddot{y}_o$	value of acceleration $\ddot{y}$ at the beginning of a timestep
y_c	cable elongation
y_m	length of cable the motor winds onto the drum
$\dot{y}_m$	rate at which the cable is wound onto the drum
y_p	upwards displacement of the payload
y_s	vertical displacement of the crane structure at the trolley
y_{s1}	vertical displacement of the first node of the multi- degree-of-freedom structure, which is the displacement at the trolley
$y_{s_{max}}$	maximum downwards deflection experienced by the crane during a particular hoisting event
$y_{s_{static}}$	static deflection of the crane when it carries the payload of mass m_p
$\{Y_s-1\}$	column vector containing all but the first structural displacements
$\{Y_s\}$	column vector containing the structural displacements
y_x	deflection of the structure at location x
$y_x(t)$	deflection at time t of the structure at location x
$y_{\Delta t}$	value of displacement y at the end of a timestep
$\dot{y}_{\Delta t}$	value of velocity $\dot{y}$ at the end of a timestep
$\ddot{y}_{\Delta t}$	value of acceleration $\ddot{y}$ at the end of a timestep

$y_{@t}$	value of displacement y at some time within a timestep
$\dot{y}_{@t}$	value of velocity $\dot{y}$ at some time within a timestep
$\ddot{y}_{@t}$	value of acceleration $\ddot{y}$ at some time within a timestep
z	a dimensioless coefficient for $\{B_s\}$ in the expressions for a_0, a_1, and x_0, z=1 when the payload is suspended by the cable, and z=0 when there is a reaction force between the floor and the payload
$Z_i(t)$	function which describes the relative change in amplitude of the i^{th} mode shape with respect to time
α	term used in the Newmark method equation for displacement at the end of a time step
α	value for $\omega_2 t + \theta_2$ at the instant the brakes are applied
β	phase shift in radians between the vibrations prior to braking and the vibrations due solely to braking
β_1	dimensionless constant used in the relation between the values for velocity and displacement at the end of a time step
β_2	dimensionless constant used in the relation between the values for acceleration and displacement at the end of a time step
δ	term used in the Newmark method equation for velocity at the end of a time step
$\langle \delta Y_s - 1 \rangle$	row vector containing all but the first virtual displacements
Δt_a	time between the last clear peak prior to braking and the first clear peak after braking
Δt_b	time between the last clear peak prior to braking and the initiation of braking
Δt	duration of one time step
$\varepsilon_{top\ south}$	strain reading at the top south side of the midspan of the bridge
$\varepsilon_{top\ north}$	strain reading at the top north side of the midspan of the bridge

$\varepsilon_{\text{bottom south}}$	strain reading at the bottom south side of the midspan of the bridge
$\varepsilon_{\text{bottom north}}$	strain reading at the bottom north side of the midspan of the bridge
$[\Phi]$	transformation matrix that produces diagonal matrices when it is pre-multiplied by [K] or [M], and the result is pre-multiplied by $[\Phi]^T$. The columns within $[\Phi]$ are the eigenvectors of the system.
$\langle\Phi_c\rangle$	row vector which relates y_c and the modal degrees of freedom

$$\langle\Phi_c\rangle = \left\langle \frac{1}{n}\langle\Phi_1\rangle - \langle\Phi_2\rangle + \langle\Phi_3\rangle \right\rangle$$

ϕ_j	j^{th} term in an eigenvector
$\Phi_i(x)$	function, calculable at location x, which describes the i^{th} orthogonal mode shape
γ_j	ratio of peak to static displacement for the undamped single degree of freedom system of the structure, subject to harmonic forcing function with frequency of ω_j
κ	ratio of the stiffness of the structure to the stiffness of the cable
λ	phase shift in radians between the vibrations prior to braking and the vibrations after braking
μ	ratio of the effective mass of the structure to the mass of the payload
Ψ	Hoist Load Spectrum Factor , from DIN 15.018
Ψ	Impact Factor , from JIS B 8821 - 1976
ρ_{drum}	velocity ratio $\frac{\omega_{drum}}{\omega_r}$
ρ_{gear}	velocity ratio $\frac{\omega_{gear}}{\omega_r}$
σ	standard deviation

σ	material strength of the cable
σ_y	yeild strength of the structure material
$\Sigma\varepsilon$	sum of the two top and two bottom strain readings from the midspan of the bridge
$\Sigma f_S\delta$	sum of the product of the spring forces and the associated virtual displacements within a system
$\Sigma f_I\delta$	sum of the product of the inertial forces and the associated virtual displacements within a system
$\Sigma f_A\delta$	sum of the product of the applied forces and the associated virtual displacements within a system
θ_2	phase shift of the vibration of the jth modal degree of freedom
ζ_0	a dimensionless constant in the expression for a_0 and a_1, $\zeta_0 = 0$ when the payload is suspended by the cable, and $\zeta_0 = \zeta_1$ when there is a reaction between the floor and the payload
ζ_1	a dimensionless constant in the expression for a_0 $\zeta_1 = \dfrac{\langle\Phi_1\rangle\{B\}}{\langle\Phi_1\rangle\{A\}}$ or $\zeta_1 = \dfrac{\langle\Phi_1\rangle\{B_s\}}{\langle\Phi_1\rangle\{A_s\}}$
ζ_2	a dimensionless constant in the expressions for a_0 and a_1 $\zeta_2 = \dfrac{\langle K_2\rangle[\Phi]\{A\}}{1 - \langle K_2\rangle[\Phi]\{B\}}$ or $\zeta_2 = \dfrac{\langle\Phi_1\rangle[D_s]}{\langle\Phi_1\rangle\{A_s\}}$
$[\omega^2]$	a diagonal matrix which has the squares of the natural frequencies of the system for its non-zero terms
ω_o	synchronous speed of the motor : the constant rate of rotation of the stator field
$\omega_{1\text{-beam}}$	first natural frequency of a simply supported beam

ω_c	natural frequency of a single degree of freedom system consisting of the cable with one end attached to the payload and the other end fixed $\omega_c = \sqrt{\frac{k_c}{m_p}}$
ω_{drum}	angular velocity of of the hoist drum
$\dot{\omega}_{drum}$	angular acceleration of the hoist drum
ω_{gear}	angular velocity of a gear within the hoist transmission
$\dot{\omega}_{gear}$	angular acceleration of a gear within the hoist transmission
ω_i	frequency of vibration of the structure prior to payload lift off with k_c constant
ω_j	j^{th} natural frequency of the system
ω_r	changing angular velocity of the rotor and its magnetic field
ω_s	natural frequency of the structure, $\sqrt{\frac{k_s}{m_s}}$
Ω^2	sum of the squares of three frequencies within the system $\Omega^2 = k_c\left(\frac{1}{n^2 m_m} + \frac{1}{m_p} + \frac{1}{m_s}\right)$

CHAPTER 1

INTRODUCTION

Bridge cranes and craneways are common structures that engineers are often asked to upgrade or design. While they have a fairly simple form, bridge cranes and craneways, because of their application, carry some unique dynamic loads which structural engineers generally are not trained to analyze. Instead of analysis, the standard practice is to account for dynamic loads by increasing static loads by some approved and accepted factor. For example, the 1977 version of CSA standard S16.1, [ref. 7] clause 7.11 states that "In the absence of a dynamic analysis ... live load which causes impact shall be increased ... 25 percent" for "Girders, and their connections, supporting power operated cranes." Designing to resist dynamic loads caused by cranes was seen as requiring a dynamic analysis for each loading case. Because of the work involved in solving that kind of problem (and it was much more of a task in 1977, when computers were not as accessible as they are in 1993) it was considered reasonable and conservative to increase instead the live, static, loads by one quarter.

Applying a factor to the results of a static analysis, to account for dynamic loading, is a labour and time saving approach. The dissatisfying feature of crane standards, and structural standards that deal with craneways, is that the expressions they prescribe for such a dynamic factor do not take into account the general parameters of the craneway structure which are normally assumed to affect the dynamic behaviour of the structure. Especially in the case of vertical hoist-induced dynamic loads, these expressions seem incomplete. Neither the stiffnesses and masses of the craneway's components, nor, in the Canadian standard to date, the properties of the hoisting motor, are considered.

In this thesis some simple closed form solutions have been derived, which describe the behaviour of a simple three degree-of-freedom bridge crane model under idealized hoist-induced vertical dynamic loading. This simple model approximates very closely the behaviour of more complicated multi-degree-of-freedom models, (which do not have simple closed form solutions for the same idealized loading cases). Tests conducted on the small bridge crane in the I. F. Morrison Structures Laboratory suggest that, with some modification, the closed-form solutions may be a good approximation to real dynamic behaviour.

1.1 Parts and Functions of a Bridge Crane

Figure 1.1 shows the parts of a typical bridge crane and craneway system. The parts of the bridge crane proper are shown in white, and the parts of the craneway are shown shaded. The bridge crane moves horizontally along the craneway; the trolley moves horizontally across the bridge; and the hoist moves the hook vertically. These three motions give the hook, and any payload attached to it, access to any point within the brick-shaped volume roughly bounded by the two rows of craneway columns and the area the bridge passes through as it travels from one end of the craneway to the other. Any point within that volume is said to be "under the craneway". The purpose of a bridge crane is to move payloads from one place under the craneway to another.

Figure 1.1 is schematic, indicating that within this format a wide range of forms exist. The bridge, the structure that spans the space between the two craneway halves, can be a single rolled section, a large welded wide flange girder, a truss, or a pair of box girders. At the ends of the bridge are endtrucks that house the wheels and drive mechanism for bridge travel. In general, the bridge can be considered a simply supported member.

The trolley generally rides on top when the bridge is made of two members, and is underslung for single girder bridges. The trolley houses wheels and some form of drive mechanism for trolley travel, and it also carries the hoist.

The hoist comprises the cable drum, the transmission, and the hoist motor. The cable drum winds up or unwinds the cable, and that, respectively, raises or lowers the hook and any attached payload.

The craneway is made up of two parallel rows of columns and the supported girders and tracks on which the endtrucks of the bridge ride. The columns may also be structural members of a building beside or over top of the craneway. Connections between girders, and between columns and

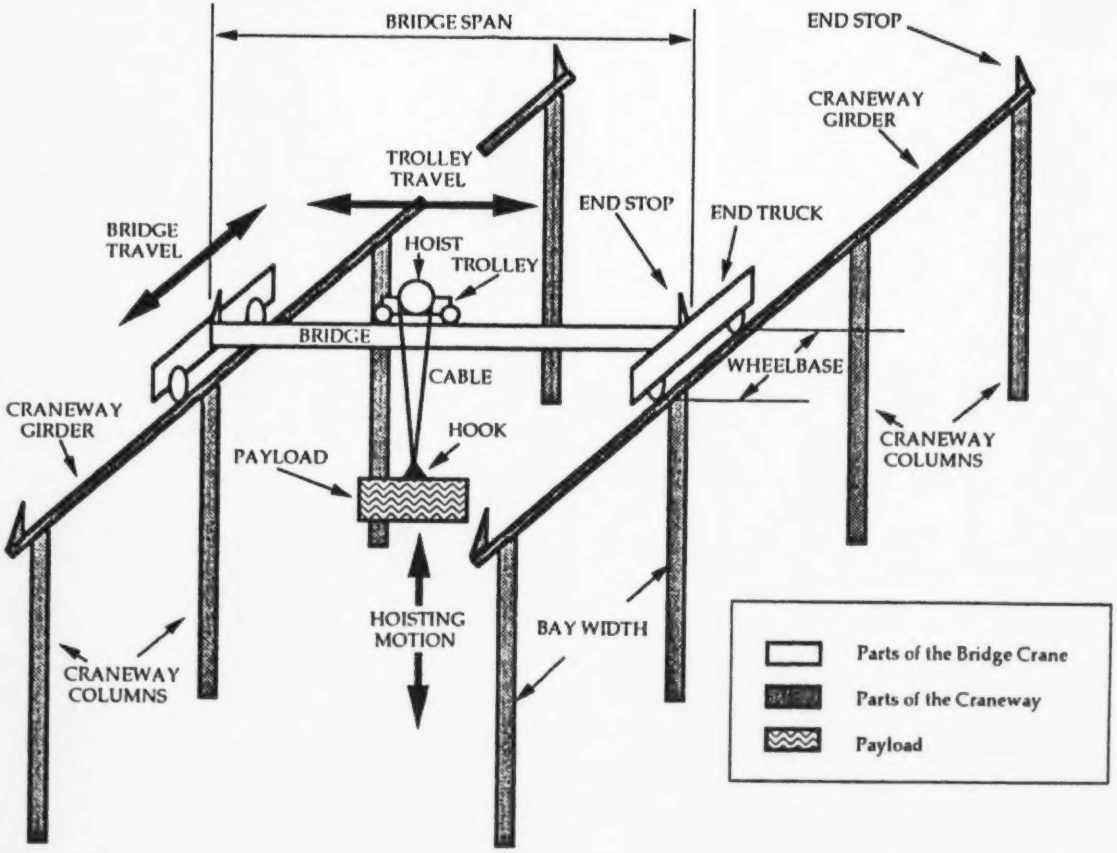
BRIDGE SPAN
END STOP
CRANEWAY GIRDER
TROLLEY TRAVEL
END STOP
END TRUCK
BRIDGE TRAVEL
HOIST
TROLLEY
BRIDGE
WHEELBASE
CABLE
CRANEWAY GIRDER
HOOK
PAYLOAD
CRANEWAY COLUMNS
HOISTING MOTION
BAY WIDTH
CRANEWAY COLUMNS
Parts of the Bridge Crane
Parts of the Craneway
Payload

Figure 1.1 Parts of a Bridge Crane and Craneway

girders, vary from craneway to craneway. The girders may be cantilevered at one or both ends. There may be a walkway beside the craneway, for service access. There may also be an attached walkway along the span of the bridge.

All three motions (hoist, trolley, and bridge travel) are usually controlled from a single control box, accessible from the ground, and attached, via electric cable, to the bridge or trolley. If the crane is radio controlled, then the control box is not physically attached to the crane. For larger cranes, the control box may be in a cab mounted on the bridge, so that an operator riding in the cab can control the crane, and can have a clear view of the hook's motion.

There are usually at least seven buttons on the control box; one for each of the two directions of each of the three motions of the crane, and an on-off switch. There may be more buttons for other features specific to a crane, such as opening doors to extend crane access, or for switching a magnet on and off, or opening and closing jaws, or a bucket, when those accessories are used instead of the hook.

1.2 Bridge Crane Loading Cases

There are a number of loading cases that bridge cranes and craneways experience that are common to most building structures. There are the dead loads of individual members, wind and snow loads on the bridge if it is outside, and, if the craneway is incorporated as part of the structural support of a building, there are the normal live and dead loads of the building, carried by the craneway girders and columns.

Along with these, there are the loads peculiar to bridge cranes. Because the purpose of the crane is to position a payload at any place under the craneway, a large vertical live load can exist anywhere on the structure. With respect to the bridge, this live load can be considered to be the weight of all the parts of the trolley, and of the cable, plus the weight of the payload the cable is supporting. This live load can be applied at any position along the span of the bridge. With respect to the craneway, the live load can be considered to be the weight of the trolley, cable, and load on the hook, plus the weight of the bridge and end trucks. The trolley can be at any point along the bridge span, and the bridge can be at any position along the length of the craneway.

Because the purpose of the crane is to move a payload, there is a large dynamic element to these live loads. There are several different dynamic loads that bridge cranes and craneway structures are subject to. Vertical unevenness in the tracks for the trolley and the endtrucks cause machinery travelling horizontally along those tracks to vibrate vertically. Horizontal unevenness of the tracks for the, and imperfect wheel alignment, cause dynamic axial loads in the bridge and dynamic lateral loads on the craneway. Starting and stopping the trolley causes the payload on the hook to swing in the plane beneath the axis of the bridge, adding tension to the cable, axial load to the bridge, and lateral load to the craneway. Starting and stopping the bridge motion causes the payload to swing in a plane perpendicular to the bridge, loading the bridge laterally and the craneway girders axially.

As the bridge changes velocity, its own mass creates inertial lateral load that it must carry, and axial load on the craneway. Similarly, as the trolley mass changes velocity the bridge must resist inertial loads acting along its axis, and the craneway must resist the lateral reactions.

When the bridge or trolley move, the acceleration up to rated speed is less than the deceleration when the brakes are applied. The mechanism of the two actions is different. Braking is usually more abrupt than starting, so the duration of the impulse and its maximum are different for the two load cases. Either of these impulse loads can occur anywhere over the craneway. Far more sudden is the deceleration when the bridge or trolley strike the respective end-stops. The wide range of lateral dynamic service loads makes it difficult to determine which case is critical. Most crane standards address this issue and give a similar recommendation; live lateral load should be taken as vertical load multiplied by some factor.

There are also less obvious dynamic loads. Moving a constant load along the bridge (or any other simply supported flexible member) causes dynamic deflection of the member, and that can produce internal forces larger than those produced by the same load if it were stationary on the bridge [ref. 2]. If the magnitude of the moving load is not constant, but varies over time, then the forces can be larger still.

All the dynamic loads mentioned above can be significant. The dynamic loads that will be addressed in detail in this thesis are the vertical dynamic loads due to hoist action only. During a hoisting event the trolley maintains a fixed position on the bridge, and the bridge maintains a fixed position on the craneway. There are two ways in which hoisting can induce vertical dynamic loads on a crane structure. The hoist motor can begin winding or unwinding cable, causing an initially stationary payload to move, or the already operating motor can stop, causing an originally moving payload to stop moving. In both cases the acceleration of the payload causes the tension in the cable to vary. The crane structure resists the varying cable tension by deflecting. As its mass accelerates, inertial loads are created which the structure must resist in addition to the cable tension. These resisting forces within the structure vary through the course of the hoisting event. The crane structure must be strong enough to carry the maximum values of these varying forces. This set of maximum forces can be called the maximum hoist-induced vertical dynamic forces.

The hoisting event, as described above, is strongly influenced by the hoist motor. It is the action of the motor that physically initiates the whole event. Structural engineers are often not familiar with how motors develop force. Nevertheless, it is apparent that this source of dynamic loading is repeatable in a way that other dynamic load sources, such as earthquakes, wind, or track unevenness, are not. Hoist-induced loading has some random aspects, and these are described in Chapter 5, but the overall behaviour can be modelled, and understood, as a repeatable dynamic event with quantitatively predictable results.

Another feature of hoist-induced vertical dynamic loads is that most of the loading action occurs at the start of the event. Once the motor reaches rated speed, its acceleration is greatly reduced. The mechanism behind this reduction is explained in Section 4.1.1. For the present, because there is no resonance, an assumption of no damping is convenient for the purposes of determining the maximum internal dynamic forces. In fact, cranes do have a very low level of damping, so an assumption of no damping is conservative and reasonable. Because damping is so low, the crane should be designed to

In undamped free vibration, the maximum force is experienced continually, but not continuously. A maximum dynamic force occurs each period only for an instant. All building materials are sensitive to rate and duration of loading [ref. 12]. Generally, the shorter the duration, and the quicker the rate, the larger the stress that can be resisted. The consequences of that increase will not be addressed in this thesis. The intent, instead, is to develop simple formulae to predict the magnitudes of the maximum forces in the crane and craneway structure, due to the actions of the hoist.

1.3 The Dynamic Factor

The weights of the trolley on the bridge, and of the bridge crane on the craneway can be referred to as live load because they fit the description of "movable equipment" as per the definition of live load given in clause 7.1.1 of CAN3-S16.1-M89 1989 [ref. 6]. However, they could also be described as a dead load. Live and dead loads are categorized as such, in Limit States Design (L.S.D.), so that each may be multiplied by a different load factor. The live load factor is generally larger, to reflect the uncertainty of the magnitude of the mass that produces the live loads. It can be argued that the bridge's mass is as certain as the mass of the craneway components, and that the dynamic effect, since it is such an important aspect of bridge crane loading, should be dealt with using a separate, dynamic factor. It can also be argued that the mass of the craneway components accelerate, as well, and add to the dynamic effect, but the craneway would generally be considered a source of dead load. For these reasons, the weight of the structural elements of the crane may be considered as a live load because it is present at some times and not at others, is subject to the L.S.D. dead load factor because of the degree of certainty of the magnitude of the mass, and is also subject to a dynamic factor because of the motion of the crane.

A dynamic factor is a coefficient that is applied to a calculated static load. The factor accounts for the effects upon the supporting structure of the acceleration of the mass used to determine the static load. The definition of a dynamic factor must, therefore, include a definition of the static load to which it is to be applied. During a hoisting event, both the mass of the crane and the mass of the payload accelerate. There are then two reasonable static loads to which the dynamic factor could be applied: the weight of the payload, or the weight of the payload and the structure combined. In this thesis the dynamic factor will be considered to apply only to the weight of the payload. This definition for the dynamic factor will be used when crane design standards are compared in Chapter 3 and when a dynamic factor formula is derived in Chapter 5.

Because the magnitude of the payload mass and the stiffness and mass of the supporting structure both influence the acceleration, they influence the dynamic factor. Two non-dynamic examples of load factors influenced by the support structure's physical properties are the factor for ponding on flat roofs, which is a function of the stiffness of the roof beams, as given in the AISC specifications [ref. 1], and the amplification factors used in the design of beam columns, as given in CAN3-S16.1-M89 [ref.6].

A given payload can be hoisted from any location under the craneway. At these different lifting locations the crane structure has different stiffnesses and different arrangements of its most massive components. Therefore, the dynamic factor varies with lifting location, even if the same payload is hoisted at each location. This is similar to roof snow load drift factors, which vary with location on the roof and are functions of the topography of the roof and other factors, as given in the National Building Code of Canada [ref. 33].

There is a limitation in the practice of approximating a dynamic load with a larger-than-applied static load. The limitation can be recognized when the differences between the responses of a linear elastic structure to static and to dynamic loading are examined. A structure subjected to a static load will assume a particular deflected shape. Changing the static load by some factor changes the deflections of all the parts of the structure by that same factor. The shape of the deflected structure remains the same. Only the amplitude of the deflection has changed. The deflection of the structure can be described by an equation such as

$$y_{\mathrm{x}} = \frac{F_x}{k(\mathrm{x},x)} \, . \tag{1.1}$$

In equation (1.1), y_{x} is the deflection of the structure at location x, F_x is the force, or group of forces, which comprise the static loading case, and which are applied at location, or set of locations, $\mathcal{x}$, and $k(x,\mathcal{x})$ is the stiffness of the structure. The stiffness is a function of both x and $\mathcal{x}$. There is a linear relationship between $F_{\mathcal{x}}$ and y_x.

Dynamic loading of a linearly elastic structure, on the other hand, can excite any or all of an infinite number of orthogonal mode shapes, as disturbing inertial forces and restoring stiffness forces cause the structure to vibrate. The characteristic equation for the displacement in the case of dynamic loading is

$$y_x(t) = \sum_{i=1}^{\infty} \Phi_i(x)\, Z_i(t) \;. \tag{1.2}$$

In equation (1.2), $y_x(t)$ is the deflection at time t of the structure at location x. Within the summation, $\Phi_i(x)$ is the function, calculable at location x, which describes the i^{th} orthogonal mode shape, and $Z_i(t)$ is the function which describes the relative change in amplitude of the i^{th} mode shape with respect to time. The function $Z_i(t)$ accounts for the effects of $F_{\mathcal{x}}(t)$, the time dependent force, or group of forces, which comprise the dynamic loading case, and which are applied at location, or set of locations, $\mathcal{x}$.

Bridge cranes and craneways generally comprise long members loaded transversely, and the shears and moments must be known in order to properly design the members. The static and dynamic shears and moments can be derived from equations (1.1) and (1.2), using

$$M_x = EI\,\frac{\partial^2 y}{\partial x^2} \;\; \text{, and } \;\; V_x = EI\,\frac{\partial^3 y}{\partial x^3} \;. \tag{1.3}$$

Two relevant differences between static and dynamic behaviour limit the number of cases in which an increased static load can adequately approximate a dynamic load. First, at any one location on a structure responding to a dynamic load in a multi-modal fashion, the ratio between displacement, moment, and shear force will not be constant over time, and the ratio of the peak to static value of any one of these parameters is generally not the same as the ratio for any other. Therefore, different dynamic factors could apply to displacements, moments, and shears. The second difference is that the ratio of displacements, moments, or shear forces between any two stations on a dynamic structure are not constant over time, and the peak to static ratios for any of those parameters are not constant from one location to another. The peak dynamic moments, shears, and displacements do not have the same relative distribution along the structure that the static moments, shears, and displacements have. Therefore, for any one hoisting location different dynamic factors could apply at different locations on the structure.

A dynamic load can only be reasonably approximated by a larger-than-applied static load if equation (1.2), and its derivatives for moment and shear, can be reasonably approximated by an equation of the form of equation (1.1) and its respective derivatives. This can only happen when one of the terms in the summation in equation (1.2) is dominant. This is the assumption made, though rarely stated, when a dynamic factor is used.

CHAPTER 2

DESCRIPTION OF THE STRUCTURES LAB SHOP CRANE

In the I. F. Morrison Structures Laboratory at the University of Alberta there is a 1.82-ton capacity overhead bridge crane servicing the shop area. In this chapter the various features of the crane are described.

2.1 Structural Configuration

A diagram of the shop crane and the craneway structure is shown in Figures 2.1 and 2.2. The section properties of the fabricated sections for the bridge and for the craneway are shown in Figures 2.3 and 2.4 respectively. Details of the end truck wheel connections are shown in Figures 6.4 and 6.5. A photograph of the crane is shown in Figure 2.5.

2.2 Trolley

The trolley is underhung. The motor and drum are on the north side, and the trolley electrical box and a box for ballast are on the south side. The ballast box is empty, however, so the center of gravity of the unloaded trolley is slightly inboard of the northern trolley wheels. The trolley is shown in Figures 2.1 and 2.2.

The mass of the trolley was determined as follows. A small frame was built which rested on a load cell on the top of the bridge rail top flange and reached under the trolley with adjustable length arms, as shown in Figure 2.6. The reading from the load cell gave the trolley weight. From the weight, its mass was calculated to be 330 kg. A second technique was later used to confirm this result. The trolley was positioned at the far east end of the bridge and the bending strain was recorded using the strain gauges mounted at centre span of the bridge. (See Section 6.2.4.) Then the crane was used to pick up and suspend a payload of 1.46 tonne with the trolley at centre span. The output from the gauges was recorded. Then the payload was placed on the shop floor so that only the trolley weight was acting on the bridge, and the

Figure 2.1 East View of Section Through Shop Crane

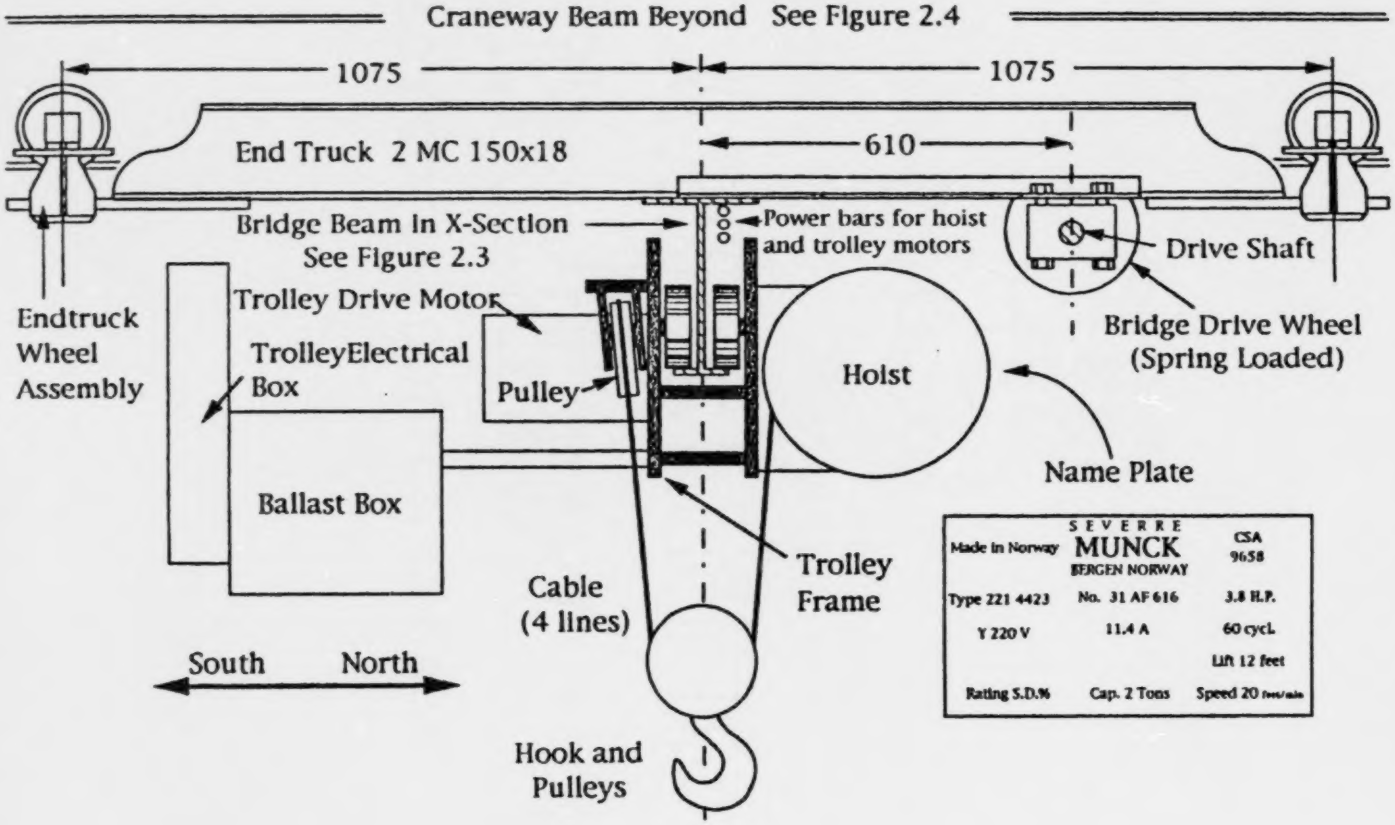
Craneway Beam Beyond See Figure 2.4
1075
1075
End Truck 2 MC 150x18
610
Bridge Beam In X-Section
See Figure 2.3
Power bars for hoist and trolley motors
Drive Shaft
Endtruck Wheel Assembly
Trolley Drive Motor
TrolleyElectrical Box
Pulley
Holst
Bridge Drive Wheel (Spring Loaded)
Name Plate
Ballast Box
Trolley Frame
Cable (4 lines)
South
North
Hook and Pulleys
Made in Norway
S E V E R R E
MUNCK
BERGEN NORWAY
CSA
9658
Type 221 4423
No. 31 AF 616
3.8 H.P.
Y 220 V
11.4 A
60 cycl.
Lift 12 feet
Rating S.D.%
Cap. 2 Tons
Speed 20 feet/min

Figure 2.2 North View of Crane and Building Structure

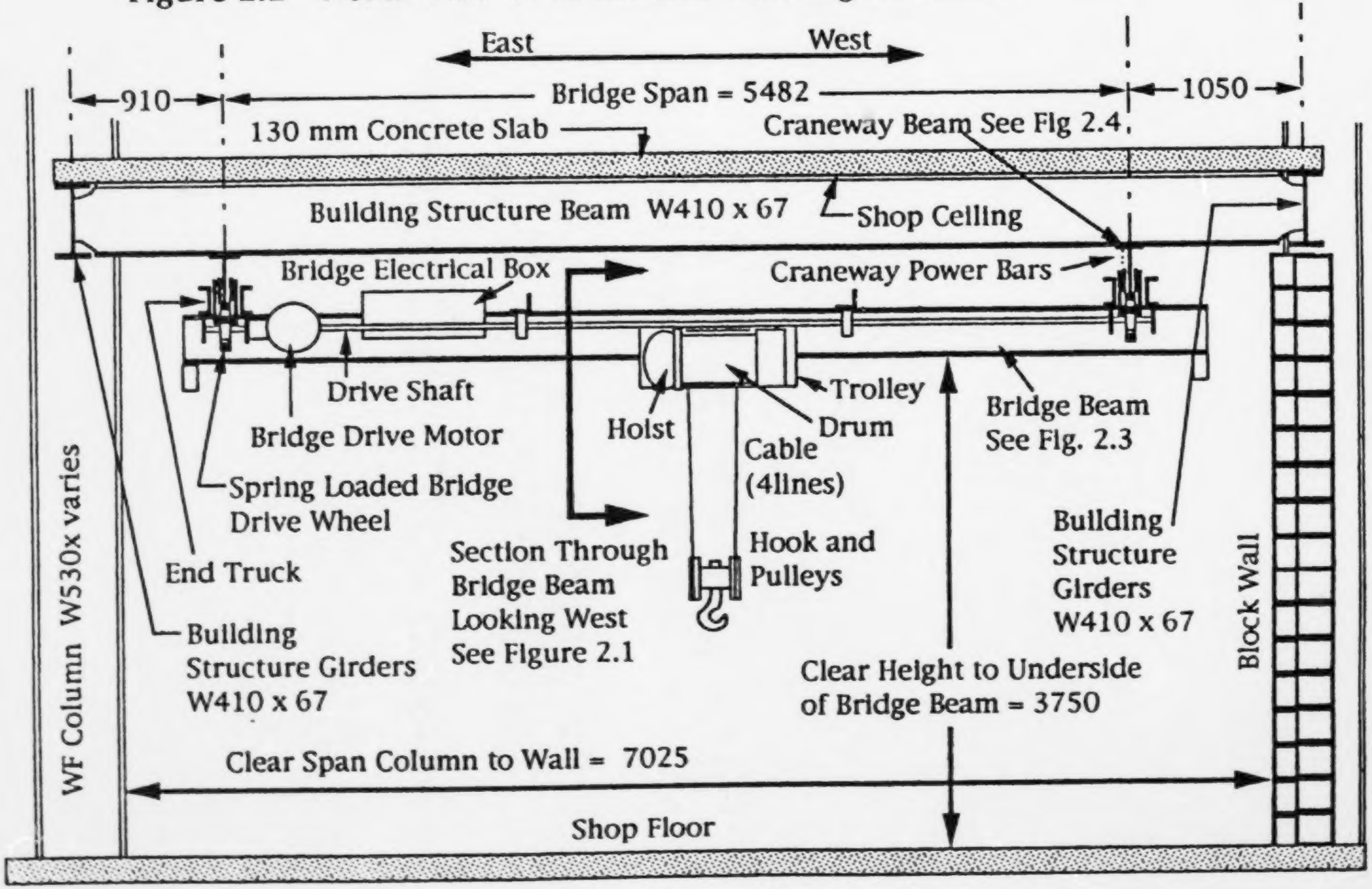
East
West
910
Bridge Span = 5482
1050
130 mm Concrete Slab
Craneway Beam See Fig 2.4
Building Structure Beam W410 x 67
Shop Ceiling
Bridge Electrical Box
Craneway Power Bars
Drive Shaft
Bridge Drive Motor
Spring Loaded Bridge Drive Wheel
End Truck
Building Structure Girders W410 x 67
Section Through Bridge Beam Looking West See Figure 2.1
Hoist
Trolley
Drum
Cable (4lines)
Hook and Pulleys
Bridge Beam See Fig. 2.3
Building Structure Girders W410 x 67
Block Wall
Clear Height to Underside of Bridge Beam = 3750
WF Column W530x varies
Clear Span Column to Wall = 7025
Shop Floor

Figure 2.3 Crane Bridge Section Properties

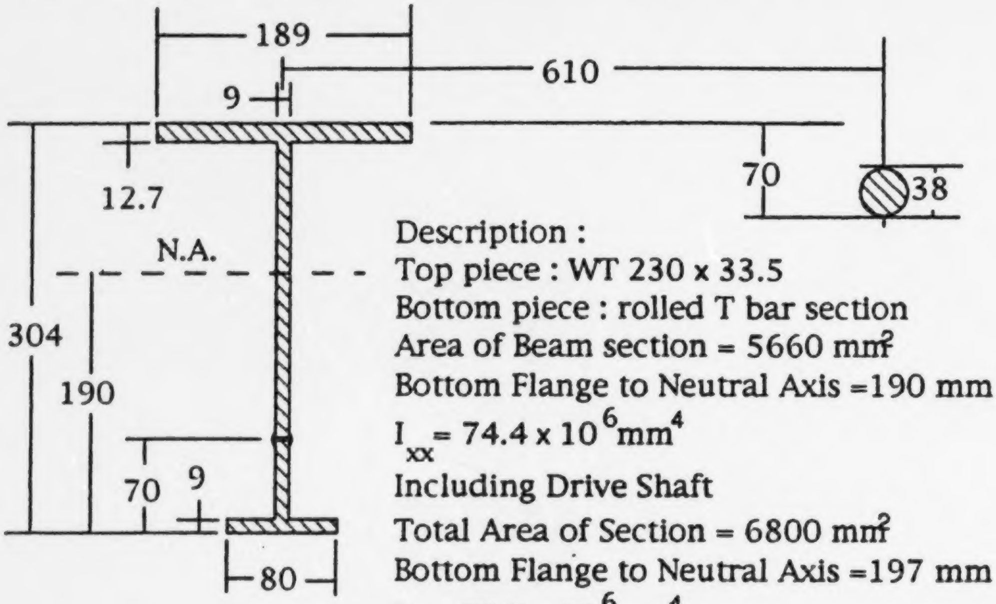
189
610
9
70
38
12.7
N.A.
304
190
70
9
80

Description :
Top piece : WT 230 x 33.5
Bottom piece : rolled T bar section
Area of Beam section = 5660 mm^2
Bottom Flange to Neutral Axis =190 mm
$I_{xx} = 74.4 \times 10^6 mm^4$
Including Drive Shaft
Total Area of Section = 6800 mm^2
Bottom Flange to Neutral Axis =197 mm
$I_{xx} = 76.2 \times 10^6 mm^4$

Figure 2.4 Craneway Beam Section Properties

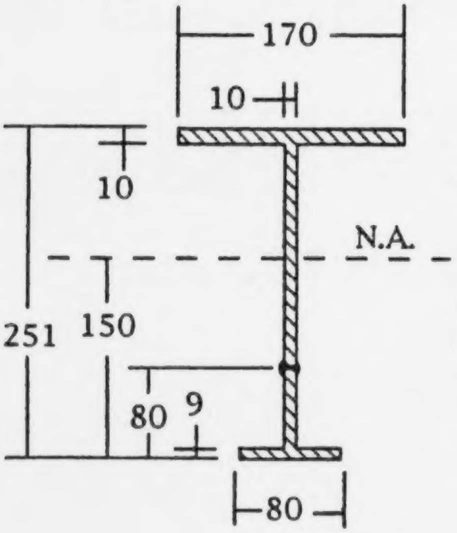
170
10
10
N.A.
251
150
80
9
80

Description :
Top piece : from W360 x 45
Bottom piece : rolled T bar section
Total Area = 4740 mm^2
Bottom Flange to
Neutral Axis =150 mm

$I_{xx} = 36.8 \times 10^6 mm^4$

Figure 2.5

Photographs of Shop Crane

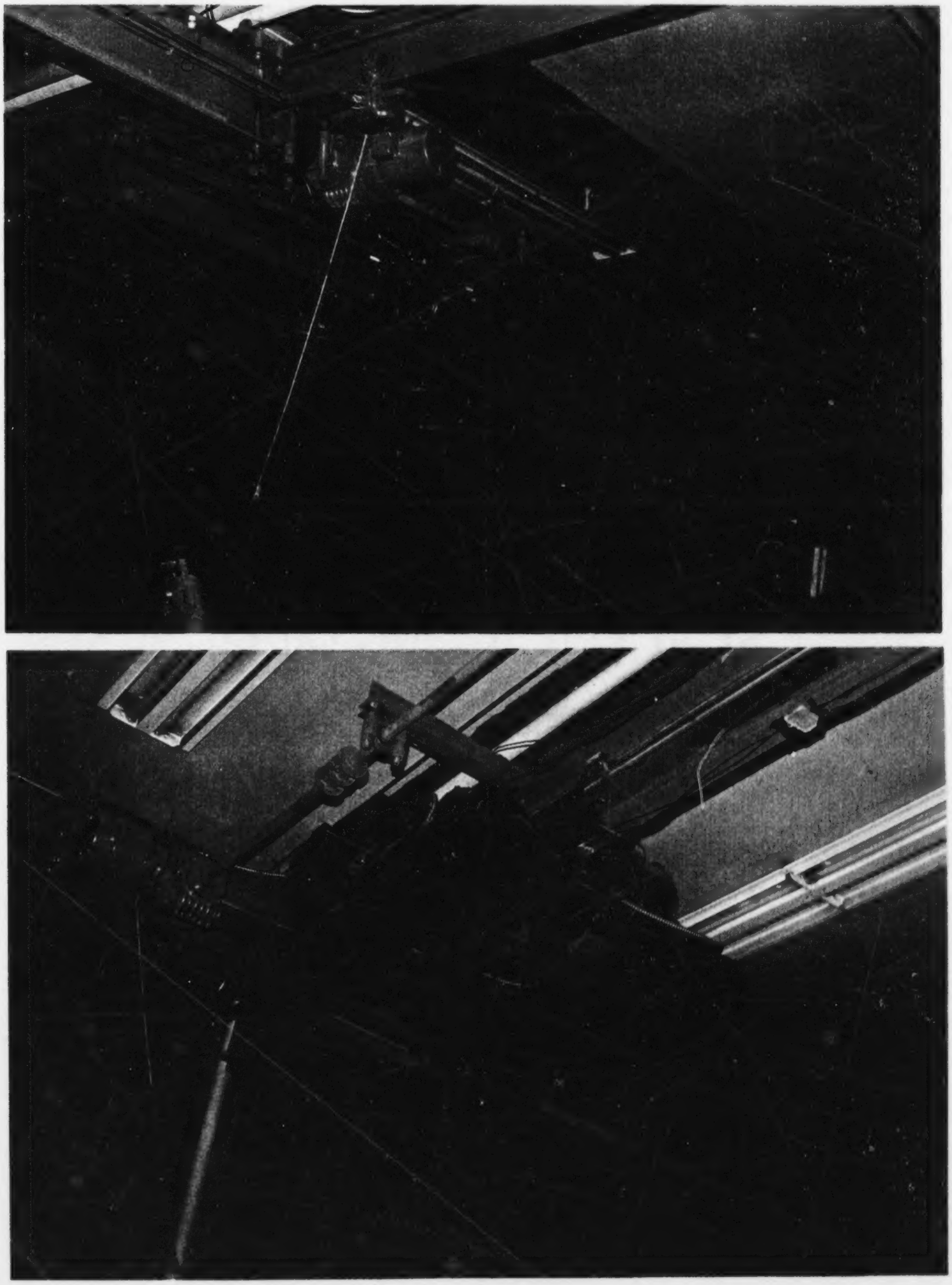

Figure 2.6 Frame for Weighing Trolley

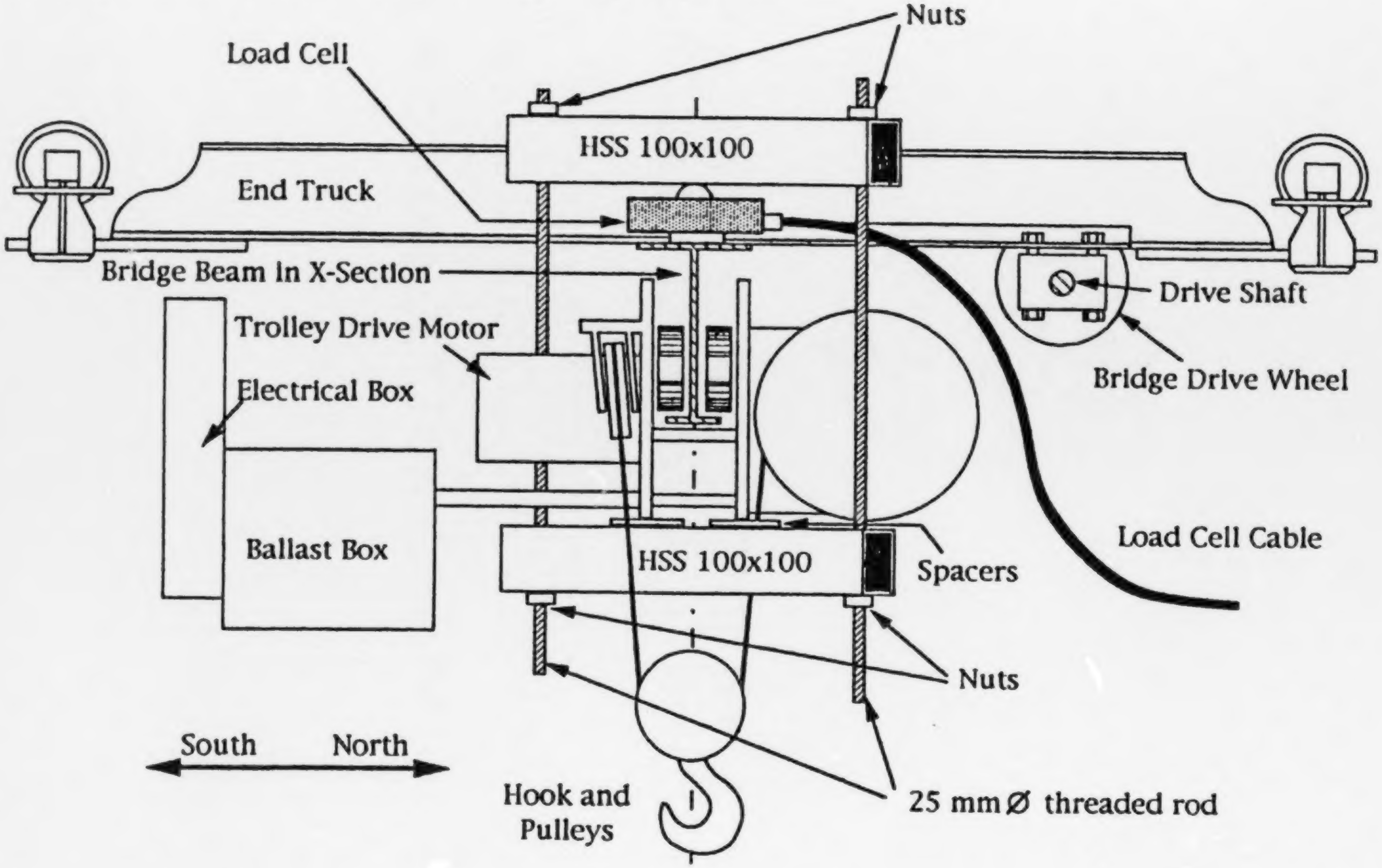
Nuts
Load Cell
HSS 100x100
End Truck
Bridge Beam In X-Section
Drive Shaft
Trolley Drive Motor
Bridge Drive Wheel
Electrical Box
Ballast Box
Load Cell Cable
HSS 100x100
Spacers
Nuts
South
North
Hook and Pulleys
25 mm Ø threaded rod

output signal was recorded again. Assuming the bridge to be linearly elastic, an estimate of the trolley mass can be made as shown in Table 2.1. The two trolley mass measurements are in reasonable agreement.

Table 2.1 Trolley Mass Calculation

Strain Gauge Output (unitless)	Condition
+18	- trolley at far end of bridge
+1855	- loaded trolley at centre of bridge
+375	- unloaded trolley at centre of bridge
Payload = 1.46 tonnes	
Estimated Trolley mass = $\frac{375 - 18}{1855 - 375}$ x 1.46 tonnes = 0.352 tonnes = 352 kg	

The values in the Strain Gauge Output column are strain gauge signals amplified by a constant. They indicate only relative strain values.

2.3 Hoist Motor

The information marked on the hoist motor is as follows. It was made in Norway by Munck Manufacturing Inc. It is a type 221-4428, serial number 31-AF-616. Its electrical rating is 11.4 amps at 220 V and 60 Hz. The rated hoisting capacity is recorded as 2 tons, which is 1.82 tonnes. The rated power is 3.8 HP, which is 2.8 kN·m/s. The motor has a lifting speed of 20 ft./min., which is 6.1 m/min. or 0·10 m/sec., and has a total lift of 12 feet, or 3.6 m.

2.4 Payload

Two sizes of payload were used in the testing program. One was a concrete and steel assembly that had been built for an earlier, unrelated, program. This assembly, referred to as the large payload, is shown in Figure 2.7, along with the calculations done to estimate its mass.

The other was a wooden box holding nine 22.7 kg ballast blocks. The box had a mass of 2 kg. Calculation of this smaller payload's weight is as follows.

$$(9 \times 22.7\ \text{kg} + 2\ \text{kg},) \times 9.81 = 2.05\ \text{kN}$$

Later the weights of both payloads were measured using a tension load cell attached in line on the crane hook. (See Section 2.5.) The large payload was found to weigh 14.35 kN, and the small payload was found to weigh 2.07 kN. Both estimates were thus confirmed.

2.5 Cable and Load Cell Assembly and Slings

The hook and its pulley are secured to the trolley through four lines of the cable, as shown in Figure 2.1 and 2.2. Therefore, the speed with which the motor rolls up the cable is four times faster than the hoisting speed.

During the testing, a tension load cell was attached beneath the hook. Several shackles were used to make this connection from the relatively small load cell to the larger hook. Beneath the load cell was another group of shackles for attaching chain or web slings. The group of lifting components, comprising the load cell and the sets of shackles above and below it, is referred to as the tension load cell assembly.

The term "sling" refers to any general purpose lifting component that attaches a payload to a hook. To secure the payloads for this test program, either 16 mm chain slings or synthetic webbing slings were used.

The elongations of the cable, tension load cell assembly, and the web or chain slings used to secure the payload, were measured. A diagram of the test setup is shown in Figure 2.8. The net stiffness of the cable, load cell assembly, and slings will be referred to as the cable stiffness, k_c.

When the payload was hanging freely from the cable above, jacks below the payload were raised, until they just touched the underside of the payload. The jacks were then raised in increments, thus reducing the cable tension. The displacements and tension were recorded at each step. When raising the

Figure 2.7 Large Payload

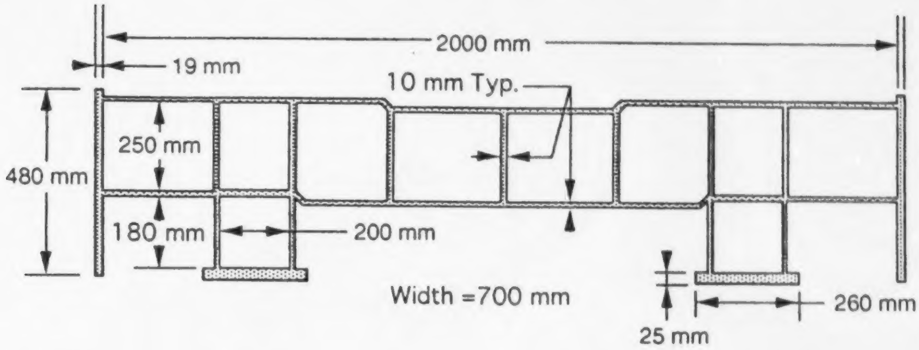
2000 mm
19 mm
10 mm Typ.
250 mm
480 mm
180 mm
200 mm
Width =700 mm
25 mm
260 mm

Large Payload is a steel frame filled with concrete

Calculations for Mass of Large Payload
Concrete Density = 2.4 tonnes/cubic metre
Steel density = 7.85 tonnes/cubic metre

Concrete :

2 legs x 180 mm x 200 mm x 700 mm x 2.4 T/m³ =	0.121 T
250 mm x 2000 mm x 700 mm x 2.4 T/m³ =	0.840 T

Steel :

2 Outboard Plates x 19 mm x 480 mm x 700 mm x 7.85 t/m³ =	0.100 T
7 Inner Panels x 10 mm x 250 mm x 700 mm x 7.85 T/m³ =	0.096 T
2 Plates x 10 mm x 2000 mm x 700 mm x 7.85 T/m³ =	0.220 T
2 Base Plates x 25 mm x 260 mm x 700 mm x 7.85 T/m³ =	0.071 T

Total Calculated Mass of Large Payload =	1.448 T

Figure 2.8 Test Setup to Measure Cable Stiffnesses

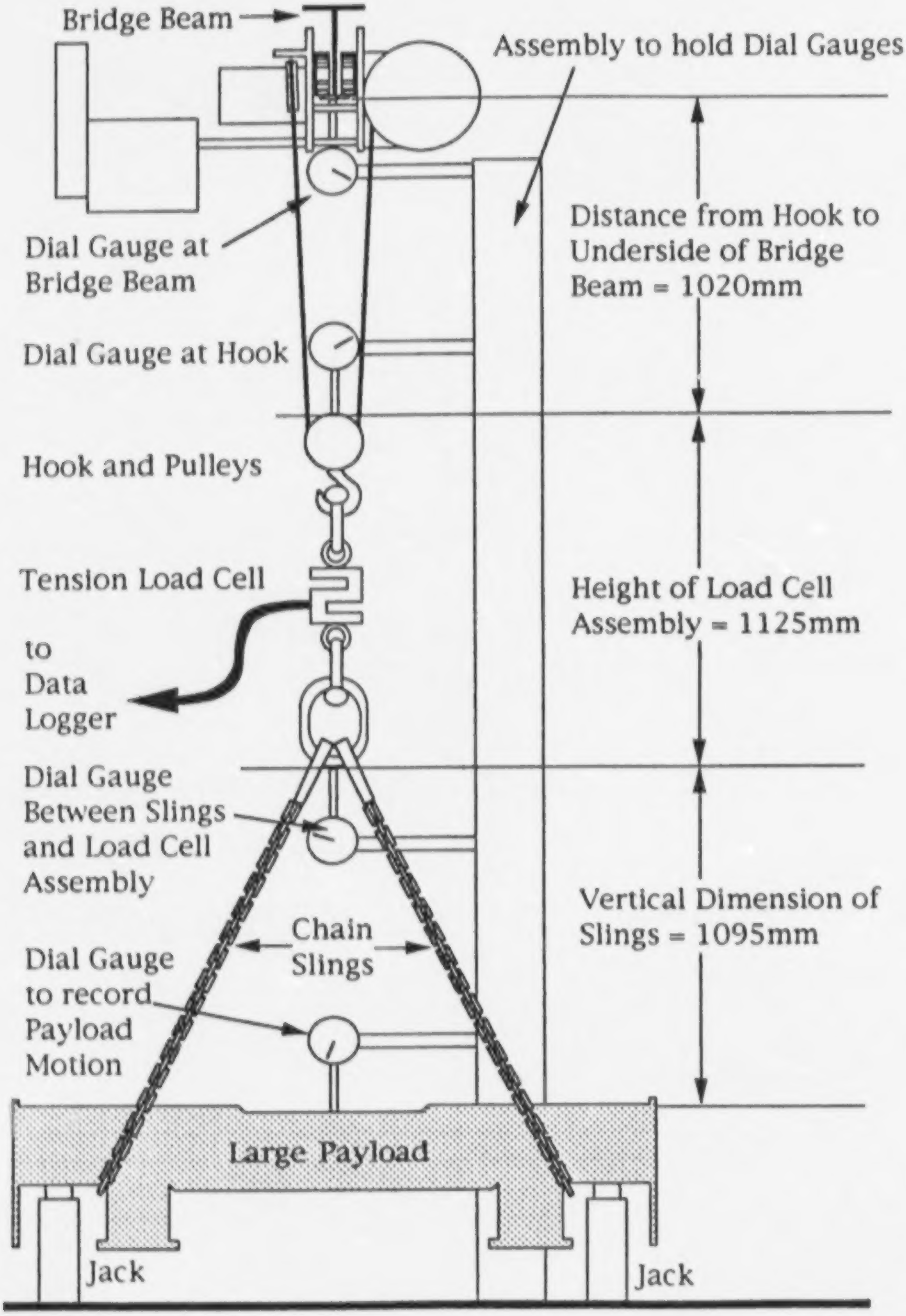
Bridge Beam
Assembly to hold Dial Gauges
Dial Gauge at Bridge Beam
Distance from Hook to Underside of Bridge Beam = 1020mm
Dial Gauge at Hook
Hook and Pulleys
Tension Load Cell
Height of Load Cell Assembly = 1125mm
to Data Logger
Dial Gauge Between Slings and Load Cell Assembly
Vertical Dimension of Slings = 1095mm
Chain Slings
Dial Gauge to record Payload Motion
Large Payload
Jack
Jack

payload produced no further decrease in tension, the cable was assumed to be completely slack. At that point the jacks were lowered incrementally, increasing the cable tension, and the displacements and tension were recorded. The graphs of the results are shown in Figures 2.9, 2.10, and 2.11. In Figure 2.9 the graphs of the net cable elongation for the web and chain slings with the small payload are shown. In Figures 2.10 and 2.11, the graphs of the elongation of wire cable, the load cell assembly, and the slings, (chain and web, respectively) with the large payload are shown. Figures 2.10 and 2.11 also show the lines for the stiffnesses from Figure 2.9 for the small payload data. The points of zero elongation for the large and small payload tests were not the same. In Figures 2.10 and 2.11, the location of the lines for the small payload along the elongation axis are chosen to fit in with the data points from the tests using the large payload.

It can be seen that there is significant hysteresis and non-linearity in the load displacement response of the cable and sling assembly. During testing it was also observed that there was a significant amount of time-dependent behaviour exhibited by the slings. The test set up was not equipped to measure this phenomenon, but some qualitative observations were made.

At the end of each step in which the payload was lowered, the measured tension did not remain constant after jacking ceased, but decreased over time. The rate of the tension reduction decreased with time. The lower dial gauge indicated that the payload was stationary, and the other dial gauges indicated upward movement at each of their respective locations. Similarly, at the end of each step in which the payload was raised, the tension increased and the upper three dial gauges indicated downward movement while the payload remained stationary. The amounts by which the positions and tensions changed were greater when the payload had just been lowered rather than raised, when the tension was high rather than low, and when web slings rather than chain slings were used. The time dependent behaviour for the chains was so slight that it would not have been noticed but for the fact that the author had been alerted to the possibility of that type of phenomenon after having tested the web slings. A simple model that represents this behaviour is shown in Figures 2.12 and 2.13. The cable and the slings can be considered to act as a spring and damper in parallel, pulling against the crane

Figure 2.9 Cable Stiffness for Small Payload

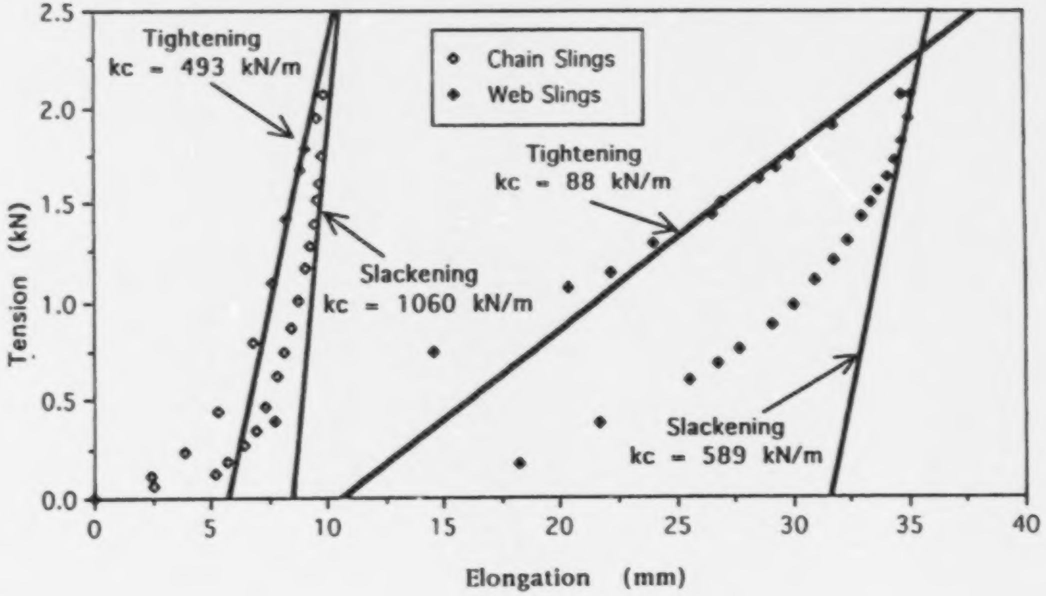

Figure 2.10 Derivation of Net Cable Stiffness

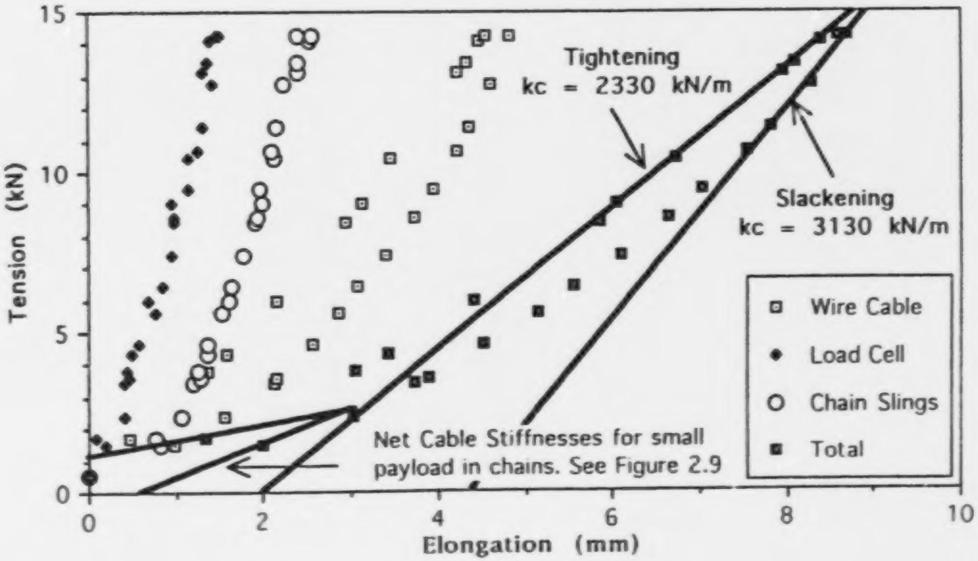

Structures Lab Shop Crane
Large Payload in Chain Slings

Figure 2.11 Derivation of Net Cable Stiffness

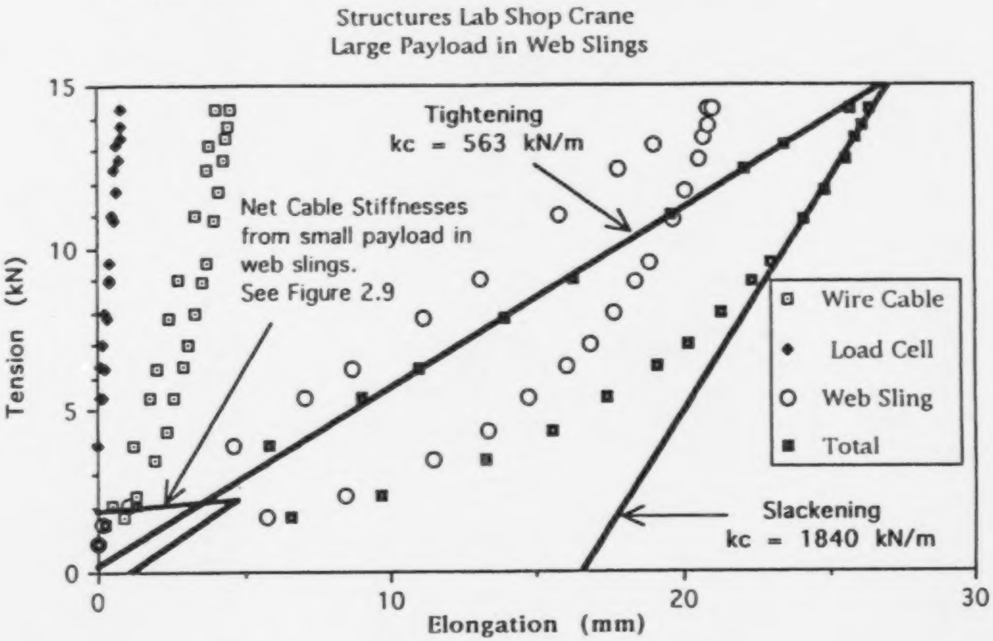

Figure 2.12 Delayed Elasticity Model for Time Dependant Behaviour Of Slings - Case of Payload Being Lowered

$T1 < T3 < T2$

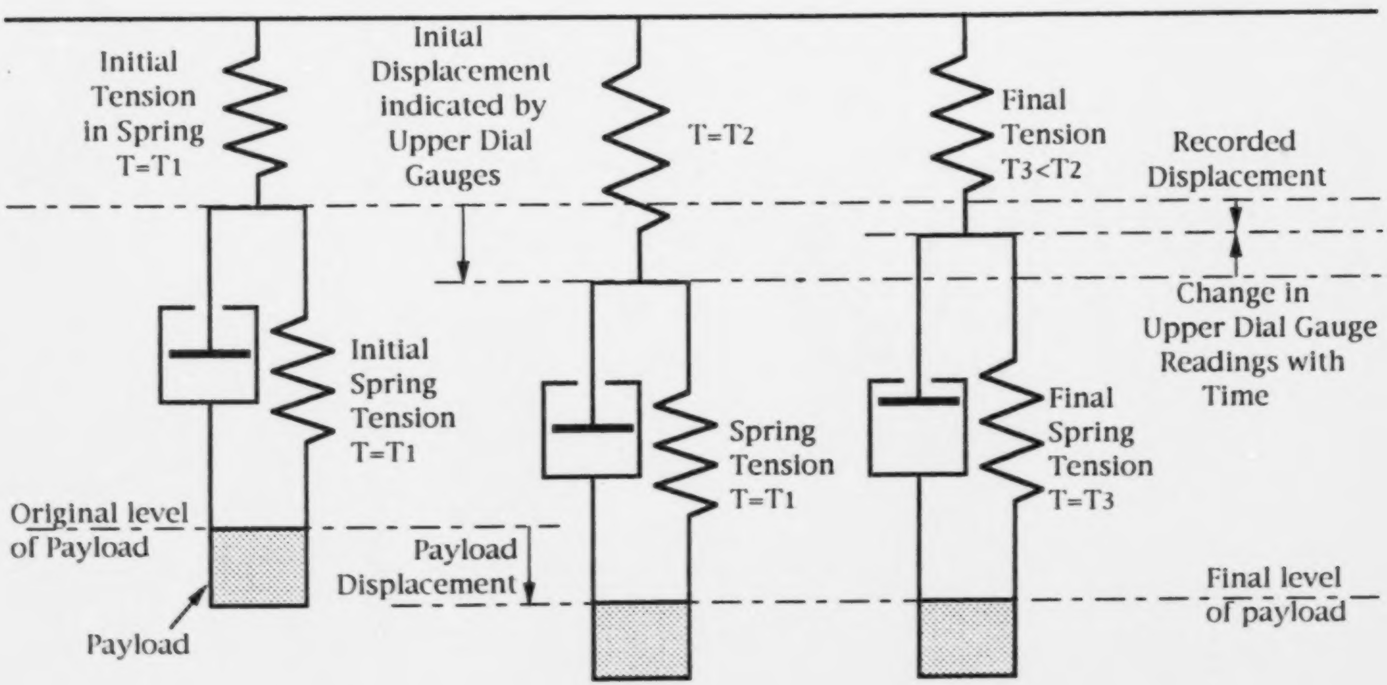
Initial
Tension
in Spring
T=T1
Inital
Displacement
indicated by
Upper Dial
Gauges
T=T2
Final
Tension
T3<T2
Recorded
Displacement
Change in
Upper Dial Gauge
Readings with
Time
Initial
Spring
Tension
T=T1
Spring
Tension
T=T1
Final
Spring
Tension
T=T3
Original level
of Payload
Payload
Displacement
Payload
Final level
of payload

Figure 2.13 Delayed Elasticity Model for Time Dependant Behaviour Of Slings : Case of Payload Being Raised

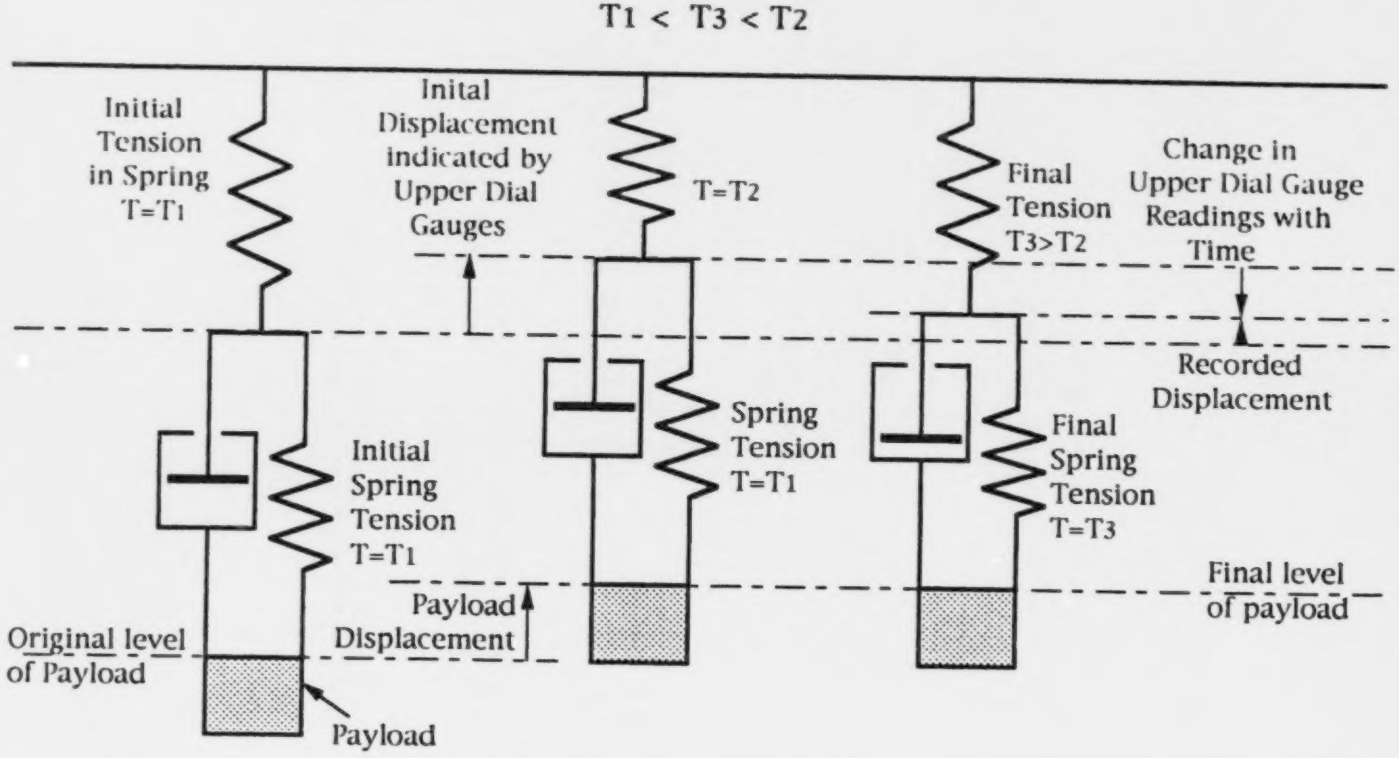
T1 < T3 < T2
Initial Tension in Spring T=T1
Inital Displacement indicated by Upper Dial Gauges
T=T2
Final Tension T3>T2
Change in Upper Dial Gauge Readings with Time
Recorded Displacement
Spring Tension T=T1
Final Spring Tension T=T3
Initial Spring Tension T=T1
Final level of payload
Payload Displacement
Original level of Payload
Payload

structure which acts as an undamped spring. This behaviour is called delayed elasticity.

To obtain the points for Figures 2.9, 2.10 and 2.11, discrete loading steps were used. There was a short delay between the establishing of a load level and the recording of displacements. For the type of dynamic loading the cable and slings are subjected to during normal use, and were subjected to during the test program, the tension varies continuously. It was assumed that the values for k_c from Figures 2.9, 2.10, and 2.11 were adequate approximations of the actual stiffnesses that occurred during testing. This will be discussed in detail in Chapters 4, 5, and 7.

The stiffness values determined near the maximum load will be used as the stiffness for the cable assembly because most of the dynamic activity occurs near that load. An estimate of the best fit line through the points near the maximum load, on the tightening and on the slackening sides of each total elongation curve is shown on the graphs. The two slopes, $k_{c_{tighten}}$ and $k_{c_{slacken}}$, were calculated. If a single value is required to describe cable stiffness, then one rationally based definition which can be used is the following. An effective stiffness, $k_{c_{effective}}$, is the stiffness which results, with a given payload mass, in the same frequency of free vibration that occurs when $k_{c_{tighten}}$ is used for the portion of each period during which the cable tension increases, and $k_{c_{slacken}}$ is used for the portion during which cable tension decreases. The expression for $k_{c_{effective}}$, given $k_{c_{slacken}}$ and $k_{c_{tighten}}$, is shown in equation (2.1).

$$k_{c_{effective}} = \left(\frac{2}{\sqrt{\frac{1}{k_{c_{slacken}}}} + \sqrt{\frac{1}{k_{c_{tighten}}}}} \right)^2 \qquad (2.1)$$

Figure 2.14 shows the relationship between the three stiffness values and the implied assumption about the shape of the hysteresis loop. Table 2.2 shows the values of $k_{c_{effective}}$. The advantages and disadvantages of using a single value for effective cable stiffness, and for using the definition given in equation (2.1) for that stiffness, is discussed in Chapter 7.

Figure 2.14 Definition of Effective Stiffness and Implied Hysteresis Loop

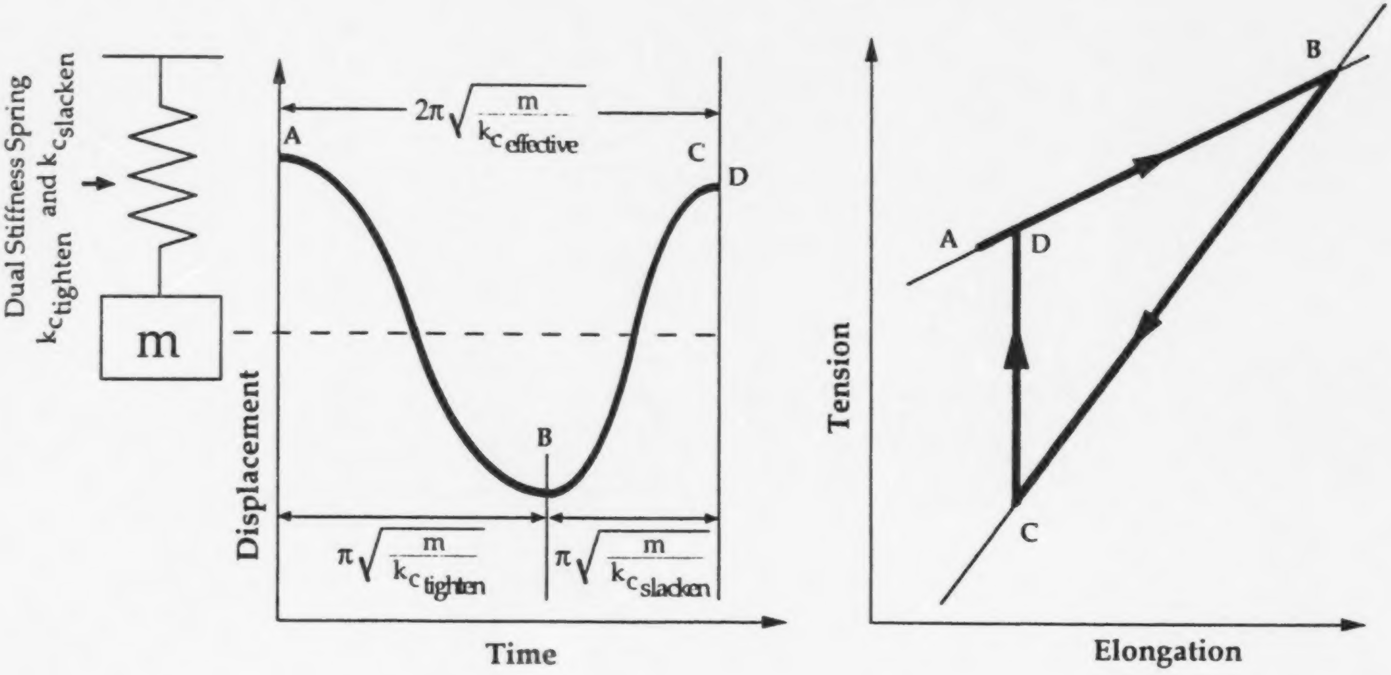
Dual Stiffness Spring
$k_{c_{tighten}}$ and $k_{c_{slacken}}$
m
Displacement
$2\pi\sqrt{\frac{m}{k_{c_{effective}}}}$
A
B
C
D
$\pi\sqrt{\frac{m}{k_{c_{tighten}}}}$
$\pi\sqrt{\frac{m}{k_{c_{slacken}}}}$
Time
Tension
Elongation
A
B
C
D

$$2\pi\sqrt{\frac{m}{k_{c_{effective}}}} = \pi\sqrt{\frac{m}{k_{c_{tighten}}}} + \pi\sqrt{\frac{m}{k_{c_{slacken}}}} \qquad \therefore k_{c_{effective}} = \left(\frac{2}{\sqrt{\frac{1}{k_{c_{tighten}}}} + \sqrt{\frac{1}{k_{c_{slacken}}}}}\right)^2$$

Table 2.2 Summary of Cable Stiffness Values

	$k_{c_{slacken}}$	$k_{c_{tighten}}$	$k_{c_{effective}}$
Small Payload Web Slings	589 kN/m	88 kN/m	183 kN/m
Small Payload Chain Slings	1060 kN/m	493 kN/m	697 kN/m
Large Payload Web Slings	1840 kN/m	563 kN/m	934 kN/m
Large Payload Chain Slings	3130 kN/m	2330 kN/m	2690 kN/m

CHAPTER 3

A REVIEW OF PRESENT STANDARDS

In this chapter the ways in which several standards deal with hoist induced dynamic loads are examined.

In the test program, described in Chapter 6 of this thesis, the shop crane in the I. F. Morrison Structures Laboratory was subjected to hoisting loads and the structural response recorded. Tests were done with the hoist at the midspan of the bridge and as far to one end of the bridge as possible. Two payloads were used. One weighed 14.35 kN, and the other weighed 2.07 kN. As the various standards are reviewed in this chapter, their application to the shop crane under those loads will be considered.

3.1 CSA Standard S16.1-1977 Steel Structures for Buildings

As the name implies, S16.1 deals with buildings and not specifically with cranes. In the 1977 version of S16.1 [ref. 7], clause 7.11 reads as follows:

> **7.11** In the absence of a dynamic analysis, or if not already specified by the authority having jurisdiction, live load which causes impact shall be increased according to the following percentages:
>
> (a) Elevator supports ....100 per cent
>
> (b) Girders, and their connections, supporting power-operated cranes ....25 per cent
>
> (c) Girders, and their connections, supporting hand-operated cranes ....10 per cent
>
> (d) Supports for light machinery, shaft or motor-driven ....20 per cent minimum
>
> (e) Supports for reciprocating machinery or power-driven units ....50 per cent minimum
>
> (f) Hangers supporting mezzanines and balconies..............33 per cent

The term "impact" is commonly used to describe an event where masses collide. The way this clause is phrased, it could be incorrectly interpreted as describing lateral impact factors, which would apply to the cases in which the trolley or the bridge drive into their respective endstops. However, factors for lateral impact are dealt with clearly in the subsequent clause 7.12. In the some codes not related to cranes, for example the Ontario Highway Bridge Design Code [ref 39], the term impact is used to describe any dynamic loading event. The reference to "girders and their connections" in part (b) of clause 7.11 therefore, can be assumed to indicate these are the items subjected to the increased vertical load due to the hoisting. The "live load which causes impact" probably refers to at least the payload weight. What is unclear is whether the weight of the trolley also "causes impact" on the bridge girder, and whether the crane weight "causes impact" on the craneway girders, since these components accelerate vertically during hoisting. It is assumed that the intent of the clause is that the factor applies only to the weight of the payload.

Therefore, the hoisted load of 14.35 kN should be treated as a static load of 1.25 x 14.35 kN = 17.94 kN, and the hoisted load of 2.07 kN should be treated as a static load of 1.25 x 2.07 kN = 2.59 kN.

3.2 CSA Standard CAN3-S16.1-M89 — Steel Structures for Buildings - Limit States Design

The more recent version of S16.1 [ref. 6] does not include any equivalent to the clause described in Section 3.1 preceding. The specifications for vertical dynamic load factors for bridge cranes was removed from later versions of S16.1, and placed in the National Building Code [ref 33], which is discussed in Section 3.3 following. There remain only two references which apply to cranes in CAN3-S16.1-M89. Under "Section 6 Dynamic Effects", clause 6.2.3.1 states the following:

> **6.2.3.1** Suitable provision shall be made in the design for the effect of live load, which induces impact or vibration, or both. In severe cases such as structural supports for heavy machinery, which causes substantial impact or vibration when in operation, the possibility of harmonic resonance, fatigue, or unacceptable vibration shall be investigated.

It is questionable whether this clause is actually intended to cover dynamic loads due to hoisting. It is almost a direct quote from clause 7.10 of the earlier version of S16.1, a clause which was not meant to deal with dynamic loads because that was handled in clause 7.11. The phrase "unacceptable vibration" implies excessive deflections that may interfere with the performance of the machinery or may damage wall or ceiling surfaces. Even if the clause is meant to cover dynamic loads due to hoisting, and "unacceptable vibrations" is intended to mean maximum dynamic stresses exceeding resisting strength, the only guidance given is that such load cases should be investigated.

The other place in CAN3-S16.1-M89 where the issue of crane loading is considered is in "Appendix I - Recommended Maximum Values for Deflections". There the suggestion is made that for industrial type buildings vertical deflections due to "Maximum wheel loads (no impact)" of simple span crane runway girders should be less than 1/600 of the span for cranes with capacity less than 225 kN, and less than 1/800 of the span for cranes with capacity of 225 kN and over. The deflection limit is probably an empirically derived check to ensure that the trough created in a girder by a fully loaded crane is not so steep that the crane cannot climb out.

3.3 National Building Code of Canada - 1992

In the National Building Code of Canada, Section 4.1.10.4. Vibrations and Impact of Machinery and Equipment, deals with dynamic loads on bridge cranes. Sentences (1) and (2) of section 4.1.10.4 states the following.

> (1) Where vibration effects, such as resonance and fatigue resulting from machinery or equipment, are likely to be significant, a dynamic analysis shall be carried out.
>
> (2) The minimum specified load due to equipment, machinery or other objects that may produce impact shall be the sum of the weight of the equipment or machinery and its maximum lifting capacity, multiplied by an appropriate factor listed in Table 4.1.10.A.

Table 4.1.10.A gives factors of 1.25 and 1.10 for impact due to the operation of motor driven and hand driven cranes respectively. It also gives a factor for the "supports for light machinery which is shaft or motor driven", of 1.20, and a factor for the "supports for reciprocating machinery (e.g. compressors) or power driven units (e.g. piston engines)" of 1.50. For elevators Table 4.1.10.A. refers to clauses in CAN/CSA-B44-M.

It is clear from sentence (2) that the factor is to be applied to more than just the payload weight. However, it is not clear which components of the crane "produce impact". The weight of the hoist and trolley probably should have the factor applied, but should the weight of the bridge crane also be factored? It is assumed that just the trolley weight is to be factored.

By applying a dynamic factor to the weight of not just the payload but the parts of the crane as well, the authors of the National Building Code are trying to take into account the inertial loads created by the motion of the bridge during hoisting. While those inertial loads should be considered, the procedure used here is not rational; the solution to a static problem should not include an increase in loads due to dynamic effects. Consider the case of a hoist lifting no payload. A dynamic factor of 1.25 would be applied to the weight of the unloaded trolley, although the trolley would not be vibrating. The method used in the National Building Code does not correctly address the general relationship between the payload weight and the size of the dynamic factor. Sentence (2) does require that the maximum lifting capacity be used, and it is possible that the weight ratios of the bridge and the maximum payload are often such that the National Building Code procedure provides accurate results. However, this is not stated explicitly in the National Building Code.

The weight of the trolley added to the weight of the large payload, and factored, is (3.24 kN + 14.35 kN) x 1.25 = 22.0 kN. This exceeds the weight of the unloaded trolley by 22.0 kN – 3.24 kN =18.75 kN.

The weight of the trolley added to the weight of the small payload, and factored, is (3.24 kN + 2.07 kN) x 1.25 = 6.64 kN. This exceeds the weight of the unloaded trolley by 22.0 kN – 3.24 kN =3.4 kN.

3.4 CSA Standard B167-1964 — General Purpose Electric Overhead Travelling Cranes

This standard, which deals exclusively with cranes, addresses vertical impact load in a more clear and perhaps more rational fashion than does S16.1. The crane is assigned to a class, based on the hours per year it is used, the proportion of loads that are above 50% of rated capacity, and the type of service the crane experiences. Tables 1, 2, 3 and 4 of section 3.4 of B167 are shown in Figures 3.1 and 3.2. There appears to be a typographical error in Table 3. In the second category, "All Loads of Rated Capacity" should probably read "Frequent Loads of Rated Capacity" to agree with the clarifying statement "Majority of Loads greater than 50 per cent of Rated Capacity". Clause 4.2.1 lists a set of seven design load descriptions, the second of which is "(b) Load impact; included in service factor (see Table 10)." Table 10 and its prefacing clause 4.2.2.1 are shown in Figure 3.3. The class system is used for several other purposes later in the standard. That is why the service factor loads are not directly placed in Table 1.

The statistical aspect of the classification system deserves some comment. Assume a payload equal in mass to the rated capacity of a crane. There is a maximum in-service, hoist-induced dynamic load to which the crane, lifting that payload, can be subjected. The load is a function of the stiffnesses and masses of the various components within the whole system, and a function of the hoist motor properties. It is a maximum service load. There is some chance involved in whether an individual hoisting event will produce the potential maximum dynamic load, or some load less than that, but the crane will not be subjected to more than that maximum, except by accident. Hoisting a payload that is heavier than the rated load, or hooking the slings to the ground or a fixed part of the craneway, for example, are accidental loading cases. These events can produce loads greater than the maximum hoist-induced load. If accidental loading could be avoided, then increasing the frequency of near capacity loads (as described in Table 3) and increasing the total number of loads per year (as described in Table 2) would not change the maximum hoist-induced dynamic load the crane will be subjected to. What increasing those two frequencies does is increase the chance of accidental loading. That is why the factor that takes dynamic loading into account is called the Service Factor, rather than the Vertical Impact, or Vertical Dynamic Factor.

Using the service factor as described in the standard, the shop crane has a "low" impact factor as per Table 4, a "low" relative impact factor as per Table 3, and a "short" operating factor as per Table 2. Thus it is designated as Class

Figure 3.1 Classification Table From CSA Standard B167-1964

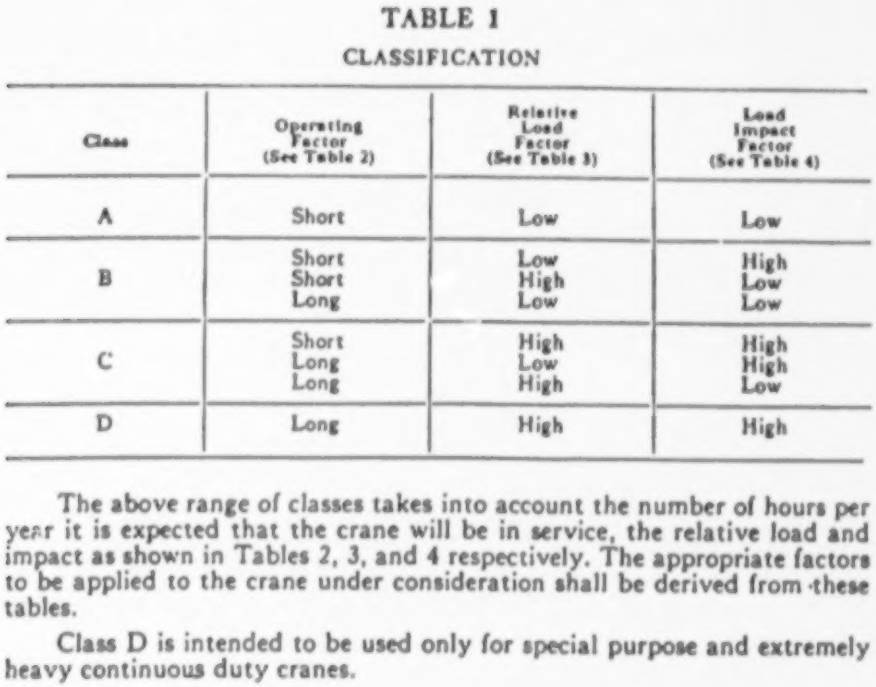

TABLE 1

CLASSIFICATION

Class	Operating Factor (See Table 2)	Relative Load Factor (See Table 3)	Load Impact Factor (See Table 4)
A	Short	Low	Low
B	Short	Low	High
	Short	High	Low
	Long	Low	Low
C	Short	High	High
	Long	Low	High
	Long	High	Low
D	Long	High	High

The above range of classes takes into account the number of hours per year it is expected that the crane will be in service, the relative load and impact as shown in Tables 2, 3, and 4 respectively. The appropriate factors to be applied to the crane under consideration shall be derived from these tables.

Class D is intended to be used only for special purpose and extremely heavy continuous duty cranes.

With the permission of the Canadian Standards Association, this material is reproduced from B167-1964 (General Purpose Electric Overhead Travelling Cranes), which is copyrighted by CSA, 178 Rexdale Boulevard, Rexdale, Ontario, Canada, M9W 1R3. This copy of CSA standard B167-1964 (General Purpose Electric Overhead Travelling Cranes), as reproduced with CSA permission, will not be updated to reflect ammendments made to the original content of the CSA Standard after November 1966. For up-to-date information, see the current edition of the CSA Catalogue of Standards.

Figure 3.2 Factor Tables From CSA Standard B167-1964

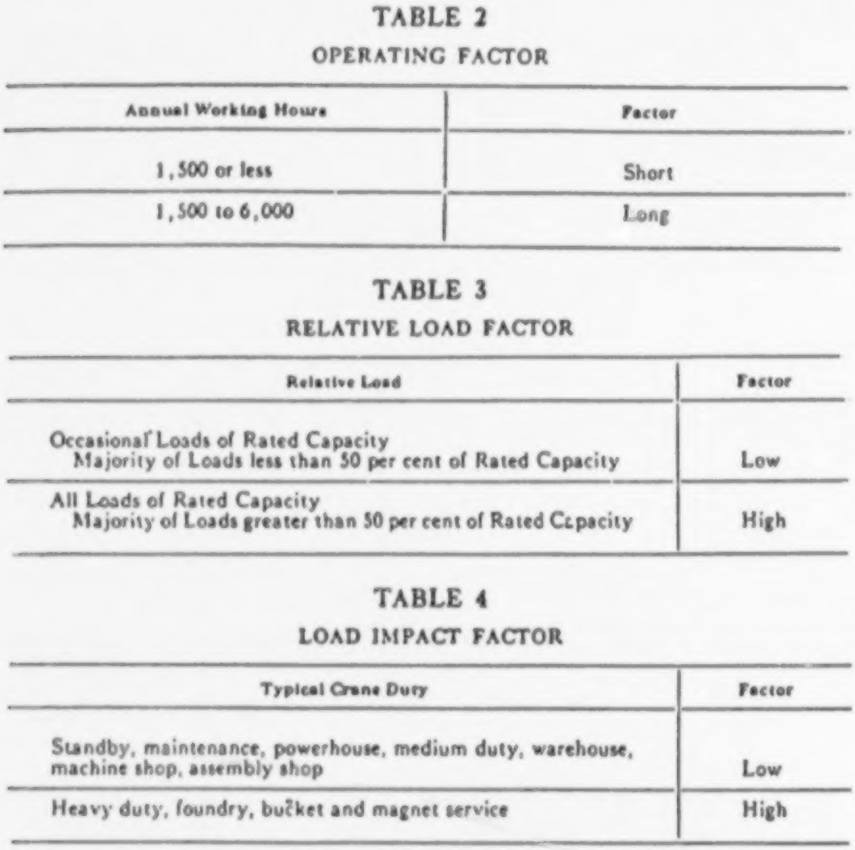

TABLE 2
OPERATING FACTOR

Annual Working Hours	Factor
1,500 or less	Short
1,500 to 6,000	Long

TABLE 3
RELATIVE LOAD FACTOR

Relative Load	Factor
Occasional Loads of Rated Capacity Majority of Loads less than 50 per cent of Rated Capacity	Low
All Loads of Rated Capacity Majority of Loads greater than 50 per cent of Rated Capacity	High

TABLE 4
LOAD IMPACT FACTOR

Typical Crane Duty	Factor
Standby, maintenance, powerhouse, medium duty, warehouse, machine shop, assembly shop	Low
Heavy duty, foundry, bucket and magnet service	High

With the permission of the Canadian Standards Association, this material is reproduced from B167-1964 (General Purpose Electric Overhead Travelling Cranes), which is copyrighted by CSA, 178 Rexdale Boulevard, Rexdale, Ontario, Canada, M9W 1R3. This copy of CSA standard B167-1964 (General Purpose Electric Overhead Travelling Cranes), as reproduced with CSA permission, will not be updated to reflect ammendments made to the original content of the CSA Standard after November 1966. For up-to-date information, see the current edition of the CSA Catalogue of Standards.

Figure 3.3 Service Factor Table From CSA Standard B167-1964

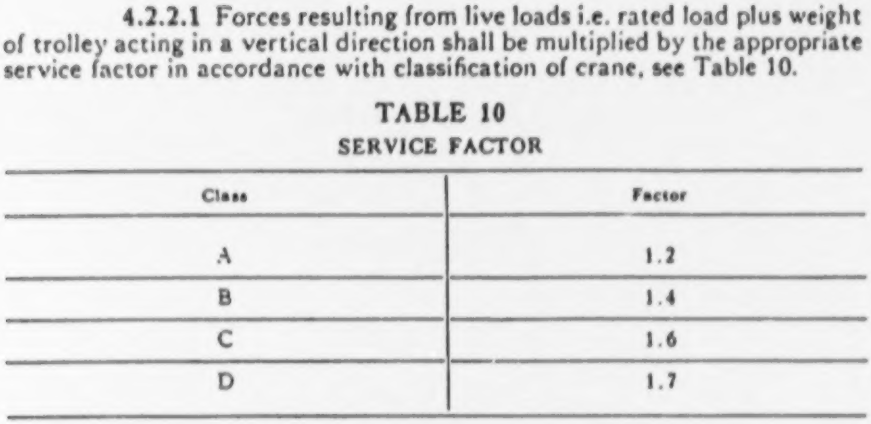

4.2.2.1 Forces resulting from live loads i.e. rated load plus weight of trolley acting in a vertical direction shall be multiplied by the appropriate service factor in accordance with classification of crane, see Table 10.

TABLE 10
SERVICE FACTOR

Class	Factor
A	1.2
B	1.4
C	1.6
D	1.7

With the permission of the Canadian Standards Association, this material is reproduced from B167-1964 (General Purpose Electric Overhead Travelling Cranes), which is copyrighted by CSA, 178 Rexdale Boulevard, Rexdale, Ontario, Canada, M9W 1R3. This copy of CSA standard B167-1964 (General Purpose Electric Overhead Travelling Cranes), as reproduced with CSA permission, will not be updated to reflect ammendments made to the original content of the CSA Standard after November 1966. For up-to-date information, see the current edition of the CSA Catalogue of Standards.

A, with a service factor of 1.2 applied to payload and trolley weight, as per Table 10.

For the large payload, The dynamic load is calculated as follows.

1.2 x (14.35 kN payload + 3.24 kN trolley weight) = 21.1 kN

This is 21.1 kN - 3.24 kN = 17.9 kN greater than the weight of the unloaded trolley.

For the small payload, the increased load is the following.

1.2 x (2.07 kN payload + 3.24 kN trolley weight) = 6.37 kN

This is 6.37 kN - 3.24 kN = 3.13 kN greater than the weight of the unloaded trolley.

The statements of permission below the tables in Figures 3.1, 3.2, and 3.3, include the comment that up-to-date information is listed in the current edition of the CSA Catalogue of Standards. However, CSA Standard B167-1964 is presently the most up to date CSA standard dealing with design loads for cranes.

3.5 DIN 15.018 part 1 - Cranes, Steel Structures, Verification and Analysis

The German standard uses a load spectrum factor Ψ to account for the vertical dynamic load factor for hoisting. The load spectrum factor is a linear function of the hoisting speed and is also a function of the lifting class of the crane. Figure 3.4 shows a plot of Ψ versus hoisting speed.

Table 23 in DIN 15.018 gives a list of lifting classes and a description of the applicable cranes. "Item No. 6 Workshop Cranes" has a designated lifting class of H_2 or H_3. There is no guidance given about the difference between an H_2 classification and an H_3 classification. The hoisting speed of the structures lab shop crane is 6.1 m/min. Substituting this value into the formula in Table 23 gives the following values for Ψ:

Figure 3.4
Graph of Dynamic Factors Ψ and 1 + (HLF) versus Hoisting Speed

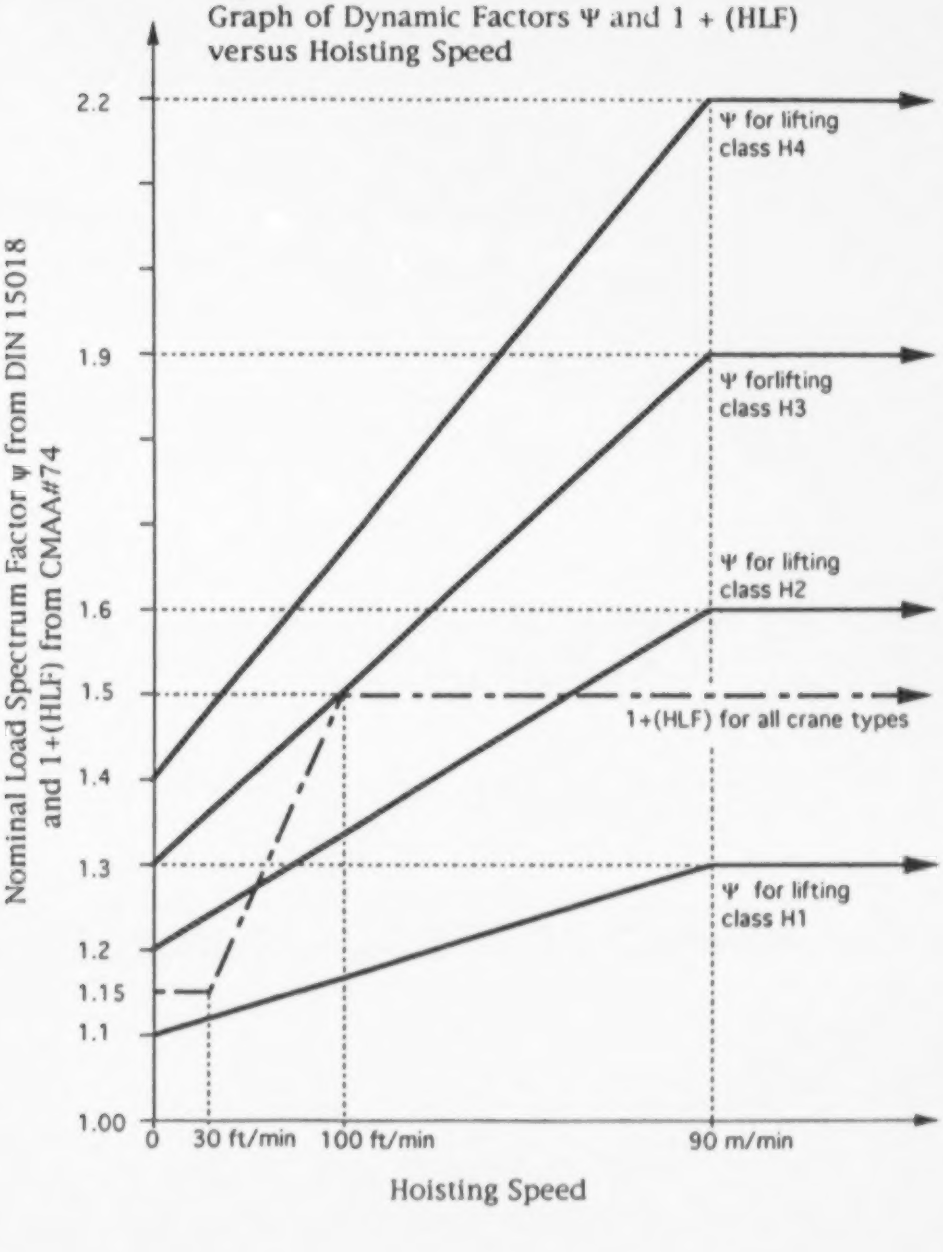

$\Psi = 1.2 + .0044 \times 6.1 = 1.23$ assuming H_2 lifting class

$\Psi = 1.3 + .0066 \times 6.1 = 1.34$ assuming H_3 lifting class

Clause 4.1.4.2 states that Ψ should be applied to the payload weight. For the larger payload, assuming the crane belongs in class H_2, the dynamic load is 1.23 x 14.35 kN = 17.7 kN. Assuming the crane belongs in class H_3, the dynamic load is 1.34 x 14.35 kN = 19.2 kN. Similarly for the smaller payload, the dynamic load is 1.23 x 2.07 kN = 2.55 kN or 1.34 x 2.07 kN = 2.77 kN, depending on whether the crane belongs in class H_2 or class H_3 respectively.

A reasonable criticism of the formula for Ψ is that as the hoisting speed approaches zero, the dynamic factor does not approach unity. It approaches values greater than one. This is despite the fact that the case of zero hoisting speed corresponds to a static situation and a dynamic factor of one would be expected.

In Clause 4.1.4.2 the following statement is found.

> "The softer the springing of the hoisting gear, the larger the elasticity of the supporting structure, the smaller the actual hoisting speed at the commencement of the hoisting of the useful load, the smaller and steadier the acceleration and deceleration during changes in the hoisting motion, the smaller the factor Ψ."

In discussing some qualitative general trends about the dynamic factor D, Barrett and Hrudey (1989) [ref. 3] stated,

"The largest D values occur when the structure is most stiff."

In Chapter 5 of this thesis, deductions are made from the mathematical model of the crane which indicate that this is not always true, and that in fact there are many real situations where decreasing the stiffness of the crane structure will increase the dynamic load factor.

3.6 DIN 4132 — Craneways, Steel Structures, Principles for Calculating Design and Construction

The German standard, DIN 4132, deals specifically with craneway structures. It refers to DIN 15.018 in several places, and the two were clearly written in conjunction with one another.

Though DIN 4132 is very thorough in its description of the loads on the craneway, it does not mention hoist-induced vertical loads. One must assume that the authors of the two standards believed either that hoist-induced vertical loads are not applied to the craneway structure, or that the factors and analysis presented in DIN 15.018 are to be used to design the craneway structure as well. The latter seems more plausible.

3.7 CMAA Specification #74 - 1987 — Specification for Top Running and Under Running Single Girder Electric Overhead Travelling Cranes

The Crane Manufacturers Association of America publishes a specification for cranes which includes a hoist load factor, (HLF). Clause 3.3.2.1.1.4.2 describes the factor.

> **3.3.2.1.1.4.2 Hoist Load Factor (HLF)** This factor applies to the motion of the rated load in the vertical direction, and covers inertia forces, the mass forces due to the sudden lifting of the hoist load and the uncertainties in allowing for other influences. The hoist load factor is 0.5 percent of the hoisting speed in feet per minute, but not less than 15 percent or more than 50 percent, except for bucket and magnet cranes for which the impact value shall be taken as 50 percent of the rated capacity of the bucket or magnet hoist.
>
> (HLF) $= .15 \leq .005 \times$ (hoist speed) $\leq .5$

The use of the term "factor" is misleading, since (HLF) is a number smaller than one. It is assumed that the actual factor, the number to multiply static weight by, is 1+ (HLF). The structures lab shop crane has a hoist speed of 20 ft./min., slow enough to require the minimum value for (HLF).

1.15 x 14.35 kN = 16.5 kN for the large payload

1.15 x 2.07 kN = 2.38 kN for the small payload

Figure 3.4 shows the dynamic factor graph from DIN 15.018 and the function 1+ (HLF) plotted so the two factors can be compared. It can be seen that there is significant difference between the two approaches. At hoisting speeds greater than 100 ft/min., the CMAA factor is constant at 1.5, which is less conservative than Ψ for H_3 and H_4 lifting class cranes at these speeds. With both formulae the static load case produces a factor greater than one, but the sloping part of the CMAA curve, above 1.15, rises proportionally to the hoisting speed. The minimum requirement of 1.15 is perhaps included because of a feeling that the uncertainty of the payload mass was worth some consideration, and it was most apparent that the uncertainty was not being addressed at low hoisting speeds. In a letter from CMAA, the chairman of the Engineering Committee suggested the formula for 1 + (HLF) was probably determined empirically. (See Appendix E.)

The two standards, CMAA#74 and DIN 15.018, use imperial and metric units for measuring hoisting velocity. In Figure 3.4 both ft/min and m/min are used, respectively, to indicate the velocities at which the formulas for 1 + (HLF) and Ψ change.

3.8 AISC Specifications for the Design, Fabrication, and Erection of Structural Steel for Buildings

The clause in the AISC specification that deals with dynamic load is shown below.

> **1.3.3 Impact**
>
> For structures carrying live loads* which induce impact, the assumed live load shall be increased sufficiently to provide for same.
>
> If not otherwise specified, the increase shall be:

For supports of elevators	100 per cent
For cab operated travelling crane support girders and their connections	25 per cent
For pendant operated travelling crane support girders and their connections	10 per cent
For supports of light machinery; shaft or motor-driven not less than	20 per cent
For supports for reciprocating machinery or power-driven units, not less than	50 per cent
For hangers supporting floors and balconies	33 per cent

---

* Live loads on crane support girders shall be taken as the maximum crane wheel loads.

This seems almost identical to clause 7.11 in the early version of CSA S16.1, but it is different in three important ways. First, the footnote makes it clear that for craneway girder design, the weight of the payload and the entire crane should be increased by the specified amount. This is a more clearly defined version of the procedure used in the National Building Code of Canada, where a dynamic factor is applied to the weight, or part of the weight, of the crane. The procedure does not correctly address the general relationship between the payload weight and the dynamic factor. (See Section 3.3) The same criticism can be made of CSA B167 (see clause 4.2.2.1 in Figure 3.3), although it is a service factor greater than one which is being applied. The service factor is intended to account for vertical hoist induced dynamic loads, as well as other in-service loads.

The second difference between AISC and CSA is that cranes are grouped into different classes; cab-operated and pendant-operated cranes in AISC, rather than power-operated and hand-operated as was done in the CSA specification. Hand-operated cranes tend to have lower hoisting accelerations than power-operated cranes, and so there is reason for having different dynamic factors for these two classes. Both cab and pendant-operated cranes are power-operated. The only difference between the two types is that the operator is either on the ground or in a cab on the bridge. Although not all large cranes are cab-operated, generally all cab-operated cranes are large. The extra mass of the operator and cab may increase the inertial loads, but that mass is very small compared to the mass of the bridge or even of the trolley and hoist motor. The AISC categories do not distinguish between cranes with higher and lower hoist accelerations, but do distinguish between cranes with marginal differences in structure mass. The small difference in structure mass does not seem to justify the fairly significant change in dynamic factor from 1.1 to 1.25, and it may be that operator safety was the primary consideration. The majority of cranes are pendant-operated and motor-driven. The dynamic factor used for this group of cranes is 1.25 by the CSA standard, but only 1.1 by the AISC standard, although the factor may be applied to different weights, as suggested above.

The third difference is that the AISC specifications do not include the option of performing a dynamic analysis.

The trolley on the shop crane can come close enough to an endtruck that one may assume the load of the trolley and payload is carried completely on the side of the craneway it is closest to. The calculation of the dynamic load using the AISC requirements is as follows.

$$\frac{\text{Weight of bridge and both end trucks}}{\text{4 pairs of wheels}} = \frac{4.88\text{ kN}}{4\text{ wheels}} = 1.22\text{ kN/wheel assembly}$$

$$\frac{\text{Weight of trolley}}{\text{2 pairs of wheels}} = \frac{3.24\text{ kN}}{2\text{wheels}} = 1.62\text{ kN/wheel assembly}$$

$$\frac{\text{Weight of large payload}}{\text{2 pairs of wheels}} = \frac{14.35\text{ kN}}{2\text{ wheels}} = 7.18\text{ kN/wheel assembly}$$

$$\frac{\text{Weight of small payload}}{\text{2 pairs of wheels}} = \frac{2.07\text{ kN}}{2\text{ wheels}} = 1.04\text{ kN/wheel assembly}$$

The weight of the unloaded trolley on the loaded side of the craneway is

$$\text{2 pairs of wheels} \times (1.22 + 1.62) = 5.68\text{ kN.}$$

For the large payload, the dynamic load on the loaded side of the craneway is

$$\text{2 pairs of wheels} \times (1.22 + 1.62 + 7.18)\text{ kN per pair of wheels} \times 1.1 = 22.0\text{ kN.}$$

The amount by which the dynamic load exceeds the weight of the unloaded trolley is 22.0 kN - 5.68 kN = 16.3 kN.

For the small payload, the dynamic load on the loaded side of the craneway is

2 pairs of wheels x (1.22 + 1.62 + 1.04) kN per pair of wheels x 1.1 = 8.54 kN,

and the amount by which the dynamic load exceeds the weight of the unloaded trolley is 8.54 kN - 5.68 kN = 2.86 kN.

3.9 JIS B 8821 - 1976 — Electric Overhead Travelling Cranes

The Japanese Industrial Standard B8821 is clear about how vertical dynamic loads are to be treated. Section 5.2.1; Impact Factors Ψ, States in part:

> **5.2.1** The impact loads caused in the hoisting operation are different in value according to the hoisting speed, deflection of the girder, rope length, and may be given in the actual measurements, but, in general, are to be given by multiplying the impact factors specified in Table 7, to the hoisting loads.

The first part of the sentence, which states that the dynamic loads due to hoisting are a function of motor speed, structure stiffness and cable stiffness, reinforces the theme of this thesis. However, the Ψ factors in Table 7 are assigned by class of crane, in similar format to that used in the German standard, and the system is less precise than the CAN B167 class designation system. Table 4, Examples of Classification of Cranes - O/H Travelling Cranes, is a list of crane designations in Roman numerals with a brief description of the type of crane. The structures lab workshop crane probably belongs in the second designation.

"II or III - Cranes for warehouse, stocking yard, machine and assembly shops, and cranes for general use."

There is no further guidance as to which of the two groups the crane belongs in.

Table 7 Impact Factors Ψ lists the impact factors that go with each of the four designations. Specifically, Ψ has values of 1.1, 1.25, 1.4 and 1.6 for Groups I, II, III, and IV respectively. Assuming that the shop crane is Class II, a factor

of 1.25 should be applied to the payload. Assuming that the shop crane is Class III, a factor of 1.4 should be applied to the payload. Therefore, the dynamic load on the crane when it hoists the large payload is

1.25 x 14.35 kN = 17.9 kN if it is a Class II crane,

and 1.40 x 14.35 kN = 20.1 kN if it is a Class III crane.

With the small payload, the dynamic load is

1.25 x 2.07 kN = 2.59 kN if it is a Class II crane,

and 1.40 x 2.07 kN = 2.90 kN if it belongs in Class III.

3.10 BS 2573 - 1983

The British Standard BS 2573 - 1983 is very similar to the Japanese Standard JIS B8821 - 1976. In Table 4 Impact and Duty Factors According to Crane Type and Application, crane duties are described and impact factors from 1.1 to 2 are assigned. The factors are to be multiplied by the payload weight. The greatest factor, 2, is to be used with forging cranes and there is a note that "this factor may be modified when an overload protection device is fitted." The remaining factors vary from 1.1 to 1.5, in increments of 0.1. The use of the structures lab workshop crane would fit best in the category of "light workshop duty (maintenance, repairs, assembly, etc.)" which has an impact factor of 1.1. Therefore, the dynamic load on the crane when the large payload is hoisted is 1.1 x 14.35 kN = 15.8 kN, and is 1.1 x 2.07 kN = 2.3 kN when the small payload is hoisted.

3.11 Other Approaches

Most texts recommend a vertical impact factor of 1.25. British texts [ref. 24.19] refer to a standard BS449, clause 7, where this value of 1.25 is recommended. The author was unable to examine a copy of this specification. The 1.25 factor is also used in AISC, Specification for Design, Fabrication, and Erection of Structural Steel for Buildings [ref. 1] so that number is used in American texts as well [ref. 13,26].

In a discussion of bridge design, Weaver [ref. 31] quotes the CMAA specification, and then says the following.

> "Actual tests have shown that impact on the crane girders rarely exceeds 5% to 7% of static load, even for relatively fast hoist speeds, due to the cushioning effect resulting from the torsion spring action of the ropes and the leaf spring action of the girders."

There are two points being conveyed in this statement. The first is that the dynamic factor tends to be less than 1.07. The tests performed for this thesis produced dynamic loads significantly higher than 1.07 times static load. The second point is that the dynamic factor increases with increased hoisting speed, and increases with increase in the stiffnesses of the two components which act as springs; the cable and the structure. In Chapter 5 of this thesis, deductions are made from the mathematical model of the crane which indicate that this is not always true, and that in fact there are many real situations where decreasing the stiffness of the crane structure will increase the dynamic load factor.

Later, in the section on craneway girders Weaver mentions the AISC standard and its 1.25 factor, and makes the point that there are a number of parameters that should influence that dynamic factor, but which are not used in its determination. He and Goldman [ref. 14] recommend adjusting the dynamic factor according to CMAA service class. Figure 3.5 shows Table 34, Runway Design Factors, from Weaver.

The CMAA classification system is the most descriptive. It is much more precise than the German, British, or Japanese standards, and is on par with

Figure 3.5 Table of Runway Design Factors from Whiting Crane Handbook

TABLE 34

RUNWAY DESIGN FACTORS

CMAA Service Class	Vertical Impact	Longitudinal	Lateral
A	10%	5%	10%
B	10% – 15%	5%	10%
C	15% – 25%	5% – 10%	15% – 20%
D	25%	10%	20%
E	25% – 50%	10% – 15%	20% – 25%
F	25% – 50%	15% – 20%	20% – 30%

Table 34 from the Whiting Crane Handbook is reproduced here
with the permission of
the Whiting Crane Corporation, 15700 Lathrop, Harvey, Illinois.

the Canadian specification B167 - 1964. The structures lab workshop crane fits in CMAA classification A2 .

> **Class A2 - (Infrequent Use)** These cranes will be used in installations such as; small maintenance shops, pumprooms, testing laboratories, and similar operations where the loads are relatively light, the speeds are slow, and a low degree of control accuracy is required. The loads may vary anywhere from no load to full capacity with a frequency of a few lifts per day or month.

For the Structures Lab shop crane the runway design factor from Table 34 from Weaver is 10%. As with CMAA, the use of the term "factor" is misleading. It will be assumed that a factor of 1.10 is meant. The dynamic loads using the large and small payloads are 1.10 x 14.35 kN = 15.8 kN, and 1.10 x 2.07 kN = 2.28 kN respectively

Although it seems a logical step, the CMAA classification system is not used by CMAA to set vertical dynamic impact factors. A single formula is used for all crane classes. (See Section 3.4.)

3.12 Summary of Standards

In all the standards, vertical dynamic loads are accounted for by increasing a static load by some dynamic factor. That different dynamic factors are not applied to moments and shear forces and deflections implies that all the standards consider the response of the structure to hoist loading to be dominated by just one mode. Only S.16.1 - 1977 and the National Building Code mention dynamic analysis, implying that multi-modal behaviour may be significant.

During a hoisting event the trolley and the payload directly below can be at any location within the craneway. For design of the bridge in bending, the critical loading case occurs when the payload and hoist are at the midspan. For design of the craneway, the critical loading case occurs when the payload and hoist are towards one end of the bridge. This is true for static or dynamic loading, but the rigidity of the structure at the point of loading has a large effect on the deflection of the structure, and thus on the dynamic forces developed. The dynamic factor used to determine the design load for the bridge crane will be different from the dynamic factor used to determine the design load for the craneway girders and columns. As it happens, the standards which are meant to be used to design the bridge are often different from the standards used to design the craneway. The bridge is covered under a specific standard for cranes, while the craneway is usually covered in a general building code. Often different authorities write the different specifications, and therefore different dynamic factor formulae are used for the bridge and for the craneway.

In most textbook examples a factor of 1.25 is used to account for vertical dynamic loading, without regard for crane properties. The stiffness of the crane and of the cable are not considered explicitly in any of the standards. It is possible that these two parameters are taken into account by grouping cranes into categories. If this is the case, then all cranes in a given category presumably have a similar structure stiffness and a similar cable stiffness, or a similar relationship between structure and cable stiffness. For all the standards but two (CSA B167 - 1964 and AISC), the categories may also group cranes with similar structure mass, another parameter expected to have an effect on dynamic behavior. No standard reviewed makes mention of such rationales for its grouping criteria.

Grouping is also used to select dynamic factors based on load frequency. This implies that there is not a specific maximum dynamic load but rather a random chance for any size of load to develop, with loads progressively larger than the mean becoming less and less likely to occur.

The German, British, and Japanese standards give category definitions which are vague. It may be unclear in which category a particular crane belongs, and what the appropriate dynamic factor is. In some cases it is not clear to which weight the dynamic factor is to be applied.

Most of the standards reviewed do not account for hoisting speed. Those two that do (DIN 15.018 and CMAA # 74), use hoisting speed differently. In both cases, at zero velocity a dynamic factor greater than one is indicated.

Table 3.1 is a summary of the dynamic loads and factors recommended in the standards reviewed in this chapter. The standards have been grouped according to whether they were meant to be used in the design of the craneway girders, or the bridge, or both. All the factors given in Table 3.1 are to be applied to the payload weight.

The dynamic factors used by the various standards range from 1.1 to 1.64. Many standards use a constant factor of 1.25. This suggests that the dynamic maximum load ratios do not vary greatly, and that 1.25 is a maximum that covers the majority of the loading cases. Therefore a dynamic factor of 1.1 may be applicable for a crane that would have a relatively light dynamic loading, and a crane subject to heavy dynamic loading would require a dynamic factor greater than 1.25, in which case a factor of 1.less than or equal to 1.64 would be adequate. By the criteria of some of the standards, the shop crane carries light dynamic loads and by the criteria of others it carries heavy dynamic loads. This applies to both the bridge and the craneway structure. The standards that recommend low factors for the structures lab crane recommend higher factors in other circumstances. Similarly, those that recommend high factors also describe applications where lower factors can be applied. There is a lack of agreement about which circumstances require relatively large dynamic factors, and which require small ones.

Table 3.1 Summary of Dynamic Loads and Factors from Various Standards Applied to the Shop Crane Carrying the Large or Small Payload

	Standard	Dynamic Load; Load beyond that of unloaded trolley		Dynamic Factor; $\frac{\text{Dynamic Load}}{\text{Payload Weight}}$	
		using 14.35 kN payload	using 2.07 kN payload	using 14.35 kN payload	using 2.07 kN payload
Standards dealing only with bridge	CSA B167 - 1964 [ref. 5]	17.9	3.13	1.25	1.51
	CMAA #74 [ref. 10]	16.5	2.38	1.15	1.15
	JIS B8821 - 1976 [ref. 16] using Class II	17.9	2.59	1.25	1.25
	JIS B8821 - 1976 [ref. 16] using Class III	20.1	2.90	1.4	1.4
	BS 2573 - 1983 [ref. 36]	15.8	2.28	1.1	1.1
Standards dealing with bridge and craneway	DIN 15.018 and DIN 4132 [ref. 35 and 34] using H_2	17.7	2.55	1.23	1.23
	DIN 15.018 and DIN 4132 [ref. 35 and 34] using H_3	19.2	2.77	1.34	1.34
Standards dealing only with craneway	CSA S16.1 - 1977 [ref. 7]	17.9	2.59	1.25	1.25
	CAN3-S16.1-M89 [ref. 6]	NA	NA	NA	NA
	National Building Code of Canada [ref 33]	18.8	3.40	1.31	1.64
	AISC [ref. 1]	16.3	2.86	1.14	1.38
	Weaver [ref. 30]	15.8	2.28	1.1	1.1

CHAPTER 4

NUMERICAL DYNAMIC ANALYSIS

Clause 7.11 of CSA S16.1-1977 specifies dynamic factors that are to be used "In the absence of a dynamic analysis...". In this chapter the steps required to perform a dynamic analysis are considered. The equations of motion for a multi-degree-of-freedom system which govern the hoisting action and structural response of the crane are developed. A computer program is described which solves the equations of motion.

4.1 Modelling of Crane Components

In order to develop a realistic model of the crane, its various parts should be examined and the behaviour of each part described by mathematical statements. The expressions can then be assembled into a set of equations of motion which can be solved for certain cases. There are four parts of the crane that should be examined: the hoist motor, the crane and craneway structure, the cable, and the payload.

Throughout the remainder of the thesis, certain variables and their derivatives with respect to time will be defined. When a dot is shown above a variable, it is the first derivative with respect to time which is being referred to. Two dots above the variable indicate its second derivative with respect to time.

4.1.1 Hoist Motor Model

Motors have two basic components; a stator which is stationary, and a rotor which rotates within the stator on a fixed axis. Both have coils through which electric current can pass. Induction motors produce torque between the stator and rotor by creating a rotating magnetic field in the coils of the stator and a corresponding magnetic field in the rotor's coils that is stationary with respect to the rotor. The magnetic field of the stator instantly attains its prescribed rate of rotation and remains at that constant angular velocity as long as the motor is turned on. As the stator's magnetic field spins, the rotor's magnetic field is compelled to follow, and it does this by spinning the rotor. Because the rotor has mass, (and may also be connected with other loads, as will be discussed later), it cannot instantly attain the constant angular velocity of the stator's field. Instead it accelerates towards that angular velocity. The constant rate of rotation of the stator field is called the synchronous speed of the motor and the symbol ω_o will be used to denote it. The changing angular velocity of the rotor and its magnetic field will be denoted by the symbol ω_r.

The difference between these two angular velocities is called slip and is denoted by s. It is defined in equation (4.1).

$$s = \frac{\omega_o - \omega_r}{\omega_o} = 1 - \frac{\omega_r}{\omega_o} \tag{4.1}$$

Under certain idealized conditions the torque between the two magnetic fields can be described as a function of slip by the following equation.

$$T = \frac{2T_{max}}{\frac{s_p}{s} + \frac{s}{s_p}} \tag{4.2}$$

In equation (4.2) T is the torque between the two magnetic fields, T_{max} is the maximum torque that can be developed between the two fields, and s_p is the pullout slip. The pullout slip is the slip at which T_{max} occurs. These two values are independent of one another and constant for any given electric motor. Figure 4.1 shows a typical torque curve.

The maximum torque is often called the "pullout torque." The term "pullout" comes from the motor's behaviour when its torque is being mechanically measured. The motor is allowed to reach and stabilize at full speed of ω_o. Then a series of known resisting torques is applied. At each increasing torque level, the motor slows down and stabilizes at a new speed, which is recorded. When the applied torque exceeds the maximum torque, the motor quickly slows to a stop. To the individual who coined the term, the motor seemed to give up, or pullout.

Figure 4.1 Typical Torque versus Motor Speed Curve

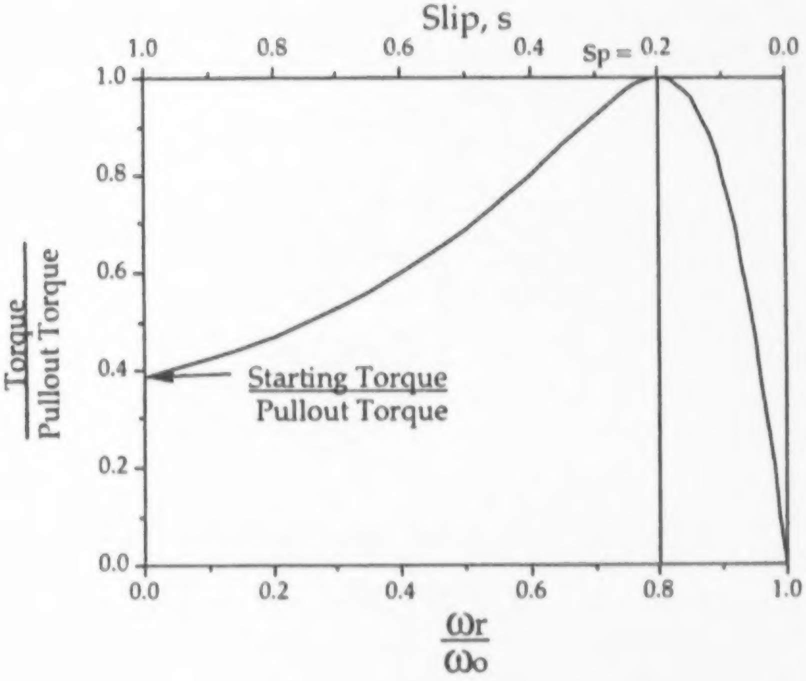

If a motor were constructed having a different value of s_p, the shape of the graph in Figure 4.1 would change. Figure 4.2 shows how the torque curve changes with respect to s_p. As the pullout slip gets smaller, and moves to the right on the graph, the torque at $\omega_r = 0$, called the starting torque, gets smaller, and the slope of the curve between $s = s_p$ and $s = 0$ gets steeper. If s_p is small, then at speeds close to ω_o the motor can deliver a wide range of torque without significantly changing speed. Figure 4.3 shows a wide range of external torques superimposed on the torque versus speed curve of Figure 4.1, and the corresponding narrow range of angular velocities. In crane applications this feature is desirable. Motors built with low values of pullout slip ($s_p<.2$) are called "constant speed" motors.

The name is inaccurate but appropriate. At the instant the motor is turned on the rotor is stationary, so $\omega_r = 0$. It is assumed a mechanical brake is released at that moment. Torque is immediately applied to the rotor by the magnetic fields. There may also be initial external torque acting on the rotor from outside sources because of the brake's release. If the motor's torque is greater than the external torque then the rotor will begin to rotate and ω_r will have a positive value. This will cause a further increase in induced torque, the rotor will accelerate, and the motor's working point will advance to the right along the curve. The torque available to accelerate the rotor is the difference between the motor's torque and the resisting torque. This is true if the resisting torque is constant or if it varies over time. Generally, after T_{max} is reached, the motor's torque approaches the resisting torque and ω_r approaches asymptotically the speed corresponding to that torque. For the majority of the running time the motor and resisting torque are nearly equal and ω_r is close to ω_o. The price that is paid for constant speed behaviour is that the starting torque is low compared to the maximum torque the motor is actually able to deliver (see Figure 4.2). An applied torque greater than the starting torque will prevent the rotor from moving forward.

Although Figures 4.1, 4.2, and 4.3, show the motor curve over the range of $1 > s > 0$, equation (4.2) applies to values of s outside of this range. When $s > 1$, $\omega_r < 0$, and the rotor is actually turning in the opposite direction to which the magnetic fields are trying to turn it. This happens when the

Figure 4.2 Torque versus Speed Curves as Pullout Slip Varies

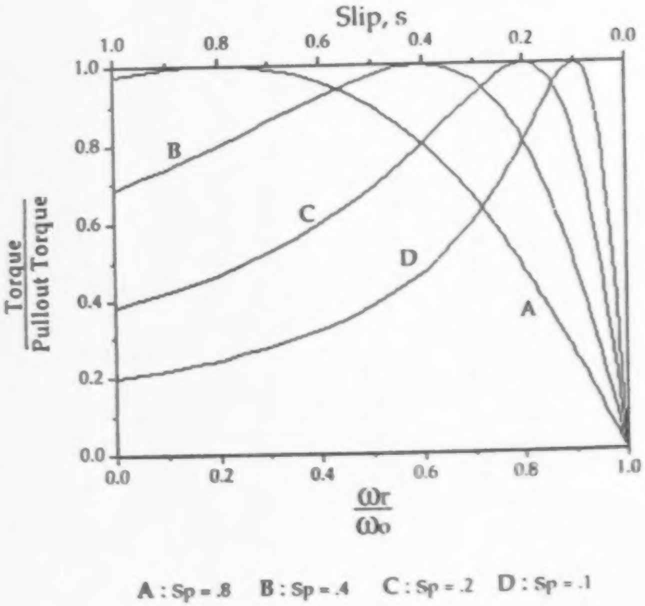

Figure 4.3 "Constant Speed" Behaviour of Typical Torque versus Motor Speed Curve

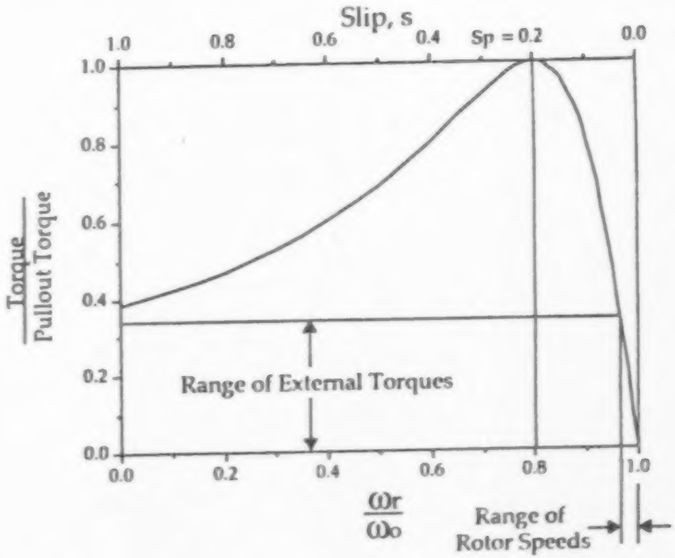

resisting torque is greater than the torque the fields provide. The motor is in "braking mode." When s is negative and $\omega_r > \omega_o$, the motor torque becomes negative and acts to slow down the rotor. This is called "generator mode". A hoist motor goes into generator mode when it is used to lower a load. Figure 4.4 shows the torque versus speed curve from equation (4.2) for a wide range of values of s.

There are two limitations to using equation (4.2) to describe real motor behaviour. The first is that the equation represents a steady state. Voltage and current in the motor's coils are assumed to be constant, and in practice this is not the case. Turning the motor on, or turning on or off other motors connected to the same power supply, will cause voltage spikes and fluctuations [ref. 37]. Any change in ω_r creates electric fluctuations, as the motor demands different power at different speeds. Although mathematical analyses exist for computing the torque versus speed curve under these circumstances [ref. 18], they require information about the internal construction of the motor that is not normally available to, or understood by, the structural engineer. It is preferable, therefore, that a design procedure for cranes not require this information. Generally these voltage changes are either very small or of extremely short duration, and only small amounts of energy are involved.

The other, and more severe, limitation on equation (4.2) is that it is for a very simple induction motor. The pullout torque is a function of coil size, and s_p is a function of the space between the stator and rotor coils. This space is called the "air gap." The radius of the rotor can be defined as the inner radius of the air gap. Equation (4.2) assumes that all the rotor's coils are at the rotor's radius. Motor manufacturers, however, can place some of the coils at that radius, and some at smaller radii. This causes the total torque delivered to be the sum of a set of smaller torques with different values of T_{max} and s_p. Figure 4.5 shows a torque versus speed curve that is the average of the four curves shown in Figure 4.2. Wound rotor motors are another variation. The resistance in the rotor coils is adjusted as a function of speed, so the motor moves through a series of torque curves with constant s_p but varying pullout torques.

Figure 4.4 Torque versus Motor Speed Curve over Extended Range of Motor Speed

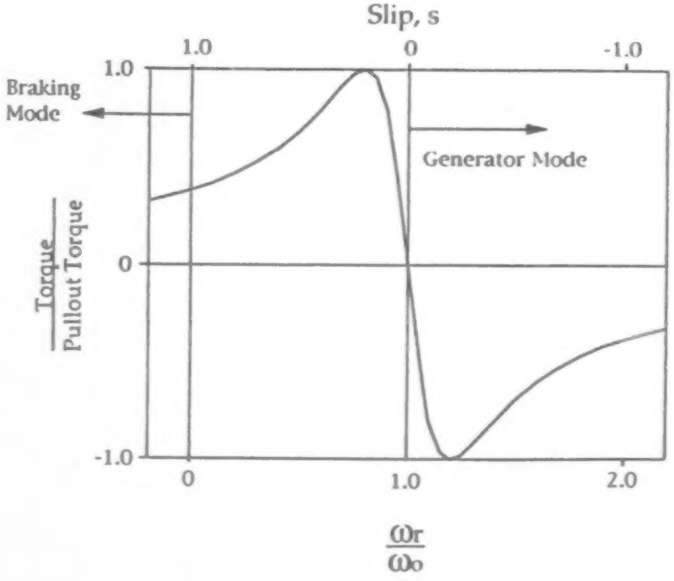

Figure 4.5 Modified Torque versus Motor Speed Curves

$$\text{Modified Curve} = \frac{A + B + C + D}{4}$$

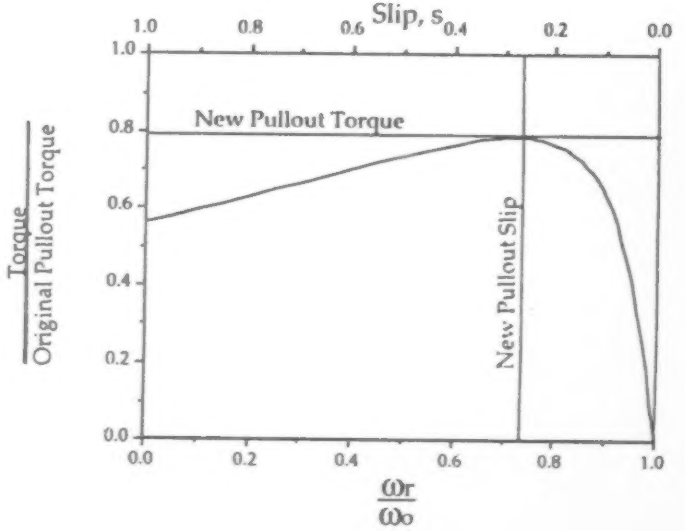

In theory the only limit on the shape of these altered torque curves is that at $s = 0, T = 0$. In practice there is also the limitation of how much wire can be fitted in at a particular radius and how expensive the motor is to make. The torque versus speed curve is generally recorded as a graph, with the points determined by making measurements of the performance of the motor.

The advantage gained by building a motor this way is significant. The "constant speed" behaviour associated with low pullout slip can be maintained while the starting torque can be made a much larger fraction of the pullout torque. The disadvantage is that these motors cost more to build. They are, nevertheless, used extensively in crane applications. Crane hoist motors are generally constant speed motors with high starting torques.

In the computer program the motor torque function is approximated as a compound curve made of two parabolas, each having the form shown below.

$$\text{Torque} = c_0 + c_1\,\omega_r + c_2\omega_r^2 \tag{4.3}$$

The two sets of coefficients, c_0, c_1 and c_2 are used to define the two parabolas. The coefficients are derived from five motor parameters: Pullout torque, initial torque, s_p, ω_o and the initial slope of the torque versus speed curve at $\omega_r = 0$. Figure 4.6 shows a graph of the compound curve approximation. The derivation of the two sets of constants, c_0, c_1 and c_2, from the five parameters is given in Appendix D.1.

All five parameters cannot be derived from the information generally given on the motor nameplate (see Figure 2.1). To obtain values for these, the motor manufacturer would need to be consulted or measurements of the motor's performance would have to be made. If the motor were changed to a different make, it is possible that all five parameters would change.

The motor is attached through a gearbox transmission to a cable drum. The hoist motor produces torque as a function of the rotor's rotational velocity. This torque causes angular acceleration of the motor's rotor, the gears and the cable drum, all of which have inertia, and it also causes tension to develop in the cable. Figure 4.7 is a diagram of the hoist's components. Let y_m be the length of cable the motor winds onto the drum. The rotational

Figure 4.6 Compound Parabolic Curve to Approximate Torque versus Motor Speed Relationship

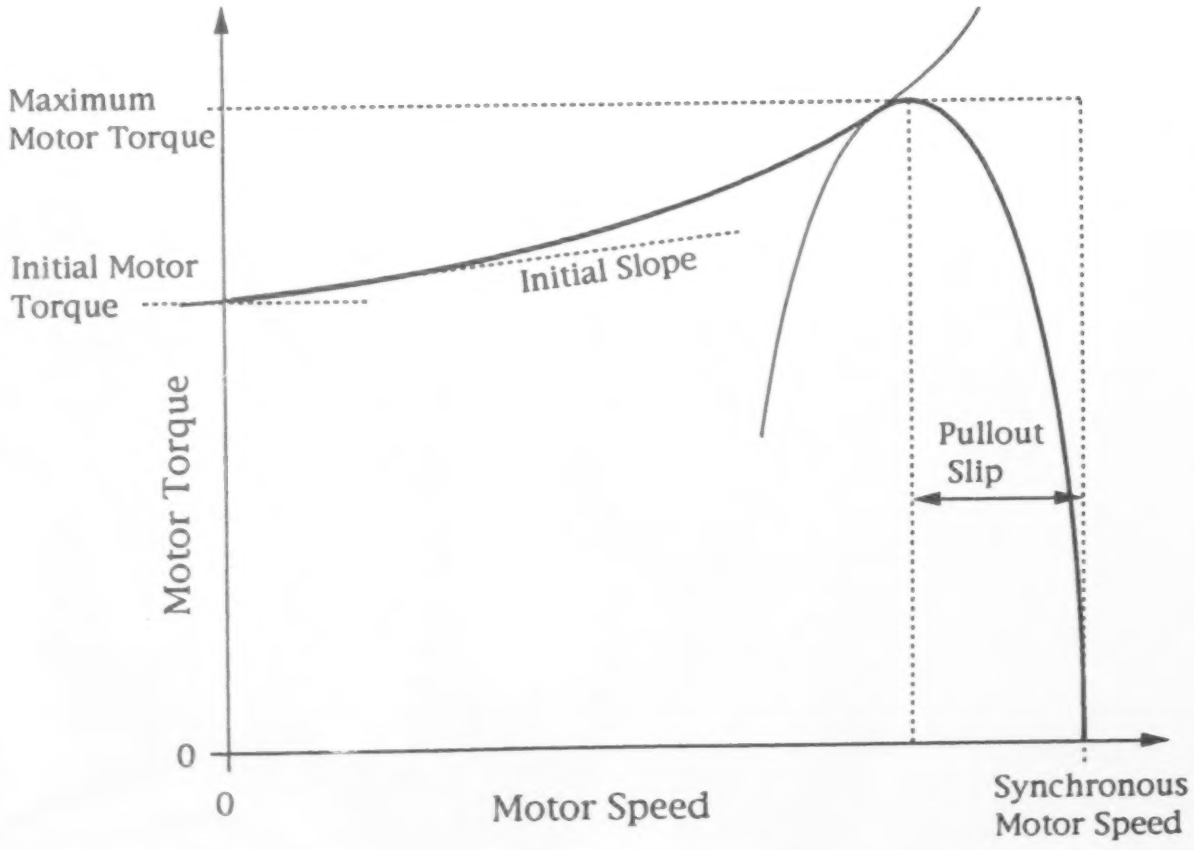

Figure 4.7 Hoist Motor, Gears, and Drum

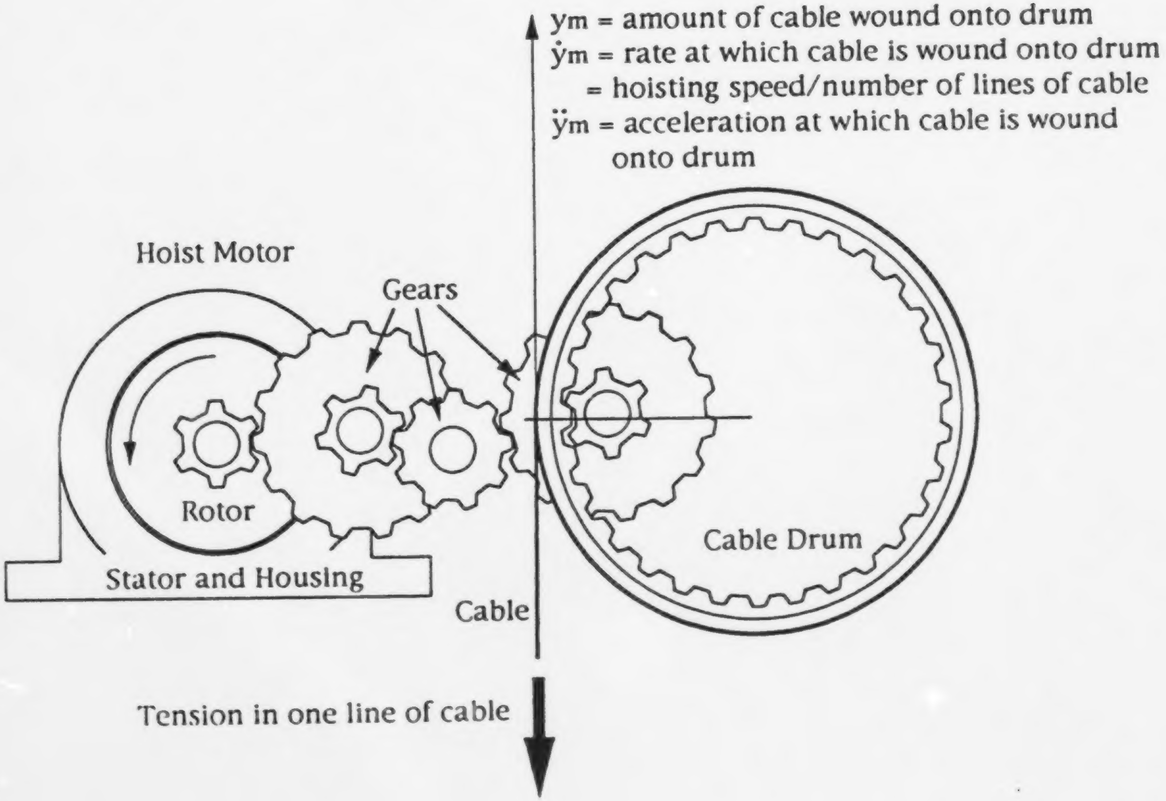
y_m = amount of cable wound onto drum
$\dot{y}_m$ = rate at which cable is wound onto drum
= hoisting speed/number of lines of cable
$\ddot{y}_m$ = acceleration at which cable is wound onto drum
Hoist Motor
Gears
Rotor
Stator and Housing
Cable
Cable Drum
Tension in one line of cable

velocities of each of the gears and of the drum are proportional for any motor velocity ω_r. Let the velocity ratio $\frac{\omega_{gear}}{\omega_r}$ be denoted as ρ_{gear}, for each gear in the transmission, and the velocity ratio $\frac{\omega_{drum}}{\omega_r}$ be denoted as ρ_{drum}. The equation of motion for this system can be written as follows.

$$\text{Torque} = I_{rotor}\,\dot{\omega}_r + \sum^{\text{all gears}} I_{gear}\,\dot{\omega}_{gear}\,\rho_{gear} + I_{drum}\,\dot{\omega}_{drum}\,\rho_{drum}$$

$$+ \left(\frac{\dot{y}_m}{\omega_r}\right) \times \text{Tension in one line of Cable} \qquad (4.4)$$

The I terms are the polar mass moments of inertia of the components named in the subscripts and the ω and $\dot{\omega}$ are their rotational speeds and accelerations respectively.

Let $r_e = \left(\frac{\dot{y}_m}{\omega_r}\right)$. The length, r_e can be considered as an effective moment arm that relates the motor torque to a force with a line of action along the cable. Dividing the terms in equation (4.4) by r_e puts the equation of motion in terms of forces and masses rather than torques and moments of inertia.

$$F_o = m_m\ddot{y}_m + \text{Tension in one line of cable} \qquad (4.5)$$

$$F_o = \frac{\text{Torque}}{r_e}$$

$$m_m = \frac{I_{rotor}}{r_e^2} + \frac{\sum^{\text{all gears}} I_{gear}\,\rho_{gear}^2}{r_e^2} + \frac{I_{drum}\,\rho_{drum}^2}{r_e^2} \qquad (4.6)$$

In equation (4.6) the largest term is $\frac{I_{rotor}}{r_e^2}$. It is always the case that the rotor has a larger polar moment of inertia than any gear and that $\frac{\omega_{gear}}{\omega_r}$ is always less than one. It is possible for the drum to have a larger moment of inertia than the rotor, but $\frac{\omega_{drum}}{\omega_r}$ is generally much smaller than one. Therefore it will generally be the case that $\frac{I_{rotor}}{r_e^2}$ will be the significant term in equation (4.6).

To estimate the magnitude of r_e, consider that constant speed motors usually have a synchronous speed of 900 or 1800 rpm. The corresponding hoisting speed will be very close to the rated hoisting speed, rarely more than 15 metres per minute. A reasonable value for r_e can be calculated as follows.

$$r_e = \frac{15 \text{ metres per minute}}{2\pi \times 900 \text{ rpm}} = .00265 \text{ metres} = 2.65 \text{ mm}$$

The moment of inertia of the rotor varies considerably with the motor's power, but even so, because of the low value of r_e, m_m calculated from equation (4.6) can be expected to be quite large compared to other masses in the system, such as the payload mass.

The term F_o represents the total force developed by the motor that would act along the line of the cable. The force F_o is proportional to the motor torque, and just as the motor torque is a function of ω_r, so F_o is a function of $\dot{y}_m$.

An approximate expression for F_o in terms of $\dot{y}_m$ can be derived which is similar to equation (4.3).

$$F_o = b_0 + b_1 \dot{y}_m + b_2 \dot{y}_m^2 \tag{4.7}$$

$$\text{where} \quad b_0 = \frac{c_0}{r_e}, \quad b_1 = \frac{c_1}{r_e^2}, \quad b_2 = \frac{c_2}{r_e^3}$$

This expression is used in the computer programs listed in Appendix C. The motor forcing function will be referred to as $F_o(\dot{y}_m)$, to indicate it is a function of the motor's speed.

The model of the hoist and motor thus far developed can be represented as shown in Figure 4.8. The motor mass m_m is acted upon by two forces; the motor force $F_o(\dot{y}_m)$, and the tension in one line of cable. The difference between these two is the inertial force of $-m_m\ddot{y}_m$.

The axis of y_m is shown horizontal, and m_m is shown on wheels. This is to indicate that there is no force due to gravity acting in the direction of y_m. The mass m_m is not the true mass of the motor, which is subject to gravitational load. It is the mass equivalent of the polar moments of inertia of the rotor and hoist gears and drum. Table 4.1 shows the calculations involved for determining m_m for the shop crane.

4.1.2 Crane and Craneway Structure Model

For a dynamic analysis, the structure is modelled as a multi-degree-of-freedom system comprising an assembly of beam elements with distributed mass and stiffness. The term "degree-of-freedom" will be used throughout the remainder of the thesis, and will be abbreviated to DoF. The plural, "degrees-of-freedom", will be abbreviated D'soF.

The beam elements used in this development are standard Hermitian, 4 DoF, elements, with local stiffness and mass matrices as shown in Figure 4.9. These beam elements do not include vertical shear deflections. Shear deflections are significant when short, thick, members are loaded at right angles to their axis. The purpose of a crane is to allow free motion of a

Figure 4.8 Forces Acting on Effective Motor Mass

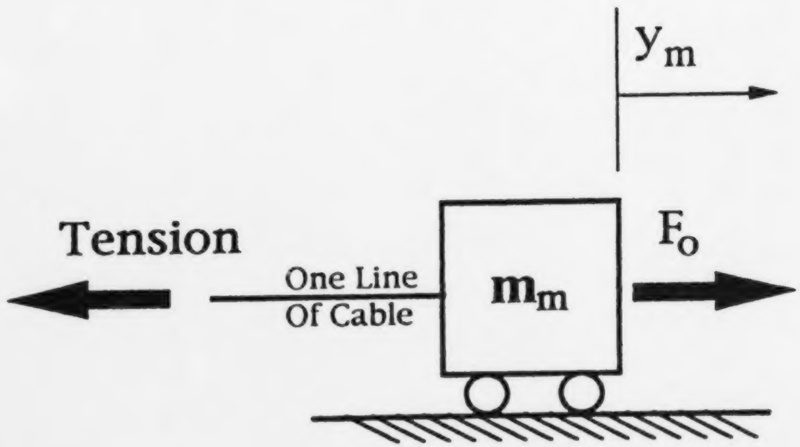
y_m
Tension
One Line
Of Cable
m_m
F_o

Table 4.1 Calculations for m_m and Motor Force

Given:

$\omega_r = 900$ rpm

stator housing and drum diameter = 300 mm

drum length = 600 mm

hoisting speed is 20 ft/min. = 0.1 m/s

4 lines of cable

rated power = 3.8 Hp = 2.8 kW = 2.8 kNm/s

Calculations

$$r_e = \frac{(.1\,m/s)(4\ lines)}{(900rpm)(60\ sec/min)(2\pi)} = 4.24\times10^{-3}\ m$$

assume rotor OD = 200 mm,
assume rotor mass = 40 kg

$$I_{rotor} = \frac{(40\ kg)(200\ mm)^2}{2} = 0.8\ kgm^2$$

assume thickness of drum = 10 mm

$$I_{drum} = 2\pi\,(300\ mm)(600\ mm)(10\ mm)(7850\ kg/m^3)(150\ mm)^2 = 1\ kgm^2$$

$$\frac{\omega_{drum}}{\omega_r} = \frac{(0.1\ m/s)(60\ sec/min)}{\pi(300\ mm)(900\ rpm)} = 1.18\times10^{-4}$$

Assume 3 gears of OD 200 mm and mass 10 kg each, at speeds of 45, 2, and 0.1 rpm when motor is at 900 rpm. For each gear,

$$I_{gear} = \frac{(10\ kg)(200\ mm)^2}{2} = 0.2\ kgm^2\ \text{each}$$

$$\sum I_{gear}\,\rho_{gear}^2 = 0.2\ kgm^2\left(\left(\frac{45rpm}{900rpm}\right)^2 + \left(\frac{2\ rpm}{900rpm}\right)^2 + \left(\frac{0.1rpm}{900rpm}\right)^2\right) = 5\times10^{-4}\ kgm^2$$

$$m_m = \frac{0.8\ kgm^2 + .5\times10^{-4}\ kgm^2 + (1\ kgm^2)(1.18\times10^{-4})^2}{(4.24\times10^{-3}\ m)^2} = 45\ \text{tonnes}$$

F_{max} Rated power is the power at which the motor runs most efficiently. Assume it corresponds to a torque delivery of about 2/3 of the pullout torque. Therefore maximum motor force is;

$$\frac{2.8\ kNm/s}{(0.1m/s)(4\ lines)} \times 1.5 = 10\ kN$$

Check

$$10\ kN - \frac{(2\ tonnes)(9.81\ m/s^2)}{4\ lines} = 5\ kN$$

5kN accelerates 45 Tonnes at 0.11 m/s^2

Therefore the motor can reach hoisting speed of 0.1 m/s in just under 1 second.

Figure 4.9 Beam Element

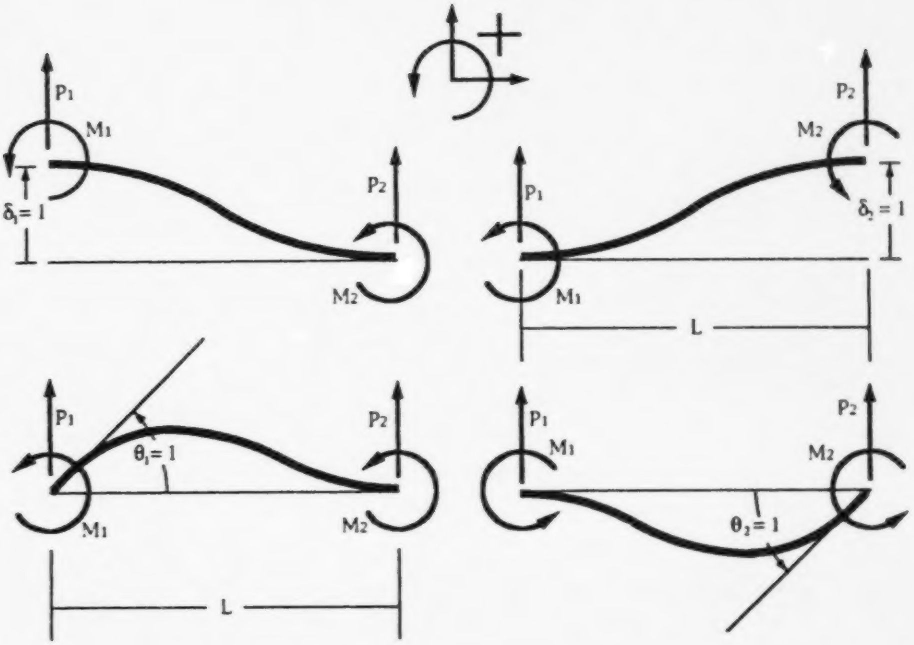

Equations of Motion for an Element

$$\begin{Bmatrix} P_1 \\ M_1 \\ P_2 \\ M_2 \end{Bmatrix} = \frac{2EI}{L^3} \begin{bmatrix} 6 & 3L & -6L & 3L \\ 3L & 2L^2 & -3L & L^2 \\ -6L & -3L & 6 & -3L \\ 3L & L^2 & -3L & 2L^2 \end{bmatrix} \begin{Bmatrix} \delta_1 \\ \theta_1 \\ \delta_2 \\ \theta_2 \end{Bmatrix}$$

$$+ \frac{\bar{m} L}{420} \begin{bmatrix} 156 & 22L & 54L & -13L \\ 22L & 4L^2 & 13L & 3L^2 \\ 54L & 13L & 156 & -22L \\ -13L & 3L^2 & -22L & 4L^2 \end{bmatrix} \begin{Bmatrix} \ddot{\delta}_1 \\ \ddot{\theta}_1 \\ \ddot{\delta}_2 \\ \ddot{\theta}_2 \end{Bmatrix}$$

E is the Young's modulus for the material
I is the moment of Inertia of the prismatic cross-section
$\bar{m}$ is the mass per unit length of the cross-section
δ represents a linear displacement
θ represents an angular displacement
P represents a linear force
M represents a moment

payload within a large, open space, so it is to be expected that the major horizontal structural components are long and thin.

The beams of the structure are supported by columns. Hoist induced vertical loading is a function of the vertical stiffness of the structure. If vertical deflections of the columns are negligible compared to the vertical deflections elsewhere on the structure, then the columns may be modelled as rigid supports for the beam elements. If column bending stiffness and mass contribute significantly to the degree of rotation of the connections between columns and beams, then the columns may also be modelled as elements subject to deflections. Elements similar to the 4 DoF Hermitian elements may be used in this case. If vertical deflections are significant, then for non-slender columns, axial stiffness may be included. The vertical stiffness of braced slender columns is not constant. The stiffness decreases with increased deflection, due to $P\Delta$ moment magnification. This may be accounted for by using elements which relate axial loading with axial and lateral displacement (Paz [ref. 21] page 251).

Unbraced slender columns are subject to column sway. When vertical load is applied mass is moved horizontally as well as vertically. The lateral displacement of the column end causes a decrease in vertical stiffness, due to $P\Delta$ moment magnification. The lateral motion is dynamic, and the inertial effects of the horizontal acceleration of the mass which the column supports must be taken into account. Therefore, the Hermitian 4 DoF elements cannot be used for the beams of a crane which is subject to column sway, because these elements do not incorporate lateral and axial D'soF. The lateral motion of the payload should also be accounted for in the case of column sway.

In the model for the shop crane, the columns are assumed to be vertically and laterally rigid, and their connections to the beams are assumed to carry no moment. The columns can therefore be considered as pin supports for the beams.

All the element stiffness and mass matrices are assembled into their two respective global matrices, $[K_S]$ and $[M_S]$, with the vertical deflection at the position of the hoist as the first DoF. Two models are used. One, designated as "E", is for the structure when it is loaded at one end of the bridge. The other, designated "2", is for the cases in which the structure is loaded at the midspan of the bridge. These cases correspond to the two loading positions used in the testing of the shop crane, described in Chapter 6. Figures 4.10 and 4.12 show the two multi-DoF models which are used. Figures 4.11 and 4.13 show the locations of the nodes and elements for "E" and "2" respectively, on isometric views of the crane and building structure. In Figures 4.10 to 4.13, node numbers are shown in circles and element numbers are underlined.

The models use transverse and axial symmetry where possible to reduce the number of D'soF. Transverse symmetry is used to reduce to half the number of elements within a member, and the number of elements needed to model the complete structure. Using half the applied load, a simply supported beam loaded symmetrically can be modelled as a beam with the same section properties but half the length, supported at one end by a pin and at the other end by a roller that allows displacement but no rotation. This cantilever will develop the same deflections and all the symmetric mode shapes which the original simply supported beam develops under symmetric loading. The full vertical reaction from the craneway is carried on node 8 by the divided element 12 in model "2". In this instance, the values of I and $\bar{m}$ for the original member are doubled and assigned to the cantilever, and this provides consistent results.

When the axis of symmetry of the complete structure divides a member axially, that member's elements are assigned section properties with values equal to half the values of the properties of the original member. Using axial symmetry does not change the number of elements within a member but does reduce the number of elements needed to model the complete structure. The bridge and element 4 of the building structure are modelled in this way in model "E".

The mass of the bridge drive motor and electrical box are assumed negligible. Load is applied to the crane structure through the cable. The first DoF of the first element is the displacement of the crane at the location of the trolley and hoist. A lumped mass at node 1 represents the trolley and hoist.

The members of the building structure are W410x67 sections which are integral with a cast 130 mm concrete floor slab above. Using the procedure outlined in CSA-S16.1-M89 [ref 6], the effective moment of inertia, I_e, of these

Figure 4.10 Multi Degree of Freedom Model for Shop Crane Loaded at East End of Bridge - Model "E"

Number of Nodes = 11
Number of Members = 11
Number of D'soF = 21

H =Hinge : Extra Rotational DoF allowed
P = Pin : Translational DoF not allowed
R = Roller : Rotational DoF not allowed
F = Fixed : Rotation and Translation not allowed

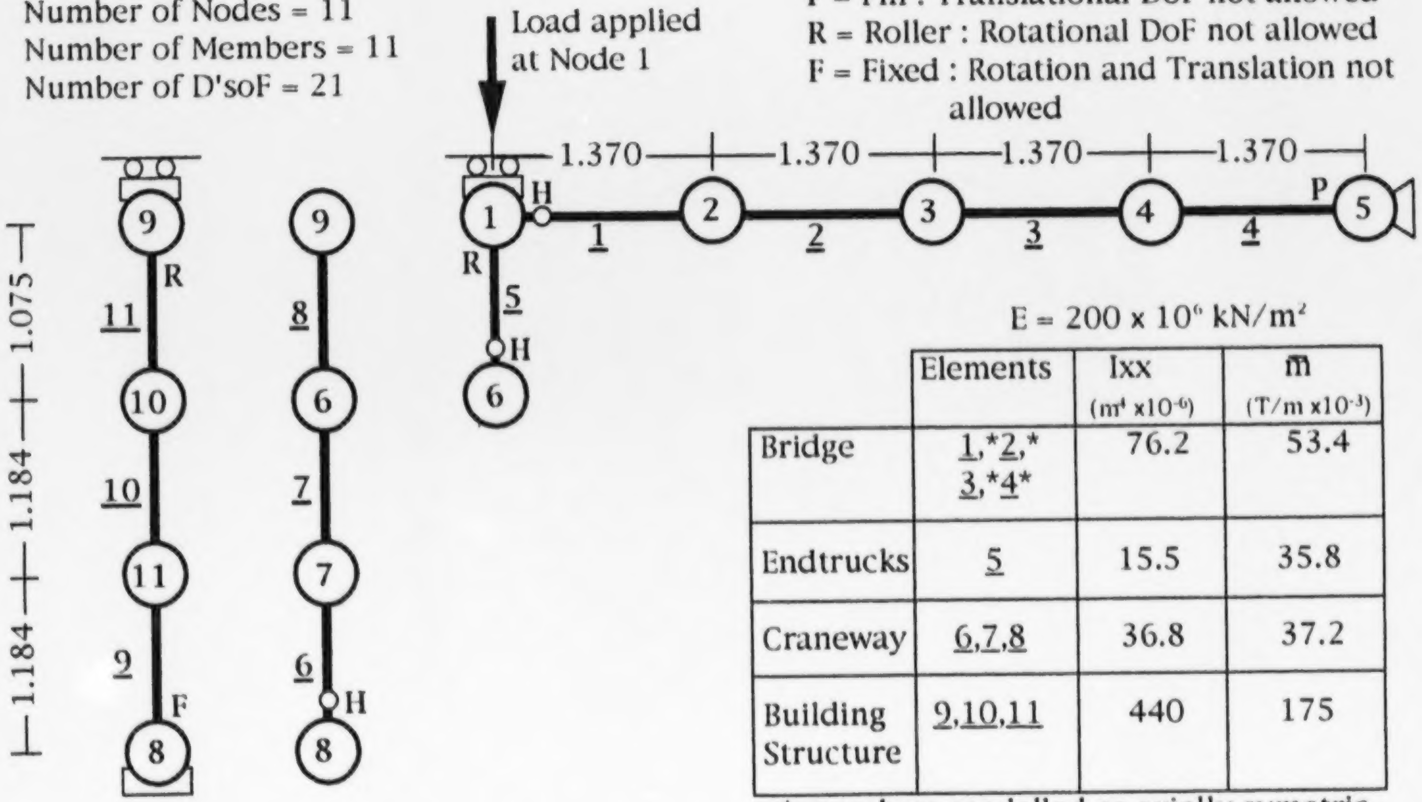
Load applied at Node 1
1.370
1.370
1.370
1.370
1
2
3
4
5
6
7
8
9
10
11
H
R
P
F
1.184
1.184
1.075

E = 200 x 10⁶ kN/m²

	Elements	Ixx (m⁴ x10⁻⁶)	m̄ (T/m x10⁻³)
Bridge	1,*2,* 3,*4*	76.2	53.4
Endtrucks	5	15.5	35.8
Craneway	6,7,8	36.8	37.2
Building Structure	9,10,11	440	175

* members modelled as axially symetric

Figure 4.11 Locations Represented by Nodes and Elements of Model "2"

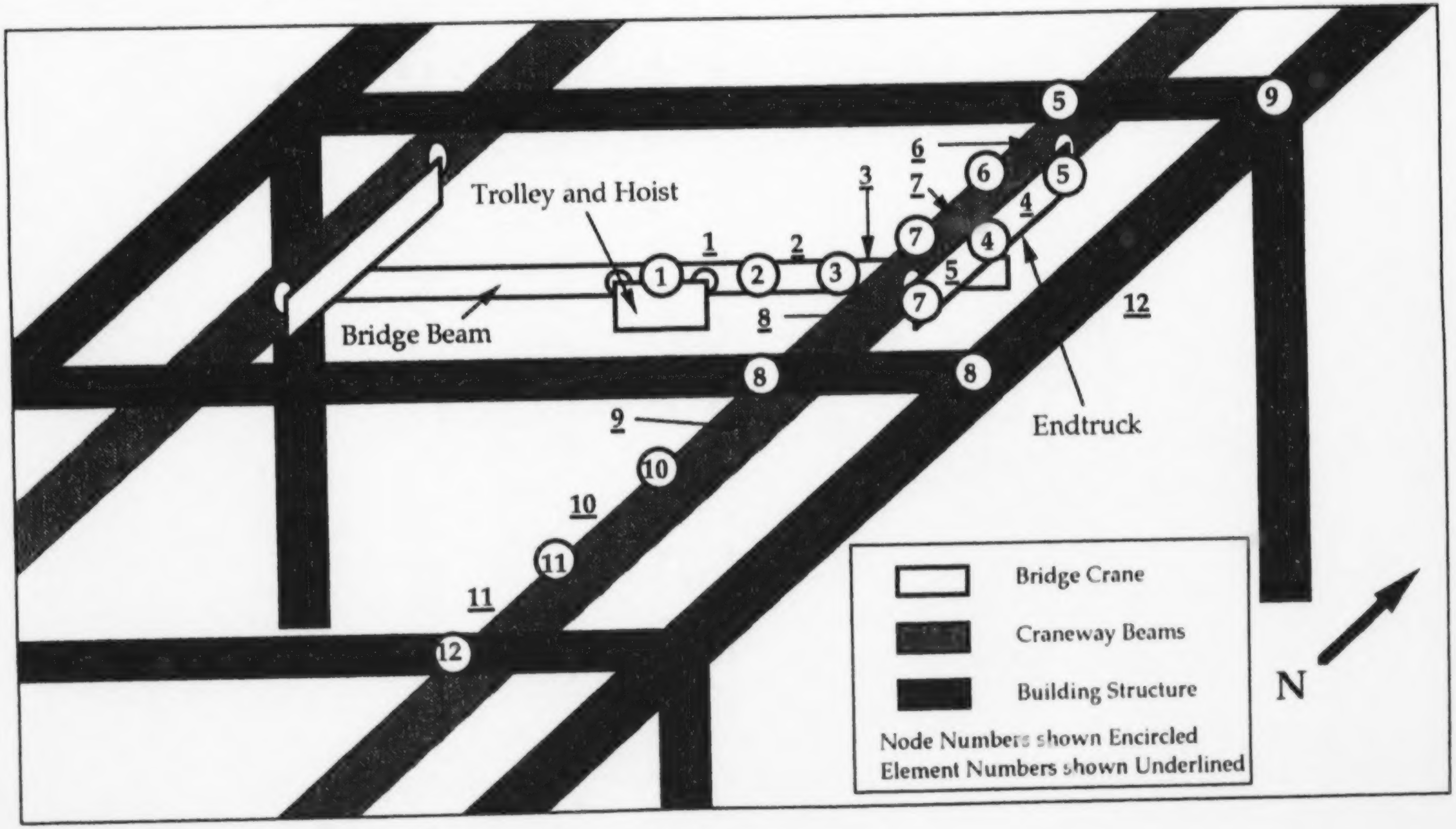
Trolley and Hoist
Bridge Beam
Endtruck
1
2
3
4
5
6
7
8
9
10
11
12
N
Bridge Crane
Craneway Beams
Building Structure
Node Numbers shown Encircled
Element Numbers shown Underlined

Figure 4.12 Multi Degree of Freedom Model for Shop Crane Loaded at Midspan - Model "2"

Number of Nodes = 12
Number of Elements = 12
Number of D'soF = 23

H=Hinge : Extra Rotational DoF allowed
P=Pin : Translational DoF not allowed
R=Roller : Rotational DoF not allowed
F=Fixed : Rotation and Translation not allowed

$E = 200 \times 10^6$ kN/m^2

	Elements	Ixx ($m^4 \times 10^{-6}$)	$\bar{m}$ ($T/m \times 10^{-3}$)
Bridge	1,2,3	76.2	53.4
Endtrucks	4,5	15.5	35.8
Craneway	6,7,8, 9,10,11	36.8	37.2
Building Structure	12*	880	350

* section properties have been doubled to account for full loading on transversely symetric element

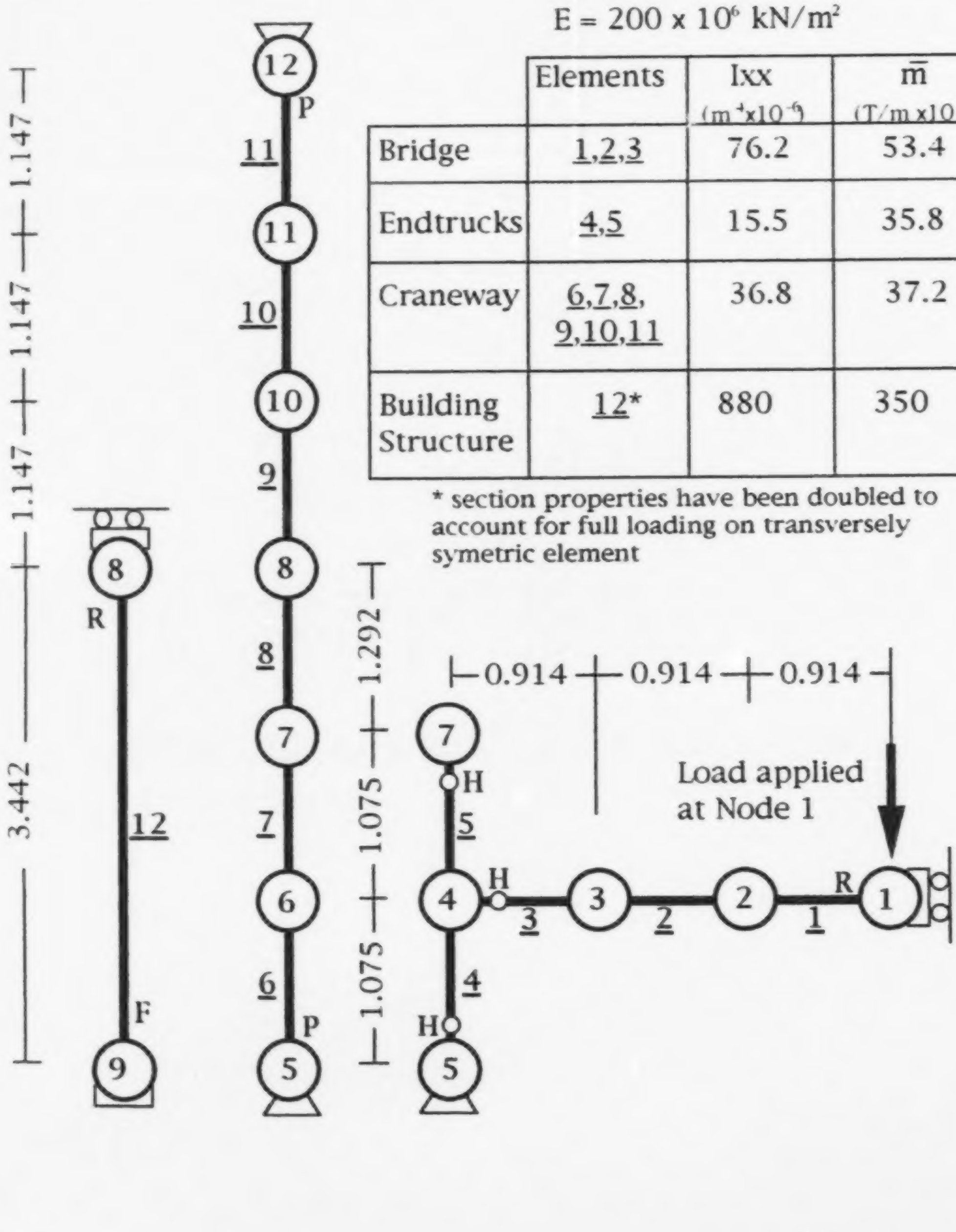
1.147
1.147
1.147
3.442
8
R
12
F
9
12
P
11
11
10
10
9
8
8
7
7
6
6
6
P
5
1.292
1.075
1.075
0.914
0.914
0.914
7
H
5
4
H
3
3
2
2
1
R
1
4
H
5
Load applied at Node 1

Figure 4.13 Locations Represented by Nodes and Elements of Model "E"

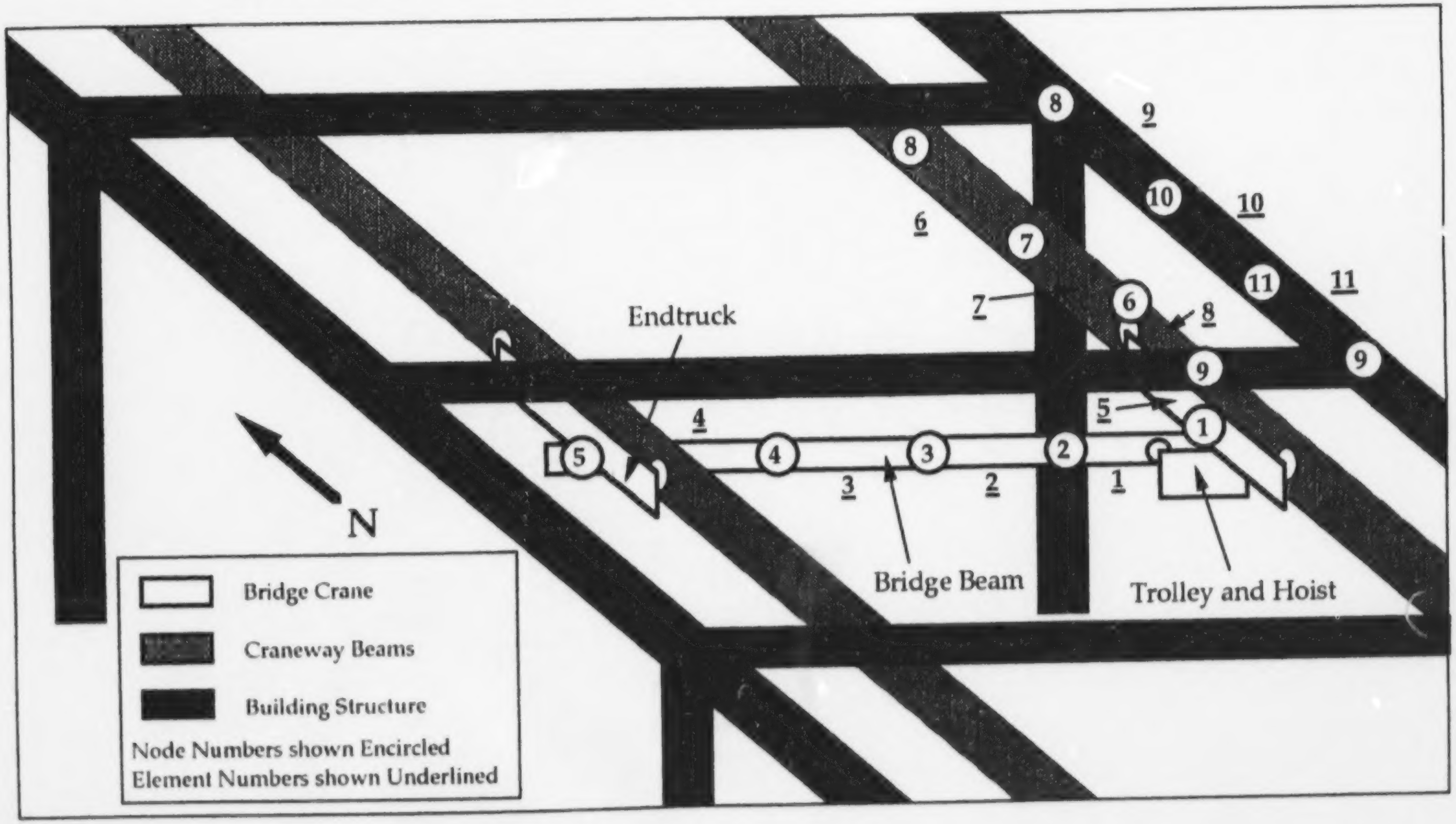

8
9
8
10
10
6
7
11
11
7
6
8
Endtruck
9
9
5
1
4
5
4
3
2
3
2
1
N
Bridge Beam
Trolley and Hoist
Bridge Crane
Craneway Beams
Building Structure
Node Numbers shown Encircled
Element Numbers shown Underlined

composite sections can be estimated from I_w, the moment of inertia of the steel section, and I_t, the moment of inertia of the transformed composite section.

$$I_e = I_w + 0.85 \sqrt[4]{p} \, (I_t - I_w) \tag{4.8}$$

The fraction of full shear connection between the concrete and the wide flange beam is accounted for by p in the formula above. For the purposes of this model, p will be assumed equal to one. The W410x67 section has a moment of inertia I_w, of 246 x 10^6mm^4. The effective width of concrete for the north-south member is a tenth of its span of 6.88m, because the beam supports the edge of the slab. The value of I_t for this transformed section is 474 x 10^6mm^4, and the effective moment of inertia is

$$I_e = 246 \times 10^6 \text{mm}^4 + 0.85(474 \times 10^6 \text{mm}^4 - 246 \times 10^6 \text{mm}^4) = 440 \times 10^6 \text{mm}^4$$

The distributed mass of the member is taken as the distributed mass of the wideflange and half the mass of the concrete assumed to act in the composite section used to calculate I_e. Concrete density is assumed to be 2400 kg/m^3 . These assumptions give the north-south building structure member a distributed masses of 175 kg/m.

The program MAKEKAM.BAS is listed in Appendix C.1. This program assembles the individual elements into stiffness and mass matrices. The program GENJAC.BAS, listed in Appendix C.2, performs the general Jacobean iteration on the two matrices from MAKEKAM.BAS and displays the natural frequencies. The stiffness and mass matrices for "E" and "2" are shown in Appendix B.1. The first seven natural frequencies are shown in Table 4.2.

Table 4.2 Frequency Data for Structure Models "2" and "E"

	Frequency Related Data for Structure Model "2" 1/2 Trolley mass = 0.176 T added at node 1				Frequency Related Data for Structure Model "E" Trolley mass = 0.352 T added at node 1			
Mode Number	ω^2 $\left(\frac{\text{radians}}{\text{second}}\right)^2$	ω $\frac{\text{radians}}{\text{second}}$	Hz $\frac{\text{cycles}}{\text{second}}$	Period $\frac{\text{seconds}}{\text{cycle}}$	ω^2 $\left(\frac{\text{radians}}{\text{second}}\right)^2$	ω $\frac{\text{radians}}{\text{second}}$	Hz $\frac{\text{cycles}}{\text{second}}$	Period $\frac{\text{seconds}}{\text{cycle}}$
1	7334	85.6	13.6	7.34E-02	10016	100	15.9	6.28E-02
2	33005	182	28.9	3.46E-02	31402	177	28.2	3.55E-02
3	111080	333	53.0	1.89E-02	59323	244	38.8	2.58E-02
4	269700	519	82.7	1.21E-02	387044	622	99.0	1.01E-02
5	417920	646	103	9.72E-03	518273	720	115	8.73E-03
6	1909600	1380	220	4.55E-03	1624694	1270	203	4.93E-03
7	2201400	1480	236	4.23E-03	2632100	1620	258	3.87E-03

4.1.3 Cable Model

The cable connects the motor to the payload and the payload to the structure. Compared to the masses of these three components, the mass of the cable is small, and is assumed insignificant. This is a reasonable assumption for most bridge cranes. A bridge crane can have a massive attachment at the lifting end of the cable, such as a ladle in a foundry, or a magnet in a junk yard. These masses can be counted as part of the payload mass. A case where the cable mass might be significant is if the cable were tremendously long, as might be the case for an elevator in a deep mine shaft.

One end of the cable is attached to the drum of the hoist and the other end is attached to either the hook or the trolley, depending on how the cable is reeved. The number of lines of cable between the hook and the structure will be called n. Below the hook the payload is secured by slings. (See Figure 2.8.) The net stiffness of the complete cable and sling arrangement is defined as k_c. This is the weight of a payload, divided by the change in the distance between that payload and the trolley, due to the application of that weight. Thus k_c comprises the stiffness of all the lines of cable between the hook and structure acting in parallel and the stiffness of the slings that secure the payload to the hook. Figure 4.14 is a schematic diagram of the cable system. It shows a single spring of stiffness k_c between the payload and the pulleys at the hook. The cable is shown as being axially rigid. This diagram satisfies the mathematical requirements of the model, but it should be remembered that the stiffness of the real cable does contribute to k_c, and that it is only a convenience to assume that the spring acts in the location indicated.

The stiffness of the cable and slings was discussed in Section 2.5. The value of k_c is not constant, and any model of the crane should take that into account. The three features to contend with are the hysteresis, the delayed elasticity, and the variability of the stiffness with respect to tension level. The first two are friction related, and could be modelled using damping. The last has to do with the changing orientation of the linear elastic members with respect to the direction of the load. This occurs with all the components in the cable and sling assembly. The cable is made of wound helical strands. Under low tension, a significant portion of the force is carried through the relatively flexible mechanism of bending moment within each wire. As the

Figure 4.14 Model for Cable

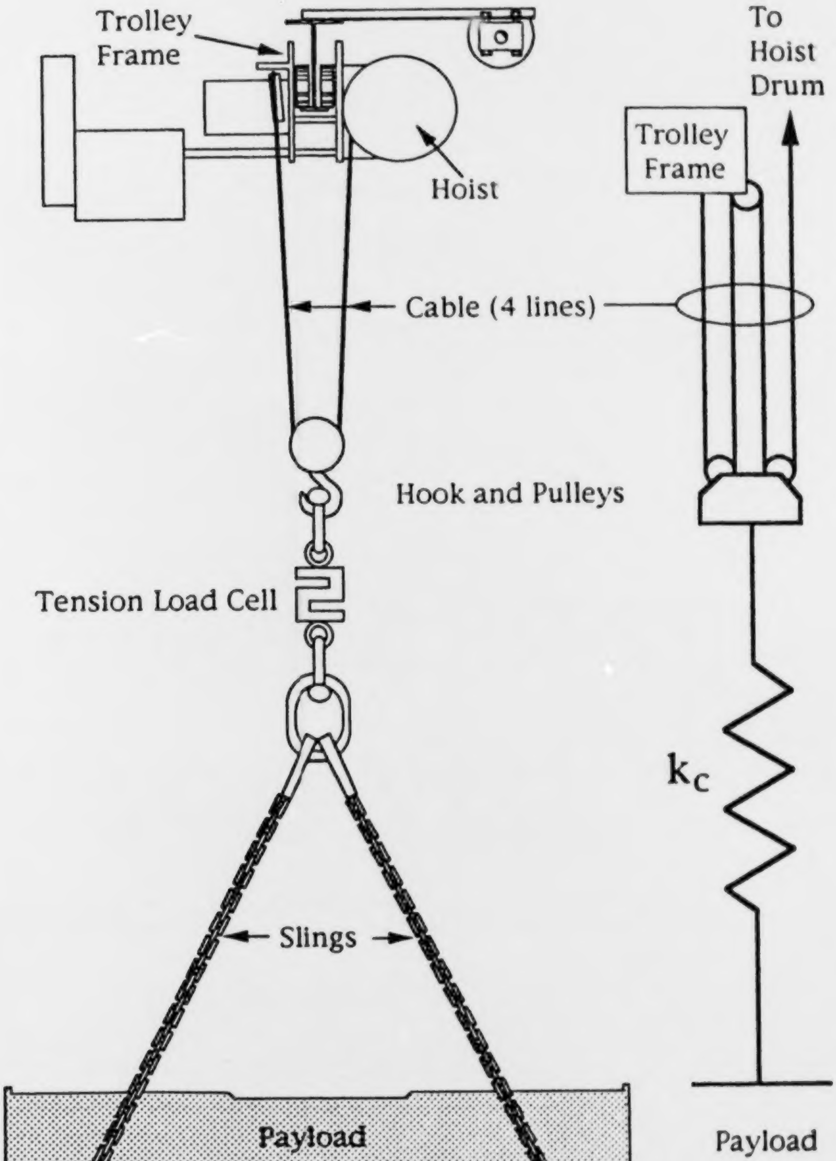
Trolley Frame
Hoist
To Hoist Drum
Trolley Frame
Cable (4 lines)
Hook and Pulleys
Tension Load Cell
k_c
Slings
Payload
Payload

tension increases in each strand, it tightens against its neighbours and no further bending moment deflection is possible. By then, the more stiff mechanism of axial elongation carries the major portion of the force. As tension increases, the cable elongates and narrows. More and more strands change from flexible bending members to stiff tension members and the net cable stiffness rises. The web sling is very similar. The strands are not helical wires but sinuous nylon fibers interwoven with one another. They must straighten out before they can elongate. A chain behaves slightly differently. Friction forces at the bearing surfaces between the links act to hold each link slightly out of line with the axis of the chain. Therefore, while the links elongate due to the chain tension, they also deflect due to shear and bending moment. As the tension load increases individual friction forces are abruptly overcome. The links slip against one another and rotate into closer alignment with the direction of the tension.

There is also friction in the pulleys, on the hook and on the trolley. Pulley friction changes the tension in each line of cable [ref. 10]. Each line of cable could be modelled as an individual spring element, and the pulleys' frictional effects could be accounted for.

For the single spring system that will be used to derive the dynamic factor, the model shown in Figure 4.14 will be used. The computer program outlined in Appendix C allows for changes in k_c with respect to tension, but does not address the issue of damping and hysteresis and delayed elasticity. The procedure used to vary k_c is explained in Section 4.3.3.

4.1.4 Payload

In the tests done on the shop crane, the payload did not deflect significantly. For the model developed in this chapter, the payload is considered as a mass attached to the cable and sling system, as shown in Figure 4.15b. If deflection is assumed significant, then the payload can be modelled as a single DoF spring and mass system, and can easily be incorporated, as shown in Figure 4.15c. If a more complex model of the payload is required, then a multi-DoF system could be devised.

Figure 4.15 Models for Payload

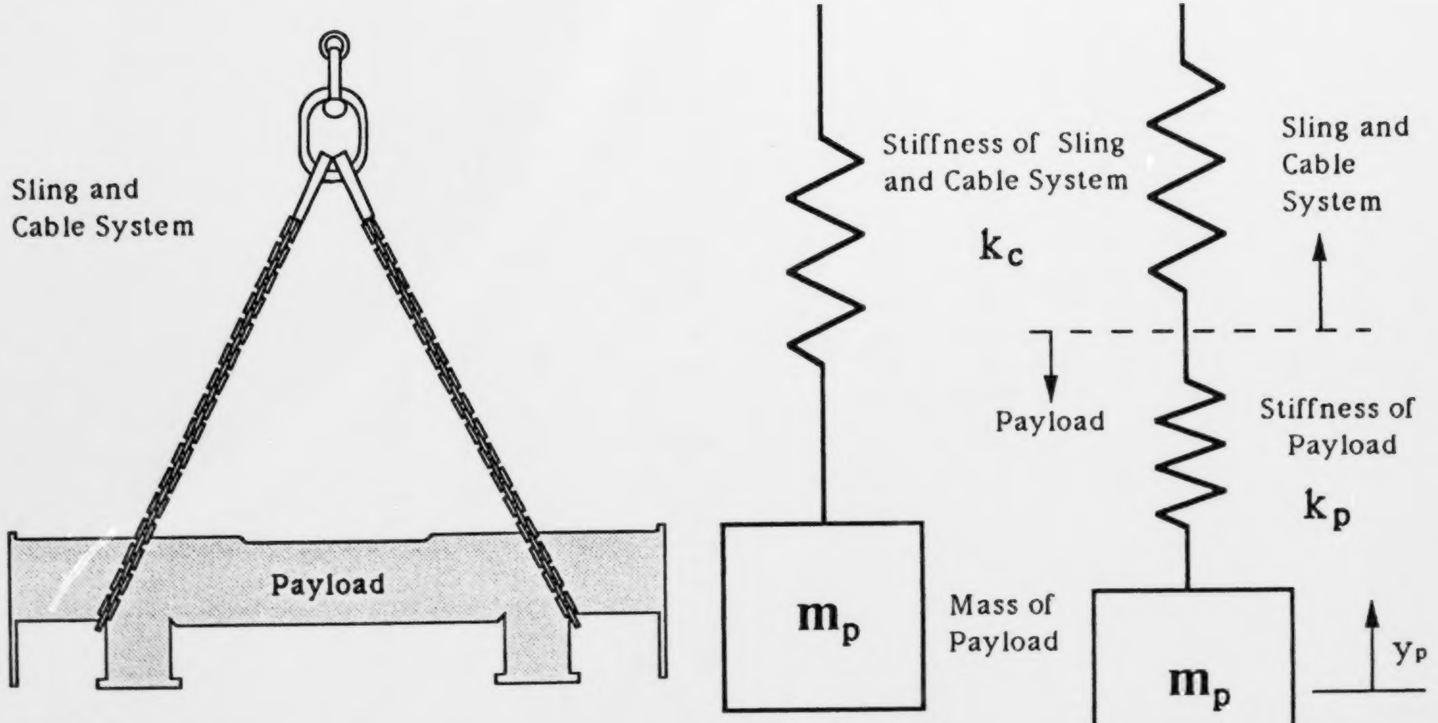
Sling and
Cable System
Payload
Stiffness of Sling
and Cable System
k_c
m_p
Mass of
Payload
Sling and
Cable
System
Payload
Stiffness of
Payload
k_p
m_p
y_p

a) Diagram of Suspended Payload

b) Model for Rigid Suspended Payload

c) Model for a Suspended Payload with Two Degrees of Freedom

The support conditions of the payload and the arrangement of the cable prior to hoisting affect the initial conditions and the dynamic factor. The range of possible starting conditions can be grouped into two types: those in which the cable has some initial tension, and those in which it does not. For those in which there is cable tension, the tension can range from zero to $m_p g$, the weight of the payload. In the limiting case, when tension equals payload weight, the payload is suspended completely by the cable. In all other cases of this first type, the payload rests on some support and the cable is taut. Any starting case of this type can be identified by specifying the initial support reaction or the initial tension in the cable. In the starting cases of the other type, the cable is slack. The tension in the cable is nominally zero, the self weight of the cable and slings being the only load carried. When the motor is turned on, there is at first no external load on it. At some time after this, the slack is used up and tension develops in the cable. The speed which the motor has reached at that moment will be between $\dot{y}_m = 0$ and $\dot{y}_m = V_o$. The value of $\dot{y}_m$ at the moment cable tension develops can be used to identify any starting case of the second type. In the border case between the two types the initial tension is zero but at the moment the motor begins to move tension begins to develop. The other limiting case for the second type is that where there is enough slack for the motor to attain full speed ($\dot{y}_m = V_o$) before any tension develops in the cable. Any further amount of slack in the cable will result in a longer wind up time before tension develops. However, when the tension does develop, V_o will have been reached and the system behaviour will be identical to the limiting case. In this limiting case, at the moment that the cable becomes tight, the difference between the vertical velocity of the structure, which equals zero, and $\dot{y}_m$, which equals V_o, is greater than for any other starting case. Because of the jerking action of the cable under this loading pattern, this starting case is called jerk-starting.

Let the force R be the floor reaction force. Whenever R does not equal zero, the payload is not moving and is in static equilibrium. Let T_c be the net cable tension and let y_p be the upwards displacement of the trolley. For the case in which the payload is moving, the dynamic equation of motion,

$$T_c - m_p g = m_p \ddot{y}_p \tag{4.9}$$

applies, and R = 0. For the case in which payload is not moving,

$$R = m_p g - T_c \tag{4.10}$$

and $0 \leq R \leq m_p g$. The case in which equation (4.10) applies cannot be referred to as the static case, although the payload is in static equilibrium. For the special case in which equation (4.9) applies, and $\ddot{y}_p = 0$, the payload is also in static equilibrium.

4.2 Assembly of the Global Matrices

The stiffness and mass terms associated with the two D'soF for the motor and the payload must be assembled with the stiffness and mass matrices $[K_s]$ and $[M_s]$ for the structure, to create the global stiffness and mass matrices. The models from Figures 4.8, 4.14, 4.15b, and one of 4.10 or 4.12, can all be brought together to give the model shown in Figure 4.16. The first degree of freedom of the structure is the vertical displacement at the node where the trolley is located. Rollers are shown on the sides of the trolley mass to indicate that only vertical displacement of the trolley is allowed. In the real system, the motor acts upon the cable through the gear box and cable drum. The action of the motor does not directly affect the structure. Therefore, the mass m_m in Figure 4.16 is assumed to be sufficiently far away from the first pulley on the trolley such that the line of cable from mass m_m to the first pulley on the trolley is horizontal. The only vertical load that is transferred from m_m to the structure and payload is the tension in one line of cable.

D'Alembert's principle states that a body is in dynamic equilibrium when the vector sum of the forces acting upon the body is equal and opposite to the inertial force, where the inertial force is the product of the mass of the body and its acceleration. Thus, the sum of the applied forces and the inertial force upon a body equals zero. Consider each of the masses of the system shown in

Figure 4.16
Assembled Multi-Degree of Freedom Model

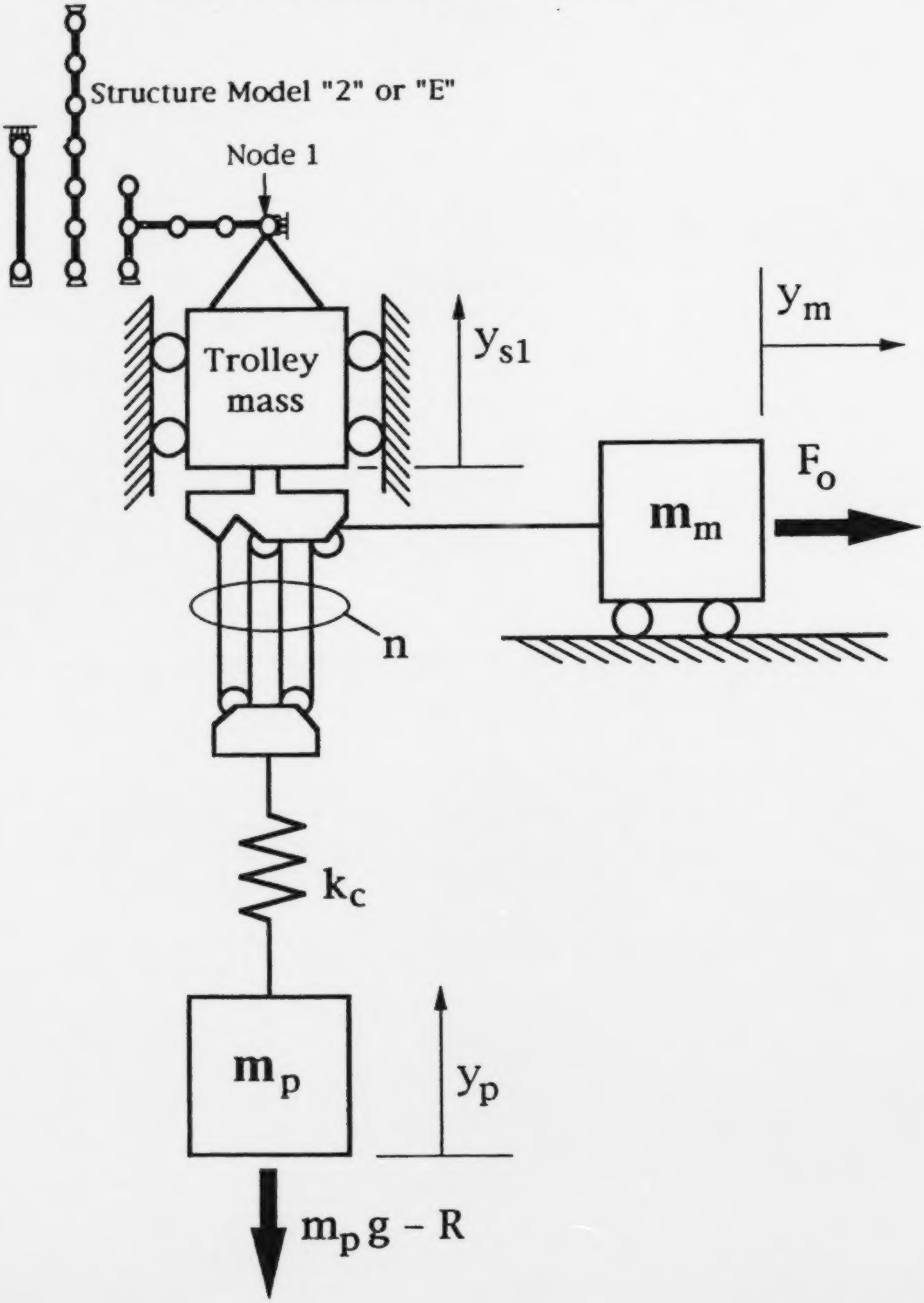
Structure Model "2" or "E"
Node 1
Trolley mass
y_{s1}
y_m
F_o
m_m
n
k_c
m_p
y_p
$m_p g - R$

Figure 4.16 as a body. The principle of virtual work is used to find the equations of motion of the system. The sum of the product of the spring forces and their virtual displacements plus the sum of the product of the inertial forces and their virtual displacements must equal the sum of the product of the applied forces and their virtual displacements. Let f_S, f_I, and f_A denote the spring, inertial, and applied forces respectively, and let δ denote the associated virtual displacements. The principle of virtual work, expressed as an equation, is shown below.

$$\Sigma f_S \delta + \Sigma f_I \delta = \Sigma f_A \delta$$

$$k_c\left(\frac{y_m}{n} - y_p + y_{s1}\right)\left(\frac{\delta y_m}{n} - \delta y_p + \delta y_{s1}\right) + \langle \delta Y_s \rangle [K_s]\{Y_s\}$$

$$+ m_m \ddot{y}_m \delta y_m + m_p \ddot{y}_p \delta y_p + \langle \delta \ddot{Y}_s \rangle [M_s]\{\ddot{Y}_s\}$$

$$= F_o\, \delta y_m + L \delta y_p \qquad (4.11)$$

Collecting together the terms which multiply δy_m and δy_p, equation (4.11) can be rewritten as the following:

$$\delta y_m \left(\frac{k_c y_m}{n^2} - \frac{k_c y_p}{n} + \frac{k_c y_{s1}}{n} + m_m \ddot{y}_m - F_o\right)$$

$$+ \delta y_p \left(\frac{-k_c y_m}{n} + k_c y_p - k_c y_{s1} + m_p \ddot{y}_p - R + m_p g\right)$$

$$+ \delta y_{s1} \left(\frac{k_c y_m}{n} - k_c y_p + k_c y_{s1}\right)$$

$$+ \langle \delta Y_s \rangle \left\{[K_s]\{Y_s\} + [M_s]\{\ddot{Y}_s\}\right\}$$

$$= 0 \quad \text{for all values of } \delta y_m, \delta y_p \text{ and all } \delta y_s. \qquad (4.12)$$

The virtual displacement δy_{s1} is the first term of the row matrix $\langle \delta Y_s \rangle$. To collect together all the terms in equation (4.12) that multiply δy_{s1}, the first term in the column vector $\left\{ [K_s]\{Y_s\} + [M_s]\{\ddot{Y}_s\} \right\}$ must be included with the terms in the third addend in (4.12) which multiply δy_{s1}. This is done using the following definitions.

Let the stiffness matrix $[K_s]$ without its first row and column be denoted by $[K_s\text{-}1]$. Similarly, $[M_s\text{-}1]$ is the structural mass matrix without its first row and column. Let the vectors $\langle \delta Y_s\text{-}1 \rangle$ and $\{Y_s\text{-}1\}$ be row and column vectors containing all but the first virtual and real structural displacements, respectively. Equation (4.12) is now rewritten.

$$\delta y_m \left(\frac{k_c y_m}{n^2} - \frac{k_c y_p}{n} + \frac{k_c y_{s1}}{n} + m_m \ddot{y}_m - F_o \right)$$

$$+ \delta y_p \left(\frac{-k_c y_m}{n} + k_c y_p - k_c y_{s1} + m_p \ddot{y}_p - R + m_p g \right)$$

$$+ \delta y_{s1} \left(\frac{k_c y_m}{n} - k_c y_p + k_c y_s + \langle K_{s1} \rangle \{Y_s\} + \langle M_{s1} \rangle \{\ddot{Y}_s\} \right)$$

$$+ \langle \delta Y_s\text{-}1 \rangle \left\{ [K_s\text{-}1]\{Y_s\text{-}1\} + [M_s\text{-}1]\{\ddot{Y}_s\text{-}1\} \right\}$$

$$= 0 \quad \text{for all values of } \delta y_m, \delta y_p \text{ and all } \delta y_s. \qquad (4.13)$$

To satisfy this requirement, the three bracketed expressions in (4.13) must each equal zero, and each of the terms in the column matrix of the fourth addend must equal zero. It can be seen that $[M_s]$ will appear within the global mass matrix. All but the first term of the stiffness matrix $[K_s]$ will appear in the global stiffness matrix. The first term will be replaced by the value $k_c + k_{s1,1}$. The matrix thus formed is $\begin{bmatrix} k_c + k_{s1.1} & \langle K_{s1}\text{-}1 \rangle \\ \{K_{s1}\text{-}1\} & [K_s\text{-}1] \end{bmatrix}$, where $\langle K_{s1}\text{-}1 \rangle$ and $\{K_{s1}\text{-}1\}$ represent all but the first term of the first row or column, respectively, of $[K_s]$. The equations of motion for the system can be written in matrix form as shown below.

$$\begin{bmatrix} \frac{k_c}{n^2} & -\frac{k_c}{n} & \frac{k_c}{n} & \langle 0 \rangle \\ -\frac{k_c}{n} & k_c & -k_c & \langle 0 \rangle \\ \frac{k_c}{n} & -k_c & k_c+k_{s1,1} & \langle K_{s1}-1 \rangle \\ \{0\} & \{0\} & \{K_{s1}-1\} & [K_s-1] \end{bmatrix} \begin{Bmatrix} y_m \\ y_p \\ \{Y_s\} \end{Bmatrix}$$

$$+ \begin{bmatrix} m_m & 0 & 0 \\ 0 & m_p & 0 \\ 0 & 0 & [M_s] \end{bmatrix} \begin{Bmatrix} \ddot{y}_m \\ \ddot{y}_p \\ \{\ddot{Y}_s\} \end{Bmatrix} = \begin{Bmatrix} F_o \\ R - m_p g \\ \{0\} \end{Bmatrix} \tag{4.14}$$

Equation (4.14) can be written more concisely as

$$[K]\{Y\} + [M]\{\ddot{Y}\} = \{F\}. \tag{4.15}$$

Two approaches are followed at this stage. In Chapter 5, equation (4.15) is modified. Simplifying assumptions are made which allow closed-form solutions for the equations of motion to be found. The solutions give expressions for the maximum displacement of the crane structure for specific hoisting events. In the remainder of this chapter, the steps required to solve equation (4.15) approximately using a time stepping technique are outlined. The results from a computer program which performs these steps are presented.

4.3 Outline of Numerical Time Stepping Procedure

Some of the terms in {F} and [K] are not constant. The approximation for the motor force term F_o in the vector {F} is the quadratic function in $\dot{y}_m$ given in equation (4.18). Thus, some of the equations of motion of the system are second order non-linear ordinary differential equations. The value of k_c varies with tension. A function for the variation of k_c has not been determined, but if k_c is not considered a constant, then that adds another level of complexity to the equations of motion. It will therefore be difficult to find a closed-form solution for the equations in (4.15). A numerical time stepping technique will be used to give an approximate solution. The time stepping technique is described in this section.

4.3.1 Degrees of Freedom Approximation Procedures

A hoisting event begins when the motor is turned on and ends when a steady state is reached in which the payload is fully suspended by the cable. For the time stepping procedure, the duration of a hoisting event is divided into discrete time steps of length Δt. Each DoF is approximated over the time step by an appropriate approximation function. The values of $\dot{y}$ and $\ddot{y}$ at the end of each time step are assumed to be linear functions of the value of y at the end of the time step. The form is as follows.

$$\dot{y}_{\Delta t} = \frac{\beta_1}{\Delta t}\left(y_{\Delta t} - y^{*}\right) \tag{4.16}$$

$$\ddot{y}_{\Delta t} = \frac{\beta_2}{\Delta t^2}\left(y_{\Delta t} - y^{**}\right) \tag{4.17}$$

In the derivations in this chapter, a variable subscripted "Δt" is the value of that variable at the end of the time step; a variable subscripted "0" is the value of that variable at the beginning of the time step; a variable subscripted "@t" is the value of that variable at any time t within the time step. The terms β_1

and β_2 are constants and y^* and y^{**} are functions of the value of y and its derivatives at the start of the time step.

If acceleration is assumed to be linear over the time step, and the acceleration changes a total of $\Delta\ddot{y}$ during Δt, then the following equation can be written.

$$\ddot{y}_{@t} = \ddot{y}_o + \frac{\Delta\ddot{y}t}{\Delta t} \tag{4.18}$$

Integrating equation (4.18) twice gives the following expressions for $y_{@t}$ and $\dot{y}_{@t}$.

$$\dot{y}_{@t} = \dot{y}_o + \ddot{y}_o t + \frac{\Delta\ddot{y}t^2}{2\Delta t} \tag{4.19}$$

$$y_{@t} = y_o + \dot{y}_o t + \frac{\ddot{y}_o t^2}{2} + \frac{\Delta\ddot{y}t^3}{6\Delta t} \tag{4.20}$$

Equations (4.18), (4.19) and (4.20) are solved when $t = \Delta t$, and written as three expressions for $\Delta\ddot{y}$.

$$\Delta\ddot{y} = \ddot{y}_{\Delta t} - \ddot{y}_o \tag{4.21}$$

$$\Delta\ddot{y} = \frac{2\,\dot{y}_{\Delta t}}{\Delta t} - \frac{2\,\dot{y}_o}{\Delta t} - 2\,\ddot{y}_o \tag{4.22}$$

$$\Delta\ddot{y} = \frac{6\,y_{\Delta t}}{\Delta t^2} - \frac{6\,y_o}{\Delta t^2} - \frac{6\,\dot{y}_o}{\Delta t} - 3\,\ddot{y}_o \tag{4.23}$$

Equating the right sides of (4.22) and (4.23) and collecting like terms gives and expression for $\dot{y}_{\Delta t}$ in terms of $y_{\Delta t}$.

$$\dot{y}_{\Delta t} = \frac{3y_{@t}}{\Delta t} - \frac{3y_o}{\Delta t} - 2\dot{y}_o - \frac{\ddot{y}_o \Delta t}{2} \qquad (4.24)$$

Equation (4.24) can be written in the form of equation (4.16),

$$\dot{y}_{\Delta t} = \frac{\beta_1}{\Delta t}\left(y_{\Delta t} - y^{*} \right) , \qquad (4.16)$$

$$\text{where} \quad \beta_1 = 3 \quad \text{and} \quad y^{*} = y_o + \frac{2\dot{y}_o \Delta t}{3} + \frac{\ddot{y}_o \Delta t^2}{6} \; . \qquad (4.25)$$

Similarly, equating the right sides of (4.21) and (4.23) and collecting like terms gives an expression for $\ddot{y}_{\Delta t}$.

$$\ddot{y}_{\Delta t} = \frac{6y_{\Delta t}}{\Delta t^2} - \frac{6y_o}{\Delta t^2} - \frac{6\dot{y}_o}{\Delta t} - 2\ddot{y}_o \qquad (4.26)$$

This can be written in the form of equation (4.17),

$$\ddot{y}_{\Delta t} = \frac{\beta_2}{\Delta t^2}\left(y_{\Delta t} - y^{**} \right) , \qquad (4.17)$$

$$\text{where } \beta_2 = 6 \quad \text{and} \quad y^{**} = y_o + \dot{y}_o \Delta t + \frac{\ddot{y}_o \Delta t^2}{3} \; . \qquad (4.27)$$

Linear acceleration does not have to be assumed. Another approach is to use the Newmark method. In the Newmark method, the displacement and its derivatives are not defined as functions over the time step Δt. Rather, their values at the end of the time step are defined in terms of initial and final values. The general form is as follows.

$$\dot{y}_{\Delta t} = \dot{y}_o + (1-\delta)\ddot{y}_o\Delta t + \delta\ddot{y}_{\Delta t}\Delta t \tag{4.28}$$

$$y_{\Delta t} = y_o + \dot{y}_o\Delta t + ((\frac{1}{2} - \alpha)\ddot{y}_o + \alpha\ddot{y}_{\Delta t})\,\Delta t^2 \tag{4.29}$$

The values of α and δ are constants selected by the user, with the constraints that $0 \leq \delta \leq 1$ and $0 \leq \alpha \leq \frac{1}{2}$. These equations are rewritten to put $\dot{y}_{\Delta t}$ and $\ddot{y}_{\Delta t}$ in terms of $y_{\Delta t}$. Equation (4.29) is rearranged to give the following:

$$\ddot{y}_{\Delta t} = \frac{y_{\Delta t}}{\alpha\Delta t^2} - \frac{y_o}{\alpha\Delta t^2} - \frac{\dot{y}_o}{\alpha\Delta t} - \frac{(1-2\alpha)\,\ddot{y}_o}{2\alpha} \tag{4.30}$$

This can be written in the form of equation (4.17),

$$\ddot{y}_{\Delta t} = \frac{\beta_2}{\Delta t^2}(\,y_{\Delta t} - y^{**})\;, \tag{4.17}$$

$$\text{where}\quad \beta_2 = \frac{1}{\alpha}\;,\quad \text{and}\quad y^{**} = y_o + \dot{y}_o\Delta t + \left(\frac{1}{2} - \alpha\right)\ddot{y}_o\Delta t^2\;. \tag{4.31}$$

Substituting the expression for $\ddot{y}_{\Delta t}$ from equation (4.32) into equation (4.30) and simplifying, gives the following.

$$\dot{y}_{\Delta t} = \frac{\delta y_{\Delta t}}{\alpha\Delta t} - \frac{\delta y_o}{\alpha\Delta t} - \left(\frac{\delta}{\alpha} - 1\right)\dot{y}_o - \left(\frac{\delta}{2\alpha} - 1\right)\ddot{y}_o\Delta t \tag{4.32}$$

Equation (4.32) can be written in the form of equation (4.16),

$$\dot{y}_{\Delta t} = \frac{\beta_1}{\Delta t}(y_{\Delta t} - y^*) \;, \tag{4.16}$$

$$\text{where } \beta_1 = \frac{\delta}{\alpha} \quad \text{and} \quad y^* = y_o + \left(1 - \frac{\alpha}{\delta}\right)\dot{y}_o\Delta t + \left(\frac{1}{2} - \frac{\alpha}{\delta}\right)\ddot{y}_o\Delta t^2 \;. \tag{4.33}$$

When $\delta = \frac{1}{2}$ and $\alpha = \frac{1}{6}$ the Newmark method is equivalent to the linear acceleration method. The most quickly converging result are achieved using the Newmark method when $\delta = \frac{1}{2}$ and $\alpha = \frac{1}{4}$. With these values the acceleration coefficient of the y^* term in (4.33) becomes zero. In this thesis the Newmark method with $\delta = \frac{1}{2}$ and $\alpha = \frac{1}{4}$ will be used.

4.3.2 Evaluating the Force Terms

The forces F_0 and R, along with the D'soF of the system and their first two derivatives with respect to time, are assumed to be known at the beginning of each time step. The two force terms vary over the time step as functions of the degrees of freedom. Specifically, F_0 is parabolic in $\dot{y}_m$ and R is governed by {Y}. If, over the time step, these two terms are approximated by some simple functions of time, then, at the end of the time step, F_0 and R will not generally have values consistent with the final values of $\dot{y}_m$ and {Y}. At this point they may be updated to consistent values. Such a procedure is simple to set up, but it is slow to converge. A procedure that maintains consistency between the forces and the degrees of freedom throughout the time step is outlined below.

The approximation procedures for the D'soF give any one derivative as a linear function of any other derivative. With some algebraic manipulation of the equations of motion, therefore, the force terms can be written as linear functions of their governing D'soF at the end of a time step. The problem reduces to solving two equations, (the now linear equations of motion and the defining forcing function), in two unknowns, (the force term and its governing degrees of freedom).

4.3.2.1 Solving for the F_0 Term

The F_0 force at the end of the time step must be expressed as a linear function of $\dot{y}_m$.

$$F_0 = a_0 + a_1\dot{y}_m \tag{4.34}$$

In this section the steps are described which are required to derive an expression for F_0 in the form shown in equation (4.34). To achieve this result, the first step is to uncouple the equations of motion in equation (4.15). The stiffness and mass matrices are diagonalized (and the equations of motion are uncoupled) through the use of a transformation matrix, $[\Phi]$. A transformation matrix $[\Phi]$ will be defined as a matrix that produces diagonal matrices when it is pre-multiplied by [K] or [M], and the result is pre-multiplied by $[\Phi]^T$. The columns within $[\Phi]$ are the eigenvectors of the system. Let the terms within $[\Phi]$ have the dimensions of mass$^{-1/2}$. The particular matrix $[\Phi]$ which will be used is the one which transforms [M] into the identity matrix [I], and transforms [K] into a diagonal matrix $[\omega^2]$ which has the squares of the natural frequencies of the system for its non-zero terms. Earlier ω was used in describing motor behaviour. This is not inconsistent. In both cases ω is a measure of rate of change of angle with respect to time. The following equations therefore apply.

$$[\omega^2] = [\Phi]^T [K] [\Phi] \quad \text{and} \quad [\,I\,] = [\Phi]^T [M] [\Phi] \tag{4.35}$$

Let {W} be the set of modal degrees of freedom of the complete system.

$$\{Y\}=[\Phi]\{W\} \tag{4.36}$$

Let all the terms in equation (4.14) be pre-multiplied by $[\Phi]^T$ and the uncoupled equations of motion result.

$$[\Phi]^T[K]\{Y\} + [\Phi]^T[M]\{\ddot{Y}\} = [\Phi]^T\{F\}$$

$$[\Phi]^T[K]\,[\Phi]\{W\} + [\Phi]^T[K]\,[\Phi]\{\ddot{W}\} = [\Phi]^T\{F\}$$

$$[\omega^2]\{W\} + \{\ddot{W}\} = [\Phi]^T\{F\} \tag{4.37}$$

All but the first two terms of {F} are zero. Therefore

$$[\Phi]^T\{F\} = \{\Phi_1\}\,F_o + \{\Phi_2\}\,(R - m_p g)\,, \tag{4.38}$$

where $\{\Phi_1\}$ and $\{\Phi_2\}$ are the first and second column of $[\Phi]$, respectively. The approximation procedures relating $\dot{y}$ and $\ddot{y}$ to y apply also to the modal degrees of freedom. Therefore, at the end of the time step, the following equation, based upon equation (4.17), applies.

$$\{\ddot{W}\} = \frac{\beta_2}{\Delta t^2}\Big\{\{W\} - \{W^{**}\}\Big\} \tag{4.39}$$

Substituting the expressions for $[\Phi]^T\{F\}$ and {W} from equation (4.38) and (4.39) into equation (4.37) gives

$$\Big[[\omega^2] + \frac{\beta_2}{\Delta t^2}[\,I\,]\Big]\{W\} = \{\Phi_1\}\,F_o + \{\Phi_2\}(R - m_p g) + \frac{\beta_2}{\Delta t^2}\{W^{**}\} \tag{4.40}$$

To rewrite (4.40) as an equation for {W}, the expression must be premultiplied by a diagonal matrix, $\Big[[\omega^2] + \frac{\beta_2}{\Delta t^2}[\,I\,]\Big]^{-1}$. The following definitions are useful. Let

$$\{A\} = \left[[\omega^2] + \frac{\beta_2}{\Delta t^2}[\,I\,]\right]^{-1}\{\Phi_1\},$$

$$\{B\} = \left[[\omega^2] + \frac{\beta_2}{\Delta t^2}[\,I\,]\right]^{-1}\{\Phi_2\},$$

$$\text{and}\quad [C] = \frac{\beta_2}{\Delta t^2}\left[[\omega^2] + \frac{\beta_2}{\Delta t^2}[\,I\,]\right]^{-1}[\,I\,]\ .$$

Equation (4.40) is now rewritten as an equation for $\{W\}$.

$$\{W\} = \{A\}F_o + \{B\}(R\text{-}mpg) + [C]\{W^{**}\} \tag{4.41}$$

The matrix [C] is a dimensionless diagonal transformation matrix whose non-zero terms are

$$c_{j,j} = \frac{1}{\dfrac{\omega_j^2\Delta t^2}{\beta_2} + 1}\ . \tag{4.42}$$

The term ω_j is the jth natural frequency of the system. As Δt becomes smaller [C] approaches the identity matrix. If a similar derivation was performed, in which the D'soF were not uncoupled, the counterpart for [C] would be a full matrix. The time required for the calculation of $\{Y\}$, rather than $\{W\}$, in each time step would increase proportionally with the number of degrees of freedom.

From equation (4.35) the expression for y_m in terms of $\{W\}$ is found.

$$y_m = \langle\Phi_1\rangle\{W\} \tag{4.43}$$

From equation (4.16), an expression for y_m in terms of $\dot{y}_m$ at the end of each time step is found.

$$y_m = \frac{\Delta t}{\beta_1}\dot{y}_m + y_m^* \tag{4.44}$$

Equating the right sides of equations (4.43) and (4.44) and substituting the expression for {W} into the result gives the following.

$$\frac{\Delta t}{\beta_1}\dot{y}_m + y_m^* = \langle\Phi_1\rangle\{A\}F_o + \langle\Phi_1\rangle\{B\}(R\text{-}mpg) + \langle\Phi_1\rangle[C]\{W^{**}\} \tag{4.45}$$

$$\text{Let } \frac{1}{\langle\Phi_1\rangle\{A\}} = k^*\text{, a stiffness term,}$$

$$\frac{\langle\Phi_1\rangle\{B\}}{\langle\Phi_1\rangle\{A\}} = \zeta_1\text{, a dimensionless constant,}$$

$$\text{and } \frac{\langle\Phi_1\rangle[C]}{\langle\Phi_1\rangle\{A\}} = \langle K^F\rangle .$$

Equation (4.45) can now be rewritten as an expression for F_o.

$$F_o = \left(\frac{k^*\Delta t}{\beta_1}\right)\dot{y}_m + \left(k^*y_m^* - \zeta_1(R\text{-}m_pg) - \langle K^F\rangle\{W^{**}\} \right) \tag{4.46}$$

The force R is zero when the payload is fully supported by the cable. Equation (4.46) then gives F_o as a linear function in terms of $\dot{y}_m$, as required in equation (4.34). When R = 0,

$$F_o = a_0 + a_1\dot{y}_m \tag{4.34}$$

$$\text{where } a_0 = k^*y_m^* + \zeta_1 m_pg - \langle K^F\rangle\{W^{**}\}$$

$$\text{and } a_1 = \frac{k^*\Delta t}{\beta_1} . \tag{4.47}$$

If the procedure used the uncoupled D'soF, the term $\langle K^F \rangle \{W^{**}\}$ would be replaced by some stiffness coefficient times y_m^{**}, and equation (4.46) would be solved more quickly. The saving in time here, however, is not as great as the gain due to the diagonal [C] matrix in (4.41).

In Section 4.3.2.2 following, it is shown that when R is not zero it is still the case that F_o can be written as a linear function in terms of $\dot{y}_m$. Thus, the value for F_o which is consistent with $\{Y\}$ at the end of each time step is found by solving two equations in two unknowns. The two equations are equation (4.47) derived from the equations of motion, and the forcing function, equation (4.7).

$$F_o = b_0 + b_1 \dot{y}_m + b_2 \dot{y}_m^2 \tag{4.7}$$

Equations (4.7) and (4.47) are combined to give

$$b_2 \dot{y}_m^2 + (b_1 - a_1) \dot{y}_m + (b_0 - a_0) = 0 \ . \tag{4.48}$$

The solution for $\dot{y}_m$ is the following.

$$\dot{y}_m = \frac{(a_1 - b_1) \pm \sqrt{(b_1 - a_1)^2 - 4 b_2 (b_0 - a_0)}}{2 b_2} \tag{4.49}$$

Equation (4.49) is solved to give a value for $\dot{y}_m$ at the end of each time step, which is substituted into (4.47) to give a consistent value for F_o at the end of each time step. The value for F_o is substituted into equation (4.41), along with the appropriate value for R, and the modal displacements are determined. These are substituted into (4.35) to give the solutions for $\{Y\}$ at the end of each time step.

4.3.2.2 Solving for the R Term

In this section a linear expression for F_o in terms of $\dot{y}_m$ is derived which accounts for changing values of R. The force R is the reaction between the payload and the floor. During the iterations in which the force R is not zero, the payload is motionless. The acceleration $\ddot{y}_p$ is equal to zero. The second equation of motion from equation (4.14) becomes the following.

$$R - m_p g = \langle K_2 \rangle \{Y\} \tag{4.50}$$

where $\langle K_2 \rangle$ is the second row of [K]. Substituting the expression for {Y} from equation (4.36) and the expression for {W} from (4.41) into equation (4.50) gives

$$R - m_p g = \langle K_2 \rangle [\Phi] \Big\{ \{A\} F_o + \{B\}(R - mpg) + [C]\{W^{**}\} \Big\} \ . \tag{4.51}$$

The following two definitions are used to simplify equation (4.51). Let

$$\frac{\langle K_2 \rangle [\Phi] \{A\}}{1 - \langle K_2 \rangle [\Phi] \{B\}} = \zeta_2 ,$$

a dimensionless constant, and let

$$\frac{\langle K_2 \rangle [\Phi][C]}{1 - \langle K_2 \rangle [\Phi] \{B\}} = \langle K^R \rangle$$

Equation (4.51) can now be rewritten as an expression for R.

$$R = \zeta_2 F_o + \langle K^R \rangle \{W^{**}\} + m_p g \tag{4.52}$$

This expression for R is substituted directly into (4.46), and the following equation results.

$$F_o = \left(\frac{k^* \Delta t}{\beta_1}\right)\dot{y}_m + \left(k^* y_m{}^* - \zeta_1\zeta_2 F_o - \zeta_1 \langle K^R \rangle \{W^{**}\} - \langle K^F \rangle \{W^{**}\}\right) \qquad (4.53)$$

Equation (4.53) is rewritten as an expression for F_o.

$$F_o = \left(\frac{k^* \Delta t}{\beta_1(1 + \zeta_1\zeta_2)}\right)\dot{y}_m + \left(\frac{k^* y_m{}^* - \left\langle \zeta_1 \langle K^R \rangle + \langle K^F \rangle \right\rangle \{W^{**}\}}{1 + \zeta_1\zeta_2}\right) \qquad (4.54)$$

Equation (4.54) is again a linear expression of F_o in terms of $\dot{y}_m$, as described by equation (4.34). When $R = -\langle K_2 \rangle \{Y\} + m_p g$,

$$F_o = a_0 + a_1 \dot{y}_m , \qquad (4.34)$$

$$\text{where} \quad a_0 = \frac{k^* y_m{}^* - \left\langle \zeta_1 \langle K^L \rangle + \langle K^F \rangle \right\rangle \{W^{**}\}}{1 + \zeta_1\zeta_2}$$

$$\text{and } a_1 = \frac{k^* \Delta t}{\beta_1(1 + \zeta_1\zeta_2)} \qquad (4.55)$$

The point at which R changes from a variable to the constant zero, will generally not fall at the end point of a time step. Within each time step R is calculated using equation (4.52). The time step during which the payload lifts off is the one that ends with the magnitude of R generated from (4.52) being greater than zero. In the real system R cannot be greater than zero because the reaction force between the payload and the floor cannot be tensile. Neither (4.47) or (4.55) are appropriate for calculating F_o for the time step in which equation (4.52) provides a positive value for R. Equation (4.47) gives a value too low for F_o, because R was not zero throughout the time step. Equation (4.55) gives a value for F_o which is too high, because R cannot in reality be positive. A simple solution is to recalculate F_o using (4.46) using the positive R value from (4.52), which gives a result between the two.

4.3.3 Solving for Variable Cable Stiffness

The preceding development in Section 4.3.2.1 gives a numeric solution for the equations of motion in which at the end of each time step the forces F_o and R are consistent with the displacements and velocities. The cable stiffness, k_c, is treated as a constant. In this section a procedure is described which treats k_c as a function of cable tension T_c. This development begins by introducing a term for the elongation of the cable. An examination of the stiffness matrix in equation (4.13) shows the net cable tension, $T_c = \frac{k_c y_m}{n} - k_c y_p + k_c y_{s1}$. If this expression for T_c is divided by the net cable stiffness k_c, then the following expression results.

$$\frac{T_c}{k_c} = \frac{y_m}{n} - y_p + y_{s1} = y_c \tag{4.56}$$

Therefore, $y_c = k_c T_c$, where the displacement y_c is the cable elongation. The expression for cable elongation in terms of the modal D'soF is

$$y_c = \left\langle \frac{1}{n}\langle\Phi_1\rangle - \langle\Phi_2\rangle + \langle\Phi_3\rangle \right\rangle \{W\} \ .$$

$$\text{Let } \langle\Phi_c\rangle = \left\langle \frac{1}{n}\langle\Phi_1\rangle - \langle\Phi_2\rangle + \langle\Phi_3\rangle \right\rangle \ . \tag{4.57}$$

If the expressions for cable tension are brought to the right side of the equations of motion in (4.14), then the following matrix equation results.

$$\begin{bmatrix} [0] & [0] \\ [0] & [K_s] \end{bmatrix} \begin{Bmatrix} y_m \\ y_p \\ \{Y_s\} \end{Bmatrix} + \begin{bmatrix} m_m & 0 & 0 \\ 0 & m_p & 0 \\ 0 & 0 & [M_s] \end{bmatrix} \begin{Bmatrix} \ddot{y}_m \\ \ddot{y}_p \\ \{\ddot{Y}_s\} \end{Bmatrix} = \begin{Bmatrix} F_o - \frac{T_c}{n} \\ R - m_p g + T_c \\ -T_c \\ \{0\} \end{Bmatrix} \tag{4.58}$$

Both sides of equation (4.58) are pre-multiplied by $[\Phi]^T$.

$$\begin{bmatrix} [0] & [0] \\ [0] & [\omega_s^2] \end{bmatrix} \{W\} + \{\ddot{W}\} = [\Phi]^T\{F\}$$

$$= \left(F_o - \frac{T_c}{n}\right)\{\Phi_1\} + (R - m_p g + T_c)\{\Phi_2\} - T_c\{\Phi_3\} \tag{4.59}$$

Substituting the expression for $\{W\}$, from equation (4.39), into equation (4.59) gives the following.

$$\left[\begin{bmatrix} [0] & [0] \\ [0] & [\omega_s^2] \end{bmatrix} + \frac{\beta_2}{\Delta t^2}[I]\right]\{W\}$$

$$= \left(F_o - \frac{T_c}{n}\right)\{\Phi_1\} + (R - m_p g + T_c)\{\Phi_2\} - T_c\{\Phi_3\} + \frac{\beta_2}{\Delta t^2}\{W^{**}\} \tag{4.60}$$

To write an equation for $\{W\}$, each of the addends in (4.60) must be pre-multiplied by a diagonal matrix $\left[\begin{bmatrix} [0] & [0] \\ [0] & [\omega_s^2] \end{bmatrix} + \frac{\beta_2}{\Delta t^2}[I]\right]^{-1}$.The following definitions are useful. Let

$$\{A_s\} = \left[\begin{bmatrix} [0] & [0] \\ [0] & [\omega_s^2] \end{bmatrix} + \frac{\beta_2}{\Delta t^2}[I]\right]^{-1}\{\Phi_1\},$$

$$\{B_s\} = \left[\begin{bmatrix} [0] & [0] \\ [0] & [\omega_s^2] \end{bmatrix} + \frac{\beta_2}{\Delta t^2}[I]\right]^{-1}\{\Phi_2\},$$

$$\{D_s\} = \left[\begin{bmatrix} [0] & [0] \\ [0] & [\omega_s^2] \end{bmatrix} + \frac{\beta_2}{\Delta t^2}[I] \right]^{-1} \{\Phi_3\} ,$$

$$\text{and} \quad [C_s] = \frac{\beta_2}{\Delta t^2} \left[\begin{bmatrix} [0] & [0] \\ [0] & [\omega_s^2] \end{bmatrix} + \frac{\beta_2}{\Delta t^2}[I] \right]^{-1} .$$

Equation (4.60) is now rewritten as an expression for {W}.

$$\{W\} = \left(F_o - \frac{T_c}{n} \right)\{A_s\} + (R - m_p g + T_c)\{B_s\} - T_c\{D_s\} + [C_s]\{W^{**}\} \quad (4.61)$$

Let the jth natural frequency of the structure be ω_{s_j}. The matrix $[C_s]$ is a dimensionless transformation matrix whose non-zero terms are

$$c_{s_{j,j}} = \frac{1}{\dfrac{\omega_{s_j}^2 \Delta t^2}{\beta_2} + 1} \quad \text{when } j \geq 3 \ ,$$

$$\text{and} \quad c_{s_{j,j}} = 1 \quad \text{when } j < 3 \ .$$

As in the preceding development in which k_c was considered constant, the right sides of (4.43) and (4.44) are equated, and the expression for {W} from (4.60) is substituted into the result.

$$y_m = \langle \Phi_1 \rangle \{W\} \qquad (4.43)$$

$$y_m = \frac{\Delta t}{\beta_1} \dot{y}_m + y_m^* \qquad (4.44)$$

$$\frac{\Delta_t}{\beta_1}\dot{y}_m + ym^* = \left(F_o - \frac{T_c}{n}\right)\langle\Phi_1\rangle\{A_s\}$$

$$+ (R - m_p g + T_c)\langle\Phi_1\rangle\{B_s\} - T_c\langle\Phi_1\rangle\{D_s\} + \langle\Phi_1\rangle[C_s]\{W^{**}\} \qquad (4.62)$$

The following definitions are used to simplify equation (4.62). Let

$$k_s^* = \frac{1}{\langle\Phi_1\rangle\{A_s\}} ,$$

$$\zeta_1 = \frac{\langle\Phi_1\rangle\{B_s\}}{\langle\Phi_1\rangle\{A_s\}} ,$$

$$\langle K_s^F\rangle = \frac{\langle\Phi_1\rangle[C_s]}{\langle\Phi_1\rangle\{A_s\}} ,$$

$$\text{and} \quad \zeta_2 = \frac{\langle\Phi_1\rangle\{D_s\}}{\langle\Phi_1\rangle\{A_s\}} .$$

Equation (4.62) is then written as an expression for F_o.

$$F_o = \frac{k_s^*\Delta t}{\beta_1}\dot{y}_m + k_s^* y_m^* + \zeta_1(R - m_p g) - \left(\zeta_2 - \frac{1}{n}\right)T_c + \langle K_s^F\rangle\{W^{**}\} \qquad (4.63)$$

The reaction force R is equal to either zero or $-T_c$. Therefore, the coefficient for T_c in (4.63) is either $-\zeta_2 + \frac{1}{n}$, or $-\zeta_2 + \frac{1}{n} - \zeta_1$, depending on whether the payload has lifted off or not. Equation (4.63) can be rewritten as

$$F_o = \frac{k_s^*\Delta t}{\beta_1}\dot{y}_m + k_s^* y_m^* - \zeta_1 m_p g - \left(\zeta_2 - \frac{1}{n} + \zeta_0\right)T_c + \langle K_s^F\rangle\{W^{**}\} , \qquad (4.64)$$

where $\zeta_0 = 0$ when $T_c \geq m_p g$, and $\zeta_0 = \zeta_1$ when $T_c < m_p g$.

In this derivation, the tension T_c is some non-linear function of cable elongation. The heavy line in Figure 4.17 is a graph of the general form of the assumed relationship between T_c and y_c which is to be approximated. It is difficult to find a closed-form solution for F_o in (4.64). If a simple expression such as

$$T_c = C y_c^2 \tag{4.65}$$

is used (where C is a constant), then the expression for T_c which would result from substituting the expression for y_c from equation (4.63) into (4.64) is a quadratic in T_c, with constants and first and second order terms. The expression for T_c would be in the form of the formula for the roots of a quadratic, with the term F_o inside the discriminant. This expression for T_c, substituted into equation (4.62) would not give a linear equation for F_o in terms of $\dot{y}_m$. It would give an expression containing first and second order terms in both F_o and $\dot{y}_m$. To find a solution for $\dot{y}_m$ which satisfies this expression and the quadratic in equation (4.8) would require finding the roots of a fourth order equation.

A more simple solution is to assume some mathematical relationship between T_c and y_c and, within each time step, solve for the two variables using an iteration procedure. The mathematical relationship assumed is the following.

$$T_c = k_c y_c + T_f (1 - e^{\frac{T_c}{\bar{T}}}) \tag{4.66}$$

The two forces T_f and $\bar{T}$ are constants. The forces T_f and $\bar{T}$ are less than zero. Figure 4.17 shows the graph of T_c versus y_c. The values for {W} from equation (4.60) are substituted into equation (4.63), and the resulting expression for y_c is substituted into equation (4.65).

Figure 4.17
Assumed Cable Tension versus
Elongation Relationship

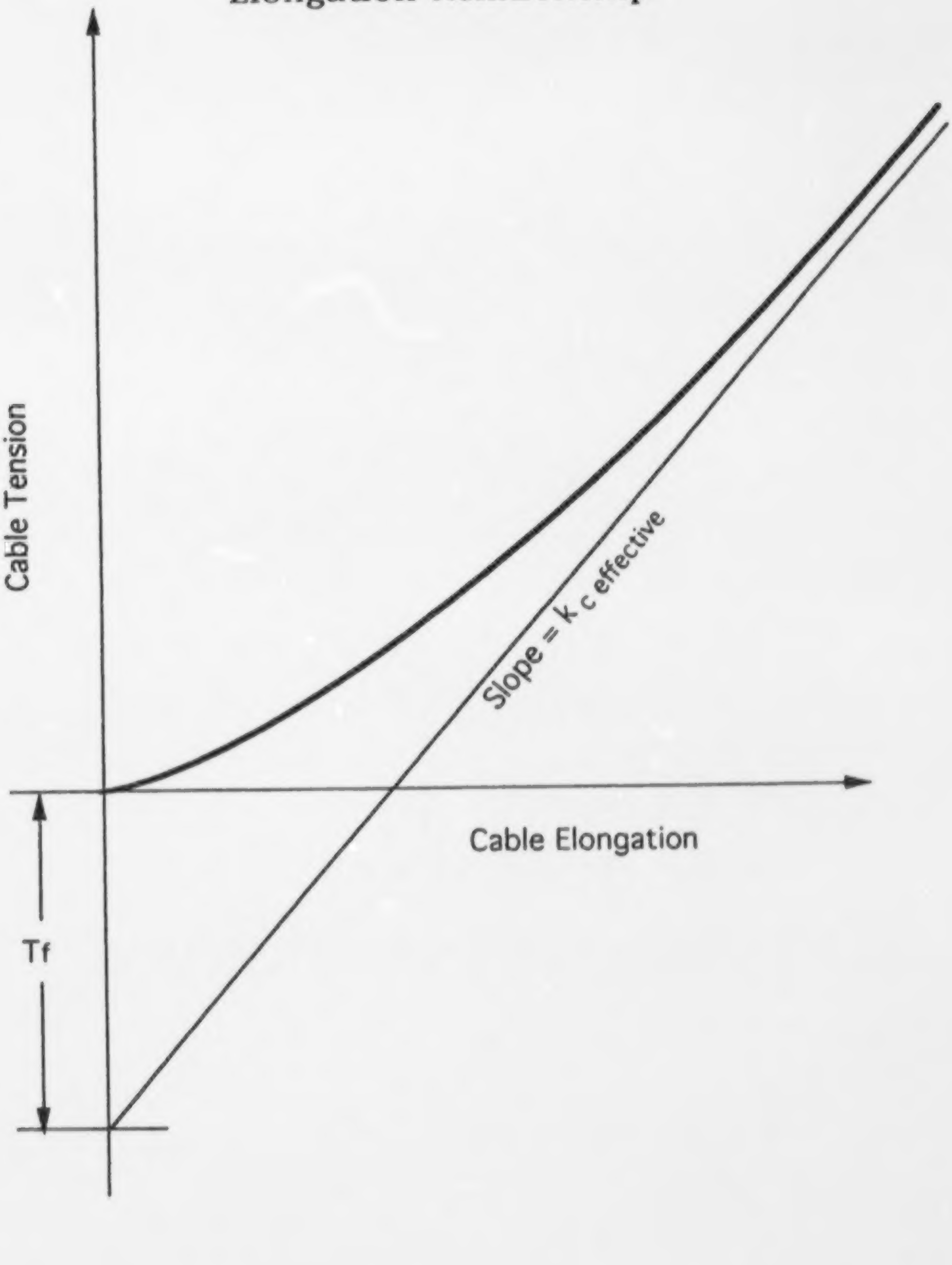

$$T_c = k_c\langle\Phi_c\rangle\left\{\left(F_o - \frac{T_c}{n}\right)\{A_s\} + (R - m_pg + T_c)\{B_s\} - T_c\{D_s\} + [C_s]\{W^{**}\}\right\}$$

$$+ T_f\,(1 - e^{\frac{T_c}{T}}) \qquad (4.67)$$

Equation (4.67) can be rewritten so that the only term on the right side involving T_c is the exponential term. The expression becomes

$$T_c = \frac{k_c\langle\Phi_c\rangle\left\{F_o\,\{A_s\} - m_pg\,\{B_s\} + [C_s]\{W^{**}\}\right\} + T_f\,(1 - e^{\frac{T_c}{T}})}{1 + k_c\langle\Phi_c\rangle\left\{\frac{1}{n}\,\{A_s\} - z\{B_s\} + \{D_s\}\right\}} \qquad (4.68)$$

where z = 1 when the payload is suspended by the cable, and z = 0 when there is a reaction force between the floor and the payload. The right side of equation (4.68) is substituted into equation (4.62). The F_o terms are collected and the following expression for F_o results.

$$F_o = a_0 + a_1\dot{y}_m + x_oT_f\,(1 - e^{\frac{T_c}{T}}), \qquad (4.69)$$

where a_0 =

$$\frac{k_s^*y_m^* - \zeta_1 m_pg - \dfrac{\left(\zeta_2 - \frac{1}{n} + \zeta_0\right)k_c\langle\Phi_c\rangle\left\{-m_pg\,\{B_s\} + [C_s]\{W^{**}\}\right\}}{1 + k_c\langle\Phi_c\rangle\left\{\frac{1}{n}\,\{A_s\} - z\{B_s\} + \{D_s\}\right\}} + \langle K_s^F\rangle\{W^{**}\}}{1 + \dfrac{\left(\zeta_2 - \frac{1}{n} + \zeta_0\right)k_c\langle\Phi_c\rangle\{A_s\}}{1 + k_c\langle\Phi_c\rangle\left\{\frac{1}{n}\,\{A_s\} - z\{B_s\} + \{D_s\}\right\}}},$$

$$\text{and } a_1 = \frac{\dfrac{k_s^* \Delta t}{\beta_1}}{1 + \dfrac{\left(\zeta_2 - \dfrac{1}{n} + \zeta_0\right) k_c \langle \Phi_c \rangle \{A_s\}}{1 + k_c \langle \Phi_c \rangle \left\{ \dfrac{1}{n}\{A_s\} - z\{B_s\} + \{D_s\} \right\}}} ,$$

$$\text{and } x_0 = \frac{1}{1 + k_c \langle \Phi_c \rangle \left\{ \dfrac{1}{n}\{A_s\} - z\{B_s\} + \{D_s\} \right\} + \left(\zeta_2 - \dfrac{1}{n} + \zeta_0\right) k_c \langle \Phi_c \rangle \{A_s\}} .$$

Both a_1 and x_0 are constant for all time steps, except in that ζ_0 and z can change values once during a hoisting event. The y_m^* and $\{W^{**}\}$ terms in the expression for a_0 are the only terms in that expression which must be calculated for each time step.

The iteration within each time step can now proceed. For each time step, an initial guess is made for the value of T_c, based on the values of T_c for the immediately preceding time steps. The acceleration $\ddot{y}_m$ is written in terms of the velocity $\dot{y}_m$ using equations (4.16) and (4.17), as shown in equation (4.70).

$$\ddot{y}_m = \frac{\beta_2 \dot{y}_m}{\beta_1 \Delta t} + \frac{\beta_2}{\Delta t^2}\left(y_m^* - y_m^{**} \right) \tag{4.70}$$

Substituting the value of $\ddot{y}_m$ from equation (4.70), and the assumed value for cable tension, into the equation of motion for the motor mass, gives a linear expression for F_o in terms of $\dot{y}_m$.

$$F_o = \frac{T_c\,\text{guess}}{n} + m_m \ddot{y}_m$$

$$= \frac{T_c\,\text{guess}}{n} + m_m \left(\frac{\beta_2 \dot{y}_m}{\beta_1 \Delta t} + \frac{\beta_2}{\Delta t^2} \left(y_m^{*} - y_m^{**} \right) \right)$$

$$= \left(\frac{\beta_2 m_m}{\beta_1 \Delta t} \right) \dot{y}_m + \left(\frac{T_c\,\text{guess}}{n} + m_m \left(\frac{\beta_2}{\Delta t^2} \left(y_m^{*} - y_m^{**} \right) \right) \right) \tag{4.71}$$

The right sides of equation (4.71) and the parabolic motor force equation (4.7) are set equal to each other. The solution for the resulting quadratic equation in $\dot{y}_m$ is found.

$$\dot{y}_m = \frac{-\left(b_1 - \left(\frac{\beta_2 m_m}{\beta_1 \Delta t} \right) \right)}{2 b_2}$$

$$- \frac{\sqrt{\left(b_1 - \left(\frac{\beta_2 m_m}{\beta_1 \Delta t} \right) \right)^2 - 4 b_2 \left(b_0 - \frac{T_c\,\text{guess}}{n} + m_m \left(\frac{\beta_2}{\Delta t^2} \left(y_m^{*} - y_m^{**} \right) \right) \right)}}{2 b_2} \tag{4.72}$$

The right sides of equation (4.68) and the parabolic motor force equation (4.7) are set equal to one another.

$$F_o = a_0 + a_1 \dot{y}_m + x_o T_f \left(1 - e^{\frac{T_c}{\dot{T}}} \right) = b_0 + b_1 \dot{y}_m + b_2 \dot{y}_m^2 \tag{4.73}$$

The value of $\dot{y}_m$ from (4.73) is substituted into equation (4.66) and a new value for T_c is determined. If this new value for T_c is not acceptably close to the previous value of T_c, then the new value of T_c is substituted into equation (4.71) and the process repeats itself. When the old and new values of T_c are acceptably close, the values for T_c and F_o are used in (4.58) to solve the modal D'soF. The procedure then follows the routine described at the end of Section 4.3.2.1.

This iteration procedure works much of the time, but there are circumstances in which the values of T_c diverge rather than converge. In these instances the iteration can be run backwards. That is, a guess for T_c is made and used in equation (4.69). The right sides of equations (4.7) and (4.69) are set equal to each other, as shown in (4.73), and the solution to the resulting quadratic equation in $\dot{y}_m$ is found.

$$\dot{y}_m = \frac{-b_1 + a_1 - \sqrt{(b_1 - a_1)^2 - 4\,b_2(\,b_0 - a_0 - x_o T_f\,(1 - e^{\frac{T_c}{\dot{T}}}))}}{2\,b_2} \qquad (4.74)$$

The resulting solution for $\dot{y}_m$ is used to calculate F_o using (4.69), and $\ddot{y}_m$ using (4.70). A new value for T_c is determined from the equation of motion for the motor mass,

$$F_o = \frac{T_c}{n} + m_m \ddot{y}_m \; . \qquad (4.75)$$

If the value for T_c from (4.75) is not acceptably close to the previous value of T_c, then the new value of T_c is substituted into equation (4.69) and the process repeats itself. When the old and new values of T_c are acceptably close, the values for T_c and F_o are used in (4.58) to solve the modal D'soF. The procedure then follows the routine described at the end of Section 4.3.2.1.

4.4 Computer Program Results

Two computer programs are listed in Appendix C which perform the steps described in the preceding sections. One, CRIMSIM.BAS, performs simulations of hoisting events using a constant value for k_c. The other, CRIS5.BAS, performs simulations of hoisting events using varying cable stiffness.

The results of eight computer simulations of hoisting events performed with the shop crane are shown in Table 4.3. The results are for varied hoisting position, sling type, and payload mass, and are all generated using CRIS5.BAS. The ratio of maximum dynamic to static displacement of the structure at the hoisting location is referred to as D. The D values from Table 4.3 are compared with values calculated for D closed-form solutions derived in Chapter 5 and the results of tests performed on the shop crane outlined in Chapter 6.

The motor values are as calculated in Table 4.1, or as assumed in Table 4.3, and the assumed F_0 versus $\dot{y}_m$ relationship is shown in Figure 4.6. The values which determine the degree of non-linearity of the relationship between cable tension and elongation are chosen such that the T_c versus y_c curves used in the simulation approximately match the tension versus elongation curves shown in Figures 2.9, 2.10, and 2.11. The tension versus elongation graphs from these figures are shown in Figures 4.18, 4.19, and 4.20 along with graphs of the assumed tension versus elongation relationships used in simulations.

Figure 4.18 Variables for Assumed Tension Elongation Relationship

Structures Lab Shop Crane
For Cases in which Small Payload is Used

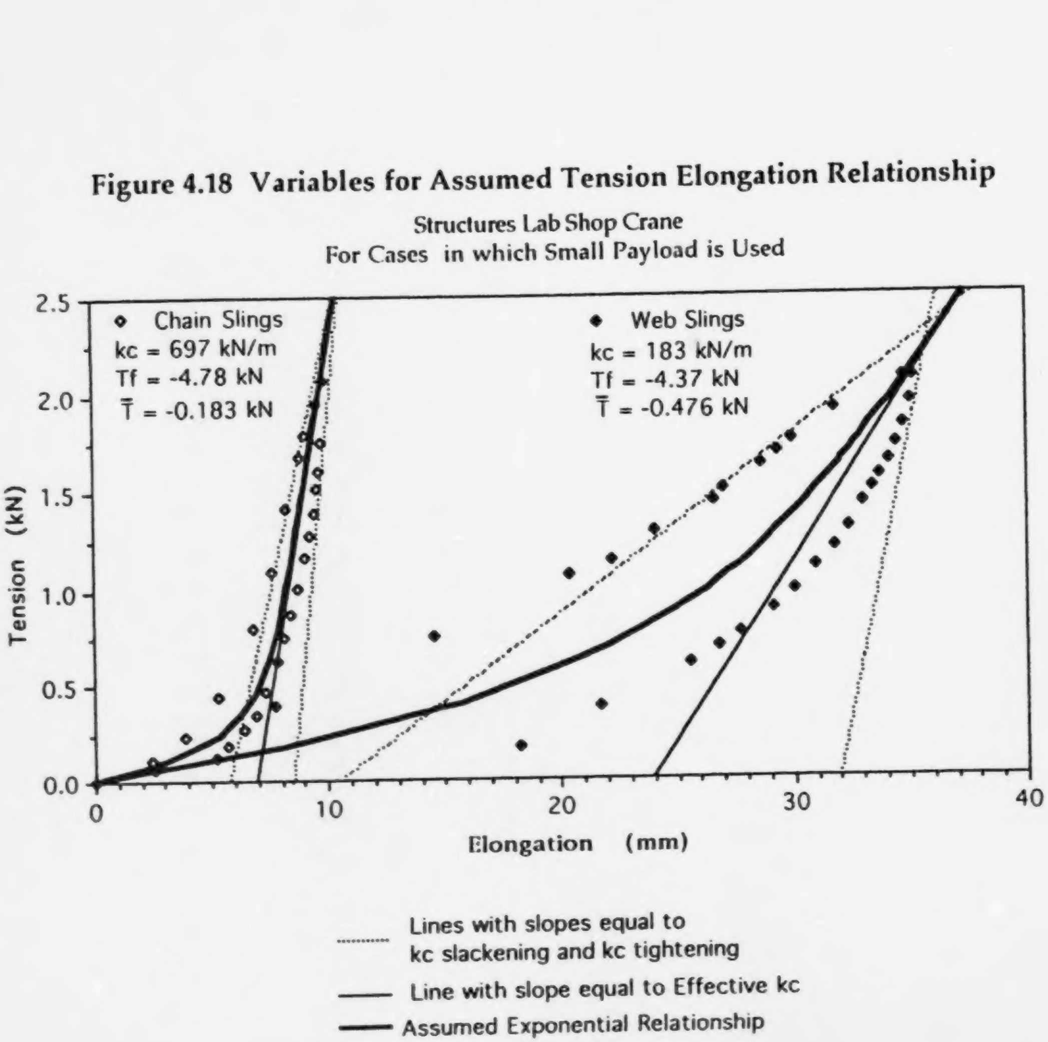

Figure 4.19 Variables for Assumed Tension Elongation Relationship

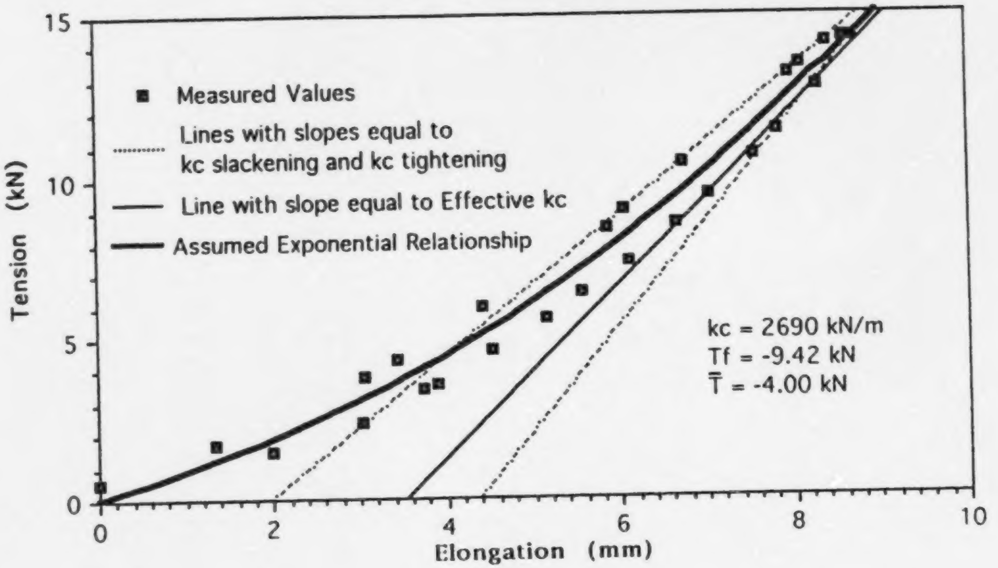

Structures Lab Shop Crane
Large Payload in Chain Slings

Figure 4.20 Variables for Assumed Tension Elongation Relationship

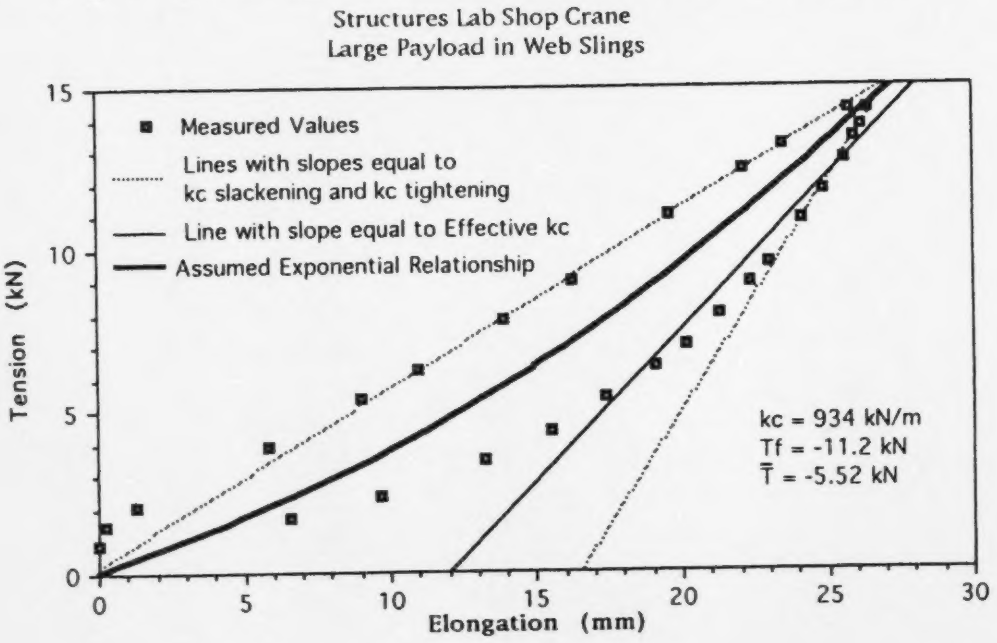

Table 4.3 Dynamic Ratios From Computer Simulations

$\Delta t = 0.001$ seconds, 5 Structural Modal D'soF Used

Motor Values : Effective Motor Mass = 45 tonnes
Maximum Motor Force = 10 kN
Initial Motor Force = 7 kN
Hoisting Speed = 0.1 m/s
Pullout Slip = 0.2
Initial Slope of Force versus Speed Curve = 0.4 kNs/m

Trolley at	midspan	midspan	east end	east end	midspan	midspan	east end	east end
Structure Model	"2"	"2"	"E"	"E"	"2"	"2"	"E"	"E"
Payload mass (tonnes)	1.46	1.46	1.46	1.46	0.211	0.211	0.211	0.211
Sling type	chain	web	chain	web	chain	web	chain	web
$k_{c\ effective}$ (kN/m)	2690	934	2690	934	697	183	697	183
T_f (kN)	-9.42	-11.2	-9.42	-11.2	-4.78	-4.37	-4.78	-4.37
$\bar{T}$ (kN)	-4.00	-5.52	-4.00	-5.52	-0.183	-0.476	-0.183	-0.476
Max' Displacement at Trolley (mm)	5.40	4.86	2.74	2.39	1.07	.755	,501	.361
Static Displacement at Trolley (mm)	3.91	3.91	1.90	1.90	.566	.566	.275	.275
Dynamic Ratio	1.38	1.24	1.44	1.25	1.89	1.34	1.82	1.31

CHAPTER 5

DERIVATION OF DYNAMIC FACTOR FORMULA

In Chapter 4 a numerical model was described and a procedure outlined with which to perform dynamic analyses of crane hoisting problems. One drawback to using this kind of dynamic analysis is that a lot of detailed information about the motor and cable is required for input. A structural engineer, doing dynamic calculations for an existing craneway system, and knowing the hoist motor to be used, could get information on the masses and diameters of the rotor and the gears and drum (or could make reasonable assumptions about those properties) and could derive the moments of inertia for those components. However, an engineer designing a new facility would generally not know the make or size of the hoist involved. Even if that information was known, hoists may be changed and systems altered as the needs of the facility change. It is dangerous to design for specific circumstances that can be easily changed when the facility is in service. In developing a procedure to determine the dynamic factor, the lack of control the designer has over future events should be considered. The tension stiffness relationships for cables, chains and web slings and motor torque versus speed curves are generally not readily available from manufacturers. Without some understanding of the sensitivity of the dynamic factor to the various input parameters, it is not good engineering practice to assume values. In this chapter a general solution will be developed for the hoisting and braking crane problem. The importance of the various parameters will be examined.

Another drawback of using the computer program to calculate the dynamic factor is that it takes time and effort to learn how the program uses the input data, and it takes time and effort to understand the results. The general solution developed in this chapter will be closed form and relatively simple to use.

The model which is used to derive the dynamic factor is described as follows. For a hoisting operation there are three D'soF. The effective mass of the hoist motor moves, the payload may move, and the bridge and the structure supporting the bridge move (deflect). These three D'soF are labeled y_m for the motor, y_p for the payload, and y_s for the structure. Similarly, m_m

denotes the equivalent mass of the motor, m_p the payload mass, and m_s the equivalent mass of the structure. (Section 4.1 contains a description of how the motor's rotational properties can be viewed as translational properties).

5.1 Reduction of Crane and Craneway Model to 1 DoF

At its simplest, the crane and craneway structure can be considered as a mass hanging on a spring, able to receive downward load through tension in the cable. This single DoF system is shown in Figure 5.1. The stiffness, k_s, of the spring is equal to the stiffness of the structure at the point of application of the load. The mass, m_s, however, is not the actual mass of the structure. The value of m_s is such that the behaviour of the single DoF system will be in some quantitative way similar to the real system. For example, the first natural frequency of the real system can be set equal to the natural frequency of the single DoF model. If the first natural frequency of the real structure is dominant in free vibration, then this model can provide acceptable results.

Consider the nature of m_s with this requirement. Let the bridge be modelled by a simply supported beam of the same span, having uniform section properties which correspond to the section properties of the bridge. The first natural frequency of the beam will be

$$\omega_{1\text{-beam}} = \pi^2 \sqrt{\frac{EI}{\bar{m} L^4}} \; . \tag{5.1}$$

The terms E, I, $\bar{m}$, and L are, respectively, Young's modulus, the moment of inertia, the distributed mass, and the span of the beam. At a particular location a distance x along the span, the vertical stiffness of the beam is

$$k_x = \frac{3LEI}{x^2(L-x)^2} \; . \tag{5.2}$$

A single DoF system consisting of a mass suspended from a spring is used to model the behaviour of the beam at location x. The stiffness of the spring is k_x, and the natural frequency of the single DoF system is the first natural

Figure 5.1 Single Degree of Freedom Model of Crane and Craneway Structure

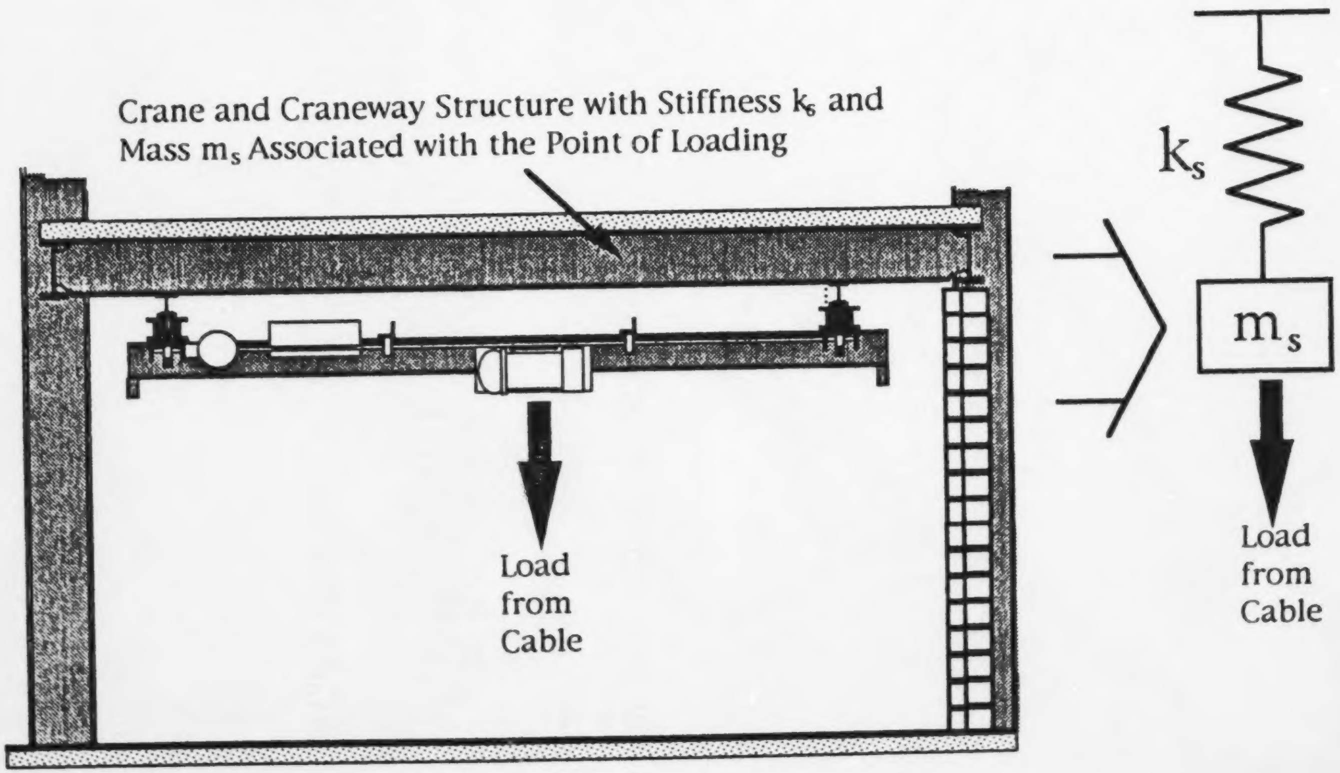

Crane and Craneway Structure with Stiffness k_s and Mass m_s Associated with the Point of Loading

Load
from
Cable
k_s
m_s
Load
from
Cable

frequency of the beam, $\omega_{1\text{-beam}}$. Therefore, the mass for the single DoF system is

$$m = \frac{k_x}{\omega^2_{1\text{-beam}}} = \frac{3L^5 \bar{m}}{\pi^4 x^2(L-x)^2} \quad . \tag{5.3}$$

It can be seen that the mass, m, which in the single DoF model accounts for the mass of the beam, is not the same magnitude as the mass of the actual beam.

To model the case of the trolley at location x on the bridge, a concentrated mass equal to the mass of the trolley is supported at location x on the beam. The first natural frequency of the beam and mass system is different from the first natural frequency of the beam alone. The difference can be approximately accounted for by adding the mass of the trolley to m, the mass of the single DoF system, because the displacements and accelerations associated with the first mode shape of the beam at location x are the same as the displacements and accelerations for the spring and mass system. The mass which accounts for the mass of the whole structure is referred to as m_s.

$$m_s = \frac{k_x}{\omega^2_{1\text{-beam}}} + \text{mass of trolley}$$

The first natural frequency of the beam with the trolley mass is

$$\omega_{1\text{-beam and trolley mass}} = \sqrt{\frac{k_x}{m_s}} = \sqrt{\frac{1}{\frac{\text{mass of trolley}}{k_x} + \frac{1}{\omega^2_{1\text{-beam}}}}} \quad . \tag{5.4}$$

Figure 5.2 shows the relative values of stiffness and effective mass along the span of a simply supported beam, and the associated natural frequencies for the single DoF system. The values used in Figure 5.2 are calculated using

Figure 5.2 Stiffness, Effective Mass, and Natural Frequency on a Simply Supported Beam

Stiffness versus Location on Span

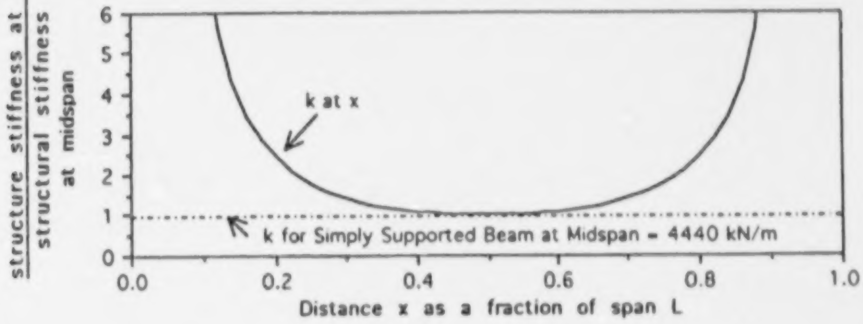

Effective Mass versus Location on Span

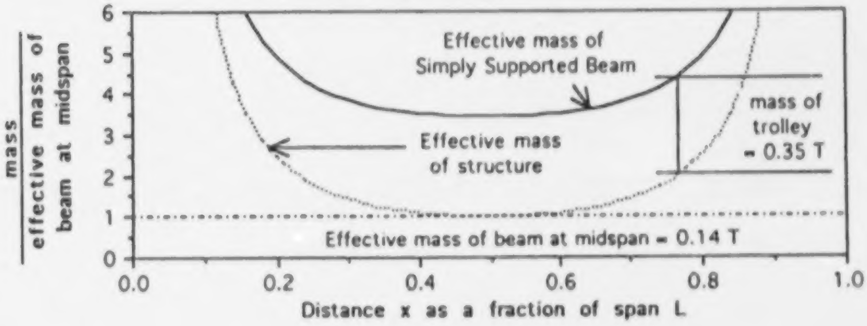

Natural Frequency versus Location on Span

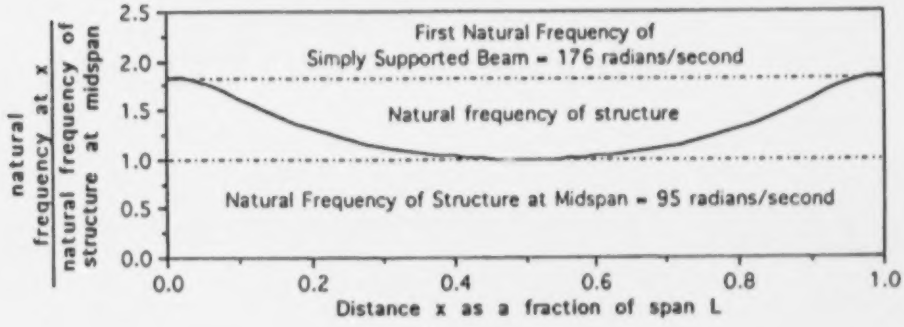

the section properties of the bridge beam of the shop crane (see Figure 2.2 and 2.3), and the mass of the trolley (see Table 2.1).

The preceding simple analogy does not account for the possibility of bridges with varying cross section, nor does it account for the finite stiffness of the craneway beams at each end of the simply supported bridge. However, the analogy does give a general impression of the values of k_s and m_s. Additional complexity in the structure does not necessarily limit the effectiveness of the single DoF model. A multi-DoF system can be developed which models the structure and accounts for craneway stiffness and other features. Stodola or Holzer iteration can be applied to the stiffness and mass matrices of such a multi-DoF system to quickly isolate a dominant first frequency [ref.9]. Table 5.1 lists the single stiffness and mass values for the two structures "E" and "2", using the first natural frequency.

Table 5.1 Effective Structure Mass from Models "2" and "E"

	Model "2"	Model "E"
Squared First Natural Frequency of Model, ω_1^2 (sec.)$^{-2}$	7334	10016
Stiffness of Model at Point of loading, k_s (kN/m)	3660	7524
Effective Structure mass, $m_s = \dfrac{k_s}{\omega^2}$ (tonnes)	0.499	0.751

Figures 5.3 shows the results from the computer program for the cases which uses the shop crane structure model "2". The hoisting event, in which the large payload is jerk-started using chain slings, is simulated. The values of the midspan bending moment and deflection of the bridge, and the reaction force of element 4 on node 5, are plotted versus time for a third of a second after the motor has been started. The first two peaks for these parameters is thus displayed. It can be seen that all the parameters are

Figure 5.3 2BC - Jerk-Starting

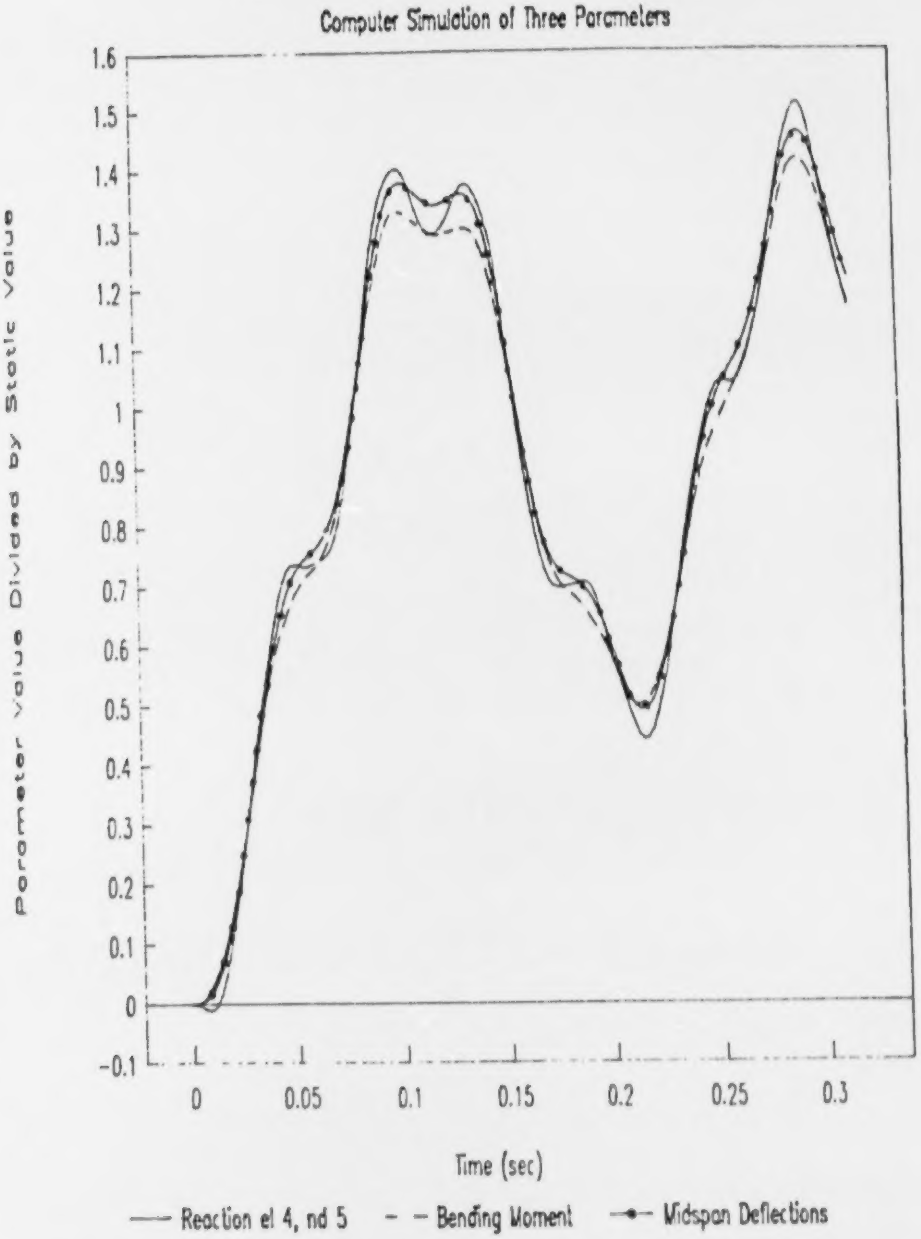
Computer Simulation of Three Parameters

roughly proportional to one another over this time interval. This implies that accurate results are obtainable when the shop crane is modelled as a single DoF system.

Let $y_s = 0$ when the crane carries no payload. The dynamic factor derived in this chapter is defined as the ratio $\frac{y_{s_{max}}}{y_{s_{static}}}$. The denominator, $y_{s_{static}}$, is the static deflection of the crane when it carries the payload of mass m_p. The numerator, $y_{s_{max}}$, is the maximum downwards deflection experienced by the crane during a particular hoisting event. Because the crane structure is modelled as a single DoF system, this ratio of deflections will be the same as the ratio of static and maximum tension in the spring representing the structure stiffness.

5.2 The Ratios κ and μ

Two dimensionless ratios, κ and μ, will be used in the discussion of various features of dynamic behaviour. They are defined below.

$$\kappa = \frac{k_s}{k_c} \qquad \text{and} \qquad \mu = \frac{m_s}{m_p} \ .$$

For a given payload and cable arrangement, the magnitudes of these two parameters vary depending on the lifting position of the trolley on the bridge and of the crane on the craneway. Crane geometry affects the value of κ. A very rough approximation of these affects can be gained by using as a model for a bridge crane, a simply supported beam on rigid supports, subject to a point load from an attached cable in tension. The stiffness of the structure is

$$k_s \propto \frac{E_s I}{L^3} \ , \qquad (5.5)$$

where E_s is Young's modulus for the structure, I is the moment of inertia of the cross section and L is the span. The cable has a stiffness roughly equal to $\frac{AE_c}{h}$, where A is the total cross sectional area of all the lines of cable, E_c is Young's modulus for the cable, and h is the length of the cable, or the height of the crane. Cable and sling sizes are selected to carry the rated load for the crane. For the purposes of this discussion, the capacity of the cable, a function of A, and the material strength σ, can be considered proportional to the rated load $m_p g$.

$$A \propto \frac{m_p g}{\sigma} \quad \text{and} \quad k_c \propto \frac{m_p g E_c}{\sigma h} \; .$$

Under these assumptions

$$\frac{k_s}{k_c} = \kappa \propto \frac{I \sigma h E_s}{L^3 m_p g \, E_c} \; . \tag{5.6}$$

This can be simplified further using the bending moment strength equation. The resisting moment should be greater than, but approximately proportional to, the sum of the dead and maximum live load moments. The maximum live load bending moment occurs when the live load is the rated capacity and is applied at midspan. For the level of this approximation, the effective mass, m_s, can be considered to be about half the actual mass of the crane.

$$(m_p + m_s)\, gL \propto \frac{\sigma_y I}{d} \; , \tag{5.7}$$

where d is the section depth and σ_y is the yield strength of the material. Multiplying the right side of expression (5.2) for κ by the constant $\dfrac{(m_p + m_s)\, gL}{\frac{\sigma_y I}{d}}$, gives the following.

$$\kappa \propto \left(\frac{I \sigma h E_s}{L^3 m_p g \, E_c}\right)\left(\frac{(m_p + m_s)\, gL}{\frac{\sigma_y I}{d}}\right) = (1+\mu)\left(\frac{hd}{L^2}\right)\left(\frac{\sigma}{\sigma_y}\right)\left(\frac{E_s}{E_c}\right) \tag{5.8}$$

The strength ratio and modulus ratio in equation (5.4) are functions of material properties. The term μ is the ratio of $\frac{m_s}{m_p}$. In general, larger cranes have greater mass and therefore a greater equivalent mass m_s, but they also have a greater rated load m_p. Although μ does vary with geometry, the change is slight, and the expression $(1+\mu)$ reduces the effect changes in μ have upon this approximation of κ. With respect to crane geometry, it can be said that the following approximate relationship holds.

$$\kappa \propto \frac{hd}{L^2} \tag{5.9}$$

Large and small cranes tend to have similar ranges for values of κ. Larger bridge cranes are generally higher and have longer spans and deeper sections. From Tables 2.2 and 5.1 the maximum and minimum values for κ associated with the tests on the shop crane are, respectively,

$$\frac{7890 \text{ kN/m}}{183\text{kN/m}} = 86.3 \text{ and } \frac{3680 \text{ kN/m}}{2686\text{kN/m}} = 1.43\,.$$

The standard range for most cranes which can use chains and web slings is probably from about 1 to 100.

The range for μ can also be examined. Considering the 1.46 tonne payload for the shop crane, the values for μ are

$$\frac{.499 \text{ tonnes}}{1.46 \text{ tonnes}} = 0.342\,, \text{ and } \frac{.751 \text{ tonnes}}{1.46 \text{ tonnes}} = 0.514.$$

(See Table 5.1.) For most bridge cranes the structure mass m_s, at center span is generally about half of the bridge's mass plus the trolley mass. The maximum value of m_s is between 1.5 and 5 times that. Small cranes with bridges fabricated from rolled sections will generally be rated to lift the equivalent of several times the bridge dead load, with this ratio decreasing as crane size increases. Cranes with box girder spans are generally rated to lift a load equal to about half their bridge dead loads. If m_p is considered the mass associated with the rated load, then μ ranges between 0.1 and 2.

5.3 Assembly of 3DoF Model

The models from Figures 4.8, 4.14, 4.15b, and 5.1, are assembled to give the model shown in Figure 5.4. This process is similar to the process outlined in Section 4.2, and Figure 5.4 is similar to Figure 4.16. The significant difference

Figure 5.4
Assembled 3 Degree of Freedom Model

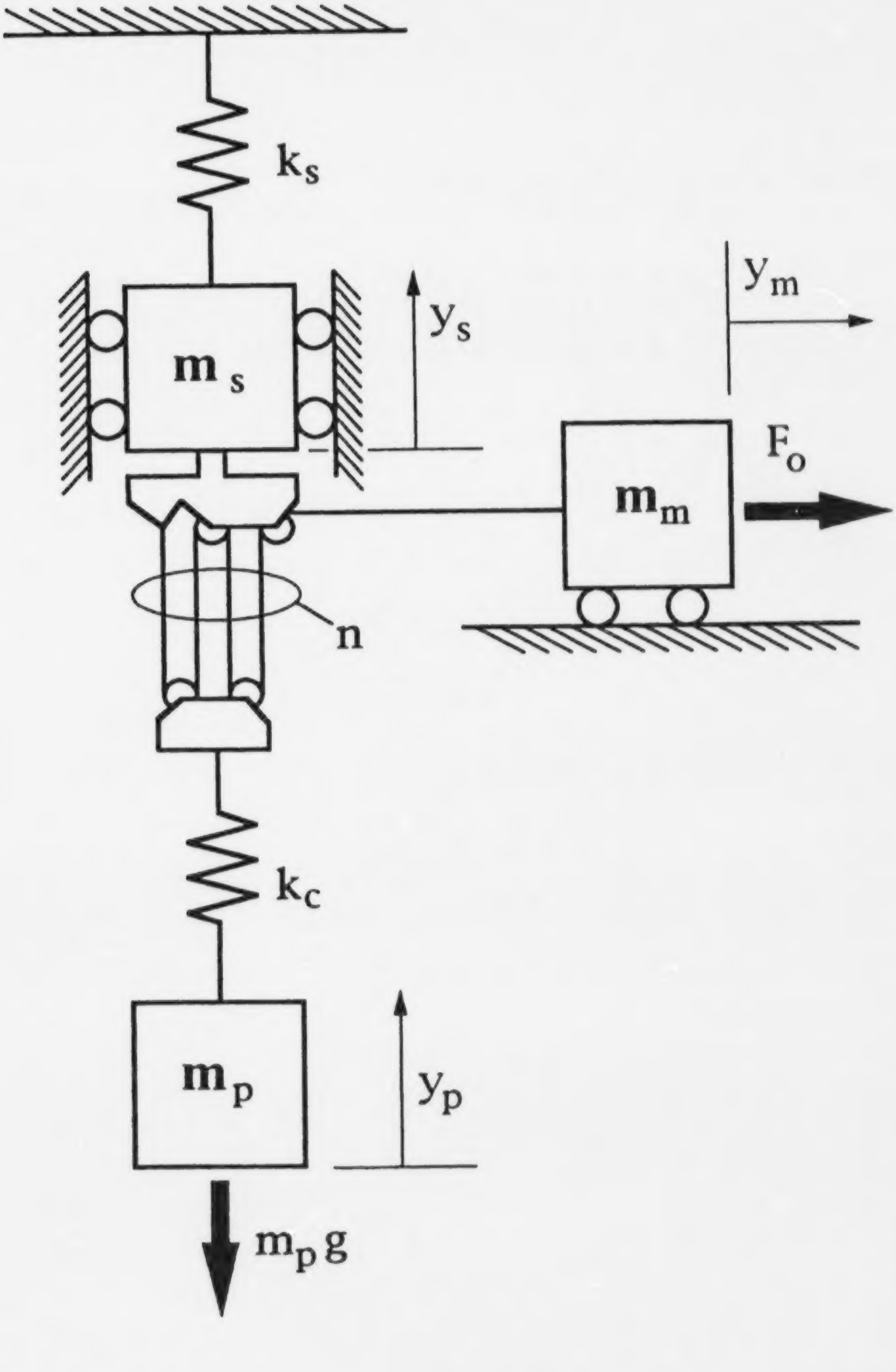
k_s
y_m
y_s
m_s
F_o
m_m
n
k_c
m_p
y_p
$m_p g$

is that the structure is now modelled as a single mass, m_s, attached to a single spring, of stiffness k_s. Rollers are included on the mass m_s to show that its motion is vertical only.

As in Section 4.2, D'Alembert's principle is invoked. Each of the three masses of the system shown in Figure 5.4 is considered as a body in dynamic equilibrium, and thus the vector sum of the inertial force and all the applied forces acting upon each of the bodies is equal to zero. The principle of virtual work is used to find the equations of motion of the system. The sum of the product of the spring forces and their virtual displacements plus the sum of the product of the inertial forces and their virtual displacements must equal the sum of the product of the applied forces and their virtual displacements. The derivation is shown below.

$$\Sigma f_S \delta + \Sigma f_I \delta = \Sigma f_A \delta$$

$$k_c\left(\frac{y_m}{n} - y_p + y_s\right)\left(\frac{\delta y_m}{n} - \delta y_p + \delta y_s\right) + k_s y_s \, \delta y_s$$

$$+ m_s \ddot{y}_s \delta y_s + m_m \ddot{y}_m \delta y_m + m_p \ddot{y}_p \delta y_p$$

$$= F_o \, \delta y_m - m_p g \delta y_p$$

$$\delta y_m \left(\frac{k_c y_m}{n^2} - \frac{k_c y_p}{n} + \frac{k_c y_s}{n} + m_m \ddot{y}_m - F_o\right)$$

$$+ \delta y_p \left(\frac{-k_c y_m}{n} + k_c y_p - k_c y_s + m_p \ddot{y}_p + m_p g\right)$$

$$+ \delta y_s \left(\frac{k_c y_m}{n} - k_c y_p + k_c y_s + k_s y_s + m_s \ddot{y}_s\right)$$

$$= 0 \quad \text{for arbitrary values of } \delta y_m, \delta y_p \text{ and } \delta y_s. \qquad (5.10)$$

To satisfy this requirement, the three bracketed expressions must each equal zero. This gives the equations of motion for the system, which can be written in matrix form as shown below.

$$\begin{bmatrix} \frac{k_c}{n^2} & -\frac{k_c}{n} & \frac{k_c}{n} \\ -\frac{k_c}{n} & k_c & -k_c \\ \frac{k_c}{n} & -k_c & k_c+k_s \end{bmatrix} \begin{Bmatrix} y_m \\ y_p \\ y_s \end{Bmatrix} + \begin{bmatrix} m_m & 0 & 0 \\ 0 & m_p & 0 \\ 0 & 0 & m_s \end{bmatrix} \begin{Bmatrix} \ddot{y}_m \\ \ddot{y}_p \\ \ddot{y}_s \end{Bmatrix} = \begin{Bmatrix} F_o \\ -m_p g \\ 0 \end{Bmatrix} \tag{5.11}$$

The three equations in (5.11) are the equations of motion for the individual masses in the 3 DoF system. It can be seen that the cable tension, denoted as T_c, can be defined by the following expression.

$$T_c = \frac{k_c}{n} y_m - k_c y_p + k_c y_s \tag{5.12}$$

A useful parameter is the cable elongation denoted as y_c, which is defined by the following expression.

$$y_c = \frac{y_m}{n} - y_p + y_s \tag{5.13}$$

Cable tension is related to the cable elongation through the cable stiffness k_c, and therefore

$$T_c = k_c y_c \, . \tag{5.14}$$

5.4 Derivation of Natural Frequencies and Mode Shapes

To find $y_{s_{static}}$ and $y_{s_{max}}$ for the dynamic factor, the system of equations in (5.11) must be solved. This is done by finding the natural frequencies and their eigenvectors and deriving the uncoupled modal D'soF. The solution for the eigenvalues and natural frequencies proceeds as follows. The expression

$$\left[[K] - \omega^2[M]\right] \{\phi\} = \{0\} \tag{5.15}$$

has non-zero solutions for an eigenvector, $\{\phi\}$, only if the determinant of $\left[[K] - \omega^2[M]\right]$ is equal to zero. That is

$$\begin{vmatrix} \frac{k_c}{n^2} - \omega^2 m_m & \frac{-k_c}{n} & \frac{k_c}{n} \\ \frac{-k_c}{n} & k_c - \omega^2 m_p & -k_c \\ \frac{k_c}{n} & -k_c & k_c + k_s - \omega^2 m_s \end{vmatrix} = 0. \tag{5.16}$$

$$\text{Let} \quad \Omega^2 = k_c\left(\frac{1}{n^2 m_m} + \frac{1}{m_p} + \frac{1}{m_s}\right), \tag{5.17}$$

and let the natural frequency of the structure, $\sqrt{\frac{k_s}{m_s}}$, be denoted by ω_s. The frequency $\sqrt{\frac{k_c}{m_p}}$ is denoted by ω_c, and is the natural frequency of a single DoF system consisting of the cable with one end attached to the payload and the other end fixed. Equation (5.16) can be rewritten as a cubic in ω^2.

$$\omega^6 - \omega^4 (\Omega^2 + \omega_s^2) + \omega^2 \omega_s^2 (\Omega^2 - \frac{\omega_s^2}{\kappa}) = 0 \tag{5.18}$$

The three roots are the squares of the three natural frequencies.

$$\omega_1^2 = 0 \tag{5.19}$$

$$\omega_2^2 = \frac{\Omega^2 + \omega_s^2 - \sqrt{(\Omega^2 + \omega_s^2)^2 - 4\omega_s^2\left(\omega_c^2 + \dfrac{k_c}{n^2 m_m}\right)}}{2} \tag{5.20}$$

$$\omega_3^2 = \frac{\Omega^2 + \omega_s^2 + \sqrt{(\Omega^2 + \omega_s^2)^2 - 4\omega_s^2\left(\omega_c^2 + \dfrac{k_c}{n^2 m_m}\right)}}{2} \tag{5.21}$$

With the frequencies determined, the non-trivial solutions to equation (5.15) can be found. For each of the three values of ω^2, equation (5.22) must be satisfied.

$$\begin{bmatrix} \dfrac{k_c}{n^2} - \omega^2 m_m & \dfrac{-k_c}{n} & \dfrac{k_c}{n} \\ \dfrac{-k_c}{n} & k_c - \omega^2 m_p & -k_c \\ \dfrac{k_c}{n} & -k_c & k_c + k_s - \omega^2 m_s \end{bmatrix} \begin{Bmatrix} \phi_1 \\ \phi_2 \\ \phi_3 \end{Bmatrix} = \begin{Bmatrix} 0 \\ 0 \\ 0 \end{Bmatrix} \tag{5.22}$$

If $k_s \neq 0$, then when $\omega^2 = 0$, there are two independent equations contained in (5.22) (The first two rows in the matrix are proportional). For the case in which $\omega^2 = 0$, let $\phi_1 = 1$. The second column is the negative of n times the first column. Therefore ϕ_2 equals $\frac{\phi_1}{n}$, or $\frac{1}{n}$, and $\phi_3 = 0$.

The solutions for $\{\phi\}$ when ω^2 is non-zero can be found, as well. Let $\phi_1 = \frac{m_s}{n m_m}$. Adding n times row 1 to row 2 gives an expression that can be solved for ϕ_2.

$$-n\omega^2 m_m \phi_1 - \omega^2 m_p \phi_2 = 0$$

$$\phi_2 = -\frac{m_s}{m_p} = -\mu \tag{5.23}$$

Subtracting n times row 1 from row 3 in equation (5.22) gives an expression that can be solved for ϕ_3.

$$n\omega^2 m_m \phi_1 + (k_s - \omega^2 m_s)\,\phi_3 = 0$$

$$\phi_3 = \frac{\omega^2}{\omega^2 - \omega_s^2} = 1 - \gamma \tag{5.24}$$

$$\text{where } \gamma = \frac{1}{1 - \frac{\omega^2}{\omega_s^2}} \tag{5.25}$$

The transformation matrix, $[\Phi]$, is a 3x3 matrix with columns comprising the three eigenvectors that correspond to the three natural frequencies. In the derivation in Chapter 4, the values of $[\Phi]$ are assigned dimensions of mass$^{-1/2}$. This was done so that the terms in $[\Phi]^T[M][\Phi]$ would be dimensionless. For the derivation in this chapter such a requirement is not advantageous. Instead, let the terms in $[\Phi]$ be dimensionless.

$$[\Phi] = \begin{bmatrix} 1 & \frac{m_s}{nm_m} & \frac{m_s}{nm_m} \\ \frac{1}{n} & -\mu & -\mu \\ 0 & 1-\gamma_2 & 1-\gamma_3 \end{bmatrix} \tag{5.26}$$

where γ_2 and γ_3 are the values for γ when the second and third natural frequencies, respectively, are substituted for ω in equation (5.25).

The ratio of peak to static displacements for an undamped single DoF system with a natural frequency ω, subjected to a harmonic forcing function of frequency $\bar{\omega}$, is $\left| \frac{1}{1 - \frac{\bar{\omega}^2}{\omega^2}} \right|$. The absolute values of γ_2 and γ_3 can therefore be seen to represent the dynamic ratios of the single DoF system of the structure, which has a natural frequency ω_s, if it were subject to harmonic forcing functions with frequencies of ω_2 and ω_3 respectively.

Each column in the $[\Phi]$ matrix, shown in equation (5.26), is associated with a mode shape. The relative magnitudes of the first, second, and third term in each column represent the relative displacements of y_m, y_p and y_s, respectively, for that mode.

For the first mode shape, if the displacement of the effective motor mass is unity, then the payload displacement is $\frac{1}{n}$, while the structure displacement is zero. This combination of displacements occurs without either of the springs in the system being stretched. The strain energy of the system is not changed as it experiences this set of displacements and the first mode is, therefore, a rigid body motion.

In Appendix D.2 it is shown that $\omega_2^2 < \omega_s^2 < \omega_3^2$. Therefore $1 - \gamma_2 < 0$ and $1 - \gamma_3 > 1$. For the second mode shape the sense (positive or negative) of the displacement of the effective motor mass is opposite to the sense of the displacement of the payload and structure. The second mode displacement of the model in Figure 5.4 has the displacement of the effective motor mass to the right with downward displacement of the payload and structure. The third mode has the payload displacement in the opposite sense to the motor and structure displacements.

Both modes two and three require elongation of the two springs in the system. The strain energy of the system changes as it undergoes displacements of the second and the third modes, which are therefore vibrational modes.

In Appendix D.3 it is shown that $\gamma_2 - 1 < \mu$. Therefore the magnitude of the second mode displacement of the payload is greater than the magnitude of the second mode displacement of the structure. Therefore, in the second mode, the structure spring and the cable spring are either both in compression or both in tension. In the third mode the sense of the movement of the structure and the payload are opposite, and so one is in compression whenever the other is in tension. The two springs are out of phase when in third mode motion.

5.5 Assumptions Concerning Motor Behaviour

In this section two assumptions are made about the behaviour of the motor. In the steady state case, the loaded motor runs at near synchronous speed. The first assumption is that once the motor is in steady state it has reached synchronous speed, and can develop the force required to put tension in the cable without changing from that speed. Therefore, y_m is a linear function of time. It follows that $\dot{y}_m$ is a constant velocity equal to $r_e\,\omega_o$, which will be called V_o. It also follows that $\ddot{y}_m$ is zero. Figure 5.5 shows a typical F_o versus $\dot{y}_m$ curve and the curve that results from this assumption.

There are two significant advantages in making this assumption. First, the differential equations have simple closed form solutions. Second, of the five parameters needed to describe the motor's forcing function, (see Section 4.1), only the hoisting speed is required, and it is the easiest to determine. The rated hoisting speed will be called H_o. It can be seen that

$$H_o = \frac{V_o}{n}\,, \tag{5.27}$$

where n is the number of lines of cable between the hook and the hoist.

The effective motor mass, m_m, is usually very large compared to the other masses, m_p and m_s. The second assumption, therefore, is that m_m approaches infinity and $\frac{1}{m_m}$ approaches zero. The advantage to using this limiting case to derive a dynamic factor is that determining a value for m_m is no longer necessary.

These two assumptions greatly simplify the derivation of the dynamic factor, but they pose an apparent paradox. Consider the first equation of motion for the 3 DoF system.

Figure 5.5 Assumption of Constant Speed Motor

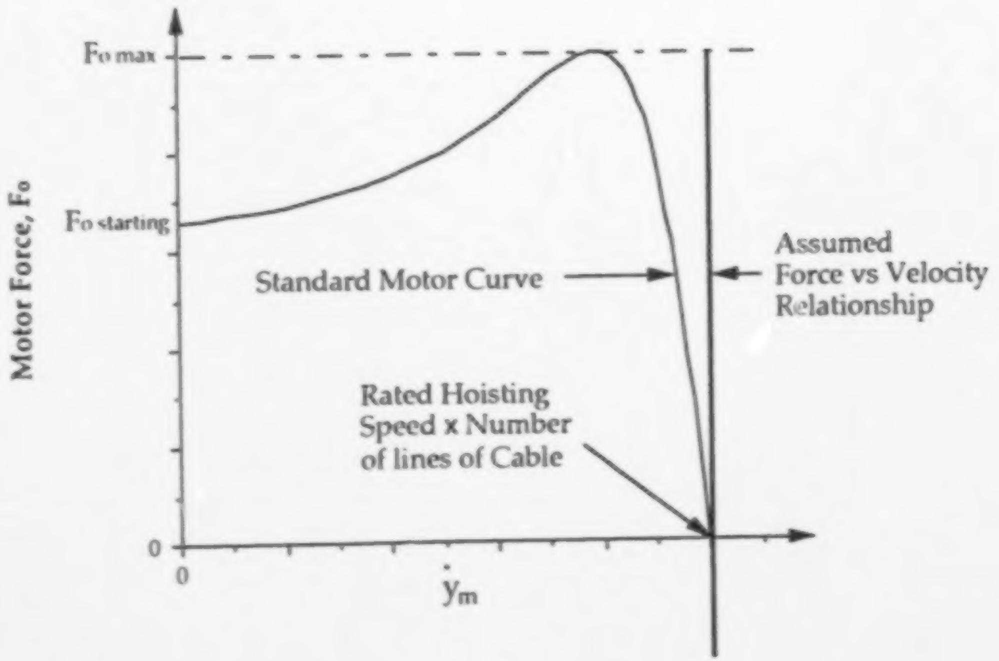

$$\frac{T_c}{n} + m_m \ddot{y}_m = F_o \tag{5.28}$$

The assumptions of constant motor speed and infinite motor mass leaves the term $m_m \ddot{y}_m$ undefined. If, in equation (5.28), the term $m_m \ddot{y}_m$ has no defined value, then T_c and F_o would be undefined as well. This is not satisfactory, and some definition of $m_m\ddot{y}_m$ is required. Two limiting definitions are compared. Figure 5.6 illustrates the two definitions which could apply to $m_m\ddot{y}_m$.

First, if a motor has an infinitely massive rotor, rotating at some rotational velocity, then applying a finite load to the cable will not alter the rotor's velocity. This defines $m_m \ddot{y}_m$ as being infinitely large. For finite values of T_c and F_o, equation (5.28) cannot apply. The cable tension and motor force are independent of one another.

However, in the real system, significantly increasing cable tension can cause an insignificant reduction in motor velocity and a significant increase in motor force. (See Figure 5.5) The second possible definition for $m_m \ddot{y}_m$ is based on the assumption that if the acceleration of the motor mass is defined as being zero, then the effective motor mass is in static equilibrium. The sum of the forces acting upon it must total zero, and therefore F_o equals $\frac{T_c}{n}$. This seems the more rational view because the motor force, F_o, is expected to influence the cable tension, T_c. By assuming that $\frac{1}{m_m}$ approaches zero while $\ddot{y}_m$ equals zero, it is implied that $m_m \ddot{y}_m$ equals zero, and that F_o equals $\frac{T_c}{n}$.

Several useful mathematical simplifications follow from the assumption that m_m approaches infinity. As m_m approaches infinity, equation (5.17) becomes the following.

$$\Omega^2 = k_c\left(\frac{1}{m_p} + \frac{1}{m_s}\right) = \omega_c^2 + \frac{k_c}{m_s} \tag{5.29}$$

The same substitution for m_m into equations (5.20) and (5.21) results in new expressions for the natural frequencies.

Figure 5.6 Two Interpretations of Infinite Mass and No Acceleration

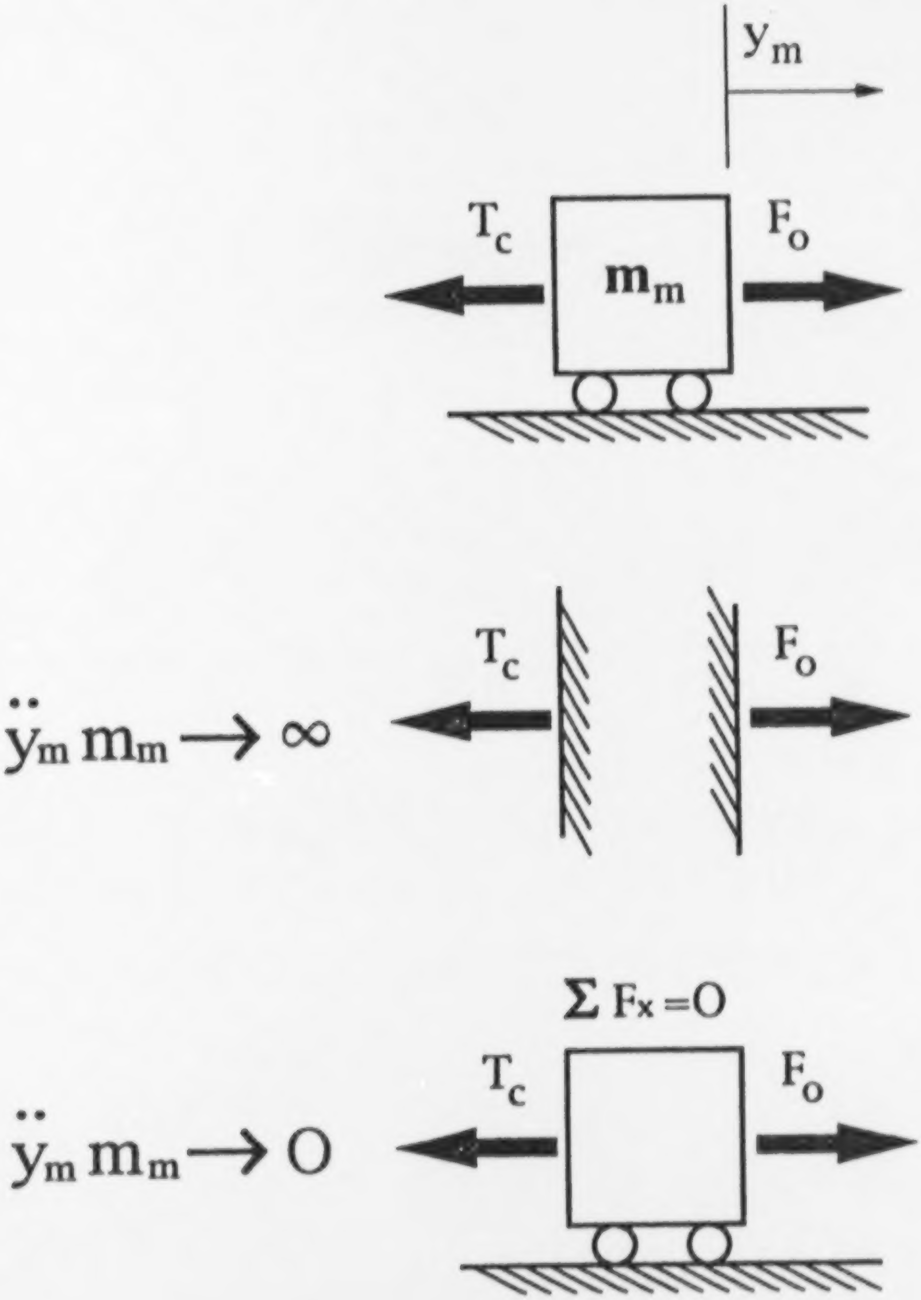
y_m
T_c
F_o
m_m
T_c
F_o
$\ddot{y}_m m_m \rightarrow \infty$
$\Sigma F_x = 0$
T_c
F_o
$\ddot{y}_m m_m \rightarrow 0$

$$\omega_2^2 = \frac{\Omega^2 + \omega_s^2 - \sqrt{(\Omega^2 + \omega_s^2)^2 - 4\omega_s^2\,\omega_c^2}}{2} \tag{5.30}$$

$$\omega_3^2 = \frac{\Omega^2 + \omega_s^2 + \sqrt{(\Omega^2 + \omega_s^2)^2 - 4\omega_s^2\,\omega_c^2}}{2} \tag{5.31}$$

5.6 Solution for Modal Degrees of Freedom

Let the three modal D'soF for the system be w_1, w_2, and w_3, such that $[\Phi]\{W\} = \{Y\}$. Expressions for the modal D'soF can be derived in terms of y_m, y_p, and y_s. The three equations from (5.26) are as follows.

$$w_1 + \frac{m_s}{nm_m}(w_2 + w_3) = y_m \tag{5.32}$$

$$\frac{w_1}{n} - \mu(w_2 + w_3) = y_p \tag{5.33}$$

$$(1 - \gamma_2)w_2 + (1 - \gamma_3)w_3 = y_s \tag{5.34}$$

Letting m_m approach infinity in equation (5.32), and substituting the resulting value for w_1 into equation (5.33), provides a solvable equation which can be used to derive expressions for the two unknowns, w_2 and w_3.

$$\mu(w_2 + w_3) = \frac{y_m}{n} - y_p \tag{5.35}$$

In Appendix D.3 it is shown that when m_m approaches infinity, $(1 - \gamma_2)(1 - \gamma_3)$ approaches $-\mu$. Using this relationship, equations (5.35) and (5.34) can be rewritten as expressions for the modal D'soF.

$$w_2 = \frac{\frac{y_m}{n} - y_p + (1-\gamma_2)\,y_s}{(1-\gamma_2)(\gamma_3-\gamma_2)} \tag{5.36}$$

and $$w_3 = \frac{\frac{y_m}{n} - y_p + (1-\gamma_3)\,y_s}{(1-\gamma_3)(\gamma_2-\gamma_3)} \tag{5.37}$$

The compatibility equation (5.13), $y_c = \frac{y_m}{n} - y_p + y_s$, can be used to put equations (5.36) and (5.37) into the following form.

$$w_2 = \frac{y_c - \gamma_2 y_s}{(1-\gamma_2)(\gamma_3-\gamma_2)} \tag{5.38}$$

$$w_3 = \frac{y_c - \gamma_3 y_s}{(1-\gamma_3)(\gamma_2-\gamma_3)} \tag{5.39}$$

5.7 General Solution for the Uncoupled Equations of Motion

Uncoupling the equations of motion in (5.11) requires premultiplying them by $[\Phi]^T$ as shown in equation (5.40) below.

$$\left[[\Phi]^T[K]\,[\Phi]\right]\{W\} + \left[[\Phi]^T[M]\,[\Phi]\right]\{\ddot{W}\} = [\Phi]^T\begin{Bmatrix} F_o \\ -\,m_p g \\ 0 \end{Bmatrix} \tag{5.40}$$

The expressions for the three modal masses are derived in Appendix D.5. The modal mass matrix is shown in equation (5.41) below.

$$[[\Phi]^T[M][\Phi]] = \begin{bmatrix} m_m + \frac{m_p}{n^2} & 0 & 0 \\ 0 & m_s(1-\gamma_2)(\gamma_3-\gamma_2) & 0 \\ 0 & 0 & m_s(1-\gamma_3)(\gamma_2-\gamma_3) \end{bmatrix} \tag{5.41}$$

Dividing each row in equation (5.40) by its modal mass gives the following set of uncoupled equations of motion.

$$\ddot{w}_1 = \frac{F_o - \frac{m_p g}{n}}{m_m + \frac{m_p}{n^2}} \tag{5.42}$$

$$\omega_2^2 w_2 + \ddot{w}_2 = \frac{\frac{m_s}{n m_m} F_o + \frac{m_s}{m_p} m_p g}{m_s(1-\gamma_2)(\gamma_3-\gamma_2)} = \frac{\frac{F_o}{n m_m} + g}{(1-\gamma_2)(\gamma_3-\gamma_2)} \tag{5.43}$$

$$\omega_3^2 w_3 + \ddot{w}_3 = \frac{\frac{m_s}{n m_m} F_o + \frac{m_s}{m_p} m_p g}{m_s(1-\gamma_3)(\gamma_2-\gamma_3)} = \frac{\frac{F_o}{n m_m} + g}{(1-\gamma_3)(\gamma_2-\gamma_3)} \tag{5.44}$$

In the limit as m_m goes to infinity, equations (5.42), (5.43), and (5.44) take the following form.

$$\ddot{w}_1 = 0 \tag{5.45}$$

$$\omega_2^2 w_2 + \ddot{w}_2 = \frac{g}{(1-\gamma_2)(\gamma_3-\gamma_2)} \tag{5.46}$$

$$\omega_3^2 w_3 + \ddot{w}_3 = \frac{g}{(1-\gamma_3)(\gamma_2-\gamma_3)} \tag{5.47}$$

To find the dynamic factor requires the solution for y_s. From equation (5.34), the solution for y_s involves w_2 and w_3 only. The general solutions for w_2 and w_3 have the following form.

$$w_2 = A_2 \sin(\omega_2 t + \theta_2) + B_2 \qquad w_3 = A_3 \sin(\omega_3 t + \theta_3) + B_3 \qquad (5.48)$$

$$\dot{w}_2 = A_2\, \omega_2 \cos(\omega_2 t + \theta_2) \qquad \dot{w}_3 = A_3\, \omega_3 \cos(\omega_3 t + \theta_3) \qquad (5.49)$$

$$\ddot{w}_2 = -A_2\, \omega_2^2 \sin(\omega_2 t + \theta_2) \qquad \ddot{w}_3 = -A_3\, \omega_3^2 \sin(\omega_3 t + \theta_3) \qquad (5.50)$$

Substituting the modal D'soF and their second derivatives from equations (5.48) and (5.50) into equations (5.46) and (5.47) respectively, gives the following solutions for B_2 and B_3.

$$B_2 = \frac{g}{\omega_2^2\,(1 - \gamma_2)\,(\gamma_3 - \gamma_2)} \qquad (5.51)$$

$$B_3 = \frac{g}{\omega_3^2\,(1 - \gamma_3)\,(\gamma_2 - \gamma_3)} \qquad (5.52)$$

Expressions for the unknowns, A and θ, can be determined from the initial conditions.

5.8 Initial Conditions

Two cases of hoist-induced dynamic loading are considered. The first is the dynamic response due to the previously stationary payload accelerating upwards. The second is the dynamic response due to the hoist motor stopping. Dynamic factors for both cases will be derived. The problems that arise in the derivations for each case are quite different.

In the starting scenario, initial conditions must be derived that can be used in the steady state equations derived in Section 5.7. The steady state equations are based upon assumptions that do not apply between the time at which the hoist motor is turned on and the time at which steady state is reached. In particular:

1) In the steady state, it is assumed that k_c is constant, but in Section 2.5 it was shown that k_c varies greatly with cable tension, and is near zero when cable tension is near zero.

2) In steady state it is assumed that motor speed $\dot{y}_m$ is constant at V_o, but this clearly is not the case during the first moments of operation of the motor.

3) In the steady state situation, F_o has been defined as being equal to cable tension. The value of F_o does not really affect the behaviour of the steady state model given that $\dot{y}_m$ is constant. However, before steady state is reached, F_o is a function of $\dot{y}_m$, and the value of F_o determines the amount of tension in the cable and the acceleration of the motor mass.

4) The motor mass is assumed infinite in the steady state case. This simplifying assumption is allowable during the steady state because $\dot{y}_m$ is assumed to be constant and $\ddot{y}_m$ is assumed equal to zero. Prior to the steady state condition, $\ddot{y}_m$ is not zero, and all the terms in the equation of motion for the motor, equation (5.28), must be finite. A value for m_m must be chosen, and the accuracy of that value will affect the accuracy of the dynamic factor.

The initial conditions should describe the most severe in service starting conditions. For example, the stationary payload may be on the ground, or partially or wholly suspended by the cable, and the starting cable tension will be between zero and $m_p g$.

Braking is the other case to be examined. Braking, in the present context, is not to be confused with the motor going into braking mode, which occurs when the motor is powered but is turning backwards under the influence of an external torque larger than the starting torque. (see Section 4.1.1). The braking event that is dealt with here occurs when the motor is turned off, and its electric field and the torque produced instantly vanish. At that moment a mechanical brake is activated which holds the rotor stationary with respect to the stator. Thus $\ddot{y}_m$ and F_o very quickly become zero and the model becomes a 2 DoF system. The various features of the motor, its $F_o(\dot{y}_m)$ function and its equivalent mass, m_m, do not have to be dealt with. The dynamic factor due to the action of braking must be derived from a different set of equations of motion from those given in equation (5.11). It is the solution to the equations of motion in (5.11) that gives the initial conditions for the braking equations of motion. The amplitude of the vibrations of the structure which occur after braking is initiated will be a function not only of the properties of the brake, but also of the vibrations present prior to braking, and the phase of those vibrations at the moment the brake was applied. The phase of the vibrations at the instant of braking may be different each time the brakes are applied during the service life of a crane. The braking event has this random aspect to it and a dynamic factor for braking should take it into account.

5.8.1 Initial Conditions for Starting

In this section a variety of starting conditions are examined. Jerk-starting is assumed to be the critical case. Assumptions are made about the behaviour of the structure prior to payload lift off, and the initial values for the D'soF are determined for the jerk-starting case. These are substituted back into the general differential equations and an expression for the dynamic factor is derived.

5.8.1.1 Assumption that Jerk-Starting is the Critical Case

In the jerk-starting case the motor is started while the payload is on the ground. There is enough slack in the cable to let the motor reach and stabilize at its synchronous speed before any tension develops in the cable. At the moment that the cable tightens the difference in speed between $\dot{y}_s$, which equals zero, and y_m, which equals V_o, is greater than for any other starting case. The assumption is made that jerk-starting is the critical starting case which causes the greatest dynamic displacements of the structure. The dynamic factor D is based upon this starting case.

Because in the jerk-starting case there is enough slack in the cable to let the motor reach and stabilize at its synchronous speed before any tension develops in the cable, the assumptions of constant motor speed and infinite motor mass are applicable. These two assumptions are only valid for the jerk-starting case. For any other starting condition, the cable develops tension and the structure deflects when $\dot{y}_m$ is less than V_o and $\ddot{y}_m$ is not zero.

For the case in which the payload is on the ground, the equations of motion in (5.11), are simplified because y_p and its derivatives are all equal to zero. That is to say, the payload is motionless. The number of D'soF of the system is reduced from three to two and the equations of motion become

$$\begin{bmatrix} \frac{k_c}{n^2} & \frac{k_c}{n} \\ \frac{k_c}{n} & k_c+k_s \end{bmatrix} \begin{Bmatrix} y_m \\ y_s \end{Bmatrix} + \begin{bmatrix} m_m & 0 \\ 0 & m_s \end{bmatrix} \begin{Bmatrix} \ddot{y}_m \\ \ddot{y}_s \end{Bmatrix} = \begin{Bmatrix} F_o \\ 0 \end{Bmatrix} . \tag{5.53}$$

Under the assumption of constant motor speed, the solution for y_m is

$$y_m = V_o\, t \ , \tag{5.54}$$

and the equation of motion for y_s, from equation (5.53), is

$$\left(\frac{k_c + k_s}{m_s}\right) y_s + \ddot{y}_s = -\frac{k_c\, V_o\, t}{n m_s} \ . \tag{5.55}$$

5.8.1.2 Assumptions Concerning Cable Behaviour

There are two ways to proceed from this point. One is to assume that the cable has a constant stiffness and is linearly elastic throughout the test. The other is to account for the changing stiffness of the cable.

1.) Consider first the development using a cable with constant k_c. Let the frequency of vibration of the structure prior to payload lift off be defined as ω_i, such that

$$\omega_i^2 = \frac{k_c + k_s}{m_s} \quad . \tag{5.56}$$

Solving equation (5.55), the expressions for y_s and its derivatives can be written as functions of time.

$$y_s = A \sin(\omega_i t + \theta) + \frac{k_c H_o t}{\omega_i^2 m_s} \tag{5.57}$$

$$\dot{y}_s = A\, \omega_i \cos(\omega_i t + \theta) + \frac{k_c H_o}{\omega_i^2 m_s} \tag{5.58}$$

$$\ddot{y}_s = -A\, \omega_i^2 \sin(\omega_i t + \theta) \tag{5.59}$$

When $t = 0$, $y_s = 0$. Therefore, from equation (5.57), $\theta = 0$, and from equation (5.58), the amplitude A is

$$A = \frac{k_c H_o}{\omega_i^3 m_s} \quad . \tag{5.60}$$

Substituting for A and θ in equations (5.57), (5.58), and (5.59) gives the following.

$$y_s = \frac{k_c H_o}{\omega_i^3 m_s} \left(\sin \omega_i t - \omega_i t \right) \tag{5.61}$$

$$\dot{y}_s = \frac{k_c H_o}{\omega_i^2 m_s} \left(\cos \omega_i t - 1 \right) \tag{5.62}$$

$$\ddot{y}_s = - \frac{k_c H_o}{\omega_i m_s} \sin \omega_i t \tag{5.63}$$

When the payload is on the verge of lift off, the cable tension, T_c, equals $m_p g$, the payload weight. Using equations (5.13) and (5.14), and given that $y_p = 0$, an expression for y_c is obtained.

$$y_c = \frac{y_m}{n} + y_s = \frac{m_p g}{k_c} \tag{5.64}$$

Substituting the expression for y_m from equation (5.54) and for y_s from equation (5.61) into equation (5.64) gives an expression from which the value of t at payload lift off can be determined.

$$H_o t + \frac{k_c H_o}{\omega_i^3 m_s} (\sin \omega_i t - \omega_i t) = \frac{m_p g}{k_c}$$

$$H_o \left(1 - \frac{k_c}{\omega_i^2 m_s} \right) t + \frac{k_c H_o}{\omega_i^3 m_s} \sin \omega_i t = \frac{m_p g}{k_c}$$

$$\left(\frac{H_o \kappa}{1 + \kappa} \right) \omega_i t + \left(\frac{H_o}{1 + \kappa} \right) \sin \omega_i t = \frac{m_p g \omega_i}{k_c}$$

$$\kappa \omega_i t + \sin \omega_i t = \frac{g}{H_o \omega_c} \sqrt{\frac{(1 + \kappa)^3}{\mu}} \qquad (5.65)$$

If the constant k_c analysis is continued, then equation (5.65) must be solved iteratively, and the value for t substituted into equations (5.61), (5.62), (5.63), and (5.54). The resulting values for y_s and its derivatives and the assumed values for $\dot{y}_m$ and $\ddot{y}_m$ would then be used as the initial conditions for the differential equations derived in Section 5.6 and 5.7.

A difficulty arising from this procedure is that there is no closed form solution for t in equation (5.65). Also, the need to solve accurately for the value of t at lift off can be questioned. The real cable is not linearly elastic. At low tensions k_c becomes very small (see Figures 2.9, 2.10, and 2.11). A small starting value for k_c will give a small starting value for the amplitude A. A small starting value for k_c will also cause the frequency ω_i, defined in equation (5.56), to be a minimum when the cable tension is lowest. If, in the real system, both the amplitude and the frequency have been increasing as cable tension approaches $m_p g$, then the value for t from equation (5.65) is not likely to be the actual time between motor actuation and payload lift off. The calculated time, t, may vary from the actual time to lift off by a significant fraction of the period $\frac{2\pi}{\omega_i}$, where ω_i is the frequency used in equations (5.61), (5.62), and (5.63). If the value of t from equation (5.65) is not related to the behaviour of the real system, then the accuracy of the values of y_s, $\dot{y}_s$, and $\ddot{y}_s$ which result from using t in equations (5.61), (5.62), and (5.63), must be suspect, especially as these equations include periodic functions.

2.) Consider now the analysis incorporating a non-constant value for k_c. If some function for k_c in terms of y_s is substituted into equation (5.55), that differential equation becomes difficult to solve. Furthermore, it is unlikely that the correct values for the constants required in such a function for k_c would be known to, or available for, a design engineer.

The simplest way to account for the variation of k_c, and the approach taken in the following development, is to assume that the motion of the structure is quasi-static prior to the time of payload lift off. The trigonometric terms in equations (5.61) (5.62) (5.63) are assumed to not contribute significantly to the values of y_s, $\dot{y}_s$, and $\ddot{y}_s$, and are set equal to zero. The equations for the velocity and acceleration of the structure at the moment of payload lift off become

$$\dot{y}_s = - \frac{k_c H_o}{\omega_1^2 m_s} = - \frac{H_o}{1 + \kappa} , \tag{5.66}$$

$$\text{and } \ddot{y}_s = 0 . \tag{5.67}$$

The value of k_c in equation (5.66) is assumed constant. The greatest changes in cable stiffness occur when cable tension is low. Payload lift off occurs when cable tension is equal to the weight of the cable. When the cable tension is near that level changes in cable stiffness are minimized. (See Figures 2.9, 2.10, and 2.11.)

The initial displacements, y_s and y_c, are determined as follows. When the payload is on the verge of motion, the tension in the cable must be $m_p g$, and, from equation (5.14), $y_c = \frac{m_p g}{k_c}$. Because $\ddot{y}_s$ is assumed equal to zero, all the tension must be resisted by the stiffness of the structure. Therefore, from equation (5.28), $y_s = -\frac{m_p g}{k_s}$.

The initial velocity, $\dot{y}_c$, is also determined. Equation (5.13) can be differentiated with respect to time. The payload is stationary and the assumption has been made that the motor's velocity will be the constant V_o, and therefore

$$\dot{y}_c = \frac{\dot{y}_m}{n} - \dot{y}_p + \dot{y}_s = \frac{V_o}{n} - 0 + \dot{y}_s = H_o + \dot{y}_s . \tag{5.68}$$

Substituting the value of $\dot{y}_s$ from equation (5.66) into (5.68) gives the solution for the rate of elongation of the cable.

$$\dot{y}_c = \frac{H_o \kappa}{1 + \kappa} \tag{5.69}$$

Since the accelerations of both the structure and the motor have been assumed equal to zero, and the payload is not yet in motion, the cable acceleration must also equal zero. Therefore, when the payload is on the verge of lifting off, the values of y_s and y_c and their derivatives, using the quasi-static analysis, are as follows.

$$y_s = -\frac{m_p g}{k_s} \qquad y_c = \frac{m_p g}{k_c}$$

$$\dot{y}_s = \frac{-H_o}{1 + \kappa} \qquad \dot{y}_c = \frac{H_o \kappa}{1 + \kappa}$$

$$\ddot{y}_s = 0 \qquad \ddot{y}_c = 0 \tag{5.70}$$

Figure 5.7 is a graph of the velocities $\dot{y}_m$, $\dot{y}_p$, $\dot{y}_s$, and $\dot{y}_c$ which result from the quasi-static approach. The curves are plotted from the time of activation of the motor till just after the payload lifts off. The advantage of the quasi-static approach over the constant k_c approach is that the time of lift off does not have to be calculated and a closed form solution for a dynamic factor can be developed.

Figure 5.7 Assumed Time Histories of Velocities for Jerk-Starting

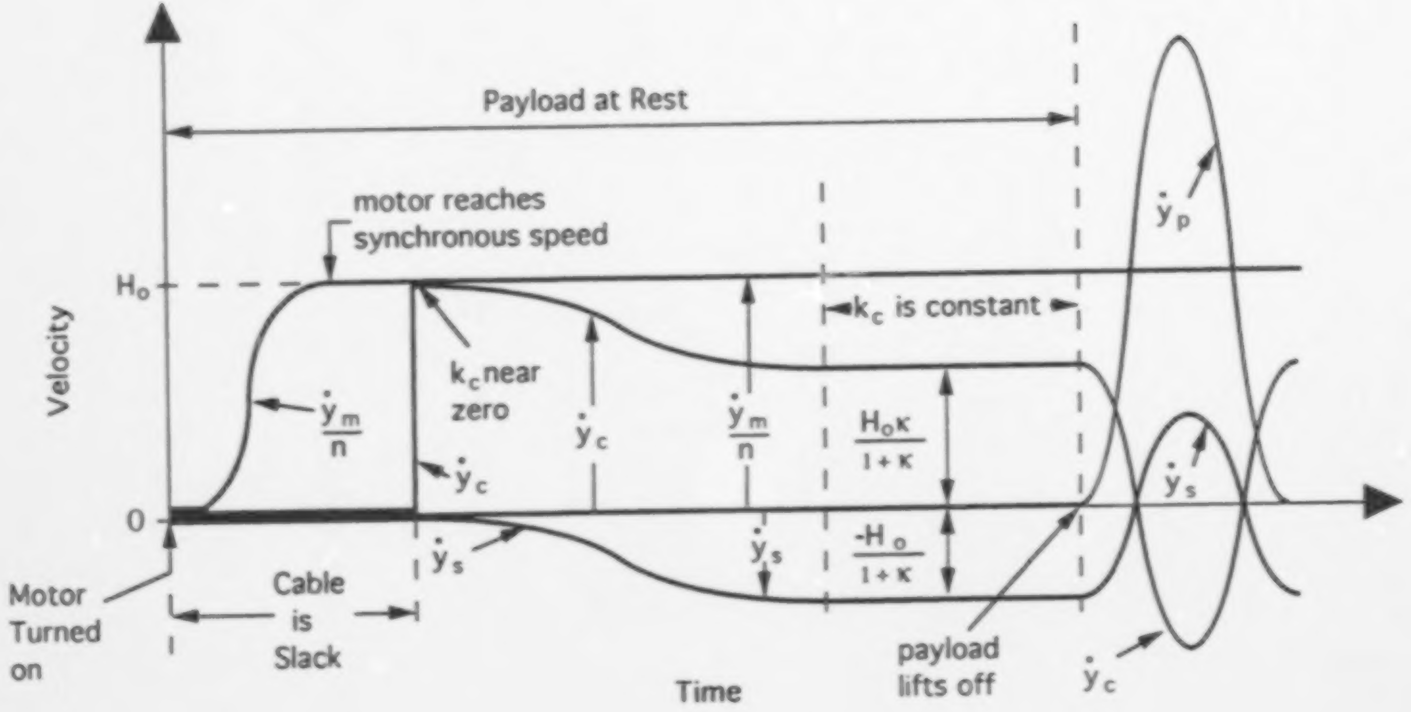

5.8.1.2.1 Validity of the Assumption of Quasi-Static Behaviour

The validity of the assumption that the structure behaves in a quasi-static manner is examined by comparing the vibrational amplitude, from equation (5.60), with $\frac{m_p g}{k_s}$, the static displacement of the structure bearing the weight of the payload. If the ratio of the amplitude to the static displacement is much less than unity, then the assumption is valid.

$$\frac{k_c\, k_s\, H_0}{\omega_1^3\, m_s\, m_p} = \frac{H_0 \omega_c}{g} \frac{\kappa\sqrt{\mu}}{\sqrt{(1+\kappa)^3}} \ll 1 \qquad (5.71)$$

The condition in (5.71) is sufficient, but not necessary, in order that the response of the structure prior to payload lift off be quasi-static. The value from equation (5.60) is an upper limit on the magnitude of the vibrational amplitude.

Table 5.2 shows the values of the left side of the inequality in (5.71) which result from various combinations of payload mass, hoisting position, and cable stiffness, for the structures lab shop crane. It can be seen that all the values are smaller than unity. At least five of the eight, and perhaps six can be considered small enough to satisfy the criterion in (5.71) above.

Values from sources other than the shop crane can also be used in (5.71) to test the validity of the assumption of quasi-static behaviour. Consider an undamped single DoF system comprising a cable of stiffness k_c fixed at one end and supporting a payload of mass m_p. When this system is subject to a free vibration in which the maximum velocity is H_0, the amplitude of the displacement of the mass about its static position is $\frac{H_0}{\omega_c}$. The static displacement of the suspended payload is $\frac{m_p g}{k_c}$. Therefore, the ratio of the amplitude to the static displacement is $\frac{H_0 \omega_c}{g}$. Cable tension and payload displacement are proportional because the system has only one DoF. Therefore the dynamic ratio also applies to the cable tension, and to the force

Table 5.2 Values of $\frac{H_o\omega_c}{g}\frac{\kappa\sqrt{\mu}}{\sqrt{(1+\kappa)^3}}$ for Test Setups for Shop Crane

Trolley at	midspan	midspan	east end	east end	midspan	midspan	east end	east end
Payload mass (tonnes)	1.46	1.46	1.46	1.46	0.211	0.211	0.211	0.211
Sling type	chain	web	chain	web	chain	web	chain	web
k_s (kN/m)	3840	3840	7590	7590	3840	3840	7590	7590
k_c effective (kN/m)	2690	934	2690	934	697	183	697	183
m_s (tonnes)	0.499	0.499	0.751	0.751	0.499	0.499	0.751	0.751
m_p (tonnes)	1.46	1.46	1.46	1.46	0.211	0.211	0.211	0.211
ω_c (radians/second)	43	25	43	25	57	29	57	29
κ	1.43	4.11	2.83	8.13	5.51	21.0	10.9	41.5
μ	0.342	0.342	0.514	0.514	2.37	2.37	3.56	3.56
$\frac{H_o\omega_c}{g}\frac{\kappa\sqrt{\mu}}{\sqrt{(1+\kappa)^3}}$	0.096	0.054	0.118	0.054	0.299	0.094	0.294	0.085

acting upon the rigid support to which the upper end of the cable is fixed. This system corresponds approximately to the real system of a crane with a hoisting speed of H_o and a high value of κ. The maximum cable tension acting upon the crane is greater than the static cable tension, $m_p g$, by a factor of $1 + \frac{H_o \omega_c}{g}$. In the standards reviewed in Chapter 3, a hoisting situation of this description would generally require a relatively high dynamic factor, such as 1.5, for example. Therefore, a value of 0.5 can be substituted into expression (5.71) for $\frac{H_o \omega_c}{g}$, for the case of cranes with high values of κ. Values of 100 and 2 can be substituted into expression (5.71) for κ and μ, respectively. Both these values are fairly high for the two parameters. A high value for κ is consistent with the conditions that lead to the assumption of a value of 0.5 for $\frac{H_o \omega_c}{g}$. A high value for μ gives a high value for the left side of the expression in (5.71). When these substitutions are made the left side of (5.71) is equal to 0.14, which may be considered significantly less than unity.

The expression $\frac{\kappa\sqrt{\mu}}{\sqrt{(1+\kappa)^3}}$ in (5.71) is a maximum with respect to κ when $\kappa = 2$. For this value of κ it is not generally the case that $\frac{H_o \omega_c}{g}$ is equal to 0.5. For the same value of μ, the maximum value for $\frac{\kappa\sqrt{\mu}}{\sqrt{(1+\kappa)^3}}$ is 3.9 times greater than the its value when $\kappa = 100$. If μ is reduced by a factor greater than $3.9^2 = 15.2$ when κ is reduced by a factor of $\frac{100}{2} = 50$, then the condition set in equation (5.71) is still met and the structure can be considered to behave in a quasi-static manner prior to payload lift off.

The validity of the assumption of quasi-static behaviour can also be considered based upon the results from computer simulations. In Figure 5.8 cable tension versus cable elongation for three jerk-starting simulations is shown. The value of the parameter T_f varies (see Figure 4.17). In one simulation the cable stiffness is the constant k_c, and in the other three, cable stiffness increases as cable tension increases, assymptotically approaching a line with slope k_c. The hoisting of a 20 kN payload is simulated.

Figure 5.8 Comparison of One Linear and Three Non-Linear Cable Tension versus Elongation Curves

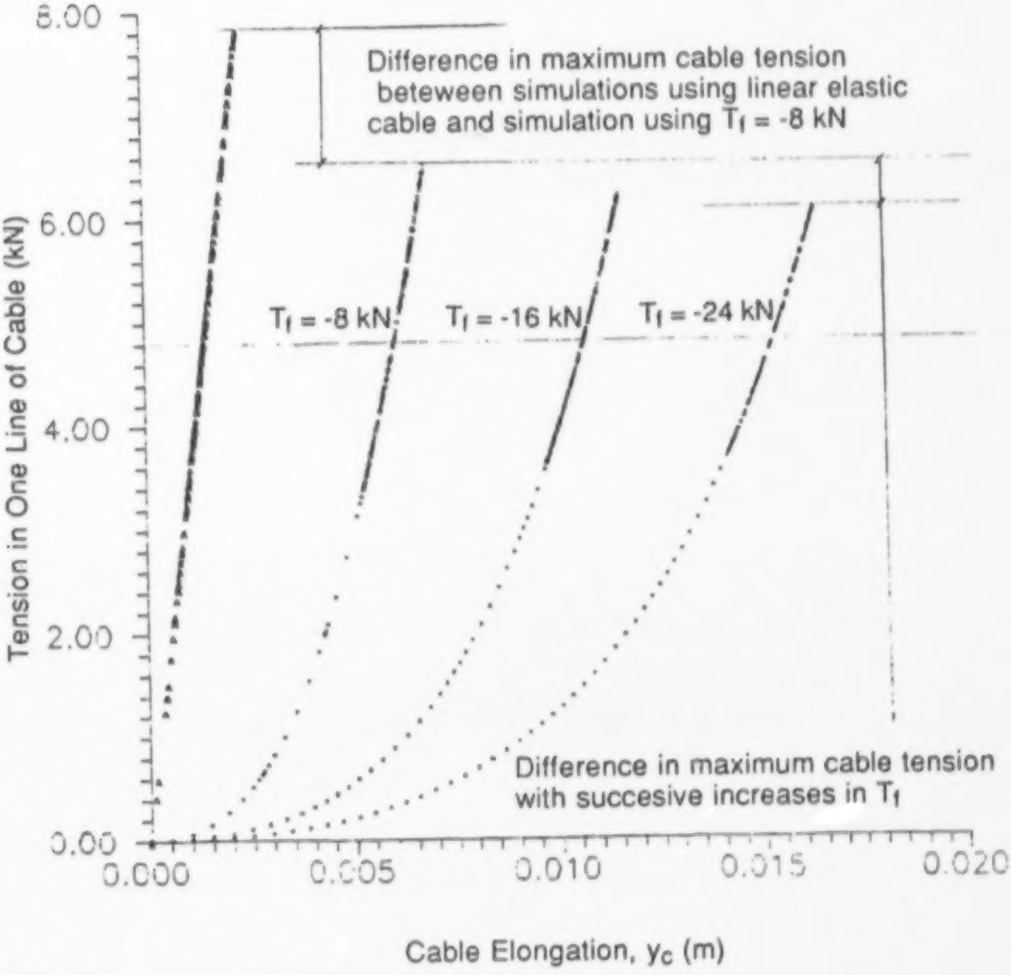

It can be seen that only a small amount of non-linearity in the relationship between T_c and y_c significantly reduces the maximum cable tension. This reinforces the argument that quasi-static behaviour of the structure prior to lift off of the payload provides consistent results

5.8.1.3 Solution Using Starting Initial Conditions

If the assumption is made that the structure behaves in a quasi-static manner prior to payload lift off, then the solution for the dynamic factor proceeds as follows. The values in equations (5.70) for y_s and y_c and their derivatives, for the instant at which the payload is on the verge of motion, are substituted into equations (5.38) and (5.39) to get the initial values of the second and third modal D'soF and their derivatives .

$$w_2 = \frac{\left(\frac{m_p g}{k_s}\right)(\kappa + \gamma_2)}{(1 - \gamma_2)(\gamma_3 - \gamma_2)} \qquad w_3 = \frac{\left(\frac{m_p g}{k_s}\right)(\kappa + \gamma_3)}{(1 - \gamma_3)(\gamma_2 - \gamma_3)} \tag{5.72}$$

$$\dot{w}_2 = \frac{\left(\frac{H_o}{1 + \kappa}\right)(\kappa + \gamma_2)}{(1 - \gamma_2)(\gamma_3 - \gamma_2)} \qquad \dot{w}_3 = \frac{\left(\frac{H_o}{1 + \kappa}\right)(\kappa + \gamma_3)}{(1 - \gamma_3)(\gamma_2 - \gamma_3)} \tag{5.73}$$

$$\ddot{w}_2 = 0 \qquad \ddot{w}_3 = 0 \tag{5.74}$$

The initial values, from equations (5.73) and (5.74) are substituted into the general solutions for w_2 and w_3 given in equations (5.49) and (5.50), and solutions for A and θ are determined. Consider first the solution for the second mode.

$$\frac{\left(\frac{H_o}{1 + \kappa}\right)(\kappa + \gamma_2)}{(1 - \gamma_2)(\gamma_3 - \gamma_2)} = A_2\, \omega_2 \cos(\omega_2 t + \theta_2) \tag{5.75}$$

$$0 = -A_2\, \omega_2^2 \sin(\omega_2 t + \theta_2) \tag{5.76}$$

From equation (5.76), a non-trivial solution for A_2 requires that $\sin(\omega_2 t + \theta_2)$ equal zero. Therefore $\cos(\omega_2 t + \theta_2) = \pm 1$. The positive value for $\cos(\omega_2 t + \theta)$ generates a positive value for the amplitude A_2 from equation (5.75).

$$\frac{\left(\frac{H_o}{1+\kappa}\right)(\kappa + \gamma_2)}{\omega_2 (1-\gamma_2)(\gamma_3-\gamma_2)} = A_2 \qquad (5.77)$$

A similar expression can be derived for the amplitude of the third mode shape.

$$\frac{\left(\frac{H_o}{1+\kappa}\right)(\kappa + \gamma_3)}{\omega_3 (1-\gamma_3)(\gamma_2-\gamma_3)} = A_3 \qquad (5.78)$$

The magnitudes A_2 and A_3 are the amplitudes of the modal degrees of freedom w_2 and w_3 respectively (at the frequencies of ω_2 and ω_3 respectively), and B_2 and B_3 are their respective mean values. Equation (5.34) is the general solution for y_s. An upper bound expression for the largest possible downwards deflection, y_{smax}, is as follows.

$$\begin{aligned} y_{smax} &= (1-\gamma_2)w_{2max} + (1-\gamma_3)w_{3max} \\ &= (\gamma_2 - 1)A_2 + (1-\gamma_2)B_2 + (\gamma_3 - 1)A_3 + (1-\gamma_3)B_3 \qquad (5.79) \end{aligned}$$

The dynamic factor, D_{3xj}, is defined as the ratio of the maximum deflection to the static deflection. The subscript "3" indicates that the dynamic factor is derived from the 3DoF model. The "x" indicates that the exact solution is used, and the "j" indicates that the dynamic factor is for the case of jerk-starting.

In Appendix D.6 it is shown that $(1 - \gamma_2)B_2 + (1 - \gamma_3)B_3 = -\frac{m_p g}{k_s}$, which is the static deflection of the crane under the weight of the payload. Dividing equation (5.79) by $\frac{m_p g}{k_s}$ gives the following expression for D_{3xj}.

$$D_{3xj} = \frac{y_{smax}}{y_{sstatic}} = 1 + \left| \frac{(1 - \gamma_2)A_2}{\left(\frac{m_p g}{k_s}\right)} \right| + \left| \frac{(1 - \gamma_3)A_3}{\left(\frac{m_p g}{k_s}\right)} \right| \qquad (5.80)$$

Substituting the values for A_2 and A_3 from (5.77) and (5.78) into equation (5.80) gives the following expression for the dynamic factor.

$$D_{3xj} = 1 + \left(\frac{H_o k_s}{m_p g}\right) \left(\left| \frac{\kappa + \gamma_2}{(1 + \kappa)\, \omega_2\, (\gamma_3 - \gamma_2)} \right| + \left| \frac{\kappa + \gamma_3}{(1 + \kappa)\, \omega_3\, (\gamma_2 - \gamma_3)} \right| \right)$$

$$= \left(\frac{H_o k_s}{m_p g}\right) \left(\frac{\left| \frac{\kappa + \gamma_2}{\omega_2} \right| + \left| \frac{\kappa + \gamma_3}{\omega_3} \right|}{(1 + \kappa)\,(\gamma_2 - \gamma_3)} \right) \qquad (5.81)$$

The sign of γ_2 is always positive. In Appendix D.7 it is proven that $\kappa > | \gamma_3 |$ for all positive values of μ. Therefore the absolute value signs in equation (5.81) may be omitted.

The term $\frac{H_o k_s}{m_p g}$ can be factored as shown below.

$$\frac{H_o k_s}{m_p g} = \frac{H_o}{g} \sqrt{\frac{k_s}{m_s}} \times \sqrt{\frac{k_c}{m_p}} \times \sqrt{\frac{k_s}{k_c}} \times \sqrt{\frac{m_s}{m_p}} = \frac{H_o \omega_c \omega_s \sqrt{\kappa \mu}}{g} \qquad (5.82)$$

Therefore, the dynamic factor can be written in a more convenient form as

$$D_{3xj} = 1 + \frac{H_o \omega_c}{g} S_{xj} \qquad (5.83)$$

$$\text{where} \quad S_{xj} = \sqrt{\kappa\mu} \left(\frac{(\kappa + \gamma_2)\left(\dfrac{\omega_s}{\omega_2}\right) + (\kappa + \gamma_3)\left(\dfrac{\omega_s}{\omega_3}\right)}{(1 + \kappa)(\gamma_2 - \gamma_3)} \right). \qquad (5.84)$$

For a given hoist, payload, and cable arrangement, $\frac{H_o \omega_c}{g}$ is constant. The natural frequency of the cable and payload system attached to a fixed rigid support is ω_c. For the limiting case of an infinitely stiff crane with a hoisting speed of H_o, the ratio of the amplitude to the static displacement is $\frac{H_o \omega_c}{g}$, and, therefore, the dynamic factor is $1 + \frac{H_o \omega_c}{g}$. Equation (5.83) shows that the change in this limiting dynamic factor, due to different lifting positions on the bridge crane, is accounted for by S_{xj}, which is called the structure coefficient. The subscript "x" indicates that the exact solution is used, and the "j" indicates that the structure coefficient is derived for the case of jerk-starting. Because S_{xj} is a function in part of cable and payload properties, changing these properties while maintaining a given lifting position on the bridge will also change the value of S_{xj}. The structure coefficient is discussed in detail in Section 5.9.

5.8.2 Initial Conditions for Braking

An analysis similar to that for jerk-starting is followed for the case of braking. The assumption is made that when braking is initiated the motor instantly stops turning. As a result of this instant deceleration, the motor displacement and its derivatives in the model are set equal to zero, and the system is reduced to only two D'soF. The equations of motion for this system are as follows.

$$\begin{bmatrix} k_c & -k_c \\ -k_c & k_c+k_s \end{bmatrix} \begin{Bmatrix} y_p \\ y_s \end{Bmatrix} + \begin{bmatrix} m_p & 0 \\ 0 & m_s \end{bmatrix} \begin{Bmatrix} \ddot{y}_p \\ \ddot{y}_s \end{Bmatrix} = \begin{Bmatrix} -m_p g \\ 0 \end{Bmatrix} \tag{5.85}$$

The natural frequencies are found by setting the determinant of the matrix $[[K] - \omega^2[M]]$ to zero and solving for the values of ω.

$$\begin{vmatrix} k_c - \omega^2 m_p & -k_c \\ -k_c & k_c+k_s - \omega^2 m_s \end{vmatrix} = 0 \tag{5.86}$$

Equation (5.86) is written below as a quadratic in ω^2.

$$\omega^4 - \omega^2(\Omega^2 + \omega_s^2) + \omega_s^2\omega_c^2 = 0 \tag{5.87}$$

where Ω^2 is as defined in equation (5.29). The two solutions to equation (5.87) are the natural frequencies for the 2 DoF system subject to braking.

$$\omega_1^2 = \frac{\Omega^2 + \omega_s^2 - \sqrt{(\Omega^2 + \omega_s^2)^2 - 4\omega_s^2\,\omega_c^2}}{2} \tag{5.88}$$

$$\omega_2^2 = \frac{\Omega^2 + \omega_s^2 + \sqrt{(\Omega^2 + \omega_s^2)^2 - 4\omega_s^2\,\omega_c^2}}{2} \tag{5.89}$$

The two natural frequencies have the same formulae, given in equations (5.30) and (5.31), as the vibrational natural frequencies for the 3 DoF system. Similarly, the matrix $[\Phi]$ is the same as for the 3 DoF system, but without the first row and column.

$$[\Phi] = \begin{bmatrix} -\mu & -\mu \\ 1-\gamma_1 & 1-\gamma_2 \end{bmatrix} \tag{5.90}$$

$$\text{where} \quad \gamma_1 = \frac{1}{1-\dfrac{\omega_1^2}{\omega_s^2}} \quad \text{and} \quad \gamma_2 = \frac{1}{1-\dfrac{\omega_2^2}{\omega_s^2}} \tag{5.91}$$

The equations for y_p and y_s can be written in terms of the modal displacements, w_1 and w_2.

$$-\frac{m_s}{m_p}(w_1 + w_2) = y_p \tag{5.92}$$

$$(1-\gamma_1)w_1 + (1-\gamma_2)w_2 = y_s \tag{5.93}$$

The two equations relating the modal displacements in terms of y_p and y_s are the following.

$$w_1 = \frac{(1-\gamma_1)y_s - y_p}{(1-\gamma_1)(\gamma_2-\gamma_1)} \qquad w_2 = \frac{(1-\gamma_2)y_s - y_p}{(1-\gamma_2)(\gamma_1-\gamma_2)} \tag{5.94}$$

The differential equations for the modal D'soF are of the same form as equations (5.46) and (5.47) for the 3 DoF system.

$$\omega_1^2 w_1 + \ddot{w}_1 = \frac{g}{(1-\gamma_1)(\gamma_2-\gamma_1)} \qquad \omega_2^2 w_2 + \ddot{w}_2 = \frac{g}{(1-\gamma_2)(\gamma_1-\gamma_2)} \tag{5.95}$$

Their general solution is of the same form as well.

$$w_1 = A_1 \sin(\omega_1 t + \theta_1) + B_1 \qquad w_2 = A_2 \sin(\omega_2 t + \theta_2) + B_2 \tag{5.85}$$

$$\dot{w}_1 = A_1\,\omega_1 \cos(\omega_1 t + \theta_1) \qquad \dot{w}_2 = A_2\,\omega_2 \cos(\omega_2 t + \theta_2) \tag{5.86}$$

$$\ddot{w}_1 = -A_1\,\omega_1^2 \sin(\omega_1 t + \theta_1) \qquad \ddot{w}_2 = -A_2\,\omega_2^2 \sin(\omega_2 t + \theta_2) \tag{5.87}$$

5.8.2.1 Solution for Braking with Static Initial Conditions

Consider first the case in which there is no vibration prior to the initiation of braking. This is the case if the time which has elapsed since the hoist motor was started is long enough for the vibrations due to hoisting to have been completely damped out. Therefore, just before the brakes are applied, the payload is moving at a constant velocity and the crane is stationary. There are no inertial forces and the 3 DoF system is in static equilibrium.

Let t = 0 at the instant braking is initiated. Because the system is still static at that time, θ_1 and θ_2 are both equal to zero. Therefore, cos $(\omega_1 t + \theta_1)$ and cos $(\omega_2 t + \theta_2)$ equal unity in equation (5.97). The initial values for the first derivatives of the modal D'soF $\dot{w}_1$ and $\dot{w}_2$ in (5.97) are determined by differentiating equation (5.94) with respect to time, and substituting the values of zero and Ho for $\dot{y}_s$ and $\dot{y}_p$, respectively.

$$\dot{w}_1 = \frac{-H_o}{(1-\gamma_1)(\gamma_2-\gamma_1)} \qquad \dot{w}_2 = \frac{-H_o}{(1-\gamma_2)(\gamma_1-\gamma_2)}$$

The solutions for the amplitudes, A_1 and A_2, when t = 0, from equation (5.97), are as follows.

$$A_1 = \frac{-H_o}{\omega_1(1-\gamma_1)(\gamma_2-\gamma_1)} \qquad A_2 = \frac{-H_o}{\omega_2(1-\gamma_2)(\gamma_1-\gamma_2)} \tag{5.99}$$

A dynamic load factor, D_{3xb}, similar to the dynamic factor in equation (5.80), can be defined. The subscript "b" in the term D_{3xb} indicates that this dynamic factor is based on an exact solution to the 3 DoF system experiencing braking.

$$D_{3xb} = \frac{y_{s\max}}{y_{s\text{static}}} = 1 + \left| \frac{(1-\gamma_1)\,A_1}{\left(\frac{m_p g}{k_s}\right)} \right| + \left| \frac{(1-\gamma_2)\,A_2}{\left(\frac{m_p g}{k_s}\right)} \right| \tag{5.100}$$

Substituting the values for A_1 and A_2 from (5.99) into equation (5.100) gives the following expression for the dynamic factor.

$$D_{3xb} = 1 + \frac{H_o k_s}{(\gamma_1 - \gamma_2) m_p g}\left(\frac{1}{\omega_1} + \frac{1}{\omega_2}\right)$$

$$= 1 + \frac{H_o \omega_c}{g} S_{xb} \tag{5.101}$$

$$\text{where } S_{xb} = \left(\frac{\sqrt{\mu\kappa}}{\gamma_1 - \gamma_2}\right)\left(\frac{\omega_s}{\omega_1} + \frac{\omega_s}{\omega_2}\right) \tag{5.102}$$

The term S_{xb} is the structure coefficient for the braking scenario. The subscript "x" indicates the exact solution was used for the derivation. As in the jerk-starting case, the structure coefficient accounts for the change in dynamic factor due to different lifting positions on the crane.

5.8.2.2 General Solution for Braking

The preceding derivation gives a dynamic factor for braking for the case in which the system is in static equilibrium prior to the initiation of braking. Now consider the braking scenario when there is some initial vibration of the payload and structure. The vibrations that exist before braking are changes in the amplitudes of the second and third mode shapes of the 3 DoF steady state model. Consider the second mode first. The expression for the second modal DoF of the steady state system in terms of the displacement of the masses is given in equation (5.36). Equation (5.36) can be differentiated with respect to time, to obtain the first and second derivative of the second modal DoF in terms of the velocities and accelerations of the masses.

$$\dot{w}_2 = \frac{\frac{\dot{y}_m}{n} - \dot{y}_p + (1 - \gamma_2)\,\dot{y}_s}{(1 - \gamma_2)\,(\gamma_3 - \gamma_2)} = \frac{H_o - \dot{y}_p + (1 - \gamma_2)\,\dot{y}_s}{(1 - \gamma_2)\,(\gamma_3 - \gamma_2)} \tag{5.103}$$

$$\ddot{w}_2 = \frac{\frac{\ddot{y}_m}{n} - \ddot{y}_p + (1 - \gamma_2)\,\ddot{y}_s}{(1 - \gamma_2)\,(\gamma_3 - \gamma_2)} = \frac{- \ddot{y}_p + (1 - \gamma_2)\,\ddot{y}_s}{(1 - \gamma_2)\,(\gamma_3 - \gamma_2)} \tag{5.104}$$

The values of $\dot{w}_2$ and $\ddot{w}_2$ from equations (5.103) and (5.104) can be substituted into equations (5.49) and (5.50) respectively.

$$A_2\,\omega_2 \cos(\omega_2 t + \theta_2) = \frac{H_o - \dot{y}_p + (1 - \gamma_2)\,\dot{y}_s}{(1 - \gamma_2)\,(\gamma_3 - \gamma_2)} \tag{5.105}$$

$$-A_2\,\omega_2^2 \sin(\omega_2 t + \theta_2) = \frac{- \ddot{y}_p + (1 - \gamma_2)\,\ddot{y}_s}{(1 - \gamma_2)\,(\gamma_3 - \gamma_2)} \tag{5.106}$$

Let the value for $\omega_2 t + \theta_2$ be α at the instant the brakes are applied. The amplitude A_2 is a function of whatever starting conditions initiated the vibrations when the hoisting event began, and may also be affected by damping. Let the amplitude A_2 in equations (5.105) and (5.106) be $\bar{A}$.

Once the brakes have been applied, the 2 DoF system is used to describe the crane's behaviour. It has been shown that the second mode shape of the 3 DoF system is the same as the first mode shape of the 2 DoF system, and that the second natural frequency of the 3 DoF system is the same as the first natural frequency of the 2 DoF system. The expressions for the velocities and accelerations of the second mode of the 3 DoF system, just before braking, written in the terms of reference of the 2 DoF system, are as follows.

$$\bar{A}\,\omega_1 \cos\alpha = \frac{H_o - \dot{y}_p + (1-\gamma_1)\,\dot{y}_s}{(1-\gamma_1)(\gamma_2-\gamma_1)} \qquad (5.107)$$

$$-\bar{A}\,\omega_1^2 \sin\alpha = \frac{-\ddot{y}_p + (1-\gamma_1)\,\ddot{y}_s}{(1-\gamma_1)(\gamma_2-\gamma_1)} \qquad (5.108)$$

The expressions for the first and second modal DoF of the 2 DoF system in terms of y_s and y_p are given in equation (5.94). If the expression for the first mode is differentiated twice, the following equations for the first and second derivative of the first after-braking mode result.

$$\dot{w}_1 = \frac{-\dot{y}_p + (1-\gamma_1)\,\dot{y}_s}{(1-\gamma_1)(\gamma_2-\gamma_1)} \qquad (5.109)$$

$$\ddot{w}_1 = \frac{-\ddot{y}_p + (1-\gamma_1)\,\ddot{y}_s}{(1-\gamma_1)(\gamma_2-\gamma_1)} \qquad (5.110)$$

Combining equation (5.109) with (5.107), and (5.110) with (5.108), expressions for the first and second derivatives of the first modal DoF can be written which do not include the structure or payload velocities and accelerations.

$$\dot{w}_1 = \bar{A}\,\omega_1 \cos\alpha - \frac{H_o}{(1-\gamma_1)(\gamma_2-\gamma_1)} \qquad (5.111)$$

$$\ddot{w}_1 = -\bar{A}\,\omega_1^2 \sin\alpha \qquad (5.112)$$

The values for $\dot{w}_1$ and $\ddot{w}_1$ in equations (5.111) and (5.112) are substituted into the differential equations (5.96) and (5.97). Let $t = 0$ at the moment braking starts.

$$A_1\,\omega_1 \cos\theta_1 \;=\; \bar{A}\,\omega_1 \cos\alpha - \frac{H_o}{(1-\gamma_1)(\gamma_2-\gamma_1)} \tag{5.113}$$

$$A_1 \sin\theta_1 \;=\; \bar{A}\sin\alpha \tag{5.114}$$

Dividing the quantities on the left and right sides of equation (5.114) by those on the left and right side, respectively, of equation (5.113), gives an expression for tan θ_1 that does not include A_1.

$$\tan\theta_1 \;=\; \frac{\sin\alpha}{\cos\alpha - \dfrac{H_o}{\bar{A}\omega_1(1-\gamma_1)(\gamma_2-\gamma_1)}} \tag{5.115}$$

Using the trigonometric identity, $\sin x = \dfrac{\tan x}{\sqrt{1+\tan^2 x}}$, the expression for sin θ_1 is written.

$$\sin\theta_1 \;=\; \frac{\sin\alpha}{\sqrt{\sin^2\alpha + \left(\cos\alpha - \dfrac{H_o}{\bar{A}\omega_1(1-\gamma_1)(\gamma_2-\gamma_1)}\right)^2}} \tag{5.116}$$

Substituting the value for sin θ_1 in equation (5.116) into equation (5.114) gives an expression for A_1.

$$A_1 = \bar{A}\sqrt{\sin^2\alpha + \left(\cos\alpha - \frac{H_o}{\bar{A}\omega_1(1-\gamma_1)(\gamma_2-\gamma_1)}\right)^2} \tag{5.117}$$

To find the maximum value of A_1 with respect to α, let the derivative of the expression under the root sign in (5.117) equal zero.

$$2 \sin\alpha \cos\alpha - 2 \sin\alpha \left(\cos\alpha - \frac{H_o}{\bar{A}\omega_1 (1-\gamma_1)(\gamma_2-\gamma_1)} \right) = 0$$

$$\sin\alpha \left(\frac{-H_o}{\bar{A}\,\omega_1 (1-\gamma_1)(\gamma_2-\gamma_1)} \right) = 0 \qquad (5.118)$$

Equation (5.118) is satisfied when $\sin\alpha = 0$, which is the case when α, in radians, is zero or some integer multiple of π. The even integer roots represent the case when the initial vibrations are in phase with the vibrations caused by braking, and the odd integer roots represent the case where the two vibrations are π radians out of phase. The maximum value for A_1 corresponds to the in-phase condition, which occurs when $\cos\alpha = +1$. The values of zero and positive one for $\sin\alpha$ and $\cos\alpha$, respectively, can be substituted into equation (5.117).

$$A_{1\,\max} = \bar{A} \left(1 - \frac{H_o}{\bar{A}\omega_1 (1-\gamma_1)(\gamma_2-\gamma_1)} \right)$$

$$= \bar{A} - \frac{H_o}{\omega_1 (1-\gamma_1)(\gamma_2-\gamma_1)} \qquad (5.119)$$

The only difference between the first mode amplitude from equation (5.119) and the first mode amplitude from equation (5.99) is the addition of $\bar{A}$, the first mode amplitude from before braking was initiated.

A similar expression is developed assuming an initial vibration of the second mode with a modal amplitude of $\bar{\bar{A}}$.

$$A_{2\,max} = \bar{\bar{A}} - \frac{H_o}{\omega_2 (1 - \gamma_2)(\gamma_1 - \gamma_2)} \tag{5.120}$$

In this derivation of the dynamic factor, it is assumed that the vibrations caused by braking are in phase with those due to some unspecified previous loading event. The dynamic factor for this case is denoted by D_{3xb+} and is given by

$$D_{3xb+} = \frac{y_{smax}}{y_{sstatic}} = 1 + \left| \frac{(1 - \gamma_1)A_{1\,max}}{\left(\frac{m_p g}{k_s}\right)} \right| + \left| \frac{(1 - \gamma_2)A_{2\,max}}{\left(\frac{m_p g}{k_s}\right)} \right| . \tag{5.121}$$

When $A_{1\,max}$ and $A_{2\,max}$ from equations (5.119) and (5.120) are substituted into (5.121), the following expression for the dynamic factor results.

$$D_{3xb+} = 1 + \frac{S_{xb} H_o \omega_c}{g} + \left| \frac{(1 - \gamma_1)\bar{A}}{\left(\frac{m_p g}{k_s}\right)} \right| + \left| \frac{(1 - \gamma_2)\bar{\bar{A}}}{\left(\frac{m_p g}{k_s}\right)} \right| \tag{5.122}$$

If it is assumed that the initial vibrations are due to jerk-starting, then $(1 - \gamma_1)\bar{A}$ and $(1 - \gamma_2)\bar{\bar{A}}$ are equal to $(1 - \gamma_2)A_2$ and $(1 - \gamma_3)A_3$, respectively, in equation (5.80). The dynamic factor D_{3xbj}, for the combined effect of braking and jerk-starting, can be written as follows.

$$D_{3xbj} = 1 + \frac{S_{xb} H_o \omega_c}{g} + \frac{S_{xj} H_o \omega_c}{g} \tag{5.123}$$

$$= 1 + \frac{H_o\, \omega_c}{g} (S_{xb} + S_{xj})$$

5.9 Discussion of Structure Coefficients

In this section it is shown that the structure coefficients S_{xb} and S_{xj} can be written solely in terms of κ and μ. Once this is established, graphs of the structure coefficients will serve to illustrate certain features of S. Some of the features of the multi-DoF system which determine the values of S are discussed. The limiting case in which μ approaches zero is examined. Some of the less obvious ways in which features of S affect the dynamic factor will also be discussed.

5.9.1 Dependence of Structure Coefficient on κ and μ

The only variables which are needed to obtain a value for the structure coefficient S are κ and μ. This is proved as follows. Equations (5.84) and (5.102) for S_{xb} and S_{xj}, respectively, are shown below.

$$S_{xj} = \sqrt{\kappa\mu}\left(\frac{(\kappa + \gamma_2)\left(\frac{\omega_s}{\omega_2}\right) + (\kappa + \gamma_3)\left(\frac{\omega_s}{\omega_3}\right)}{(1 + \kappa)\,(\gamma_2 - \gamma_3)}\right) \tag{5.84}$$

$$S_{xb} = \left(\frac{\sqrt{\mu\kappa}}{\gamma_1 - \gamma_2}\right)\left(\frac{\omega_s}{\omega_1} + \frac{\omega_s}{\omega_2}\right) \tag{5.102}$$

In each, the expression for S contains κ and μ, in addition to γ terms and the ratios of the modal and structural natural frequencies. The general form of the equation for the γ terms is given in (5.25).

$$\gamma = \frac{1}{1 - \frac{\omega^2}{\omega_s^2}} \tag{5.25}$$

It can be seen that γ is also a function of the ratio of modal and structural natural frequencies.

This ratio of modal and structural natural frequencies can be expressed as a function which has only κ and μ as its variables. This is shown as follows. The form of the equations for the squares of the modal natural frequencies is shown below.

$$\omega^2 = \frac{\Omega^2 + \omega_s^2 \pm \sqrt{(\Omega^2 + \omega_s^2)^2 - 4\omega_s^2\,\omega_c^2}}{2} \tag{5.124}$$

When $\Omega^2 + \omega_s^2$ is divided by ω_s^2, the following expression, in terms of κ and μ, results.

$$\left(\frac{\Omega^2 + \omega_s^2}{\omega_s^2}\right) = \left(\frac{ms}{ks}\right)\left(\frac{k_c}{mp} + \frac{k_c}{ms} + \frac{ks}{ms}\right) = \frac{1 + \mu + \kappa}{\kappa} \tag{5.125}$$

The discriminant which appears in equations (5.124) can be divided by $\Omega^2 + \omega_s^2$.

$$\frac{\sqrt{(\Omega^2 + \omega_s^2)^2 - 4\omega_s^2\,\omega_c^2}}{\Omega^2 + \omega_s^2} = \sqrt{1 - 4\left(\frac{\omega_s^2}{\Omega^2 + \omega_s^2}\right)\left(\frac{\omega_c^2}{\Omega^2 + \omega_s^2}\right)}$$

$$= \sqrt{1 - \frac{4\mu\kappa}{(1 + \mu + \kappa)^2}} \tag{5.126}$$

When the expressions of the right sides of equations (5.125) and (5.126) are substituted into equation (5.124), the following equation for modal natural frequencies results.

$$\omega^2 = \omega_s^2\left(\frac{1 + \mu + \kappa}{2\kappa}\right)\left(1 \pm \sqrt{1 - \frac{4\mu\kappa}{(1 + \mu + \kappa)^2}}\right) \tag{5.127}$$

It can be seen from equation (5.127) that the ratio of modal and structural natural frequencies can be expressed using only κ and μ as variables. The only variables in equations (5.84) and (5.102) for S, which do not involve κ or μ explicitly, can be expressed as the ratio of modal and structural natural frequencies. Therefore, S can be expressed using only κ and μ as variables .

Figure 5.9 shows the structure coefficient, S_{xj}, from equation (5.84) plotted against a wide range of values for κ, with μ as a parameter. Figure 5.10 shows S_{xb} for the same range of κ and μ values.

The preceding argument proves that the ratios μ and κ are the only variables needed to determine the structure coefficients. It might be expected that S_{xj} and S_{xb} can also be expressed using only the frequencies ω_s and ω_c as variables. However, this is not the case. Consider the following identities.

$$\frac{\omega_s^2}{\omega_c^2} = \frac{k_s m_p}{m_s k_c} = \frac{\kappa}{\mu}$$

A particular value for ω_s and a particular value for ω_c define a value for the ratio $\frac{\kappa}{\mu}$, but do not determine individual values of κ and μ. However, individual values for κ and μ are required to define a single value for the structure coefficient. With two trivial exceptions, any one ratio of κ to μ, and the particular values for ω_s and ω_c associated with that ratio, defines a line on the S versus κ graph which passes through all values of S. Figure 5.11 illustrates this by showing the locus of points for S_{xj}, for which $\kappa = 2\mu$.

One of the trivial exceptions is the limiting case in which κ is zero. Under that condition, $S = 0$. The other exception is the limiting case in which μ is zero. In this case κ can assume any value without altering the magnitude of the ratio $\frac{\kappa}{\mu}$. The line associated with $\mu = 0$ on the S versus κ graph passes through all values of $S < 1$. The limiting case of μ approaching zero is discussed further in Section 5.9.2.

The expression for S_{xj} is long and complicated if expressed strictly in terms of μ and κ. An approximation that gives acceptable results is the following.

Figure 5.9 Jerk-Starting Structure Coefficient versus κ

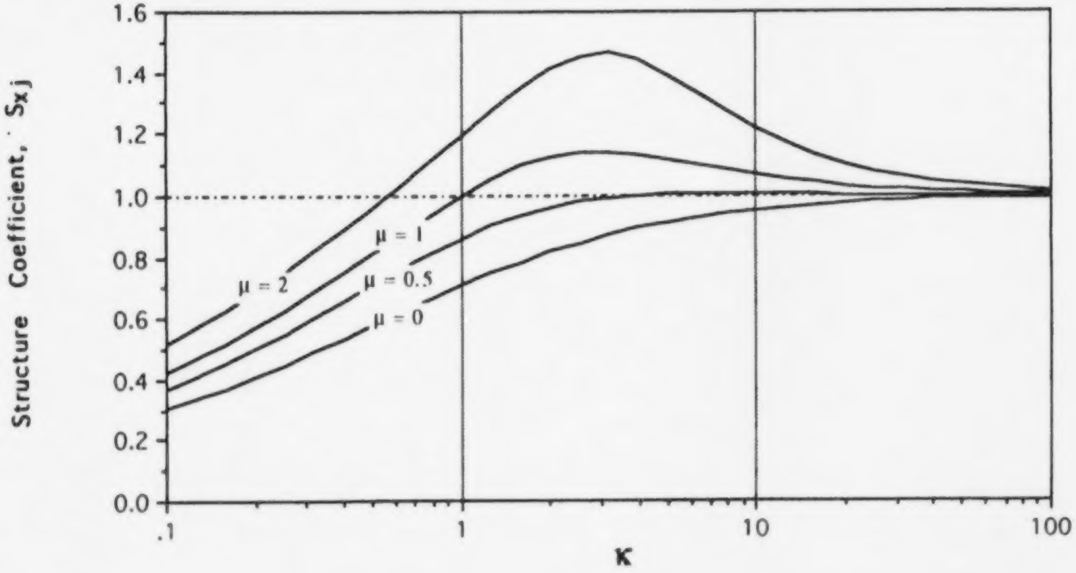

Figure 5.10 Structure Coefficient for Braking, versus κ

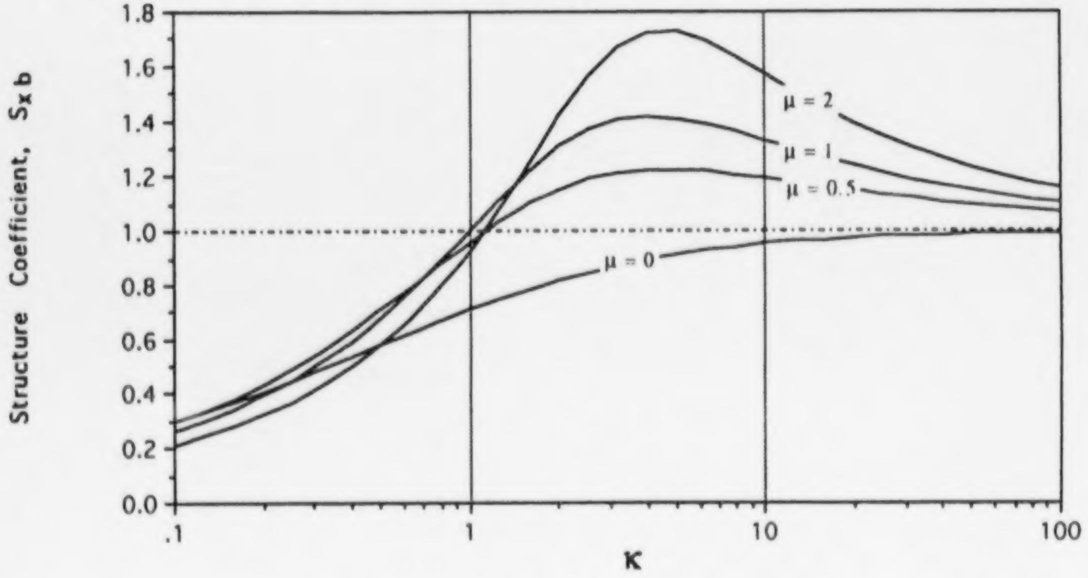

Figure 5.11 Path of Values for S_{xj} when $\kappa = 2\mu$

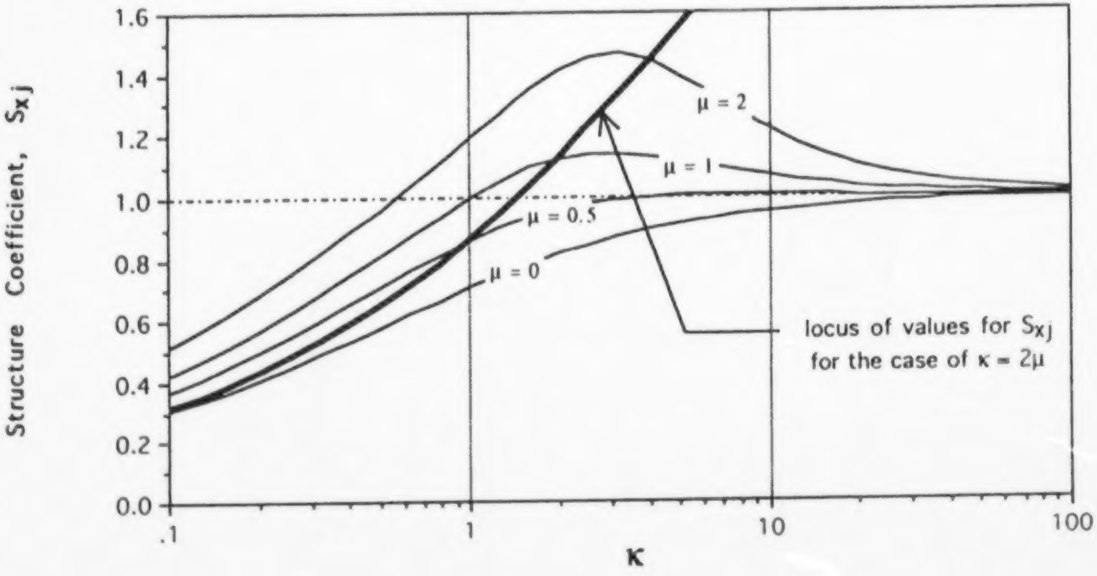

$$S_{aj} = \frac{\sqrt{\kappa(1+\mu+\kappa)}}{\kappa+1}\left(1 + \frac{2\mu\kappa}{(1+\mu+\kappa)^2}\right) \qquad (5.128)$$

The subscript "a" indicates this value for the structure coefficient is an approximation. The expression in (5.128) was found through trial-and-error, and is not based on any derivation. Figure 5.12 shows a graph comparing the approximate and exact solutions for S_{xj}, and shows a graph of the ratio of the approximate to exact values of S_{xj}, plotted against κ. The approximate value stays reasonably close to the exact value for a practical range of κ and μ values.

Similarly, the equation for S_{xb} when written strictly in terms of κ and μ, is not convenient to use. It may be approximated by the following.

$$S_{ab} = \left(1 + \frac{2\mu\kappa}{(1+\mu+\kappa)^2}\right)^3 \sqrt{\frac{\kappa}{1+\mu+\kappa}} \qquad (5.129)$$

This expression was also found through trial-and-error. Figure 5.13 shows the approximation S_{ab} from (5.129) plotted with the exact values of S_{xb} from equation (5.102). The graphs in Figure 5.13 compare the approximation to the exact value of S_{xb}. The approximation stays acceptably close to the exact value.

5.9.2 Solution for S when μ Approaches Zero

In this section solutions for the equations for S are derived for the limiting case in which μ approaches zero. This corresponds to the case in which the payload is much more massive than the mass of the crane. Consider first the solutions for S_{xj} in this limiting case. Equation (5.84) for S_{xj} is shown below.

$$S_{xj} = \sqrt{\kappa\mu}\left(\frac{(\kappa+\gamma_2)\left(\frac{\omega_s}{\omega_2}\right) + (\kappa+\gamma_3)\left(\frac{\omega_s}{\omega_3}\right)}{(1+\kappa)(\gamma_2-\gamma_3)}\right) \qquad (5.84)$$

Figure 5.12 Approximation for S_{xj}

Graph of S_{xj} and S_{aj} versus κ

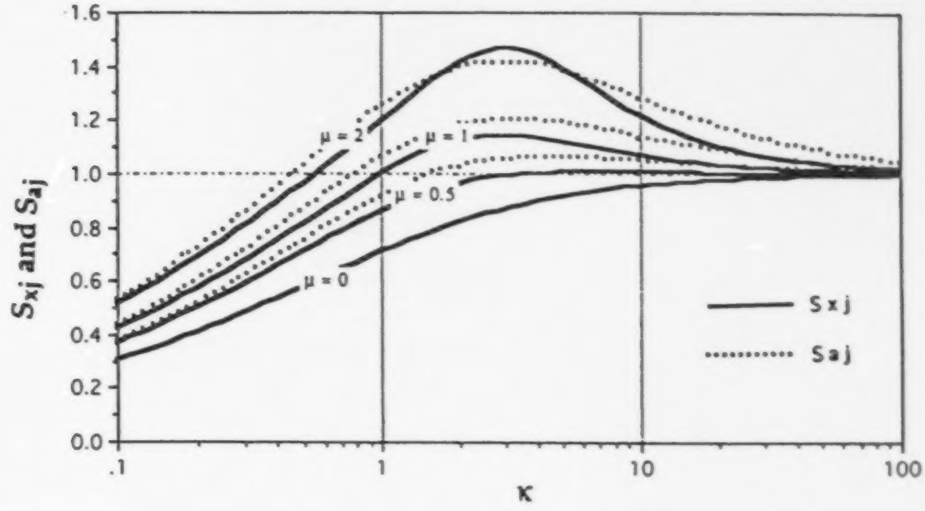

Ratio of S_{xj} and S_{aj}

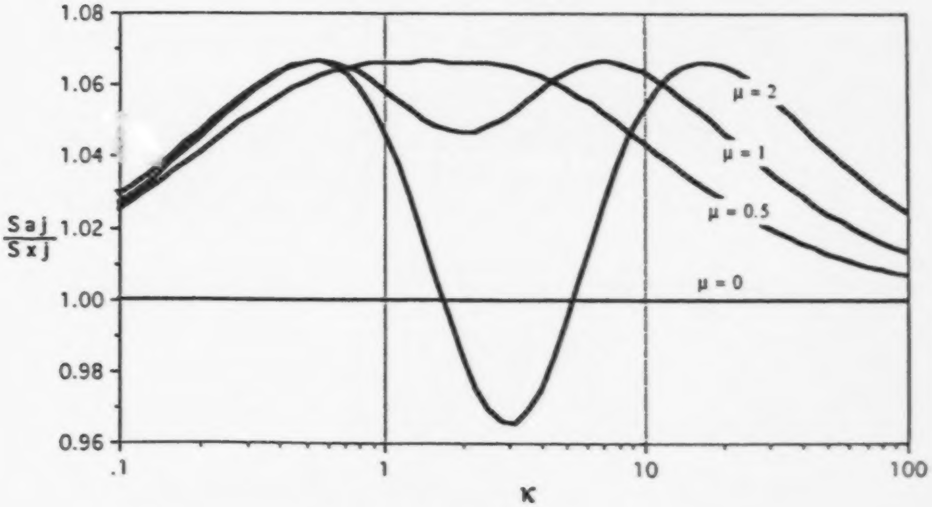

Figure 5.13 Approximation for S_{xb}

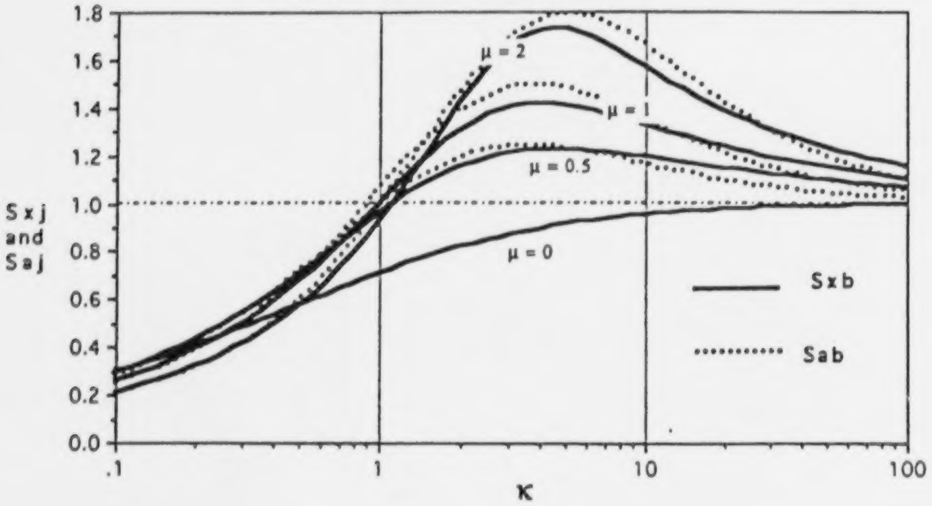

Graph of S_{xb} and S_{ab} versus κ

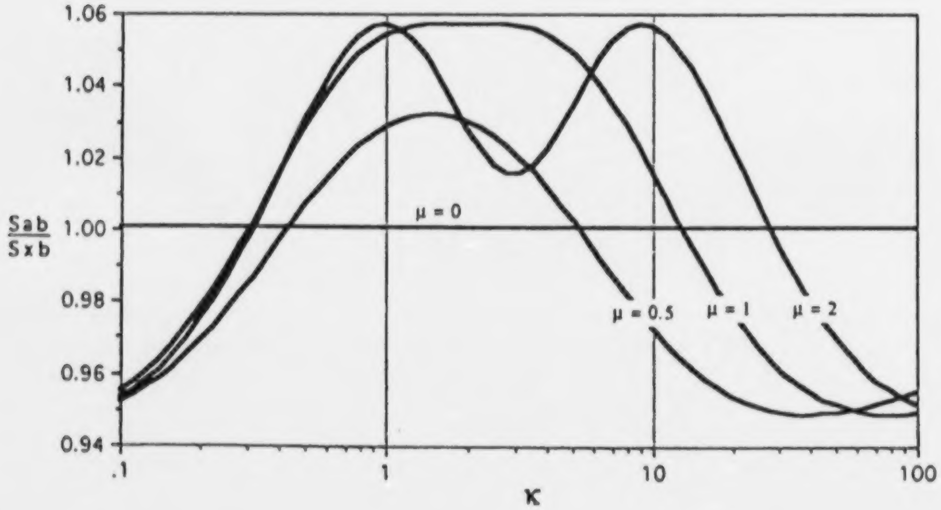

Ratio of S_{xb} and S_{ab}

To solve for S_{xj} as μ approaches zero, the values of $\frac{\omega_s}{\omega_2}$, $\frac{\omega_s}{\omega_3}$, and $\gamma_2 - \gamma_3$ must be evaluated as μ approaches zero.

From equation (5.127), an expression for $\frac{\omega_s}{\omega}$ is written.

$$\frac{\omega_s}{\omega} = \frac{1}{\sqrt{\left(\frac{1 + \mu + \kappa}{2\kappa}\right)\left(1 \pm \sqrt{1 - \frac{4\mu\kappa}{(1 + \mu + \kappa)^2}}\right)}} \tag{5.130}$$

The solution for $\frac{\omega_s}{\omega_3}$ results when the sign of the discriminant in equation (5.130) is positive. A direct substitution of $\mu = 0$ in equation (5.30) gives the following.

$$\frac{\omega_s}{\omega_3} = \sqrt{\frac{\kappa}{1 + \kappa}} \tag{5.131}$$

The solution for $\frac{\omega_s}{\omega_2}$ results when the sign of the discriminant in equation (5.130) is negative. From equation (5.130) it can be seen that when μ approaches zero, $\frac{\omega_s}{\omega_2}$ approaches infinity. Therefore, the expression for S_{xj} in equation (5.84), as μ approaches zero, contains the undefined term $\frac{\omega_s\sqrt{\mu}}{\omega_2}$. A value for the undefined term can be found using the relationship that $\sqrt{1 - x} \approx 1 - \frac{x}{2}$ when $x \ll 1$. Applying this relationship to the discriminant in equation (5.116), it can be seen that

$$\sqrt{1 - \frac{4\mu\kappa}{(1 + \mu + \kappa)^2}} \approx 1 - \frac{2\mu\kappa}{(1 + \mu + \kappa)^2} \tag{5.132}$$

when $\frac{2\mu\kappa}{(1+\mu+\kappa)^2} \ll 1$, which is the case as μ approaches zero. Substituting the expression for the discriminant from (5.132) into equation (5.130) gives the following expression for ω_2^2.

$$\lim_{\mu\to 0} \frac{\omega_s\sqrt{\mu}}{\omega_2} = \lim_{\mu\to 0} \frac{\sqrt{\mu}}{\sqrt{\left(\frac{1+\mu+\kappa}{2\kappa}\right)\left(1 - 1 + \frac{2\mu\kappa}{(1+\mu+\kappa)^2}\right)}} = \sqrt{1+\kappa} \tag{5.133}$$

To solve the right side of equation (5.84) for S_{xj} as μ approaches zero, a solution is still required for $\gamma_2 - \gamma_3$. From equation (5.130) it can be seen that when μ approaches zero, $\frac{\omega_s}{\omega_2}$ approaches infinity. Substituting zero for the inverse of this frequency ratio into equation (5.25) gives the following for γ_2.

$$\gamma = \gamma_2 = \frac{1}{1-0} = 1 \tag{5.134}$$

Substituting the value from equation (5.131) for the frequency ratio $\frac{\omega_s}{\omega_3}$ into equation (5.25) gives the following for γ_3.

$$\gamma = \gamma_3 = \frac{1}{1 - \frac{1+\kappa}{\kappa}} = -\kappa \tag{5.135}$$

Substituting the values from equations (5.131), (5.133), (5.134), and (5.135) for $\frac{\omega_s}{\omega_3}$, $\frac{\omega_s\sqrt{\mu}}{\omega_2}$, γ_2, and γ_3 , respectively, into equation (5.84) , the expression for S_{xj} as μ approaches zero is found.

$$\lim_{\mu\to 0} S_{xj} = \lim_{\mu\to 0} \sqrt{\kappa\mu}\left(\frac{(\kappa+\gamma_2)\left(\frac{\omega_s}{\omega_2}\right) + (\kappa+\gamma_3)\left(\frac{\omega_s}{\omega_3}\right)}{(1+\kappa)(\gamma_2 - \gamma_3)}\right)$$

$$= \sqrt{\kappa}\left(\frac{(\kappa + 1)\sqrt{1 + \kappa} + 0}{(1 + \kappa)\,(1 + \kappa)}\right)$$

$$= \sqrt{\frac{\kappa}{\kappa + 1}} \qquad (5.136)$$

The preceding development gives an expression for the jerk-starting structure coefficient as μ approaches zero. A similar development gives the solution for the structure coefficient for braking, S_{xb}, for the case in which μ approaches zero. Equation (5.102) for S_{xb} is shown below.

$$S_{xb} = \left(\frac{\sqrt{\mu\kappa}}{\gamma_1 - \gamma_2}\right)\left(\frac{\omega_s}{\omega_1} + \frac{\omega_s}{\omega_2}\right) \qquad (5.102)$$

To solve for S_{xb} as μ approaches zero, the values of $\frac{\omega_s}{\omega_1}$, $\frac{\omega_s}{\omega_2}$, and $\gamma_1 - \gamma_2$ must be evaluated as μ approaches zero. The first and second natural frequencies of the 2 DoF system developed for the braking scenario are equal to the second and third natural frequencies of the 3 DoF steady state system, respectively. Therefore, ω_2, ω_3, γ_2, and γ_3, in equation (5.84) are equal, respectively, to ω_1, ω_2, γ_1, and γ_2, in equation (5.102). Equations (5.131), (5.133), (5.134), and (5.135) for the 3 DoF steady state case are rewritten below in the terms of reference of the 2 DoF system.

$$\frac{\omega_s}{\omega_2} = \sqrt{\frac{\kappa}{1 + \kappa}} \qquad (5.137)$$

$$\lim_{\mu \to 0} \frac{\omega_s\sqrt{\mu}}{\omega_1} = \sqrt{1 + \kappa} \qquad (5.138)$$

$$\gamma_1 = \frac{1}{1 - 0} = 1 \qquad (5.139)$$

$$\gamma_2 = \frac{1}{1 - \frac{1+\kappa}{\kappa}} = -\kappa \tag{5.140}$$

The values for $\frac{\omega_s}{\omega_2}$, $\frac{\omega_s\sqrt{\mu}}{\omega_1}$, γ_1, and γ_2 in equations (5.137), (5.138), (5.139), and (5.140) are substituted into equation (5.102) to provide the solution for S_{xb} as μ approaches zero.

$$\lim_{\mu\to 0} S_{xb} = \lim_{\mu\to 0} \left(\frac{\sqrt{\mu\kappa}}{\gamma_1 - \gamma_2}\right)\left(\frac{\omega_s}{\omega_1} + \frac{\omega_s}{\omega_2}\right)$$

$$= \left(\frac{\sqrt{\kappa}}{1+\kappa}\right)\left(\sqrt{1+\kappa} + 0\right)$$

$$= \sqrt{\frac{\kappa}{\kappa + 1}} \tag{5.141}$$

Comparing equations (5.141) and (5.136), it can be seen that, for the case in which μ approaches zero, the structural coefficient for both braking and jerk-starting is $\sqrt{\frac{\kappa}{\kappa+1}}$. This expression approaches a maximum of one as κ approaches infinity. For small non-zero values of μ the maximum structure coefficient occurs at large but finite values of κ, and the smaller μ is, the larger the value of κ at the structure coefficient peak.

The S versus κ constant μ curves shown in Figures 5.9 and 5.10 have certain common features. When κ approaches infinity, ($k_s \gg k_c$), the value of S approaches one. At some finite value of κ, S rises to a maximum, and this maximum is greater for larger values of μ. That maximum exists, and is greater than one, for all values of μ greater than zero. Let the value of κ when S is a maximum, with respect to κ, be called κ_{max}.

Figures 5.14 and 5.15 show the locus of the maxima for each of the structure coefficients. In the case of S_{xj}, an analytical solution for the maxima was not found. For Figure 5.14 the points of maximum value of S_{xj} with respect to κ were found for discrete values of μ. The points were plotted and a curve was passed through them. An expression for the maximum values of S_{xb} was derived. The maximum value of $S_{xb} = \sqrt{\mu + 1}$ occurs when $\kappa = \kappa_{max} = \dfrac{(\mu + 1)^2}{\mu}$.

It can be seen that for S_{xb} and S_{xj} the value of κ_{max} varies widely with μ. The conditions that cause S to assume a maximum value can be understood when the crane structure is considered as a single DoF system isolated from the rest of the model. Consider the single DoF crane subject to a independent and external forcing function comprising two harmonic frequencies of $\bar{\omega}_1$ and $\bar{\omega}_2$, with respective amplitudes of F_1 and F_2. The particular solution for the displacement of the structure would be

$$y_s = \frac{F_1}{k_s}\left(\frac{1}{1 - \frac{\bar{\omega}_1^2}{\omega_s^2}}\right)\sin(\bar{\omega}_1 t + \theta_1) + \frac{F_2}{k_s}\left(\frac{1}{1 - \frac{\bar{\omega}_2^2}{\omega_s^2}}\right)\sin(\bar{\omega}_2 t + \theta_2). \quad (5.142)$$

The bracketed terms containing the frequency ratios are γ terms, as defined in equation (5.25). It can be seen that the response of the crane structure, when subjected to two independent harmonic forcing functions, increases when one or both the forcing frequencies approach ω_s, the natural frequency of the crane structure. When either of the applied frequencies is equal to ω_s, the model is in resonance.

If the cable tension is considered to act upon the structure as an external load comprising two harmonic forcing functions, then the two frequencies for the forcing function are the two vibrational natural frequencies of the complete system, (either the 3 DoF steady state system, or the 2 DoF system derived for the braking scenario). The equation for the forcing function

Figure 5.14 Path of Maximum Values for S_{xj}

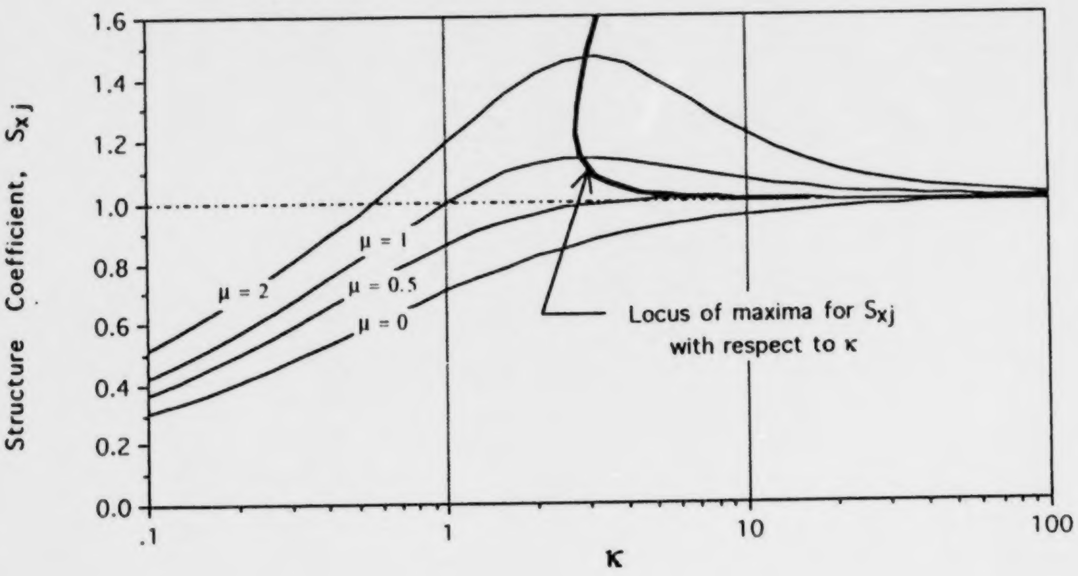

Figure 5.15 Path of Maximum Values for S_{xb}

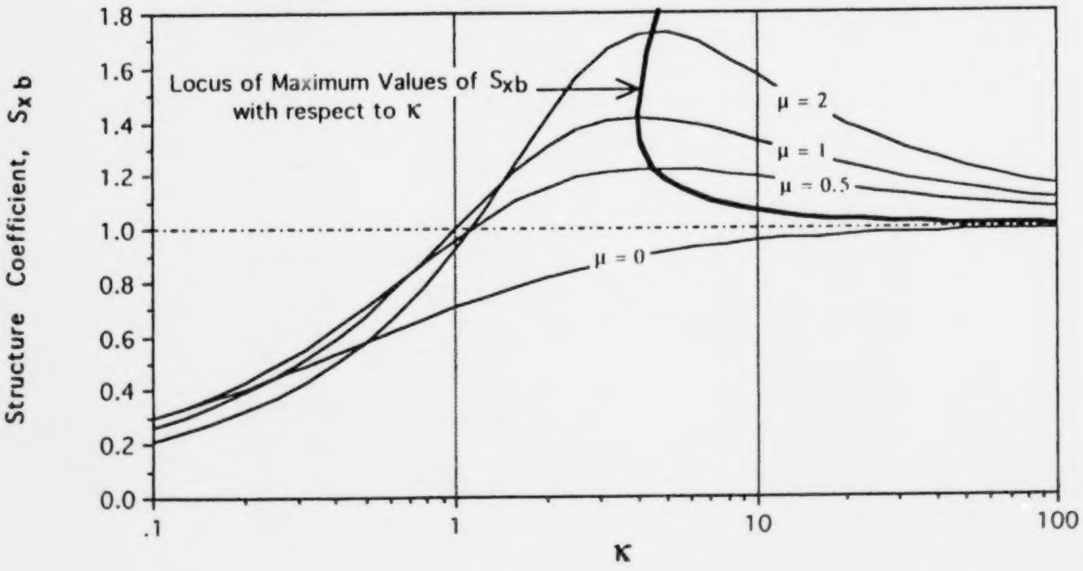

acting upon the structure is obtained by substituting equations (5.28), (5.29), and (5.30) for y_m, y_p, and y_s, into equation (5.12) for T_c.

$$w_1 + \frac{m_s}{nm_m}(w_2 + w_3) = y_m \tag{5.32}$$

$$\frac{w_1}{n} - \mu(w_2 + w_3) = y_p \tag{5.33}$$

$$(1 - \gamma_2)w_2 + (1 - \gamma_3)w_3 = y_s \tag{5.34}$$

$$T_c = \frac{k_c}{n} y_m - k_c y_p + k_c y_s \tag{5.12}$$

$$\begin{aligned} T_c = {} & \frac{k_c}{n}\left(w_1 + \frac{m_s}{nm_m}(w_2 + w_3)\right) \\ & - k_c\left(\frac{w_1}{n} - \mu(w_2 + w_3)\right) \\ & + k_c\big((1 - \gamma_2)w_2 + (1 - \gamma_3)w_3\big) \end{aligned} \tag{5.143}$$

It is assumed that $\frac{1}{m_m}$ approaches zero. Using the relationship, from Appendix D.4, that $(1 - \gamma_2)(1 - \gamma_3) = -\mu$ when $\frac{1}{m_m}$ approaches zero, equation (5.143) can be rewritten as the following.

$$T_c = k_c\big(\gamma_3(1 - \gamma_2)w_2 + \gamma_2(1 - \gamma_3)w_3\big) \tag{5.144}$$

The response of the structure to this loading is given in equation (5.34). A comparison of equations (5.34) and (5.144) shows that for each mode there is a difference between the coefficient used in the expression for T_c and the coefficient used in the expression for y_s. The tension T_c and the displacement y_s are not proportional to each other over time. A dynamic factor different from the one derived in this chapter would be required for cable design.

From equation (5.144) it can be seen that the cable tension, T_c, is comprised of two harmonic forcing functions, but they are not independent of the properties of the structure. The frequencies and magnitudes are determined by the properties of the complete multi-DoF system which includes the crane. The crane structure, subjected to T_c, cannot go into resonance. However, some insight into the mechanism which causes maximum values of S can be gained by examining the cases in which one or both the natural frequencies of the complete system approach the natural frequency of the crane structure.

Consider first the situation when the value of μ is low. Equation (5.133) indicates that ω_2, the lower of the two natural frequencies of the multi-DoF system, approaches $\omega_s\sqrt{\frac{\mu}{1+\kappa}}$. Thus, when μ is low, ω_2 is small compared to ω_s. Equation (5.131) shows that ω_3, the higher of the two natural frequencies, approaches $\omega_s\sqrt{\frac{1+\kappa}{\kappa}}$ when μ is low. As κ increases, ω_3 approaches the natural frequency of the structure. For low values of μ, the S curves reach a maximum at high values of κ, and the lower the value of μ, the higher the value of κ at which the maximum value of S occurs.

For higher values of μ, the case exists in which the natural frequency of the structure is approached by both of the natural frequencies of the complete system, rather than just the higher of the two. The closer the two frequencies are to ω_s, the greater will be the dynamic response. In Appendix D.2 it is proven that the lower natural frequency is always less than ω_s and ω_c, and the upper natural frequency is always higher than ω_s and ω_c. The two natural frequencies approach one another (and therefore ω_s, which they bound), as the discriminant in equation (5.130) approaches zero. This occurs when $\frac{4\mu\kappa}{(1+\mu+\kappa)^2}$ approaches one. The value of $\frac{4\mu\kappa}{(1+\mu+\kappa)^2}$ is less than one for all positive values of μ and κ, and approaches one only when both μ and κ approach infinity. However, the value of κ at which $\frac{4\mu\kappa}{(1+\mu+\kappa)^2}$ is a maximum can be determined by taking the first derivative of $\frac{4\mu\kappa}{(1+\mu+\kappa)^2}$ with respect to κ, and setting it equal to zero.

$$\frac{d}{d\kappa}\left(\frac{4\mu\kappa}{(1+\mu+\kappa)^2}\right) = 0$$

$$\frac{4\mu(1+\mu+\kappa)^2 - 8\mu\kappa(1+\mu+\kappa)}{(1+\mu+\kappa)^4} = 0$$

Dividing both sides of equation (5.145) by $\frac{4\mu}{(1+\mu+\kappa)^3}$ gives

$$(1+\mu+\kappa) - 2\kappa = 0$$

$$\kappa = 1 + \mu \tag{5.146}$$

When equation (5.146) is satisfied, the two natural frequencies are as close to each other as possible for a given value of μ. That $\frac{4\mu\kappa}{(1+\mu+\kappa)^2}$ approaches unity only when both κ and μ approach infinity indicates that the action of the cable tension cannot make the crane structure resonate.

Figures 5.16 and 5.17 are the graphs of the structure coefficients for jerk-starting and for braking, respectively, plotted against κ. In each of these figures two of the curves are shown in a heavy line. The first is a plot of the function

$$S = \sqrt{\frac{\kappa}{\kappa+1}}\ ,$$

which applies for the case in which μ approaches zero. For this case, as κ increases, the lower of the two natural frequencies of the multi-DoF system becomes very small compared to ω_s, while the higher of the two approaches

Figure 5.16 Influences Upon the Path of Maximum Values of S_{xj}

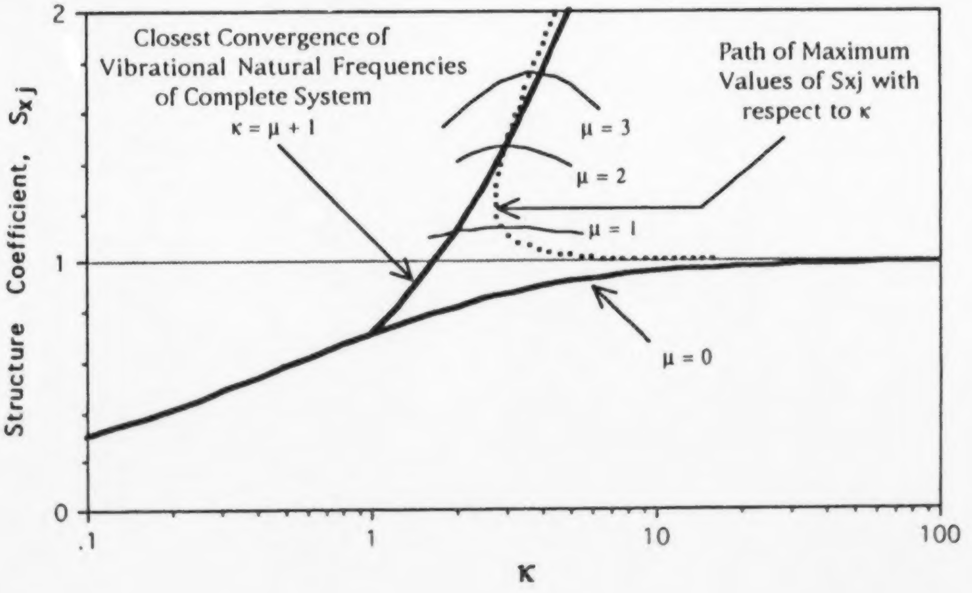

Figure 5.17 Influences Upon the Path of Maximum Values of S_{xb}

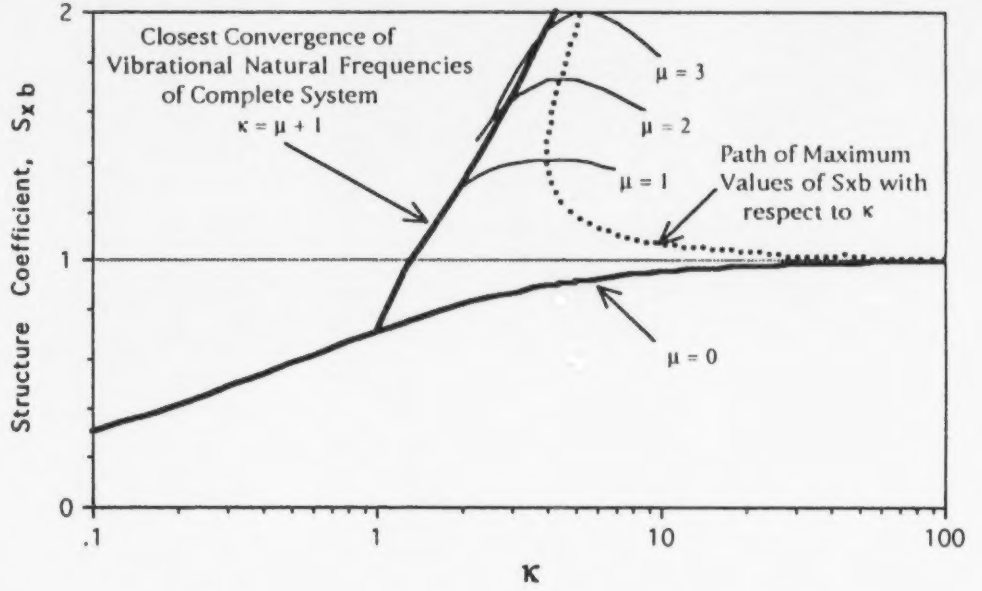

ω_s. The second curve is the locus of values of S which satisfy the condition that $\kappa = 1 + \mu$. This corresponds to the case of the closest convergence of the two natural frequencies of the multi-DoF system, for a given value of μ. The locus of points of maximum values of S with respect to κ is shown as a dotted line. The curve representing the maxima is close to the curve for μ approaching zero when the value of μ is low, and approaches the curve of closest convergence when the value of μ is not low.

If μ is not low, the highest structural coefficients with respect to κ occur near where the two vibrational natural frequencies reach their closest converge to one another. If μ is low, then at large values of κ the higher of the two natural frequencies approaches the natural frequency of the structure and cause the structural coefficients to reach their maxima with respect to κ.

5.9.4 Effects of Varying κ on the Dynamic Factor

In this section some of the effects that varying κ has on the dynamic factor will be examined. A value of μ for which the maximum value of S is 1.1 or less is referred to as a low value of μ. For low values of μ the curves representing the locus of maximum values of S in Figures 5.9 and 5.10 are nearly level and close to unity. A reduction in κ when μ is low will not significantly increase the value of S. It may reduce the value of S, or it may leave it relatively unchanged at a value near unity. If the reduction in κ is accomplished by reducing only k_s, then ω_c remains constant in the general expression for the dynamic factor,

$$D = 1 + \frac{H_0 \omega_c S}{g} \tag{5.147}$$

Therefore, under the condition that μ is low, D either decreases or remains roughly constant in response to the change in S as k_s is reduced. This is the situation described in DIN 15.018 [ref. 35] in clause 4.1.4.2 , where it is stated that " ... the larger the elasticity [flexibility] of the supporting structure, ... the smaller the [dynamic] factor Ψ." It is also the situation described by Barrett and Hrudey [ref. 3], where it was stated that "The largest D values occur when the structure is most stiff." Cranes are designed and built to lift and move payloads which are too massive to be moved conveniently in some other fashion. It is a natural simplification to focus on the payload mass, and to assume that $m_p \gg m_s$, and that μ is low, for the purposes of a dynamic investigation. However, this is not always true. Any reduction in k_s for which κ remains greater than κ_{max} will cause an increase in the dynamic factor. That increase occurs for all values of μ greater than zero, and it can be considered significant for values of μ which are not low. Reducing structure stiffness does not always reduce the dynamic factor.

In the same clause in DIN 15.018 the statement is also made that "The softer the springing of the hoisting gear...the smaller the [dynamic] factor Ψ." The term hoisting gear is assumed to apply to slings and below hook attachments. The claim is made that reducing the value of k_c reduces the dynamic factor. If this is so, then design engineers could always assume the stiffest likely values for k_c in their calculations without concern that this is not the critical case. If, when the crane is in service, web slings are substituted for chain slings, then k_c is reduced, and the dynamic loads due to hoisting are reduced. If the claim is not always true, then standards should give guidelines indicating the circumstances under which less than maximum k_c values should be investigated.

In the remainder of this section, the circumstances, if any, under which reducing k_c will reduce D, are determined. When k_c is reduced, κ is increased, and the structure coefficient S is either increased or decreased. Reducing k_c also reduces ω_c, which is a factor multiplied by S in the general formula

$$D = 1 + \frac{H_o \omega_c S}{g} \qquad (5.147)$$

Reducing k_c will increase D only for the case in which there is an increase in S, and only if that increase is great enough to compensate for the corresponding decrease in ω_c. The restriction on the rate of increase of S with respect to k_c is determined by first finding an expression for $\frac{dD}{dk_c}$.

$$\frac{dD}{dk_c} = \frac{d\,\dfrac{H_o\omega_c S}{g}}{dk_c}$$

$$= \frac{H_o\omega_c}{g}\frac{dS}{dk_c} + \frac{H_oS}{g}\frac{d\omega_c}{dk_c}$$

$$= \frac{H_o\omega_c}{g}\frac{dS}{d\kappa}\frac{d\kappa}{dk_c} + \frac{H_oS}{g\sqrt{m_p}}\frac{d\sqrt{k_c}}{dk_c} \qquad (5.148)$$

The ratio κ is defined as $\frac{k_s}{k_c}$, and therefore $d\kappa = -\frac{k_s}{k_c^2}\,dk_c$.

$$\frac{dD}{dk_c} = -\left(\frac{H_o\omega_c k_s}{g\,k_c^2}\right)\frac{dS}{d\kappa} + \frac{H_oS}{2g\sqrt{m_p\,k_c}} \qquad (5.149)$$

Reducing k_c will increase D when $\frac{dD}{dk_c} < 0$.

$$-\left(\frac{H_o\omega_c k_s}{g\,k_c^2}\right)\frac{dS}{d\kappa} + \frac{H_oS}{2g\sqrt{m_p\,k_c}} < 0$$

$$\frac{H_oS}{2g\sqrt{m_p\,k_c}}\,\frac{g\,k_c^2}{H_o\omega_c\,k_s} < \frac{dS}{d\kappa}$$

$$\frac{S}{2\kappa} < \frac{dS}{d\kappa} \qquad (5.150)$$

If the condition in (5.150) is satisfied, then a reduction in k_c will cause an increase in D.

Figures 5.18 and 5.19 show overlying graphs of values for $\frac{S}{2\kappa}$ and approximate values for $\frac{dS}{d\kappa}$ plotted against the log of κ. The curves are for jerk-starting and braking respectively, with μ set to a value of 1.5. The

Figure 5.18 Example Case in Which Decreasing k_c Increases Dynamic Factor

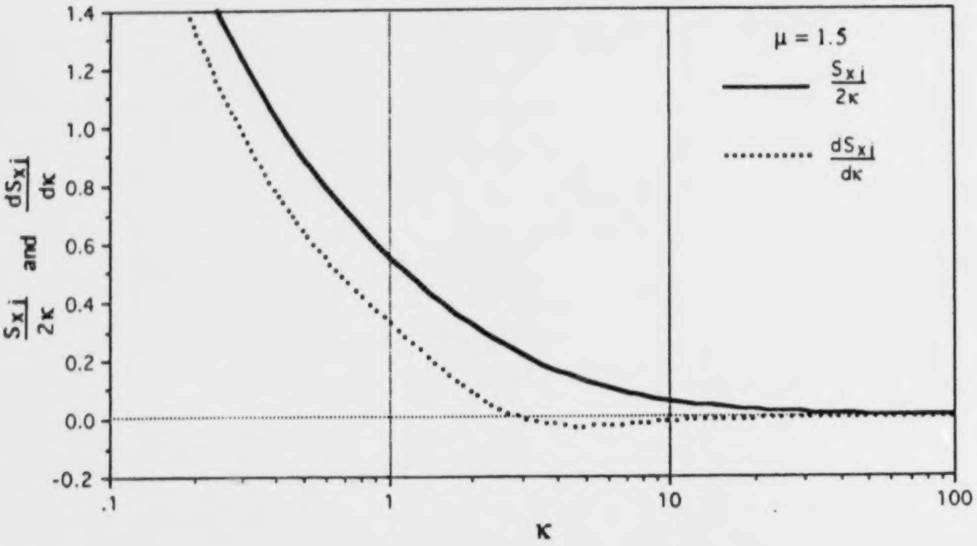

Figure 5.19 Example Case in Which Decreasing k_c Decreases Dynamic Factor

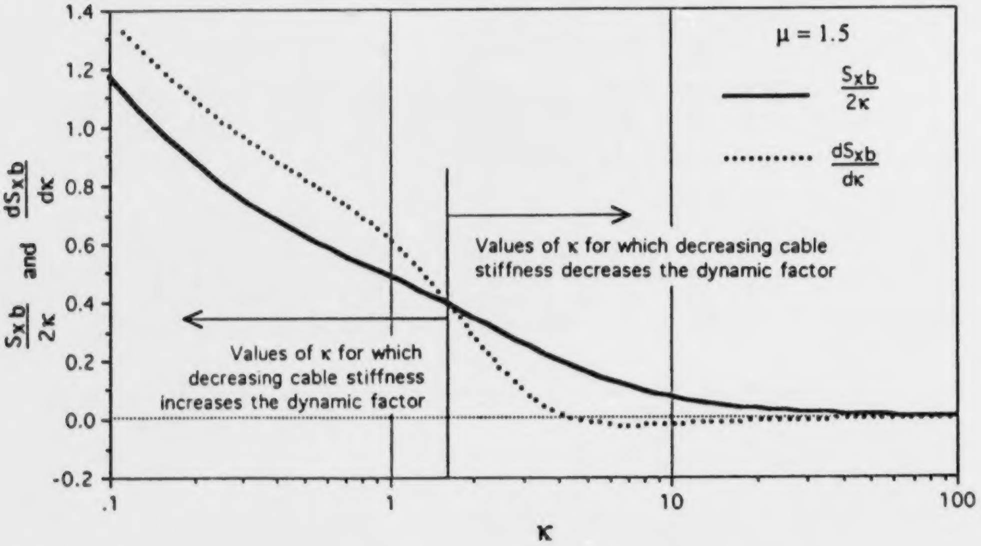

approximate $\frac{dS}{d\kappa}$ values are generated by calculating changes in rise over changes in run of the appropriate S versus κ curves over 60 evenly spaced points.

In the graph for jerk-starting, it is never the case that $\frac{S}{2\kappa} < \frac{dS}{d\kappa}$ and therefore, when $\mu = 1.5$ it is never the case that jerk-stating with less stiff slings will cause a higher dynamic factor. In the graph for braking, $\frac{S}{2\kappa} < \frac{dS}{d\kappa}$ when $\kappa < 1.7$. If the 3DoF model is accurate, then there are some situations in which the use of less stiff slings will cause increased dynamic loads.

5.10 Summary of Derived Dynamic Factors

Analysis of a simple 3 DoF model provides dynamic factor formulae. The dynamic factors are applied to the weight of the payload. The dynamic effects of starting are taken into account by the following formula.

$$D_{3xj} = 1 + \frac{S_{xj} H_o \omega_c}{g}$$

$$\text{where} \quad S_{xj} = \sqrt{\kappa\mu}\left(\frac{(\kappa + \gamma_2)\left(\frac{\omega_s}{\omega_2}\right) + (\kappa + \gamma_3)\left(\frac{\omega_s}{\omega_3}\right)}{(1+\kappa)(\gamma_2 - \gamma_3)}\right) \qquad (5.84)$$

The effects due to braking are taken into account by the expression below.

$$D_{3xb} = 1 + \frac{S_{xb} H_o \omega_c}{g}$$

$$\text{where } S_{xb} = \left(\frac{\sqrt{\mu\kappa}}{\gamma_1 - \gamma_2}\right)\left(\frac{\omega_s}{\omega_1} + \frac{\omega_s}{\omega_2}\right) \qquad (5.102)$$

Both dynamic factors approach 1 for the static case where hoisting speed is zero. Both factors are greater than one by an amount proportional to the hoisting speed. A number of assumptions were made in the derivations for the dynamic factors. They are listed below.

1. The crane structure acts as a single DoF spring and mass system.
2. The payload acts as a rigid mass.
3. The motor's mass is infinitely large compared to the other masses in the system.
4. While the motor is operating and under load, it has a constant speed of V_o.
5. Jerk-starting is the most severe starting case. Jerk-starting is defined as the case in which the payload is initially stationary and there is enough slack in the cable to allow the motor to achieve full speed before any tension develops in the cable.
6. The crane structure behaves in a quasi-static manner prior to lift off of the payload. Therefore, at the moment the payload lifts off, the acceleration of the crane structure is zero, and the velocity of the crane structure is downwards and equal to $\frac{H_o}{1 + \kappa}$.
7. When the brake is applied, the motor stops instantly.

The structure coefficients S_{xj} and S_{xb} depend upon κ, the ratio of the stiffnesses of the crane structure and the cable, and μ, the ratio of the masses of the crane and the payload. Generally, each structure coefficient reaches a maximum at some finite value of κ. In the limiting theoretical case in which μ approaches zero, the two structure coefficients approach the same value, given by $S = \sqrt{\frac{\kappa}{\kappa + 1}}$. The dynamic factor which accounts for the case where the vibrations due to braking and the vibrations due to jerk-starting act in phase has the formula

$$D_{3xbj} = 1 + \frac{(S_{xj} + S_{xb})H_o\omega_c}{g}. \qquad (5.123)$$

The formulas for of S_{xj} and S_{xb} when expressed in terms of μ and κ are unwieldy, and more convenient approximate expressions have been found. They are

$$S_{aj} \approx \frac{\sqrt{\kappa\,(1 + \mu + \kappa)}}{\kappa + 1}\left(1 + \frac{2\mu\kappa}{(1 + \mu + \kappa)^2}\right), \qquad (5.74)$$

and $$S_{ab} \approx \left(1 + \frac{2\mu\kappa}{(1 + \mu + \kappa)^2}\right)^3 \sqrt{\frac{\kappa}{1+\mu+\kappa}}\,. \qquad (5.91)$$

There are instances where decreasing the stiffness of the crane structure will increase the dynamic factor. There are also situations in which decreasing the stiffness of the cable or slings will also cause an increase in the dynamic factor.

Tables 5.2 and 5.3 show the frequencies and dynamic factors predicted by the 3DoF model for eight test setups. The derived values in Table 5.4 values are calculated from the effective cable stiffness (see Section 2.5).

Table 5.3 Summary of Calculated Frequencies

Trolley at	midspan	midspan	east end	east end	midspan	midspan	east end	east end
Payload mass, m_p (tonnes)	1.46	1.46	1.46	1.46	0.211	0.211	0.211	0.211
Sling type	chain	web	chain	web	chain	web	chain	web
k_s (kN/m)	3840	3840	7590	7590	3840	3840	7590	7590
k_c effective (kN/m)	2690	934	2690	934	697	183	697	183
m_s (tonnes)	0.499	0.499	0.751	0.751	0.499	0.499	0.751	0.751
κ	1.43	4.11	2.83	8.13	5.51	21.0	10.9	41.5
μ	0.342	0.342	0.514	0.514	2.37	2.37	3.56	3.56
ω_s (radians/second)	87.7	87.7	101	101	87.7	87.7	101	101
ω_c (radians/second)	42.9	25.3	42.9	25.3	57.5	29.5	57.5	29.5
ω_2 (radians/second)	31.9	22.5	36.2	23.8	50.9	28.7	54.1	29.1
ω_3 (radians/second)	118	98.5	119	107	99.0	90.0	107	102

Table 5.4 Summary of Predicted Dynamic Ratios

Trolley at	midspan	midspan	east end	east end	midspan	midspan	east end	east end
Payload mass, m_p (tonnes)	1.46	1.46	1.46	1.46	0.211	0.211	0.211	0.211
Sling type	chain	web	chain	web	chain	web	chain	web
k_s (kN/m)	3840	3840	7590	7590	3840	3840	7590	7590
k_c effective (kN/m)	2690	934	2690	934	697	183	697	183
m_s (tonnes)	0.499	0.499	0.751	0.751	0.499	0.499	0.751	0.751
κ	1.43	4.11	2.83	8.13	5.51	21.0	10.9	41.5
μ	0.342	0.342	0.514	0.514	2.37	2.37	3.56	3.56
$\frac{H_o \omega_c}{g}$ (m/s)	0.437	0.258	0.437	0.258	0.586	0.300	0.586	0.300
S_{xj}	0.870	0.964	0.992	1.01	1.48	1.13	1.48	1.10
D_{3xj}	1.38	1.25	1.43	1.26	1.86	1.34	1.87	1.33
S_{xb}	1.02	1.15	1.21	1.21	1.82	1.43	1.91	1.38
D_{3xb}	1.45	1.30	1.53	1.31	2.07	1.43	2.12	1.41

CHAPTER 6

TESTING PROGRAM

Dynamic tests were performed on the shop crane in the I. F. Morrison Structures Laboratory. The dynamic response was measured during a number of hoisting events. In this chapter the test procedure is described and the resulting data are presented and discussed.

There are four physical properties of the crane and payload system which affect the dynamic factors derived in Chapter 5. They are crane structure stiffness, crane structure mass, payload mass, and cable stiffness. To examine the effects these parameters have upon the dynamic response of a real crane, the test setup was varied in three ways.

1) The position of the hoist was a varied. In roughly half the tests, the hoist was located at the midspan of the crane bridge beam with the northern end truck wheels as near as possible to the craneway support column. This position corresponds to the structure computer model "2" in Chapter 4. In the other half of the tests, the trolley was positioned at the east end of the bridge, and the bridge was located equidistant from the craneway support columns. This position corresponds to the model "E" in Chapter 4. By varying the trolley location, the effect of changing the structure stiffness k_s could be measured. Varying the trolley location also changes the natural frequencies of the structure. The structure mass, as defined in Chapter 5, can be considered to be the stiffness of the structure divided by the square of the dominant frequency. In general, the rate at which k_s changes with respect to position is different from the rate at which the dominant frequency changes (see Figure 5.2). Therefore, varying the hoisting position between positions "2" and "E" also changed the structure mass.

2) Two different payloads were hoisted; a large payload weighing 14.35 kN, and a small payload weighing 2.07 kN. Changes in dynamic response due to variation in payload mass could therefore be examined. The large payload was chosen because its weight of 14.35 kN was near the crane's rated capacity of 17.8 kN. The small payload was chosen to investigate dynamic behaviour for higher values of μ.

3) Both web and chain slings were used for each hoisting location and for each payload. The effects of variations in k_c, and in the ratio κ, could thus be observed. For the large payload, 100 mm wide web slings were used. These slings were too bulky for the smaller payload, and 25 mm wide web slings were used instead. For the tests in which chain slings were required, No. 16 chains were used to hoist both payloads.

The dynamic factor is dependent upon the physical attributes of the structure, cable, and payload, and also upon the hoisting procedure. In Chapter 5, two dynamic factors, D_{3xj} and D_{3xb}, were derived, to account for hoisting and braking behaviour respectively. The factor D_{3xj} was derived specifically for the jerk-starting case, which was assumed to be the most severe starting case.

The test procedure was designed to verify the assumption that jerk-starting was the most severe starting case. For each combination of payload, sling, and hoisting position, three different starting conditions were tested.

1) The payload was suspended by the cable.

2) The payload rested upon the shop floor and the cable had some initial tension in it.

3) The payload was fully supported by the shop floor, and the cable was slack. For these tests the assumption was made that there was enough slack that the hoist motor could reach synchronous speed before tension developed in the cable. These tests are considered to represent the jerk-starting case.

For the three starting cases described above, the crane and payload were static at the beginning of each test. The motor was turned on and allowed to run for one to two seconds, and then turned off. Turning the motor off automatically initiated braking. Therefore each test also provided a sample of after-braking dynamic behaviour, and the accuracy of D_{3xb} could be examined.

Along with the three starting cases, a fourth variation of the test procedure was performed.

4) With the cable initially taught, and the crane structure static, the motor was turned on and off several times in quick succession. This procedure is called "plugging". It was performed to determine whether a random mix of

starting and braking could produce a more severe dynamic effect than jerk-starting.

A five symbol code was used to name, and to identify the features of each test. The code is summarized in Table 6.1. The following convention is used. Any group of tests with the same setup, as described by the first three symbols of the test name, is referred to as a test set. Any group of tests with the same starting condition, as indicated by the lower case fourth letter in the test name, is referred to as a test series.

Several stations were established on the crane. At each a number of parameters were recorded throughout the duration of each test. By comparing the maximum to the static values in this data, the dynamic ratios could be determined. Other aspects of the structure behaviour could also be examined and compared with the behaviour predicted by the 3DoF model.

Because displacements, moments, and shears were measured at different locations, the assumption that the structure can be considered as a single mode system, could be tested. If the structure can be modelled by a single mode system, then the ratios between displacements, moments, and shears should remain constant, at any one location and between different locations on the structure, throughout the testing time.

To test whether the motor delivers a constant hoisting speed, the payload displacement was recorded. The cable tension was also measured so that the assumptions relating to the variability of k_c could be examined.

Often data was recorded after braking, and in the cases of "plugging", after the last time the brakes were applied. The rate of damping during the ensuing free vibration of the crane and payload could be determined, and the assumption, that damping was not significant, could therefore be tested.

Figure 6.1 shows the two hoisting locations and indicates the stations and what parameters were recorded at each. Figure 6.2 is a diagram of the test set up. Figure 6.3 is a schematic diagram of the data collection and analysis system.

Table 6.1 Test Name Designations

Each test was assigned a five symbol code to identify the features of that test. For example: E B C t 3

First Symbol - indicates Hoisting Position.
E - trolley positioned at east end of bridge
2 - trolley positioned at midspan of bridge

Second Symbol - indicates Payload Size
B - large payload (14.35 kN) used
L - small payload (2.07 kN) used

Third Symbol - indicates Type of Slings
S - Web Slings used,
100 mm wide with large payload,
25 mm wide with small payload
C - No.16 Chain Slings used

Fourth Symbol - indicates Hoisting Process
h - payload hanging from slings when motor started
t - payload on floor and cable and slings tight when motor started
s - payload on floor with cable and slings slack enough to allow motor to attain full speed before significant tension develops
b - same as s but with improvements to test setup
p - motor "plugged"; turned off and on in quick, random spurts

Fifth Symbol - indicates Test Run Number
1 - First test in series
2 - Second test in series
3 - Third test in series

Figure 6.1 Schematic Plan View of Shop Crane Showing Locations of Data Collecting Stations

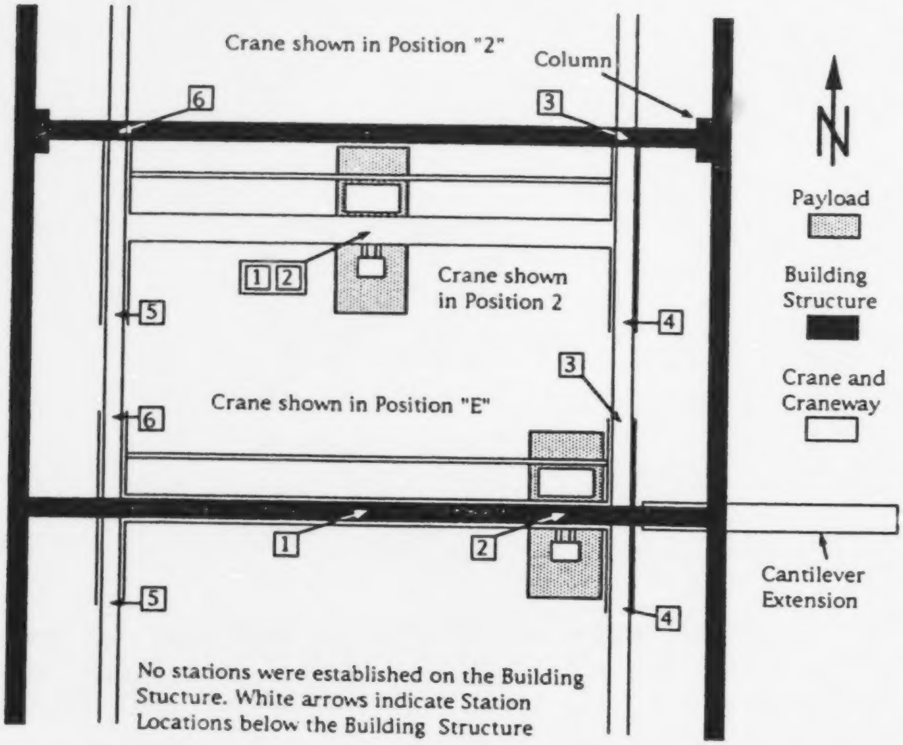
Crane shown in Position "2"
Column
6
3
1 2
Crane shown in Position 2
5
4
3
Crane shown in Position "E"
6
1
2
5
4
N
Payload
Building Structure
Crane and Craneway
Cantilever Extension

No stations were established on the Building Stucture. White arrows indicate Station Locations below the Building Structure

Station 1	Strain Gauges on Bridge at Midspan to record Bending Moment Strain, and Accelerometer on Bridge at Midspan to record Bridge Midspan Accellerations
Station 2	LVDTs to record Payload Displacement, and Bridge Displacement, and Tension Load Cell to record Cable Tension
Station 3	Fabricated Load Cell on Northeast End Truck Wheel Assembly to record Reaction Forces between Crane and Craneway
Station 4	LVDT under Craneway at Southeast End Truck Wheel Assembly to record Craneway Displacement, and Fabricated Load Cell on Southeast End Truck Wheel Assembly to record Reaction Forces between Crane and Craneway, and Accelerometer at Southeast End Truck Wheel Assembly to record Accelerations
Station 5	Fabricated Load Cell on Southwest End Truck Wheel Assembly to record Reaction Forces between Crane and Craneway
Station 6	Fabricated Load Cell on Northwest End Truck Wheel Assembly to record Reaction Forces between Crane and Craneway

Figure 6.2 Typical Test Setup

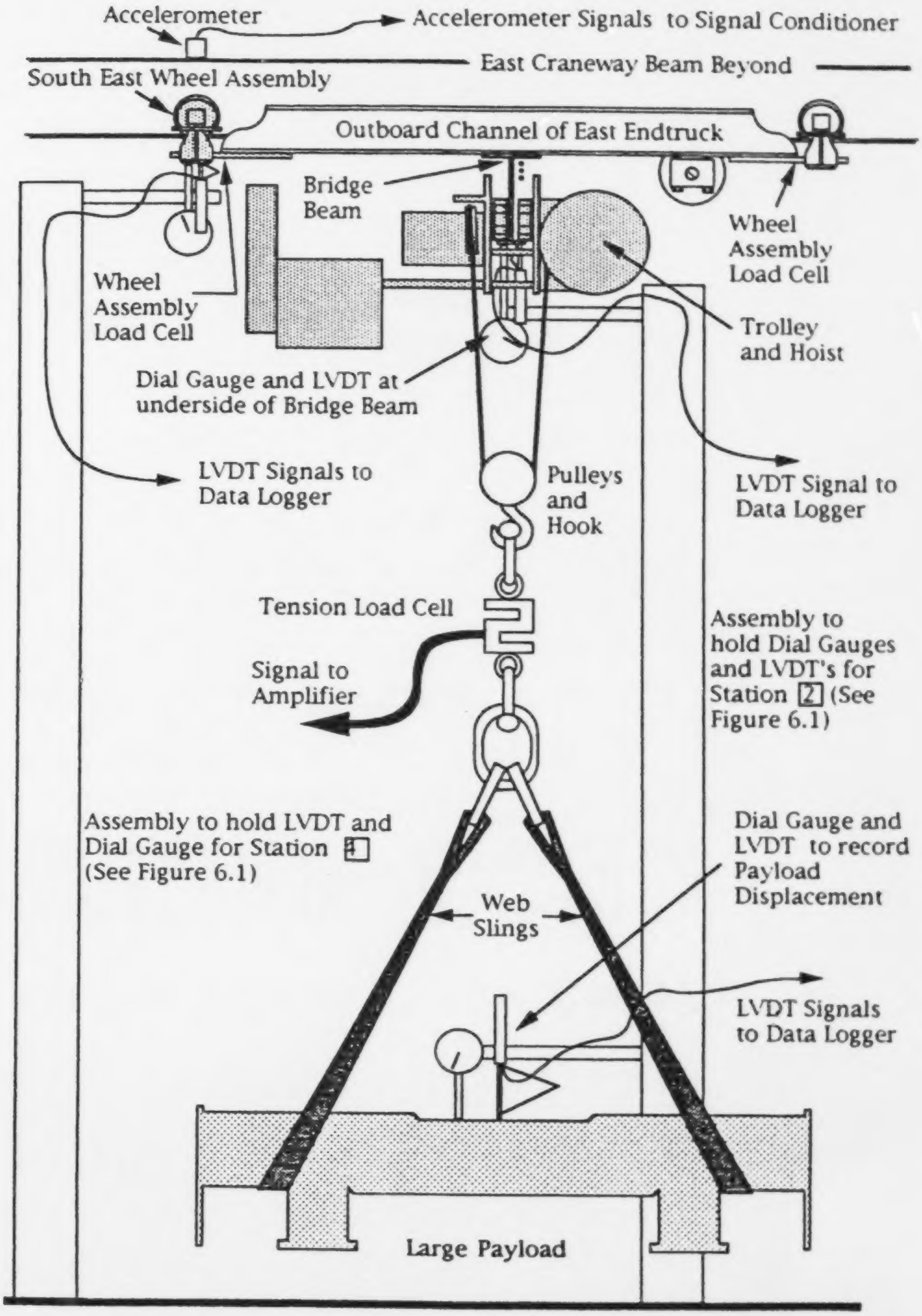

Accelerometer
Accelerometer Signals to Signal Conditioner
East Craneway Beam Beyond
South East Wheel Assembly
Outboard Channel of East Endtruck
Bridge Beam
Wheel Assembly Load Cell
Wheel Assembly Load Cell
Trolley and Hoist
Dial Gauge and LVDT at underside of Bridge Beam
LVDT Signals to Data Logger
Pulleys and Hook
LVDT Signal to Data Logger
Tension Load Cell
Signal to Amplifier
Assembly to hold Dial Gauges and LVDT's for Station 2 (See Figure 6.1)
Assembly to hold LVDT and Dial Gauge for Station 4 (See Figure 6.1)
Dial Gauge and LVDT to record Payload Displacement
Web Slings
LVDT Signals to Data Logger
Large Payload

Figure 6.3 Processing and Data Analysis Steps

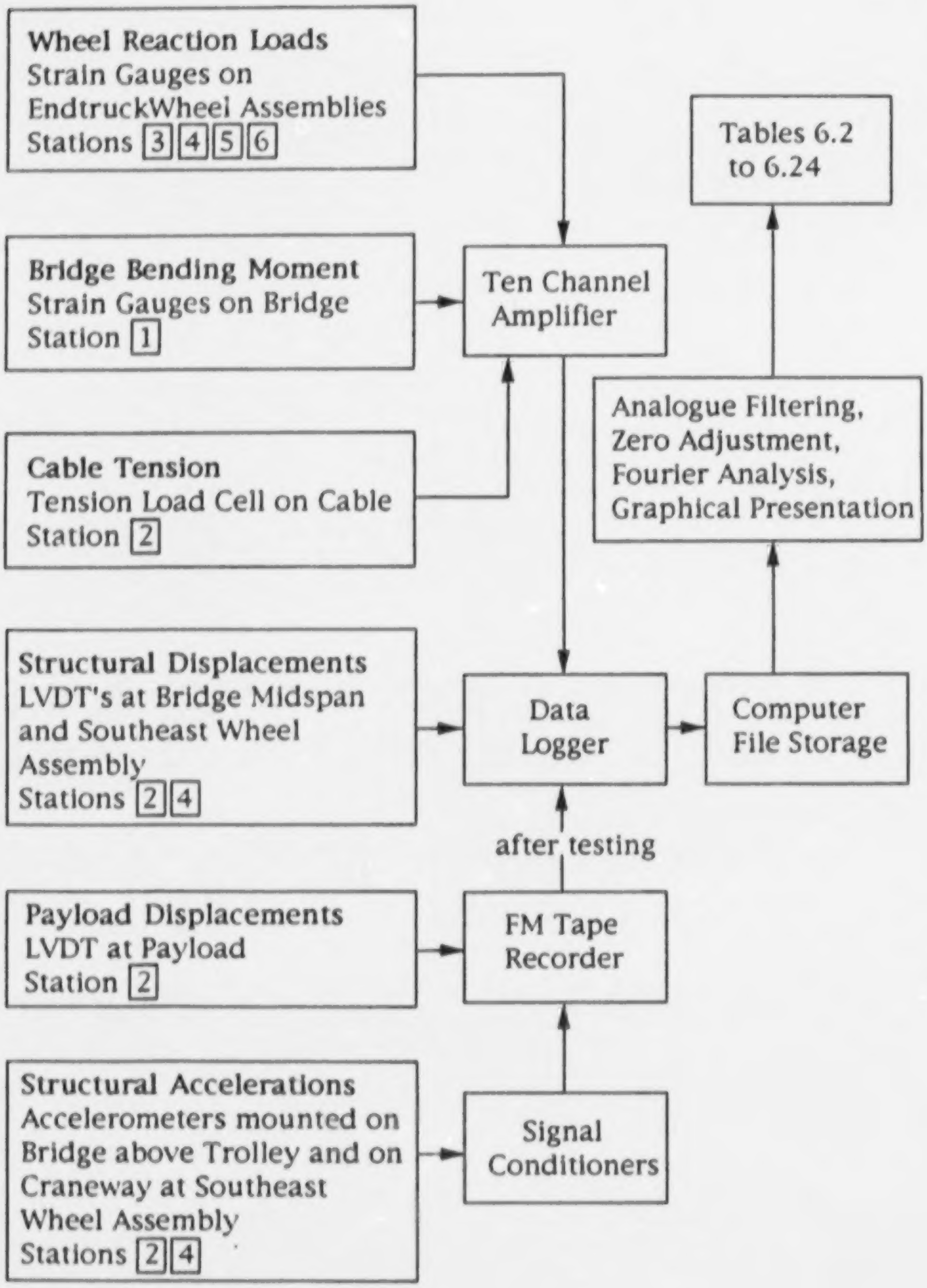
Wheel Reaction Loads
Strain Gauges on
EndtruckWheel Assemblies
Stations 3 4 5 6
Bridge Bending Moment
Strain Gauges on Bridge
Station 1
Cable Tension
Tension Load Cell on Cable
Station 2
Structural Displacements
LVDT's at Bridge Midspan
and Southeast Wheel
Assembly
Stations 2 4
Payload Displacements
LVDT at Payload
Station 2
Structural Accelerations
Accelerometers mounted on
Bridge above Trolley and on
Craneway at Southeast
Wheel Assembly
Stations 2 4
Ten Channel
Amplifier
Data
Logger
after testing
FM Tape
Recorder
Signal
Conditioners
Computer
File Storage
Analogue Filtering,
Zero Adjustment,
Fourier Analysis,
Graphical Presentation
Tables 6.2
to 6.24

6.1 Setup and Calibration

6.1.1 Acceleration Measurement

Bruel and Kjaer type 4370 accelerometers were used to monitor the acceleration of the crane structure, and to provide frequency data that could be compared with the data from the LVDT's and strain gauges.

The accelerometers comprise a layer of piezoelectric material sandwiched between two pieces of steel, one of which acts as a base, the other as a cantilevered mass. The shear deflections of the layer of piezoelectric material cause its capacitance to change [ref. 25]. Coaxial cables connected the accelerometers to Bruel and Kjaer type 2635 charge amplifiers, referred to as signal conditioners. The signal conditioners measured the capacitance of the piezoelectric layer, and produced a corresponding voltage signal which was recorded.

The accelerometers, conditioners, and cables were calibrated in tests for a previous project [ref. 20]. The conditioners were set to deliver a signal of $1\ \mathrm{V}/1\mathrm{m}/\mathrm{s}^2$, and to apply a 0.2 Hz high pass filter and a 0.1 kHz low pass filter to the signal.

The filtered signal was passed to an FM tape recorder. The channels on the tape recorder were set to cut off at ±1.0 volts, corresponding to an acceleration range of $\pm 1\mathrm{m}/\mathrm{s}^2$. This limit was determined by assuming that the dynamic factor would be around 1.3, and so the largest displacement amplitude would be

$$\frac{14.35\ \mathrm{kN}}{3680\ \mathrm{kN/m}} \times 0.3 = 1.1\ \mathrm{mm}.$$

The second natural frequency of the crane and payload system was expected to be about 30 radians/sec. (see Table 5.2). Therefore, the maximum accelerations were estimated to be

$$1.1\ \mathrm{mm} \times (30\ \mathrm{radians/second})^2 = 1\mathrm{m}/\mathrm{s}^2.$$

It was found that this limit was too restrictive and as a result the peaks of some of the acceleration signals were not recorded. However, the acceleration signals obtained were satisfactory for determining frequency.

6.1.2 Displacement Measurement

Linear Voltage Displacement Transducers (LVDT's), were used to measure the displacements of the payload, the bridge directly above the payload, and the U bracket directly under the southeast wheels of the end truck. Frames, separate from the crane, were used to hold the LVDT's in place during testing. At first 2 x 4 wooden columns jacked against the ceiling were used. These were light and easy to set up and rigid enough to hold the LVDT's steady, but it was found during testing that the ceiling near the crane deflected with the crane. The wooden columns moved slightly, but enough to alter the LVDT readings significantly. Once this was discovered, free standing steel posts with base plates were used to hold the LVDT's. These posts were quite stable and so massive that they were inconvenient to move. But once set up they provided a rigid platform from which reliable displacement measurements could be taken. All the "b" series tests and all the tests using the smaller payload were conducted using the steel posts.

All the cores of the LVDT's were spring loaded, rather than being glued to the structure. This was done to facilitate disassembly of the test apparatus, a task which had to be done many times. Also, the movements of the crane were not exclusively vertical. There was some lateral movement and some rotation. Had the cores been glued to the structure, they would have been subjected to bending forces that would have hindered their smooth movement within their respective LVDT bodies, and this might have caused them to be damaged. The springs for the two LVDT's on the structure had stiffnesses of about 0.1 kN/m. The core had a mass of about 3 grams. The natural frequency of the LVDT system was, therefore, 180 radians/second, which is higher than the expected highest natural frequency of 118 radians/second for the EBC test set (see Table 5.2). The third LVDT was used to measure payload motion, and required greater travel than did the other LVDT's. The spring arrangement used was relatively flexible. The mass of the core for the payload LVDT was about 8 grams but the stiffness of the spring was about 0.02 kN/m. If damping due to friction between the core and body of the LVDT is ignored, then the natural frequency of the spring and core system is 50 radians/second. This is lower than the third natural frequencies, and some of the second natural frequencies, listed in Table 5.2. However, the frequency of vibration of the payload was not of concern. This data was intended to give approximate payload position and to be used to confirm hoisting speed. The low stiffness of the LVDT spring did not interfere with those purposes.

The core end of the LVDT at the end truck rested against a smooth piece of sheet metal glued in place to the underside of the U bracket. The core end of the LVDT at the payload rested on a smooth piece of sheet metal as well. A dial gauge was mounted beside each LVDT. Its readings were used to verify the initial and final displacements recorded by the LVDT.

The LVDT's were calibrated after all the testing was completed. During calibration, all three LVDT's remained in the same electric circuit used during testing. Each LVDT in turn was mounted on a frame that also held a micrometer. The micrometer was situated in line with the LVDT so that adjusting the micrometer would move the core of the LVDT. The calibration signals were passed directly to the data logger. Appendix A.2 gives the calibration curves and the resulting calibration factors.

6.1.3 Wheel Loads

Four identical endtruck wheel assemblies supported the crane upon the craneway. A typical wheel assembly is shown in Figure 6.4. The two wheels of each assembly rode on the upper surface of the lower flange of the craneway rail, and were held in place by a stiff U shaped bracket that hung beneath the craneway rail. A flame cut Y shaped plate rested in a ball and socket cradle at the bottom of the U bracket. The Y plate was welded to the bottom flanges of the two channels that made up the end truck.

The vertical reactions between the wheels and the bottom flange of the crane rail could not be measured directly. Instead, signals generated by bending strains in the Y plates were used to generate the wheel load data. An assumption was made that during testing the bending strains in the Y plate were proportional to the reactions at the wheels. This assumption implied that the inertial forces acting upon the assembly were negligible. Figure 6.5

Figure 6.4 Endtruck Wheel Assembly

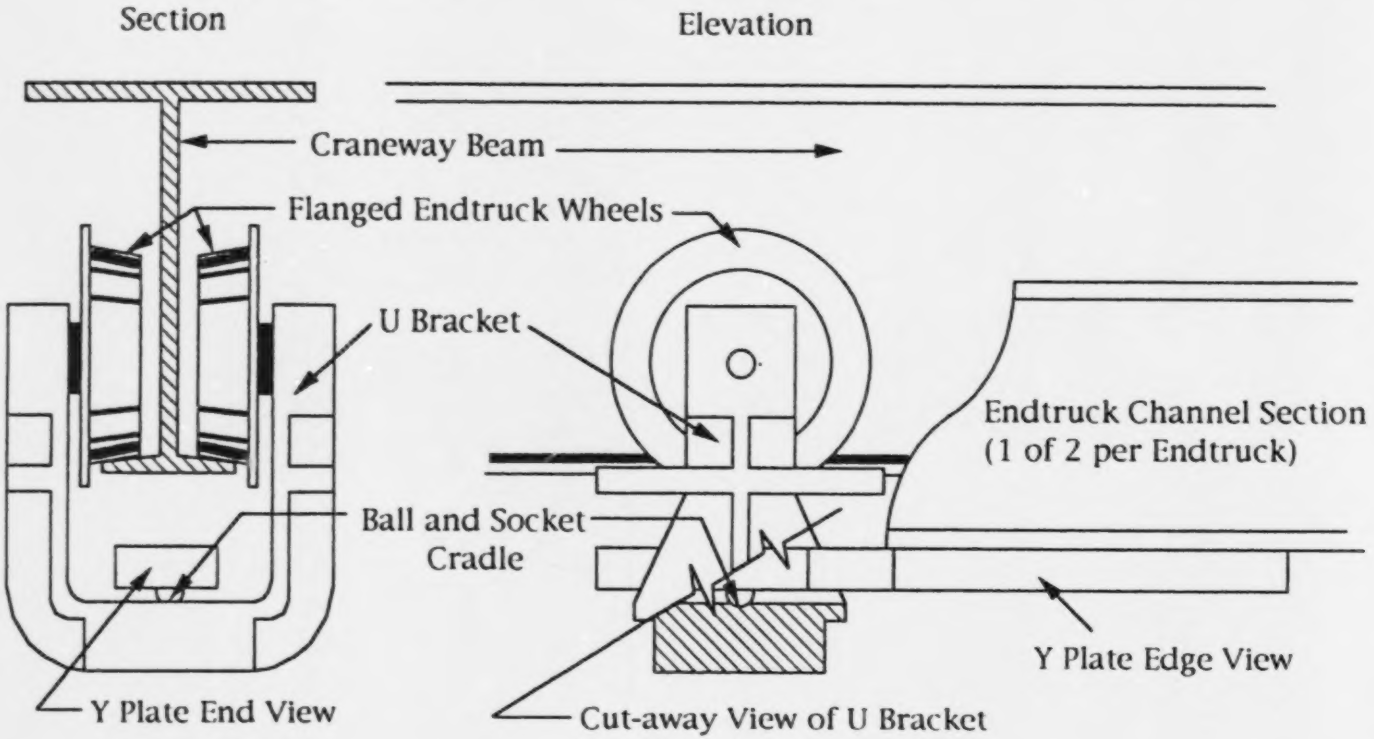
Section
Elevation
Craneway Beam
Flanged Endtruck Wheels
U Bracket
Ball and Socket Cradle
Endtruck Channel Section (1 of 2 per Endtruck)
Y Plate End View
Y Plate Edge View
Cut-away View of U Bracket

Figure 6.5 Free Body Diagram of Endtruck Wheel Assembly

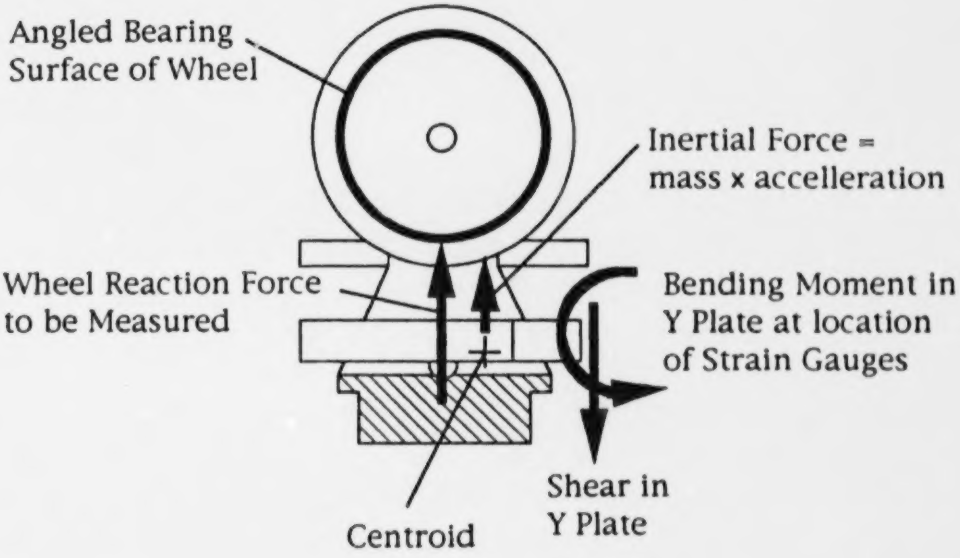
Angled Bearing
Surface of Wheel
Inertial Force =
mass x accelleration
Wheel Reaction Force
to be Measured
Bending Moment in
Y Plate at location
of Strain Gauges
Shear in
Y Plate
Centroid

Cut-away View of Endtruck Wheel Assembly shows a free body diagram of the wheel assembly. The mass of the whole assembly was estimated to be less than 20 kg, and the accelerations were estimated to be about 1m/s^2. Therefore, the maximum anticipated inertial loads were about 20 N. The static load held by one pair of wheels at one corner of the crane under the weight of the small payload was $\frac{2.07 \text{ kN}}{4 \text{ pairs of wheels}}$ = 520 N, which is 26 times the expected inertial load. The inertial load was therefore considered insignificant.

Strain gauges were mounted on the upper and lower surfaces of the Y plate, aligned to the estimated direction of principal strains, and located where the strains were expected to be maximum. The gauges were wired in a full Wheatstone bridge circuit, as shown in Figure 6.6.

Each wheel assembly Wheatstone bridge was individually calibrated using the following procedure. A standard, pre-calibrated, load cell was fixed to one end of a threaded piece of steel pipe, and a jack was fixed to the other. This assembly was tall enough to reach from the floor to the underside of the U bracket. The jack raised the pipe, which lifted the end truck wheels a few millimeters off the crane rail. Then the 1.46 tonne payload was hoisted, putting load onto the pipe and load cell. The signal from the load cell was recorded, as was the signal received through the Wheatstone bridge by the data logger. Three levels of loading were obtained by moving the loaded hoist to different locations. The wheels of the assembly being calibrated were examined to be sure they were not touching the crane rail, and that all load transferred to that U bracket was being carried by the load cell and pipe (see Figure 6.7).

The bridge drive wheels (see Figure 2.1) were spring loaded. They pushed up on the underside of the crane rail bottom flange. This gave a high enough normal load to develop a friction force sufficient to drive the crane. During the calibration the wheel springs were slackened to the point where the drive wheels did not touch the crane rail. During the testing, however, the springs were tight and the drive wheels remained operational. This was done to ensure in-service conditions when the crane's dynamic response was measured.

Figure 6.6 Y Plate Load Cell

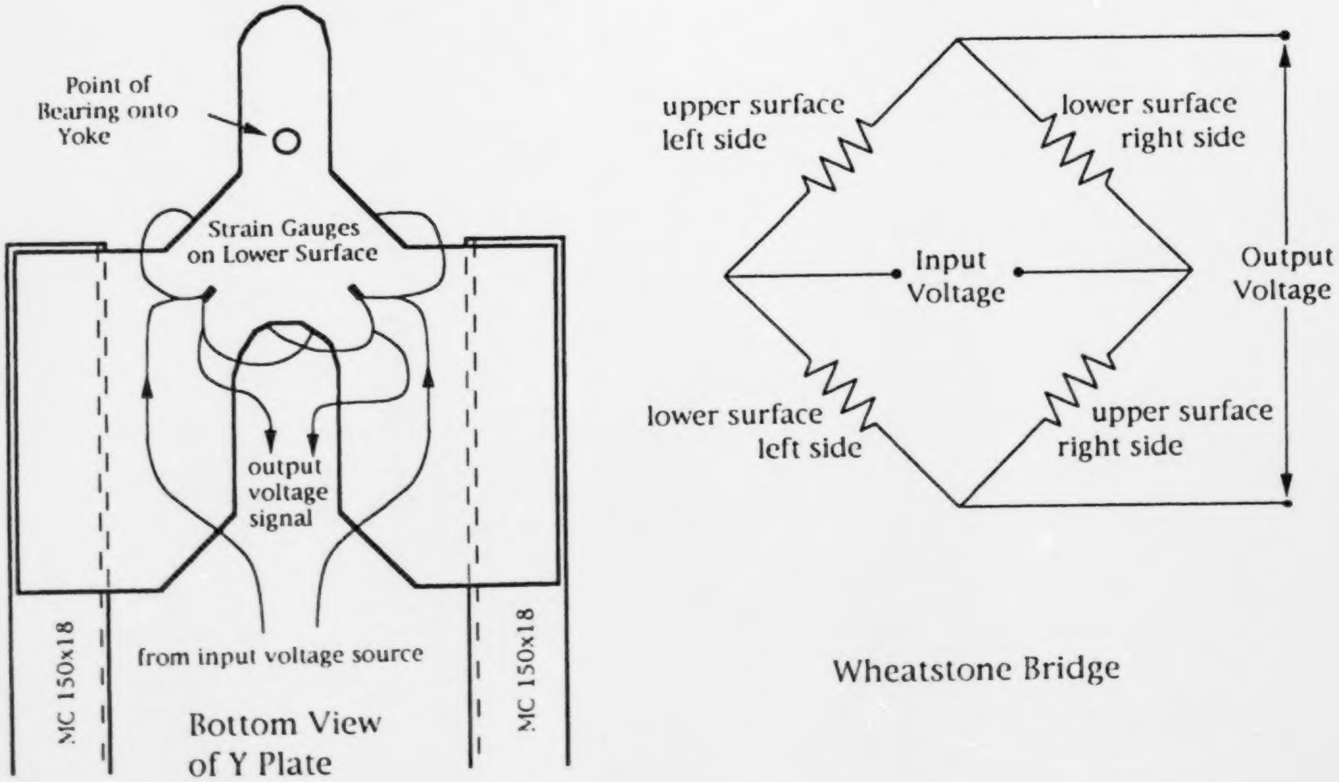
Point of
Bearing onto
Yoke
Strain Gauges
on Lower Surface
output
voltage
signal
from input voltage source
MC 150x18
MC 150x18
upper surface
left side
lower surface
right side
Input
Voltage
Output
Voltage
lower surface
left side
upper surface
right side

Bottom View of Y Plate

Wheatstone Bridge

Figure 6.7 Wheel Assembly Load Cell Calibration

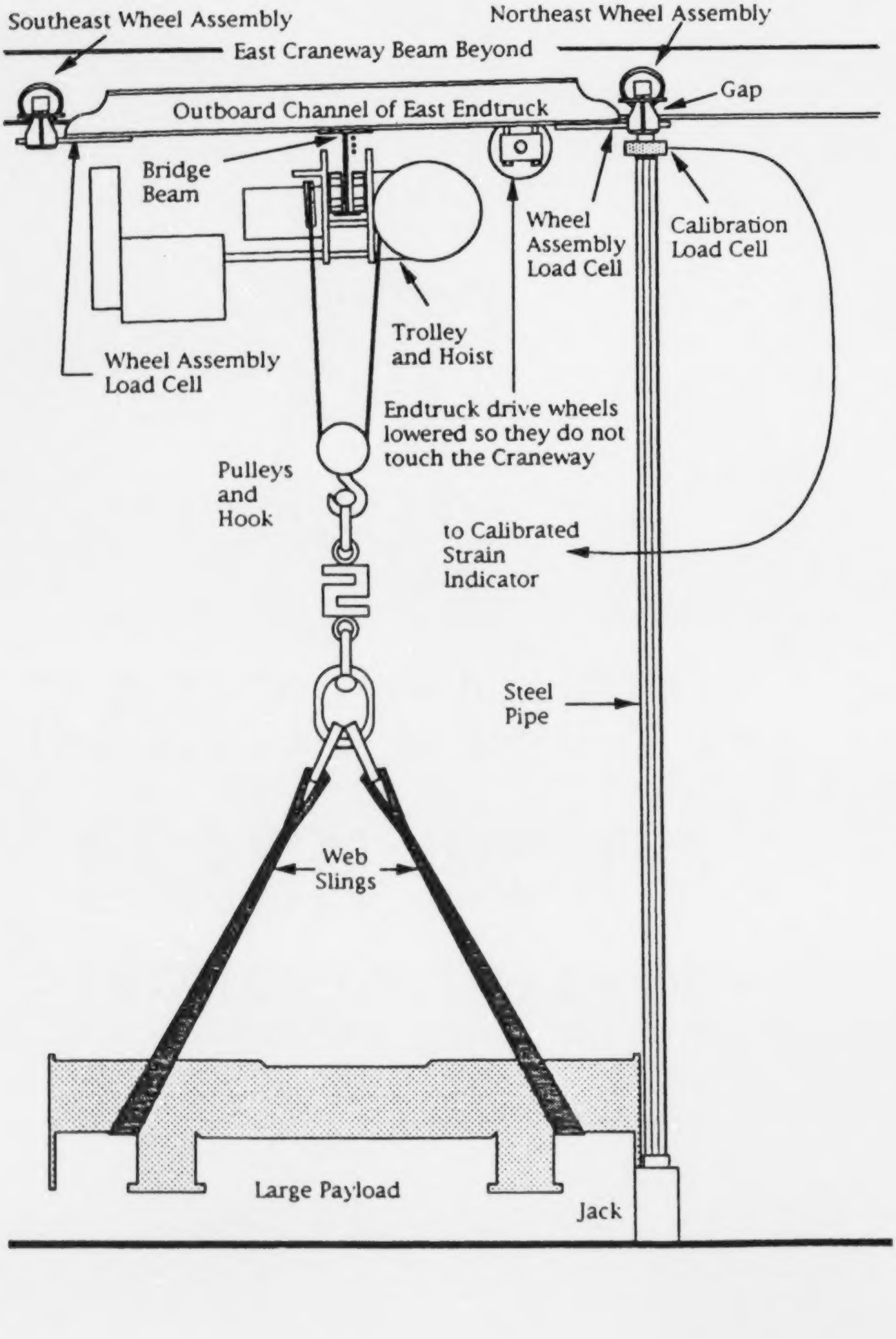
Southeast Wheel Assembly
Northeast Wheel Assembly
East Craneway Beam Beyond
Gap
Outboard Channel of East Endtruck
Bridge Beam
Wheel Assembly Load Cell
Calibration Load Cell
Trolley and Hoist
Wheel Assembly Load Cell
Endtruck drive wheels lowered so they do not touch the Craneway
Pulleys and Hook
to Calibrated Strain Indicator
Steel Pipe
Web Slings
Large Payload
Jack

Appendix A.3 contains the calibration graphs for these four load cells. As with the other strain gauge measurements, the wheel load cell voltage was passed through a multi-channel amplifier. An amplification factor of 1000 was used for each of the signals.

The amplifier was set up at the west end of the craneway, and north of the testing locations for the crane. Therefore, the input and output voltage wires for both the wheel load cells on the east side had to run on top of the bridge beam, parallel to the hoist and trolley power bars for the whole 5.5 m span. The signals from both these wheel assemblies were subject to electrical interference when the crane motor was operating. Therefore, on the amplifier channel for the southeast wheel the amplifier's low pass filter was set to 10 Hz, or 63 radians per second. This was high enough to allow recording of second mode vibration signals, but filter out third mode vibrations.

6.1.4 Bridge Bending Moment

The bridge bending strains were measured using a full Wheatstone bridge with four active strain gauges, two mounted on the top surface, and two on the bottom surface of the bridge beam at center span. Because the crane had to available for other tasks between tests, all the lead wires for these strain gauges had to traverse half the span of the crane bridge beam so as not to interfere with the motion of the trolley, and to avoid being severed between the trolley wheels and the top surface of the bottom flange of the bridge. The leads were connected to form a Wheatstone bridge at the connection to the amplifier. Figure 6.8 shows the wiring arrangement. The wires that ran along the underside of the bridge beam were secured with 75x75 mm pads of ceiling panel material glued to the bottom surface of the bottom flange.

The factor used to convert the data logger signal to bridge bending moment was determined as follows. The expected bridge moment developed under static weight of the large payload, 14.35 kN, was calculated.

$$M = \frac{(14.35\text{ kN})(5.482\text{ m bridge span} - 0.204\text{ m trolley span})}{4} = 18.93\text{ kN}\cdot\text{m}$$

The strain gauge signal was set to zero with the unloaded trolley at midspan. When the 14.35 kN payload was lifted, the signal returned by the data logger was 1167. The factor, therefore, was $\frac{18.93\text{ kN}\cdot\text{m}}{1167} = 16.20 \times 10^{-3}\text{ kN}\cdot\text{m}$.

Figure 6.8 Wiring Arrangement for Strain Gauges on Bridge Beam

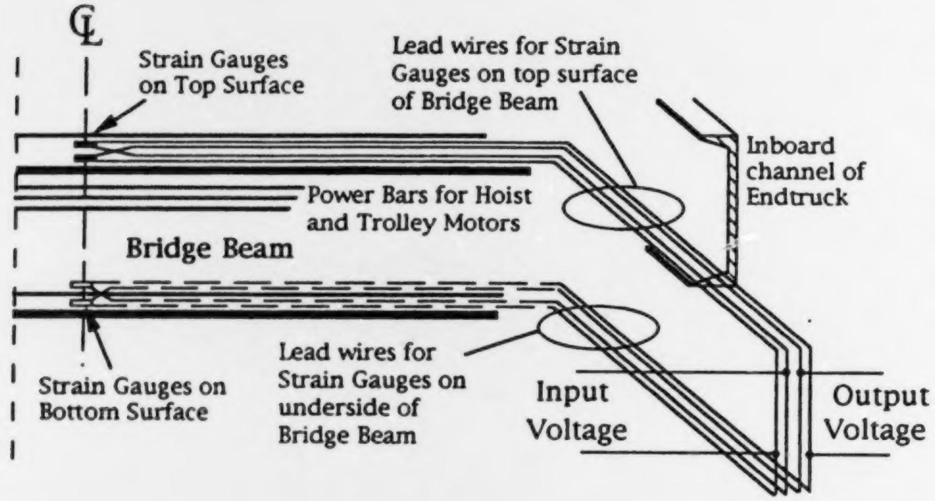
℄
Strain Gauges on Top Surface
Lead wires for Strain Gauges on top surface of Bridge Beam
Inboard channel of Endtruck
Power Bars for Hoist and Trolley Motors
Bridge Beam
Lead wires for Strain Gauges on underside of Bridge Beam
Strain Gauges on Bottom Surface
Input Voltage
Output Voltage

Section View of Bridge Beam and Trolley

Wheatstone Bridge Wiring Diagram

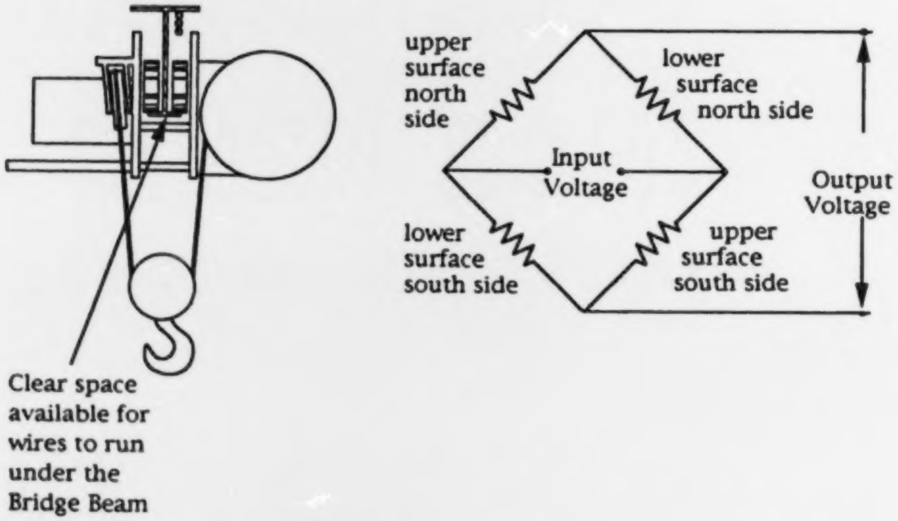
Clear space available for wires to run under the Bridge Beam
upper surface north side
lower surface north side
Input Voltage
Output Voltage
lower surface south side
upper surface south side

This figure is confirmed by calculating the amplification of the signal. The sum of the strains at each of the four strain gauge locations on the bridge section is

$$\begin{aligned}\Sigma\varepsilon &= \varepsilon_{\text{top south}} + \varepsilon_{\text{top north}} + \varepsilon_{\text{bottom south}} + \varepsilon_{\text{bottom north}} \\ &= \frac{2My_{\text{top}}}{EI} + \frac{2My_{\text{bottom}}}{EI} \\ &= \frac{2Md}{EI}\ ,\end{aligned}$$

where y_{top} and y_{bottom} are the distances from the centroid of the member to the top and bottom surfaces respectively, and d is the member depth.

The member depth was 304 mm, Young's modulus is 200 GPa, the moment of inertia, I_{xx}, for the member was 76.2 x 106 mm^4, and M was the bridge beam moment. Therefore, the sum of the strains is

$$\begin{aligned}\Sigma\varepsilon &= \frac{2M(304\text{ mm})}{(200\text{ GPa})(76.2 \times 10\text{-}6\text{ mm}^4)} \\ &= (39.9 \times 10^{-6}/\text{kN}\cdot\text{m})\ M\ .\end{aligned}$$

The gauge factor for these strain gauges was 2.07. The input voltage from the amplifier (see Section 6.2.2) was 5V, and the amplification factor was set to 750. The amplifier can be set to compensate for a full bridge, rather than half bridge circuit. The data logger converts a 5V signal to the number 2048. Therefore, the moment factor can be derived as follows.

$$\begin{aligned}&\frac{M}{\text{data logger signal}} \\ &= \frac{\left(\frac{5V}{2048}\text{ data logger ratio}\right)(2\text{ for Full Bridge Setting})}{(\text{ 750 amplification})(5\text{ V input})(39.9 \times 10^{-6}/\text{kN}\cdot\text{m})(2.07\text{ gauge factor})} \\ &= 15.8 \times 10^{-3}\text{ kN}\cdot\text{m}\end{aligned}$$

The previously derived value of 16.2 x 10^{-3} kN·m is about 3% greater.

A check on the individual strain gauge readings revealed that when the bridge was loaded at midspan, the southern strain gauges produced slightly lower signals than did the northern strain gauges. It was assumed this was due to some axial rotation of the bridge, brought on by the influence of the drive shaft on the location of the shear centre. This was not confirmed through calculation. The moment of inertia used in the calculations above includes the effect of the drive shaft. (See Figure 2.3)

6.1.5 Cable Tension

Cable tension was measured using an HBM USB 10 kip tension load cell, attached through the amplifier to the data logger. The cell was first connected to a Vishay Ellis-20 Digital Strain Indicator and calibrated on the MTS machine in the I. F. Morrison Structures Lab. The load cell was then attached to the shop crane and the large and small payloads were weighed (see Section 2.4). Then the cell was connected through the amplifier to the data logger. The signal was zeroed when the cell was unloaded, and when the cell carried the 14.35 kN payload, the data logger produced a signal of 1055. Therefore the calibration factor for the cable tension is

$$\frac{14.35\text{ kN}}{1055} = 13.6 \times 10^{-3}\text{ kN.}$$

A low pass filter of 10 Hz, or 63 radians/second was set on the amplifier channel that carried the tension signal.

6.2 Recording and amplifying equipment

6.2.1 FM Tape Recorder

A four channel FM Tape Recorder received the craneway accelerometer signal on channel one, the bridge accelerometer signal on channel two, and the payload LVDT signal on channel three. Channels one and two had their maximum ranges set at ±1V. The maximum range for channel three was set at ±5V. Channel four was not used. A tape speed of $3\frac{1}{3}$ fpm was selected for the testing. The tape position for each set of test data was recorded with the position counter. Later, the tape signal was played back into the data logger for analogue-to-digital conversion.

6.2.2 Validyne Amplifier

The Validyne Amplifier was a ten channel amplifier. Each channel was controlled by a removable cassette, called a CD19 carrier demodulator. Each carrier demodulator sent an input potential of 5V AC to its connected Wheatstone bridge and sent a DC output signal to the data logger. The output signal was equal to the set amplification factor times the output signal the carrier demodulator received from the strain gauge bridge. The electrical bridge was balanced by turning two adjustment screws on the front face of each carrier demodulator unit.

The Validyne amplifier seemed suitable for this application because many signals could be amplified using a single piece of equipment that was easy to adjust and run. However, failure of some of its components due to age or poor initial design caused problems during testing. On some channels electrical bridge balance could not be maintained. The balance adjustment screws were built in such a way that their connections to the carrier demodulator control board broke during adjustment. The error did not manifest itself in an obvious way, and unless a careful check was made on the affected channel, the error could go unnoticed throughout the test. Some remedial repairs were done on these connections, but results were never satisfactory for many of the channels. Therefore, the zero points for the strain gauge signals had to be adjusted when the data was reduced to Lotus files. (See section 6.3.1.)

6.2.3 Dash 8 Data Logger

The Dash 8 data logger was a computer component which performed high speed analogue to digital conversion and storage. A number of handling subroutines were written by Dale Lathe of the Civil Engineering electronics lab.

For this testing program the data logger was set to take 20 000 readings per test at a rate of 12 000 readings per second. The bridge bending moment, the four wheel loads, the cable tension, and the displacements at the trolley and at the southeast wheel were recorded by the data logger during testing. Therefore eight channels were used, and the rate of data acquisition was

$$\frac{12\,000 \text{ readings per second}}{8 \text{ channels}} = 1500 \text{ readings per second on each channel.}$$

The duration of each test was

$$\frac{20\,000 \text{ readings per test}}{12\,000 \text{ readings per second}} = 1\frac{2}{3} \text{ seconds per test.}$$

Over the full duration of a test, each channel received

$$1\frac{2}{3} \text{ sec/test} \times 1500 \text{ readings/sec/channel} = 2500 \text{ readings/test/channel.}$$

When this data was transferred to IBM Lotus files, only every third data point was used. This made the Lotus files a more convenient size for data manipulation. For each parameter, the time interval between adjacent data points in the file was 0.002 seconds. The maximum frequency of vibration that could be defined by the data on file was 250 radians per second, or 39 Hz, which is much higher than any expected third natural frequency, from Table 5.2. Higher frequency signals will be subject to aliasing and their frequencies will not be determinable with this data sampling rate.

6.3. Data Reduction

6.3.1 Setting Zero Points

It was intended that the data would be recorded such that zero displacement, tension, moment, and reaction forces occurred for the static case of the trolley positioned over the payload with the cable slack. Because of the failure of the amplifier to maintain a balanced bridge, techniques had to be developed after testing that would determine the zero points for the amplified data. The techniques were required for signals from the reaction forces at the four wheels, the bending moment at midspan, and the cable tension.

It was assumed that the drift of the zero points was small over the duration of one complete set of tests. Since all the sets included at least one series of tests where the cable was initially slack, ("s" or both "b" and "s"), the starting data values of these tests were assumed to be the zero points applicable to all the tests in that set. All the data values for the test set would be increased or decreased the same amount as the "slack" test series data values needed to be increased or decreased. The static load values from the tests where the payload was initially suspended were compared to the mean values recorded during free vibrations, and were found to be approximately equal. The zeroing procedure was therefore assumed to give accurate results.

In a few cases, this simple procedure was not possible. In some instances initial free vibrations having small but significant amplitude obscured the static values of the signals affected. In these cases, the duration of a free vibration period was estimated by examining the graph, and the data was averaged over an integer number of periods. In other instances the zero point was difficult to determine because the cable tension was some small but significant amount before data logging was started. Thus the first values recorded would not in general be zero point values. Also, some of the data collecting equipment was very sensitive to electrical interference from the nearby power bars of the crane. That data was effectively masked during the duration of the time that the crane power was on. (Section 6.3.2 describes this problem further.) In these cases, the average value of the free vibration phase at the end the hoisting event was set equal to the static value. The static value was determined from the "hanging" series test, in which the payload was initially suspended. The procedure of averaging over integer numbers of periods of free vibration was again used.

6.3.2 Electrical Interference and Filtering

Some of the wires carrying data signals ran near and parallel to the power bars that serviced the trolley and hoist motors. When the hoist motor was activated electric current ran through the power bars, in some cases causing induced voltage in the parallel signal wires. The induced voltage interfered with the voltage signals from the measuring devices.

Some of the electrical interference in the signals proved useful in one sense. Many of the data records show momentary spikes which correspond to the voltage peaks that occurred when the motor was turned on or off. In the recorded data the activation of the motor and the initiation of braking became events that were located temporally relative to the crane response. However, some of the recorded data was completely obscured by superimposed high frequency signals of varying amplitude. This interference was at about 60 Hz, and was only recorded at the times when the hoist motor was on.

The load data from the two wheel assemblies on the east side of the crane were most affected. The wires carrying these signals travelled the length of one endtruck and the length of the bridge parallel to the power bars. The strain gauge signals from the bridge midspan were carried on wires right beside those which carried the eastern wheel load signals, but were only beside the power bars for half the distance. The signal wires from the southwestern wheel assembly ran alongside power bars for only the span of the western endtruck, and those for the northwestern assembly did not travel any length parallel to power bars. The midspan signals and the signals from the western wheel assemblies were not significantly affected by the interference.

The wheel load data presented in Figure 6.9 illustrates electrical interference and filtering. The signal for the southeast wheel load was passed through a 10 Hz low pass filter. The filtered signal shows three interesting features. First, frequencies greater than 10 Hz, (63 radians/second), are not part of the signal. This frequency cut off is lower than the expected third natural frequencies listed in Table 5.2. The third mode contribution to the magnitude of the dynamic ratio is smaller than the contribution from the second mode. In Chapter 7 dynamic ratios from filtered and unfiltered signals will be compared.

Second, when compared with the other wheel load data, it can be seen that the southeast signal has been shifted out of phase and lags behind the others by approximately 0.015 seconds. The filtered signal voltage at any time t is a function of the voltage levels that occurred on the input side of the filter during the interval just prior to t. The lower the low pass frequency, the longer the interval required to produce a filtered voltage signal.

This leads to the third interesting feature. There is often a change of value in the southeast wheel load signal when the motor is switched on or off. These dips are voltage spikes that have been filtered. They are of much smaller magnitude and much greater duration than are the spikes the other wheel load signals display at those times. Generally the dips begin at the same

Figure 6.9 2BSb2 – Wheel Loads

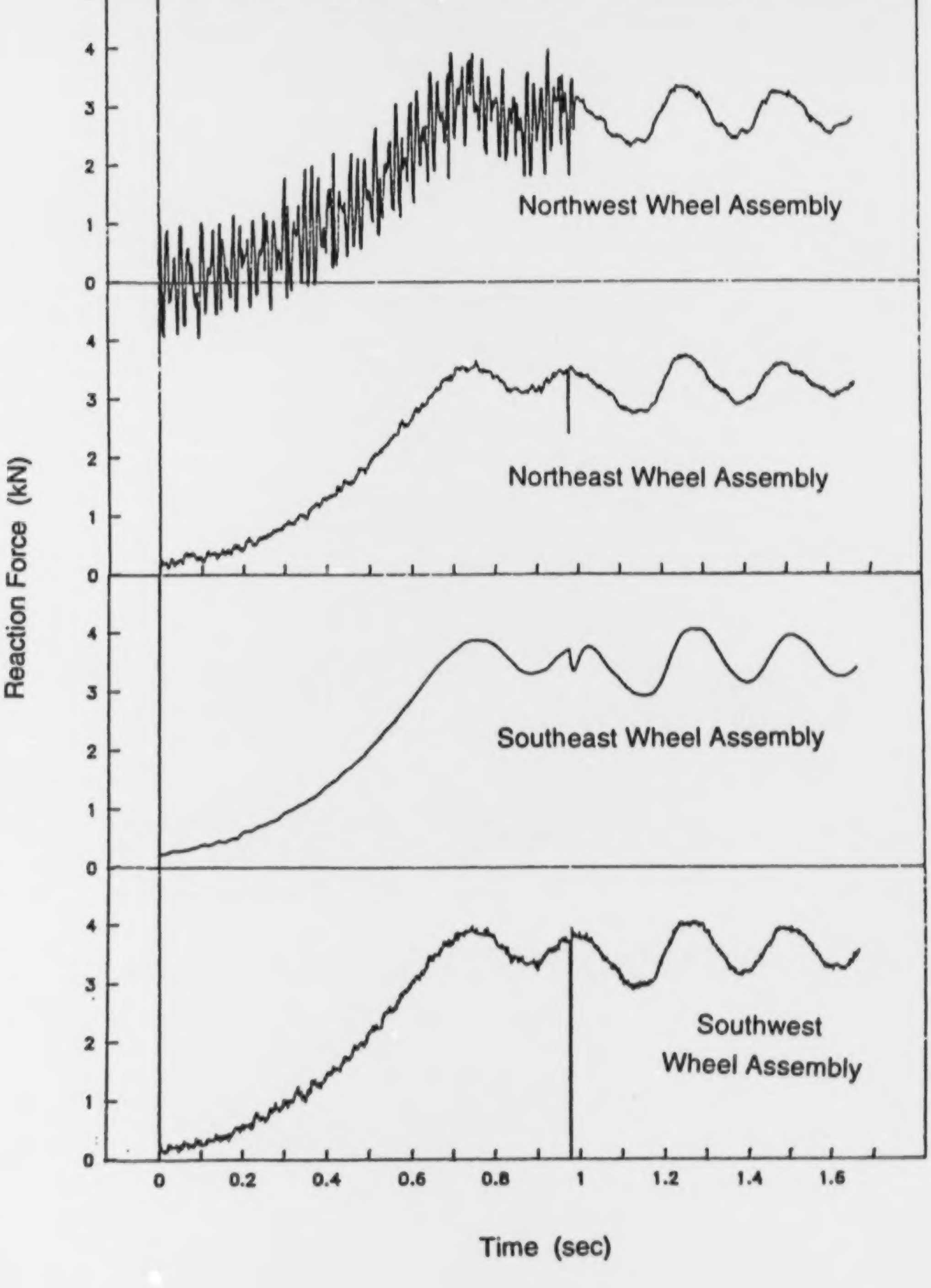

time as the spikes, and then fade out over about 0.03 seconds. This is another example of filtering causing a signal lag.

The unfiltered signal from the northeast wheel assembly was masked by electrical interference induced by the operation of the hoist motor. To get an estimate of the true value of the dynamic wheel load, a moving average of the unfiltered data was computed, and the results graphed. The data points for a moving average are generated using the following formula.

$$x_i = \sum_{j=i}^{i+n} \frac{x_j}{n} \tag{6.1}$$

In equation (6.1) x_i is the i^{th} moving average data point, and x_j is the j^{th} unfiltered data point. The number of unfiltered data points used to calculate a single averaged point is n. The total number of moving average points that can be generated, the maximum value for i, is n-1 less than the total number of unfiltered data points available.

It was found that performing this moving average technique with the unfiltered signals from the northeast wheel assembly, using a value of 15 for n, generated curves which are similar to the unfiltered signals from the two western wheel assemblies. Fifteen data points corresponds to a time span of 0.03 seconds, which is about twice as long as the period of the electrical interference obscuring the northeast wheel assembly signal. If the moving average data set is graphed such that each point, x_i, is plotted with the same abscissa as x_{i+n}, the graph displays all three of the qualities of the electronically filtered signal which were described previously.

Figure 6.9 is a graph of the four wheel load signals for test 2BSb2, showing the filtered south east signal and the unfiltered, masked, north east signal, and the two relatively clean signals from the two western wheel loads. The features described in the preceding discussion are indicated. Figure 6.10 shows the northeast wheel load signal, as originally recorded, and when filtered using an averaged band of 15 data points, with the averaged value plotted at the end of the band.

Figure 6.10 2BSb2 – NE Wheel Load

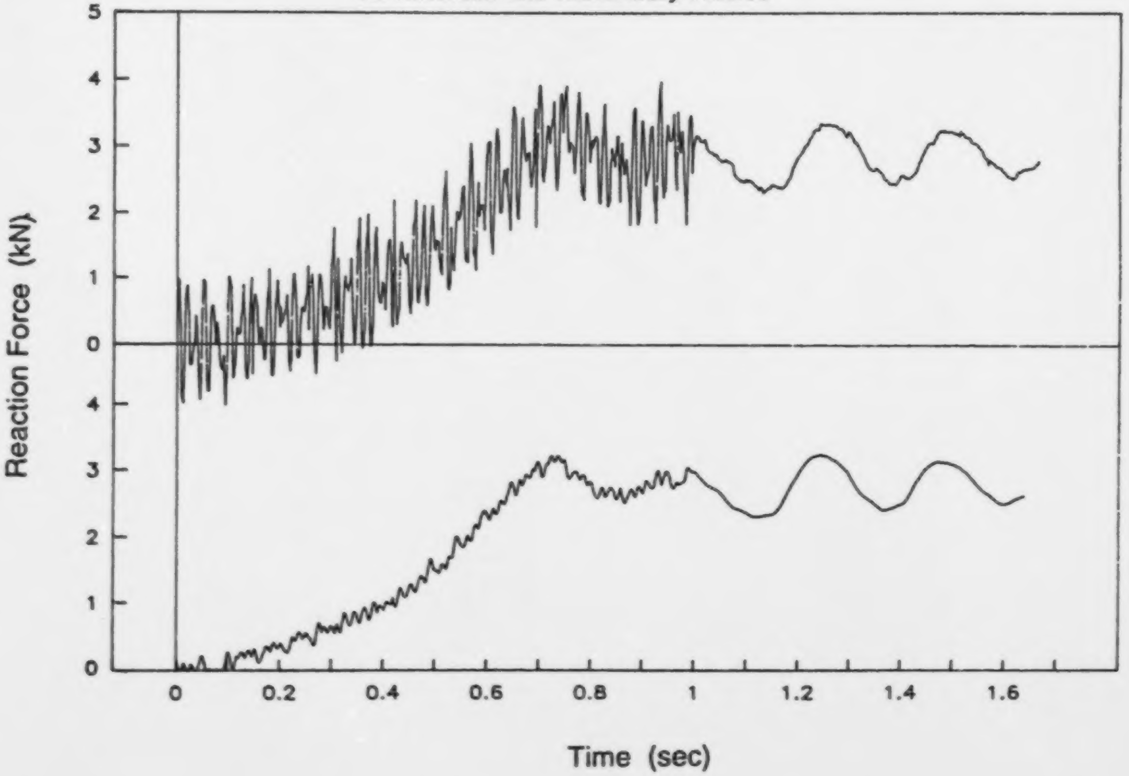

As Recorded and Numerically Filtered

For the tests which used the smaller payload, the western signals were also smoothed with numerical averaging using a 5 data point averaged band width. Tables 7.2 to 7.10 are based upon the filtered signals.

6.3.3 Acceleration Signals

The accelerometer signals show intervals in which high frequency signals mask the expected lower frequency structural response. Although the high frequency signals were generated at times when the hoist motor was running, and sometimes for short periods after, this interference does not appear to be due to induced voltage from the hoist motor. The interference does not have defined spikes bounding the times of hoist motor operation, and the interference is often present at times when the motor was not running. The coaxial cables connecting the accelerometers to the signal conditioners are resistant to induced voltages, and care was taken that those cables not travel any distance parallel to the power bars on the bridge or the craneway. The source of the interference is not known, but may be high frequency vibrations carried by the crane structure, and due to play in the bearings or gears of the transmission of the hoist.

Because the tape recorder channel was set to limit the signal at ±1.0V, or $\pm 1.0 m/s^2$, and the acceleration amplitudes during hoisting were sometimes greater than this, these sections of the accelerometer signals cannot be numerically filtered to reveal the first and second mode accelerations.

6.3.4 Displacement Signals

All the tests conducted using the large payload, except for the "b" series, have displacement graphs which are assumed to be invalid. It was this set of tests for which the wooden columns were used to hold the LVDT's. That data was not used in assembling the data summary charts that appear at the end of this chapter.

With the introduction of the steel columns as a base for the LVDT's, the displacement measurement system performed well. There are two exceptions to this. Figure 6.11 and 6.12 show the displacement graph for ELSs1 and ELSs3 respectively. The displacement graphs for the two tests are very different. The

Figure 6.11 ELSs1 - Structure Displacement versus Time

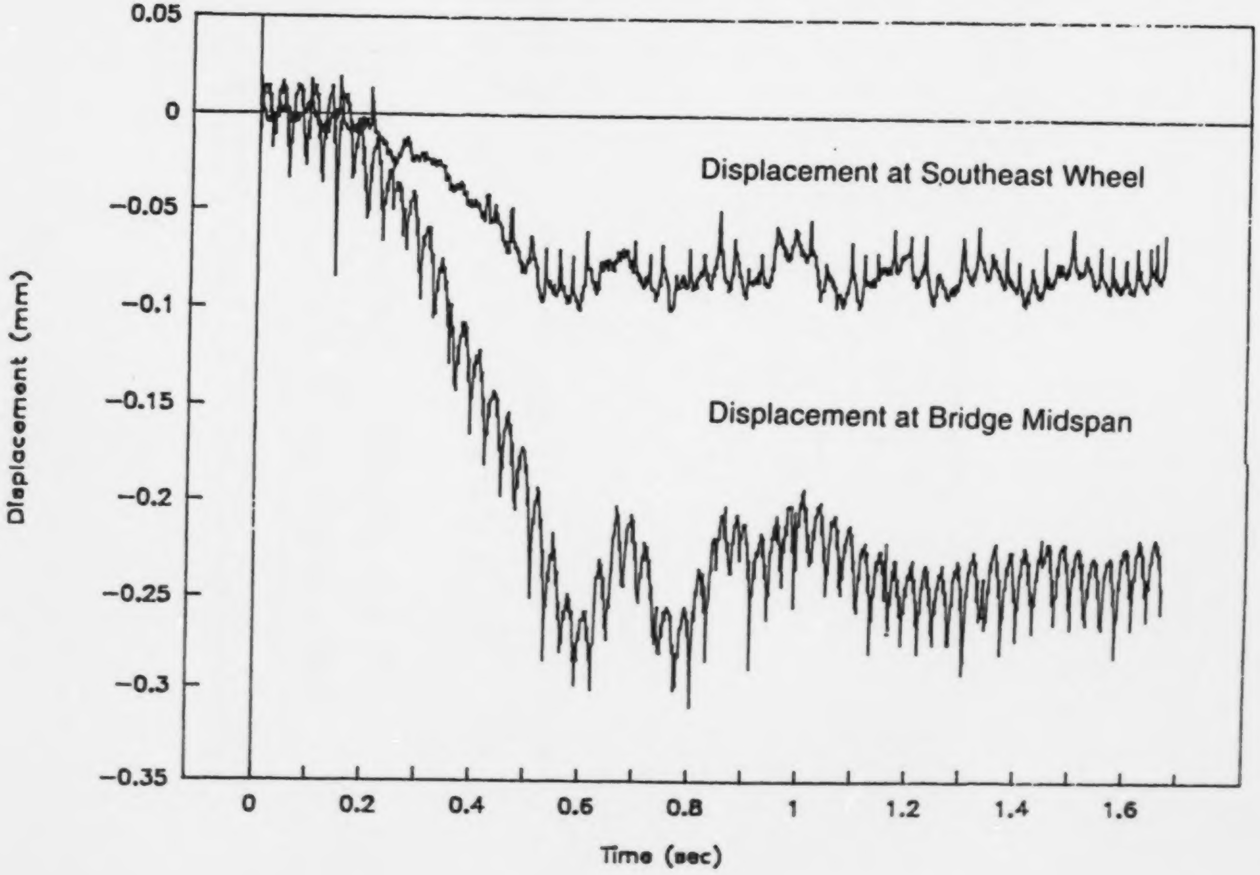

Figure 6.12 ELSs3 - Structure Displacement versus Time

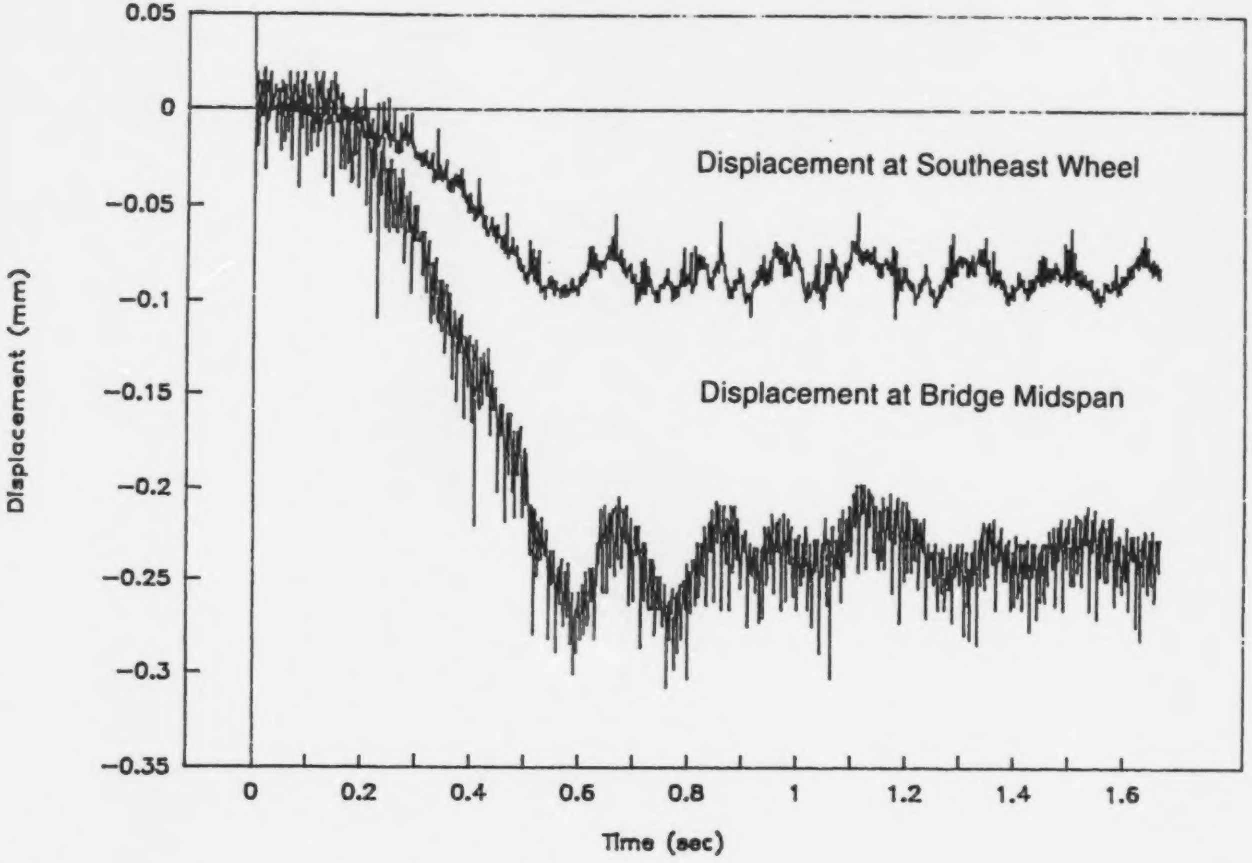

signals from ELSs3 seem to be contaminated with some high frequency interference which continues throughout the duration of the test, not just when the motor is on. No explanation was found for this curious phenomenon.

6.5 Data Presentation

For each test and for each parameter measured, the data was collected and plotted versus time. Figures 6.14 to 6.23, at the end of this section, show the graphs for one jerk-starting hoisting event from two of the eight test set, as examples. The peak values and the natural frequencies and other salient features have been determined from the graphical data from all the tests. These are shown in Tables 6.2 to 6.24, which appear at the end of this chapter.

6.5.1 Natural Frequency Data

The symbols ω_2 and ω_3 stand respectively for the first and second vibrational frequency during free vibration, or when the motor was running and the payload was not touching the shop floor. Because it was generally dominant, it was usually possible to determine ω_2 directly from the graphs. The locations of the peaks and valleys were generally well defined and the time lapse for an integer number of half periods was easily determined. The second vibrational frequency was not always well defined and when it could not be determined using the above procedure, a Fourier analysis was used to analyze sections of the data from the free vibration stages of the test. The Fourier analysis process produced graphs of amplitude versus frequency for the sets of data points which were analyzed. From these graphs the dominant frequencies within the data could be more easily determined. In some cases even this process did not produce clear results, and the Fourier analysis generated a cluster of similarly sized spikes. Table 6.2 shows the natural frequencies measured from the test data. In the tests where there was no clear value for the natural frequency, a blank space was left on Table 6.2.

6.4.2 Peak Values

In Tables 6.3 to 6.24, the data for peak values is arranged by test set. For each of the eight test sets (2BC, 2BS, EBC, EBS, 2LC, 2LS, ELC, ELS), the designation for each individual test is listed and the peak values for

Table 6.2 Measured Natural Frequencies

Test	ω2	ω3
2BC b1	32.1	
2BC b2	31.8	130
2BC b3	31.6	132
2BC h1	32.2	
2BC h2	32.5	137
2BC h3	32.9	135
2BC p1	31.9	
2BC p2		
2BC p3		
2BC s1	31.6	
2BC s2		
2BC s3	31.4	
2BC t1	31.9	
2BC t3	32.8	
Average	32.1	134
σ	0.495	3.11
C.of Var.	2%	2%

Test	ω2	ω3
2BS b1		
2BS b2	27.2	
2BS b3	27.2	150
2BS h1		126
2BS h2	29.7	126
2BS h3	28.1	
2BS p1	26.8	
2BS p2		126
2BS p3		
2BS s1	26.8	
2BS s2	26.6	127
2BS s3	27.4	
2BS t1	27.3	125
2BS t2		
2BS t3		126
Average	27.5	129
σ	0.949	9.09
C.of Var.	3%	7%

Test	ω2	ω3
EBC b1	36.3	183
EBC b2	36.3	182
EBC b3	36.9	
EBC h1	37.9	176
EBC h2	38	
EBC h3	38.1	173
EBC p1	37	
EBC p3	37.4	
EBC s1	37.6	184
EBC s2	36.3	
EBC s3	36.3	181
EBC t1a		
EBC t1	37.8	
EBC t2	37.6	
EBC t3	38.6	175
Average	37.3	179
σ	0.778	4.38
C.of Var.	2%	2%

Test	ω2	ω3
EBS b1	30.1	185
EBS b2	30.9	181
EBS b3	30.9	184
EBS h1	32.2	
EBS h2	32.5	185
EBS h3	32.5	
EBS p1	32	
EBS p2	32	
EBS p3	32.1	
EBS s1	32	184
EBS s2	32	183
EBS s3	30.4	181
EBS t1	31	
EBS t2	31.4	
EBS t3	31.7	178
Average	31.6	183
σ	0.753	2.45
C.of Var.	2%	1%

Excluding 2BSb3		
Average	27.5	126
σ	1.01	0.632
C.of Var.	4%	1%

Test	ω2	ω3
2LC s1	60.7	121
2LC s2	60.6	122
2LC s3	60.7	125
2LC h1	60.2	123
2LC h2	59.4	126
Average	60.3	123
σ	0.554	2.07
C.of Var.	1%	2%

Test	ω2	ω3
2LS s1	37.4	118
2LS s2	36.3	126
2LS s3	37.4	132
2LS h1	39	138
2LS h2	39.8	139
2LS h3	39	
Average	38.2	131
σ	1.32	8.76
C.of Var.	3%	7%

Test	ω2	ω3
ELC s1		
ELC s2	78.5	
ELC s3	65	
Average	71.8	
σ	9.55	
C.of Var.	13%	

Test	ω2	ω3
ELS s1	40	183
ELS s3	39.8	190
Average	39.9	187
σ	0.141	4.95
C.of Var.	0%	3%

displacements, moments, and wheel reactions, are shown. The corresponding static values that apply to each group of tests are shown below that group. The peak values are divided by the static values and the average and the standard deviation of these ratios are recorded as D for each test. Also, two measures of the coefficient of variation are given. The first is the standard deviation of D divided by D and recorded as a percentage. The second is the standard deviation of D divided by D-1 and recorded as a percentage. A peak, by definition, must be greater than the static value, and therefore D always exceeds unity. This second coefficient of variation gives a measure of the predictability of the amount by which the ratio D exceeds unity.

For the test in which the large payload was used, all except the "b" series do not have peak displacement measurements recorded (see Section 6.1.2). For all the tests in which the payload and the trolley were at the east end of the bridge, the reactions at the northwest and southwest wheel assemblies were not shown in the charts because the loads were too small to be accurately recorded by the test equipment. The peak moments at the centre of the bridge were considered too small to be of value in determining D. Graphs of the midspan moment for the tests in which the load was not applied at midspan, did not show the same dominant frequency displayed by the other parameters. This is discussed further in Section 7.21 . Therefore, the midspan moment and the north and south west reaction peaks for EBC, EBS, ELC, and ELS, are not shown in Tables 6.3 to 6.24.

Peak cable tension is not presented in Tables 6.3 to 6.24. Cable tension is generally not proportional to crane displacements. This is shown by comparing equation (5.34) for structure displacement and equation (5.144) for cable tension.

For most of the test sets, three kinds of peaks were recorded, and are displayed in different tables. The first type are the peaks due to jerk-starting. This includes all the tests in the "b" and "s" series and some of the "p" series tests. For the jerk-starting cases the average dynamic ratio, the standard deviation, and the two coefficients of variation, are calculated for each parameter. The average dynamic ratio, the average standard deviation, and the averages of the two coefficients of variation, are calculated using all the jerk-starting tests in the set. These averages are displayed at the bottom right side of the tables.

The second type comprise peaks for starting conditions other than jerk-starting. This includes the "h" and "t" series and the remainder of the "p" series tests. In these tables the initial cable tension has also been recorded. For all the tests where the small payload was used, only the jerk-starting condition was tested. Therefore, for test sets 2LC, 2LS, ELC, and ELS, there is no table for other than jerk-starting peaks

The third type of peak presented in the Tables in 6.3 to 6.24 is caused by braking. Peaks which occurred after braking were recorded in some tests in each of the test sets. Along with the magnitudes of the peaks, two time measures are included in the tables which deal with braking. The time between the last clear peak during which the motor was running and the first clear free vibration peak after braking, is recorded as the parameter Δt_a. The time between the last clear peak during which the motor was running and the data spike caused by the motor turning off, is recorded as the parameter Δt_b. The spike is assumed to represent the initiation of braking. Both these time measures will be used in the analysis of the braking data.

Test set 2LC is exceptional in that, for all the parameters, the peaks induced by jerk-starting do not occur in the first period immediately following payload lift off. They occur within the second or later periods. In no other test set is this behaviour present. Figure 6.13 shows the midspan displacement, bending moment, and cable tension, for 2LCs3, as an example. All the 2LC jerk-starting test results show a similar pattern. Table 6.15 displays the values of the first peaks after payload lift off, and Table 6.16 displays the values for the largest peaks immediately following.

Figure 6.13

2LCs3 - Example Where Second Peak after Payload Liftoff is Greatest

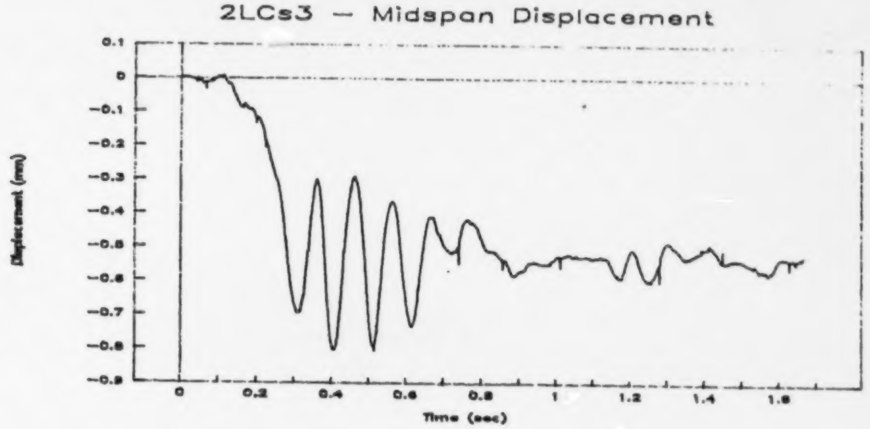

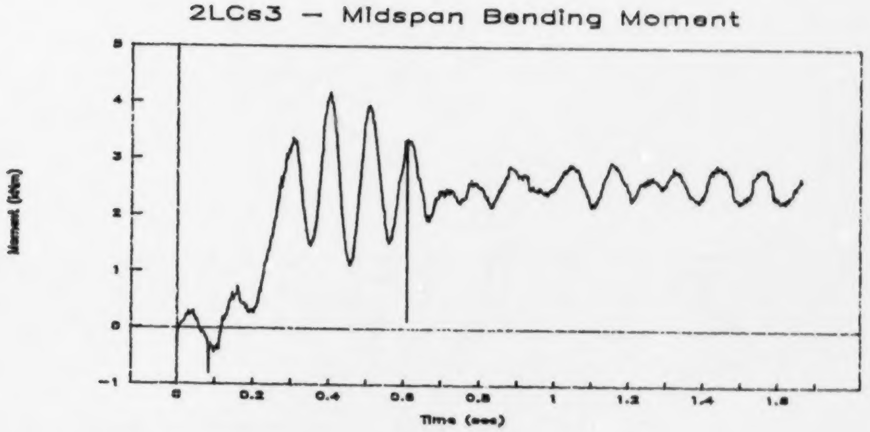

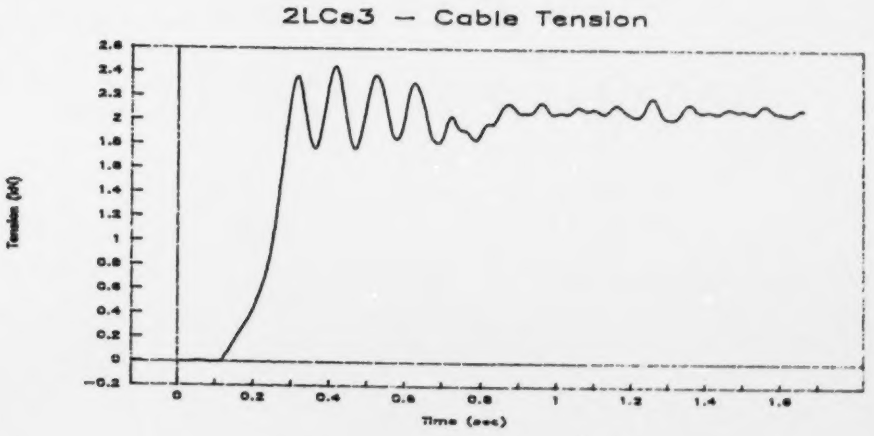

Figure 6.14 2BCb2 - Structure Displacement versus Time

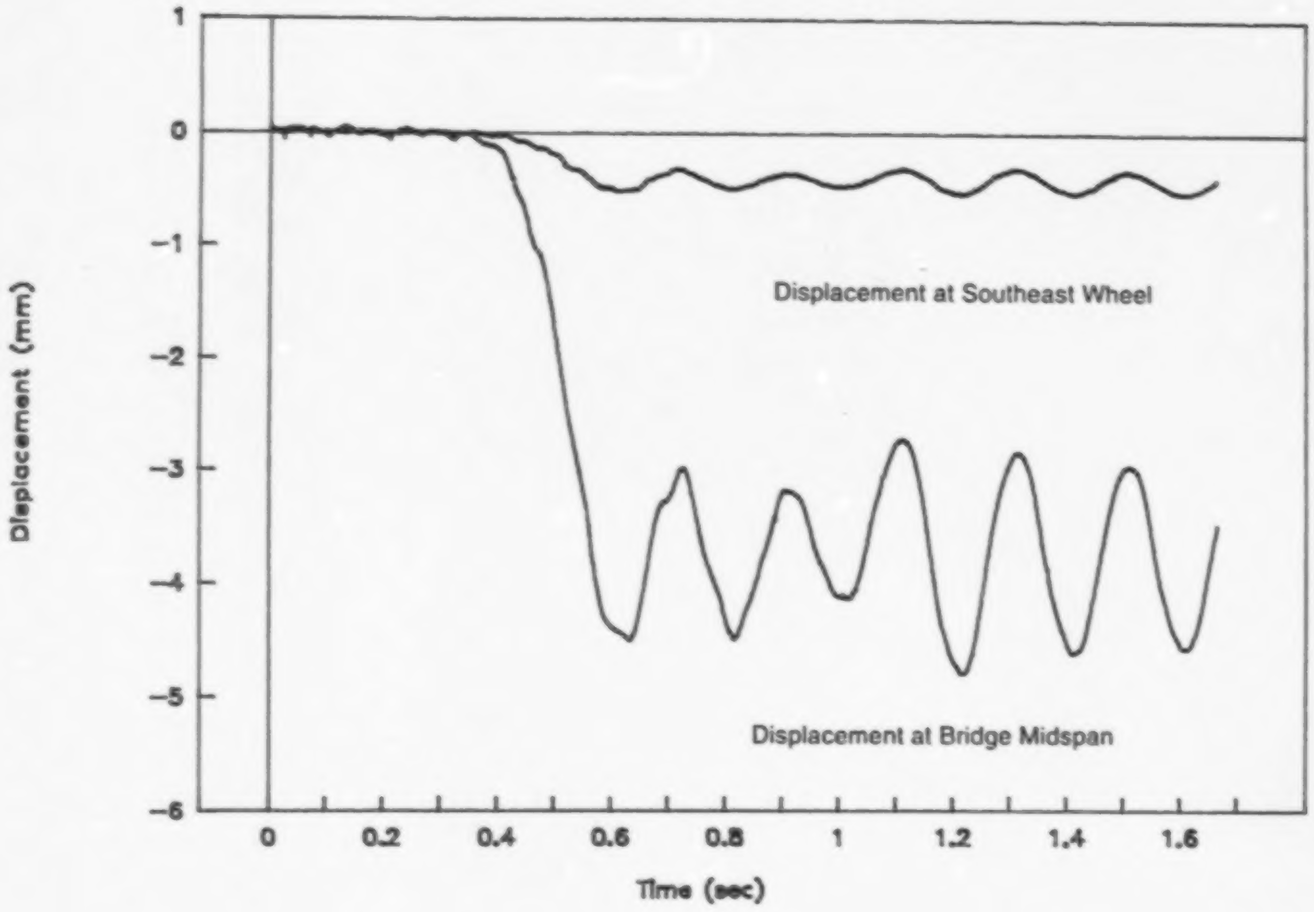

Figure 6.15 2BCb2 - Cable Tension versus Time

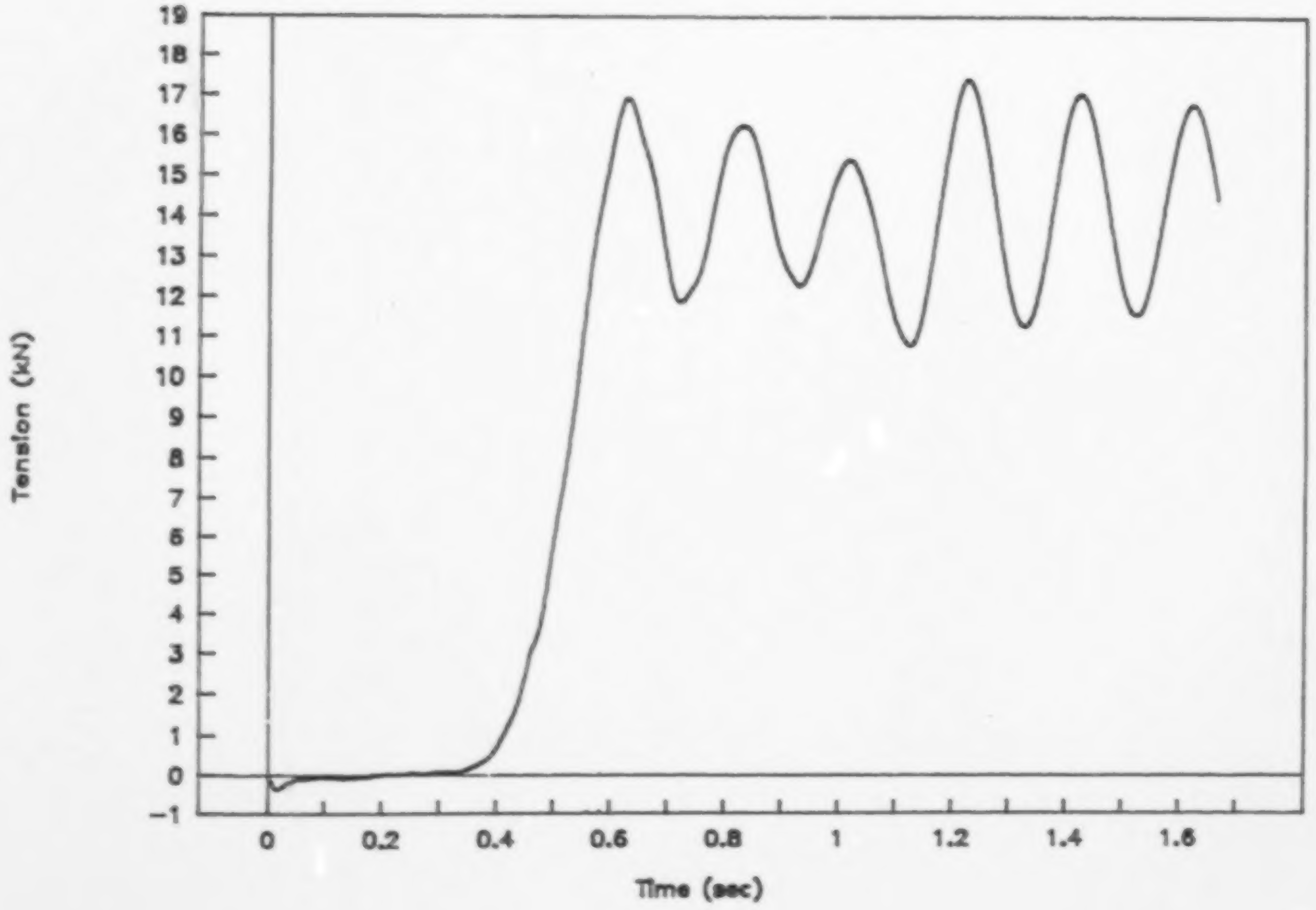

Figure 6.16 2BCb2 - Midspan Bridge Bending Moment versus Time

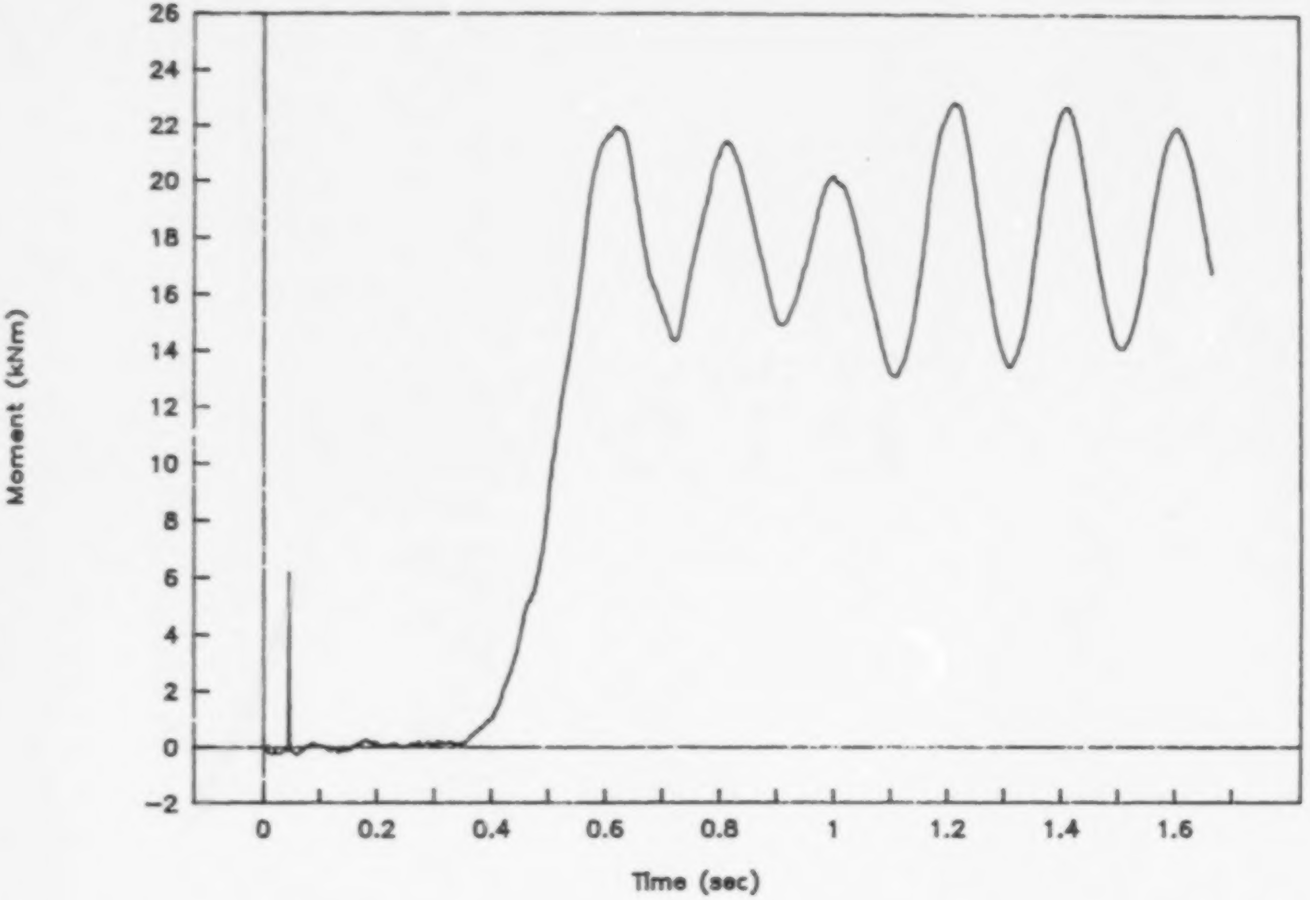

Figure 6.17 2BCb2 - Wheel Loads versus Time

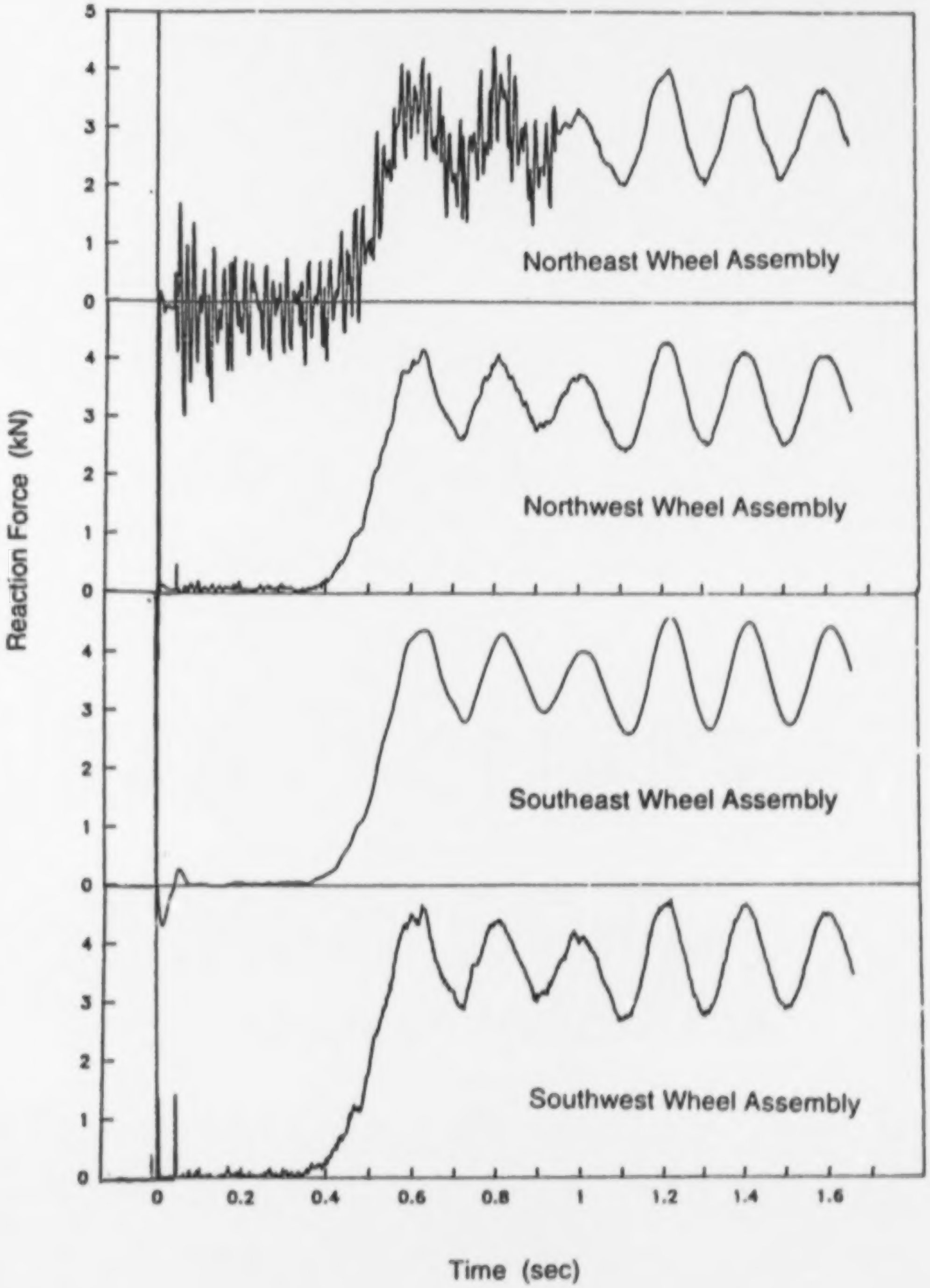

Figure 6.18 2BCb2 - Accelerations and Payload Displacement

2BCb2 — Acceleration at Bridge Midspan

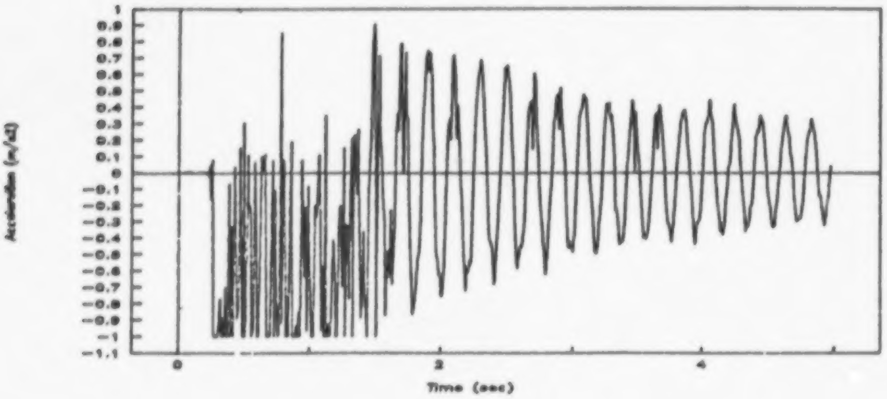

2BCb2 — Acceleration at SE wheel

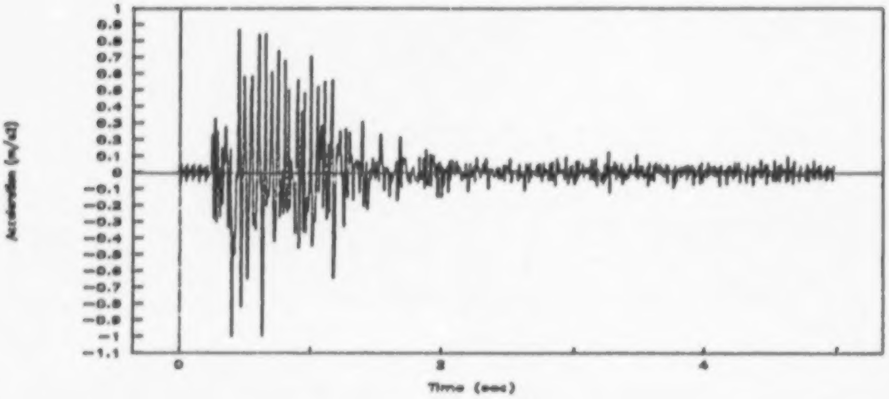

2BCb2 — Payload Displacement

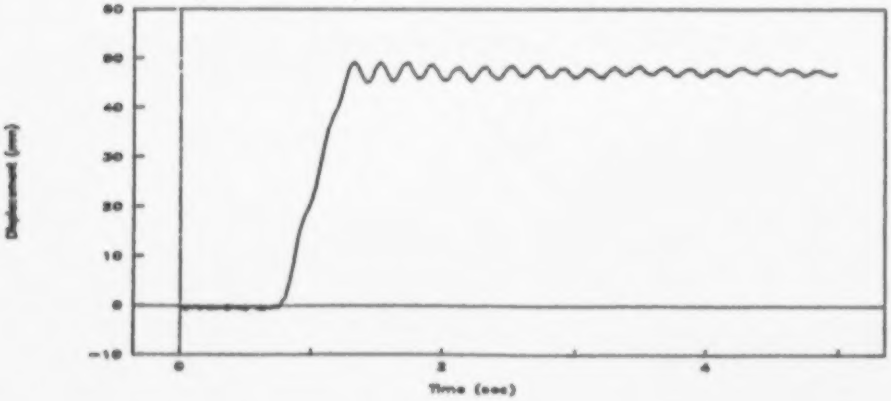

Figure 6.19 EBSb3 - Structure Displacement versus Time

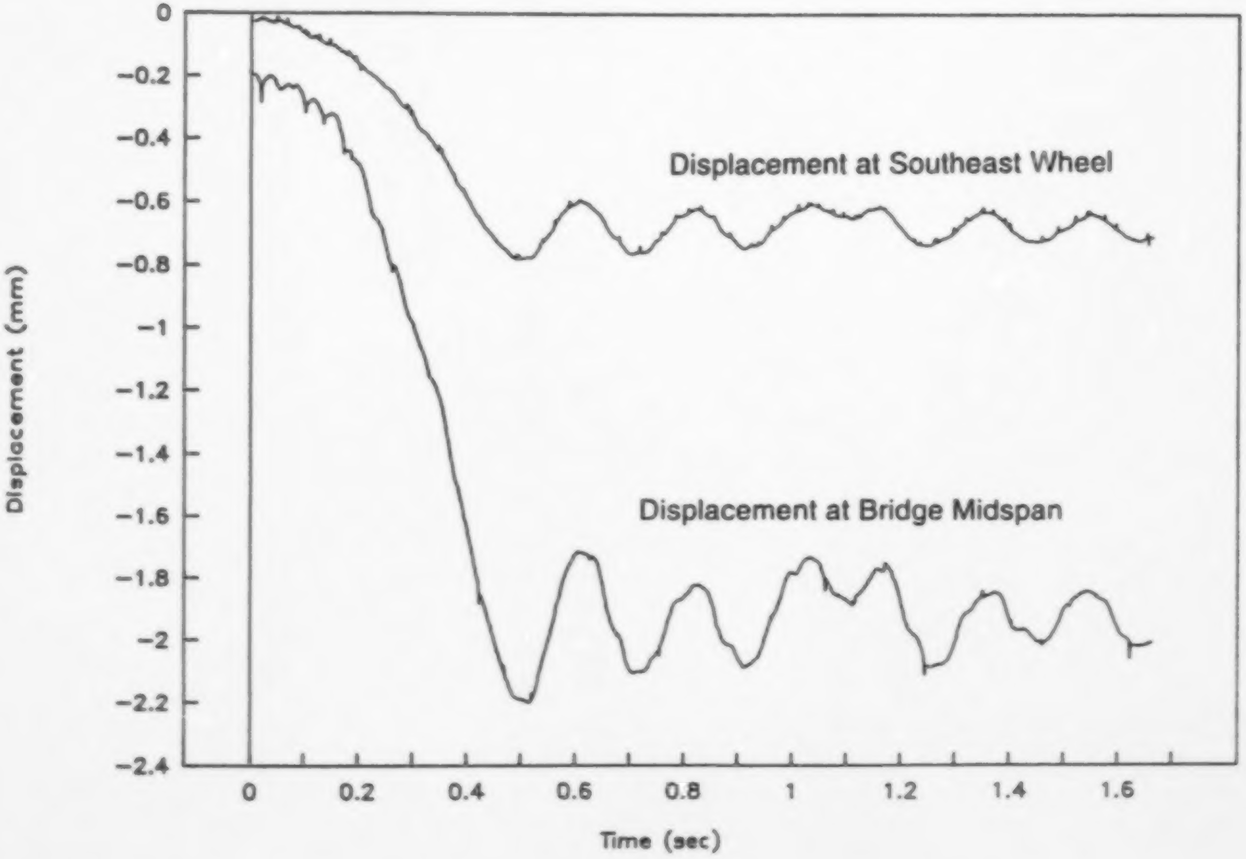

Figure 6.20 EBSb3 - Cable Tension versus Time

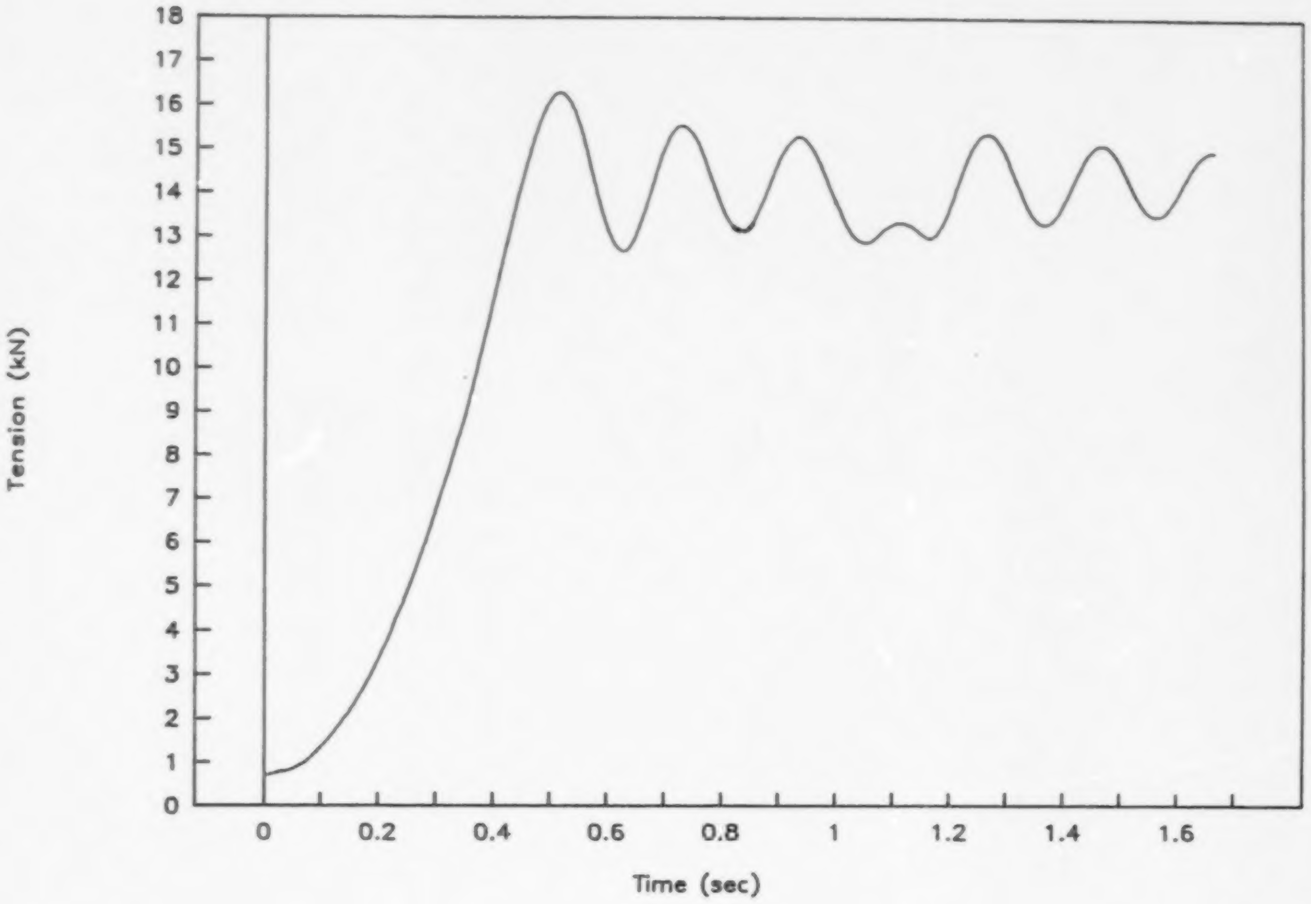

Figure 6.21 EBSb3 - Midspan Bridge Bending Moment versus Time

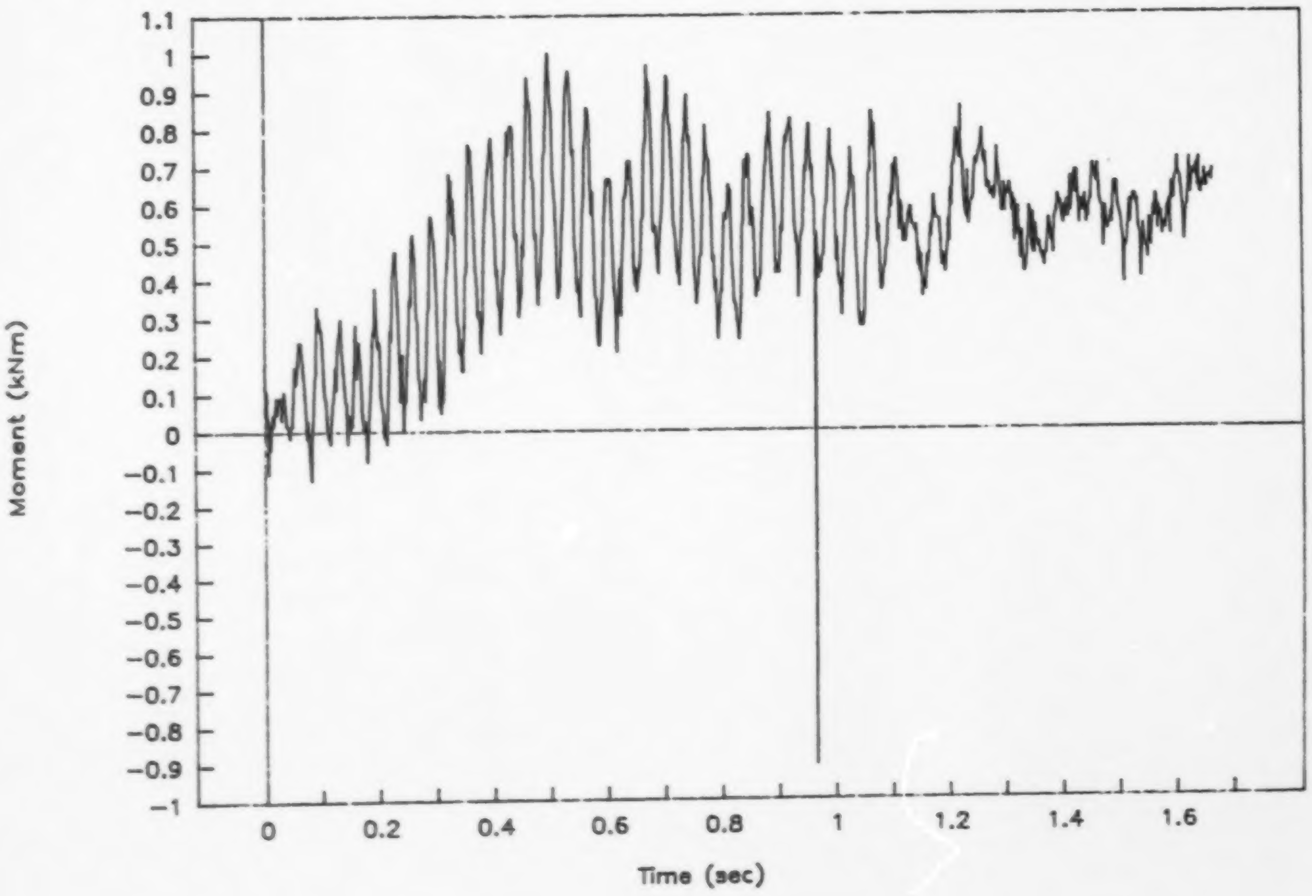

Figure 6.22 EBSb3 - Wheel Loads versus Time

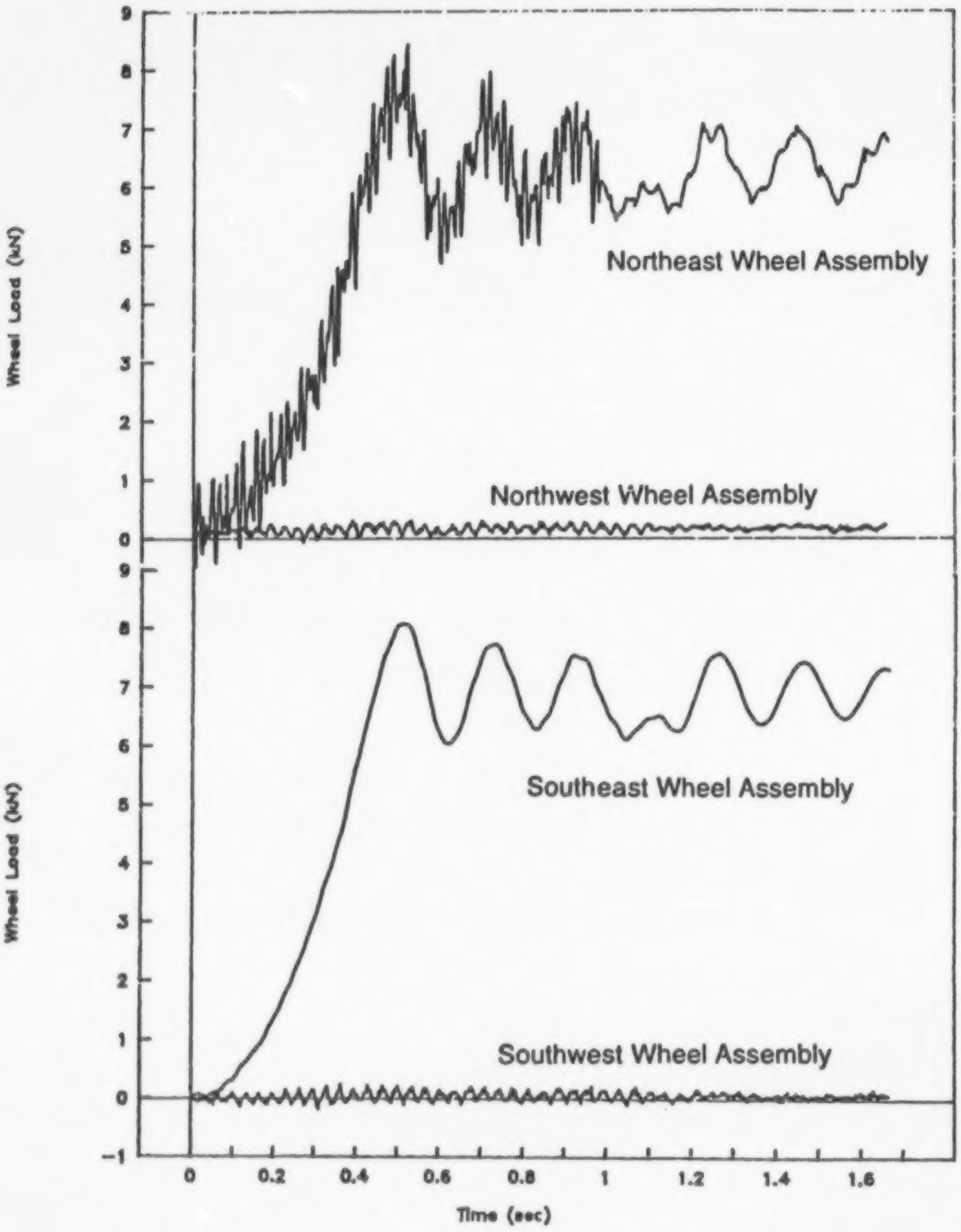

Figure 6.23 EBSb3 - Accelerations and Payload Displacement

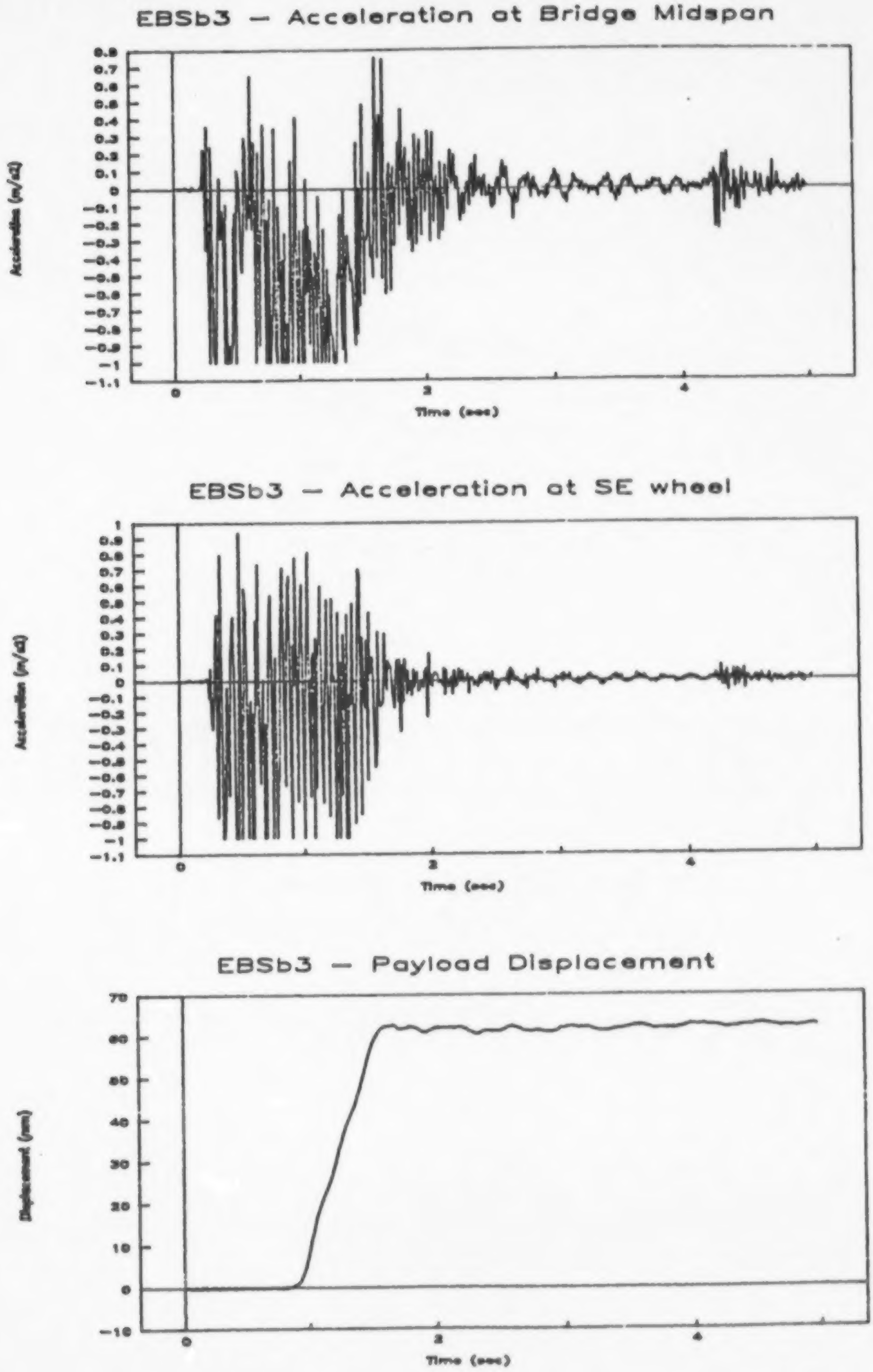

Table 6.3 Peak Values due to Jerk-Starting for 2BC

Test	Displacement(mm)		Moment	Reactions at Wheels (kN)				Ave. D,	σ,	$\frac{\sigma}{D}$	$\frac{\sigma}{D-1}$
	Trolley	SE Wheel	(kN m)	NE	NW	SE	SW	by Test	by Test		
2BC b1	-4.58	-0.53	22.42	3.91	4.16	4.46	4.72	1.26	4.1E-02	3%	16%
b2	-4.49	-0.52	21.98	3.50	4.15	4.42	4.56	1.22	2.9E-02	2%	13%
b3	-4.49	-0.52	21.95	3.86	4.24	4.41	4.50	1.24	3.9E-02	3%	16%
Static Values	-3.76	-0.43	17.96	2.96	3.34	3.63	3.60				
2BC s1			23.98	3.88	3.84	4.53	4.80	1.24	1.6E-02	1%	6%
s2			23.40	3.65	3.79	4.55	4.80	1.22	1.8E-02	1%	8%
s3			23.70	3.91	3.91	4.63	4.89	1.26	1.7E-02	1%	7%
p1			23.38	3.96	3.85	4.65	4.81	1.25	2.8E-02	2%	11%
p3			23.41	3.71	3.87	4.58	4.86	1.24	2.0E-02	2%	8%
Static Values	-3.76	-0.46	19.22	3.06	3.09	3.70	3.87				
Ave. Dynamic Ratio, D, by parameter	1.20	1.2	1.23	1.26	1.25	1.23	1.26				
σ, by parameter	1.4E-02	1.3E-02	1.3E-02	5.3E-02	1.4E-02	1.5E-02	2.3E-02				
$\frac{\sigma}{D}$	1%	1%	1%	4%	1%	1%	2%				
$\frac{\sigma}{D-1}$	7%	6%	6%	21%	5%	6%	9%				

2BC	
Average Dynamic Ratio, D	1.24
σ	3.0E-02
$\frac{\sigma}{D}$	2.5%
$\frac{\sigma}{D-1}$	12.7%

Table 6.4 Peak Values due to Starting Conditions Other Than Jerk-Starting, for 2BC

Test	Init. Tens. (kN)	Moment (kN m)	Reactions at Wheels (kN)				Average D by Test	σ, by Test	$\frac{\sigma}{D}$	$\frac{\sigma}{D-1}$
			NE	NW	SE	SW				
2BC h1	14.35	22.08	3.70	3.63	4.29	4.58	1.18	2.3E-02	2%	13%
h2	14.35	20.92	-	3.25	3.76	4.08	1.05	3.0E-02	3%	56%
h3	14.35	21.75	-	3.49	4.20	4.43	1.14	6.7E-03	1%	5%
p2	no peak while motor running									
t1	2.62	24.32	3.92	3.94	4.72	4.96	1.28	6.5E-03	1%	2%
t3	11.99	21.08	3.26	3.29	3.97	4.24	1.08	1.6E-02	1%	20%
Static		19.22	3.06	3.09	3.70	3.87				

Table 6.5 Peak Values After Braking for 2BC

Test	Displacement(mm)		Moment	Reactions at Wheels (kN)				Ave. D	σ,	$\frac{\sigma}{D}$	$\frac{\sigma}{D-1}$	Δt a	Δt b
	Trolley	SE Wheel	(kN m)	NE	NW	SE	SW	by Test	by Test			(seconds)	(seconds)
2BC b1	-4.45	-0.50	21.83	3.75	3.98	4.24	4.52	1.21	4.1E-02	3%	20%	0.37	0.07
b2	-4.79	-0.53	22.87	4.04	4.24	4.58	4.67	1.28	4.1E-02	3%	15%	0.40	0.13
b3	-4.36	-0.50	21.07	3.59	3.87	4.25	4.28	1.18	2.0E-02	2%	11%	0.44	0.13
Static	-3.76	-0.43	17.96	2.96	3.34	3.63	3.60						
2BC h1			21.80	3.50	3.58	4.24	4.47	1.15	9.6E-03	1%	7%	0.43	0.12
h2			22.52	3.35	3.45	4.00	4.29	1.11	3.5E-02	3%	30%	0.38	0.13
h3			19.92	3.26	3.21	3.83	4.03	1.04	1.2E-02	1%	29%	0.49	0.1
p1			no braking peak during test										0.01
p2			24.15	4.06	4.00	4.71	4.97	1.29	2.6E-02	2%	9%	-	-
p3			no braking peak during test										0.06
s1			21.08	3.47	3.46	4.08	4.30	1.11	1.5E-02	1%	13%	0.57	0.04
s2			no braking peak during test										-
s3			21.21	3.23	3.41	4.06	4.33	1.10	2.4E-02	2%	25%	0.64	0.19
t1			23.38	3.75	3.69	4.51	4.73	1.22	1.2E-02	1%	6%	0.38	0.06
t3			21.76	3.43	3.49	4.16	4.40	1.13	6.3E-03	1%	5%	0.35	0.05
Static	-3.76	-0.46	19.22	3.06	3.09	3.70	3.87						

Table 6.6 Peak Values due to Jerk-Starting for 2BS

Test	Displacement(mm)		Moment	Reactions at Wheels (kN)				Ave. D,	σ,	$\frac{\sigma}{D}$	$\frac{\sigma}{D-1}$
	Trolley	SE Wheel	(kN m)	NE	NW	SE	SW	by Test	by Test		
2BS b1	-4.07	-0.47	20.80	3.37	3.47	3.91	4.14	1.10	3.1E-02	3%	32%
b2	-4.01	-0.47	19.91	3.45	3.64	3.87	4.06	1.09	2.6E-02	2%	28%
b3	-4.14	-0.47	20.70	3.39	3.61	4.02	4.18	1.11	1.9E-02	2%	17%
Static Values	-3.82	-0.42	18.32	3.07	3.30	3.60	3.68				
2BS s1			21.29	3.47	3.41	4.18	4.49	1.14	1.4E-02	1%	10%
s2			21.21	3.56	3.42	4.19	4.44	1.15	1.3E-02	1%	9%
s3			21.37	3.45	3.43	4.13	4.35	1.14	7.3E-03	1%	5%
p3			21.37	3.40	3.42	4.26	4.50	1.15	2.3E-02	2%	16%
Static Values	-3.76	-0.46	18.62	3.05	3.02	3.65	3.85				
Ave. Dynamic Ratio, D, by parameter	1.07	1.1	1.13	1.13	1.11	1.12	1.14				
σ, by parameter	1.7E-02	0.0E+00	2.1E-02	2.3E-02	3.1E-02	3.4E-02	2.4E-02				
$\frac{\sigma}{D}$	2%	0%	2%	2%	3%	3%	2%				
$\frac{\sigma}{D-1}$	26%	0%	16%	19%	28%	27%	17%				

2BS	
Average Dynamic Ratio, D	1.12
σ	3.0E-02
$\frac{\sigma}{D}$	2.7%
$\frac{\sigma}{D-1}$	24.6%

Table 6.7 Peak Values due to Starting Conditions Other Than Jerk-Starting, for 2BS

Test	Init. Tens. (kN)	Moment (kN m)	Reactions at Wheels (kN)				Average D by Test	σ, by Test	$\frac{\sigma}{D}$	$\frac{\sigma}{D-1}$
			NE	NW	SE	SW				
2BS h1	14.35	21.24	3.46	3.44	4.16	4.42	1.14	4.9E-03	0%	3%
h2	14.35	20.70	3.52	3.38	4.06	4.38	1.13	1.2E-02	1%	10%
h3	14.35	21.04	3.49	3.46	4.15	4.46	1.14	1.2E-02	1%	9%
p2	no peak while motor running									
t1	9.28	21.32	3.51	3.41	4.12	4.37	1.14	9.8E-03	1%	7%
t1	6	21.25	3.60	3.49	4.20	4.47	1.16	1.5E-02	1%	9%
t3	0.7	21.21	3.56	3.42	4.19	4.44	1.15	1.3E-02	1%	9%
Static		18.62	3.05	3.02	3.65	3.85				

Table 6.8 Peak Values After Braking for 2BS

Test	Displacement(mm)		Moment	Reactions at Wheels (kN)				Ave. D	σ,	$\frac{\sigma}{D}$	$\frac{\sigma}{D-1}$	Δt a	Δt b
	Trolley	SE Wheel	(kN m)	NE	NW	SE	SW	by Test	by Test			(seconds)	(seconds)
2BS b1	no braking peak during test											-	0.07
b2	-4.22	-0.47	20.58	3.32	3.75	4.06	4.07	1.11	1.8E-02	2%	16%	0.52	0.20
b3	-4.4	-0.50	21.31	3.45	3.82	4.21	4.24	1.16	2.0E-02	2%	13%	0.46	0.15
Static	-3.82	-0.42	18.32	3.07	3.30	3.60	3.68						
2BS h1			22.81	3.65	3.65	4.49	4.70	1.22	1.4E-02	1%	6%	0.45	0.12
h2			21.96	3.64	3.53	4.32	4.62	1.19	1.2E-02	1%	7%	0.44	0.04
h3			22.23	3.60	3.59	4.33	4.59	1.19	5.3E-03	0%	3%	0.49	0.18
p1			20.42	3.21	3.26	3.91	4.22	1.08	1.9E-02	2%	23%	0.54	-
p2			22.50	3.85	3.80	4.42	4.84	1.24	2.7E-02	2%	11%	-	-
s1	no braking peak during test											-	2.20
s2			21.16	3.39	3.39	4.11	4.32	1.12	9.0E-03	1%	7%	0.53	0.03
s3	no braking peak during test											-	-
t1			21.30	3.45	3.40	4.13	4.38	1.13	6.9E-03	1%	5%	0.51	0.01
t3			21.14	3.44	3.37	4.12	4.35	1.13	7.1E-03	1%	6%	-	0.02
Static	-3.76	-0.46	18.62	3.05	3.02	3.65	3.85						

Table 6.9 Peak Values due to Jerk-Starting, for EBC

Test	Displacement (mm)		Reactions at Wheels (kN)		Average D	σ,	$\frac{\sigma}{D}$	$\frac{\sigma}{D-1}$
	Trolley	SE Wheel	NE	SE	by Test	by Test		
EBC b1	-2.30	-0.86	8.12	9.24	1.25	3.7E-02	3%	15%
b2	-2.31	-0.86	8.48	9.23	1.25	3.8E-02	3%	15%
b3	-2.29	-0.89	8.56	9.26	1.26	1.9E-02	1%	7%
Static Values	-1.83	-0.72	6.35	7.31				
EBC s1			7.82	9.21	1.27	1.3E-02	1%	5%
s2			7.98	9.19	1.27	1.5E-02	1%	6%
s2			8.30	9.43	1.28	8.0E-03	1%	3%
Static Values	-1.9	-0.74	6.33	7.25				
Ave. Dynamic Ratio, D, by parameter	1.26	1.2	1.29	1.27				
σ, by parameter	5.5E-03	2.4E-02	4.4E-02	1.4E-02				
$\frac{\sigma}{D}$	0%	2%	3%	1%				
$\frac{\sigma}{D-1}$	2%	12%	15%	5%				

EBC	
Average Dynamic Ratio, D	1.27
σ	4.0E-02
$\frac{\sigma}{D}$	3.2%
$\frac{\sigma}{D-1}$	15%

Table 6.10 Peak Values due to Starting Conditions Other Than Jerk-Starting, for EBC

Test	Initial Tension (kN)	Displacement (mm)		Reactions at Wheels (kN)		Average D by Test	σ, by Test	$\frac{\sigma}{D}$	$\frac{\sigma}{D-1}$
		Trolley	SE Wheel	NE	SE				
EBC t1	8.2			7.10	8.01	1.11	1.2E-02	1%	11%
t2	8.46			7.24	8.02	1.12	2.7E-02	2%	21%
t3	9.79			7.44	8.23	1.16	2.8E-02	2%	18%
h1	14.35			7.41	8.26	1.15	2.2E-02	2%	14%
h2	14.35	no peak while motor running							
h3	14.35			7.19	8.11	1.13	1.2E-02	1%	10%
p1	14.24			7.40	8.28	1.16	1.9E-02	2%	12%
p2	14.24			-	8.09	1.12	-	-	-
p3	14.24	no peak while motor running							
Static Values		-1.9	-0.74	6.33	7.25				

Table 6.11 Peak Values After Braking, for EBC

Test	Displacement (mm)		Reactions at Wheels (kN)		Average D	σ,	$\frac{\sigma}{D}$	$\frac{\sigma}{D-1}$	Δt a	Δt b
	Trolley	SE Wheel	NE	SE	by Test	by Test			(seconds)	(seconds)
EBC b1	-2.28	-0.84	8.03	8.93	1.22	4.2E-02	3%	19%	0.34	0.03
b2	-2.33	-0.87	8.40	9.19	1.27	4.7E-02	4%	18%	0.54	0.09
b3	-2.31	-0.91	8.50	9.35	1.29	3.6E-02	3%	13%	0.34	0.03
Static Values	-1.83	-0.72	6.35	7.31						
EBC s1			7.46	8.48	1.17	6.3E-03	1%	4%	-	0.09
s2			7.22	8.21	1.14	5.8E-03	1%	4%	0.37	0.19
s3			7.22	8.32	1.14	4.9E-03	0%	3%	0.33	0.04
t1			7.04	7.83	1.10	2.3E-02	2%	24%	0.66	0.00
t2			7.24	8.20	1.14	9.0E-03	1%	7%	0.37	0.10
t3			6.87	7.68	1.07	1.8E-02	2%	25%	0.57	0.16
h1			7.26	8.09	1.13	2.2E-02	2%	17%	0.46	0.02
h2			7.29	8.00	1.13	3.4E-02	3%	27%	0.61	-
h3			7.51	8.07	1.15	5.2E-02	5%	35%	0.37	0.10
p1			8.04	9.01	1.26	1.9E-02	2%	8%	-	-
p2			8.01	8.80	1.24	3.6E-02	3%	15%	0.36	-
p3			8.25	9.31	1.29	1.4E-02	1%	5%	1.39	-
Static Values	-1.9	-0.74	6.33	7.25						

Table 6.12 Peak Values due to Jerk-Starting, for EBS

Test	Displacement (mm)		Reactions at Wheels (kN)		Average D by Test	σ, by Test	$\frac{\sigma}{D}$	$\frac{\sigma}{D-1}$
	Trolley	SE Wheel	NE	SE				
EBS b1	-2.06	-0.78	7.52	8.47	1.14	1.7E-02	1%	12%
b2	-2.07	-0.79	7.23	8.46	1.15	1.2E-02	1%	8%
b3	-2.14	-0.77	7.51	8.45	1.15	2.3E-02	2%	16%
Static Values	-1.83	-0.69	6.49	7.33				
EBS s1			7.58	8.24	1.14	2.4E-02	2%	17%
s2			7.70	8.35	1.15	1.4E-02	1%	9%
s2			7.66	8.48	1.16	1.3E-03	0%	1%
Static Values	-1.9	-0.74	6.38	7.34				
Ave. Dynamic Ratio, D, by parameter	1.14	1.1	1.17	1.15				
σ, by parameter	2.4E-02	1.4E-02	3.5E-02	1.3E-02				
$\frac{\sigma}{D}$	2%	1%	3%	1%				
$\frac{\sigma}{D-1}$	17%	11%	20%	9%				

EBS	
Average Dynamic Ratio, D	1.15
σ	2.7E-02
$\frac{\sigma}{D}$	2.4%
$\frac{\sigma}{D-1}$	18%

Table 6.13 Peak Values due to Starting Conditions Other Than Jerk-Starting, for EBS

Test	Initial	Displacement (mm)		Reactions at Wheels (kN)		Average D	σ,	$\frac{\sigma}{D}$	$\frac{\sigma}{D-1}$
	Tension (kN)	Trolley	SE Wheel	NE	SE	by Test	by Test		
EBS t1	1.33			7.81	8.60	1.20	3.7E-02	3%	19%
t2	6.74			7.65	8.65	1.19	1.5E-02	1%	8%
t3	3.5			7.76	8.60	1.19	3.2E-02	3%	16%
h1	14.3			7.24	8.06	1.12	2.6E-02	2%	22%
h2	14.3			6.98	7.96	1.09	6.8E-03	1%	8%
h3	14.3			7.52	8.41	1.16	2.3E-02	2%	14%
p1	14.37	no peak while motor running							
p2	14.37			7.28	8.13	1.12	2.4E-02	2%	19%
p3	14.37	no peak while motor running							
Static Values		-1.9	-0.74	6.38	7.34				

Table 6.14 Peak Values After Braking, for EBS

Test	Displacement (mm)		Reactions at Wheels (kN)		Average D	σ,	$\frac{\sigma}{D}$	$\frac{\sigma}{D-1}$	Δt a	Δt b
	Trolley	SE Wheel	NE	SE	by Test	by Test			(seconds)	(seconds)
EBS b1	-1.96	-0.73	6.86	7.88	1.07	9.1E-03	1%	14%	0.32	0.03
b2	-2.14	-0.79	7.48	8.52	1.13	5.2E-02	5%	39%	0.43	0.11
b3	-2.07	-0.73	6.92	7.99	1.08	3.5E-02	3%	42%	0.34	0.05
Static Values	-1.83	-0.69	6.49	7.33						
EBS s1	no braking during test								-	-
s2			7.47	8.44	1.10	6.7E-02	6%	64%	0.39	0.07
s3	no braking during test								-	0.17
t1			7.74	8.54	1.11	7.6E-02	7%	69%	0.37	0.06
t2			7.34	8.27	1.09	5.0E-02	5%	54%	0.37	0.05
t3			7.02	7.90	1.07	1.5E-02	1%	22%	0.32	0.03
h1			7.48	8.34	1.10	5.7E-02	5%	59%	0.34	0.04
h2			7.40	8.49	1.11	7.2E-02	6%	67%	-	-
h3			7.22	8.12	1.08	3.6E-02	3%	44%	0.34	0.05
p1			8.67	9.66	1.19	1.8E-01	16%	98%	-	-
p2			8.57	9.54	1.18	1.7E-01	15%	96%	-	-
p3			8.87	9.78	1.20	2.0E-01	16%	100%	-	-
Static Values			6.38	7.34						

Table 6.15 First Peak Values due to Jerk-Starting, for 2LC

Test	Displacement(mm)		Moment	Reactions at Wheels (kN)				Average D	σ,	$\frac{\sigma}{D}$	$\frac{\sigma}{D-1}$
	Trolley	SE Wheel	(kN m)	NE	NW	SE	SW	by Test	by Test		
2LC s1	-0.68	-0.08	3.33	0.46	0.63	0.64	0.68	1.30	1.0E-01	8%	34%
s2	-0.66	-0.08	3.35	0.41	0.56	0.63	0.68	1.25	1.0E-01	8%	41%
s3	-0.69	-0.07	3.27	0.43	0.58	0.66	0.70	1.26	9.5E-02	8%	37%
Static Values	-0.55	-0.06	2.54	0.39	0.42	0.51	0.53				
Ave. Dynamic Ratio, D, by parameter	1.23	1.3	1.31	1.11	1.40	1.26	1.30				
σ, by parameter	2.8E-02	9.6E-02	1.6E-02	6.5E-02	8.6E-02	3.0E-02	2.2E-02				
$\frac{\sigma}{D}$	2%	8%	1%	6%	6%	2%	2%				
$\frac{\sigma}{D-1}$	12%	35%	5%	58%	21%	11%	7%				

2LC, first peak	
Average Dynamic Ratio, D	1.27
σ	9.7E-02
$\frac{\sigma}{D}$	7.6%
$\frac{\sigma}{D-1}$	36%

Table 6.16 Later Peak Values due to Jerk-Starting, for 2LC

Test	Displacement(mm)		Moment	Reactions at Wheels (kN)				Average D	σ,	$\frac{\sigma}{D}$	$\frac{\sigma}{D-1}$
	Trolley	SE Wheel	(kN m)	NE	NW	SE	SW	by Test	by Test		
2LC s1	-0.69	-0.09	3.44	0.47	0.64	0.64	0.80	1.37	1.4E-01	10%	37%
s2	-0.77	-0.1	3.85	0.49	0.60	0.68	0.75	1.43	1.3E-01	9%	31%
s3	-0.79	-0.1	4.19	0.45	0.65	0.75	0.79	1.49	1.7E-01	12%	35%
Static Values	-0.55	-0.06	2.54	0.39	0.42	0.51	0.53				
Ave. Dynamic Ratio, D, by parameter	1.36	1.6	1.51	1.21	1.50	1.35	1.47				
σ, by parameter	9.6E-02	9.6E-02	1.5E-01	5.1E-02	6.3E-02	1.1E-01	5.0E-02				
$\frac{\sigma}{D}$	7%	6%	10%	4%	4%	8%	3%				
$\frac{\sigma}{D-1}$	26%	16%	29%	25%	13%	31%	11%				

2LC, later peak	
Average Dynamic Ratio, D	1.43
σ	1.5E-01
$\frac{\sigma}{D}$	10.4%
$\frac{\sigma}{D-1}$	35%

Table 6.17 Peak Values due to Starting Conditions Other Than Jerk-Starting, for 2LC

Test	Displacement(mm)		Moment	Reactions at Wheels (kN)				Average D	σ,	$\frac{\sigma}{D}$	$\frac{\sigma}{D-1}$
	Trolley	SE Wheel	(kN m)	NE	NW	SE	SW	by Test	by Test		
2LC h1	-0.68	-0.08	3.14	-	0.59	-	0.66	1.29	7.6E-02	6%	26%
p1	-0.78	-0.10	3.82	-	0.67	0.73	0.90	1.55	1.2E-01	8%	22%
Static	-0.55	-0.06	2.54	0.39	0.42	0.51	0.53				

Table 6.18 Peak Values After Braking, for 2LC

Test	Displacement(mm)		Moment	Reactions at Wheels (kN)				Average D	σ,	$\frac{\sigma}{D}$	$\frac{\sigma}{D-1}$	Δt a	Δt b
	Trolley	SE Wheel	(kN m)	NE	NW	SE	SW	by Test	by Test			(seconds)	(seconds)
2LC s1	-0.74	-0.1	3.43	0.52	0.58	0.64	0.75	1.39	1.3E-01	9%	33%	0.33	0.01
s2	-0.64	-0.08	3.05	0.49	0.54	0.60	0.68	1.24	6.4E-02	5%	26%	0.33	0.05
s3	-0.62	-0.08	3.07	0.50	0.48	0.56	0.64	1.20	8.5E-02	7%	43%	0.96	0.10
h1	-0.77	-0.09	3.81	0.57	0.66	0.71	0.76	1.47	6.4E-02	4%	14%	0.54	-
p1	-0.75	-0.08	3.62	0.57	0.58	0.70	0.76	1.40	4.5E-02	3%	11%	0.34	0.10
Static	-0.55	-0.06	2.54	0.39	0.42	0.51	0.53						

Table 6.19 Peak Values due to Jerk-Starting, for 2LS

Test	Displacement(mm)		Moment	Reactions at Wheels (kN)				Average D	σ,	$\frac{\sigma}{D}$	$\frac{\sigma}{D-1}$
	Trolley	SE Wheel	(kN m)	NE	NW	SE	SW	by Test	by Test		
2LS s1	-0.58	-0.07	3.31	-	0.49	0.57	0.70	1.18	1.0E-01	9%	59%
s2	-0.61	-0.08	3.17	-	0.49	0.58	0.72	1.21	1.1E-01	9%	53%
s3	-0.61	-0.08	3.27	-	0.51	0.59	0.71	1.23	9.9E-02	8%	44%
Static Values	-0.53	-0.06	2.57	0.36	0.45	0.52	0.53				
Ave. Dynamic Ratio, D, by parameter	1.13	1.3	1.26	-	1.10	1.12	1.34				
σ, by parameter	3.3E-02	9.6E-02	2.8E-02	-	2.6E-02	1.9E-02	1.9E-02				
$\frac{\sigma}{D}$	3%	8%	2%	-	2%	2%	1%				
$\frac{\sigma}{D-1}$	25%	35%	11%	-	25%	17%	6%				

2LS	
Average Dynamic Ratio, D	1.21
σ	1.0E-01
$\frac{\sigma}{D}$	8.5%
$\frac{\sigma}{D-1}$	50%

Table 6.20 Peak Values After Braking, for 2LS

Test	Displacement(mm)		Moment	Reactions at Wheels (kN)				Average D	σ,	$\frac{\sigma}{D}$	$\frac{\sigma}{D-1}$	Δt_a	Δt_b
	Trolley	SE Wheel	(kN m)	NE	NW	SE	SW	by Test	by Test			(seconds)	(seconds)
2LS s1	-0.57	-0.07	3.00	-	0.49	0.56	0.61	1.12	4.5E-02	4%	37%	0.42	0.10
s2	-0.58	-0.08	3.02	0.39	0.53	0.57	0.60	1.16	8.7E-02	8%	56%	0.43	-
s3	-0.59	-0.08	3.16	0.43	0.48	0.60	0.73	1.21	1.1E-01	9%	54%	0.59	-
h1	-0.63	-0.08	3.25	0.47	0.54	0.65	0.70	1.27	5.7E-02	5%	22%	-	0.07
h2	-0.6	-0.08	3.18	0.45	0.54	0.63	0.68	1.24	6.4E-02	5%	27%	0.44	-
Static	-0.53	-0.06	2.57	0.36	0.45	0.52	0.53						

Table 6.21 Peak Values due to Jerk-Starting, for ELC

Test	Displacement (mm)		Reactions at Wheels (kN)		Average D by Test	σ, by Test	$\frac{\sigma}{D}$	$\frac{\sigma}{D-1}$
	Trolley	SE Wheel	NE	SE				
ELC s1	-0.28	-0.10	0.86	1.15	1.09	6.7E-02	6%	75%
s2	-0.30	-0.11	0.95	1.16	1.14	2.7E-02	2%	20%
s3	-0.31	-0.12	0.89	1.12	1.16	4.1E-02	4%	25%
Static Values	-0.26	-0.10	0.76	1.00				
Ave. Dynamic Ratio, D, by parameter	1.14	1.1	1.2	1.14				
σ, by parameter	5.9E-02	1.0E-01	6.0E-02	2.1E-02				
$\frac{\sigma}{D}$	5%	9%	5%	2%				
$\frac{\sigma}{D-1}$	42%	100%	33%	15%				

ELC	
Average Dynamic Ratio, D	1.14
σ	6.4E-02
$\frac{\sigma}{D}$	5.6%
$\frac{\sigma}{D-1}$	45%

Table 6.22 Peak Values After Braking, for ELC

Test	Displacement (mm)		Reactions at Wheels (kN)		Average D	σ,	$\frac{\sigma}{D}$	$\frac{\sigma}{D-1}$	Δt a	Δt b
	Trolley	SE Wheel	NE	SE	by Test	by Test			(seconds)	(seconds)
ELC s1	-0.27	-0.11	0.99	1.23	1.17	1.2E-01	10%	72%	-	-
s2	-0.30	-0.12	0.90	1.14	1.20	7.4E-02	6%	37%	-	-
s3	-0.28	-0.11	0.91	1.21	1.17	1.0E-01	9%	61%	0.34	-
Static Values	-0.26	-0.10	0.76	1.00						

Table 6.23 Peak Values due to Jerk-Starting, for ELS

Test	Displacement (mm)		Reactions at Wheels (kN)		Average D by Test	σ, by Test	$\frac{\sigma}{D}$	$\frac{\sigma}{D-1}$
	Trolley	SE Wheel	NE	SE				
ELS s1	-0.28	-0.10	0.99	1.14	1.24	1.1E-01	9%	46%
s3	-0.28	-0.10	0.82	1.14	1.24	1.1E-01	9%	46%
Static Values	-0.24	-0.08	0.71	0.99				
Ave. Dynamic Ratio, D, by parameter	1.17	1.3	1.3	1.15				
σ, by parameter	0.0E+00	0.0E+00	1.7E-01	0.0E+00				
$\frac{\sigma}{D}$	0%	0%	13%	0%				
$\frac{\sigma}{D-1}$	0%	0%	62%	0%				

ELS	
Average Dynamic Ratio, D	1.21
σ	8.5E-02
$\frac{\sigma}{D}$	7.0%
$\frac{\sigma}{D-1}$	40%

Table 6.24 Peak Values After Braking, for ELS

Test	Displacement (mm)		Reactions at Wheels (kN)		Average D	σ,	$\frac{\sigma}{D}$	$\frac{\sigma}{D-1}$	Δt_a	Δt_b
	Trolley	SE Wheel	NE	SE	by Test	by Test			(seconds)	(seconds)
ELS s1	-0.26	-0.10	0.83	1.07	1.15	8.1E-02	7%	55%	0.35	-
s2	-0.25	-0.10	0.86	1.08	1.14	9.1E-02	8%	66%	0.34	-
Static Values	-0.24	-0.08	0.71	0.99						

CHAPTER 7

COMPARISON OF TEST RESULTS AND PREDICTED BEHAVIOUR

In Chapter 7 the predicted and measured dynamic factors are compared for the two cases: jerk-starting and braking. The predicted and measured natural frequencies will also be compared, and the test results will be examined for patterns that support or refute the various assumptions used in formulating the 3 DoF model.

7.1 Dynamic Ratios

7.1.1 Comparison of D_{3xj} with Measured Dynamic Ratios for Jerk-Starting Tests

Table 7.1 shows the average jerk-starting dynamic ratio for each test set. The test values used here for set 2LC are from Table 6.16 and are for the largest dynamic factor occurring during the time the motor was running. The predicted-to-measured ratios for the dynamic factors for each test set are shown in the third row of Table 7.1. All but two of the ratios are less than 1.15. The values of 1.32 and 1.65, for 2LC and ELC, respectively, are the two highest predicted-to-measured ratios. These two test sets correspond to the two cases, described in Section 5.8.1.2.1, which give values for $\frac{H_0\omega_c}{g}\,\frac{\kappa\sqrt{\mu}}{\sqrt{(1+\kappa)^3}}$ which do not satisfy the requirement given in (5.71).

The dynamic factor is the factor by which the maximum dynamic response of the structure exceeds the static response. The dynamic factor is, therefore, always greater than one. The ratio of the amount by which the predicted and measured values of D exceed unity are compared in the fourth row of Table 7.1. It can be seen that for all the test sets but ELC, this ratio is 2.01 or less. The ratio of $\frac{D_{3xj}-1}{D-1}$ for ELC is three times greater than the next largest of these ratios.

Figure 7.1 shows a graph of the predicted values for each test set plotted against the measured dynamic ratio for jerk-starting. The best-fit line

Figure 7.1
Predicted versus Measured
Dynamic Ratios for Jerk-Starting

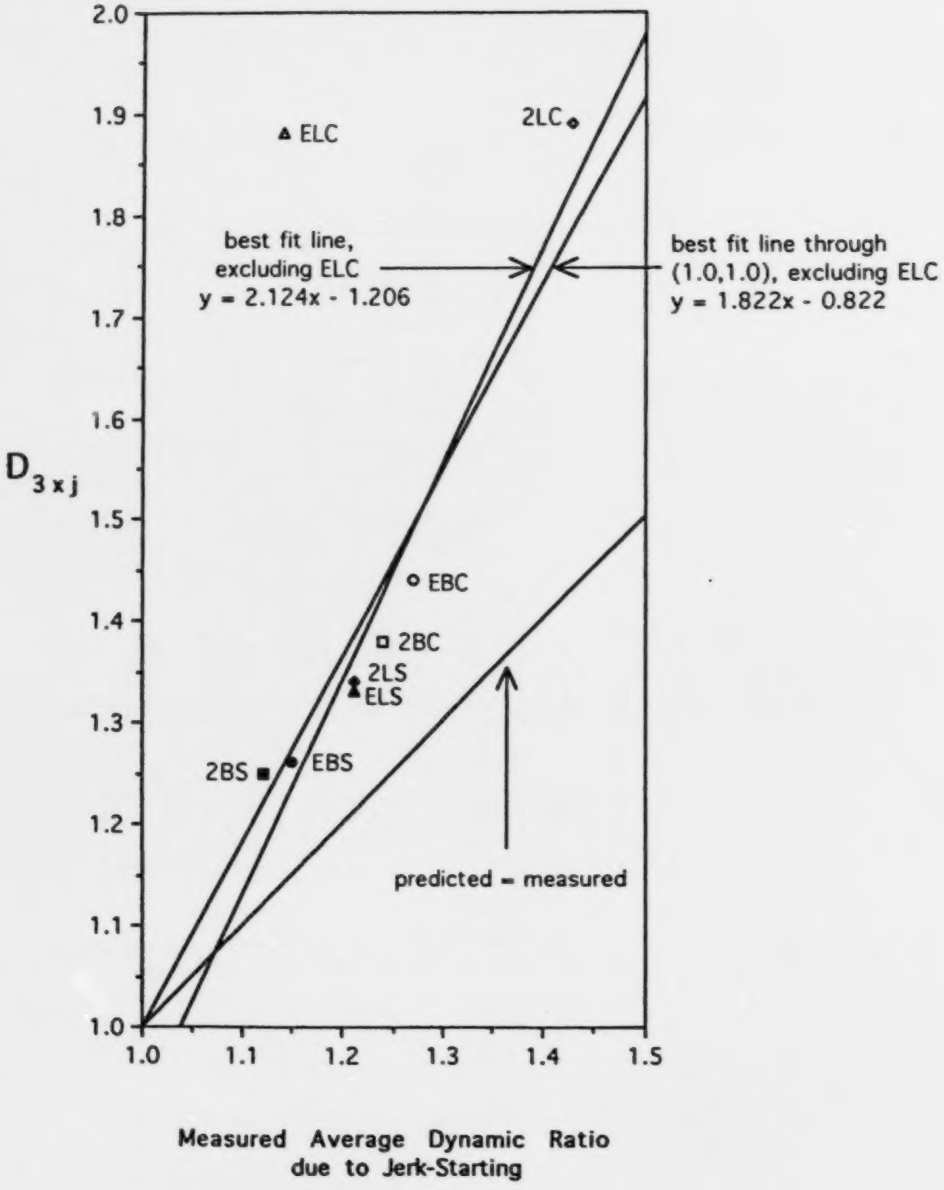

through all but the point for ELC very nearly passes through (1.0, 1.0). Again omitting the data for ELC, the best-fit line constrained to pass through (1.0, 1.0) has a slope of 1.822.

Table 7.1 Comparison of D_{3xj} and Measured Dynamic Ratio

	2BC	2BS	EBC	EBS	2LC	2LS	ELC	ELS
D_{3xj}	1.38	1.25	1.43	1.26	1.86	1.34	1.87	1.33
Measured Dynamic Ratio, D	1.24	1.12	1.27	1.15	1.43	1.21	1.14	1.21
$\frac{D_{3xj}}{D}$	1.11	1.11	1.13	1.10	1.30	1.11	1.64	1.10
$\frac{D_{3xj}-1}{D-1}$	1.59	2.07	1.61	1.73	2.01	1.61	6.19	1.58

7.1.1.1 The Anomaly of the Results for Set ELC

The results displayed in Figure 7.1 and Table 7.1 show a reasonable correspondence between predicted and measured values for all the test sets except ELC. For ELC, the predicted dynamic ratio is greater than the measured dynamic ratio by a factor of 1.65, which is the largest for all the test sets. The ratio of $\frac{D_{3xj}-1}{D-1}$ for ELC is about three times greater than the next largest of these ratios.

If it is assumed that the 3 DoF model can be used to predict real bridge crane behaviour within acceptable limits, then some feature of the testing procedure for the ELC test set did not conform to the conditions that were assumed in the development of the 3 DoF model and the factor D_{3xj}. One explanation for these test results is suggested by examining the graph of the cable tension versus time. The graphs for the three ELC tests are shown in Figures 7.2, 7.3 and 7.4. In each, shortly after the motor has been actuated, tension in the cable first starts rising and then remains constant at a value of

Figure 7.2 ELCs1

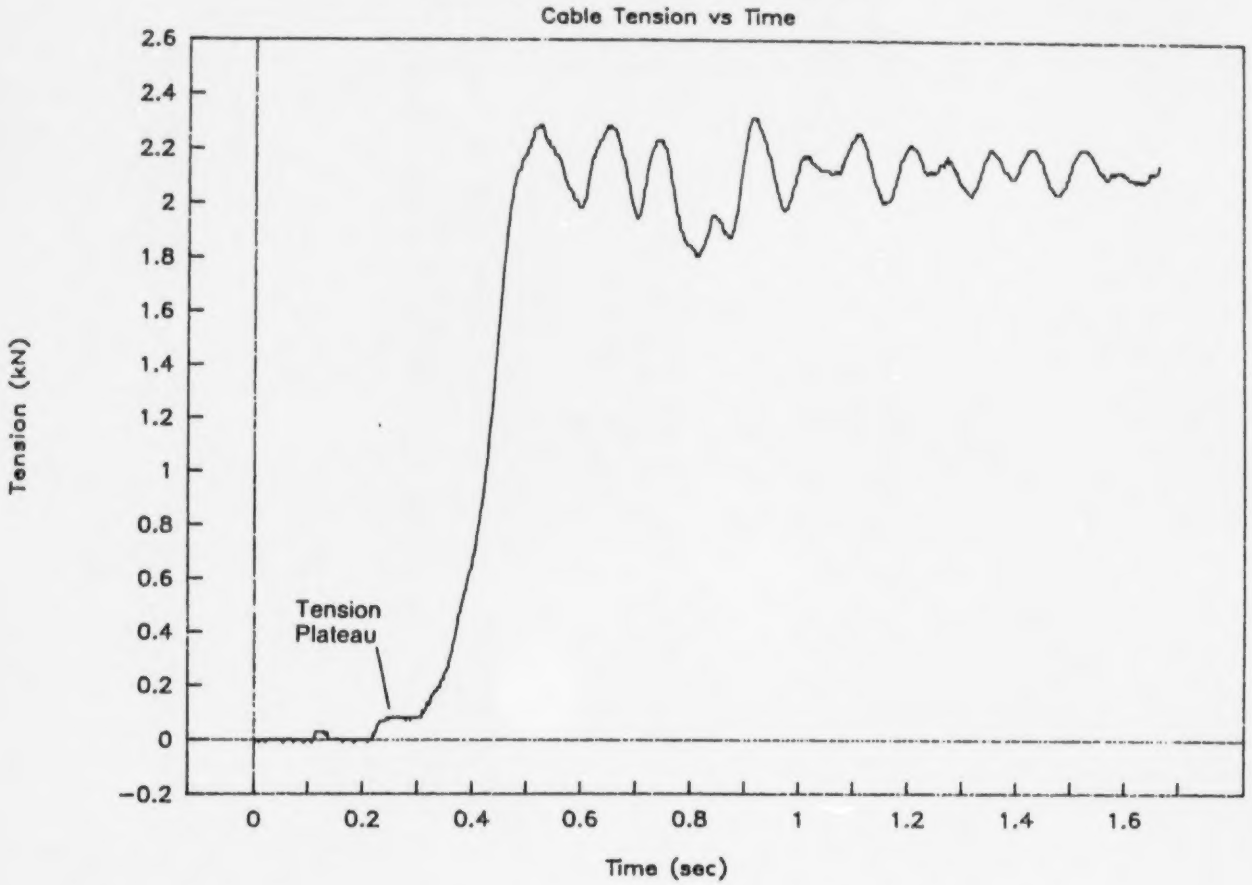

Figure 7.3 — ELCs2

Cable Tension vs Time

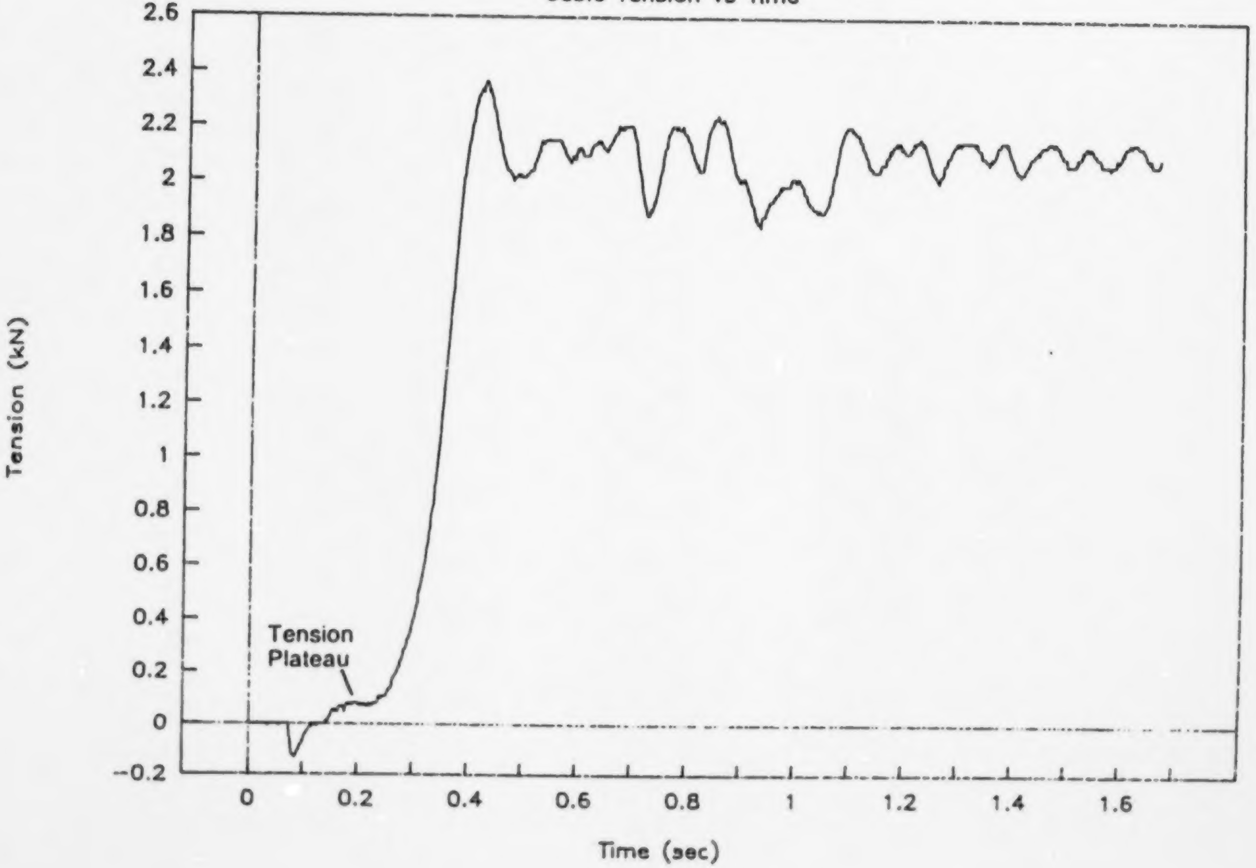

Figure 7.4 – ELCs3

Cable Tension vs Time

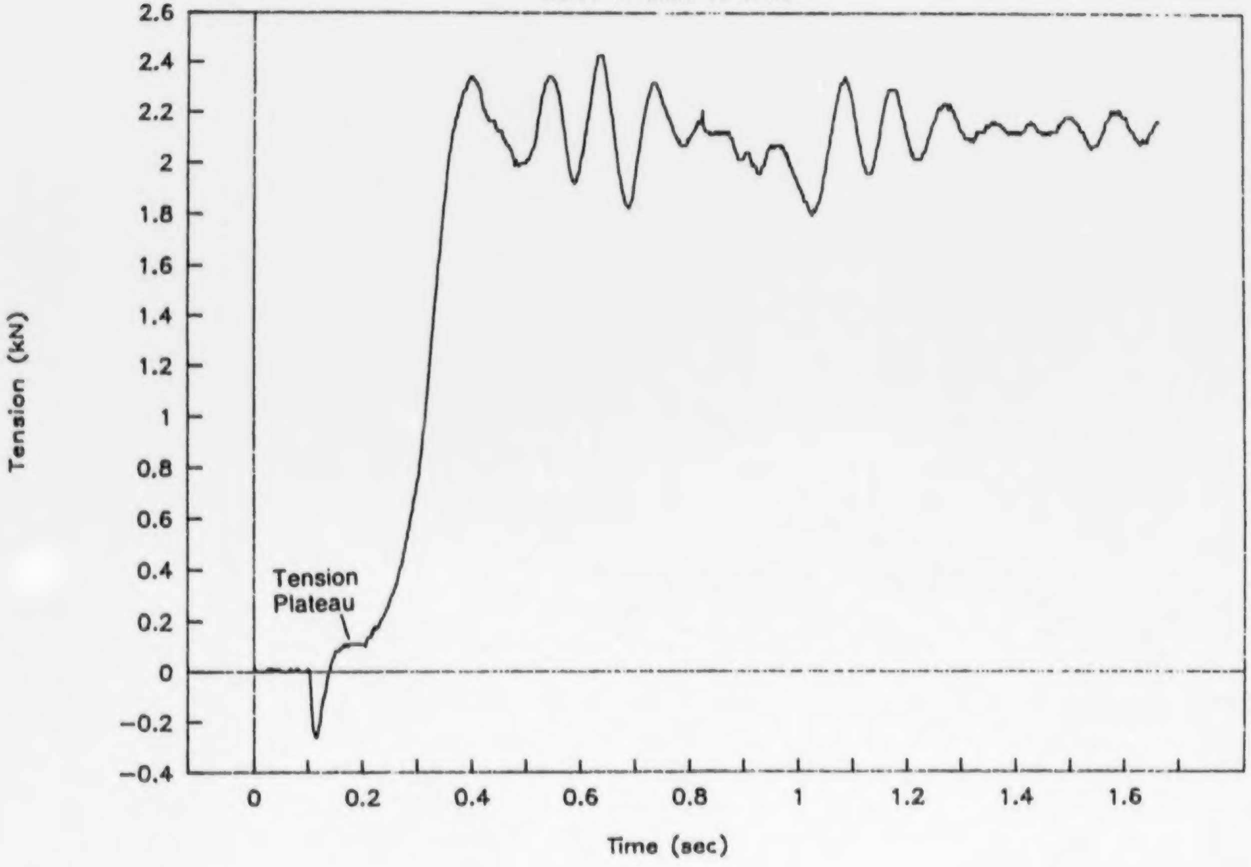

approximately 0.1 kN for a duration of approximately 0.1 seconds. After, tension rises to equal roughly the weight of the payload. In no other test in any other test set is this constant tension observed.

The constant tension could have been caused by the payload teetering before lift off. This happens when one side of one of the two slings is tighter than the others and begins lifting first. Nothing in the graphs indicates that the motor was not running continuously throughout the hoisting event, and therefore the hook was rising continuously at the hoisting speed. That the tension remained constant for some length of time implies that the cable was not being stretched for the duration of the plateau. If the cable was not being stretched, then the payload was moving upwards. If the payload was moving before it was lifted right off the ground (if it was teetering), then the jerk-starting assumptions are too conservative to describe the hoisting events that occurred during the ELC tests.

7.1.2 Comparison of Measured Dynamic Ratios for Braking Conditions and D_{3xb}

Figure 7.5 is a graph of the dynamic ratios before braking, plotted against the dynamic ratios after braking. In the majority of tests, braking decreased the dynamic ratio.

A distinction is made between the dynamic ratio due solely to braking, and the dynamic ratio which results after braking has occurred. As a result of hoisting, the crane and payload vibrate. At some arbitrary time during the cycle of these vibrations, braking is initiated. The two vibrations, due to hoisting and due to braking, are superimposed on each other and are not generally in phase, although they are of the same frequency (see Section 7.2.3). The dynamic ratio due solely to braking cannot be determined by the test procedure. It is the ratio which D_{3xb} is meant to account for.

Although it cannot be isolated from the data recorded after braking, there is a technique for estimating the dynamic ratio due solely to braking. For this technique, the gross assumption is made that the whole multi-DoF system vibrates at the dominant frequency only. Therefore the initial structure vibration can be described with the following equation.

Figure 7.5 Comparison of Dynamic Ratios Before and After Braking

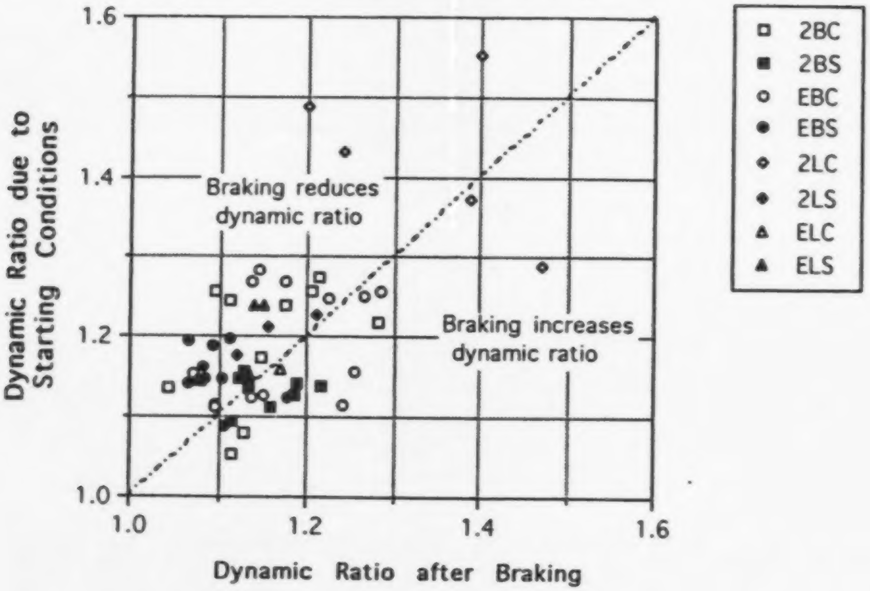

$$y_s \text{ (before braking)} = A \sin \omega t \tag{7.1}$$

where A is the vibration amplitude of the crane prior to braking, and ω is the dominant frequency of the 3 DoF system.

After braking has occurred, the vibration is described as follows.

$$y_s \text{ (after braking)} = C \sin(\omega t + \lambda) \tag{7.2}$$

The term λ is the phase shift between the vibrations which were present before braking, and those which occur after. The amplitude of the vibrations present after the initiation of braking is C, and ω is the dominant frequency for the 2 DoF system associated with braking. The frequencies in equations (7.1) and (7.2) are assumed to be equal.

The vibrations, that occur after the braking event, can be considered as the sum of two harmonic motions, as shown in equation (7.3).

$$y_s \text{ (after braking)} = A \sin \omega t + B \sin(\omega t + \beta) \tag{7.3}$$

where B is the amplitude of the vibrations due solely to braking, and β is the phase shift between the initial vibrations and braking vibrations which are added on. The amplitude A is as it was defined for equation (7.2). Figure 7.6 shows the assumed relationship between the vibrations.

The identity for the sine of the sum of two angles is applied in equations (7.2) and (7.3), as shown below.

$$y_s \text{ (after braking)} = (C \cos \lambda) \sin \omega t + (C \sin \lambda) \cos \omega t \tag{7.4}$$

$$y_s \text{ (after braking)} = A \sin \omega t + (B \cos \beta) \sin \omega t + (B \sin \beta) \cos \omega t \tag{7.5}$$

The right sides of equations (7.4) and (7.5) must be equal for all values of t, and therefore

Figure 7.6
Assumed Displacement Vibrations due Solely to Braking

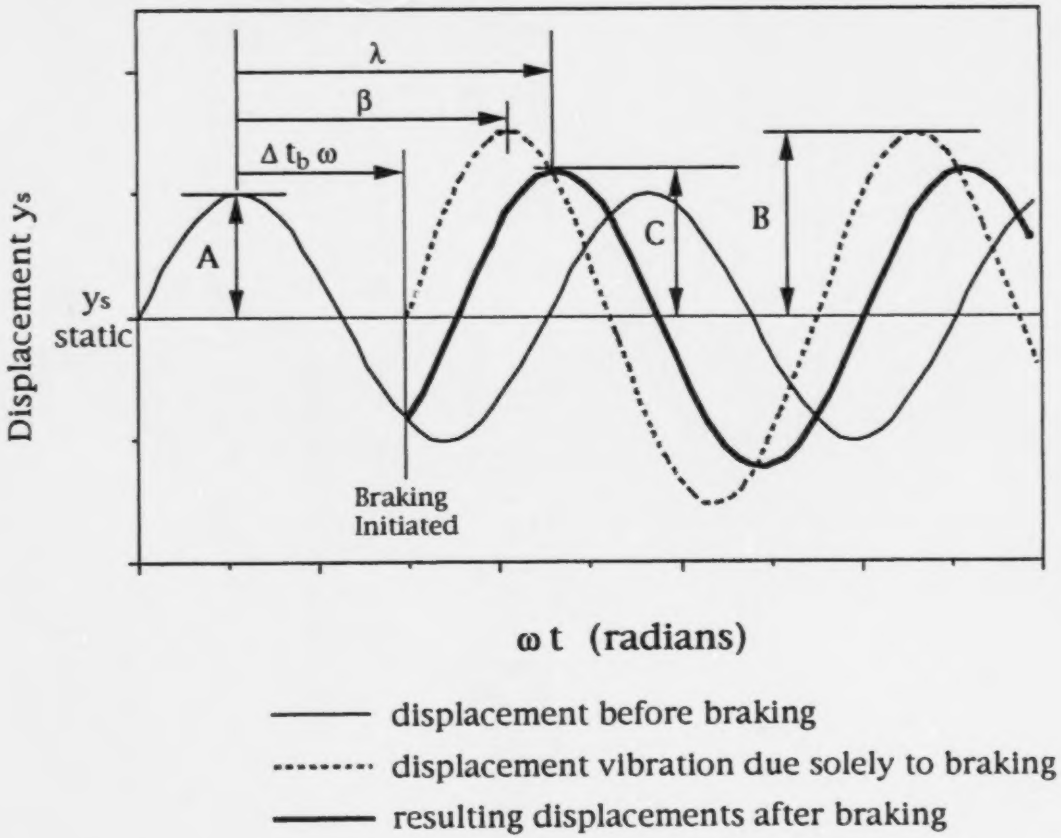

$$C \cos \lambda = A + B \cos \beta \quad , \tag{7.6}$$

$$\text{and} \quad C \sin \lambda = B \sin \beta \quad . \tag{7.7}$$

A solution for the two unknowns, B and β is found.

$$\beta = \tan^{-1} \frac{C \sin \lambda}{C \cos \lambda - A} \tag{7.8}$$

$$B = \frac{C \sin \lambda}{\sin \beta} \tag{7.9}$$

Equation (7.9) is the solution for B, the amplitude due solely to braking. In Figure 7.7 the value of $1 + \frac{|B|}{y_{s\,\text{static}}}$ is compared with the values for D_{3xb} for each test set. The amplitude, A, used in equation (7.8) for the points in Figure 7.7, is the initial amplitude which was recorded in Tables 6.3 to 6.24. It is not the amplitude just before braking, which in general is slightly less than the initial amplitude due to the small effects of damping. Values of λ are calculated by measuring the time between a peak before braking and a peak after braking, and multiplying that time duration by the second natural frequency for that test.

Figure 7.8 shows a graph of the average dynamic ratio due solely to braking, calculated as outlined above, plotted against D_{3xb} for each test set. This graph can be compared to the graph in Figure 7.1. The correlation between the test results and the predicted values calculated for the braking case in this fashion, is not as good as the correlation for the jerk-starting case. There are several potential reasons why this is so. First, the procedure for determining B is based upon a major simplification of the multi-DoF system, and that introduces inaccuracies. Second, the assumption underlying the derivation of D_{3xb} may not be appropriate. The assumption used to determine the initial conditions for the braking scenario is that at the instant

Figure 7.7
Dynamic Ratios due Solely to Braking

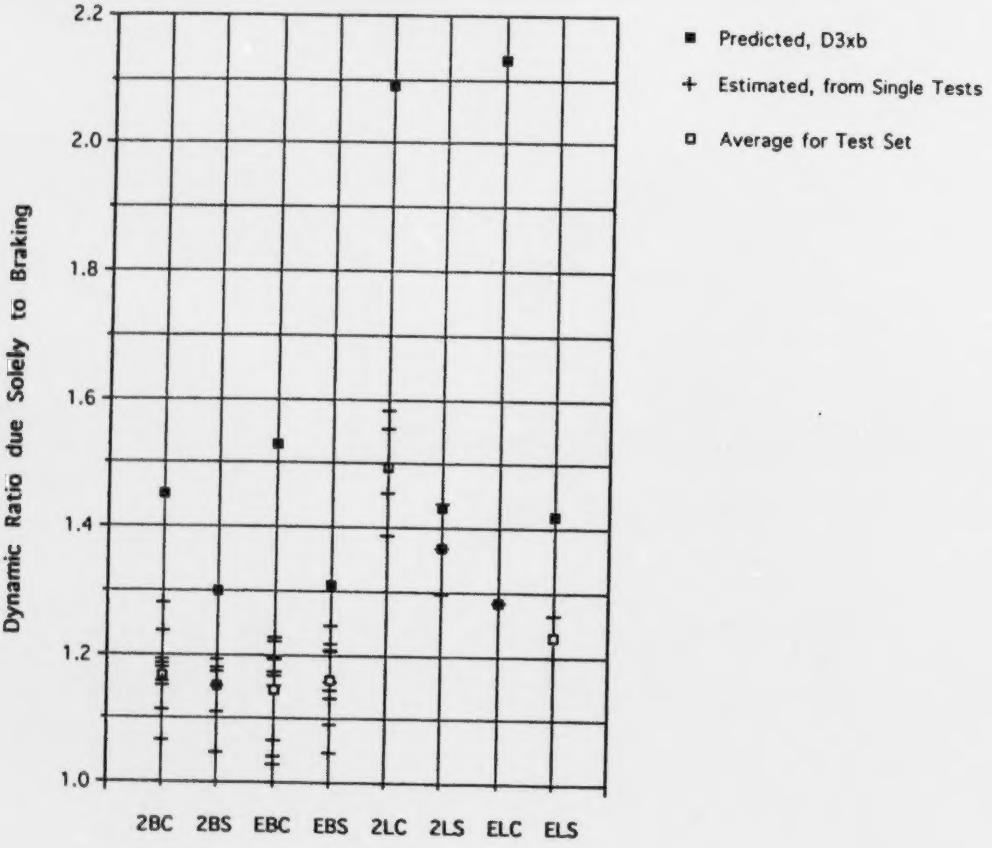

Figure 7.8
Predicted versus Measured Dynamic Ratios due Solely to Braking

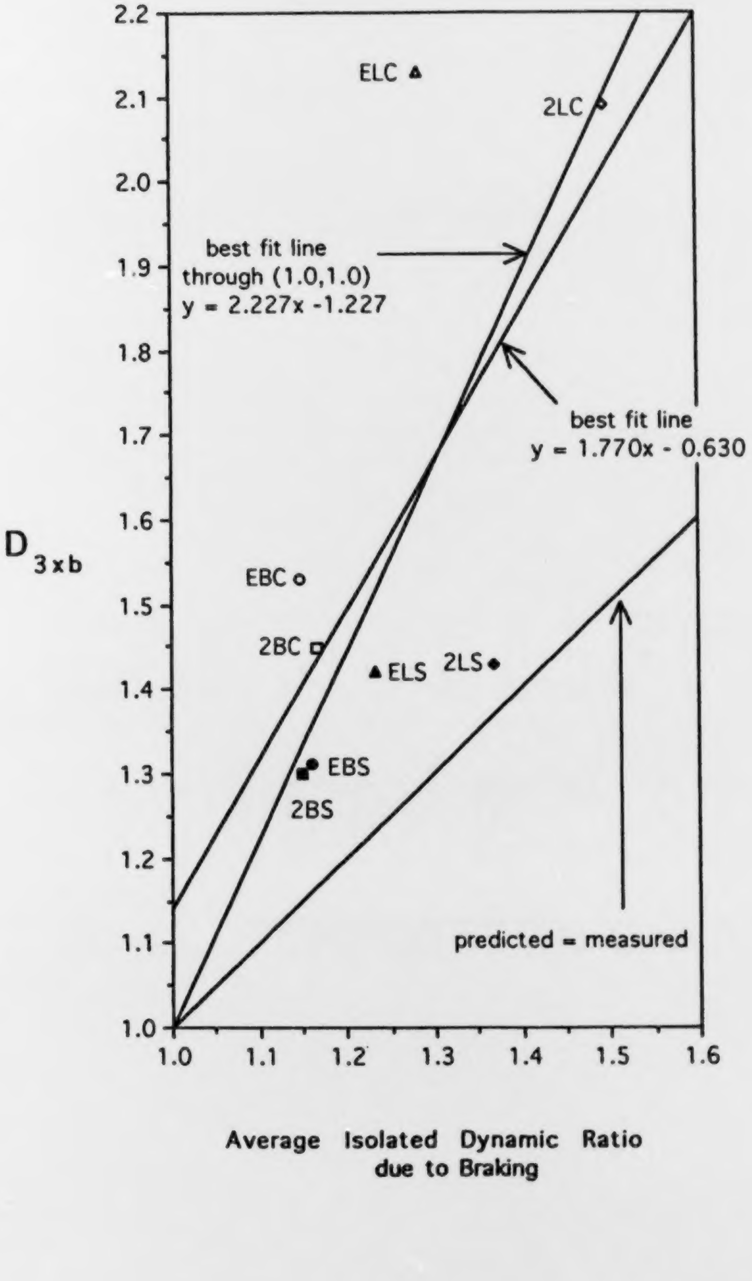

the brake is applied, the motor mass stops moving. This is a conservative assumption, and the predicted dynamic factors based on that assumption are much higher than the test results. Aside from the magnitude, some features of the data from the tests indicates that slippage during braking affects the dynamic ratio.

Consider the graph in Figure 7.9, which is a plot of the phase shift, β, versus B, the magnitude of the dynamic ratio due solely to braking. Because the time at which braking was initiated was chosen without reference to the phase of the vibrations of the structure or payload, the points in Figure 7.9 would be expected to have a uniform angular distribution, but clearly this is not the case. Of the 46 data points, 41 are between $\frac{\pi}{2}$ and $\frac{3\pi}{2}$.

The distribution of the phase of the structure vibrations at the instant when the motor power was turned off can be determined from the collected data. The time between the last peak of the structure vibrations prior to braking, and the data spike which marks the instant the motor was turned off, is determined from the graphs and recorded as the variable Δt_b in Tables 6.5, 6.8, 6.11, 6.14, 6.18, 6.20, 6.22, and 6.24, which deal with braking. If, when the motor power is turned off, the brake is applied and the rotor stops instantly, and if the technique for finding β and B is valid, then the angle β should equal the angle $\Delta t_b \omega + \frac{\pi}{2}$, as can be seen in Figure 7.5. If there is some uniform delay between the time the power to the motor is shut off and the instant the rotor suddenly stops turning, then the difference between angles β and $\Delta t_b \omega$ would be greater than $\frac{\pi}{2}$, and that difference would be the same for each test within a test set.

Figure 7.10 is a graph of $\Delta t_b \omega + \frac{\pi}{2}$ plotted against the angle β associated with positive values for B. It can be seen that the difference between each corresponding pair of angles β and $\Delta t_b \omega$ is not constant for each test set. Therefore, there is not a constant delay between the time the power to the motor is shut off and the instant the rotor suddenly stops turning. The standard deviation of the angle $\Delta t_b \omega + \frac{\pi}{2}$ about the mean of 1.02π is 0.498π. If

Figure 7.9
Phase Shift β versus Dynamic Ratio due Solely to Braking

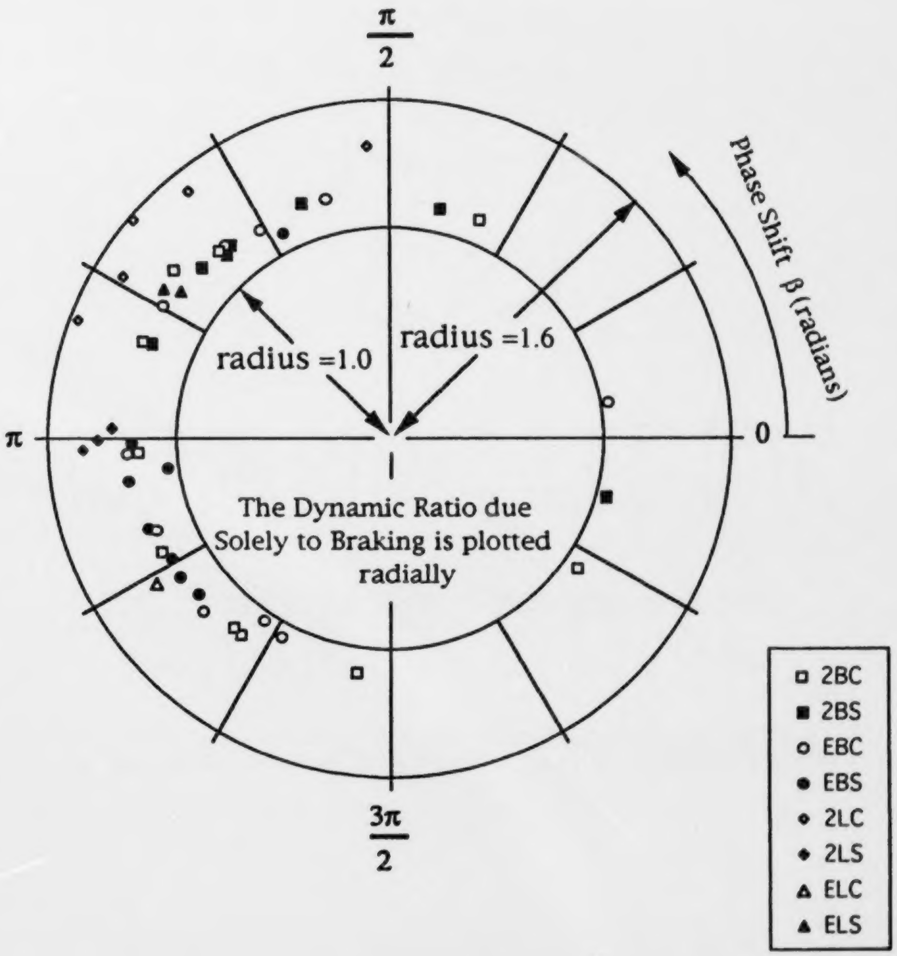

Figure 7.10

Comparison of Angles β and $\Delta t_b\omega + \frac{\pi}{2}$

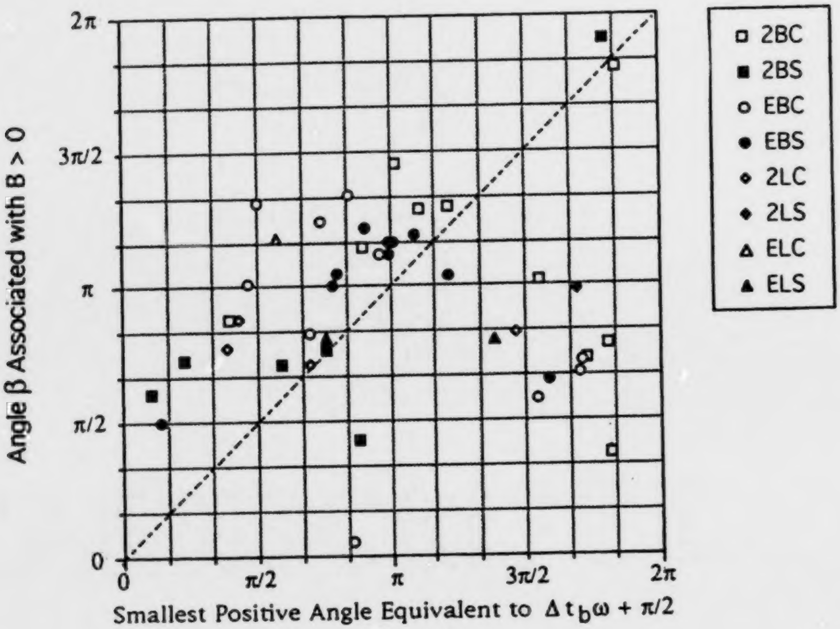

$\Delta t_b\omega + \frac{\pi}{2}$ had a uniform angular distribution, then it would have a standard deviation of $\frac{\pi}{\sqrt{3}}$ which is approximately 0.58π. Therefore the distribution of the phase of the structure vibrations at the instants at which the motor power was turned off are, as expected, roughly uniformly distributed. The standard deviation of the angle β about the mean of $.953\pi$ is 0.353π. The concentration of the values of β between $\frac{\pi}{2}$ and $\frac{3\pi}{2}$ may indicate that the brake slips before the rotor completely ceases to turn, and that it slips more when activated at one phase of the vibrations than at another. In developing the formula for D_{3xb} the assumption was made that the rotor stopped turning the instant the brakes were applied. If the amount the brake slips has a significant effect upon the dynamic factor, then this assumption is not valid. The slipping of the brake may account for the less accurate predictions from D_{3xb} .

7.1.3 Comparison of Measured Dynamic Ratios and Dynamic Factors from the Standards

In Figures 7.11 to 7.14 the measured dynamic ratios and dynamic factors from the standards reviewed in Chapter 3, are compared. The standards specify dynamic factors, but do not describe the type of hoisting event which the dynamic factors are for. It is reasonable to assume that the factors from the standards are meant to account for the largest dynamic responses of the crane during in-service operation. Therefore, in Figures 7.11 to 7.14, it is the largest dynamic ratio from each test, whether due to braking or starting conditions, which is compared to the dynamic factors from Table 3.1. The value of D_{3xj} is also included in these figures as a reference, although D_{3xj} was derived specifically for jerk-starting hoisting events and not for combined starting and braking scenarios. In Table 3.1, the first group of standards was meant to apply to the bridge beam, and the later group was meant to apply to the building structure that supports the craneway. In the test sets prefixed with "2" the bridge beam was most severely loaded. The results from these sets are compared to the factors specified in the first group of standards. In the test sets prefixed with an "E", the building members were most severely

Figure 7.11
Comparison of Measured Dynamic Ratios with Specified Dynamic Factors

Case of Bridge Beam and Large Payload

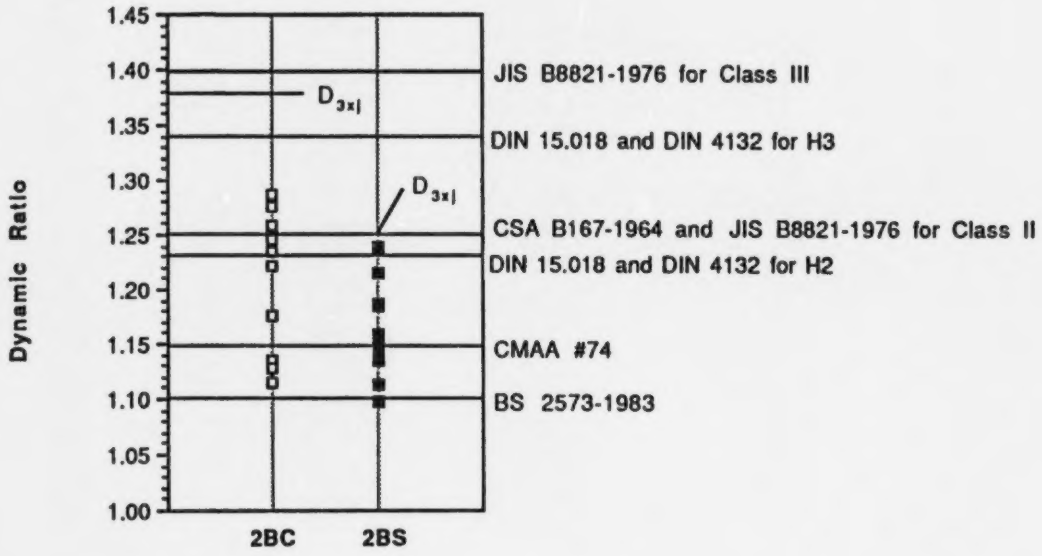

Figure 7.12
Comparison of Measured Dynamic Ratios with Specified Dynamic Factors

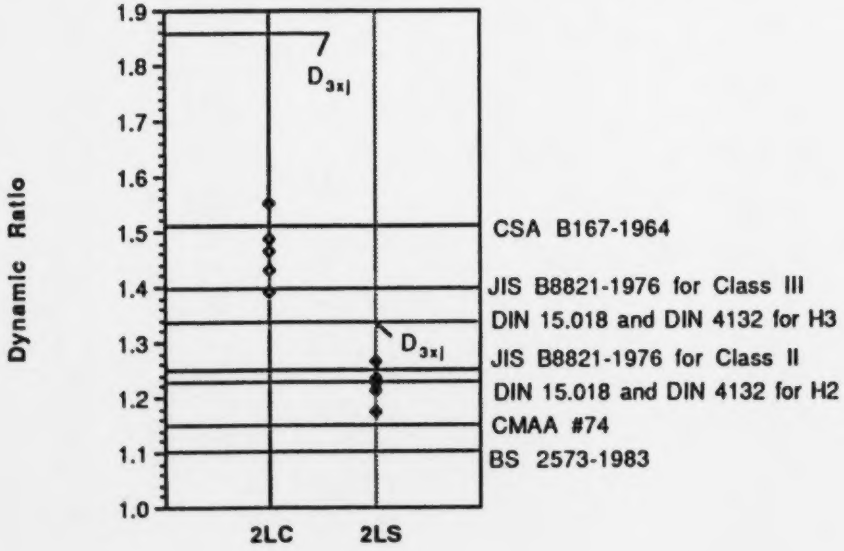
Case of Bridge Beam and Small Payload

Figure 7.13
Comparison of Measured Dynamic Ratios with Specified Dynamic Factors

Case of Craneway Structure and Large Payload

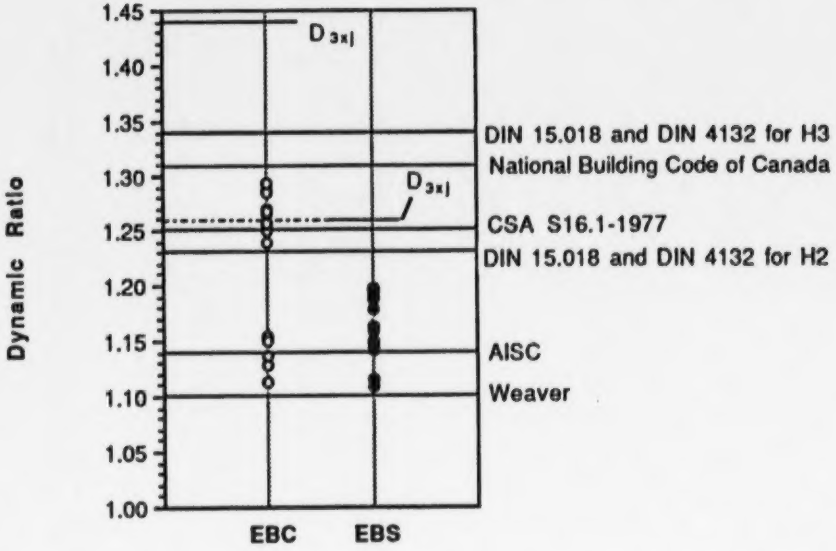

Figure 7.14
Comparison of Measured Dynamic Ratios with Specified Dynamic Factors

Case of Craneway Structure and Small Payload

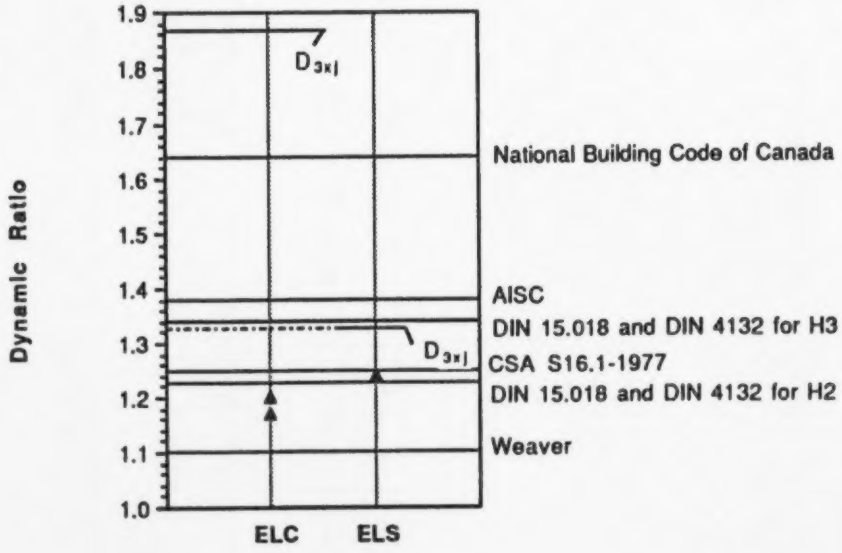

loaded, and the results from these sets are compared to the dynamic factors from the latter group of standards.

The standards are applied to the cases in which the shop crane hoists the large payload, and in which it hoists the small payload. The purpose of using the shop crane and the small payload, in the testing and in the calculations with the standards, is to simulate the case of a relatively heavier crane lifting its rated load. Larger cranes tend to be heavier relative to their rated loads. Therefore, their values of μ, where m_p is the rated load, are higher. Using the shop crane to hoist the small payload, which has a small value for m_p, provided hoisting events in which the value of m_p was relatively low, and the values for μ were relatively high. In Figures 7.11 to 7.14 the results for the large and small payloads are compared to the specifications from the standards for these two cases.

None of the standards take into account differences between chain slings and web slings. Therefore, in Figures 7.11 to 7.14, the test results for both types of slings are displayed together and compared with the specified dynamic factors meant to apply to both.

In Figures 7.11 and 7.12, it can be seen that CMAA # 74 and BS 2573.1988 specify dynamic factors lower than those measured during tests. The same is true of Weaver's values in Figures 7.13 and 7.14. This does not mean that a design process that includes any of these three dynamic factors will necessarily produce unconservative results. Other parts of the process may be conservative enough to compensate adequately. It does mean that the factor meant to account for dynamic loads is unconservative.

The H3 designation in the German standards DIN 15.018 and DIN 4132 gives dynamic factors slightly higher than the highest measured ratios for the tests using the large payload. Therefore, the classification that would best fit the shop crane is H3. In Figure 7.11, the Class II designation from JIS B 8821. 1976 gives a dynamic factor slightly lower than the test results, and the Class III factor is much higher than the test results. It is not clear which Class should apply.

For the case of the small payloads, the Class III designation for JIS B8821.1976 and the H3 designation from DIN 15.018 and DIN 4132 specify factors which are much less than the dynamic ratios for the 2LC tests. The ELC test results are low, probably due to errors in the test procedure (see Section 7.1.1.1). The values for D_{3xj} from test sets 2LC and ELC are close to each other, and it may be that, had the errors not occurred in the ELC tests, the dynamic ratios for sets ELC and 2LC would have been similar. If the ELC tests had provided dynamic ratios of similar magnitude to those from the 2LC tests, then it would be seen that the H3 and Class III designations consistently give factors that are too low. This may not mean that the two standards are unconservative. The designation system in each is based on qualitative descriptions of the crane and its uses. The purpose of using the small payload was to simulate a different type of crane from the shop crane. Such a crane would have a high value of μ when lifting its rated load, and would, for example, have a double box girder bridge. Each of the two standards might place such a crane in a category which is different from that for the shop crane. The different categories might be associated with higher dynamic factors.

Both DIN 15.018 and CMAA # 74 provide formulae that, for particular ranges of hoisting speed, give the dynamic factor as a linear function of the hoisting speed. The 3 DoF analysis provides formulae for D_{3xj} and D_{3xb} which also are linear functions of hoisting speed. However, the 3 DoF analysis provides no limit for the range of positive hoisting speeds for which the linear relationship holds. Figure 7.15 is a graph of dynamic factors versus hoisting speed. The values for the dynamic factors from DIN 15.018 and CMAA # 74 are plotted. The test results from the eight test sets are also plotted, at the shop crane hoisting speed of 0.1m/s. If it is assumed that the dynamic factor is unity when the hoisting speed is zero, and that the relationship between the factor and the hoisting speed is linear, then lines can be drawn from the point (1.0 , 0.0) through the points representing the measured dynamic ratios. The shaded area in Figure 7.15 indicates the range through which those lines would pass. It can be seen that the lines would be steeper than those proposed by either standard, although the lower dynamic ratios do approach the rate recommended in CMAA # 74.

From Figures 7.13 and 7.14. it can be seen that the dynamic factor of 1.25 from CSA S.16.1.1977 is adequate. As mentioned earlier, it may be that the dynamic ratios from the test set ELC should be approximately equal to those

Figure 7.15 Graph of Dynamic Factors and Measured Dynamic Ratios versus Hoisting Speed

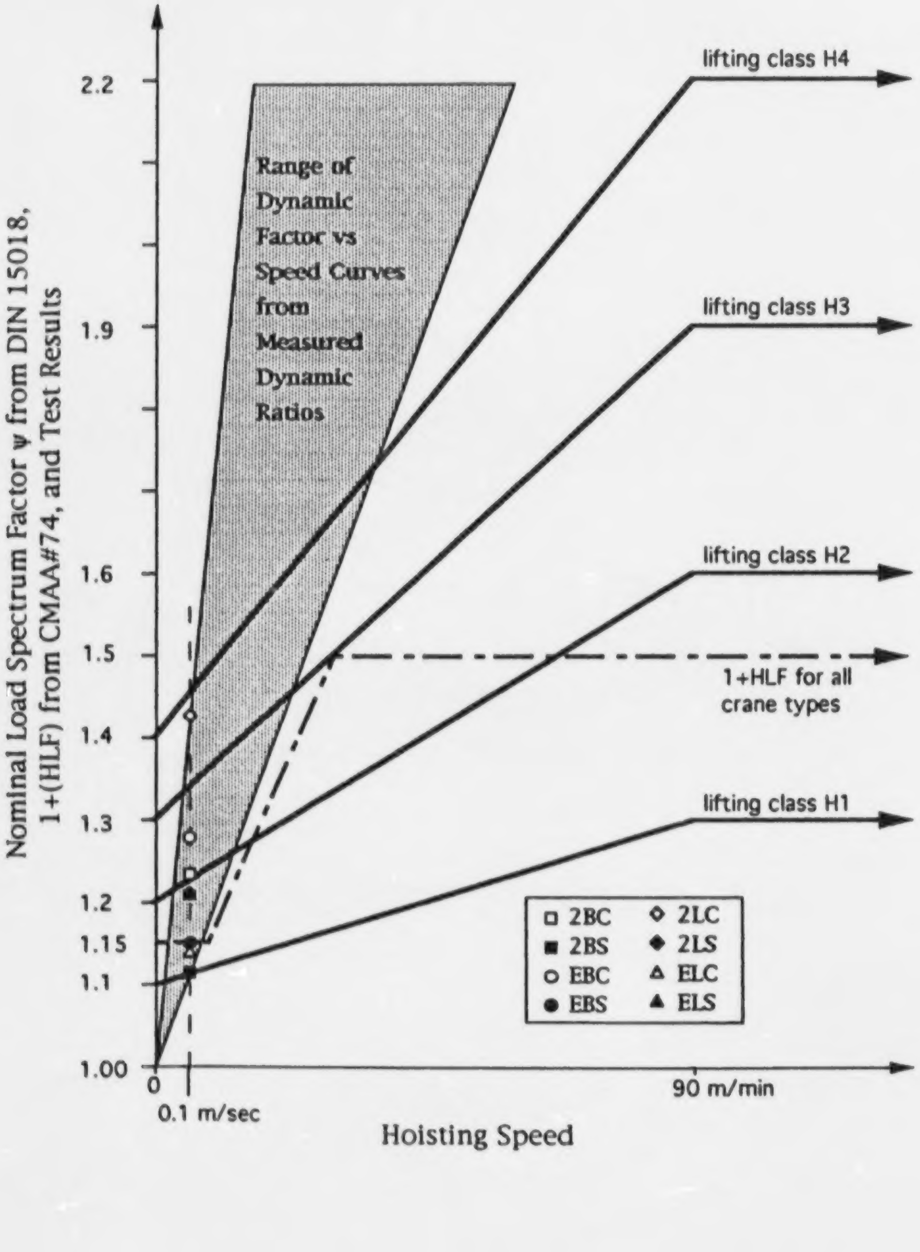

from 2LC. If that is so, then S16.1.1977 is not adequate, because it specifies a constant factor of 1.25 and does not account for changes in μ and the corresponding significant changes in value of D. The AISC factor and the factor used in the National Building Code of Canada do change with respect to μ, and that change can be seen between Figures 7.13 and 7.14. Again, if it is assumed that the ELC results should be between 1.4 and 1.5, then the AISC specified factor is low by about 0.15 in each instance, and the National Building Code factor is slightly high in each instance.

7.2 Evaluation of Assumptions Underlying 3 DoF Model

Some of the assumptions made in developing the 3 DoF model and the D_{3xj} and D_{3xb} factors can be evaluated using the test results.

7.2.1 Single DoF System Structure Assumption

The crane structure can be considered to behave as a single DoF system if all the moments, shears, and displacements are proportional over time. If that is the case, then for any hoisting event, the time histories of all the moments, shears, and displacements are in phase, and have the same frequencies and the same relative amplitudes. An examination of Figures 6.14 to 6.23 shows that when the plotted parameters have significant amplitude, their time histories are proportional. The wheel load graphs show correlation from station to station. The displacements of the trolley and the south east wheel are also proportionally related. The bending moment and midspan downwards deflections are proportional, as are the south east wheel displacements and the south east wheel reaction forces.

Figure 7.16 shows a plot of the jerk-starting dynamic ratios for all of the tests, arranged by parameter type and station. The values are normalized relative to the average dynamic ratios for each test. The spread in peak values for different parameters is 30%, and the coefficient of variation is 5.01% from a mean of 0.998. From these test results it is reasonable to conclude that the structure behaves like a single DoF system.

Some of the test results indicate the limitations of the single DoF model of the structure. For each of the test sets in which the crane was loaded at the

Figure 7.16
Normalized Jerk-Starting Dynamic Ratio Plotted by Parameter

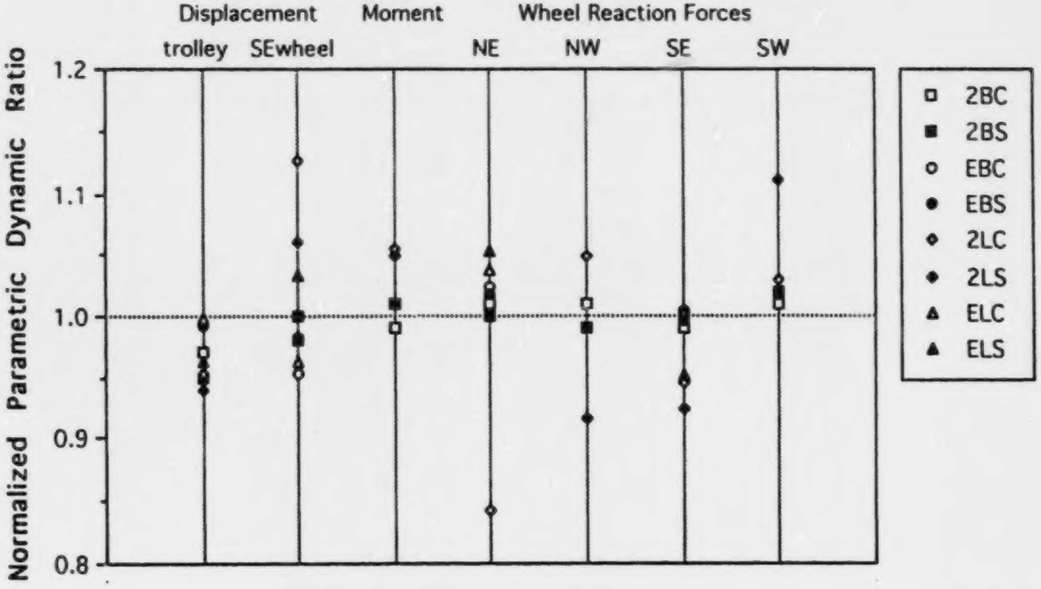

east end, (those test sets prefixed with an "E" rather than an "2"), the moment recorded at the midspan of the bridge had a frequency much higher than the dominant natural frequency. The dominant natural frequency for these tests shows clearly in the displacements and reactions. It is also observed in Figures 6.12 to 6.17 that the higher frequency content of the displacement time histories is less than that of the moment or wheel load time histories. This is expected for multi-DoF systems. Both the amplitude of the midspan moment for the tests where the trolley was at the east end, and the differences between the higher frequency amplitudes of different parameters, are small. They are insignificant in magnitude compared with the magnitudes of the maximum moments, displacements and shears which occurred in the same tests.

7.2.2 Assumption of No Damping

Damping was assumed to have an insignificant effect on the magnitudes of the dynamic factors. An examination of the graphs shows a decay in the amplitudes during free vibration. Calculations of the equivalent viscous damping ratio ξ, were carried out, and the results are presented in Table 7.2. The viscous damping ratio is assumed to be small if tan ξ is approximately equal to ξ, which is the case in these tests.

Table 7.2 Measured Damping Ratios

	2BC	2BS	EBC	EBS	2LC	2LS	ELC	ELS
Equivalent Viscous Damping Ratio, ξ	0.013	0.020	0.022	0.016	0.033	0.025	-	-

As shown in the Table 7.2, the damping is very small and can be considered insignificant when peak amplitude ratios are considered. The maximum dynamic responses occur shortly after loading, before the effects of this low level of damping can become significant.

The cable system shows hysteresis, and delayed elasticity. These features are caused by damping. Therefore, although damping does not produce significant rates of decay of amplitude, it does affect the value of k_c, which is used to calculate the dynamic factor.

7.2.3 Assumption of Infinite Motor Mass and Constant Motor Speed

A comparison of the time histories, shown in Figures 6.14 to 6.23, of the various parameters before and after braking has occurred, indicates that the assumption of constant speed motor and infinite motor mass is valid. The frequencies that occur when the motor is running, and the free vibration frequencies after braking, are not measurably different. If the brake is not faulty, then the changes in cable tension do not rotate the hoist drum once the rotor has stopped moving, and the system has two D'soF. If the frequencies associated with those two D'soF are nearly the same as the frequencies that are active when the motor is running, then the changes in the cable tension do not significantly alter the rate of rotation of the hoist, which is the condition that follows from the assumption that V_0 is constant and m_s approaches infinity.

7.2.4 Assumption that Jerk-Starting is the Most Severe Starting Case

By definition, for this testing program any non-jerk-starting test began with tension in the cable. Figure 7.17 shows a graph of the dynamic ratio plotted against the initial cable tension for each test done using the large payload. (Only jerk-starting tests were performed in test sets ELS and ELC, and only jerk-starting and hanging tests were performed in test sets 2LC and 2LS.) To compare the results from different test sets, the dynamic ratios for each test were normalized relative to the average dynamic ratio for their test set. The following formula was used.

$$p = \frac{d - 1}{a - 1} + 1 \tag{7.12}$$

where d is the dynamic ratio for each test, a is the average dynamic ratio for that test set, and p is the point which is plotted against the initial cable tension. Equation (7.12) generates values that are normalized with respect to

Figure 7.17 Dynamic Ratio versus Initial Cable Tension

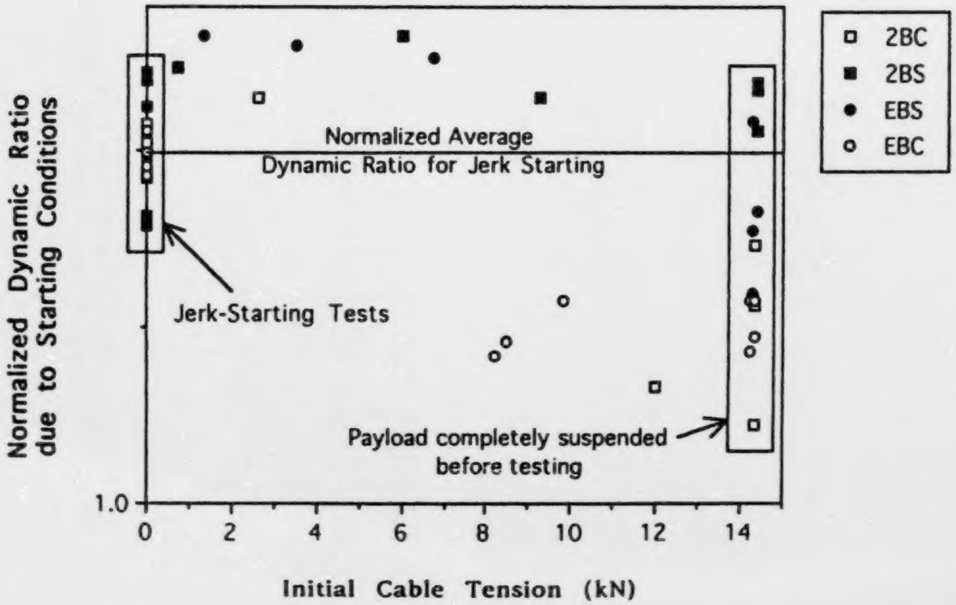

unity as well as with respect to the average dynamic ratio for that test set. For the limiting case in which d equals one, the solution for p is one.

It can be seen from the graph in Figure 7.17 that the highest dynamic ratios are attained with initial cable tension values that are low but greater than zero. Jerk-starting is not the most severe starting case.

That jerk-starting is not the critical case can be explained as follows. For the theoretical case of a linearly elastic cable, jerk-starting is the most severe condition because any other starting condition involves loading the motor before hoisting speed is reached. In general, that will cause lower cable tension for longer durations, and that tends to produce smaller dynamic ratios. However, the stiffness of the real cable is not constant. Consider a hoisting event in which the amount of initial cable tension is exactly that required to produce the maximum dynamic ratio. If the initial tension were reduced, then the initial cable stiffness would be reduced. The acceleration of the motor would be greater, but the crane structure would not be pulled as quickly because the cable would stretch more. If the initial tension were increased, then the initial cable stiffness would be increased. The acceleration of the motor would be less because the initial load upon it is increased. The velocity of the crane structure and the motor mass would more closely match, but the velocity of the motor would be less. At some particular initial tension a balance is reached, between the effect on the motor and the effect on the structure, which causes the dynamic ratio to be a maximum.

In Chapter 5, the non-constant cable stiffness was accounted for by assuming that at the instant of payload lift off the structure was at its static deflection with no acceleration and a velocity of $\frac{Ho}{1+k}$ downwards. These assumptions are meant to describe the circumstances associated with jerk-starting, but they do not explicitly preclude initial tension in the cable. They do require that for some length of time before the payload lifts off, the motor must maintain synchronous speed, and the cable must maintain the stiffness associated with the tension m_pg. Therefore, D_{3xj} can still be used to describe the critical starting case.

None of the dynamic ratios from the test results was greater than the values of D_{3xj} calculated for the test set.

7.2.5 Assumptions Regarding the Values of k_c and m_s

In section 2.5 a procedure was introduced to deal with the significant hysteresis of the cable. The slopes of the loading and unloading curves for the cable tension versus elongation graphs were used to define $k_{c_{effective}}$, the effective stiffness assumed to apply during free vibration of the system.

The measured natural frequencies from Table 6.2 and the calculated natural frequencies from Table 5.2. are compared in Table 7.3. There are significant differences between the two sets of values. If the 3DoF model can provide results that accurately match the response of a real bridge crane, then the discrepancies between the measured and calculated natural frequencies can be explained in terms of incorrect data being used in the formula for ω_2 and ω_3. Of the four variables used, k_s, m_s, k_c, and m_p, two are not measured

Table 7.3 Comparison of Measured and Predicted Natural Frequencies

	2BC	2BS	EBC	EBS	2LC	2LS	ELC	ELS
Predicted Second Natural Frequency, (radians/second)	31.9	22.5	36.2	23.8	50.9	28.7	54.1	29.1
Measured Second Natural Frequency, (radians/second)	32.0	27.5	37.3	31.6	60.3	38.2	71.8	40.0
Ratio of Predicted to Measured	0.997	0.819	0.970	0.753	0.845	0.751	0.753	0.727
Predicted Third Natural Frequency, (radians/second)	118	98.5	119	107	99.0	90.0	107	102
Measured Third Natural Frequency, (radians/second)	134	129	179	183	123	131	-	187
Ratio of Predicted to Measured	0.880	0.763	0.667	0.584	0.805	0.687	-	0.545

values. Both m_s and k_c are estimated on the basis of certain assumptions and are not measured directly.

The test results can be used to check the assumed values of m_s and k_c. The tests provide measured values of ω_2 and ω_3 . Thus there are four measured variables: m_p, k_s, ω_2, and ω_3. These are sufficient in order to solve for the two assumed variables, m_s and k_c. Expressions for m_s and k_c in terms of ω_2 and ω_3 are derived for the 3 DoF model from equations (5.30) and (5.31). Adding these two equations together gives the following.

$$\omega_3^2 + \omega_2^2 = \Omega^2 + \omega_s^2 = \omega_s^2 + \omega_c^2 + \frac{k_c}{k_s}$$

$$\frac{k_c}{m_p} + \frac{k_s}{m_s} + \frac{k_c}{m_s} = \omega_3^2 + \omega_2^2 \tag{7.10}$$

The difference between the squares of the two natural frequencies is also of value.

$$\omega_3^2 - \omega_2^2 = \sqrt{(\Omega^2 + \omega_s^2)^2 - 4\omega_s^2\,\omega_c^2}$$

$$(\omega_3^2 - \omega_2^2)^2 = (\Omega^2 + \omega_s^2)^2 - 4\omega_s^2\,\omega_c^2$$

$$\omega_3^2\,\omega_2^2 = \omega_s^2\,\omega_c^2$$

$$\omega_3^2\,\omega_2^2 = \frac{k_s k_c}{m_s m_p}$$

$$k_c = \omega_3^2\,\omega_2^2\,\frac{m_s m_p}{k_s} \tag{7.11}$$

Substituting equation (7.11) into (7.10) leads to the following expression for m_s .

$$\omega_3^2\,\omega_2^2\,\frac{m_s}{k_s} + \frac{k_s}{m_s} + \omega_3^2\,\omega_2^2\,\frac{m_p}{k_s} = \omega_3^2 + \omega_2^2$$

$$m_s^2 + m_s\left(m_p - \frac{(\,\omega_3^2 + \omega_2^2\,)k_s}{\omega_3^2\,\omega_2^2}\right) + \frac{k_s^2}{\omega_3^2\,\omega_2^2} = 0$$

$$m_s = \frac{\dfrac{(\,\omega_3^2 + \omega_2^2\,)k_s}{\omega_3^2\,\omega_2^2} - m_p - \sqrt{\left(m_p - \dfrac{(\,\omega_3^2 + \omega_2^2\,)k_s}{\omega_3^2\,\omega_2^2}\right)^2 - \dfrac{4k_s^2}{\omega_3^2\,\omega_2^2}}}{2} \tag{7.12}$$

Using the measured values of ω_2, ω_3, k_s, and m_p, the validity of the values assumed for k_c and m_s can be judged. Table 7.4 shows the values calculated for k_c and m_s from (7.11) and (7.12), and the values that have been assumed till this point.

The cable stiffness, k_c, is affected by the choice of chain or web slings, and by whether the large or small payload was hoisted. Thus, it is expected that there are four distinct values of k_c calculated from equation (7.11): one for each of the pair of tests 2BC and EBC, 2BS and EBS, 2LC and ELC, and 2LS ELS. It can be seen in Table 7.4 that this is the case. Similar results appear for each pair of test sets in which the same payload and slings were used.

Only in the case of 2BC and EBC is the value k_c from (7.11) close to the value of $k_{c_{effective}}$. This results can be explained as follows. During the measurement of $k_{c_{slacken}}$ and $k_{c_{tighten}}$ the cable and sling assembly had time between each load step to move to its steady state elongation. The much higher loading rates that occurred during the dynamic testing did not allow time for changes in cable stiffness due to delayed elasticity to develop. During the cable stiffness measurements, the chain slings holding the large payload were only marginally subject to the effects of delayed elasticity at each load step. The initial and final stiffness at each load step were nearly equal. The change in loading rate, therefore, has little effect on the chain slings holding the large payload. Therefore, for EBC and 2BC, the value of k_c from equation (7.11) is similar to the value of $k_{c_{effective}}$.

The web slings did not have time to experience delayed elasticity during the high loading rates they were subjected to in the dynamic tests. Thus, they displayed a stiffness higher than $k_{c_{effective}}$ in the dynamic tests. In test sets 2LS and ELS, the values of k_c derived from the natural frequencies are roughly midway between $k_{c_{effective}}$ and $k_{c_{slacken}}$. The values of k_c derived from the natural frequencies, for test sets 2BS and EBS, are approximately equal to $k_{c_{slacken}}$.

All but the cable stiffness calculations for the test with the small payload and chain slings, have been explained in the preceding discussion. In 2LC the value of k_c derived from the natural frequencies is slightly greater than $k_{c\ slacken}$. There does not seem to be a consistent way to explain these results

Table 7.4 Recalculation of Cable Stiffness and Effective Structure Mass Using Measured Natural Frequencies

Test Set	2BC	2BS	EBC	EBS	2LC	2LS	ELC	ELS
Structure Stiffness k_s (kN/m)	3840	3840	7590	7590	3840	3840	7590	7590
Payload mass, m_p (tonnes)	1.46	1.46	1.46	1.46	0.211	0.211	0.211	0.211
Measured ω_2 (radians/second)	32.1	27.5	31.6	31.6	60.3	38.2	71.8	39.9
Measured ω_3 (radians/second)	134	126	179	183	123	131	-	187
Trolley at	midspan	midspan	east end	east end	midspan	midspan	east end	east end
m_s (tonnes), from computer models	0.499	0.499	0.751	0.751	0.499	0.499	0.751	0.751
m_s (tonnes), from natural frequencies	0.382	0.349	0.331	0.284	0.363	0.247	-	0.229
Sling type	chain	web	chain	web	chain	web	chain	web
$k_{c\ \text{slacken}}$ (kN/m)	3130	1840	3130	1840	1060	589	1060	589
$k_{c\ \text{tighten}}$ (kN/m)	2330	563	2330	563	493	88	493	88
$k_{c\ \text{effective}}$ (kN/m)	2690	934	2690	934	697	183	697	183
k_c (kN/m), from natural frequencies	2660	1590	2840	1820	1100	337	-	352

given the information available. It may be that the data used to determine k_c has not been correctly interpreted, or it may mean that the 3DoF model is not adequate.

It would be expected that the values of m_s for the test sets 2BC, 2BS, 2LC, and 2LS should be the same, since in these tests the loads were applied at the same position, midspan on the bridge. Similarly, m_s for EBC, EBS, ELC, and ELS should be constant, because these tests were all performed with the trolley at the east end of the bridge. However, the recalculated values for m_s given in Table 7.4 do not show this. Between the sets of tests prefixed with "E" and those prefixed with "2", the values of m_s are not distinctly different. In Section 2.2 the mass of the trolley alone was determined to be 0.35 tonnes. The value for m_s must be greater than the trolley mass because more than the mass of the trolley moves when the crane deflects. Yet m_s calculated from the measured natural frequencies is less than the trolley mass for five of the seven test sets in which the calculations were possible. This may be the result of slight errors in the measurement of k_s, m_p, ω_2, and especially of ω_3, which is the most difficult to measure accurately and to which m_s, from equation (7.12), is most sensitive. However, if the measurements are assumed to have been done to a reasonable degree of accuracy, then the discrepancy calls into question the validity of the 3 DoF model.

In retrospect, the testing program should have included a test in which the unloaded crane was given a dynamic load. The resulting dominant natural frequency would have served as the value of ω_s, and m_s would have been determinable from the two measured values, k_s and ω_s.

7.2.6 Assumptions Relating to Structure Motion

In the development of D_{3xj} the assumptions were made that at the instant of payload lift off $y_s = -\frac{m_p g}{k_s}$, $\dot{y}_s = -\frac{H_o}{1+k}$, and $\ddot{y}_s = 0$. Because the payload displacement was recorded on tape rather than by the data logger, the moment of payload lift off cannot be correlated with the crane displacement or the cable tension. The accelerometer signals do not indicate zero acceleration just prior to payload lift off (see Section 6.3.3) .

Approximate values for the velocity of the structure $\dot{y}_s$, are generated by numerical differentiation of the displacement data. Values for the approximate cable stretch rate, $\dot{y}_c$, are generated in a similar fashion, using the cable tension data divided by a constant value for k_c. The velocity values, calculated for all the jerk-starting tests in which reliable structure displacement data was recorded, are plotted versus time in Figures 7.18 to 7.25, shown at the end of this chapter.

Certain features of the velocity curves can be compared with the assumed velocity curves shown in Figure 5.7. Near $t = 0$, the $\dot{y}_c$ curves in Figures 7.18 to 7.25 and the curve for $\dot{y}_c$ shown in Figure 5.7. do not match. The curves generated from the test data start near zero and approach the maximum, whereas in Figure 5.7, $\dot{y}_c$ moves instantly to H_o and then decreases to a plateau. This is because the velocity represented in Figure 5.7 is that of a cable which has a stiffness that varies from zero, at low cable tension, to k_c when cable tension is near m_pg. The rate of elongation generated using the measured data uses a constant value of k_c. Therefore, when the rate of change of cable tension is zero, the rate of elongation is also zero.

Another feature of the curves in Figure 5.7 is the plateau that occurs at the time during which k_c becomes constant just prior to the payload lifting off. A plateau is apparent in Figures 7.18 to 7.25 . The velocities from test sets 2LS, ELS and ELC are too small in magnitude for conclusions about curve shape to be drawn. For the remaining test sets, the only consistent pattern is that there is a trough around the point of maximum downward velocity of the structure and that the curves enter the trough less steeply from the left than leaving it from the right. In most of the cases the presence of a plateau is masked by vibrations that are smaller in amplitude and higher in frequency than the dominant ω_2 vibrations that occur after the payload lifts off. In theory these vibrations before lift off have a frequency of ω_i (see Section 5.6.1), but the frequency of the vibrations was not measured to confirm this. In general, the tests in which web slings were used have troughs of longer duration than do the tests in which chain slings were used.

For the quasi-static model of the structure, downward velocity of the structure just prior to the lift off of the payload is, from equation (5.70), $\frac{H_o}{1+\kappa}$, where H_o is the hoisting speed and κ is the ratio of the stiffnesses of the cable and structure, $\frac{k_s}{k_c}$. For the shop crane, the value of $H_o = 0.1\text{m/sec}$, and k_s is as measured for the two different hoisting locations. Table 7.5 gives the maximum downward velocity of the crane from the graphs in Figures 7. 18 to 7. 25. If it is assumed that this velocity represents $-\frac{H_o}{1+\kappa}$, then κ and k_c can be calculated from this measurement. This new value for k_c, which will be referred to as cable stiffness calculated from structure velocity, is presented in Table 7.5 along with the other values that have been assumed or calculated for k_c. The cable stiffness calculated from structure velocity gives results close to $k_{c_{tighten}}$ for all the test sets. Only with test set EBS is the value of k_c calculated from structure velocity closer to the value of $k_{c_{effective}}$ than $k_{c_{tighten}}$.

It is reasonable that the value of $\dot{y}_s$ just before payload lift off should yield a value of k_c approximately equal to the value of $k_{c_{tighten}}$. The similarity between $k_{c_{tighten}}$ and k_c calculated from structure velocity would seem to validate the use of $k_{c_{tighten}}$ in the equations for the dynamic factor. However, that seems contrary to the reasoning in Section 7.2.4 in which values of k_c are derived from the measured natural frequencies. In Section 7.2.4, the observation is made that, for web slings, the values for k_c derived from frequencies is greater than the value of $k_{c_{tighten}}$. The argument presented in that section is that the measurements of $k_{c_{tighten}}$ were done using a procedure in which the effects of delayed elasticity were significant. Because the dynamic tests involved quick reversals in cable tension rates, delayed elasticity was not a factor, and the $k_{c_{tighten}}$ values are therefore too low and not appropriate in calculations for D. However, the k_c values calculated from the structure velocity are close to the $k_{c_{tighten}}$ values. An examination of the cable tension curves in Figures 7.18 to 7.25 reveals that before lift off there is a length of time during which the cable is steadily being tightened, and that this length of time is long compared to the half period of the dominant vibrations after lift off. If, before lift off, the tightening of the cable is of sufficient duration that delayed elasticity will have significant effect on the value of the cable stiffness, then the two arguments above do not contradict each other.

If there is no contradiction, then the question remains; What value of k_c should be used to calculate the dynamic factor for jerk-starting? During jerk-starting, the cable tightens till the maximum load is reached, shortly after payload liftoff. On that basis, $k_{c_{tighten}}$ should be used, because it gives the correct structure velocity just prior to payload lift off. However, once the payload has lifted off, and the structure reaches its maximum dynamic deflection, using the values of k_c derived from the natural frequencies seems appropriate. The values for k_c derived from the natural frequencies are greater than $k_{c_{tighten}}$. Table 7.6 shows the calculation of the dynamic factor D_{3xj} using $k_{c_{effective}}$, $k_{c_{tighten}}$, and k_c derived from the natural frequencies. It can be seen that in general a reduction in k_c causes a reduction in D_{3xj}. Because the formula for D_{3xj} gives conservative results, lower values of k_c give values of D_{3xj} which are closer to the measured dynamic factors. However, this does not mean that the lowest values of k_c are the most appropriate. The fact that the D_{3xj} formula produces conservative results may be due to conservative assumptions being used in deriving the model rather than in inappropriate values being used in the formula.

The values of the rate of cable elongation in Figures 7.18 to 7.25 are calculated from the following expression

$$\dot{y}_c = \frac{\dot{T}_c}{k_c} \quad . \tag{713}$$

Up to the maximum value of the cable rate, the value of $k_{c_{tighten}}$ is used in equation (7.13). After the maximum, the value of $k_{c_{effective}}$ is used. The sum of the absolute value of $\dot{y}_s$ and $\dot{y}_c$ is also shown in Figures 7.18 to 7.25. In general, the sums are less than but close to the value of H_o, which is 0.1 m/s.

Table 7.5 Recalculation of Cable Stiffness Using Structure Velocity

Test Set		2BC	2BS	EBC	EBS	2LC	2LS	ELC	ELS
Measured structure velocity (mm/s) from test	b or s 1	-38.0	-	-23.9	-9.6	-11.5	-2.5	-4.2	-
	b or s 2	-37.7	-12.0	-22.0	-10.3	-9.3	-	-4.5	-
	b or s 3	-35.1	-13.5	-20.9	-9.7	-10.2	-2.2	-3.7	-1.3
average structure velocity (mm/sec)		-36.9	-12.7	-22.3	-9.9	-10.3	-2.4	-4.1	-1.3
$\kappa = \dfrac{-H_o}{\text{str. velocity}} - 1$		1.71	6.87	3.49	9.14	8.70	41	23	79
Structure Stiffness k_s (kN/m)		3840	3840	7590	7590	3840	3840	7590	7590
Sling type		chain	web	chain	web	chain	web	chain	web
k_c (kN/m), from structure velocity		2248	559	2175	831	442	94	327	96
$k_{c\ slacken}$ (kN/m)		3130	1840	3130	1840	1060	589	1060	589
$k_{c\ tighten}$ (kN/m)		2330	563	2330	563	493	88	493	88
$k_{c\ effective}$ (kN/m)		2690	934	2690	934	697	183	697	183
k_c (kN/m), from natural frequencies		2660	1590	2840	1820	1100	337	-	352

Table 7.6 Comparison of Predicted Dynamic Ratios Using Various Values of Cable Stiffness

Test Set	2BC	2BS	EBC	EBS	2LC	2LS	ELC	ELS
Trolley at	midspan	midspan	east end	east end	midspan	midspan	east end	east end
Payload (tonnes)	1.46	1.46	1.46	1.46	0.211	0.211	0.211	0.211
Sling type	chain	web	chain	web	chain	web	chain	web
measured dynamic ratio, D	1.24	1.12	1.27	1.15	1.43	1.21	1.14	1.21
D_{3xj} using $k_{c\ \mathrm{effective}}$	1.38	1.25	1.43	1.26	1.86	1.34	1.87	1.33
$\frac{D_{3xj}}{D}$	1.11	1.11	1.13	1.10	1.30	1.11	1.64	1.10
$\frac{D_{3xj}-1}{D-1}$	1.59	2.07	1.61	1.73	2.01	1.61	6.19	1.58
D_{3xj} using k_c & m_s from frequencies	1.37	1.30	1.41	1.34	2.01	1.44	-	1.43
$\frac{D_{3xj}}{D}$	1.10	1.16	1.11	1.17	1.41	1.19	-	1.18
$\frac{D_{3xj}-1}{D-1}$	1.54	2.50	1.52	2.26	2.35	2.10	-	1.90
D_{3xj} using $k_{c\ \mathrm{tighten}}$	1.36	1.20	1.41	1.20	1.68	1.22	1.66	1.22
$\frac{D_{3xj}}{D}$	1.10	1.07	1.11	1.04	1.18	1.01	1.45	1.01
$\frac{D_{3xj}-1}{D-1}$	1.52	1.64	1.51	1.34	1.59	1.05	4.70	1.04

Figure 5.7 Assumed Time Histories of Velocities for Jerk-Starting

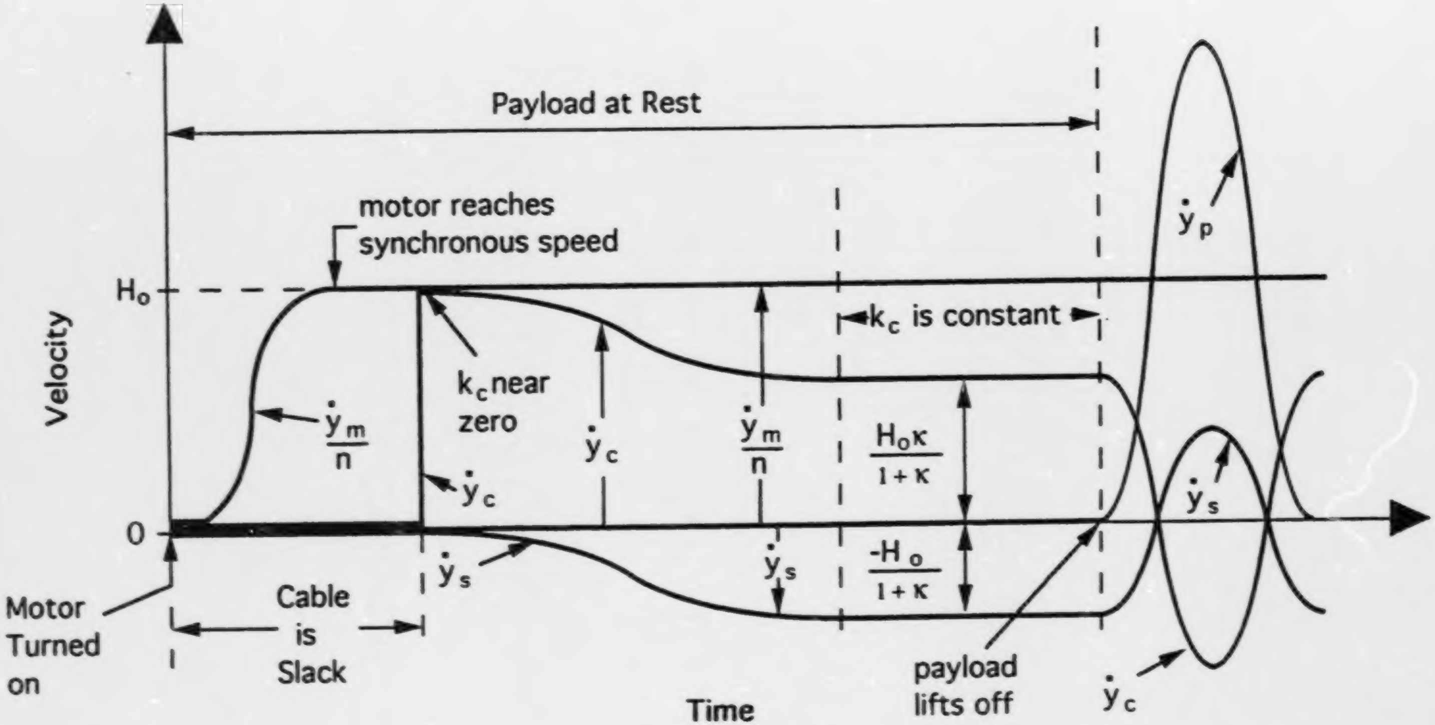

Figure 7.18 2BCb1 - Structure Velocity and Cable Elongation Rate

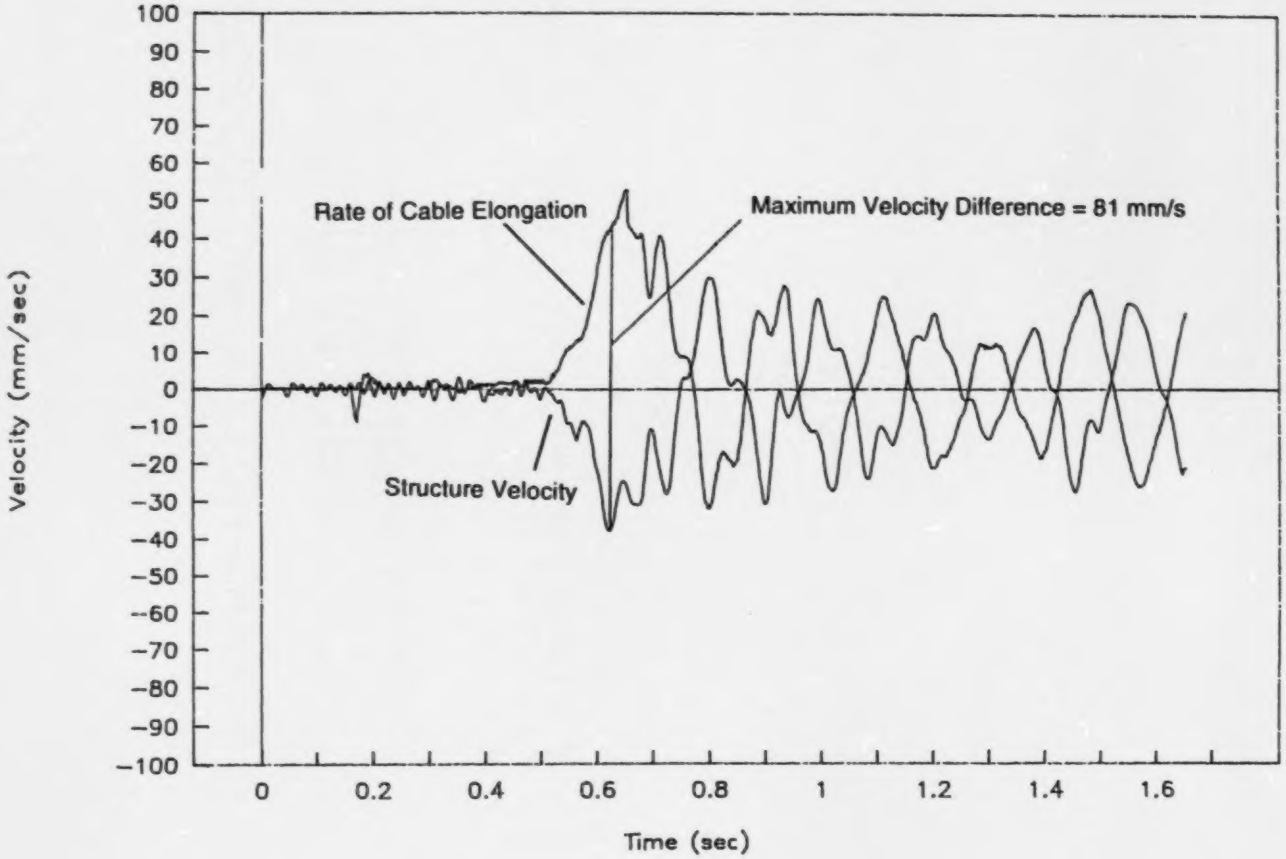

Figure 7.19 2BSb2 - Structure Velocity and Cable Elongation Rate

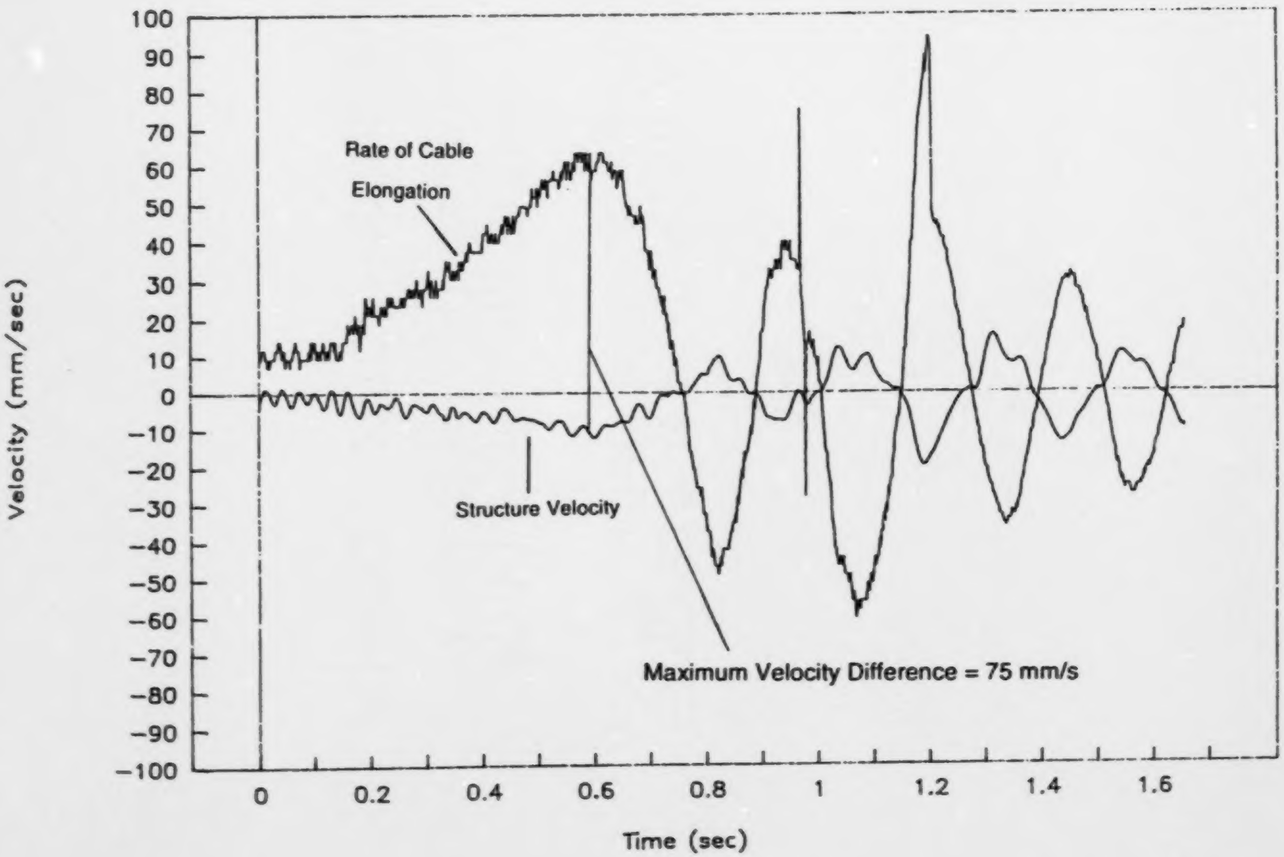

Figure 7.20 EBCb1 - Structure Velocity and Cable Elongation Rate

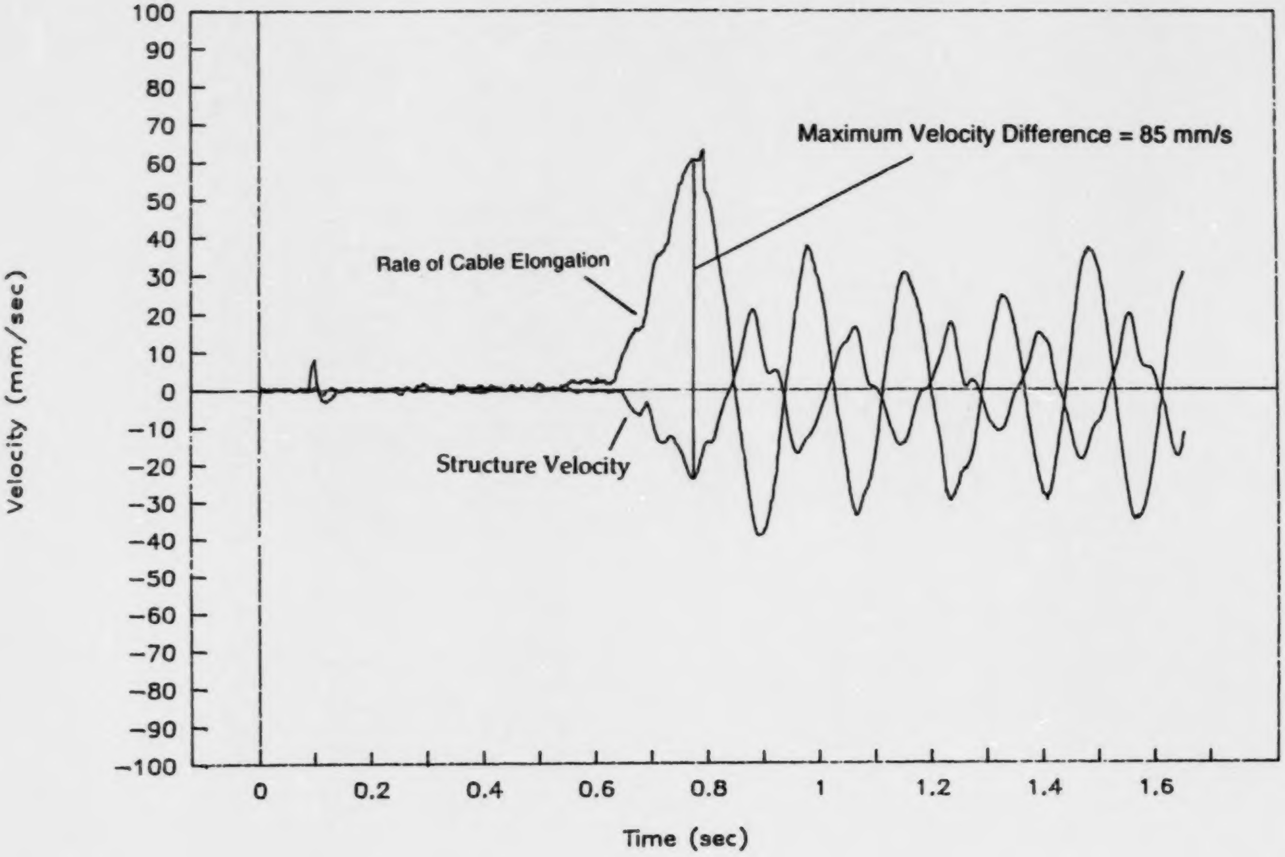

Figure 7.21 EBSb1 - Structure Velocity and Cable Elongation Rate

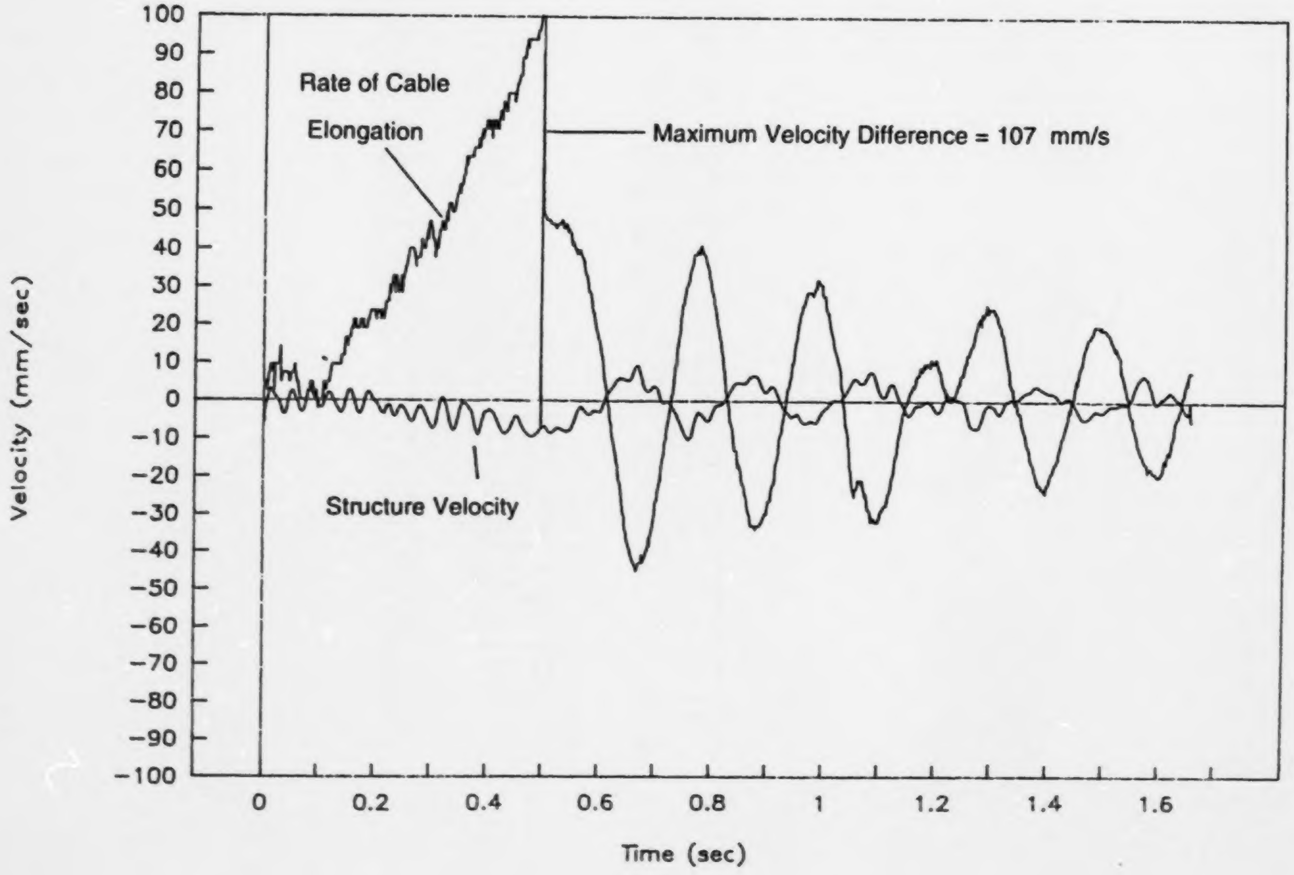

Figure 7.22 2LCs1 - Structure Velocity and Cable Elongation Rate

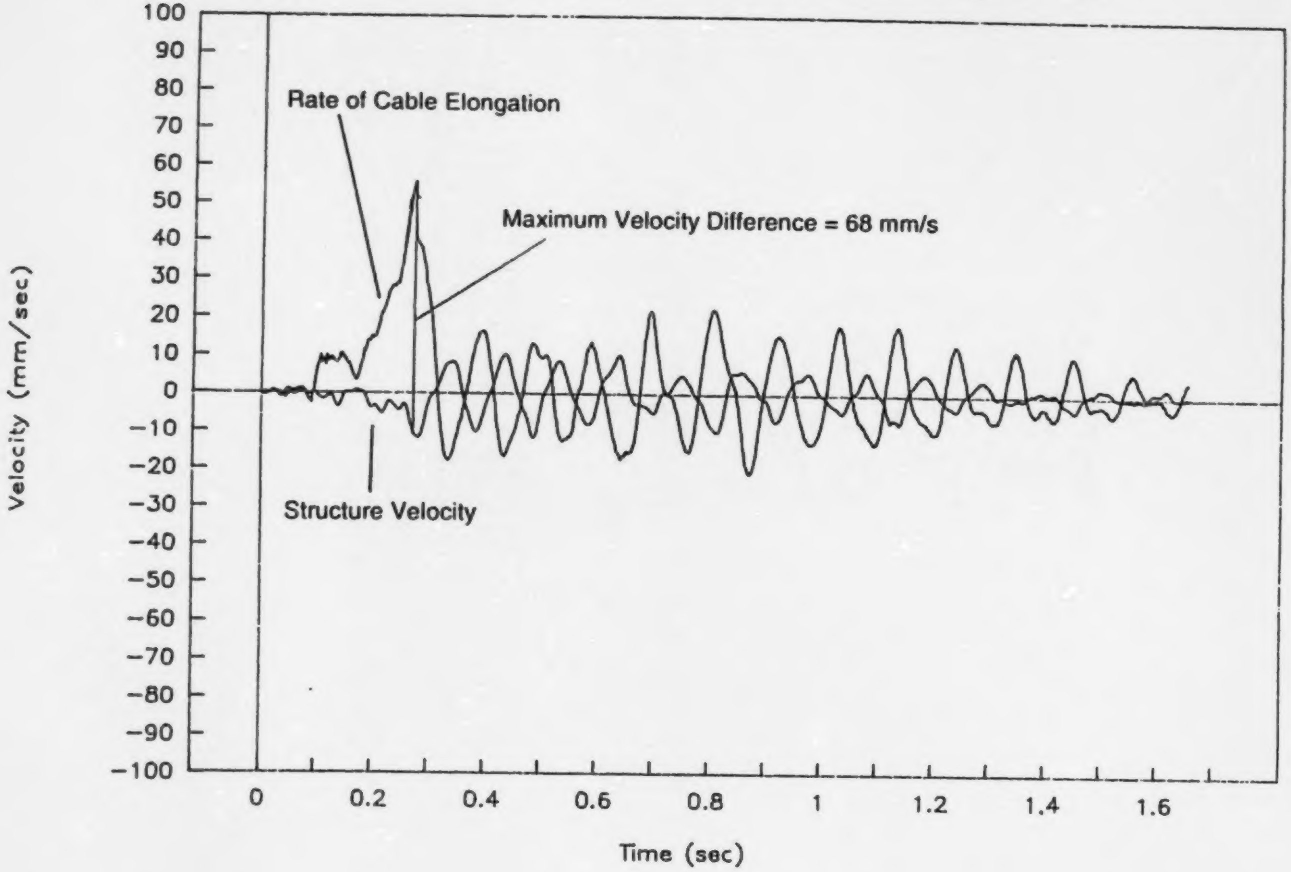

Figure 7.23 2LSs1 - Structure Velocity and Cable Elongation Rate

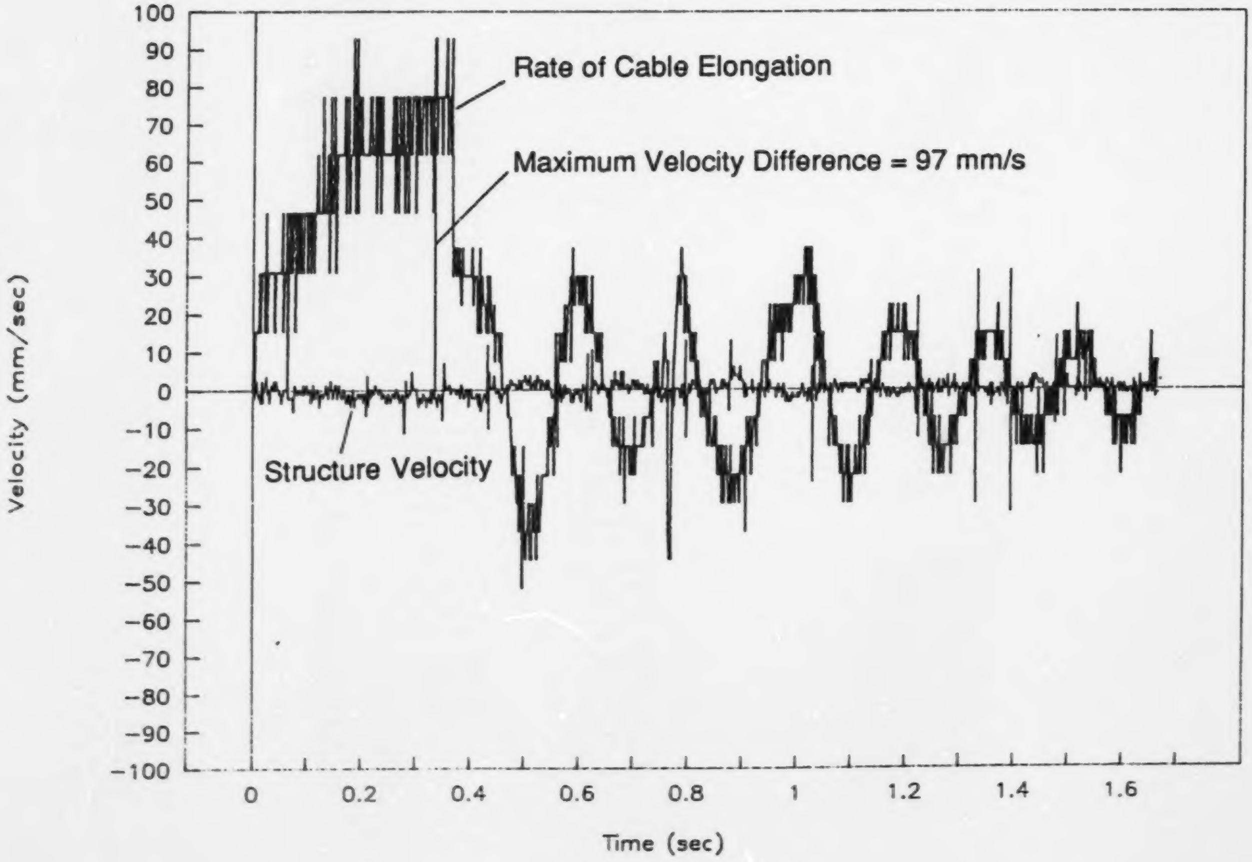

Figure 7.24 ELCs1 - Structure Velocity and Cable Elongation Rate

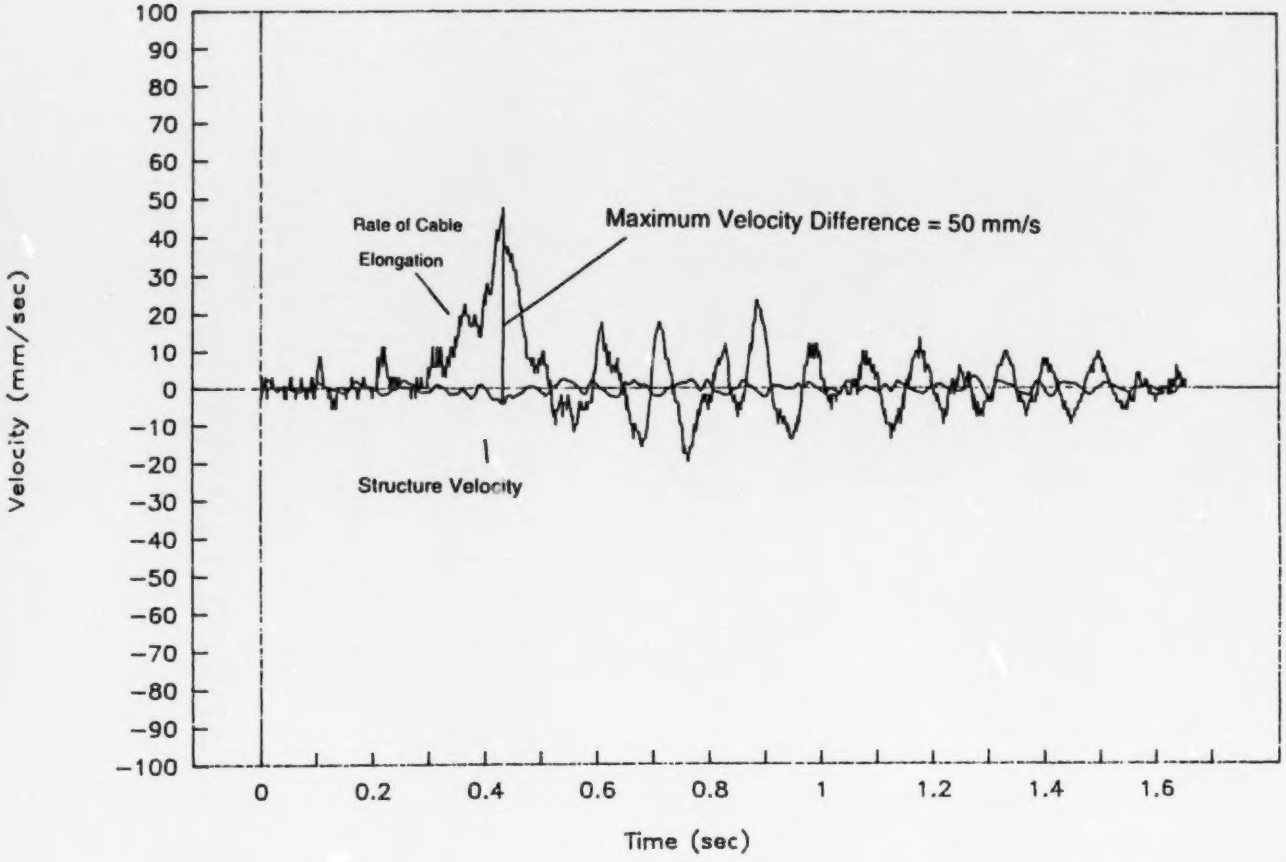

Figure 7.25 ELSs3 - Structure Velocity and Cable Elongation Rate

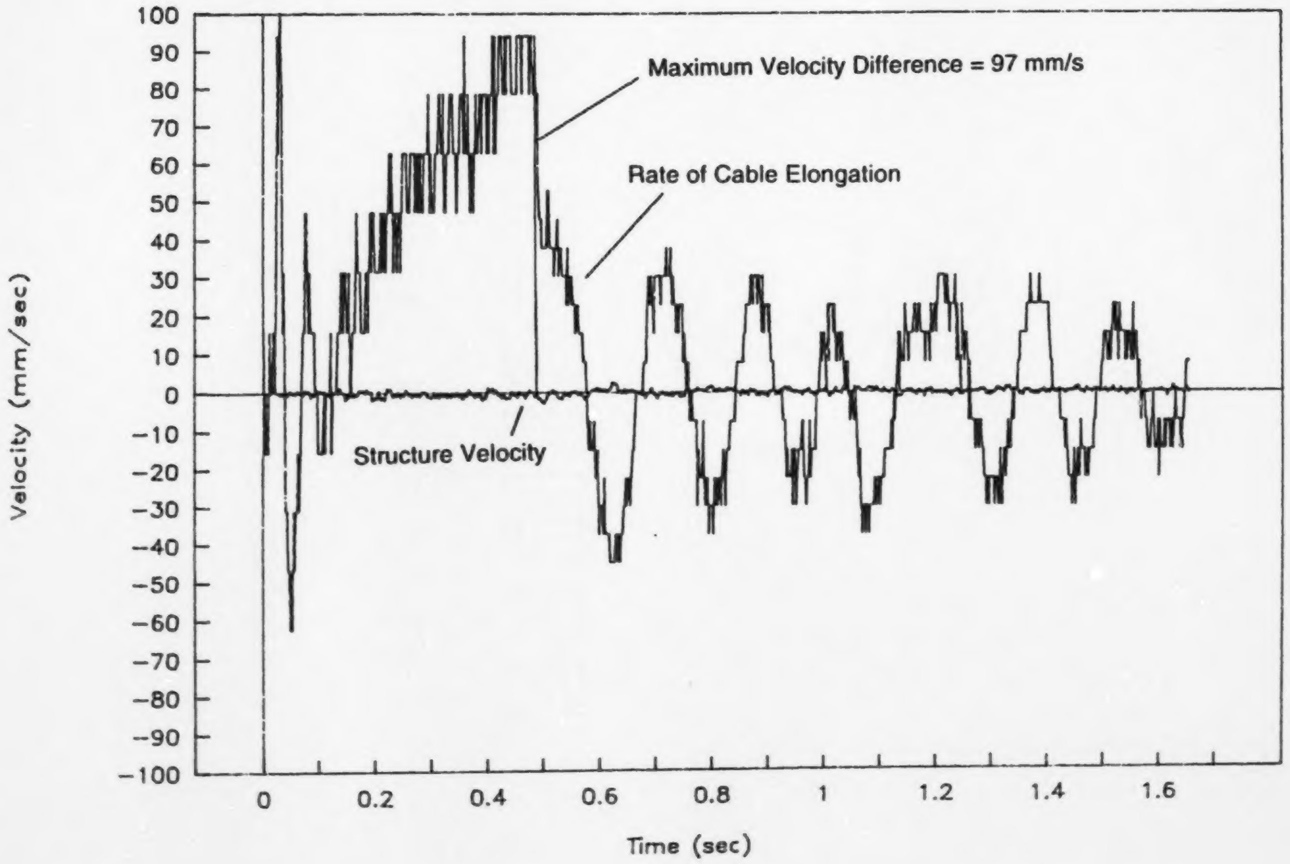

CHAPTER 8

CONCLUSIONS AND RECOMMENDATIONS

8.1 Conclusions

(1.) The test results show that, subject to a variety of hoist-induced loads, the multi-modal nature of the response from the structures lab shop crane was insignificant. The crane can be considered to behave as a single DoF structure. This suggests that other, and perhaps all, bridge cranes can be considered as single DoF structures for the purpose of dynamic analysis.

(2.) The test results show that the dynamic response of the structure was a function of the hoist's location on the crane, the stiffness of the slings, and the mass of the payload.

(3.) The test results show that the dynamic response was a function of the conditions that existed prior to hoisting. Specifically, a small amount of tension in the cable and slings before hoisting caused a greater dynamic response from the crane than did any other initial condition. The dynamic response from jerk-starting the crane was slightly less than the maximum response. The smallest dynamic response occurred when the payload was initially fully suspended by the cable.

(4.) The test results show that the dynamic response of the crane to braking was a function of the amplitude of the vibrations of the crane prior to braking, and of the displacement and velocity of the structure at the moment braking was initiated.

(5.) The 3DoF model, and the formula for D_{3xj} derived from it, predict the dynamic response to jerk-starting more consistently and accurately than any of the standards examined.

(6.) The 3DoF model, and the formula for D_{3xb} derived from it, do not predict the dynamic response to braking as well, because the formula for D_{3xb} does not take into account the displacement and velocity of the structure at the moment braking is initiated.

(7.) A standard based on the 3DoF model would include a formula with the following form.

$$D = 1 + \frac{H_o \omega_c S}{g}$$

where g is the acceleration due to gravity, and D is the dynamic factor to be applied to the forces, moments, and deflections, which occur for the static case in which the payload is suspended by the cable of the crane.

(8.) The three variables which affect D are the hoisting velocity, H_o; the frequency ω_c; and the structure coefficient, S. The frequency ω_c is the square root of the ratio of the net stiffness of cable and slings, k_c, to the mass of the payload, m_p. The structure coefficient S is a function of the ratio of structure stiffness, k_s, to net cable stiffness, k_c, and of the ratio of effective structure mass, m_s, to payload mass, m_p. The structure coefficient S is also a function of the type of hoisting event being considered.

(9.) The factor D is greater than one by an amount proportional to the hoisting speed, and equals unity in the static case.

(10.) The 3DoF model predicts that, under certain conditions, decreasing the stiffness of the crane structure will increase the dynamic factor.

(11.) The 3DoF model predicts that, under certain conditions, decreasing the net stiffness of the cable and slings will increase the dynamic factor.

(12.) None of the standards reviewed present a dynamic factor that explicitly accounts for effects due to the four parameters: structure stiffness k_s, net cable stiffness k_c, effective structure mass m_s, and payload mass m_p. Furthermore, some do not explicitly account for the effects of hoisting speed, H_o.

(13.) Given the good agreement between the 3DoF model and the test results, and the disagreement between the standards, and the relatively poor predictions from them, further study on this topic is justified.

8.2 Recommendations

8.2.1 Recommendations for Further Study

(1.) By using two payloads of different mass, the effect of varying the ratio of effective structure mass to payload mass could be examined. Future testing should be done with cranes that have high ratios of structure mass to payload mass when payloads equal to the rated capacity of the cranes are lifted. These would be cranes with long spans and stiff cross sections. Box girder cranes, when loaded to capacity, probably have the highest structure-to-payload mass ratios. Tests on this type of crane could verify the presence of the structure coefficient maximum with respect to the stiffness ratio of the structure and cable, because the maximum is more pronounced with higher structure masses.

(2.) Much work remains to be done on the dynamic behavior of cables, especially relating to changes in stiffness. The 3DoF model uses the ratio of stiffnesses of the structure to the cable as an important parameter, and any design standard based on the 3DoF model will need to account for the cable stiffness. Further study should be performed to answer the following questions. In calculating the dynamic factor, should cable stiffness be taken as some average of the static loading and unloading stiffnesses, or should it use one or the other? Should the same value of cable stiffness be used for starting and braking? How can a dynamic value for cable stiffness be measured? How can the correct value for cable stiffness be presented in an accessible form to a structural engineer designing a facility that includes a bridge crane?

(3.) Again, relating to the net cable stiffness, none of the standards take into account differences between chain and web slings. In the tests performed there was only one case where using web slings produced higher dynamic ratios than using chain slings, and that was between sets ELC and ELS. It is possible the test results for ELC are not valid, and that had this test been done correctly much higher dynamic ratios would have resulted. If this is the case, then is there any reason to design for web sling usage? In Section 5.9.4 it was shown that the derived dynamic factor for braking can be higher with less stiff slings. This should be confirmed or refuted through some testing program.

(4.) The predictions using the formula for D_{3xb} were not as accurate as were the predictions using the formula for D_{3xj}. This may be due to the way the dynamic braking ratio was determined from the test results, and it may also be due to inappropriate assumptions made in the derivation of D_{3xb}. Further testing and theoretical work should be done on the time history of the braking force produced by bridge crane hoisting motors. Also, further testing and theoretical work should be done on how to combine the effects of braking and the effects of the vibrations that occur before braking. Adding the two together, as was done in this thesis, seems to produce results that are too conservative to be useful.

(5.) It is a common feature to have two hoists on a bridge crane. The hoists can act independently or in unison. Further testing and theoretical work should be done to determine how the 3 DoF system can be modified to include more than one hoist.

(6.) The strength of a material generally increases when the material is loaded dynamically rather than statically. Further testing and theoretical work should be done to determine how this increase in strength can be taken into account in the case of dynamic loading of bridge cranes.

(7.) The effective structure mass values of 0.525 tonnes and 0.768 tonnes, when the payload was at midspan and at the east end of the bridge respectively, were derived by dividing the stiffness of the structure by the square of the first natural frequency of the structure. The first natural frequency was determined by building a finite element model of the structure, and then finding the eigenvalues of the system. This process is rather long. A standard formula could be developed for the single stiffness and single mass of a simple multi-DoF system loaded at a distance x from one side, as shown in Figure 8.1. Static condensation or the first frequency approach could be used. In many cases the stiffness and mass on the left and right side of the crane would be the same, and that would simplify such a formula further.

Figure 8.1
Proposed Multi-DoF System With Which to Derive Effective Structure Mass

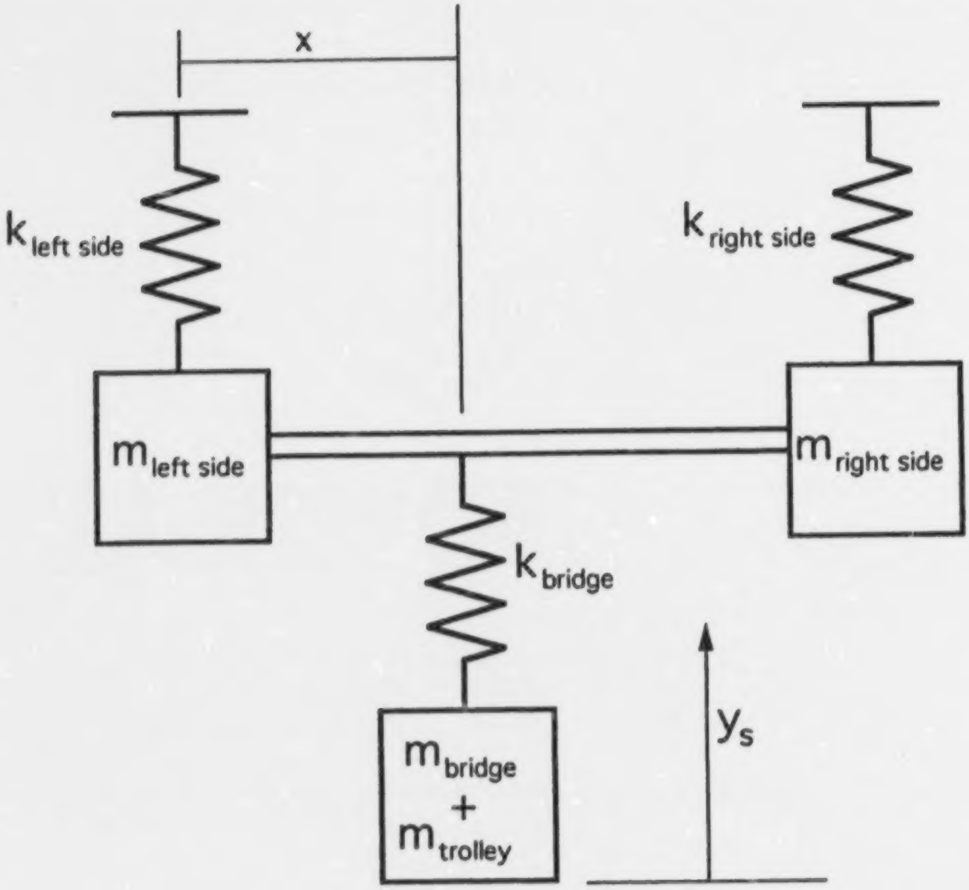
x
$k_{\text{left side}}$
$k_{\text{right side}}$
$m_{\text{left side}}$
$m_{\text{right side}}$
k_{bridge}
y_s
$m_{\text{bridge}} + m_{\text{trolley}}$

(8.) In the German standard DIN 15.018 and in CMAA #74, upper limits are specified for the dynamic factor, beyond which, increases in hoisting speed will have no effect on the structure. The 3DoF model derived in Chapter 5 does not predict such a limit, but in the testing program the test set, ELC, produced results much lower than predicted by the 3DoF model. In the discussion of ELC in Section 7.1.1.1, and throughout Chapter 7, the implication has been that the discrepancy between the test results and the prediction from the 3DoF model was due to some mistake in preparing the payload and slings before hoisting, and that greater care on the part of the experimenter would have avoided the problem. It is, however, possible that the test results indicate a consistent phenomenon which the authors of DIN 15.018 and CMAA #74 recognized. It may be that, under circumstances that would be expected to produce the highest dynamic factors, a mechanism that significantly reduces the dynamic factor becomes so likely to occur that it becomes practically unavoidable. Teetering may be such a mechanism. Further testing and theoretical work should be done to establish the upper limit of the dynamic factor.

8.2.2 Recommendations Relating to Procedures for Numerical Dynamic Analysis

The following recommendations relate to the design of the computer programs used to perform dynamic analysis for this thesis.

(1.) The computer program CRIS5.BAS uses a continuous function to relate cable tension and cable elongation. This requires an iteration within each time step to give values for the cable tension, motor force, and cable elongation, that are consistent with each other at the end of the time step. As mentioned in Section 4.4.4, using discrete changes in cable stiffness at prescribed tensions would be a better approach. It would be faster than using a continuous nonlinear stiffness tension function and an extra level of iteration, and it would lend itself easily to the introduction of hysteresis. Another approach that should be investigated is to include damping in the model for the cable. Hysteresis and delayed elasticity could be accounted for using a spring and damper in parallel, as shown in Figures 2.13 and 2.14. To

Figure 8.2 Alternate Model for Cable

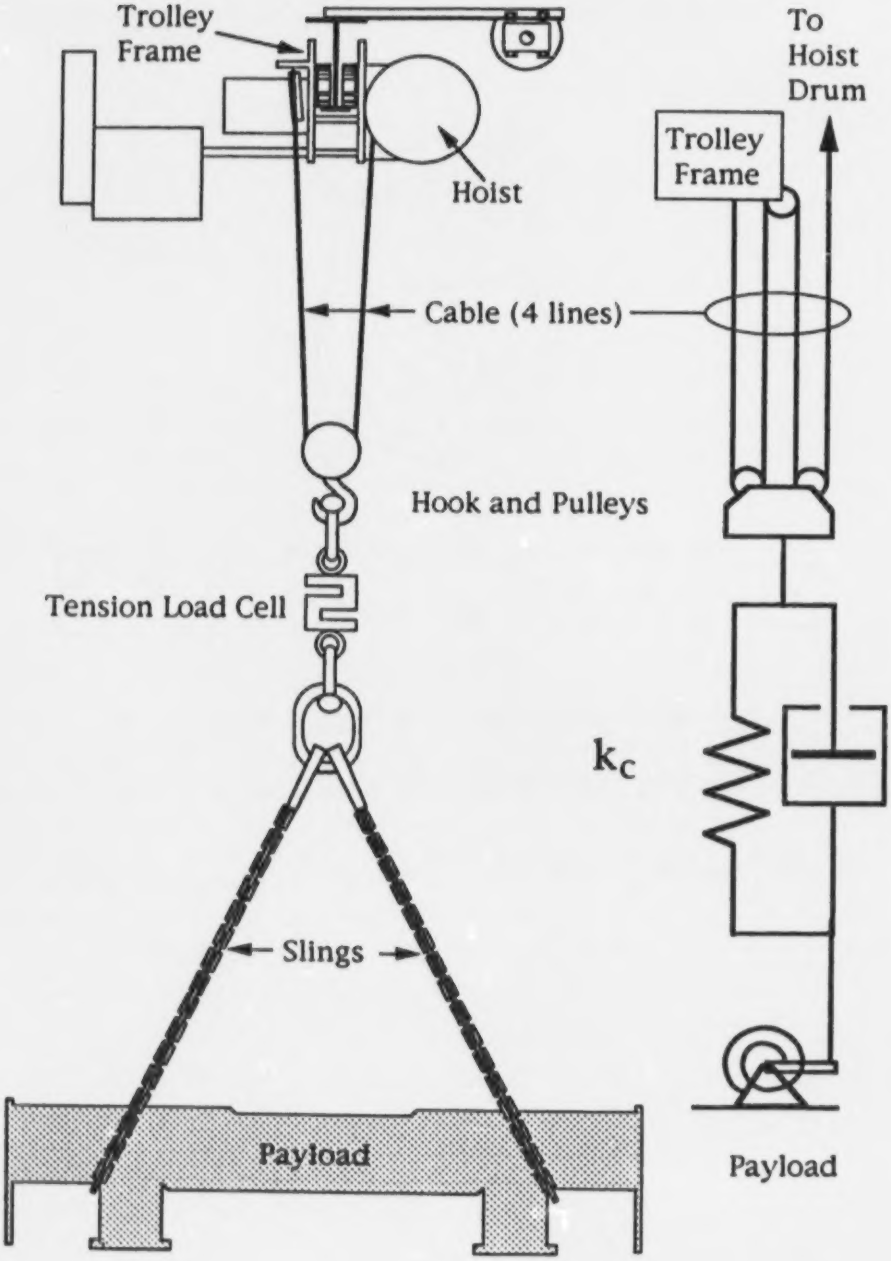
Trolley Frame
Hoist
To Hoist Drum
Trolley Frame
Cable (4 lines)
Hook and Pulleys
Tension Load Cell
k_c
Slings
Payload
Payload

account for the variation of cable stiffness with cable tension, a radial spring attached to a lever could be used in series with the delayed elasticity mechanism. The model for the cable would be as shown in Figure 8.2.

(2.) The program MAKEKAM.BAS is used for entering beam element data and assembling the global stiffness and mass matrices. It has the limitation that when a hinge is specified at one node of an element, the rotational DoF of that end of the element is independent of the rotations of the other elements which share that node. The connection between two continuous members which are joined within their lengths, and which have a common vertical displacement, but independent rotations, cannot be modelled. The program MAKEKAM.BAS would be improved if it allowed extra D'soF between pairs of elements at a node, rather than just between individual elements.

8.2.3 Recommendations Relating to Test Procedure

The following recommendations relate to the test procedure.

(1.) The cable stiffness and the structure mass are two important parameters that were not precisely determined in the present testing program. Two fairly simple procedures could and should have been performed to get these two values.

The first procedure is to record the motion of the crane when it is vibrating without a payload. This could be done by attaching the hook to some quick-release mechanism fixed to the ground at a point directly below the hoist. The motor would be turned on briefly to put the cable in tension and load the structure. Then the hook could be released and the ensuing vibrations recorded. The measured stiffness of the structure, k_s , can be divided by the square of the dominant frequency of these vibrations to give a working value for the effective mass of the structure, m_s.

To obtain a value for cable stiffness, a stiff support could be placed such that it braces the unloaded bridge beam. The support should not interfere with the lifting of the payload. When the payload is lifted, the support prevents the beam from deflecting measurably. The case of an infinitely high structural stiffness is approximated. The square of the vibration frequency of a crane with the payload on the cable, multiplied by the known payload mass, gives the value for cable stiffness. Also, with this test set-up, the damping of the cable, which is the major component of the damping of the complete crane system, could be determined.

(2.) The assembly used for holding the LVDT's must be very rigid and self supporting; therefore, in general, such an assembly will be heavy. For ease in setting up the tests, it would have been worthwhile to equip the assembly with locking wheels so that it could be manually moved into position then locked into place.

It would also have helped to have some kind of fine vertical adjustment for the LVDT's on the assembly, and a fixed spirit level with which to check that the LVDT's were vertical.

At the beginning of the testing program, the use of lasers for measuring displacements was considered. This idea was abandoned because it was felt that the LVDT's would serve the purpose adequately, were readily available, and would not require a holding assembly that was not too large to build. However, for taller cranes which might require a holding assembly too large and awkward to be practical, deflection measurements using a laser could be considered.

(3.) The custom-built load cells on the wheel assemblies of the shop crane worked very well. Because they were set up permanently, the crane could move along the craneway without interfering with them. Time was saved because the crane did not have to be jacked up and a load cell inserted beneath each wheel for each test. It was fortunate that the shop crane had the Y plate which supported the end trucks on the wheel assemblies. Most end trucks are hollow sections with the wheel inside, and the axle mounted spanning the two webs. The strains on this kind of endtruck are generally very small. Even so, it is worth trying to measure a strain signal that corresponds to the reaction force acting on the wheel.

(4.) All the data should have been collected on one recording medium, either the tape recorder, or the data logger. Then all the different parameters could be compared temporally. This would have helped with understanding the teetering that may have occurred with test set ELC. It would have helped with calculating y_c and $\dot{y}_c$, because the payload displacement data could then be on the same graph as the rest of the displacement data.

(5.) Both the accelerometer signals and the north east wheel reaction load signal should have been filtered, and the cable tension signal need not have been. Having at least one unfiltered signal is useful because the times at which the motor is switched on and off is then recorded.

(6.) It would be worthwhile to actually measure $\dot{y}_m$, perhaps with a tachometer attached to the drum. This would help with the measurement of $\dot{y}_c$, it would confirm the constant speed assumption, and it would help with understanding what happens during braking.

REFERENCES

1. American Institute of Steel Construction, Specifications for the Design, Fabrication and Erection of Structural Steel Buildings. 1973.

2. Agarwal, A.C., On the Applicability of Fatigue Laboratory Tests on Moving Loads. CANCAM 89. Twelfth Canadian Congress of Applied Mechanics, pg. 234.

3. Barrett, D.A., and Hrudey, T.M., An Investigation of Hoist Induced Dynamic Loads on Bridge Crane and Craneway Structures. CANCAM 89. Twelfth Canadian Congress of Applied Mechanics, pg. 240.

4. Banford, Experimental Measurements: Precision, Error and Truth. Second Edition. Imperial College, London. John Wiley and Sons, March 1986.

5. Canadian Standards Association, General Purpose Electric Overhead Travelling Cranes. CSA Standard B167, 1964.

6. Canadian Standards Association, Steel Structures for Buildings — Limit States Design. CAN 3-S16.1-M89 , 1989.

7. Canadian Standards Association, Steel Structures for Buildings. CSA Standard S16.1, 1974.

8. Chein and Ritchie, Design and Construction of Composite Floors. Canadian Institute of Steel Construction, 1984.

9. Clough, R. and Penzien, J., Dynamics of Structures. McGraw-Hill, 1975.

10. Construction Safety Association of Ontario, Rigging Manual. June 1982.

11. Crane Manufacturers Association of America, Specification for top running and under running single girder electric overhead travelling cranes. Specification #74-1987.

12. Garlicki, A.M. and McCormack J.E., Dynamic Loads in Chains (An Exploratory Study). NRC Canada Division of Mechanical Engineering Vehicle Dynamics Laboratory. Controlled technical report. May 1989.

13. Gaylord, Edwin H.Jr., and Gaylord, Charles V., Design of Steel Structures. 2nd ed. McGraw-Hill, 1972.

14. Goldman, Carl, Design of Crane Runway Girders for Top Running and Under Running Cranes and Monorails. Proceedings of 1988 Annual Conference, CSCE, pg. 425.

15. Gutkowski, Richard M., Structures — Fundamental Theory and Behaviour. Van Nostrand Reinhold Co. Inc., 1981.

16. Hornbeck, Numerical Methods. Quantum Publishers Inc., 1975.

17. Japanese Standards Association, Electric Overhead Travelling Cranes. JISB8821, 1976.

18. Kovács, Pál, Transient Phenomena in Electrical Machines. Elsevier, 1984.

19. MacGinley, T.J., Steel Structures — Practical Design Studies. E & FN Spon, London, 1981.

20. Matthews and Montgomery and Murray, Designing Floor Systems for Dynamic Response. Structural Engineering Report No. 106, Dept. of Civil Eng. University of Alberta, Edmonton, Alberta, Oct. 1982.

21. Paz, Mario, Structural Dynamics — Theory and Computation. Van Nostrand Reinhold Co. Inc., 1980.

22. Pearson, Carl E., Numerical Methods in Engineering and Science. Van Norstrand Reinhold Co. Inc., 1986.

23. Podolny, Walter, Construction and Design of Cable Stayed Bridges. Copyright 1976 by John Wiley & Sons, Inc.

24. Robb, Ian, Steel Frame Design Examples. Macmillan, 1972.

25. Serridge and Licht, Piezoelectric Accelerometers and Vibration Preamplifiers. Theory and Application Handbook. Bruel and Kjaer Publication, Naerum, Denmark, Oct. 1986.

26. Shedd, T.C., Structural Design in Steel. John Wiley and Sons Inc., 1934.

27. Troitsky, M.S., Cable-Stayed Bridges — Theory and Design. Second Edition. BSP professional Books, London, 1988.

28. Validyne Engineering Corporation, Instruction Manual 10/20 channel Module Case Model MCI 10/20, 19414 Londelius St. Northridge, Calif. 91324, Oct. 1975.

29. Validyne Engineering Corporation, Instruction Manual Model CD19 Carrier Demodulator. A unit of the MCI Module Case System. 19414 Londelius St. Northridge, Calif. 91324, Oct. 1975.

30. Vaughan, Application of B & K Equipment to Strain Measurement. Bruel and Kjaer Publication. Naeruim, Denmark, Oct. 1975.

31. Weaver, Wm. M, Overhead Crane Handbook. Whiting Crane Corp., Harvey, Illinoise, 1985.

32. Canadian Portland Cement Association, Concrete Design Handbook. Part 1 CSA Standard CAN3 - A23.3 - M84 "Design of Concrete Structures for Buildings, with Explanatory Notes." Canadian Portland Cement Association,. 1985.

33. Canadian Commission on Building and Fire Codes, National Building Code of Canada 1990, second revisions and errata 1992. National Research Council of Canada, Ottawa, 1992.

34 Deutsche Norm, DIN 4132 Craneways, Steel Structures, Principles for Calculation, Design and Construction. Beuth Verlag GmbH. Berlin 30, Feb. 1981.

35 Deutsche Norm, DIN 15.018 Part 1 Cranes, Steel Structures, Verification and Analysis. Beuth Verlag GmbH. Berlin 30, Nov. 1984.

36. British Standard, BS 2573 Part1. 1983.

37. Reuland Electric Company, Voltage Transients; the Unseen Assasin. Technotes Issue No. 2. Nov 1973.

38. Levi, Enrico, Polyphase Motors; A Direct Approach to their Design. Wiley Interscience Library. John Wiley and Sons Inc. 1984.

39. Ontario Highway Engineering Division, Ontario Highway Bridge Design Code 1983. 2nd edition. Ontario Highway Engineering Division, Downsview, 1983.

APPENDIX A

CALIBRATIONS

Appendix A.1 Calibration Curves for Wheel Assembly Load Cells

Figure A.1
Calibration Curve for
N.W. Wheel Load

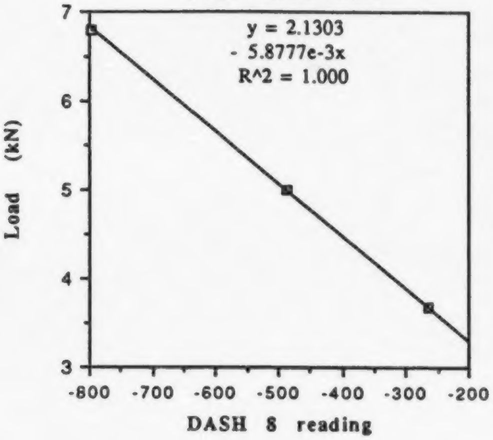

Figure A.2
Calibration Curve for
N.E. Wheel Load Cell

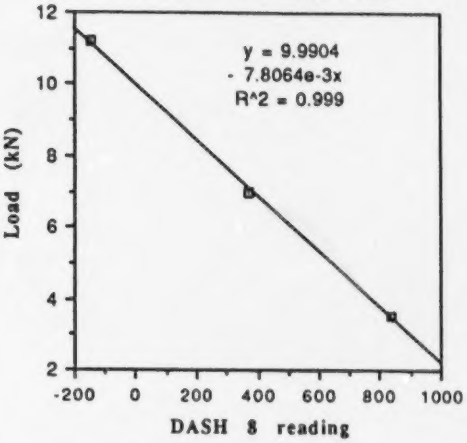

Figure A.3
Calibration Curve for
S.W. Wheel Load cell

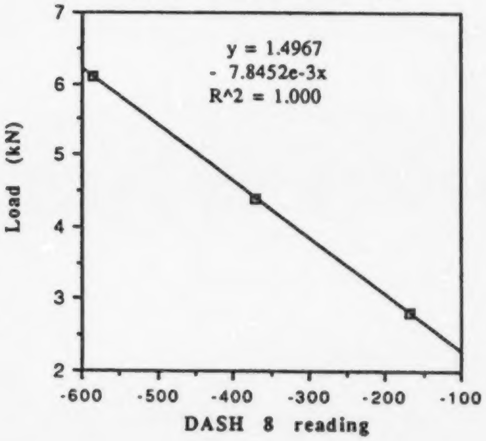

Figure A.4
Calibration Curve for
S.E. Wheel Load Cell

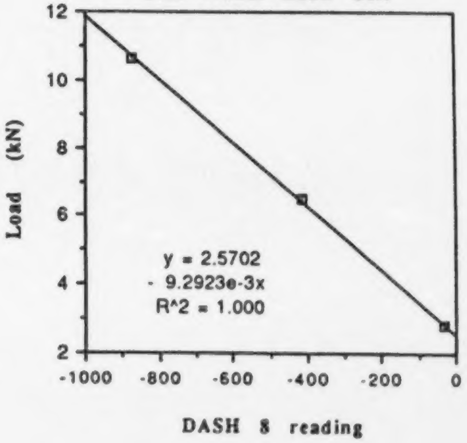

Appendix A.2 Calibration Curves for LVDT's

Figure A.5
Calibration Curve for LVDT 24T 1010 at SE Wheel

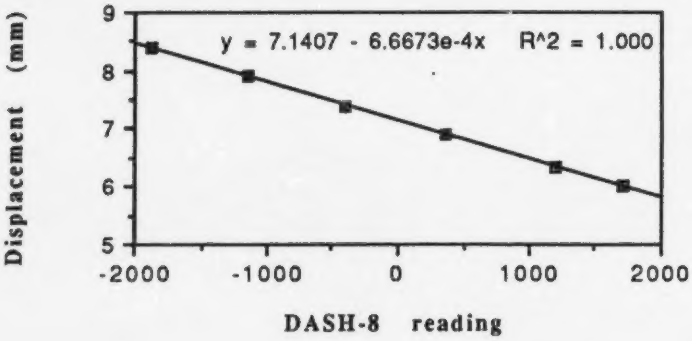

Figure A.6
Calibration Curve for LVDT 24T 2501 at Trolley

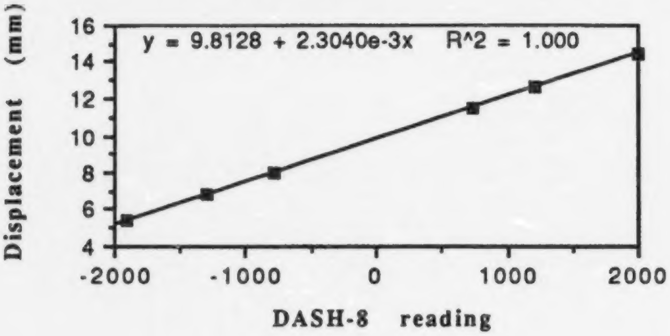

Figure A.7
Calibration Curve for LVDT 6T 3005 at Payload

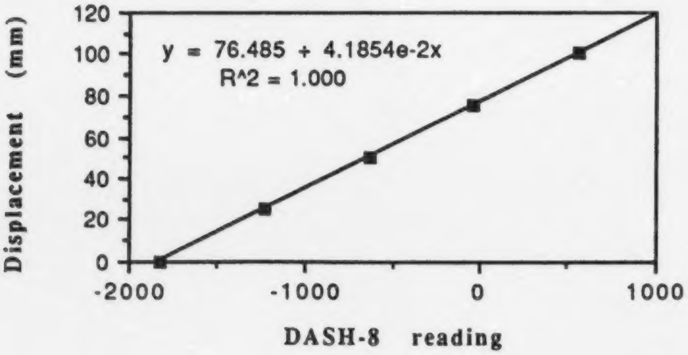

APPENDIX A.3

MEASURED STATIC DISPLACEMENT OF CRANE STRUCTURE

The following are measurements from dial gauges attached to the crane structure. The gauges read positive downwards in units of.01 mm. The craneway dial gauge was positioned directly under the SE end truck wheel. The bridge dial gauge was positioned directly under the trolley.

Table A.1 Dial Gauge Readings from Jerk-Starting Tests in which 2.11 kN Payload was Used

Test Name	Craneway Dial Gauge			Bridge Dial Gauge		
	Unloaded	Loaded	Displ.	Unloaded	Loaded	Displ.
ELC s1	910	920	10	2201	2228	27
ELC s2	910	920	10	2203	2228	25
ELC s3	910	920	10	2202	2228	26
	ELC average -0.10 (mm, + up)			ELC average -0.26 (mm, + up)		
ELS s1	908	917	9	2080	2104	24
ELS s2	908	917	9	2080	2104	24
ELS s3	908	917	9	2079	2104	25
	ELS average -0.09 (mm, + up)			ELS average -0.24 (mm, + up)		
2LC s1	3641	3648	7	956	1013	51
2LC s2	3641	3648	7	962	1014	52
2LC s3	3641	3648	7	962	1016	54
	2LC average -0.07 (mm, + up)			2LC average -0.54 (mm, + up)		
2LS s1	3640	3646	6	966	1015	49
2LS s2	3640	3647	7	964	1016	52
2LS s3	3640	3647	7	964	1016	52
	2LS average -0.07 (mm, + up)			2LS average -0.51 (mm, + up)		

Table A.2 Dial Gauge Readings from Jerk-Starting Tests in which 14.35 kN Payload was Used

Test Name	Craneway Dial Gauge			Bridge Dial Gauge		
	Unloaded	Loaded	Displ.	Unloaded	Loaded	Displ.
EBC b1	912	986	74	1595	1786	191
EBC b2	912	986	74	1595	1785	190
EBC b3	913	986	73	1595	1785	190
	EBC average -0.74 (mm, + up)			EBC average -1.90 (mm, + up)		
EBS b1	917	986	69	1599	1787	188
EBS b2	917	989	72	1601	1788	187
EBS b3	917	989	72	1598	1788	190
	EBS average -0.71 (mm, + up)			EBS average -1.88 (mm, + up)		
2BC b1	3643	3690	47	1462	1837	375
2BC b2	3644	3690	46	1460	1834	376
2BC b3	3645	3691	46	1460	1833	377
	2BC average -0.46 (mm, + up)			2BC average -3.76 (mm, + up)		
2BS b1	3645	3690	45	1465	1839	374
2BS b2	3644	3690	46	1460	1837	373
2BS b3	3645	3690	45	1464	1834	370
	2BS average -0.45 (mm, + up)			2BS average -3.72 (mm, + up)		

From ELC and ELS,

structure stiffness at craneway dial gauge $= \dfrac{2.11\text{kN}}{2 \times 0.10\text{mm}} = 11{,}000$ kN/m

From ELC and ELS,

structure stiffness at trolley, corresponding to k_s, $= \dfrac{2.11\text{kN}}{0.25\text{mm}} = 8{,}400$ kN/m

From 2LC and 2LS,

structure stiffness at craneway dial gauge $= \dfrac{2.11\text{kN}}{4 \times 0.07\text{mm}} = 7{,}500$ kN/m

From 2LC and 2LS,

structure stiffness at trolley, corresponding to k_s, $= \dfrac{14.35\text{kN}}{0.52\text{mm}} = 4{,}100$ kN/m

From EBC and EBS,

structure stiffness at craneway dial gauge $= \dfrac{14.35\text{kN}}{2 \times 0.73\text{mm}} = 10{,}000$ kN/m

From EBC and EBS,

structure stiffness at trolley, corresponding to k_s, $= \dfrac{14.35\text{kN}}{1.89\text{mm}} = 7{,}590$ kN/m

From 2BC and 2BS,

structure stiffness at craneway dial gauge $= \dfrac{14.35\text{kN}}{4 \times 0.46\text{mm}} = 7{,}800$ kN/m

From 2BC and 2BS,

structure stiffness at trolley, corresponding to k_s, $= \dfrac{14.35\text{kN}}{1.89\text{mm}} = 3{,}840$ kN/m

APPENDIX B

The following pages contain the stiffness and mass matrices for the structural models "E" and "2" described in Chapter 4. The file containing the matrices for model "E" is called "ESTR4", and the file containing the the matrices for "2" is called "2STR".

The matrices are sparse. Most of the terms within each of the matrices are zero. Only the non-zero terms for each matrix are listed, along with their location within the matrix. As the matrices are symmetrical, only half the non-diagonal terms are displayed. The other half can be generated by switching the row and column numbers.

```
The stiffness matrix for the file :estr4
K( 1 , 1 ) =  65505.58
K( 1 , 2 ) =  24359.32
K( 1 , 3 ) = -35561.05
K( 1 , 4 ) =  24359.32
K( 1 , 10 ) = -29944.53
K( 1 , 12 ) = -16095.19
K( 2 , 2 ) =  22248.18
K( 2 , 3 ) = -24359.32
K( 2 , 4 ) =  11124.09
K( 3 , 3 ) =  71122.1
K( 3 , 5 ) = -35561.05
K( 3 , 6 ) =  24359.32
K( 4 , 4 ) =  44496.35
K( 4 , 5 ) = -24359.32
K( 4 , 6 ) =  11124.09
K( 5 , 5 ) =  71122.1
K( 5 , 7 ) = -35561.05
K( 5 , 8 ) =  24359.32
K( 6 , 6 ) =  44496.35
K( 6 , 7 ) = -24359.32
K( 6 , 8 ) =  11124.09
K( 7 , 7 ) =  71122.1
K( 7 , 9 ) =  24359.32
K( 8 , 8 ) =  44496.35
K( 8 , 9 ) =  11124.09
K( 9 , 9 ) =  22248.18
K( 10 , 10 ) =  154250
K( 10 , 11 ) =  6711.987
K( 10 , 12 ) =  16095.19
K( 10 , 13 ) = -53211.32
K( 10 , 14 ) = -31501.1
K( 10 , 17 ) = -71094.11
K( 11 , 11 ) =  52250.91
K( 11 , 13 ) =  31501.1
K( 11 , 14 ) =  12432.43
K( 11 , 17 ) = -38213.08
K( 12 , 12 ) =  11534.88
K( 13 , 13 ) =  106422.6
K( 13 , 16 ) = -31501.1
K( 14 , 14 ) =  49729.73
K( 14 , 16 ) =  12432.43
K( 15 , 15 ) =  297297.3
K( 15 , 18 ) = -376643.5
K( 15 , 19 ) =  148648.7
K( 16 , 16 ) =  24864.87
K( 17 , 17 ) =  921132.4
K( 17 , 20 ) = -850038.2
K( 17 , 21 ) = -456895.6
K( 18 , 18 ) =  1272444
K( 18 , 20 ) = -636222.2
K( 18 , 21 ) =  376643.5
K( 19 , 19 ) =  594594.6
K( 19 , 20 ) = -376643.5
K( 19 , 21 ) =  148648.7
K( 20 , 20 ) =  1486261
K( 20 , 21 ) =  80252.06
K( 21 , 21 ) =  624739.1
```

```
K( 21 , 21 ) =  117057.4
K( 21 , 23 ) =  33566.21
K( 22 , 22 ) =  51333.92
K( 22 , 23 ) =  12833.46
K( 23 , 23 ) =  25666.96
```

```
The mass matrix for the file :estr4
M( 1 , 1 ) =  2.788092E-02
M( 1 , 2 ) =  2.624978E-03
M( 1 , 3 ) =  4.703014E-03
M( 1 , 4 ) = -1.551124E-03
M( 1 , 10 ) =  4.948072E-03
M( 1 , 12 ) =  1.280543E-03
M( 2 , 2 ) =  6.538583E-04
M( 2 , 3 ) =  1.551124E-03
M( 2 , 4 ) = -4.903937E-04
M( 3 , 3 ) =  2.717297E-02
M( 3 , 5 ) =  4.703014E-03
M( 3 , 6 ) = -1.551124E-03
M( 4 , 4 ) =  1.307717E-03
M( 4 , 5 ) =  1.551124E-03
M( 4 , 6 ) = -4.903937E-04
M( 5 , 5 ) =  2.717297E-02
M( 5 , 7 ) =  4.703014E-03
M( 5 , 8 ) = -1.551124E-03
M( 6 , 6 ) =  1.307717E-03
M( 6 , 7 ) =  1.551124E-03
M( 6 , 8 ) = -4.903937E-04
M( 7 . 7 ) =  2.717297E-02
M( 7 , 9 ) = -1.551124E-03
M( 8 . 8 ) =  1.307717E-03
M( 8 , 9 ) = -4.903937E-04
M( 9 , 9 ) =  6.538583E-04
M( 10 , 10 ) =  4.550736E-02
M( 10 , 11 ) = -4.797986E-04
M( 10 , 12 ) =  2.167073E-03
M( 10 , 13 ) =  5.662903E-03
M( 10 , 14 ) =  1.614137E-03
M( 10 . 17 ) =  5.141572E-03
M( 11 , 11 ) =  1.028171E-03
M( 11 , 13 ) = -1.614137E-03
M( 11 , 14 ) = -4.41032E-04
M( 11 , 17 ) =  1.33062E-03
M( 12 , 12 ) =  4.235642E-04
M( 13 , 13 ) =  3.271899E-02
M( 13 , 16 ) =  1.614137E-03
M( 14 , 14 ) =  1.176085E-03
M( 14 , 16 ) = -4.41032E-04
M( 15 , 15 ) =  2.766329E-03
M( 15 , 18 ) =  7.593387E-03
M( 15 , 19 ) = -2.074747E-03
M( 16 , 16 ) =  5.880426E-04
M( 17 , 17 ) =  8.472842E-02
M( 17 , 20 ) =  .0241875
M( 17 , 21 ) =  6.259636E-03
M( 18 , 18 ) =  .15392
M( 18 , 20 ) =  .02664
M( 18 , 21 ) = -7.593387E-03
M( 19 , 19 ) =  5.532659E-03
M( 19 , 20 ) =  7.593387E-03
M( 19 , 21 ) = -2.074747E-03
M( 20 , 20 ) =  .146835
M( 20 . 21 ) = -2.257117E-03
M( 21 , 21 ) =  4.836825E-03
```

```
M( 21 , 21 ) =  3.169653E-02
M( 21 , 23 ) = -1.51483E-03
M( 22 , 22 ) =  1.069237E-03
M( 22 , 23 ) = -4.009638E-04
M( 23 , 23 ) =  5.346184E-04
```

```
The stiffness matrix for the file :2str
K( 1 , 1 ) =  239512.2
K( 1 , 2 ) = -239512.2
K( 1 , 3 ) =  109457.1
K( 2 , 2 ) =  479024.5
K( 2 , 4 ) = -239512.2
K( 2 , 5 ) =  109457.1
K( 3 , 3 ) =  133391.7
K( 3 , 4 ) = -109457.1
K( 3 , 5 ) =  33347.92
K( 4 , 4 ) =  479024.5
K( 4 , 6 ) = -239512.2
K( 4 . 8 ) =  109457.1
K( 5 , 5 ) =  133391.7
K( 5 , 6 ) = -109457.1
K( 5 , 8 ) =  33347.92
K( 6 , 6 ) =  299401.3
K( 6 , 8 ) = -109457.1
K( 6 , 10 ) = -16095.19
K( 6 , 13 ) = -29944.53
K( 6 , 15 ) =  16095.19
K( 7 , 7 ) =  23069.77
K( 7 , 10 ) =  5767.442
K( 7 , 13 ) = -16095.19
K( 7 , 15 ) =  5767.442
K( 8 , 8 ) =  66695.85
K( 9 . 9 ) =  27386.05
K( 9 , 11 ) = -38213.08
K( 9 , 12 ) =  13693.02
K( 10 , 10 ) =  11534.88
K( 11 , 11 ) =  142188.2
K( 11 , 13 ) = -71094.11
K( 11 , 14 ) =  38213.08
K( 12 , 12 ) =  54772.09
K( 12 , 13 ) = -38213.08
K( 12 , 14 ) =  13693.02
K( 13 . 13 ) =  141990.3
K( 13 , 14 ) = -11758.31
K( 13 , 15 ) = -16095.19
K( 13 , 16 ) = -40951.66
K( 13 , 17 ) =  26454.77
K( 14 , 14 ) =  50172.42
K( 14 , 16 ) = -26454.77
K( 14 , 17 ) =  11393.19
K( 15 , 15 ) =  11534.88
K( 16 , 16 ) =  151272.2
K( 16 , 17 ) =  7111.436
K( 16 , 18 ) = -89133.75
K( 16 , 19 ) = -58528.7
K( 16 , 20 ) =  33566.21
K( 17 , 17 ) =  48453.34
K( 17 , 19 ) = -33566.21
K( 17 , 20 ) =  12833.48
K( 18 , 18 ) =  204532.2
K( 19 , 19 ) =  117057.4
K( 19 , 21 ) = -58528.7
K( 19 , 22 ) =  33566.21
K( 20 , 20 ) =  51333.92
K( 20 , 21 ) = -33566.21
K( 20 , 22 ) =  12833.48
```

```
The mass matrix for the file :2str
M( 1 , 1 ) =  1.812854E-02
M( 1 , 2 ) =  6.275263E-03
M( 1 , 3 ) = -1.38079E-03
M( 2 , 2 ) =  3.625707E-02
M( 2 , 4 ) =  6.275263E-03
M( 2 , 5 ) = -1.38079E-03
M( 3 , 3 ) =  7.766413E-04
M( 3 , 4 ) =  1.38079E-03
M( 3 , 5 ) = -2.912405E-04
M( 4 , 4 ) =  3.625707E-02
M( 4 , 6 ) =  6.275263E-03
M( 4 , 8 ) = -1.38079E-03
M( 5 , 5 ) =  7.766413E-04
M( 5 , 6 ) =  1.38079E-03
M( 5 , 8 ) = -2.912405E-04
M( 6 , 6 ) =  .0467174
M( 6 , 8 ) = -2.336722E-03
M( 6 , 10 ) =  1.280543E-03
M( 6 , 13 ) =  4.948072E-03
M( 6 , 15 ) = -1.280543E-03
M( 7 , 7 ) =  8.471283E-04
M( 7 , 10 ) = -3.176731E-04
M( 7 . 13 ) =  1.280543E-03
M( 7 , 15 ) = -3.176731E-04
M( 8 , 8 ) =  3.883207E-04
M( 9 , 9 ) =  4.401281E-04
M( 9 , 11 ) =  1.33062E-03
M( 9 , 12 ) = -3.300961E-04
M( 10 , 10 ) =  4.235642E-04
M( 11 , 11 ) =  2.970686E-02
M( 11 , 13 ) =  5.141572E-03
M( 11 , 14 ) = -1.33062E-03
M( 12 , 12 ) =  8.802562E-04
M( 12 , 13 ) =  1.33062E-03
M( 12 , 14 ) = -3.300961E-04
M( 13 , 13 ) =  4.699961E-02
M( 13 , 14 ) =  1.000862E-03
M( 13 , 15 ) = -2.167073E-03
M( 13 , 16 ) =  6.179452E-03
M( 13 , 17 ) = -1.922039E-03
M( 14 , 14 ) =  1.204212E-03
M( 14 , 16 ) =  1.922039E-03
M( 14 , 17 ) = -5.730632E-04
M( 15 , 15 ) =  4.235642E-04
M( 16 , 16 ) =  .48116
M( 16 , 17 ) = -6.891226E-04
M( 16 , 18 ) = -.2172017
M( 16 , 19 ) =  5.485937E-03
M( 16 , 20 ) = -1.51483E-03
M( 17 , 17 ) =  1.298703E-03
M( 17 , 19 ) =  1.51483E-03
M( 17 , 20 ) = -4.009638E-04
M( 18 , 18 ) =  .1359288
M( 19 , 19 ) =  3.169653E-02
M( 19 , 21 ) =  5.465937E-03
M( 19 , 22 ) = -1.51483E-03
M( 20 , 20 ) =  1.069237E-03
M( 20 , 21 ) =  1.51483E-03
M( 20 , 22 ) = -4.009638E-04
```

APPENDIX C

COMPUTER PROGRAM LISTINGS

Appendix C contains the listing of the various computer programs written for this thesis. The programs are written in Basic

Appendix C.1 Listing for MAKEKAM.BAS

The program MAKEKAM.BAS assembles the global stiffness and mass matrices for a structure composed of beam elements, and enters each assembled matrix into a file with the suffix ".1" and ".2" , respectively. It also creates a file with the suffix ".P" which contains the locations of the degrees of freedom of the individual elements within the global structure matrix.

```
10 ' MAKEKAM.BAS - make [K] and [M]
20 '
30 ' This programme makes a stiffness matrix [K] and a mass matrix [M] for
40 'a structure made of beams and columns. Assumptions made to construct this
50 'model are :
60 '     All members exhibit only elastic behavior
70 '     All members have only flexural response
80 '     All members exhibit only in plane behavior
90 '     All columns are braced against lateral motion at their ends
100 '     Each member is prismatic, having its own material and x-sectional
110 '       properties constant throughout its length
120 '
130 'Each member starts and ends at a numbered node.
140 'Free degrees of freedom are kept in the upper left corner of the matrices,
150 'and fixed degrees of freedom are stored in the remainder. Another
160 'matrix [P] keeps track of which nodal D'soF are in which positions.
170 '[P] has dimensions (nn,4), where the 4 columns contain:
180 '    #1  the δ DoF associated with that node
190 '    #2  the θ DoF associated with that node
200 '    #3  an extra δ DoF for if there is a slide at that node
210 '    #4  an extra θ DoF for if there is a hinge at that node
220 'The structures assembled [K] and [M] matrices are stored
230 ' in filename.1 and filename.2 respectively.
240 'Each members properties and the global positions of its 4 DsoF
250 'are stored serially in filename.L  (for Local)
260 'From this data another program can recreate each 4x4 member
270 'stiffness matrix and calculate the member forces.
280 '
290 '     Variables list
300 '
310 '     N            NODE
320 '     M            MEMBER
330 '     NN           number of nodes
340 '     NM           number of members
350 '     NFR          number of free D'soF
360 '     NDOF         total number of D'soF
370 '     NFIL         node for impact load
380 '     K(NDOF,NDOF) stiffness matrix
390 '     W(NDOF,NDOF) mass matrix  ( m is used as integer for member )
400 '     P(NN,4)   stores nodal DoF positions in [K] and [M]
410 '     NODE1(M)     first node of member M
420 '     NODE2(M)     last node of member M
430 '     IEND(m)    end condition flag at first node of member M
440 '     IIEND(m)   end condition flag at last node of member M
450 '     L,E,DM,X(M) length,Young's modulus, distributed mass, and Ixx
460 '                  respectively for member M
470 '     CST          Coefficient for element stiffness matrix
480 '     CMS          Coefficient for element mass matrix
485 '     ISM(m)       symetry factor for CET and CMS
490 '     SMALLK       local stiffness entry
500 '     SMALLM       local mass entry
510 '
520 '****************** Initialize and Set Up Screen ************************
530 '
540 INPUT "Shall we do this in colour?(y,n)",A$
550 SCREEN 0,1
560 KEY OFF
570 Z$="##.#^^^^^"
580 DEFINT F,I,J,M,N,P,Q
590 IF A$="y" OR A$="Y" THEN ICLR=1
```

```
600 BAR$=STRING$(80,CHR$(220))
610 LIN$=STRING$(80,CHR$(219))
620 CLR$=STRING$(60," ")
630 SUP$=" HSRPF"
640 NUM$="0123456789"
650 Q(1)=20:Q(2)=1:Q(3)=15:Q(4)=3:Q(5)=3:Q(6)=5
660 ARO$=CHR$(17)+CHR$(196)+CHR$(196)+CHR$(217)
670 IF ICLR =1 THEN COLOR 2,6,2
680 CLS
690 LOCATE 25,1 :PRINT LIN$
700 LOCATE 4,1 : PRINT BAR$;
710 IF ICLR =1 THEN COLOR 15
720 IF FINISH=1 GOTO 890
730 LOCATE 1,1,1
740 INPUT;" Output Filename : ",SFN$
750 OPEN SFN$+".1" FOR OUTPUT AS #1
760 OPEN SFN$+".2" FOR OUTPUT AS #2
770 OPEN SFN$+".1" FOR OUTPUT AS #3
771 IF FLAG=1 GOTO 800
780 LOCATE 1,45 : INPUT " Number of nodes : ",NN
790 DIM P(NN,4),PLACE(4)
800 INPUT;"     Node for Impact Load : ",NFIL
810 PRINT
811 IF FLAG=1 GOTO 830
820 INPUT " Number of Members : ",NM
830 PRINT #3, MKI$(NM);SPACE$(14);
835 IF FLAG=1 THEN SWAP P(NFIL,1),P(NFILO,1):GOTO 2950
840 DIM NODE1(NM),NODE2(NM),NE(NM),L(NM),E(NM),DM(NM),X(NM),
      IEND(NM),IIEND(NM),NWH(2*NM),NWS(2*NM),ISM(NM)
850 '
860 '**************** Input Loop for each Member ************************
870 '
880 FOR M=1 TO NM
890 LOCATE 6,1,1
900 PRINT " MEMBER NUMBER ";M
910 IF FINISH =1 THEN NMDOF=NMDOF-NE(M)+1
920 PRINT
930 INPUT " Devided Member? (1 or 2)" ;ISM(M)
932 IF ISM(M)=0 THEN ISM(M)=ISM(M-1):LOCATE 8,27:PRINT ISM(M)
935 PRINT
940 PRINT " Beam or Column ?";
950  A$=INKEY$ : IF A$="" GOTO 950
960 KEY(15) ON
970 IF A$=CHR$(13) GOTO 1010
980 TP=INSTR("BbCc",A$)
990 IF TP=0 THEN KEY(15) OFF : GOTO 950
1000 TP=(TP+1)\2-1
1010 LOCATE ,2,1
1020 IF TP=0 THEN PRINT "Beam                "
1030 IF TP=1 THEN PRINT "Column              "
1040 PRINT
1050 KEY(15) OFF
1060 INPUT;" Member Length  ",L(M)
1070 IF L(M)=0 THEN L(M)=L(M-1) : PRINT L(M);
1080 PRINT :PRINT
1090 INPUT;" E  ",E(M)
1100 IF E(M)=0 THEN E(M)=E(M-1)  :  PRINT E(M);
1110 PRINT : PRINT " _"
1120 INPUT;" m  ",DM(M)
1130 IF DM(M)=0 THEN DM(M)=DM(M-1)  :  PRINT DM(M);
```

```
1140 PRINT :PRINT
1150 INPUT;" Ixx  ",X(M)
1160 IF X(M)=0 THEN X(M)=X(M-1)  :  PRINT X(M);
1170 PRINT:PRINT
1180 PRINT"                         Ends            Supports"
1190 PRINT"                     hinge  slide   roller  pin  fixed"
1200 PRINT" from node "
1210 PRINT" to node   "
1220 LOCATE 22,12,1
1230 INPUT;"",NODE2(M)
1240 IF NODE2(M)<=0 GOTO 1230
1250 IF TP<>0 GOTO 1320
1260 LOCATE ,24,1
1270 A$=INKEY$ : IF A$="" GOTO 1270
1280 IF A$<>CHR$(13) THEN IIEND(M)=1:PRINT "*";:GOTO 1500
1290 LOCATE ,31,1
1300 A$=INKEY$ : IF A$="" GOTO 1300
1310 IF A$<>CHR$(13) THEN IIEND(M)=2:PRINT "*";:GOTO 1500
1320 LOCATE ,40,1
1330 A$=INKEY$ : IF A$="" GOTO 1330
1340 IF A$<>CHR$(13) THEN IIEND(M)=3:PRINT "*";:GOTO 1440
1350 LOCATE ,46,1
1360 A$=INKEY$ : IF A$="" GOTO 1360
1370 IF A$<>CHR$(13) THEN IIEND(M)=4:PRINT "*";:GOTO 1440
1380 LOCATE ,52,1
1390 A$=INKEY$ : IF A$="" GOTO 1390
1400 IF A$<>CHR$(13) THEN IIEND(M)=5:PRINT "*";:GOTO 1440
1410 '
1420 '****************** Column special case **********************
1430 '
1440 IF TP=0 GOTO 1500
1450 IF IIEND(M)=0 THEN IIEND(M)=4
1460 IF IIEND(M)=3 THEN IIEND(M)=5
1470 '
1480 '****************** Switch front to back *********************
1490 '
1500 IF NODE1(M)>0 GOTO 1580
1510 NODE1(M)=NODE2(M) : NODE2(M)=0
1520 IEND(M)=IIEND(M) : IIEND(M)=0
1530 LOCATE 23,12,1
1540 GOTO 1230
1550 '
1560 '***************** Option to Change Member Data *********************
1570 '
1580 LOCATE 25,1,0
1590 IF ICLR =1 THEN COLOR ,2
1600 PRINT " Data for Member ";M;"  If OK press ";ARO$;
1610 A$=INKEY$ : IF A$="" GOTO 1610
1620 LOCATE 25,1 : PRINT CLR$;
1630 IF ICLR =1 THEN COLOR ,6
1640 LOCATE 23,12 : PRINT CLR$
1650 LOCATE 22,12 : PRINT CLR$
1660 FOR I=1 TO 6
1670 LOCATE I*2+6,Q(I) : PRINT CLR$
1680 NEXT
1690 IF A$=CHR$(32) THEN NODE1(M)=0 : IIEND(M)=0 : GOTO 890
1700 IF FINISH=1 GOTO 1740
1710 NEXT
1720 FINISH=1
1730 '
```

```
1740 '***************** Input Data Summary ************************
1750 '
1760 CLS
1770 LOCATE 25,1,0
1780 IF ICLR =1 THEN COLOR 2
1790 PRINT LIN$
1800 IF ICLR =1 THEN COLOR 15,6
1810 LOCATE 1,1 : PRINT "INPUT DATA SUMMARY ";SFN$
1820 LOCATE 2,58 :PRINT "_":LOCATE 2,14 :PRINT "nodes"
1830 LOCATE 3,1 : PRINT "member    from      to       length        E
  m            Ixx"
1840 IS=0 : IH=0
1850 FOR M=1 TO NM
1860 IF INT(M\5)*5=M THEN PRINT
1870 PRINT USING " ###";M;
1880 PRINT USING SPACE$(4)+" ### "+MID$(SUP$,IEND(M)+1,1);NODE1(M);
1890 PRINT USING SPACE$(3)+" ### "+MID$(SUP$,IIEND(M)+1,1);NODE2(M);
1900 PRINT USING SPACE$(5)+"###.###";L(M);
1910 PRINT USING SPACE$(5)+"##.#^^^^";E(M);
1920 PRINT USING SPACE$(5)+"##.###^^^^" ;DM(M);
1930 PRINT USING SPACE$(5)+"##.###^^^^";X(M)
1940 '
1950 '*************** Check Hinges and Slides *************
1960 '
1970 IF IEND(M)=1 THEN IH=IH+1 : NWH(IH)=NODE1(M)
1980 IF IIEND(M)=1 THEN IH=IH+1 : NWH(IH)=NODE2(M)
1990 IF IEND(M)=2 THEN IS=IS+1 : NWS(IS)=NODE1(M)
2000 IF IIEND(M)=2 THEN IS=IS+1 : NWS(IS)=NODE2(M)
2010 NEXT
2020 '
2030 FOR I=1 TO IH-1
2040 FOR J=I+1 TO IH
2050 IF NWH(I)<>NWH(J) GOTO 2080
2060 PRINT :PRINT "Node";NWH(I);"has Hinge specd twice!"
2070 GOTO 2260
2080 NEXT
2090 NEXT
2100 '
2110 FOR I=1 TO IS-1
2120 FOR J=I+1 TO IS
2130 IF NWS(I)<>NWS(J) GOTO 2160
2140 PRINT :PRINT "Node";NWS(I);"has Slide specd twice!"
2150 GOTO 2260
2160 NEXT
2170 NEXT
2180 '
2190 '*************** Option to Change Data ****************************
2200 '
2210 LOCATE 25,1,0
2220 IF ICLR =1 THEN COLOR ,2
2230 PRINT " Data Summary  If OK press ";ARO$;
2240 A$=INKEY$ : IF A$="" GOTO 2240
2250 IF A$=CHR$(13) GOTO 2411
2260 LOCATE 25,1,0
2270 IF ICLR =1 THEN COLOR 15,2,2
2280 PRINT CLR$;
2290 LOCATE 25,1,0
2300 PRINT  " Member Number to change  ";
2310 I=27 : MN$=""
2320 A$=INPUT$(1)
```

```
2330 IF INSTR(NUM$,A$)=0 GOTO 2370
2340 MN$=MN$+A$
2350 LOCATE 25,I : PRINT A$; : I=I+1
2360 GOTO 2320
2370 IF A$<>CHR$(13) GOTO 2320
2380 M=VAL(MN$)
2390 NODE1(M)=0 : IIEND(M)=0
2400 ERASE NWH, NWS
2405 DIM NWH(2*NM),NWS(2*NM)
2410 GOTO 670
2411 LOCATE 25,1,0
2412 PRINT"PrtSc or any key to continue      ";
2413 A$=INKEY$ : IF A$="" GOTO 2413
2420 '
2430 '************** End of Input Loop * Begin Calcs ***************
2440 '
2450 NFR=0
2460 FOR M=1 TO NM
2470 N=NODE1(M)
2480 ON IEND(M) GOSUB 2530,2540,2550,2560,2570
2490 N=NODE2(M)
2500 ON IIEND(M) GOSUB 2530,2540,2550,2560,2570
2510 NEXT
2520 GOTO 2610
2530 P(N,4)=1   :  NFR=NFR+1  :  RETURN
2540 P(N,3)=1   :  NFR=NFR+1  :  RETURN
2550 P(N,2)=-1  :  NFR=NFR-1  :  RETURN
2560 P(N,1)=-1  :  NFR=NFR-1  :  RETURN
2570 P(N,1)=-1  :  P(N,2)=-1  :  NFR=NFR-2  :  RETURN
2580 '
2590 '******************** Assign DoF positions for [K] and [M] ***********
2600 '
2610 I=1 : J=1
2620 NFR=2*NN+NFR
2630 FOR N=1 TO NN
2640 FOR H=1 TO 2
2650 IF P(N,H)=-1 THEN P(N,H)=NFR+I : I=I+1 : ELSE P(N,H)=J : J=J+1
2660 IF P(N,H+2)= 1 THEN P(N,H+2)=J     : J=J+1
2670 NEXT
2680 NEXT
2690 NDOF=NFR+I-1
2700 '
2710 '**************** Put DoF for Impact at start *********************
2720 '
2730 IF P(NFIL,1)<>0 OR P(NFIL,3)<>0 GOTO 2790
2740 LOCATE 25,1
2750 IF ICLR =1 THEN COLOR 15,4,4
2760 PRINT "No available DoF for Impact Load. If OK press ";ARO$;
2770 A$=INPUT$(1)
2780 IF A$<>CHR$(13) THEN ERASE P : GOTO 2260
2790 IF P(NFIL,3)<>0 AND P(NFIL,1)=0 THEN IDOF=3 : GOTO 2880
2800 IF P(NFIL,3)=0 AND P(NFIL,1)<>0 THEN IDOF=1 : GOTO 2880
2810 LOCATE 25,1
2820 IF ICLR =1 THEN COLOR 15,4,4
2830 PRINT "Put Impact on Node ";NFIL;" or Slide at Node ";NFIL;"? (N/S)"
2840 A$=INPUT$(1)
2850 IF INSTR("nN",A$)>0 THEN IDOF=1 : GOTO 2880
2860 IF INSTR("sS",A$)>0 THEN IDOF=3 : GOTO 2880
2870 GOTO 2840
2880 I=1
```

```
2890 IF P(I,1)=1 THEN J=1 : GOTO 2920
2900 IF P(I,2)=1 THEN J=2 : GOTO 2920
2910 I=I+1 : IF I<=NN GOTO 2890
2920 P(I,J)=P(NFIL,IDOF)
2930 P(NFIL,IDOF)=1
2940 '
2950 '***************** DIMension [K] and [M] and sizing ******************
2960 '
2970 DIM K(NDOF,NDOF)
2980 DIM W(NDOF,NDOF)
2990 '
3000 '******************* Calc Local stiffnesses and masses *****************
3010 '
3020 FOR M=1 TO NM
3030 L=L(M)
3040 CST=2*E(M)*X(M)/(L*L*L)/ISM(M)
3050 PRINT #3, MKS$(CST*ISM(M));MKS$(L);
3060 CMS=DM(M)*L/420/ISM(M)
3070 GOTO 3190
3080 SMALLK=6        :SMALLM=156      :RETURN
3090 SMALLK=3*L      :SMALLM=22*L     :RETURN
3100 SMALLK=-6       :SMALLM=54       :RETURN
3110 SMALLK=3*L      :SMALLM=-13*L    :RETURN
3120 SMALLK=2*L*L    :SMALLM=4*L*L    :RETURN
3130 SMALLK=-3*L     :SMALLM=13*L     :RETURN
3140 SMALLK=L*L      :SMALLM=-3*L*L   :RETURN
3150 SMALLK=-3*L     :SMALLM=-22*L    :RETURN
3160 '
3170 '************* Locate local in global [K] and [M] ************
3180 '
3190 J=0:N=NODE1(M):IND=IEND(M)
3200 PLACE(1+J)=P(N,1)
3210 PLACE(2+J)=P(N,2)
3220 IF IND=1 THEN PLACE(2+J)=P(N,4)
3230 IF IND=2 THEN PLACE(1+J)=P(N,3)
3240 PRINT #3, MKI$(PLACE(1+J));MKI$(PLACE(2+J));
3250 IF J=0 THEN J=2:N=NODE2(M):IND=IIEND(M):GOTO 3200
3260 '
3270 '************* Assemble global [K] and [M] ************
3280 '
3290 NZ=0
3300 FOR IR=1 TO 4
3310 IF PLACE(IR) > NFR GOTO 3400
3320 FOR IC=IR TO 4
3330 IF PLACE(IC) > NFR GOTO 3390
3340 ON NZ+IC GOSUB 3080,3090,3100,3110,3120,3130,3140,3080,3150,3120
3350 PR=PLACE(IR):PC=PLACE(IC)
3360 IF PR>PC THEN SWAP PR,PC
3370 K(PR,PC)=K(PR,PC)+SMALLK*CST
3380 W(PR,PC)=W(PR,PC)+SMALLM*CMS
3390 NEXT IC
3400 NZ=NZ+4-IR
3410 NEXT IR
3420 ERASE PLACE
3430 NEXT M
3440 CLOSE #3
3450 '
3460 '********************** Print [K] *******************************
3470 '
3480 IF ICLR =1 THEN COLOR 15,6
```

```
3490 CLS
3500 LOCATE 1,1
3510 PRINT "  [K]":PRINT
3520 FOR I=1 TO NFR
3530 FOR J=1 TO I-1
3540 IF ICLR =1 THEN IF INT(J/2)*2=J THEN COLOR ,2  ELSE COLOR ,6
3550 IF ICLR =1 THEN IF K(J,I)<>0 THEN COLOR 14
3560 PRINT USING Z$ ;K(J,I); :IF ICLR =1 THEN COLOR 15
3570 NEXT J
3580 FOR J=I TO NFR
3590 IF ICLR =1 THEN IF INT(J\2)*2=J THEN COLOR ,2  ELSE COLOR ,6
3600 IF K(I,J)<>0 THEN NVK=NVK+1 :IF ICLR =1 THEN COLOR 14
3610 PRINT USING Z$ ;K(I,J); :IF ICLR =1 THEN COLOR 15
3620 NEXT J
3630 PRINT
3640 NEXT I
3650 COLOR 15:LOCATE 25,1:PRINT "Press any key to see [M] ";
3660 A$=INKEY$ : IF A$="" GOTO 3660
3670 LOCATE 25,1:PRINT CLR$
3680 '
3690 '*********************** Print [M] *******************************
3700 '
3710 IF ICLR =1 THEN COLOR 15,6
3720 CLS
3730 LOCATE 1,1
3740 PRINT "  [M]":PRINT
3750 FOR I=1 TO NFR
3760 FOR J=1 TO I-1
3770 IF ICLR =1 THEN IF INT(J/2)*2=J THEN COLOR ,2  ELSE COLOR ,6
3780 IF ICLR =1 THEN IF W(J,I)<>0 THEN COLOR 14
3790 PRINT USING Z$ ;W(J,I); :IF ICLR =1 THEN COLOR 15
3800 NEXT J
3810 FOR J=I TO NFR
3820 IF ICLR =1 THEN IF INT(J\2)*2=J THEN COLOR ,2  ELSE COLOR ,6
3830 IF W(I,J)<>0 THEN NVM=NVM+1 :IF ICLR =1 THEN COLOR 14
3840 PRINT USING Z$ ;W(I,J); :IF ICLR =1 THEN COLOR 15
3850 NEXT J
3860 PRINT
3870 NEXT I
3880 IF ICLR =1 THEN COLOR 15
3890  LOCATE 25,1:PRINT "Press any key to continue";
3900 A$=INKEY$ : IF A$="" GOTO 3900
3910 LOCATE 25,1:PRINT CLR$
3920 '
3930 '***************** Store [K] and [M] on file ********************
3940 '
3950 PRINT #1, MKS$(NFR);MKS$(NVK);: PRINT #2, MKS$(NFR);MKS$(NVM);
3960 FOR I=1 TO NFR
3970 FOR J=I TO NFR
3980 IF K(I,J)<>0 THEN PRINT #1, MKS$(K(I,J));MKI$(I);MKI$(J);:LPRINT USING "K(#
##_,###)=##.###^^^^";I,J,K(I,J)
3990 IF W(I,J)<>0 THEN PRINT #2, MKS$(W(I,J));MKI$(I);MKI$(J);:
4000 NEXT J
4010 NEXT I
4011 FOR I=1 TO NFR
4012 FOR J=I TO NFR
4013 IF W(I,J)<>0 THEN LPRINT USING "M(###_,###)=##.###^^^^";I,J,W(I,J)
4014 NEXT J
4015 NEXT I
4020 CLOSE #1 : CLOSE #2
```

```
4025 '
4030 '**************** Option to change NFIL *******************
4035 '
4037 LOCATE 25,1,0
4040 INPUT "Another Loading Case? (y/n)",A$
4050 IF A$="n" OR A$="N" THEN END
4060 FLAG=1 : FINISH=0 :ERASE K :ERASE W:NFILO=NFIL
4065 NVK=0 : NVM=0
4070 GOTO 670
```

Appendix C.2 Listing for GENJAC.BAS

Appendix C.2 contains the listing for the basic program GENJAC.BAS. Given a stiffness and mass matrix, this program performs a general jacobian iteration and determines the eigenvalues and eigenvectors that generate modal masses equal to unity and modal stiffnesses equal to the squared natural frequencies of the system.

```
10 '
20 '++++++++++++ Input [K] and [M] +++++++++++++++++
30 '
40 DEFDBL A-Z
50 DEFINT H,I,J,N,S
60 CLS
70 INPUT "INPUT File name  ";F$
80 OPEN F$+".k" AS #1 LEN=8
90 OPEN F$+".M" AS #2 LEN=8
100 FIELD #1, 4 AS NDOFK$,4 AS NVK$
110 FIELD #2, 4 AS NDOFM$,4 AS NVM$
120 GET #1 : GET #2
130 IF NDOFK$ <> NDOFM$ THEN CLOSE #1:CLOSE #2:GOTO 70
140 NVK=CVS(NVK$) : NVM=CVS(NVM$)
150 N=CVS(NDOFK$)
160 DIM K(N,N),M(N,N),EVEC(N,N),EVAL(N),OLDEVAL(N)
170 '
180 '++++++++++++ Put [K] in Matrix Format ++++++++++++++
190 '
200 FIELD #1, 4 AS K$,2 AS R$,2 AS C$
210 FOR I=1 TO NVK
220 GET #1
230 K(CVI(R$),CVI(C$))=CVS(K$)
240 NEXT
250 CLOSE #1
260 '
270 '++++++++++++ Put [M] in Matrix Format ++++++++++++++
280 '
290 FIELD #2, 4 AS M$.2 AS R$,2 AS C$
300 FOR I=1 TO NVM
310 GET #2
320 M(CVI(R$),CVI(C$))=CVS(M$)
330 NEXT
340 CLOSE #2
350 '
360 '++++++++ Initialize <Eval> and [Evec] and Limits ++++++++++
370 '
380 FOR I=1 TO N
390 EVAL(I)=K(I,I)/M(I,I)
400 EVEC (I,I)=1
410 NEXT
420 NSWMAX=20
430 LIM=1E-09
440 LMS=LIM*LIM
450 '
460 '++++++++ Start Sweep ++++++++++++++
470 '
480 FOR SW=1 TO NSWMAX
490 LOCATE 3,1 : PRINT SW;
500 '
510 '++++++++++++++++ Update Old<Eval> +++++++++++++++++++++
520 '
530 FOR I=1 TO N
540 OLDEVAL(I)=EVAL(I)
550 NEXT
560 '
570 '++++++ Check if M(i,j) and K(i,j) are Large Enough to Zero ++++++++
580 '
590 THR=10^(-2*SW)
600 FOR I=1 TO N-1
```

```
605 IF K(I,I)=0 GOTO 1200
610 FOR J=I+1 TO N
615 IF K(J,J)=0 GOTO 1190
620 IF K(I,J)*K(I,J)<THR*K(I,I)*K(J,J) AND
       M(I,J)*M(I,J)<THR*M(I,I)*M(J,J)     GOTO 1190
630 '
640 '+++++++++ Calc Rotation Matrix Values A and G +++++++++++
650 '
660 KII=K(I,I)*M(I,J)-K(I,J)*M(I,I)
670 KJJ=K(J,J)*M(I,J)-K(I,J)*M(J,J)
680 IF KII=0 AND KJJ=0 THEN A=0:G=-K(I,J)/K(J,J):GOTO 750
690 KM=K(I,I)*M(J,J)-K(J,J)*M(I,I)
700 X=SQR(KM*KM/4+KII*KJJ)+SGN(KM)*KM/2
710 IF KM<>0 THEN X=X*SGN(KM)
720 A=KJJ/X   : G=-KII/X
730 'PRINT"(";I;",";J;") ";A,G
740 '
750 '++++++++++ Zero Element 1,j ++++++++++++++++
760 '
770 FOR H=1 TO I-1
780 KI=K(H,I) : MI=M(H,I)
790 KJ=K(H,J) : MJ=M(H,J)
800 K(H,I)=KI+G*KJ  :  M(H,I)=MI+G*MJ
810 K(H,J)=KJ+A*KI  :  M(H,J)=MJ+A*MI
820 NEXT
830 '
840 FOR H=J+1 TO N
850 KI=K(I,H) : MI=M(I,H)
860 KJ=K(J,H) : MJ=M(J,H)
870 K(I,H)=KI+G*KJ  :  M(I,H)=MI+G*MJ
880 K(J,H)=KJ+A*KI  :  M(J,H)=MJ+A*MI
890 NEXT
900 '
910 FOR H=I+1 TO J-1
920 KI=K(I,H) : MI=M(I,H)
930 KJ=K(H,J) : MJ=M(H,J)
940 K(I,H)=KI+G*KJ  :  M(I,H)=MI+G*MJ
950 K(H,J)=KJ+A*KI  :  M(H,J)=MJ+A*MI
960 NEXT
970 '
980 KJ=K(J,J) :  MJ=M(J,J)
990 K(J,J)=KJ+2*A*K(I,J)+A*A*K(I,I)
1000 M(J,J)=MJ+2*A*M(I,J)+A*A*M(I,I)
1010 K(I,I)=K(I,I)+2*G*K(I,J)+G*G*KJ
1020 M(I,I)=M(I,I)+2*G*M(I,J)+G*G*MJ
1030 '
1040 K(I,J)=0 : M(I,J)=0
1050 '
1060 'FOR IR=1 TO N:FOR IC=1 TO N:PRINT USING " ##.#^^^^";K(IR,IC);:NEXT :PRINT
:NEXT:PRINT
1070 'FOR IR=1 TO N:FOR IC=1 TO N:PRINT USING "###.###";M(IR,IC);:NEXT :PRINT :N
EXT:PRINT
1080 'STOP
1090 '
1100 '++++++++ Update [Evec] ++++++++++++++
1110 '
1120 FOR H=1 TO N
1130 EI=EVEC(H,I)
1140 EJ=EVEC(H,J)
1150 EVEC(H,I)=EI+G*EJ
```

```
1160 EVEC(H,J)=EJ+A*EI
1170 NEXT
1180 '
1190 NEXT J
1200 NEXT I
1210 '
1220 '++++++++++ Update <Eval> +++++++++++++
1230 '
1240 FOR H=1 TO N
1250 EVAL(H)=K(H,H)/M(H,H)
1260 NEXT
1270 '
1280 '+++++++++ First Convergence Check ++++++++++++
1290 '
1300 FOR I=1 TO N
1310 IF ABS(EVAL(I)-OLDEVAL(I))>ABS(LIM*OLDEVAL(I)) GOTO 1460
1320 NEXT
1330 '
1340 '++++++++++ Second Convergence Check +++++++++++
1350 '
1360 FOR I=1 TO N-1
1370 FOR J=I+1 TO N
1380 IF K(I,J)*K(I,J)>ABS(LMS*K(I,I)*K(J.J)) OR
             M(I.J)*M(I,J)>LMS*M(I,I)*M(J,J)     GOTO 1460
1390 NEXT J
1400 NEXT I
1410 PRINT "System Converged"
1420 GOTO 1500
1430 '
1440 '++++++++++ Next Sweep ++++++++++++++++++
1450 '
1460 NEXT SW
1470 PRINT "System did not converge after ";NSWMAX;" sweeps"
1480 END
1490 '
1500 '+++++++++ Normalize [M] +++++++++++++++
1505 '
1510 FOR I=1 TO N
1515 IF EVAL(I)<0 THEN EVAL(I)=0
1520 FOR J=1 TO N
1530 EVEC(J,I)=EVEC(J,I)/SQR(M(I,I))
1540 NEXT
1550 NEXT
1560 '
1570 '+++++++++ Sort <Eval> smallest to largest ++++++++++++
1580 '
1590 FOR I=1 TO N-1
1610 FOR J=I TO N
1620 IF EVAL(I)>EVAL(J) THEN GOSUB 1670
1630 NEXT
1640 NEXT
1650 GOTO 1730
1660 '
1670 SWAP EVAL(I),EVAL(J)
1680 FOR H=1 TO N
1690 SWAP EVEC(H,I),EVEC(H,J)
1700 NEXT
1710 RETURN
1720 '
1730 '++++++++ Print to Screen ++++++++++++++
1740 '
1750 PRINT "mode      w²            Hz         Period"
1760 FOR I=1 TO N
1770 FR=SQR(EVAL(I))/2/3.1415927#
1780 PRINT USING "##  ";I; :
     PRINT USING " ##.####^^^^ "; EVAL(I);FR;
1790 IF EVAL(I)=0 THEN PRINT "      "+CHR$(236):GOTO 1820
1800 PER=1/FR
1810 PRINT USING " ##.###^^^^ ";PER
1820 NEXT
1830 PRINT:PRINT:PRINT"If all is OK, press ENTER "
1840  A$=INPUT$(1)
1850 IF A$<>CHR$(13) GOTO 2070
1860 '
1870 FOR I=1 TO N
1880 FOR J=1 TO N
1890 PRINT USING "##.##^^^^ "; EVEC(I,J);
1900 NEXT :PRINT :NEXT
1910 PRINT:PRINT:PRINT"If all is OK, press ENTER "
1920  A$=INPUT$(1)
1930 IF A$<>CHR$(13) GOTO 2070
1940 '
1950 '++++++++++ Store Data ++++++++++++++++++
1960 '
1970 OPEN F$+".N" FOR OUTPUT AS #1
1980 OPEN F$+".P" FOR OUTPUT AS #2
1990 PRINT #1, MKS$(N);MKS$(N);
2000 PRINT #2, MKS$(N);MKS$(N);
2010 FOR I=1 TO N
2020 PRINT #1, MKD$(EVAL(I));
2030 FOR J=1 TO N
2040 PRINT #2, MKD$(EVEC(I,J));
2050 NEXT
2060 NEXT
2070 END
```

Appendix C.3 Listing for CRIMSIM.BAS

The program CRIMSIM.BAS is listed in Appendix C.3. This program performs the time stepping numerical analysis described in Chapter 4, using a constant cable stiffness.

```
 'CRIMSIM  Crane Impact Simulation
20 '
30 'This programme simulates the dynamic behavior of a craneway system
40 'subject to hoist motor loads.
50 'A structural stiffness matrix and a structural mass matrix are read
 0 'and assembled with cable and motor DsoF to form the overall [K] and
 0 '[M] system of equations such that
80 '
90 '                                    "
100 '                 [K](Y)+[M](Y)=(F)
110 '
120 'Position and acceleration are made dependent over a small timestep DT
130 'such that [K] and [M] can be combined into a single effective stiffness
140 'matrix [Ke]. This matrix is inverted and is used to solve for (Y).
150 '
160 '                                         "
170 '                 (Y)=1/[Ke]((F)+[M](Y*))
180 '
190 'Because of the nature of (F) this can further be simplified to
200 '
210 '                 (Y)=(1/[Ke])Fo+(Y*)
220 '
230 'The value Fo is a function of motor speed. By earlier assumptions,
240 'velocity is also dependent on position. Therefore there are two
250 'equations relating Fo and motor speed;
260 '  the one from the dynamic matrix equation aboveand
270 '  the motor function
280 'These two equations are solved for the end of the timestep and
290 'the predicted value of Fo is used in the dynamic matrix above to
300 'solve for the vector (Y). The procedure is then repeated for
 10 'new "starting" conditions.
 20 'This type of iteration is a Leading Point Iteration
330 ' For a more detailed description of the programme and the theory
340 'behind it, see section      of Hoist Induced Dynamic Load Factors for
350 'Craneway Structures, a thesis required for completion of the degree
360 'of MSc in Civil Engineering at the University of Alberta
370 COLOR 15,1,2
380 CLS
390 KEY OFF
400 DEFDBL A-Z
410 DEFINT I,J,L,G,N,R,C,P
420 PRINT "press Ctrl-Print Screen for hardcopy of all screen in-and-output."
430 PRINT"Detailed output to screen=1, Data to file=2, Both=3"
440 INPUT "Type of Output";ITOOP
450 IF ITOOP=1 GOTO 470
460 INPUT "file name  ";DATAFILE$
470 Z1$=" +#.##^^^^ "
480 Z$=" +#.##^^^^ "
490 '
500 '▓▓▓▓▓▓▓▓▓▓▓▓▓▓▓▓▓▓▓▓▓▓▓▓▓▓▓▓▓▓▓▓▓▓▓▓▓▓▓▓▓▓▓▓▓▓▓▓▓ Input math data █
510 '
520 PRINT"Newmark=1  Constant Acceleration=2  Linear Acceleration=3
530 INPUT "Approximation method";I
540 ON I GOSUB 3420,3540,3620
550 INPUT "Timespan to analize";TIMESPAN
560 INPUT "Timestep deltaT";DT
 70 INPUT "Filename with [K] in it ";FILEK$
 80 INPUT "Filename with [M] in it ";FILEM$
590 OPEN FILEK$ AS #1  LEN=8
600 OPEN FILEM$ AS #2  LEN=8
610 FIELD #1,4 AS K$,4 AS NVK$
620 FIELD #2,4 AS M$,4 AS NVM$
630 GET #1,1 : GET #2,1
640 IF K$<>M$ THEN CLOSE #1 : CLOSE #2 : GOTO 570
```

```
650 NVK=CVS(NVK$) : NVM=CVS(NVM$)
660 NDOF=CVS(K$)+2
670 DIM KE(NDOF,NDOF),Z(NDOF,NDOF),YSTAR(NDOF),Y(NDOF),DY(NDOF),DDY(NDOF),
        YSTATIC(NDOF),H1(NDOF),H2(NDOF)
680 DIM  K(NVK+5), RK(NVK+5), CK(NVK+5)
690 '
700 '[redacted] Input [Ks] █
 10 '
720 FIELD #1,4 AS K$, 2 AS IK$, 2 AS JK$
730 FOR I=1 TO NVK
740 GET #1
750 K(I+5)=CVS(K$) : RK(I+5)=CVI(IK$)+2  : CK(I+5)=CVI(JK$)+2
760 NEXT
770 CLOSE #1
780 '
790 '[redacted] Assemble [K] █
800 '
810 INPUT  "Cable stiffness, kc ";KC
820 FOR I=1 TO 6
830 K(I)=KC+K(I)
840 RK(I)=INT(1+I^2/13)
850 CK(I)=I-(RK(I)-1)*2
860 IF I=6 THEN CK(I)=3
870 IF I=2 OR I=5 THEN K(I)=-KC
880 NEXT
890 '
900 '[redacted] Invert [K] to get (Ystatic) █
910 '
920 W=1
930 GOSUB 3690
940 IJK=2 : GOSUB 3060
950 YSTATIC(2)=1
960 N=2
 70 GOSUB 2460
980 FOR I=1 TO NDOF
990 PRINT YSTATIC(I);
1000 NEXT
1010 PRINT
1020 '
1030 '[redacted] Put [K] into [Ke]  █
1040 '
1050 ERASE KE
1060 W=SQR(BETA2)/DT
1070 GOSUB 3690
1080 IJK=2 : GOSUB 3060
1090 '[redacted] Input [Ms] and put into [Kes]  █
1100 '
1110 FIELD #2,4 AS M$, 2 AS IM$, 2 AS JM$
1120 FOR I=1 TO NVM
1130 GET #2
1140 Z(CVI(IM$)+2,CVI(JM$)+2)=CVS(M$)*W
1150 IF IM$<>JM$ THEN Z(CVI(JM$)+2,CVI(IM$)+2)=Z(CVI(IM$)+2,CVI(JM$)+2)
1160 KE(CVI(IM$)+2,CVI(JM$)+2)=CVS(M$)*W+KE(CVI(IM$)+2,CVI(JM$)+2)
1170 IF IM$<>JM$ THEN KE(CVI(JM$)+2,CVI(IM$)+2)=KE(CVI(IM$)+2,CVI(JM$)+2)
1180 NEXT
1190 CLOSE #2
1200 '
1210 '[redacted] Assemble [M] and [Ke] █
 220 '
1230 INPUT "Apparent motor mass, mm ";MM
1240 INPUT "Mass of Load, ml ";ML
1250 Z(2,2)=Z(2,2)+ML*W
1260 Z(1,1)=Z(1,1)+MM*W
1270 KE(2,2)=KE(2,2)+ML*W
1280 KE(1,1)=KE(1,1)+MM*W
1290 IJK=1 : GOSUB 3060
```

```
1300 IJK=2 : GOSUB 3060
1310 '
1320 '[redacted] Calc [Z]=[M]/[Ke] and {H1} and {H2} █
1330 '
1340 N=1
1350 H1(1)=1/W : H2(2)=-ML*9.810001/W
1360 GOSUB 2460
 370 FOR I=1 TO NDOF
 380 FOR J=1 TO NDOF
1390 Z(I,J)=Z(I,J)/(W*W)
1400 NEXT :NEXT
1410 IJK=1 : GOSUB 3060
1420 '
1430 '[redacted] Input motor data and Calc parabola coefficients █
1440 '
1450 INPUT "Max Motor Force, Fp ";FP
1460 INPUT "Initial Motor Force, Fi ";FI
1470 INPUT "Pullout Slip, sp ";SP
1480 INPUT "Hoisting speed, Vo ";VO
1490 INPUT;"Initial slope, mi ";MI$
1500 IF LEN(MI$)=0 THEN  MI=2*(FP-FI)*SP*(SP+1)/((1-SP)*(SP*SP+1)):PRINT MI/VO
                   ELSE  MI=VAL(MI$)*VO
1510 A2=((FI+MI)*(FP/(SP*SP))-(FP/SP+MI/2)^2)/(2*FP/SP-FP/(SP*SP)-FI)
1520 AOP(1)=FP*(2*SP-1)/(SP*SP)       : AOP(2)=FI
1530 A1P(1)=2*FP*(1-SP)/(VO*SP*SP)    : A1P(2)=MI/VO
1540 A2P(1)=-FP/(VO*SP)^2             : A2P(2)=A2/(VO*VO)
1550 VC=2*(AOP(1)-AOP(2))/(A1P(2)-A1P(1))
1560 P=2
1570 '
1580 '[redacted] Check step size adequate █
1590 '
1600 A1=DT/(BETA1*H1(1))
1610 MAXSLOPE=2*FP*(1+VC/VO-SP)/(VO*SP*SP)
 620 IF A1<MAXSLOPE THEN COLOR 0,4 : PRINT A1,MAXSLOPE : GOTO 2450
1630 '
1640 '[redacted] Input initial conditions █
1650 '
1660 INPUT "initial {Y} vector   -Static?(y/n)";A$
1670 FOR I=1 TO NDOF
1680 IF A$="n" OR A$="N" THEN INPUT Y(I)
                          ELSE Y(I)=-ML*9.810001*YSTATIC(I):PRINT Y(I)
1690 NEXT
1700 PRINT "        ."
1710 INPUT "initial {Y} vector  -Stationary?(y/n)";A$
1720 IF A$="y" OR A$="Y" GOTO 1760
1730 FOR I=1 TO NDOF
1740 INPUT DY(I)
1750 NEXT
1760 FO=FI
1770 FA=KC*(Y(1)-Y(2)+Y(3))
1780 IF FA<0 THEN FA=0
1790 DDY(1)=(FI-FA)/MM
1800 PRINT "           ";CHR$(34)
1810 PRINT "initial {Y} vector. (";CHR$(152);"m already established)";
1820 INPUT "  -others Stationary?(y/n) ";A$
1830 IF A$="y" OR A$="Y" GOTO 1900
1840 FOR I=2 TO NDOF
1850 INPUT DDY(I)
 860 NEXT
 870 '
1880 '[redacted] Print Data █
1890 '
1900 IF ITOOP=1 GOTO 2000
1910 OPEN DATAFILE$ FOR OUTPUT AS #3
1920 RCLN=(NDOF+1)*12
1930 PRINT #3, MKI$(RCLN);SPACE$(RCLN-2);
```

```
1940 IF ITOOP=1 GOTO 2000
1950 PRINT#3, MKS$(T);MKS$(FA);MKS$(FO);
1960 FOR I=1 TO NDOF
1970 PRINT#3, MKS$(Y(I));MKS$(DY(I));MKS$(DDY(I));
1980 NEXT
1990 IF ITOOP=2 GOTO 2010
2000 GOSUB 3200
2010 LOCATE 25,1 : PRINT "t=";:PRINT USING "##.##^^^^";T;:PRINT " step=";E;
2020 '
2030 '████████████████████████████ Assemble {Y*} vector █
2040 '
2050 ERASE YSTAR
2060 FOR I=1 TO NDOF
2070 FOR J=I+1 TO NDOF
2080 YSTAR(I)=YSTAR(I)+Z(I,J)*FNACCSTAR(J)
2090 YSTAR(J)=YSTAR(J)+Z(J,I)*FNACCSTAR(I)
2100 NEXT
2110 YSTAR(I)=YSTAR(I)+H2(I)+Z(I,I)*FNACCSTAR(I)
2120 NEXT
2130 '
2140 '██████████████████████████████████████ Calculate Fo █
2150 '
2160 A0=FNVELSTAR(1)*A1-YSTAR(1)/H1(1)
2170 DYM=(A1-A1P(P)-SQR((A1-A1P(P))*(A1-A1P(P))-4*A2P(P)*(A0P(P)-A0)))
        /(2*A2P(P))
2180 IF P=2 AND DYM>VC THEN P=1 : GOTO 2170
2190 IF P=1 AND DYM<VC THEN P=2 : GOTO 2170
2200 FO=A0+A1*DYM
2210 '
2220 '██████████████████████████████████████ Solve {Y} vector █
2230 '
2240 FOR I=1 TO NDOF
2250 DYSTAR=FNVELSTAR(I)
2260 DDYSTAR=FNACCSTAR(I)
2270 Y(I)=FO*H1(I)+YSTAR(I)
2280 FA=KC*(Y(1)-Y(2)+Y(3))
2290 '
2300 '███████████████████████████████████ Solve {Ẏ} and {Ÿ} vectors █
2310 '
2320 DY(I)=Y(I)*BETA1/DT-DYSTAR
2330 DDY(I)=Y(I)*BETA2/(DT*DT)-DDYSTAR
2340 NEXT I
2350 '
2360 '███████████████████████████████████ Iterate next step █
2370 '
2380 E=E+1
2390 T=T+DT
2400 IF ITOOP=2 GOTO 2430
2410 E$=INKEY$ : IF E$=CHR$(13) GOTO 1940
2420 GOTO 2410
2430 IF T =< TIMESPAN GOTO 1940
2440 CLOSE #3
2450 END
2460 '
2470 '█████████████████████████████████ Invert matrix subroutine █
2480 '
2490 'find largest value in column j of [Ke] for pivot
2500 '
2510 FOR J=N TO NDOF
2520 MAX=KE(J,J) : ITOJ=J
2530 FOR I=J+1 TO NDOF
2540 IF ABS(KE(I,J))>ABS(MAX) THEN MAX=KE(I,J) : ITOJ=I
2550 NEXT
2560 IF ITOJ=J GOTO 2650
2570 FOR L=N TO NDOF
2580 SWAP KE(J,L),KE(ITOJ,L)
```

```
2590 IF N=1 THEN SWAP Z(J,L),Z(ITOJ,L)
2600 NEXT
2610 IF N=2 THEN SWAP YSTATIC(J),YSTATIC(ITOJ)
          ELSE SWAP H1(J),H1(ITOJ) : SWAP H2(J),H2(ITOJ)
2620 '
2630 'make values in column j of [Ke] equal
2640 '
 650 G=1
 660 FOR I=N TO NDOF
2670 IF I=J GOTO 2760
2680 KDEN=KE(I,J)
2690 IF KDEN=0 THEN OMIT(G)=I : G=G+1 : GOTO 2760
2700 KFAC=KE(J,J)/KDEN
2710 FOR L=N TO NDOF
2720 KE(I,L)=KE(I,L)*KFAC
2730 IF N=1 THEN Z(I,L)=Z(I,L)*KFAC
2740 NEXT L
2750 IF N=2 THEN YSTATIC(I)=YSTATIC(I)*KFAC
          ELSE H1(I)=H1(I)*KFAC : H2(I)=H2(I)*KFAC
2760 NEXT I
2770 '
2780 'subtract row j to get 0's in column j of [Ke]
2790 '
2800 G=1
2810 FOR I=N TO NDOF
2820 IF I=J GOTO 2890
2830 IF OMIT(G)=I THEN G=G+1 : GOTO 2890
2840 FOR L=N TO NDOF
2850 KE(I,L)=KE(I,L)-KE(J,L)
2860 IF N=1 THEN Z(I,L)=Z(I,L)-Z(J,L)
2870 NEXT L
2880 IF N=2 THEN YSTATIC(I)=YSTATIC(I)-YSTATIC(J)
          ELSE H1(I)=H1(I)-H1(J) : H2(I)=H2(I)-H2(J)
 890 NEXT I
2900 ERASE OMIT
2910 NEXT J
2920 '
2930 'normalize
2940 '
2950 FOR I=N TO NDOF
2960 IF N=2 THEN YSTATIC(I)=YSTATIC(I)/KE(I,I) : GOTO 3010
2970 FOR J=N TO NDOF
2980 Z(I,J)=Z(I,J)/KE(I,I)
2990 NEXT J
3000 H1(I)=H1(I)/KE(I,I) : H2(I)=H2(I)/KE(I,I)
3010 NEXT I
3020 RETURN
3030 '
3040 '█████████████████████████████████████████████████████████ Print matrix █
3050 '
3060 FOR R=1 TO NDOF
3070 FOR C=1 TO NDOF
3080 ON IJK GOSUB 3150,3170
3090 NEXT C
3100 PRINT
3110 NEXT R
3120 PRINT
3130 A$=INKEY$ : IF A$ <> CHR$(13) GOTO 3130
 160 RETURN
 150 PRINT USING Z1$;Z(R,C);
3160 RETURN
3170 PRINT USING Z1$;KE(R,C);
3180 RETURN
3190 '
3200 '████████████████████████████████████████████████ Step by step Output █
3210 '
```

```
3220 PRINT "Step #";E;" T=";T;" ";STRING$(20,CHR$(219))
3230 PRINT
3240 PRINT "ym  ";Y(1);"     dym  ";DY(1);"    ddym ";DDY(1)
3250 PRINT "yl  ";Y(2);"     dyl  ";DY(2);"    ddyl ";DDY(2)
3260 PRINT "ys  ";Y(3);"     dys  ";DY(3);"    ddys ";DDY(3)
3270 PRINT
3280 PRINT "ddym*";FNACCSTAR(1);"     dym* ";FNVELSTAR(1)
 290 PRINT "ddyl*";FNACCSTAR(2);"     dyl* ";FNVELSTAR(2)
3300 PRINT "ddys*";FNACCSTAR(3);"     dys* ";FNVELSTAR(3)
3310 PRINT
3320 PRINT "parabola#";P
3330 PRINT A0P(P);" + ";A1P(P);"w + ";A2P(P);"w^2"
3340 PRINT "Slope= ";A1,"Intercept= ";A0
3350 PRINT "Fo= ";FO
3360 PRINT "Fa= ";FA
3370 PRINT
3380 RETURN
3390 '
3400 '██████████████████████████████████████████████ Approximation Procedures █
3410 '
3420 'Newmark Method
3430 '
3440 PRINT "In general  α=.25 and δ=.5"
3450 INPUT " α=";ALPHA
3460 INPUT " δ=";DELTA
3470 BETA1=DELTA/ALPHA
3480 BETA2=1/ALPHA
3490 BETA3=(1-2*ALPHA)/(2*ALPHA)
3500 DEF FNACCSTAR(I)=BETA2*(Y(I)/(DT*DT)+DY(I)/DT)+BETA3*DDY(I)
3510 DEF FNVELSTAR(I)=BETA1*Y(I)/DT+(BETA1-1)*DY(I)+(BETA1/2-1)*DDY(I)*DT
3520 RETURN
3530 '
3540 'Constant Acceleration Method
 550 '
3560 BETA1=2
3570 BETA2=2
3580 DEF FNACCSTAR(I)=2*Y(I)/(DT*DT)+2*DY(I)/DT
3590 DEF FNVELSTAR(I)=2*Y(I)/DT+DY(I)
3600 RETURN
3610 '
3620 'Linear Acceleration Method
3630 '
3640 BETA1=3
3650 BETA2=6
3660 DEF FNACCSTAR(I)=6*Y(I)/(DT*DT)+6*DY(I)/DT+2*DDY(I)
3670 DEF FNVELSTAR(I)=3*Y(I)/DT+2*DY(I)+.5*DDY(I)*DT
3680 RETURN
3690 '
3700 '████████████████████████████████████ Put [K] into [Ke] subprogramme █
3710 '
3720 FOR I=1 TO NVK+5
3730 KE(RK(I),CK(I))=K(I)/W
3740 IF RK(I)<>CK(I) THEN KE(CK(I),RK(I))=K(I)/W
3750 NEXT
3760 RETURN
```

Appendix C.4 Listing for CRIS5.BAS

The program CRIS5.BAS is listed in Appendix C.4. This program performs the time stepping numerical analysis described in Chapter 4, using a non-constant cable stiffness. An iteration within each time step is used to determine values for the forces acting on the system.

```
10 'CRIS5    Crane Impact Simulation
20 '
30 'This programme simulates the dynamic behavior of a craneway system
40 'subject to hoist motor loads.
50 'Normal stiffness and mass matrices are read in
60 'The system of equations is
70 '
80 '                          ..
90 '               [Kn]{W}+[Mn]{W}={F}
100 '
110 ' {W} are the normal DsoF of the system.
120 'Displacement, velocity and acceleration are made dependent
130 'over a small timestep DT, so {F} can be expressed
140 'in terms of velocities.
150 'The motor forcing function in {F} is expressed in terms of
160 'motor velocity in a seperate equation.
170 'These two equations are solved for the end of the timestep and
180 'the predicted {F} is used in the dynamic matrix above to
190 'solve for the vector {W}. The procedure is then repeated for
200 'new "starting" conditions.
210 'This type of iteration is a Leading Point Iteration
220 ' For a more detailed description of the programme and the theory
230 'behind it, see section      of Hoist Induced Dynamic Load Factors for
240 'Craneway Structures, a thesis required for completion of the degree
250 'of MSc in Civil Engineering at the University of Alberta
260 '
270 ':::::::::::::: Initialize ::::::::::::::::::::::
280 '
290 DEFDBL A-Z
300 DEFINT N,I,J,Q,H
310 Z$="##.###^^^^ "
320 '
330 PRINT "press Ctrl-Print Screen for hardcopy of all screen in-and-output."
340 '
350 '::::::::::::::::: Input Structural Data ::::::::::::::::
360 '
370 INPUT "Input Test Name ",NTF$
380 INPUT "Structure filename  ";NSF$
390 INPUT "Input Symetry Factor" ;ISF
400 '
410 'Get Masses
420 '
430 T$=".M" :GOSUB 630
440 GET #1
450 MM=CVS(V$)
460 GET #1
470 MLG=CVS(V$)*9.810001
480 ML=CVS(V$)
490 CLOSE #1
500 '
510 'Get [w²]
520 '
530 T$=".N" :GOSUB 630
540 DIM KN(NDOF)
550 FIELD #1, 8 AS V$
560 FOR I=1 TO NDOF
570 GET #1
580 KN(I)=CVD(V$)
590 NEXT
600 CLOSE #1
```

```
610 GOTO 710
620 '
630 'Open Input Files Subroutine
640 '
650 OPEN NSF$+T$ AS #1  LEN=8
660 FIELD #1,4 AS V$,4 AS NV$
670 GET #1,1
660 NDOF=CVS(V$) : NV=CVS(NV$)
690 RETURN
700 '
710 'Get [*]
720 '
730 T$=".P" : GOSUB 630
740 DIM P(NDOF,NDOF)
750 FIELD #1, 8 AS V$
760 FOR I=1 TO NDOF
770 FOR J=1 TO NDOF
780 GET #1
790 P(I,J)=CVD(V$)
800 NEXT
810 NEXT
820 CLOSE
830 '
840 ':::::::::: Open Test Output Files :::::::::::::::
850 '
860 OPEN NTF$+".W" FOR OUTPUT AS #1
870 OPEN NTF$+".S" FOR OUTPUT AS #2
880 OPEN NTF$+".I" FOR OUTPUT AS #3
890 PRINT #3, "Test Filename = ";NTF$
900 PRINT #3, "Structure Filename = ";NSF$
910 PRINT #3, "Symetry Factor =";ISF
920 '
930 ':::::::::::::: Input Cable Data :::::::::::::::
940 '
950 LIM=.000001
960 CNV=MLG
970 ICNV=2
980 INPUT "Cable Maximum Stiffness, kc max ";KC
990 INPUT "Tension Offset, Tf ";TF
1000 IF TF>0 THEN TF=-TF
1010 INPUT "Tension Rate, Tbar ";TB
1020 IF TB>0 THEN TB=-TB
1030 INPUT "Number of Lines ";NL
1040 PRINT #3, "kc max=";KC,"Tf =";TF,"Tbar =";TB
1050 PRINT #3, "Number of Lines =";NL
1060 KC=KC/ISF/NL:TF=TF/ISF/NL:TB=TB/ISF/NL
1070 '
1080 '::::::: Input motor data and Calc parabola coefficients ::::::::
1090 '
1100 INPUT "Max Motor Force, Fp ";FP
1110 INPUT "Initial Motor Force, Fi ";FI
1120 INPUT "Pullout Slip, sp ";SP
1130 INPUT "Hoisting speed, Vo ";VO
1140 PRINT #3,"Fp = ";FP,"Fi = ";FI,"sp = ";SP :
     PRINT #3,"Vo = ";VO ;
1150 VO=VO*NL
1160 INPUT "Initial slope, mi ";MI$
1170 IF LEN(MI$)=0 THEN  MI=2*(FP-FI)*SP*(SP+1)/((1-SP)*(SP*SP+1))/VO:PRINT MI
 ELSE  MI=VAL(MI$)
1180 PRINT #3,"mi = ";MI
```

```
1190 FP=FP/ISF : FI=FI/ISF: MI=MI/ISF
1200 A0P(1)=FP*(2*SP-1)/(SP*SP)       : A0P(2)=FI
1210 A1P(1)=2*FP*(1-SP)/(V0*SP*SP)    : A1P(2)=MI
1220 VC=2*(A0P(2)-A0P(1))/(A1P(1)-A1P(2))
1230 A2P(1)=-FP/(V0*SP)^2             : A2P(2)=(A1P(1)-A1P(2))/(2*VC)+A2P(1)
1240 '
1250 ':::::::::: Select Approximation Procedure ::::::::::::::
1260 '
1270 PRINT"Newmark=1  Constant Acceleration=2  Linear Acceleration=3
1280 INPUT "Approximation method";I
1290 ON I GOTO  1310,1430,1520
1300 '
1310 'Newmark Method
1320 '
1330 PRINT #3, "Newmark"
1340 PRINT "In general  α=.25 and δ=.5"
1350 INPUT " α=";ALPHA
1360 INPUT " δ=";DELTA
1370 BETA1=DELTA/ALPHA
1380 BETA2=1/ALPHA
1390 DEF FNSS(D,V.A)=D+V*DT+(.5-ALPHA)*A*DT*DT
1400 DEF FNS(D,V,A)=D+(1-1/BETA1)*V*DT+(.5-1/BETA1)*A*DT*DT
1410 GOTO 1600
1420 '
1430 'Constant Acceleration Method
1440 '
1450 PRINT #3, "Constant"
1460 BETA1=2
1470 BETA2=2
1480 DEF FNSS(D,V,A)=D+V*DT
1490 DEF FNS(D,V,A)=D+V*DT/2
1500 GOTO 1600
1510 '
1520 'Linear Acceleration Method
1530 '
1540 PRINT #3, "Linear"
1550 BETA1=3
1560 BETA2=6
1570 DEF FNSS(D,V,A)=D+V*DT+A*DT*DT/3
1580 DEF FNS(D,V,A)=D+2*V*DT/3+A*DT*DT/6
1590 '
1600 ':::::::::: Input Time Data :::::::::::::
1610 '
1620 INPUT "Input number of timesteps ";NTS
1630 INPUT "Timestep deltaT";DT
1640 '
1650 'Select Reading step
1660 '
1670 PRINT "Frequency of data saved."
1680 INPUT "(Default = 1)",STP%
1690 IF STP%=0 THEN STP%=1
1700 '
1710 '::::::::::::: Filter Number of DsoF ::::::::::::::::
1720 '
1730 FOR NEDOF=NDOF TO 1  STEP -1
1740 IF SQR(KN(NEDOF))<1/DT GOTO 1760
1750 NEXT
1760 IF NEDOF=NDOF GOTO 1780
1770 PRINT "Only the first";NEDOF;" modal D'soF will be used !"
1780 DIM W(NEDOF),A(NEDOF),B(NEDOF),C(NEDOF),D(NEDOF),DW(NEDOF),DDW(NEDOF), KO(
EDOF),KG(NEDOF),PC(NEDOF),KPD(NEDOF)
1790 '
1800 ':::::::::::::: Calculate Constants ::::::::::::::
1810 '
1820 PRINT"         {A}           {B}           {C}          [D]          <Φc>"
1830 FOR I=1 TO NEDOF
1840 PC(I)=P(3,I)-P(2,I)+P(1,I)/NL
1850 A(I)=P(1,I)/(KN(I)+BETA2/(DT*DT))
1860 B(I)=P(2,I)/(KN(I)+BETA2/(DT*DT))
1870 C(I)=PC(I)/(KN(I)+BETA2/(DT*DT))
1880 D(I)=BETA2/(BETA2+DT*DT*KN(I))
1890 PRINT I;
1900 PRINT USING " ##.####^^^^ ";A(I);B(I);C(I);D(I);PC(I)
1910 '
1920 Z1=PC(I)*C(I)+Z1
1930 NEXT
1940 Z2=Z1-PC(2)*C(2)
1950 '
1960 Z1=1+NL*KC*Z1
1970 ZG=1-KC*DT*DT/(Z1*BETA2*MM*NL)
1980 FG=KC*9.810001*DT*DT/(BETA2*Z1*ZG)
1990 PRINT
2000 PRINT"       z1          zg          Fg "
2010 PRINT USING " ##.####^^^^ ";Z1;ZG;FG
2020 PRINT
2030 '
2040 Z2=1+NL*KC*Z2
2050 ZO=1-KC*DT*DT/(Z2*BETA2*MM*NL)
2060 PRINT
2070 PRINT"       z2          zO "
2080 PRINT USING " ##.####^^^^ ";Z2;ZO
2090 PRINT
2100 '
2110 PRINT"        kc<Φc>[D] "
2120 FOR I=1 TO NEDOF
2130 KPD(I)=KC*PC(I)*D(I)
2140 PRINT I;
2150 PRINT USING " ##.####^^^^ ";KPD(I)
2160 NEXT
2170 PRINT
2180 '
2190 PRINT "L=-m2g   a1=";
2200 A1F=MM*BETA2/(DT*BETA1)
2210 KS=MM*BETA2/(DT*DT)
2220 PRINT USING " ##.####^^^^ ";A1F/ZG
2230 PRINT USING " ks= ##.####^^^^ ";KS/ZG
2240 PRINT "L=CT     a1=";
2250 PRINT USING " ##.####^^^^ ";A1F/ZO
2260 PRINT USING " ks= ##.####^^^^ ";KS/ZO
2270 '
2280 ':::::::::::::: Check Slope ::::::::::::::
2290 '
2300 A1MX=A1F/ZG : IF ZG>ZO THEN  A1MX=A1F/ZO
2310 MXS=2*A2P(1)*VC+A1P(1)
2320 IF A1MX<MXS THEN PRINT A1MX;"<";MXS;" Choose smaller timestep" :
                  GOTO 1600
2330 PRINT #3, "Number of time steps = ";NTS,
           "Timestep = ";DT
2340 PRINT #1,MKI$(NEDOF+3);MKI$(NTS/STP%);MKS$(DT*STP%);SPACE$((NEDOF+1)*4);
2350 '
```

```
2360 ':::::::::: Input Initial Conditions ::::::::::::::::
2370 '
2380 PRINT "Case 1 - Load hanging in the air, all vels=0, all accs=0":PRINT
2390 PRINT "Case 2 - Load on the ground, cable in tension,"
2400 PRINT "         all vels=0, all accs=0":PRINT
2410 PRINT "Case 3 - Load on the ground, cable slack,"
2420 PRINT "         all vels=0, all accs=0":PRINT
2430 PRINT "Case 4 - All disp, vels, accs, are prescribed.":PRINT
2440 INPUT "select a case number.",ISC
2450 PRINT #3, "Starting Case ";ISC;
2460 ON ISC GOTO 2480,2580,2840,3040
2470 '
2480 'Case 1 - Load hanging
2490 '
2500 PRINT #3, : CLOSE #3
2510 CT=MLG/NL
2520 DY1=0
2530 TO=MLG/NL
2540 L=-MLG
2550 GOSUB 2700
2560 GOTO 3070
2570 '
2580 'Case 2 - Load on ground. cable in tension
2590 '
2600 PRINT "Input cable tension, CT.  0<CT<";MLG/NL*ISF;
2610 INPUT CT
2620 PRINT #3, "  Cable Tension = ";CT : CLOSE #3
2630 CT=CT/ISF
2640 DY1=0
2650 L=-CT*NL
2660 IF CT<=0 THEN CT=0:GOTO 2900
2670 GOSUB 2700
2680 GOTO 3070
2690 '
2700 'Cable in Tension Subroutine
2710 '
2720 X=TF*(1-EXP(CT/TB))
2730 Q=2 : Y3=0
2740 FOR I=3 TO NEDOF
2750 W(I)=-P(3,I)*CT*NL/KN(I)
2760 Y3=Y3+P(3,I)*W(I)
2770 NEXT
2780 YC=(CT-X)/KC
2790 W(2)=(Y3-YC)/P(2,2)
2800 FO=FI
2810 GOSUB 2980
2820 RETURN
2830 '
2840 'Case 3 - Cable slack
2850 '
2860 PRINT "Input motor speed attained at which "
2870 PRINT "all slack is used up. ( dy(1) synchronous =";VO;")";
2880 INPUT DY1
2890 PRINT #3, "  dy1 at start = ";DY1: CLOSE #3
2900 Q=2 :IF DY1>VC THEN Q=1
2910 DW(1)=DY1/P(1,1)
2920 FO=A0P(Q)+A1P(Q)*DY1+A2P(Q)*DY1*DY1
2930 CT=0
2940 L=0
2950 GOSUB 2980
```

```
2960 GOTO 3070
2970 '
2980 '::::::::: Initial Motor Acc Subroutine :::::::::::::
2990 '
3000 DDY1=(F0-CT)/MM
3010 DDW(1)=DDY1/P(1,1)
3020 RETURN
3030 '
3040 'Case 4 - Prescribed
3050 PRINT "Case 4 is not written yet. Sorry" : GOTO 2360
3060 '
3070 ':::::::::: Save Starting Conditions :::::::::::
3080 '
3090 CTB=CT : CTC=CT
3100 BDY1(1)=A1P(1)-MM*BETA2/DT/BETA1
3110 BDY1(2)=A1P(2)-MM*BETA2/DT/BETA1
3120 PRINT #2, MKI$(3);MKI$(NEDOF+1);MKS$(1);SPACE$(4);
3130 FOR I=1 TO NEDOF
3140 PRINT #2, MKS$(W(I));MKS$(DW(I));MKS$(DDW(I));
3150 NEXT
3160 PRINT #2, MKS$(Y1);MKS$(DY1);MKS$(DDY1);
3170 CLOSE #2
3180 '
3190 '::::::::::: Loop for Each Time Step :::::::::::::
3200 '
3210 FOR ITS=1 TO NTS
3220 LOCATE 24,60 : PRINT ITS;
3230 '
3240 ':::::::::: Print Data :::::::::::::
3250 '
3260 IF FIX((ITS-1)/STP%)*STP%<>ITS-1 GOTO 3310
3270 FOR I=1 TO NEDOF
3280 PRINT #1, MKS$(W(I));
3290 NEXT
3300 PRINT #1, MKS$(CT);MKS$(F0);MKS$(YC);
3310 IT =0
3320 '
3330 'Calculate First Guess for CT
3340 '
3350 IF TF=0 THEN X=0 :GOTO 3430
3360 CTA=CTB : CTB=CTC : CTC=CT
3370 CT=CTA-3*CTB+3*CTC
3380 IF CT<0 THEN CT=0
3390 ICNV=1
3400 '
3410 ':::::::::: Calc y1* and y1** :::::::::::::::
3420 '
3430 Y1S=FNS(Y1,DY1,DDY1)
3440 Y1SS=FNSS(Y1,DY1,DDY1)
3450 '
3460 ':::::::::: Calc kc<Φc>[D]{W**} :::::::::::::::
3470 '
3480 KPDWSS=0
3490 FOR I=1 TO NEDOF
3500 KPDWSS=KPDWSS+KPD(I)*FNSS(W(I),DW(I),DDW(I))
3510 NEXT
3520 '
3530 ':::::::::: Check if Load is hanging ::::::::::::::::
3540 '
3550 IF T0=MLG/NL GOTO 3780
```

```
3560 '
3570 ':::::::::: Calc a0 and a1 ::::::::::::::::::::
3580 '
3590 'Load Supported
3600 '
3610 A1=A1F/Z0
3620 A0LX=KS/Z0*(Y1S-Y1SS)+KPDWSS/(Z2*Z0)
3630 ZZ=Z2*Z0
3640 GOSUB 3880
3650 L=-NL*CT
3660 IF CT<MLG/NL GOTO 4370
3670 '
3680 'Load Changing from Supported to Hanging
3690 '
3700 T0=CT: TG=CT:F01=F0: GOTO 3780
3710 T4=CT
3720 CT=(T0-MLG/NL)*(T4-T1)/(T0-T1)+MLG/NL
3730 F0=F01+(F0-F01)*(CT-T0)/(T4-T0)
3740 L=-MLG
3750 T0=MLG/NL
3760 GOTO 4370
3770 '
3780 'Load Hanging
3790 '
3800 A1=A1F/ZG
3810 A0LX=KS/ZG*(Y1S-Y1SS)+FG+KPDWSS/(Z1*ZG)
3820 ZZ=Z1*ZG
3830 GOSUB 3880
3840 L=-MLG
3850 IF T0>MLG/NL GOTO 3710
3860 GOTO 4370
3870 '
3880 '::::::::::::::Iteration Procedure for CT ::::::::::::
3890 '
3900 'Constant kc case
3910 '
3920 IF TF=0 THEN X=0 : GOTO 4000
3930 '
3940 '
3950 '          Iteration  : Calc DY1 from equation of motion and
3960 '                       CT from parabolic motor equation
3970 '
3980 CDY1=A0P(Q)-MM*BETA2*(Y1S-Y1SS)/DT^2-CT
3990 DY1=(-BDY1(Q)-SQR(BDY1(Q)^2-4*A2P(Q)*CDY1))/2/A2P(Q)
4000 IF Q=2 AND DY1>VC THEN Q=1 : GOTO 3980
4010 IF Q=1 AND DY1<VC THEN Q=2 : GOTO 3980
4020 A0=A0P(Q)-(A1-A1P(Q))*DY1+A2P(Q)*DY1^2
4030 X=(A0-A0LX)*ZZ
4040 IF X<TF THEN ICNV=2 :GOTO 4120
4050 CT2=CT
4060 CT=TB*LOG(1-X/TF)
4070 GOTO 4240
4080 F0=A0+A1*DY1
4090 DDY1=BETA2*(DY1*DT/BETA1+Y1S-Y1SS)/(DT*DT)
4100 RETURN
4110 '
4120 'backwards iteration
4130 '
4140 X=TF*(1-EXP(CT/TB))
4150 A0=X/ZZ+A0LX
```

```
4160 DY1=(A1-A1P(Q)-SQR((A1-A1P(Q))^2-4*A2P(Q)*(A0P(Q)-A0)))/2/A2P(Q)
4170 IF Q=2 AND DY1>VC THEN Q=1 : GOTO 4160
4180 IF Q=1 AND DY1<VC THEN Q=2 : GOTO 4160
4190 FO=A0+A1*DY1
4200 DDY1=BETA2*(DY1*DT/BETA1+Y1S-Y1SS)/(DT*DT)
4205 CT2=CT
4210 CT=FO-MM*DDY1
4230 '
4240 'Check for convergence
4250 '
4270 IF ABS(CT-CT2)<LIM THEN GOTO 4080
4280 IT=IT+1
4290 IF IT=1 THEN CTG=(CT2+CT)/2 : GOTO 4310
4300 CTG=(CT2/(CT-CT2)+A/(A-B))/(1/(CT-CT2)+1/(A-B))
4310 A=CT2
4320 B=CT
4330 CNV=ABS(CT-CT2)
4340 CT=CTG
4350 ON ICNV GOTO 3950,4120
4360 '
4370 ':::::::: Calc y1, {W}, {dW}, {ddW} and yc :::::::::
4380 '
4390 CNV=MLG
4400 YCOLD=YC
4410 Y1=DT*DY1/BETA1+Y1S
4420 W(1)=Y1/P(1,1)
4430 DW(1)=DY1/P(1,1)
4440 DDW(1)=DDY1/P(1,1)
4450 YC=PC(1)*W(1)
4460 FOR I=2 TO NEDOF
4470 WS=FNS(W(I),DW(I),DDW(I))
4480 WSS=FNSS(W(I),DW(I),DDW(I))
4490 W(I)=B(I)*L-NL*CT*C(I)+D(I)*WSS
4500 DW(I)=BETA1/DT*(W(I)-WS)
4510 DDW(I)=BETA2/(DT*DT)*(W(I)-WSS)
4520 YC=YC+PC(I)*W(I)
4530 NEXT
4540 NEXT ITS
4550 CLOSE
4560 '
4570 'W2Y
4580 '
4590 'This program calcs {Y} = [Φ]{W}
4600 ' where {W} has been generated from CRIS and [Φ] from GENJAC
4610 '
4620 'Get [Φ]
4630 '
4640 DEFSNG P,D,Y
4650 '
4660 OPEN NSF$+".P" AS #1  LEN=8
4670 FIELD #1, 4 AS V$
4680 GET #1
4690 NDOF=CVS(V$)
4700 FIELD #1, 8 AS V$
4710 DIM P(NDOF,NDOF)
4720 FOR I=1 TO NDOF
4730 FOR J=1 TO NDOF
4740 GET #1
4750 P(I,J)=CVD(V$)
4760 NEXT
```

```
4770 NEXT
4780 CLOSE
4790 '
4800 'Get {W} size
4810 '
4820 OPEN NTF$+".W" AS #1  LEN = 8
4830 FIELD #1, 2 AS N$, 2 AS NPT$, 4 AS DT$
4840 GET #1
4850 N=CVI(N$)-3
4860 IF N<> NDOF THEN PRINT"[Φ] and {W} not the same size! ":PRINT"Extra {W}s as
sumed to be 0s."
4870 NPTS=CVI(NPT$)
4880 DT=CVS(DT$)
4890 CLOSE
4900 DIM W$(N)
4910 '
4920 'Set up {Y} output files
4930 '
4940 OPEN NTF$+".Y" FOR OUTPUT AS #2
4950 OPEN NTF$+"Y.DAT" FOR OUTPUT AS #3
4960 '
4970 'Order {W} data
4980 '
4990 OPEN NTF$+".W" AS #1  LEN=4*N+12
5000 FOR I=1 TO N
5010 FIELD #1, (I-1)*4 AS NULL$, 4 AS W$(I)
5020 NEXT
5030 FIELD #1, N*4 AS NULL$, 4 AS CT$, 4 AS F0$, 4 AS YC$
5040 GET #1
5050 PRINT #2, MKI$(NDOF);NPT$;DT$;SPACE$((NDOF-2)*4);
5060 '
5070 'Loop for each reading
5080 '
5090 FOR H=1 TO NPTS
5100 GET #1, H+1
5110 '
5120 'Calc {Y}=[Φ]{W}
5130 '
5140 PRINT #3, USING "##.###^^^^^";DT*(H-1);
5150 FOR I=1 TO NDOF
5160 Y=0
5170 FOR J=1 TO N
5180 Y=P(I,J)*CVS(W$(J))+Y
5190 NEXT
5200 '
5210 'Store {Y}
5220 '
5230 PRINT #2, MKS$(Y);
5240 IF I<4 THEN PRINT #3, USING ", ##.###^^^^^";Y;
5250 NEXT
5260 PRINT #3, USING ", ##.###^^^^^";ISF*CVS(CT$);ISF*CVS(F0$);CVS(YC$)
5270 NEXT
5280 '
5290 CLOSE
5300 '
5310 ' VMSES
5320 '
5330 'This program calcs shears,moments, and strain energy
5340 'for beam members created by MAKEKAM and {Y} from
5350 'W2Y.   Part of thesis for Doug Barrett. (me)
```

```
5360 '
5370 'Open Member Datafile
5380 '
5390 DEFINT P
5400 DEFSNG V,M,S,D,A,T
5410 OPEN NSF$+".L" AS #2  LEN=16
5420 FIELD #2, 2 AS NM$
5430 GET #2,1
5440 NM=CVI(NM$)
5450 FIELD #2, 4 AS CST$, 4 AS L$,
 AS P$(1), 2 AS P$(2), 2 AS P$(3), 2 A
S P$(4)
5460 '
5470 'Open Y data and get size
5480 '
5490 OPEN NTF$+".Y" AS #1   LEN=8
5500 FIELD #1,2 AS NDOF$, 2 AS NPTS$, 4 AS DT$
5510 GET #1,1
5520 NDOF=CVI(NDOF$) : NPTS=CVI(NPTS$) : DT=CVS(DT$)
5530 CLOSE #1
5540 OPEN NTF$+".Y" AS #1  LEN=4*(NDOF)
5550 '
5560 'Loop for each member
5570 '
5580 OPEN NTF$+"MX.DAT" FOR OUTPUT AS #4
5590 FOR M%=1 TO NM
5600 '
5610 'Get Member Data
5620 '
5630 GET #2
5640 FOR I=1 TO 4 : P(I)=CVI(P$(I)) : NEXT
5650 L=CVS(L$) : CST=CVS(CST$)
5660 '
5670 'Select Ys Required
5680 '
5690 FOR I=1 TO 4
5700 IF P(I)+2>NDOF THEN Y$(I)=MKS$(0) : GOTO 5720
5710 FIELD #1, (P(I)+1)*4 AS NULL$, 4 AS Y$(I)
5720 NEXT
5730 '
5740 'Loop for Each Timestep
5750 '
5760 OPEN NTF$+RIGHT$(STR$(M%),(FIX(LOG(M%)/LOG(10))+1))+".DAT" FOR OUTPUT AS #3
5770 FOR  PT=1 TO NPTS-1
5780 '
5790 'Get y values
5800 '
5810 GET #1,PT+1
5820 FOR I=1 TO 4
5830 Y(I)=CVS(Y$(I))
5840 NEXT
5850 '
5860 'Calculate Forces and Energy
5870 '
5880 V1=CST*(6*Y(1)+3*Y(2)*L-6*Y(3)+3*L*Y(4))
5890 M1=CST*L*(3*Y(1)+2*Y(2)*L-3*Y(3)+L*Y(4))
5900 M2=CST*L*(3*Y(1)+Y(2)*L-3*Y(3)+L*2*Y(4))
5910 SE=((Y(1)-Y(3))*V1+Y(2)*M1+Y(4)*M2)/2
5920 D1=Y(1):A1=Y(2):D2=Y(3):A2=Y(4)
5930 '
```

```
5940 'Check for Max
5950 '
5960 T=DT*(PT-1)
5970 IF PT>1 GOTO 6060
5980 V1MAX=ABS(V1)
5990 M1MAX=ABS(M1)
6000 M2MAX=ABS(M2)
6010 SEMAX=ABS(SE)
6020 D1MAX=ABS(D1)
6030 A1MAX=ABS(A1)
6040 D2MAX=ABS(D2)
6050 A2MAX=ABS(A2)
6060 IF ABS(V1)>V1MAX THEN V1MAX=ABS(V1) : TV1MAX=T
6070 IF ABS(M1)>M1MAX THEN M1MAX=ABS(M1) : TM1MAX=T
6080 IF ABS(M2)>M2MAX THEN M2MAX=ABS(M2) : TM2MAX=T
6090 IF ABS(SE)>SEMAX THEN SEMAX=ABS(SE) : TSEMAX=T
6100 IF ABS(D1)>D1MAX THEN D1MAX=ABS(D1) : TD1MAX=T
6110 IF ABS(A1)>A1MAX THEN A1MAX=ABS(A1) : TA1MAX=T
6120 IF ABS(D2)>D2MAX THEN D2MAX=ABS(D2) : TD2MAX=T
6130 IF ABS(A2)>A2MAX THEN A2MAX=ABS(A2) : TA2MAX=T
6140 '
6150 'Store Data
6160 '
6170 PRINT #3,USING "##.###^^^^, "; T,V1,M1,M2,SE,D1,A1,D2,A2
6180 '
6190 NEXT  PT
6200 '
6210 'print Max data
6220 '
6230 PRINT #4, USING "###,";M%;
6240 PRINT #4, USING "##.###^^^^,";V1MAX,TV1MAX,M1MAX,TM1MAX,M2MAX,TM2MAX,SEMAX,
TSEMAX;
6250 PRINT #4, USING "##.###^^^^,";D1MAX,TD1MAX,D2MAX,TD2MAX,A1MAX,TA1MAX,A2MAX,
TA2MAX
6260 CLOSE #3
6270 NEXT M%
6280 '
6290 CLOSE
6300 KILL NTF$+".W"
6310 KILL NTF$+".Y"
6320 CLEAR
6330 GOTO 290
```

APPENDIX D

DERIVATIONS

Appendix D contains the mathematical derivations and proofs referred to in Chapters 4 and 5

Appendix D.1 Derivation of Parabolic Compound Curve

Figure D.1 shows the compound parabolic curve used to approximate the force versus motor speed relationship. Parabola #1 passes through $F = 0$ when $V = V_o$, and passes through $F = F_p$ when $V = V_p = V_o(1 - S_p)$, with slope of zero. By symetry,

$$F_1 = C(V_o - V)\,(V_o(1 - 2s_p) - V) \quad , \qquad \text{(D.1.1)}$$

where C is a constant. When $V = V_p$,

$$F_1 = F_p = C(V_o - V_p)(2V_p - V_o - V_p) \, ,$$

$$F_p = -C(V_o - V_p)^2 \, ,$$

$$\text{and therefore} \quad C = \frac{-F_p}{(V_o - V_p)^2} \; . \qquad \text{(D.1.2)}$$

The expression for C in (D.1.2) is substituted into equation (D.1.1).

$$F_1 = \frac{-F_p}{(V_o - V_p)^2}\,(V_o - V)(2V_p - V_o - V)$$

$$= \frac{-F_p}{(V_o - V_p)^2}\,V^2 + \frac{F_p}{(V_o - V_p)^2}\,(2V_p - V_o + V_o)V$$

$$- \frac{F_p}{(V_o - V_p)^2}\,(Vo(2V_p - V_o))$$

The coefficients for the first parabola are the following.

$$b_{0p1} = \frac{F_p\,V_o}{(V_o - V_p)^2}\,(V_o - 2V_p) = \frac{F_p(2sp - 1)}{sp^2}$$

Figure D.1 Derivation of Compound Parabolic Curve to Approximate Force versus Motor Speed Relationship

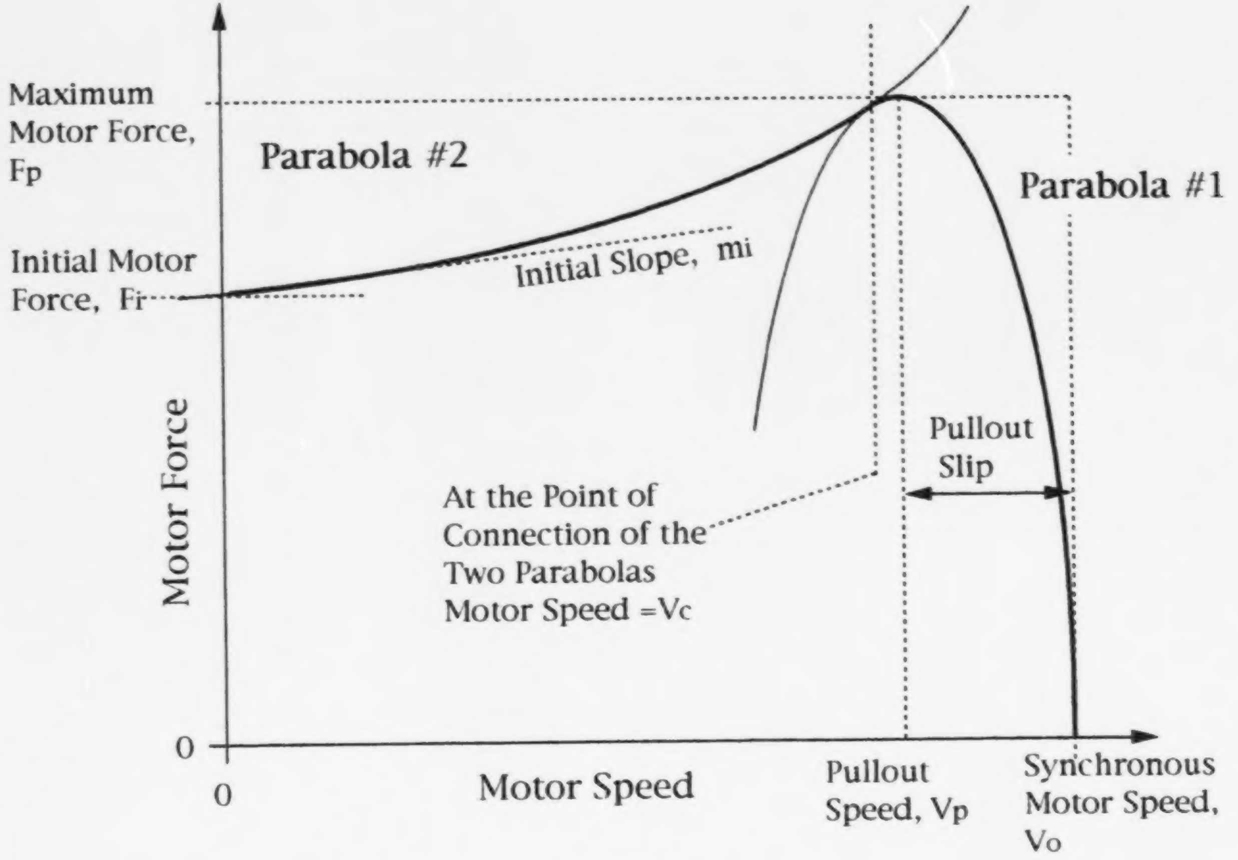

$$b_{1p1} = \frac{2F_p\, V_p}{(V_o - V_p)^2} = \frac{2F_p\, V_p}{V_o^2 - sp^2}$$

$$b_{2p1} = \frac{-F_p}{(V_o - V_p)^2} = \frac{-F_p}{V_o^2 - V_p^2}$$

The subscript "p1" refers to the fact that these coefficients are for the first parabola of the compound curve.

Parabola #2 passes through $F = F_i$ when $V = 0$, with slope m_i.

$$F_2 = F_i + m_i V + b_{2p2}\, V^2$$

The subscript "p2" refers to the fact that the coefficient is for the second parabola of the compound curve.

Parabola #1 and #2 meet at $V = Vc$ with same slope.

$$\frac{dF_2}{dV} \text{ at } V_c = m_i + 2b_{2p2}\, Vc \qquad \text{(D.1.3)}$$

$$\text{and } \frac{dF_1}{dV} \text{ at } V_c = \frac{2F_pV_p}{V_o^2 sp^2} - \frac{2F_pV_c}{V_o^2 sp^2} = \frac{2F_p}{V_o^2 sp^2}(V_p - V_c) \qquad \text{(D.1.4)}$$

From (D.1.3) and (D.1.4), the following expression for b_{2p2} results.

$$b_{2p2} = \frac{\frac{2F_p}{V_o^2 sp^2}(V_p - V_c) - m_i}{2V_c} \qquad \text{(D.1.5)}$$

When $V = V_c$,

$$F_1 = \frac{-F_p}{V_o^2 sp^2}(V_c^2 - 2V_pV_c + V_o(2V_p - V_o)), \qquad \text{(D.1.6)}$$

$$\text{and} \quad F_2 = F_i + m_i V_c + b_{2p2}\, Vc^2 . \qquad \text{(D.1.7)}$$

Equating the right sides of (D.1.6) and (D.1.7), and using the expression for b_{2p2} from (D.1.5), gives the following.

$$\frac{-F_p}{(V_o - V_p)^2}\,(V_c^2 - 2V_pV_c\ + 2V_oV_p - V_o^2)$$

$$= \ F_i + m_i\,V_c + \frac{F_p}{V_o sp^2}\,(Vp - Vo)Vc\ - \frac{miVc}{2}$$

$$V_c\left(\frac{2F_pV_p}{V_o^2sp^2} + m_i - \frac{m_i}{2} + \frac{F_pV_p}{V_o^2sp^2}\right) = \frac{F_p}{V_o^2sp^2}\,(V_o^2 - 2V_oV_p)\ -\ F_i \qquad \text{(D.1.8)}$$

Equation (D.1.8) is rewritten as an expression for V_c.

$$V_c\ =\ \frac{\frac{F_p}{sp^2}\,(2sp - 1\,)\ -\ F_i}{\frac{-\,F_pV_p}{V_o^2sp^2} + \frac{m_i}{2}}\ =\ \frac{b_{0p1}\ -\ F_i}{\frac{-\,b_{1p1}}{2} + \frac{m_i}{2}} \qquad \text{(D.1.9)}$$

Appendix D.2 Proof that ω_2^2 and ω_3^2 Bound ω_s^2 and ω_c^2

The expressions for the natural frequencies of the 3DoF system are given in Equations (5.20) and (5.21).

$$\omega_2^2 = \frac{\Omega^2 + \omega_s^2 - \sqrt{(\Omega^2 + \omega_s^2)^2 - 4\omega_s^2\left(\omega_c^2\ +\ \frac{k_c}{n^2m_m}\right)}}{2} \qquad (5.20)$$

$$\omega_3^2 = \frac{\Omega^2 + \omega_s^2 + \sqrt{(\Omega^2 + \omega_s^2)^2 - 4\omega_s^2\left(\omega_c^2\ +\ \frac{k_c}{n^2m_m}\right)}}{2} \qquad (5.21)$$

The product of the natural frequencies is the following.

$$\omega_2^2\omega_3^2 = \frac{(\Omega^2 + \omega_s^2)^2 - (\Omega^2 + \omega_s^2)^2 + 4\omega_s^2\left(\omega_c^2 + \dfrac{k_c}{n^2 m_m}\right)}{4}$$

$$= \omega_s^2\omega_c^2 + \frac{\omega_s^2 k_c}{n^2 m_m} \qquad \text{(D.2.1)}$$

When m_m approaches infinity, equation (D.2.1) becomes

$$\omega_2^2\omega_3^2 = \omega_2^2\omega_c^2 \, . \qquad \text{(D.2.2)}$$

The sum of the natural frequencies is the following.

$$\omega_2^2 + \omega_3^2 = \Omega^2 + \omega_s^2 = \omega_c^2 + \omega_2^2 + \frac{k_c}{m_s} + \frac{k_c}{n^2 m_m} \qquad \text{(D.2.3)}$$

Because the sum of ω_2^2 and ω_3^2 is greater than the sum of ω_s^2 and ω_c^2, it must be the case that $\omega_3^2 > \omega_s^2$ and ω_c^2, and that $\omega_2^2 < \omega_s^2$ and ω_c^2 .

Appendix D.3 Proof that $(1 - \gamma_2)(1 - \gamma_3) = -\mu$

The following is a proof that when m_m approaches infinity, $(1 - \gamma_2)(1 - \gamma_3)$ approaches $-\mu$. From equations (D.2.1) and (D.2.3) of Appendix D.2, the product and sum of the natural frequencies is the following.

$$\omega_2^2\omega_3^2 = \omega_s^2\omega_c^2 + \frac{\omega_s^2 k_c}{n^2 m_m} \qquad \text{(D.3.1)}$$

$$\omega_2^2 + \omega_3^2 = \Omega^2 + \omega_s^2 = \omega_c^2 + \omega_s^2 + \frac{k_c}{m_s} + \frac{k_c}{n^2 m_m} \qquad \text{(D.3.2)}$$

The product of $(1 - \gamma_2)$ and $(1 - \gamma_3)$ is written in terms of frequencies.

$$(1 - \gamma_2)(1 - \gamma_3) = \left(\frac{\omega_2^2}{\omega_2^2 - \omega_s^2}\right)\left(\frac{\omega_3^2}{\omega_3^2 - \omega_s^2}\right) \qquad \text{(D.3.3)}$$

The denominator in equation (D.3.3) is expanded and simplified using equations (D.3.1) and (D.3.2).

$$(\omega_2^2 - \omega_s^2)(\omega_3^2 - \omega_s^2) = \omega_2^2\omega_3^2 - \omega_s^2(\omega_2^2 + \omega_3^2) + \omega_s^4$$

$$= \omega_s^2\omega_c^2 + \frac{\omega_s^2 k_c}{n^2 m_m} - \omega_s^2\left(\omega_c^2 + \omega_s^2 + \frac{k_c}{m_s} + \frac{k_c}{n^2 m_m}\right) + \omega_s^4$$

$$= \omega_s^2\left(\omega_c^2 + \frac{k_c}{n^2 m_m} - \omega_c^2 - \omega_s^2 - \frac{k_c}{m_s} - \frac{k_c}{n^2 m_m} + \omega_s^2\right)$$

$$= -\,\omega_s^2\frac{k_c}{m_s} \qquad \text{(D.3.4)}$$

Therefore, the product of $(1 - \gamma_2)$ and $(1 - \gamma_3)$ is

$$(1 - \gamma_2)(1 - \gamma_3) = \frac{\omega_c^2 + \dfrac{k_c}{n^2 m_m}}{\dfrac{k_c}{m_s}}$$

$$= -\frac{m_s}{m_p} - \frac{m_s}{n^2 m_m} \quad .$$

When m_m approaches infinity, the following equation holds.

$$(1 - \gamma_2)(1 - \gamma_3) = -\frac{m_s}{m_p} = -\mu \qquad \text{(D.3.5)}$$

Appendix D.4 Proof that $\mu > \gamma_2 - 1$

Equation (D.3.5) from Appendix D.3 is the following.

$$(1 - \gamma_2)(1 - \gamma_3) = -\mu \tag{D.3.5}$$

This can be rewritten as shown below.

$$1 - \gamma_3 = \frac{\mu}{\gamma_2 - 1} \tag{D.4.1}$$

If $\mu > \gamma_2 - 1$, then from (D.4.1) it follows that

$$1 - \gamma_3 > 1 \ , \quad \text{or} \quad \gamma_3 < 0 \ .$$

The expression for γ_3 from (5.25), is

$$\gamma_3 = \frac{1}{1 - \frac{\omega_3^2}{\omega_s^2}} \ .$$

Because $\omega_3^2 > \omega_s^2$, it must be that $\gamma_3 < 0$, and therefore $\mu > \gamma_2 - 1$.

Appendix D.5 Modal Masses

The modal masses are derived by finding the solution to $[\Phi]^T\,[M]\,[\Phi]$. The product of the first two factors $[\Phi]^T\,[M]$ follows.

$$\begin{bmatrix} 1 & \frac{1}{n} & O \\ \frac{m_s}{nm_m} & -\mu & 1-\gamma_2 \\ \frac{m_s}{nm_m} & -\mu & 1-\gamma_3 \end{bmatrix} \begin{bmatrix} m_m & O & O \\ O & m_p & O \\ O & O & m_s \end{bmatrix} = \begin{bmatrix} m_m & \frac{m_p}{n} & O \\ \frac{m_s}{n} & -m_s & (1-\gamma_2)m_s \\ \frac{m_s}{n} & -m_s & (1-\gamma_3)m_s \end{bmatrix}$$

This matrix is multiplied by $[\Phi]$ as shown below.

$$\begin{bmatrix} m_m & \frac{m_p}{n} & O \\ \frac{m_s}{n} & -m_s & (1-\gamma_2)m_s \\ \frac{m_s}{n} & -m_s & (1-\gamma_3)m_s \end{bmatrix} \begin{bmatrix} 1 & \frac{1}{n} & O \\ \frac{m_s}{nm_m} & -\mu & 1-\gamma_2 \\ \frac{m_s}{nm_m} & -\mu & 1-\gamma_3 \end{bmatrix} =$$

$$\begin{bmatrix} m_m + \frac{m_p}{n^2} & \frac{m_s}{n} - \frac{m_s}{n} & \frac{m_s}{n} - \frac{m_s}{n} \\ \frac{m_s}{n} - \frac{m_s}{n} & \frac{m_s^2}{n^2 m_m} + \frac{m_s^2}{m_p} + (1-\gamma_2)^2 m_s & \frac{m_s^2}{n^2 m_m} + \frac{m_s^2}{m_p} + (1-\gamma_2)(1-\gamma_3)m_s \\ \frac{m_s}{n} - \frac{m_s}{n} & \frac{m_s^2}{n^2 m_m} + \frac{m_s^2}{m_p} + (1-\gamma_2)(1-\gamma_3)m_s & \frac{m_s^2}{n^2 m_m} + \frac{m_s^2}{m_p} + (1-\gamma_3)^2 m_s \end{bmatrix}$$

In Appendix D.4 it was shown that

$$(1 - \gamma_2)(1 - \gamma_3) = -\frac{m_s}{m_p} - \frac{m_s}{n^2 m_m} \quad .$$

Therefore, the solutions to the expressions in positions (2,3) and (3,2) of the matrix $[\Phi]^T$ [M] $[\Phi]$ are zero. It can be seen that all the other non-diagonal terms also solve to zero. Using the relationship

$$(1 - \gamma_2)(1 - \gamma_3) = -\frac{m_s}{m_p} - \frac{m_s}{n^2 m_m} \quad ,$$

the second diagonal term can be simplified.

$$\frac{{m_s}^2}{n^2 m_m} + \frac{{m_s}^2}{m_p} + (1 - \gamma_2)^2 m_s$$

$$= -(1 - \gamma_2)(1 - \gamma_3)\, m_s + (1 - \gamma_2)^2 m_s$$

$$= m_s(1 - \gamma_2)(\gamma_3 - \gamma_2)$$

Similarly, the third diagonal term can be rewritten as follows.

$$\frac{{m_s}^2}{n^2 m_m} + \frac{{m_s}^2}{m_p} + (1 - \gamma_3)^2 m_s$$

$$m_s(1 - \gamma_3)(\gamma_2 - \gamma_3)$$

The resulting modal mass matrix is the following.

$$\begin{bmatrix} m_m + \frac{m_p{}^2}{n^2} & 0 & 0 \\ 0 & m_s(1-\gamma_2)(\gamma_3-\gamma_2) & 0 \\ 0 & 0 & m_s(1-\gamma_3)(\gamma_3-\gamma_2) \end{bmatrix}$$

Appendix D.6 Proof that $(1-\gamma_2)B_2 + (1-\gamma_3)B_3 = \frac{-m_p g}{k_s}$

Expressions for B_2 and B_3 are given in Equations (5.51) and (5.52)

$$B_2 = \frac{g}{\omega_2^2\,(1-\gamma_2)\,(\gamma_3-\gamma_2)} \tag{5.51}$$

$$B_3 = \frac{g}{\omega_3^2\,(1-\gamma_3)\,(\gamma_2-\gamma_3)} \tag{5.52}$$

The proof proceeds as follows.

$$(1-\gamma_2)B_2 + (1-\gamma_3)B_3 = \frac{g}{\omega_2^2(\gamma_3-\gamma_2)} + \frac{g}{\omega_3^2\,(\gamma_2-\gamma_3)}$$

$$= \frac{(\omega_3^2-\omega_2^2)\;g}{\omega_2^2\omega_3^2\;(\gamma_3-\gamma_2)} \tag{D.6.1}$$

The term $(\gamma_3-\gamma_2)$ can be expressed as a function of frequencies.

$$\gamma_3 - \gamma_2 = \frac{1}{1 - \frac{\omega_3^2}{\omega_s^2}} - \frac{1}{1 - \frac{\omega_2^2}{\omega_s^2}}$$

$$= \frac{\omega_s^2}{\omega_s^2 - \omega_3^2} - \frac{\omega_s^2}{\omega_s^2 - \omega_2^2}$$

$$= \frac{(\omega_3^2 - \omega_2^2)\,\omega_s^2}{(\omega_s^2 - \omega_3^2)\,(\omega_s^2 - \omega_2^2)} \qquad \text{(D.6.2)}$$

The expression for $\gamma_3 - \gamma_1$ in equation (D.6.2) is substituted into equation (D.6.1).

$$(1 - \gamma_2)B_2 + (1 - \gamma_3)B_3 = \frac{g(\omega_3^2 - \omega_2^2)\,(\omega_s^2 - \omega_3^2)\,(\omega_s^2 - \omega_2^2)}{\omega_2^2\omega_3^2\,(\omega_3^2 - \omega_2^2)\omega_s^2}$$

$$\frac{g(\omega_s^2 - \omega_3^2)\,(\omega_s^2 - \omega_2^2)}{\omega_2^2\;\omega_3^2\;\omega_s^2} \qquad \text{(D.6.3)}$$

The expression for the product $(\omega_s^2 - \omega_3^2)\,(\omega_s^2 - \omega_2^2)$ is simplified as follows.

$$(\omega_s^2 - \omega_3^2)\,(\omega_s^2 - \omega_2^2) = \omega_s^4 - \omega_3^2\omega_s^2 - \omega_2^2\omega_s^2 + \omega_2^2\omega_3^2$$

$$= \omega_s^4 - \omega_s^2(\omega_2^2 + \omega_3^2) + \omega_2^2\omega_3^2$$

From equations (D.1.1) and (D.1.3) in Appendix D.2,

$$\omega_2^2\omega_3^2 = \omega_s^2\omega_c^2 \qquad \text{(D.6.5)}$$

$$\omega_2^2 + \omega_3^2 = \omega_2^2 + \omega_3^2 + \frac{k_c}{m_s} \qquad \text{(D.6.6)}$$

Using equations (D.6.5) and (D.6.6), equation (D.6.3) can be simplified.

$$(\omega_s^2 - \omega_3^2)(\omega_s^2 - \omega_2^2) = \omega_s^4 - \omega_s^2(\omega_c^2 + \omega_s^2 + \frac{k_c}{m_s}) + \omega_s^2\omega_c^2$$

$$= \omega_s^2(\omega_s^2 - \omega_c^2 - \omega_s^2 - \frac{k_c}{m_s} + \omega_c^2)$$

$$= -\,\omega_s^2 \frac{k_c}{m_s} \qquad \text{(D.6.7)}$$

Equations (D.6.5) and (D.6.7) are used in equation (D.6.3).

$$(1 - \gamma_2)B_2 + (1 - \gamma_3)B_3 = \frac{-g\,\omega_s^2 \frac{k_c}{m_s}}{\omega_s^4\omega_c^2}$$

$$= -\,g\frac{k_c\, m_s\, m_p}{m_s\, k_s k_c} = \frac{-m_p g}{k_s}$$

Appendix D.7 Proof that $\kappa > |\gamma_3|$

The proof that $\kappa > |\gamma_3|$ is done by proving that the statement $\kappa < |\gamma_3|$ is false. The expression for γ_3 is given in equation (5.25).

$$\gamma_3 = \frac{1}{1 - \frac{\omega_3^2}{\omega_s^2}} \tag{5.25}$$

Because $\omega_3^2 > \omega_s^2$, γ_3 is negative. The absolute value for γ_3 is as follows.

$$|\gamma_3| = \frac{1}{\frac{\omega_3^2}{\omega_s^2} - 1}$$

If $\kappa > |\gamma_3|$, then

$$\kappa < \frac{1}{\frac{\omega_3^2}{\omega_s^2} - 1} ,$$

$$\text{and} \quad \frac{1 + \kappa}{\kappa} > \frac{\omega_3^2}{\omega_s^2} . \tag{D.7.1}$$

From Equation (5.127)

$$\frac{\omega_3^2}{\omega_s^2} = \left(\frac{1 + \mu + \kappa}{2\kappa}\right)\left(1 + \sqrt{1 - \frac{4\mu\kappa}{(1 + \mu + \kappa)^2}}\right) .$$

This expression for the frequency ratio can be substituted into (D.7.1) and the following inequality results.

$$\frac{1+\kappa}{\kappa} > \left(\frac{1+\mu+\kappa}{2\kappa}\right)\left(1+\sqrt{1-\frac{4\mu\kappa}{(1+\mu+\kappa)^2}}\right)$$

$$\frac{2(1+\kappa)}{1+\mu+\kappa} - 1 > \sqrt{1-\frac{4\mu\kappa}{(1+\mu+\kappa)^2}}$$

$$\frac{1-\mu+\kappa}{1+\mu+\kappa} > \sqrt{1-\frac{4\mu\kappa}{(1+\mu+\kappa)^2}}$$

$$\frac{(1-\mu+\kappa)^2}{(1+\mu+\kappa)^2} > 1-\frac{4\mu\kappa}{(1+\mu+\kappa)^2}$$

$$(1-\mu+\kappa)^2 > (1+\mu+\kappa)^2 - 4\mu\kappa$$

$$1+\mu^2+\kappa^2-2\mu-2\mu\kappa+2\kappa > 1+\mu^2+\kappa^2+2\mu+2\kappa-2\mu\kappa$$

$$-2\mu > +2\mu$$

Therefore, if $\kappa < |\gamma_3|$, then $-2\mu > +2\mu$. For positive values of μ, this cannot be, and therefore $\kappa > |\gamma_3|$.

APPENDIX E

LETTER FROM CMAA

Appendix E contains a copy of a letter from the Chair of the Engineering Committee of the CMAA, regarding thoughts on how the factor HLF was derived.

KRANCO
INCORPORATED
Excellence in Material Handling
P.O. Box 40400 • Houston, Texas 77240 • 10543 Fisher Road • (713) 466-7541 • 800-527-3248

February 5, 1990

University of Alberta
220, Civil/Electrical Building
Edmonton, Alberta T6G 2G7

Attn: Doug Barrett

Dear Mr. Barrett,

The equation you referenced in your letter to MHI on January 16, 1990 is the result of many years of study and committee discussion and may very well be empirical.

I can only direct you to other specifications which are sometimes referenced for you to compare and draw your own conclusions.

AISE Standard #6 (tentative) - May 1, 1969
ANSI B30.2d - 1988
Federation Europeenne De La Manutention
(FEM) 2nd edition - Dec. 1970
ASME NOG - 1 - 1989

These may be of some assistance. Your local technical publication book store of library as your best source for locating the above.

Very truly yours,

RJ Kroll

R.J. Kroll
Chairman
CMAA Engineering Committee

RJK/mv

cc: Bill Capps
MHI